International Journal of Physics, 2016, Vol. 4, No. 1, 1-4
Available online at http://pubs.sciepub.com/ijp/4/1/1

DOI:10.12691/ijp-4-1-1

Laser Effect on the Activation Energies, Bulk Etch Rate and Track Etch Rate of CR-39 Polymeric Detector

Ahmed A. Ibrahim*, Sozan Bhaa-al-deen

Department Physics, College of Science, Kirkuk University, Kirkuk, Iraq
*Corresponding author: Ahmedabd71@yahoo.com

Abstract The aim of this paper is to find the effect of Nd: YAG laser of wavelength (532 nm), laser power 150 MW on the CR-39 polymer. Twenty three detectors were divided in to three sets. The first set (ten detectors) (post-exposed) was first exposed to alpha radiation from ^{241}Am source at 3MeV and then treated in air with laser at different exposure time started from 10 minutes to 100 minutes with ten minutes differ between them (alpha + laser). For the second set (ten detectors) (pre-exposed), the process was reversed (laser +alpha) under the same conditions, for the last set (three detectors) (un-exposed to laser), used as a control set, was irradiated with an alpha source (241Am). Alpha track diameters, bulk etching velocity (V_B), track etching velocity (V_T), etching efficiency (η), etching ratio (V) were determined. The activation energies of bulk etch (E_B) and track etch (E_T) for unexposed, post-exposed and pre-exposed are found to be equal to 1.10, 0.92, 0.82 eV and 1.07, 0.86, 0.79 eV respectively.

Keywords: *nuclear track detectors, CR-39, activation energy of bulk etch (EB) and track etch (ET), etching conditions*

Cite This Article: Ahmed A. Ibrahim, and Sozan Bhaa-al-deen, "Laser Effect on the Activation Energies, Bulk Etch Rate and Track Etch Rate of CR-39 Polymeric Detector." *International Journal of Physics*, vol. 4, no. 1 (2016): 1-4. doi: 10.12691/ijp-4-1-1.

1. Introduction

Nuclear track techniques are very important in many fields of science and technology. A solid state nuclear track detector namely CR-39 [poly-allyl-diglycol carbonate (C12H18O7)] is widely used for the detection of low Z and high Z particles. [1]. The interaction of electromagnetic radiation with the detector material results in structural changes. These changes depend on several factors such as detector structure, exposure condition, radiation type and energy, irradiation condition, etching process etc. Two competing processes, bond secession and crosslink, occur as a result of irradiation with (LLET) radiation. Bond secession lead to the degradation of the surface and as a result increases the bulk and track etch rates while crosslink results in hardening of the

Surface and subsequently decreases the bulk and track etch rates.[2]. The laser effect on the (SSNTDs) depends on laser properties (laser wavelength, laser repetition rate and energy density) and on the detector properties (density, thickness, etc). In general, infrared (IR) laser interaction with SSNTDs can induce thermal effects [3], while ultraviolet (UV) laser will give rise to photoablation or photodecomposition [4]. Many authors reported the effects of incoherent UV radiation on the etching properties of SSNTDs. These effects depend on several factors: radiation parameters, detector property and irradiation condition [5]. Activation energy of CR-39 polymer detector (bulk or track) is defined as the energy required to activate the reaction between the detector material and the etchant solution. Many works studied the activation energy of the CR-39 polymer detector [6,7]. The effect of gamma irradiation on the activation energy of CR-39 polymer detector was reported by [8].

2. Materials and Method

2.1. To find Laser effect on CR-39

CR-39 detector (1cm2) of thickness (0.5 mm). Twenty three detectors were divided into three sets, The third set(three detectors) served as a control set and its samples were exposed only to alpha radiation with close contact to 241 Am, The first set (ten detectors) (post-exposed) was first exposed to alpha radiation from 241Am source and then treated in air with laser at different exposure time started from 10 minutes to 100 minutes with ten minutes differ between them (alpha + laser). For the second set (ten detectors) (pre-exposed), the process was reversed (laser +alpha) under the same conditions. All the samples were etched in 6.25 M NaOH solution at 343 ^{o}K.

2.1.1. To Find the Activation Energy:

Fifteen detectors were divided into three sets, The first set (five detectors) (post-exposed) was first exposed to alpha radiation from 241Am source and then treated in air with laser at 60 minutes (alpha + laser), the second set (Five detectors) (pre-exposed), the process was reversed (laser +alpha) under the same conditions and the the third set served as a control set and its samples were exposed only to alpha radiation with close contact to 241 Am,. All the samples were etched in 6.25 M NaOH solution at five different temperatures, ranging from 338 K to 358 K, for 3

h. An equal temperature increment of 5 K was used. After etching, CR-39 detectors were thoroughly washed with distilled water and dried in open air. The thickness of the removed layer as a result of etching was found using a sensitive micrometer with digital camera. The bulk etch rate, V_B, is calculated by

$$V_B = (d1 - d2 / 2t) \quad (1)$$

Where d1 and d2 are the detector thickness (in mm) before and after etching;
t: is the etching time (in h).

The track etching rate VT for a given alpha particle was determined by measuring the etch –cone length Le after an etching time t, such that

$$Le = V_T t - V_B t \quad (2)$$

with V_B and t known [9], the measured value of Le immediately yields the value V_T.

The etch rate (sensitivity) V for circular tracks is given by

$$V = (V_B / V_T) \quad (3)$$

The dependence of VB, VT on temperature follows the Arrhenius

Type of law and is given by

$$V_B (V_T) = Ae - E_B / Kt \quad (4)$$

Where E_B is the activation energy for bulk etch rate and A is a constant.

K is the Boltzmann constant, A similar equation applies for track etch rate, VT, by replacing EB by ET by taking a natural log of above equation and plotting the graph between ln V_B (V_T) and $10^3/Tk^{-1}$, the slope gives the value of E_B (E_T).

3. Result and Discussion

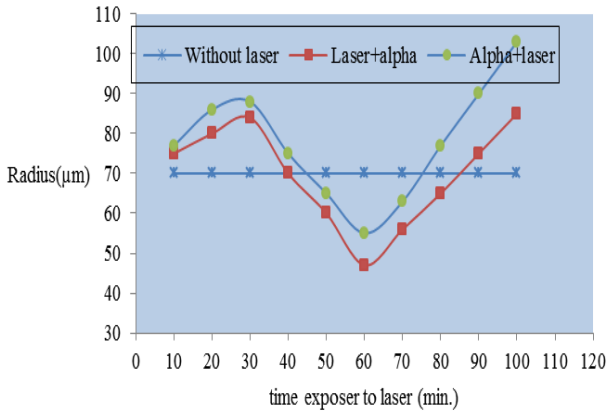

Figure 1. laser effect on CR-39

Figure 1 shows the effect laser radiation on CR-39 at different exposure time, The results showed that we have obtained an increase in the response of the detector irradiated with alpha particles and exposure to lasers, the increasing the size and speed of growth diameters effects formed a gradual increase with increasing to laser exposure time that value reached the highest value at exposure time is equal to 30min This indicates an increase in ductility Detector and get the decomposition in molecular chains and resulted in the acceleration of the process of the emergence of impact, and increase the time of exposure to a laser beam at 60min began diameters decreasing gradually until it reached a minimum value close to the diameters Detector record, which is due to increase in the complexity of chains of polymeric (Cross Linking) and hardening Detector this results agree with results in [10] references.

Table 1 and Table 2 shows the V_B and V_T value under at 60 minutes exposure time for laser radiation at different solution temperatures of three cases (laser+ alpha), (alpha +laser) and alpha only

Table 1. The value of V_B under laser radiation at different temperatures

	Laser + alpha	laser + Alpha	alpha
T °K	V_B(µm/hr)	V_B(µm/hr)	V_B(µm/hr)
338	0.4	0.813	1.152
343	0.813	1.08	1.355
348	1.49	2.168	2.64
353	2.168	2.71	3.25
358	2.64	3.32	4.065

Table 2. The value of V_T under laser radiation at different temperatures

	Laser + alpha	laser + Alpha	alpha
T °K	V_T(µm/hr)	V_T(µm/hr)	V_T(µm/hr)
338	0.424	0.839	1.184
343	0.876	1.1344	1.418
348	1.529	2.21	2.697
353	2.2	2.76	3.35
358	2.696	3.421	4.177

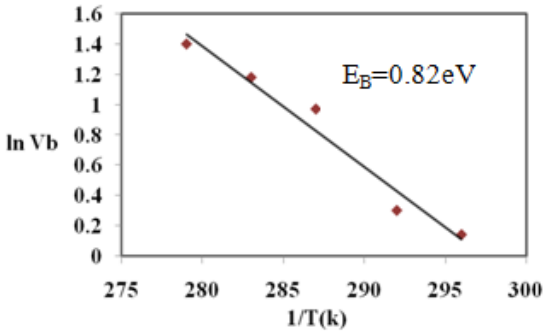

Figure 2. The activation energies for bulk (E_B) etch rate for alpha

The linear dependence of ln V_B and ln V_T versus reciprocal temperature, for reference, post-exposed and pre-exposed samples are depicted in Figs. Figure 2 and Figure 3 shows the variation of ln (vb) versus 1/T for alpha + laser, laser +alpha and alpha only of tracks to find the activation energies bulk in CR-39 by using the Arrhenius equation, the results of alpha only case is equal to 0.82 eV was less than from the another two cases alpha+ laser and laser + alpha there were 0.92 eV and 1.01eV respectively. The differences in value because the laser effects on the CR-39 polymer detector such as the (Cross Linking) and hardening Detector these effects lead to increase in activation energies of bulk etching. Again we can shows in Figure 5, Figure 6 and Figure 7 the variation of ln (V_T) versus 1/T for alpha + laser, laser +alpha and alpha only of tracks to find the activation energies track etching in CR-39 by using the Arrhenius equation, the results of alpha only case is equal to 0.79 eV

was less than from the another two cases alpha+ laser and laser + alpha there were 1.07 eV and 0.86eV respectively. The activation energies for bulk (E_B) and track (E_T) etch rates, for each set, were calculated from the slopes of these linear plots. These values are listed in Table 3.

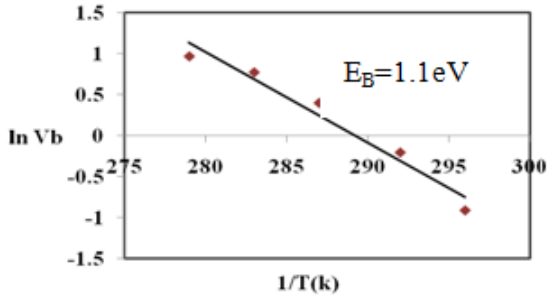

Figure 3. The activation energies for bulk (E_B) etch rate for laser+alpha

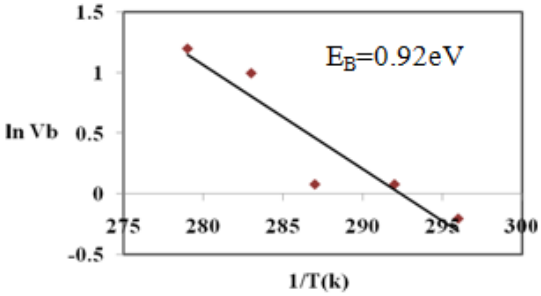

Figure 4 The activation energies for bulk (E_B) etch rate for alpha + laser

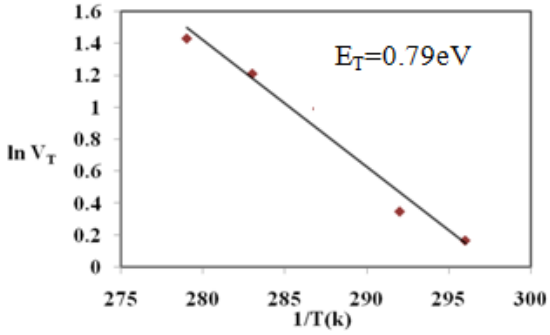

Figure 5. The activation energies for bulk (E_T) etch rate for alpha

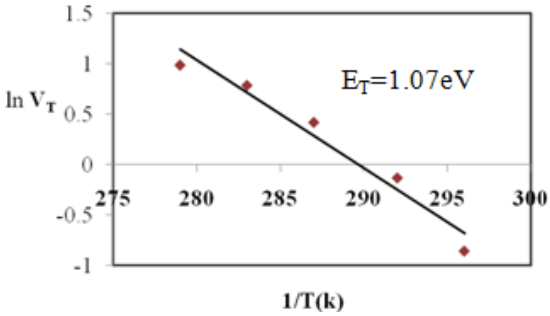

Figure 6. The activation energies for bulk E_T etch rate for laser+ alpha

Table 3. The values of The activation energies for bulk (E_B) and track (E_T) etch rates, for each set

Type of case	E_B (ev)	E_T(ev)
Laser+alpha	1.10	1.07
Alpha+ laser	0.92	0.86
Only alpha	0.82	0.79

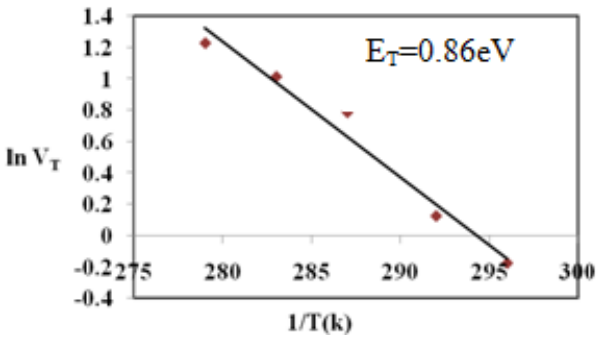

Figure 7. The activation energies for bulk (E_T) etch rate for alpha +laser

The measured values shows change in the activation energy of bulk etch rate for the irradiated samples as compared to the reference un-exposed sample. The activation energy of track etch rate for pre-exposed sample show an appreciable increases compared to that corresponding to the unexposed sample. This observed increase is indicative of the increase in hardening of CR-39 polymer detector resulting from the increase in cross-linking in the polymer. Also, the obtained values of E_T, in each set, are found to be less than those of E_B. This implies that the downward etch rate along the track is larger than that of bulk etch rate.

4. Conclusions

1: The activation energy of bulk etch rate, E_B, of CR-39 polymer detector is slightly affected by the laser treatment, This supports the proposal that E_B is a characteristic of the bulk material of the detector.

2: The significant increase in E_T for pre-exposed samples, compared to un-exposed and post-exposed samples, Track activation energy, E_T, has found to be lower than the bulk activation energy, E_B, for CR-39 detector in all different cases.

References

[1] Fleischer R.L, Price R.B and Walker R.M, *Nuclear Tracks in Solids: Principles and Applications*, University of California Press, Berkeley, USA, 1975.

[2] Saffarini G., NidalD waikat, Mousa El-Hasan, Fuminobu Sato, Yushi Kato and Toshiyu kiIida "The effect of infrared laser on the activation energy of CR-39 polymeric detector" *Nuclear Instruments and Methods in Physics Research*" (A 680), 82-85, 2012.

[3] Durrani S.M.A and. Abu-Jarad F., "The heat effect on CR-39 nuclear track detectors irradiated by a pulsed IR laser" *Nuclear Instruments and Methods* 100 (1), 97-102, 1995.

[4] Babak Jaleh, Parviz Parvin, Kavoos Mirabaszadeh, and Mehran Katouz, KrF laser irradiation effects on nuclear track recording properties of polycarbonate," *Radiation Measurements*, 38,(2), 137-254, April, 2004.

[5] Benton E.V, and HenkeR.P, *Charged particle tracks in polymers no. 7: sensitivity enhancement of lexan. Naval Radiological Defense Lab.(NRDL)*, San Francisco, CA, Report Number(s):AD-682922; USNRDL-TR(1968) 68-136.

[6] Awad E.M and EL-Samman H.M, Activation energy of etching for CR-39 as a function of linear energy transfer of the incident ions. *"Radiation Measurements*" 31, 109-114, 1999.

[7] Virk H.K, Modgil S.K and Bhatia R.K, Activa -tion energy for the annealing of radiation damage in CR-39: An intrinsic property of the detector," Nuclear Tracks and Radiation Measurements", 11(6) 323 -325, 1986.

[8] Surinder S. and Neerja. The effect of gamma-irradiation on the activation energy of bulk and track etching in CR-39 plastic track detector "Radiation Measurements ", 42, 1507-1507, 2007.

[9] Khayrat A. H.and ; Durrani, S.A., variation of alpha-particle track diameter in CR-39 as a function of residual energy and etching "Radiation measurements", 30, 15-18, 2012.

[10] G.Saffarini, D. Nidal, M.El-Hassan. Kato and T.Lida, Discovery new solution etchant, "*Nucl.Instr.and math in phy. Research*"', A. 680., 82-85, 2012.

International Journal of Physics, 2016, Vol. 4, No. 1, 5-10
Available online at http://pubs.sciepub.com/ijp/4/1/2

DOI:10.12691/ijp-4-1-2

An IBM-2 Calculation of E2/M1 Multipole Mixing Ratios of Transitions in $^{90\text{-}96}$Sr

Saad Naji Abood[1], Laith Ahmed Najim[2,*]

[1]Department of Physics, College of Science, AL-Nahrain University, Baghdad, IRAQ
[2]Department of Physics, College of Science, Mosul University, Mosul, IRAQ
*Corresponding author: Prof.lai2014@gmail.com

Abstract The interacting boson model is applied to the even strontium isotopes, $^{90\text{-}96}$Sr. Excitation energies, electromagnetic transition strengths, quadrupole and δ(E2/M1) multipole mixing ratios have been described systematically. It is seen that the properties of low-lying levels in these isotopes, for which the comparison between experiment and theory is possible, can be epistemologically satisfied by the Interacting Boson Model-2 (IBM-2).

Keywords: *interacting boson model, the electric transition probability, multipol mixing ratios, nuclear shell model, Sr Isotopes*

Cite This Article: Saad Naji Abood, and Laith Ahmed Najim, "An IBM-2 Calculation of E2/M1 Multipole Mixing Ratios of Transitions in $^{90\text{-}96}$Sr." *International Journal of Physics*, vol. 4, no. 1 (2016): 5-10. doi: 10.12691/ijp-4-1-2.

1. Introduction

The neutron-proton interaction is known to play a dominant role in quadrupole correlations in nuclei. As a consequence, the excitation energies of collective quadrupole excitations in nuclei near a closed shell are strongly dependent on the number of nucleons outside the closed shell.

The $^{90\text{-}92\text{-}94\text{-}96}$Sr isotopes (Z=38), with neutron number varies from 52 to 58 are known to exhibit have N_π=1 and N_ν varies from 1 to 4. Lie in the transitional region that occurred at the lower limit of the range of deformed nuclei.

The interacting boson approximation has been quite successful at describing the collective properties of several medium nuclei. The interacting boson model (IBM) presented by Arima and Iachello [1,2,3,4] and Casten [5] has become widely accepted as a tractable theoretical scheme of correlating, describing and predicting low-energy collective properties of complex nuclei. In this model, the low-energy states of even–even nuclei are described in terms of interactions between s (J=0) and d (J=2) bosons. The corresponding Hamiltonian is diagonalized in this boson space by employing somewhat powerful and effective group theory methods.

The outline of the remaining part of this paper is as follows: It starts from an approximate IBM-2 formulation for the Hamiltonian, reviewing the theoretical background of the study. Previous experimental and theoretical data are compared with estimated values when the general features of Sr isotopes in the range A= 90-96.

In recent years many works have had been done on the structure of Sr nucleus. In this work we extended the available systematic IBM-2 calculations of Strontium region.

2. The Interacting Boson Model

It is proposed that the change from spherical to deformed structure is related to an exceptionally strong neutron-proton interaction. It is also suggested that the neutron-proton effective interactions have a deformation producing tendency, while the neutron-neutron and proton-proton interactions are of spheriphying nature [6,7]. Within the region of medium-heavy and heavy nuclei, a large of nuclei exhibit properties that are neither close to an harmonic quadrupole vibrational spectra nor to deformed rotors [8]. While defining such nuclei in a geometric description [9], these phenomena will have a standard description that is given in terms of nuclear triaxiality [10], going from rigid triaxial shapes to softer potential energy surfaces. In the first version of the interacting boson model (IBM-1) [11], no distinction is made between proton and neutron variables while describing triaxiality explicitly. This can be done by introducing the cubic terms in the boson operators [12]. This is a contrast to the recent work of Dieperink and Bijker [13,14] which showed triaxiality occurs in particular dynamic symmetries of the IBM-2 that distinguish between protons and neutrons.

In the present work, the IBM-2 states that the low lying collective state of even-even nuclei can be described by the interaction of s and d−bosons, carrying angular momentum l = 0 and l = 2, respectively.

The IBM-2 Hamiltonian is written [9]:

$$H = \varepsilon_d (n_{dv} + n_{d\pi}) + KQ_\nu^{(2)}.Q_\pi^{(2)} + V_{\pi\pi} + V_{\nu\nu} + M_{\nu\pi} \quad (1)$$

$$Q_\rho = (s_\rho^{+} d_\rho + d_\rho^{+} s_\rho)^{(2)} + \chi_\rho (d_\rho^{+} d_\rho)^{(2)} \qquad \rho = \nu, \pi \quad (2)$$

where κ is the quadrupole-quadrupole strength and $V_{\rho\rho}$ is the boson-boson interaction, which is given by the equation:

$$V_{\rho\rho} = \frac{1}{2}\sum_{L=0,2,4} C_{\rho}^{L}\left(\left[d_{\rho}^{+}d_{\rho}^{+}\right]^{(L)}.\left[\tilde{d_{\rho}}\tilde{d_{\rho}}\right]^{(L)}\right).$$

and

$$M_{\nu\pi} = \tfrac{1}{2}\xi_2(s_{\nu}^{+}d_{\pi}^{+} - d_{\nu}^{+}s_{\pi}^{+})^{(2)}.(\tilde{s}_{\nu}\tilde{d}_{\pi} - \tilde{d}_{\nu}\tilde{s}_{\pi})^{(2)} - \sum_{k=1,3}\xi_k(d_{\nu}^{+}.d_{\pi}^{+})^{(k)}.(\tilde{d}_{\nu}.\tilde{d}_{\pi})^{(2)} \quad (3)$$

The Majorana term $M_{\pi\nu}$ shifts the states with mixed proton-neutron symmetry with respect to the totally symmetric ones. Since little experimental information is known about such states with mixed symmetry , we did not attempt to fit the parameters appearing in equation (3) , but rather that took constant values for all *Sr* isotopes.

The general one-body E2 transition operator in the IBM-2 is [18]:

$$T(E2) = e_{\pi}Q_{\pi} + e_{\nu}Q_{\nu} \quad (4)$$

Where Q_{ρ} is in the form of equation (2). For simplicity, the χ_{ρ} has the same value as in the Hamiltonian. This is also suggested by the single j-shell microscopy. In general, the E2 transition results are not sensitive to the choice of e_{ν} and e_{π}, whether $e_{\nu} = e_{\pi}$ or not.

The B(E2) strength for E2 transitions is given by:

$$B(E2; J_i \to J_f) = 1/(2J_i+1)\ \left(\left|< J_f \left\|T(E2)\right\| J_i >\right|^2\right) \quad (5)$$

In the IBM-2, the M1 transition operator up to the one-body term is

$$T(M1) = \sqrt{\frac{3}{4\pi}}(g_{\nu}.L_{\nu} + g_{\pi}.L_{\pi}).$$

The g_{ν} and g_{π} are the boson g-factors in nuclear magneton units, that depend on the nuclear configuration. They should be different of different nuclei. Where $L_{\upsilon}(L_{\pi})$ is the neutron and (proton) angular momentum operator $L_p^{(1)} = \sqrt{10}(d^{+}d)^{(1)}$.

$$T(M1) = \sqrt{\frac{3}{4\pi}}\left[\begin{array}{l}\frac{1}{2}(g_{\pi}+g_{\nu})\left(L_{\pi}^{(1)}+L_{\nu}^{(1)}\right)\\ +\frac{1}{2}(g_{\pi}-g_{\nu})\left(L_{\pi}^{(1)}+L_{\nu}^{(1)}\right)\end{array}\right] \quad (6)$$

The B(M1) strength for M1 transitions is given by:

$$B(M1; J_i \to J_f) = 1/(2J_i+1)\left(\left|< J_f \left\|T(M1)\right\| J_i >\right|^2\right) \quad (7)$$

Instead of evaluate the E2 and M1 matrix elements for the Sr isotopes under study which are essential in the theoretical mixing ratio calculations, it is possible to determine these ratios in an analytical form. The calculated *E2/M1* mixing ratio:

$$\delta(E2/M1) = 0.835E_{\gamma}\frac{\langle I_f \left\|T(E2)\right\| I_i\rangle}{\langle I_f \left\|T(M1)\right\| I_i\rangle} \quad (8)$$

Where E_{γ} is called the transition energy and in MeV and $\Delta(E2/M1)$ is in (eb/μ_n).

3. Results and Discussion

3.1. IBM-2 Hamiltonian Parameters

The computer program NPBOS [19] was used to make the Hamiltonian diagonal. In principle, all parameters can be varied independently in fitting the energy spectrum of one nucleus. However, in order to reduce the number of free parameters and in agreement with microscopic calculations of Guilu *et al.*, [20], only ε and κ are vary as a function to both of N_{π} and N_{ν} *i.e.* ε = ε(N_{π}, N_{ν}) and κ = κ(N_{π}, N_{ν}) are allowed . The other parameters depend only on N_{π} or N_{ν}, *i.e.* $\chi_{\pi} = \chi_{\pi}(N_{\pi})$, $\chi_{\nu} = \chi_{\nu} = (N_{\nu})$, $C_{L\pi} = C_{L\pi}(N_{\pi})$ and $C_{L\nu} = C_{L\nu}(N_{\nu})$. Thus, in isotopes chain, χ_{π} is kept constant , whereas for two isotonic Sr isotopes, χ_{ν}, $C_{L\pi}$ and $C_{L\nu}$ are kept constant (see Table 1).

In principle, the boson numbers N_{π} and N_{ν} can be treated as parameters, but they are taken to be fixed here, counted as half the number of particles and holes outside of the nearest closed shell. We have considered the Z = 28 and 50 as closed shell for this calculation as large quadruple deformations were measured for Z = N= 40 nuclei [2] and therefore no N = 40 spherical sub-shell closure exists in this region.

The isotopes $^{90-96}$Sr have $N_{\pi} = 1$, and N_{ν} varies from 2 to 5, while the parameters κ, χ_{ν}, and ε were treated as free parameters and their values were estimated by fitting to the measured level energies. This procedure was made by selecting the "traditional" values of the parameters and then allowing one parameter to vary while keeping the others constant until a best fit was obtained. This was carried out iteratively until an overall fit was achieved. The best fit values for the Hamiltonian parameters are given in Table 1.

Table 1. IBM-2 Hamiltonian parameters , all parameters in MeV units except χ_{π} and χ_{ν} are dimensionless

Isotopes	N_{ν}	ε	κ	χ_{π}	χ_{ν}	$C_{0\nu}$	$C_{2\nu}$	$C_{4\nu}$	ξ_1	ξ_2	ξ_3
$^{90}_{38}Sr_{52}$	1	1.040	-0.148	1.038	0.01	0.002	0.003	0.002	-0.76	0.21	-0.16
$^{92}_{38}Sr_{54}$	2	1.126	-0.122	1.038	0.01	0.002	0.003	0.002	-0.76	0.21	-0.16
$^{94}_{38}Sr_{56}$	3	1.198	-0.095	1.038	0.02	0.002	0.003	0.002	-0.76	0.21	-0.16
$^{96}_{38}Sr_{58}$	4	1.114	-0.086	1.038	0.02	0.002	0.003	0.002	-0.76	0.21	-0.16

3.2. Energy Levels

Using the parameters in Table 1, the estimated low-lying energy levels are shown in Table 2, along with experimental energy levels. As can be seen, the agreement

between experiment and IBM-2 results is quite good and the general features are reproduced well. The discrepancy between IBM-2 results and experiment for high spin states is observed. But one must be careful in comparing theory with experiment, since all calculated states have a collective nature, whereas some of the experimental states may have a particle-like structure. Behavior of the ratio $R_{4/2} = E(4_1^+)/E(2_1^+)$ of the energies for the first 4^+ and 2^+ states are good criteria for the shape transition. The value of $R_{4/2}$ ratio has the calculated values which change from 3 to 2 by increasing the neutron number, $R_{4/2}$ remains greater than 2 or all the isotopes. It implies that this structure seems to be varying from deformed rotor to very near harmonic vibrator ($SU(3)$ to $SU(5)$).

In our calculation, the nuclei are nearly spherical with vary small oblate deformation. This is consistent with the work of Hirata *et al*., [21]. At the beginning of the shell from N = 50, the nucleus is close to the vibrational limit. As the neutron number increases, the nucleus is slowly becoming gamma unstable or O(6) limit.

IBM-2 provides a good agreement with the available experimental data for the energy levels and transition probabilities. It shows a strong evidence of transition from SU(3) to SU(5) symmetry when neutron number increases from $N = 52$ to 58.

Table 2. Low Lying Energy Levels for $^{90\text{-}96}$Sr (in MeV unit)

J_i^π	Sr^{90}		Sr^{92}		Sr^{94}		Sr^{96}	
	Exp.	***IBM-2***	*Exp.*	***IBM-2***	*Exp.*	***IBM-2***	*Exp.*	***IBM-2***
0_1^+	0.0	0.0	0.0	0.0	0.0	0.0	0.0	0.0
2_1^+	0.831	0.833	0.814	0.812	0.836	0.835	0.814	0.749
4_1^+	1.635	1.639	1.673	1.674	2.146	2.141	1.792	1.787
6_1^+	-	2.569	3.128	3.331	-	2.241	-	2.262
2_2^+	1.892	1.782	1.384	1.278	2.271	2.220	1.506	1.492
0_2^+	2.674	2.550	2.088	1.964	-	2.003	1.229	1.310
4_2^+	-	1.721	1.957	2.109	-	2.211	1.792	1.831
2_3^+	2.586	2.391	2.053	1.347	2.292	2.320	1.628	1.597
3_1^+	5.840	3.320	2.224	2.623	-	2.575	-	2.851

Experimental data are taken from ref. [22].

In this work the 2_3^+ state in these isotopes are well described by the lowest mixed symmetry state in the vibrational limit of IBM-2. The validity of this limit is related to the proximity to the closed neutron shell at N =50 and a more detailed calculation would be necessary for large N allowing departures from the vibrational limit. One should also allow admixture between states of full symmetry and mixed symmetry, i.e., states of different F-spin , but both of these generalizations introduce many unknown interaction parameters.

3.3. Electric Quadrupole Transition Probability B(E2)

In order to find the value of the effective charge we have fitted the calculated absolute strengths ($B(E2; 2_1^+ \to 0_1^+)$) the transitions ground state band to the experimental ones. The values of the boson effective charges for all isotopes, following the work of Subber *et al*., [23] were determined by the experimental $B(E2; 2_1^+ \to 0_1^+)$, effective charges were obtained that $e_\nu = 0.0851$ e.b and $e_\pi = 0.060$ e.b. Table 3 given the electric transition probability. The relative B(E2) values are proportional to these effective charges.

Table 3. Electric transition probability for Sr$^{90\text{-}96}$ in e^{2}b^2 units

$J_i^\pi \to J_f^\pi$	Sr^{90}		Sr^{92}		Sr^{94}		Sr^{96}	
	Exp.	***IBM-2***	*Exp.*	***IBM-2***	*Exp.*	***IBM-2***	*Exp.*	***IBM-2***
$2_1^+ \to 0_1^+$	0.020(3)	0.02	0.018(4)	0.018	0.020(5)	0.020	0.034(9)	0.0306
$4_1^+ \to 2_1^+$	0.064(11)	0.0708	0.00711(11)	0.00541	-	0.331	-	0.501
$2_2^+ \to 2_1^+$	-	0.00338	>0.0321	0.0289	-	0.0432	> 0.0033	0.0087
$2_2^+ \to 0_1^+$	-	0.0548	-	0.003	-	0.0011	-	0.00087
$3_1^+ \to 2_1^+$	-	0.0009	-	0.0031	>0.00006	0.00364	-	0.00051
$3_1^+ \to 4_1^+$	-	0.0029	-	0.0060	>0.0122	0.009	-	0.023
$Q(2_1^+)$ e.b	-	0.088	-	0.084	-	0.083	-	0.032

Experimental data are taken from [22,25,26,27].

The $B(E2;2_1^+ \to 0_1^+)$ and $B(E2;4_1^+ \to 2_1^+)$ values decrease as neutron number increases toward the middle of the shell as the value of $B(E2;2_2^+ \to 2_1^+)$ has small value because contain mixtures of M1 and The calculated $B(E2)$ value of $2_2^+ \to 2_1^+$ transition is between the error limit. For $B(E2;4_1^+ \to 2_1^+)$ transition, the difference between the experimental and theoretical values is very small.

The value of $B(E2;2_2^+ \to 0_1^+)$ is small because there are not deformed nuclei.

However the calculated values in Table 3 are in agreement with the experimental results, there are some difference between the $B(E2)$ values of $2_2^+ \to 0_1^+$ transition because there is not enough data and certain result for this transition. The other experimental B(E2) values of some transitions does not exist.

The quadrupole moment for first excited state in *Sr* isotopes is very well described. The quadrupole moment of the first excited state 2_1^+ is also decreasing toward as neutron number increases. As mentioned above, the calculated values of $Q(2_1^+)$ indicated this nucleus has oblate shape in first excited states 2_1^+.

3.4. Magnetic Transition Probability *B(M1)*

To evaluate the magnetic transition probability, the work depend on the Eqs.6 and 7, and determine the values of g_π and g_ν. It is interesting to note that the matrix element is approximately proportional to $N_\pi/(N_\pi+N_\nu)$ and $N_\nu/(N_\pi+N_\nu)$, respectively , and directly to the number of active proton and neutron bosons. This leads to a approximate expression [8]:

$$g = g_\pi N_\pi/(N_\pi+N_\nu) + g_\nu N_\nu/(N_\pi+N_\nu) \qquad (9)$$

and $g = Z/A$, where Z is the atomic number, and A is the mass number.

Therefore the values of g-factor are given as $g_\nu = 0.223\mu_N$ and $g_\pi = 0.841\mu_N$. Table 4 gives the values of B(M1) for some transitions, there is a very little experimental data to compare with IBM-2 results.

Table 4. Magnetic transition probability for $^{90\text{-}96}$Sr in μ_N^2 units

$J_i^\pi \to J_f^+$	Sr^{90}		Sr^{92}		Sr^{94}		Sr^{96}	
	Exp.	***IBM-2***	*Exp.*	***IBM-2***	*Exp.*	***IBM-2***	*Exp.*	***IBM-2***
$1^+ \to 0_1^+$	-	0.123	-	0.341	-	0.789	-	0.951
$1^+ \to 2_1^+$	-	0.0032	0.001253	0.00247	-	0.923		0.0005
$2_2^+ \to 2_1^+$	-	0.0520	0.02506	0.0752	-	0.000345	>0.00030	0.000335
$3_1^+ \to 2_1^+$	-	0.002231	-	0.00639	>1.3x10^{-4}	4.4x10^{-5}	-	0.00431
$2_3^+ \to 2_1^+$	-	0.00423	-	0.00084	-	0.00076	-	0.000329
$2_3^+ \to 2_2^+$	-	0.0019	0.05191	0.0710	-	0.000871	-	0.000432
$g(2_1^+)$	-	0.82	-	0.75	-	0.62	-	0.58

Experimental data are taken from [22].

1. The transitions between low-lying collective states (e.g., $2_1^+, 2_2^+$) are relatively weak since the arise from antisymmetric component in the wave functions introduced by *F*-spin breaking in the Hamiltonian.
2. Strong transitions connecting a symmetric states, $|F_{\max}\rangle$ with one proton-neutron boson mixed symmetry (e.g., $B(M1;1^+ \to 0_1^+)$).
3. The magnitude of M1 values increases with increasing spin for $\gamma \to g$ and $\gamma \to \gamma$ transitions.

3.5. Mixing Ratio $\delta(E2/M1)$

Evaluating the mixing ratio $\delta(E2/M1)$ for *Sr* isotopes, depend on the equation (8), Table 5, shows the variation of 6 for the group of $2^+ \to 2_1^+$ transitions and it is seen that both the magnitude and sign of $\delta(E2/M1)$ are correctly obtained for the three transitions a summary of the results where the experimental data have sufficient precision for a useful comparison and also when there is no ambiguity in the nature of the levels. (At higher energies where the level density is great the order of the experimental levels may differ from the calculated order). These results exhibit disagreement in some cases, with one case showing disagreement in sign. However, it is a ratio between very small quantities and any change in the dominator that will have a great influence on the ratio. The large calculated value for $\delta(3_3^+ \to 4_1^+)$ is not due to a dominate *E*2 transition, but may be under the effect of very small *M*1 component in the transition.

The reduced E2 and M1 matrix elements have been evaluated for a selection of transitions in tungsten isotopes (A = 90,92,94,96); their dependence on ξ_2 is striking. A sudden change in sign is sometimes observed in M1; it occurs when the E2 matrix element is small. It may be attributed to a very low value of the E2 reduced matrix element; even though the program has an arbitrary sign choice, the sign is consistent for all results within a calculation, and the sign of the ratio of the matrix elements which determine the sign of the multipole mixing ratio is not arbitrary.

The δ -mixing ratios were calculated for some selected transitions in $^{90\text{-}96}$***Sr*** Tables 5 show comparisons with experimental results. The parameters χ_ρ, ξ_2 and ξ_k ,

and were kept at their best-fit values and the g_ρ were fine-tuned in order to fit the experimental data. In particular, g_π was found to be very sensitive to the δ-mixing ratios. Good agreement was achieved with the set of parameters (see Table 1). We are now in a position to use these Hamiltonian parameters confidently to ***o*** calculate δ-mixing ratios for any transition in these isotopes.

The variations in sign of the E2/M1 mixing ratios from nucleus to nucleus for the same class transitions and within a given nucleus for transitions from different spin states suggest that a microscopic approach is needed to explain the data theoretically. For that reason, we did not take into consideration the sign of mixing ratios. Sign convention of mixing ratios had explained in detail by *J. Lang et al.*, [27].

Table 5. Mixing ratios for $^{90\text{-}96}$Sr in eb/μ_N units

Transition $J_i^\pi \to J_f^+$	Sr^{90}		Sr^{92}		Sr^{94}		Sr^{94}	
	Exp.	IBM-2	*Exp.*	IBM-2	*Exp.*	IBM-2	*Exp.*	IBM-2
$2_2^+ \to 2_1^+$	+0.50(3)	0.775	+0.12(2)	-2.560		-6.981	+2.0(11)	2.562
$4_2^+ \to 4_1^+$	-	-0.784		-0.210	-0.35(8)	-0.64		3.290
$2_3^+ \to 2_1^+$	-	0.0301	+1.7	0.981		0.0002	$0.58^{+1.7}_{-1}$	1.331
$2_3^+ \to 2_2^+$		-0.998		2.98		2.569		2
$4_3^+ \to 4_1^+$	-	2.98		0.461	-	0.982	-	-4.45
$3_1^+ \to 2_1^+$	0.53^{+18}_{-11}	1.30	-	0.0028	-	0.0022	-	0.0096
$3_1^+ \to 4_1^+$	-	-17.6	-	0.002	-	0.0097	-	1.567
$4_3^+ \to 4_2^+$	-	0.987	-	3.890	-	-0.452	-	2.431
$3_3^+ \to 4_1^+$	-	-0.33	-	-2.765	-	2.984	-	1.940
$3_3^+ \to 2_2^+$	-	0.657	-	0.861	-	0.567	-	1.320
$1_1^+ \to 2_1^+$	-	20.34	-0.27(5)	-0.434	-	0.657	-	5.556
$5_1^+ \to 4_1^+$	-	0.00022	-	0.0532	-	0.0432	-	0.00035
$5_1^+ \to 6_1^+$	-	0.00023	-	0.0002	-	0.00022	-	0.0003
$6_2^+ \to 6_1^+$	-	0.00005	-	0.0251	-	0.00023	-	0.0004

Experimental data are taken from [22].

4. Conclusions

In this work we have carried out an analysis for the even mass *Sr* isotopes based on the IBM-2. The boson core parameters have been obtained and the main results for energy levels and quadrupole transition probabilities agree very well with experiment. In general, good agreement was obtained when compared with experiment. The boson-boson interaction parameters were fixed by the calculations on the boson core nuclei. The results indicate that the energy spectra of all different quasibands of the even-even Sr isotopes can be reproduced quite well. It is noticed, however, that the results of $B(E2)$ calculations for even-even *Sr* nuclei were in better agreement with the existing experimental data. The best fit values for the Hamiltonian parameters for even-even Sr isotopes are given in Table 1, and the calculated energy values which are compared with the experimental data are given in Table 1, *Sr* isotopes. The agreement is good for member of ground state, ground and beta bands.

The calculated values in this study show that the transitions connect the levels with the same parity and the $E2$ transitions are predominant. A sensitive test of our projection is provided by comparing calculated $B(E2)$ values with experimental predictions. The agreement between the values obtained in this analysis and the experimental results is good for ground state band, hoping that if the other parameters are normalized by means of this projection it can be considerably improved for gamma band and beta band for further work**.**

In this work, the mixing ratio $\delta(E2/M1)$ of transitions linking the gamma and ground state bands have been examined. The transitions which link low spin states and that obtained in the present work are in good agreement and show a little bit irregularities.

References

[1] F. Iachello and A. Arima, *The Interacting Boson Model*, (Camb. Univ. Press, (1987).

[2] A. Arima and F. Iachello, Ann. *Phys. NY*, 99 (1976) 253.

[3] A. Arima and F. Iachello, Ann. *Phys. NY*, 111 (1978) 201.

[4] A. Arima and F. Iachello, Ann. *Phys. NY*, 123 (1979) 468.

[5] R. F. Casten, *Nucl. Phys.*, A 347 (1980) 173.

[6] C. K. Nair, A. Ansari and L. Satpathy, Phys. Lett., 71B, (1977), 257-261.

[7] A. Sevrin, K. Heyde, and J. Jolie, *Phys. Rev.* C 36, (1987) 2631-2638.

[8] M. Sambataro, O. Scholten, A. E. L.Dieperink and G. Piccitto, Nucl. Phys. A423 (19984) 333.

[9] A. Bohr and B. Mottelson, "Nuclear Structure', Vol. II (Benjamin), New York, (1969).

[10] O. Schoten, A. Arima and F. Iachello, Interacting Ann. Phys. (N.Y.), 99 (1976) 468-473.

[11] K. Hayde, P. Van Isacker, M. Waroquier and J. Moreau, Phys. Rev., C 29, (1984), 1420-1426.
[12] J. Y. Zhang, R. F. Casten, and N. V. Zamfir, Phys. Lett. B 407, (1997) 201-206.
[13] A. E. L. Dieperink and R. Bijker, Phys. Lett., 116B, (1982), 77-81.
[14] A. E. L. Dieperink, Progress in Particle and Nuclear Physics, edited by D. Wilkinson, Plenum, New York, 9, (1983).
[15] A. Arima, T. Otsuka, F. Iachello, T. Talmi, Phys.Lett., 66B, (1977), 205-209.
[16] T. Tagziria, M. Elahrash, W. D. Hamilton, M. Finger, J. John, and V. N. Pavlov, J. Phys. G: Nucl. Part. Phys., 16 (1990) 1323-1328.
[17] Van Isacker and G. Puddu, Nucl. Phys A348 (1980) 125.
[18] Y. X. Liu, G. L. Long and H. Z. Sun, J. Phys. G: Nucl. Part. Phys., 17 (1991) 877-880.
[19] T. Otsuka and N. Yoshida, the IBA-2 computer program NPBOS, University of Tokyo (1985), and Japan Atomic Energy Research Institute Report,(1985) JAERI-M85-094.
[20] Long Gulilu, Zhang Jinyu and Tian Lin, Commun. Theor. Phys. 29 (1998) 249.
[21] D. Hirata, H. Taki, I. Tanihata and P. Ring, Phys. Lett. B 314 (1993) 168.
[22] *ENSDF*, http:// www.nndc.bnl.gov/ensdf (*Nuclear data sheet*) (2011).
[23] A. R. Subber, P. Park, W. D. Hamilton, K. Kumar, K. Schreckenbash and G. Colvin, J. Phys. G: Nucl. Phys. 12 (1986) 881
[24] H. Mach et al., Nucl. Phys. A 523 (1991) 197.
[25] C. M. Baglin, Nucl. Data Sheets 66 (1962) 347.
[26] J. K. Tuli. Nucl. Data Sheets 66 (1992) 1.
[27] J. Lang, K. Kumar and J. H. Hamilton, Rev. Mod. Phys. Vol.54 No. 1 (1982).

International Journal of Physics, 2016, Vol. 4, No. 1, 11-20
Available online at http://pubs.sciepub.com/IJP/4/1/3

DOI:10.12691/ijp-4-1-3

Transmission of Information and Interaction in the Mutual Motion of Two Physical Bodies MSR (Motion Shapes Reality)

Mihailo M. Jeremić*

Mihailo Jeremić, independent Researcher, Mladenovac, Serbia
*Corresponding author: nacrtmika@gmail.com

Abstract When two bodies are in mutual motion, it should not be considered that one of them is stationary while the other moves or vice versa, but that both bodies move in relation to the center of mass (which is motionless, conditionally) and that they move at speeds dependent on the relationships of their masses, which is the consequence of the law of conservation of momentum. The time of a light signal travelling between two bodies A and B in mutual motion at the velocity of v_0 depends on the relationship between the masses of these bodies m_A and m_B, so light signal travel time from the body A to the body B differs from the light signal travel time from the body B to the body A. In accordance with this, the following notions are defined: the relationship of the time difference (interval) between two successively emitted light signals from one body and the time difference (interval) of receiving these two signals by the other body, as well as the intensity and relationship between the relative velocities v of the two bodies measured from one body and from the other body. In addition, the expressions are derived for the Doppler shift in the function of velocity v_0 of the mutual motion of two bodies A and B and the relationship between the masses of these bodies m_A and m_B. The results of this study prove that the formulae of the special theory of relativity (STR) have not been duly derived (since they disregard the masses of the bodies in mutual motion) and that they do not offer correct results.

Keywords: *physics, the special theory of relativity*

Cite This Article: Mihailo M. Jeremić, "Transmission of Information and Interaction in the Mutual Motion of Two Physical Bodies MSR (Motion Shapes Reality)." *International Journal of Physics*, vol. 4, no. 1 (2016): 11-20. doi: 10.12691/ijp-4-1-3.

1. Introduction

The information about a phenomenon is obtained on the basis of recording the information which has reached either our senses or the devices used for registering that phenomenon. This information is transmitted at the final velocity dependent on the information transmitter and the medium through which the information is transmitted.

Also, the interactions between individual bodies (particles) are transmitted at the final velocity which depends on the information transmitter and the medium through which the interaction is transmitted.

When it comes to the bodies which are mutually motionless, the information and interactions are received at the same rate as they are emitted since successive signals travel the same distance. However, when it comes to the bodies which are in mutual motion, the rate of receiving and emitting information (interaction) is not identical because each forthcoming information (interaction) travels a different distance length.

Thus, considering the bodies in mutual motion, it is necessary to find the dependence of the sent and received information (interactions) in the function of the speed of transmitting this information (interactions) and the speed of the movement of the bodies.

The special theory of relativity (hereinafter referred to as STR), proposed by Albert Einstein at the beginning of the 20th century, is generally accepted nowadays.

STR regards the mutual motion of two inertial systems WITH NO MASS assuming that it is irrelevant whether one system is motionless and the other is moving or the second system is stationary while the first system is moving [1]. Thus, bodies are regarded as mathematical points with no mass, and not as physical bodies with mass, which does not correspond to reality.

The subject of this paper is proposing a new theory named MSR (Motion Shapes Reality) on the transmission of light signals between two bodies in mutual motion, based on the law of conservation of momentum.

When talking about the motion of two bodies, it is necessary to bear in mind that each body has its mass!

So, while two bodies are moving, one of them should not be considered to be still while the other is moving and vice versa, but both bodies should be considered to be moving in relation to the center of mass (which is motionless, conditionally) and that they move at velocities dependent on the relationships of their masses, which is the consequence of the law of conservation of momentum [2], which is a consequence of Newton's third law [3].

2. Transmitting Information and Interactions during Motion

The information about a phenomenon is obtained on the basis of recording the information which has reached either our senses or the devices used for registering that phenomenon. This information is transmitted at the final velocity dependent on the information transmitter and the medium through which the information is transmitted.

Also, the interactions between individual bodies (or particles) are transmitted at the final velocity which depends on the information transmitter and the medium through which the interaction is transmitted.

When it comes to the bodies which are mutually motionless, the information and interaction are received at the same rate as they are emitted since successive signals travel the same distance. However, when it comes to the bodies which are in mutual motion, the rate of receiving and emitting information (interaction) is not identical because each upcoming information (interaction) covers a different distance length.

Thus, in relation to the bodies in mutual motion it is necessary to find the dependence of the sent and received information (interactions) in the function of the speed of transmitting this information (interactions) and the speed of the bodies.

2.1. The Motion of Two Bodies in the Same Line

When talking about the motion of two bodies, it is necessary to bear in mind that each body has its mass.

Figure 2.1 illustrates the motion of two bodies A and B having the masses m_A and m_B.

According to the law of conservation of momentum, it follows: $m_A v_A = m_B v_B$

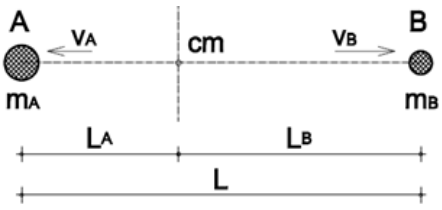

cm – the center of mass for m_A and m_B

$v_0 = v_A + v_B$	$L = L_A + L_B$
$v_A = v_0 m_B/(m_A+m_B)$	$L_A = L\, m_B/(m_A+m_B)$
$v_B = v_0 m_A/(m_A+m_B)$	$L_B = L\, m_A/(m_A+m_B)$

(1.1)

Figure 2.1.

Thus, when it comes to the motion of two bodies with masses m_A and m_B where one of them moves at the velocity of v_0 in relation to the other, one of them should not be considered to be still while the other is moving and vice versa, but both bodies should be considered to be moving in relation to the center of mass (which is motionless, conditionally) and that they move at the velocities of v_A and v_B which are dependent on the relationship of the masses m_A and m_B.

2.1.1. Light Signals between Two Bodies in Motion

Let us consider the travel time of a light signal with the speed of c_0 between two bodies A and B in mutual motion at the speed of v_0, according to the Figure 2.1. It has been accepted that the plus sign is used for the velocity when the bodies move away from each other. So, if the bodies approach each other, the sign in front of the velocity symbol should be changed in the following expressions.

a) The light signal from the body A towards the body B

A light signal emitted from the body A at the speed of c_0 reaches the body B during the time t_A; the body B needs the same time (t_A) to move away for the additional distance of $\Delta L_B = t_A v_B$, moving at the speed of v_B in relation to the center of mass cm, so that the total distance covered by the light signal amounts to:

$$L'_B = t_A c_0 = L + \Delta L_B = L + t_A v_B$$

Solving for t_A, the travel time of the light signal from A to B is obtained:

$$t_A = L/(c_0 - v_B) \qquad (2.1.1.a)$$

b) The light signal from body B towards body A

When a light signal emitted from the body B at the speed of c_0 reaches the body A during the time t_B, the body A needs the same time to move away for the additional distance of $\Delta L_A = t_B v_A$, moving at the speed of v_A in relation to the center of mass cm, so that the total distance covered by the light signal amounts to:

$$L'_A = t_B c_0 = L + \Delta L_A = L + t_B v_A$$

Solving for t_B, the travel time of the light signal from B to A is obtained:

$$t_B = L/(c_0 - v_A) \qquad (2.1.1.b)$$

c) The relationship of signals from A to B and from B and A

Comparing the travel times of t_A and t_B of light signals from the body A to the body B and from the body B to the body A, it is perceived that they are different, i.e. $t_A \neq t_B$ (except for the bodies of identical masses $m_A = m_B$ when both $v_A = v_B$ and $L_A = L_B$):

$$t_A / t_B = (c_0 - v_A)/(c_0 - v_B). \qquad (2.1.1.c)$$

2.1.2. Time Intervals of Two Bodies In Motion

Let us consider the time difference (interval) between two successively emitted light signals from the body A and the time difference (interval) of receiving these signals by the body B, according to Figure 2.1.

In order to simplify the text, all 'A' marks will be replaced by 'E' (emitter), and all 'B' marks will be replaced by 'R' (receiver).

As seen in section 2.1.1.a, the travel time of the first light signal from E to R is:

$$t_1 = L/(c_0 - v_R).$$

Let us define the travel time from the body E to the body R of the second light signal emitted from the body E after particular time Δt_E in relation to the first signal.

During the time Δt_E the body E covers the additional distance of $\Delta L_E = \Delta t_E v_E$ and the body R covers the additional distance of $\Delta L_{R1} = \Delta t_E v_R$. While the light signal travels from the body E to the body R during the time t_2, the body R covers the additional distance of $\Delta L_{R2} = t_2 v_R$; thus, the total distance covered by the second light signal from the body E to the body R amounts to:

$$\begin{aligned} L'_2 &= t_2 c_0 = L + \Delta L_{R1} + \Delta L_{R2} + \Delta L_E \\ &= L + \Delta t_E v_R + t_2 v_R + \Delta t_E v_E \end{aligned}$$

Solving it for t_2, the following is obtained:

$$t_2 = (L + \Delta t_E v_0)/(c_0 - v_R).$$

The difference in the duration of the travelling of the first and second signal from E to R amounts to:

$$\begin{aligned} t_2 - t_1 &= (L + \Delta t_E v_0)/(c - v_R) - L/(c_0 - v_R) \\ &= \Delta t_E v_0/(c_0 - v_R) \end{aligned}$$

thus, the time interval of the signal reception is:

$$\begin{aligned} \Delta t_R &= \Delta t_E + (t_2 - t_1) = \Delta t_E \left[1 + v_0/(c_0 - v_R)\right] \\ &= \Delta t_E (c_0 + v_E)/(c - v_R) \end{aligned}$$

$$\Delta t_R = \gamma \Delta t_E \qquad \gamma = (c_0 + v_E)/(c_0 - v_R) \quad (2.1.2.1)$$

If light signals are simultaneously emitted from the end points of a line segment of L_E length on the body E towards the body R, they will reach the body R at the same time and the same length $L_R = L_E$ will be recorded on the body R. Thus, there is no contraction of the length.

However, the body A's crossing the distance $\Delta L_E = v_E \Delta t_E$ at the speed of v_E during the time Δt_E will be read out on the body R as the crossing of the distance (ΔL_E) during the time Δt_R, so the velocity of the body E in relation to the center of mass will be read out on the body R:

$$\begin{aligned} v'_E &= v_E (c_0 - v_R)/(c_0 + v_E) = v_E/\gamma \\ \Delta v_E &= v_E' - v_E = v_E (1 - 1/\gamma) \end{aligned} \quad (2.1.2.1a)$$

Since the body R moves at the velocity v_R in relation to the center of mass, the total velocity of movement of the body E in relation to the body R will be recorded on the body R:

$$\begin{aligned} v &= v_R + v'_E = v_R + v_E/\gamma \\ v &= v_0 + v_E (1 - 1/\gamma) \end{aligned} \quad (2.1.2.1b)$$

In the case when m_R is insignificantly small in relation to m_E, an approximate expression is obtained:

$$\begin{aligned} \Delta t_R &= \gamma \Delta t_E \\ \gamma &= c_0/(c_0 - v_0) \\ v &= v_0 \end{aligned} \quad (2.1.2.2)$$

In the case when m_E is insignificantly small in relation to m_R, an approximate expression is obtained:

$$\begin{aligned} \Delta t_R &= \gamma \Delta t_E \\ \gamma &= (c_0 + v_0)/c_0 \\ v &= v_0 c_0/(c_0 + v_0) \end{aligned} \quad (2.1.2.3)$$

The previous formulae are derived for the situation of the two bodies moving away from each other. As already mentioned in the introductory part of chapter 2.1.1, if the bodies approach each other, the sign before the velocity symbol should be changed in the previous expressions. Thus, the expressions are as follows:

$$\begin{aligned} \Delta t_R &= \gamma \Delta t_E \\ \gamma &= (c_0 - v_E)/(c_0 + v_P) \\ v &= v_0 c_0/(c_0 - v_E) \end{aligned} \quad (2.1.2.4)$$

In the case when m_R is insignificantly small in relation to m_E, an approximate expression is obtained:

$$\begin{aligned} \Delta t_R &= \gamma \Delta t_E \\ \gamma &= c_0/(c_0 + v_0) \\ v &= v_0 \end{aligned} \quad (2.1.2.5)$$

In the case when m_E is insignificantly small in relation to m_R an approximate expression is obtained:

$$\begin{aligned} \Delta t_R &= \gamma \Delta t_E \\ \gamma &= (c_0 - v_0)/c_0 \\ v &= v_0 c_0/(c_0 - v_0) \end{aligned} \quad (2.1.2.6)$$

2.1.3. The Doppler Shift

The Doppler shift z is defined in the expression [4]:

$$z = \Delta f / f_R = (f_E - f_R)/f_R = f_E/f_R - 1$$

where:

f_E emitted frequency $f_E = 1/\Delta t_E$

f_R observed frequency $f_R = 1/\Delta t_R$

Δf the difference between the emitted and observed frequency $\Delta f = f_R - f_E$

$$f_E/f_R = (1/\Delta t_E)/(1/\Delta t_R) = \Delta t_R/\Delta t_E$$

$$z = \Delta t_R/\Delta t_E - 1 = \gamma - 1. \quad (2.1.3)$$

a) The Doppler shift when E and R are moving away from each other

Applying the formulae (2.1.2.1), we have:

$$z = \left[1 + v_0/(c_0 - v_R)\right] - 1 \quad z = v_0/(c_0 - v_R)$$

$$z = \frac{v_0 (m_E + m_R)}{c_0 (m_E + m_R) - v m_E} \qquad v = \frac{z c_0 (m_E + m_R)}{(z+1) m_E + m_R} \quad (2.1.3.1)$$

In the case when m_R is insignificantly small in relation to m_E, an approximate expression is obtained:

$$z \approx v_0/(c_0 - v_0) \qquad v_0 \approx z c_0/(z+1) \quad (2.1.3.2)$$

In the case when m_E is insignificantly small in relation to m_R, an approximate expression is obtained:

$$z \approx v_0/c_0 \qquad v_0 \approx z c_0 \quad (2.1.3.3)$$

b) The Doppler shift when E and R are approaching each other

Applying the formulae (2.1.2.4), we have:

$$z = \left[1 - v_0/(c_0 + v_R)\right] - 1 \quad z = -v_0/(c_0 + v_R)$$

$$z = \frac{-v (m_E + m_R)}{c_0 (m_E + m_R) + v_0 m_E} \qquad v = \frac{-z c_0 (m_E + m_R)}{(z+1) m_E + m_R} \quad (2.1.3.4)$$

In the case when m_R is insignificantly small in relation to m_E, an approximate expression is obtained:

$$z \approx -v_0/(c_0+v_0) \qquad v_0 \approx -zc_0/(z+1) \quad (2.1.3.5)$$

In the case when m_E is insignificantly small in relation to m_R, an approximate expression is obtained:

$$z \approx -v_0/c_0 \qquad v_0 \approx -zc_0 \quad (2.1.3.6)$$

c) The Doppler shift in astronomy

When the Earth receives light signals from massive stars, the Earth's mass m_R is insignificantly small in relation to the mass of stars m_E, so the approximate expressions can be applied (2.1.3.2):

$$z \approx v_0/(c_0-v_0) \text{ and } v_0 \approx zc_0/(z+1).$$

Table 2.1.3 offers a comparative description of the relationship between the Doppler shift z and the velocity v_0 calculated according to the relativistic Doppler Effect (STR) [5] and according to the formulae of MSR (Movement Shapes Reality).

It can be noticed that STR calculates a smaller Doppler shift for the same velocities, i.e. it calculates bigger velocities for the same Doppler shift. The bigger the velocity, the bigger the error in calculating the Doppler shift according to STR.

Table 2.1.3. The Doppler shift in astronomy according to STR and MSR

v_0/c	z' (STR)	z (MSR)	Δz=z-z'	z/z'
0,01	0,0101	0,0101	0,0001	1,0050
0,02	0,0202	0,0204	0,0002	1,0101
0,05	0,0513	0,0526	0,0013	1,0257
0,10	0,1055	0,1111	0,0056	1,0528
0,20	0,2247	0,2500	0,0253	1,1124
0,30	0,3628	0,4286	0,0658	1,1814
0,40	0,5275	0,6667	0,1391	1,2638
0,50	0,7321	1,0000	0,2679	1,3660
0,60	1,0000	1,5000	0,5000	1,5000
0,70	1,3805	2,3333	0,9529	1,6902
0,80	2,0000	4,0000	2,0000	2,0000
0,90	3,3589	9,0000	5,6411	2,6794
0,93	4,2509	13,2857	9,0349	3,1254
0,96	6,0000	24,0000	18,0000	4,0000
0,98	8,9499	49,0000	40,0501	5,4749
0,99	13,1067	99,0000	85,8933	7,5534

2.2. The Motion of Two Bodies on Parallel Lines

Let us consider the mutual movement of two bodies A and B on parallel lines at the relative velocity of v_0, according to Figure 2.2.

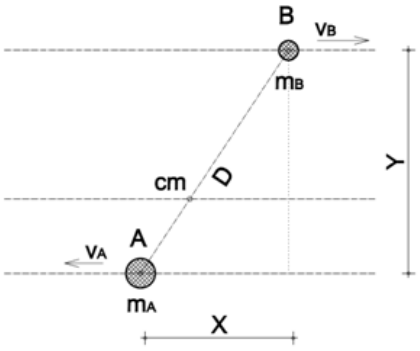

cm–the center of mass for m_A and m_B

$v_0 = v_A + v_B$

$v_B = v_0 m_A/(m_A+m_B)$

$v_A = v_0 m_B/(m_A+m_B)$

Figure 2.2.

2.2.1. Light Signals Between Two Bodies in Motion

Let us think about the travel time of a light signal of the emitted speed of c_0 between bodies A and B, according to Figure 2.2.1. It has been accepted that the positive sign of the velocity is used when two bodies move away from each other. So, if the bodies approach each other, in the following formulae the sign before the velocity symbol should be altered.

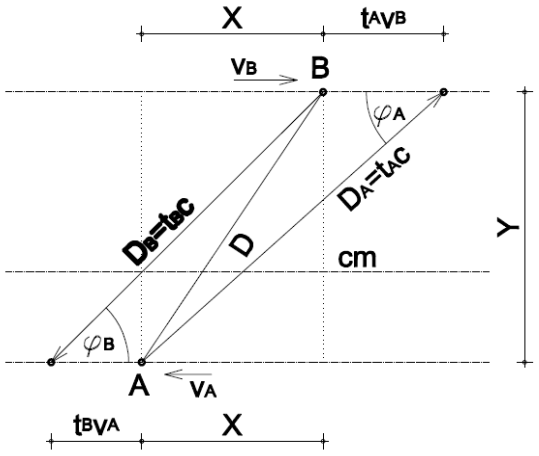

Figure 2.2.1.

a) The light signal from the body A towards the body B

While a light signal travels from A towards B at the speed c during a particular time t_A, the body B covers the distance of $\Delta X_B = t_A v_B$ in that time, so the light signal covers the distance of $D_A = t_A c_0 = (X+t_A v_B)/\cos\varphi_A$. Solving this for t_A, it is obtained as follows:

$$t_A = X/(c_0\cos\varphi_A - v_B) \quad (2.2.1.a)$$

b) The light signal from the body B towards the body A

While a light signal travels from B towards A at the speed c during a particular time t_B, the body A covers the distance $\Delta X_A = t_B v_A$ in that time, so the light signal covers the distance of $D_B = t_B c_0 = (X+t_B v_A)/\cos\varphi_B$. Solving this for t_B, it is obtained as follows:

$$t_B = X/(c_0\cos\varphi_B - v_A) \quad (2.2.1.b)$$

c) The relationship of the signal from A to B and from B to A

Comparing the travel times of t_A and t_B of light signals from the body A to the body B and from the body B to the body A, it is perceived that they are different, i.e. $t_A \neq t_B$ (except for the bodies of identical masses $m_A=m_B$ when both $v_A=v_B$ and $\varphi_A=\varphi_B$):

$$t_A/t_B = (c_0\cos\varphi_B - v_A)/(c_0\cos\varphi_A - v_B) \quad (2.2.1.c)$$

2.2.2. Time Intervals of Two Bodies in Motion

Let us consider the time difference (interval) between two successively emitted light signals from the body B and the time difference (interval) of receiving these same signals by the body A, according to the Figure 2.2.

In order to simplify the text, all 'B' marks will be replaced by 'E' (emitter), and all 'A' marks will be replaced by 'R' (receiver), according to Figure 2.2.2.

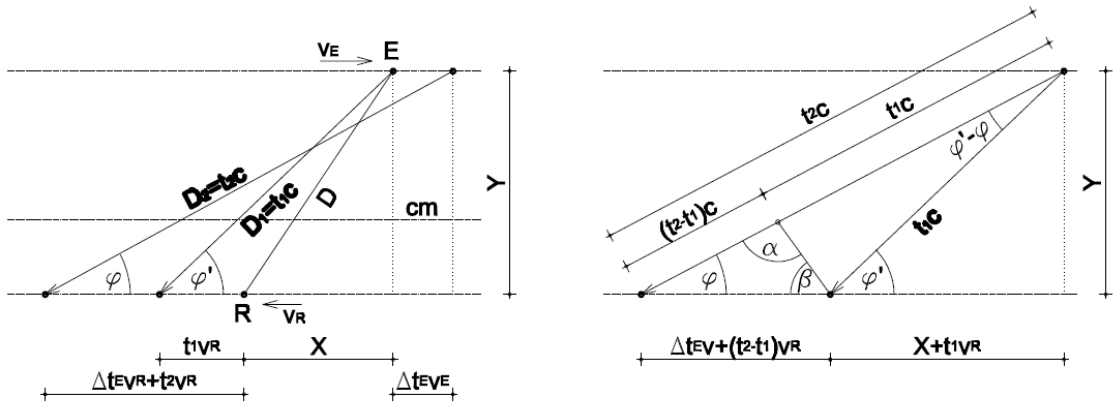

Figure 2.2.2.

The total distance covered by the body R from the emission of the first signal to the reception of the first signal amounts to $\Delta X_1 = t_1 v_R$.

Let us define the travel time from the body E to the body R of the second light signal emitted from the body E after particular time Δt_E in relation to the first signal.

During the time Δt_E the body E covers the additional distance of $\Delta X_E = \Delta t_E v_E$ and the body R covers the additional distance of $\Delta X_{R1} = \Delta t_E v_R$.

While the light signal travels from the body E to the body R during the time t_2, the body R covers the additional distance of $\Delta X_{R2} = t_2 v_R$; thus, the total distance of moving away of the bodies E and R on the motion line (x-axis) from the emission of the first signal to the reception of the second signal amounts to:

$$\Delta X_2 = \Delta X_E + \Delta X_{R1} + \Delta X_{R2}$$
$$= \Delta t_E v_E + \Delta t_E v_R + t_2 v_R .$$

Since $v_E + v_R = v_0$, the previous expression becomes: $\Delta X_2 = \Delta t_E v_0 + t_2 v_R$ so

$$\Delta X_2 - \Delta X_1 = \Delta t_E v_0 + (t_2 - t_1) v_R$$

Applying the law of sine to Figure 2.2.2, we have:

$$(t_2 - t_1) c_0 / \sin\beta = \left[\Delta t_E v_0 + (t_2 - t_1) v_R\right] / \sin\alpha$$

Changing

$$\alpha = \pi/2 + (\varphi' - \varphi)/2 \qquad \sin\alpha = \cos\left[(\varphi' - \varphi)/2\right]$$
$$\beta = \pi/2 - (\varphi' + \varphi)/2 \qquad \sin\beta = \cos\left[(\varphi' + \varphi)/2\right]$$

in the previous expression and solving for $(t_2 - t_1)$, we have:

$$t_2 - t_1 = \Delta t_E \frac{v_0\left(1 - \tan\frac{\varphi'}{2}\tan\frac{\varphi}{2}\right)}{c_0\left(1 + \tan\frac{\varphi'}{2}\tan\frac{\varphi}{2}\right) - v_R\left(1 - \tan\frac{\varphi'}{2}\tan\frac{\varphi}{2}\right)}$$

that is, introducing the relation $k = \dfrac{\tan\left(\frac{\varphi'}{2}\right)}{\tan\left(\frac{\varphi}{2}\right)}$

$$t_2 - t_1 = \Delta t_E \frac{v_0\left(1 - k\tan^2\frac{\varphi}{2}\right)}{c_0\left(1 + k\tan^2\frac{\varphi}{2}\right) - v_R\left(1 - k\tan^2\frac{\varphi}{2}\right)} \qquad (*)$$

Since the time interval between the reception of the first and second signal equals

$$\Delta t_R = \Delta t_E + (t_2 - t_1)$$

we have:

$$\Delta t_R = \Delta t_E \left[1 + \frac{v_0\left(1 - k\tan^2\frac{\varphi}{2}\right)}{c_0\left(1 + k\tan^2\frac{\varphi}{2}\right) - v_R\left(1 - k\tan^2\frac{\varphi}{2}\right)}\right]$$

that is:

$$\Delta t_R = \gamma\, \Delta t_E \quad v = v_R + v_E/\gamma \quad v = v_0 + v_E(1 - 1/\gamma)$$

$$\gamma = 1 + \frac{v_0\left(1 - k\tan^2\frac{\varphi}{2}\right)}{c_0\left(1 + k\tan^2\frac{\varphi}{2}\right) - v_R\left(1 - k\tan^2\frac{\varphi}{2}\right)} \qquad (2.2.2.1)$$

Applying the law of sine to Figure 2.2.2, we have:

$$\frac{D_2}{\sin\varphi'} = \frac{D_2 - (t_2 - t_1)c_0}{\sin\varphi}$$

$$(t_2 - t_1) = \frac{D_2}{c_0}\left(1 - \frac{\sin\varphi}{\sin\varphi'}\right) = \frac{D_2}{c_0}\left[1 - \frac{\tan\frac{\varphi}{2}\left(1 + \tan^2\frac{\varphi'}{2}\right)}{\tan\frac{\varphi'}{2}\left(1 + \tan^2\frac{\varphi}{2}\right)}\right]$$

Equalizing the previous expression with the expression (*) and solving for k, we have:

$$k=\frac{\left[\begin{array}{l}\left(c_0+v_R+\dfrac{v_0c_0\Delta t_E}{D_2}\right)\tan^2\dfrac{\varphi}{2}\\ -\left(c_0-v_R-\dfrac{v_0c_0\Delta t_E}{D_2}\right)\end{array}\right]}{2(c_0+v_R)\tan^2\dfrac{\varphi}{2}}$$

$$+\frac{\sqrt{\left\{\begin{array}{l}\left[\begin{array}{l}\left(c_0+v_R+\dfrac{v_0c_0\Delta t_E}{D_2}\right)\tan^2\dfrac{\varphi}{2}\\ -\left(c_0-v_R-\dfrac{v_0c_0\Delta t_E}{D_2}\right)\end{array}\right]^2\\ +4({c_0}^2-{v_R}^2)\tan^2\dfrac{\varphi}{2}\end{array}\right\}}}{2(c_0+v_R)\tan^2\dfrac{\varphi}{2}}.$$

Introducing the change $1/\Delta t_E = f_E$ (the frequency of the emitted signal), we have:

$$k=\frac{\left[\begin{array}{l}\left(c_0+v_R+\dfrac{v_0c_0}{D_2f_E}\right)\tan^2\dfrac{\varphi}{2}-\left(c_0-v_R-\dfrac{v_0c_0}{D_2f_E}\right)\\ +\sqrt{\left\{\begin{array}{l}\left[\begin{array}{l}\left(c_0+v_R+\dfrac{v_0c_0}{D_2f_E}\right)\tan^2\dfrac{\varphi}{2}\\ -\left(c_0-v_R-\dfrac{v_0c_0}{D_2f_E}\right)\end{array}\right]^2\\ +4({c_0}^2-{v_R}^2)\tan^2\dfrac{\varphi}{2}\end{array}\right\}}\end{array}\right]}{2(c_0+v_R)\tan^2\dfrac{\varphi}{2}}$$

$$\tan\left(\frac{\varphi'}{2}\right)=k\ tan\left(\frac{\varphi}{2}\right)\quad \phi'=2\text{atan}\left[k\ tan\left(\frac{\varphi}{2}\right)\right] \quad (2.2.2.2)$$

The above mentioned shows that the relationship between the time intervals Δt_R and Δt_E does not depend only on the angle φ and velocity v_0 but also on the distance between E and M (D_2) and on the time interval of the emitted signals, i.e. on the frequency of the emitted signals f_E.

In the case of long distances and high signal frequency, the member $\frac{v_0c_0}{D_2f_E}$ can be disregarded.

2.2.2.1. Time Intervals for φ << π/2

In the case of long distances for the angle φ<<π/2 and the small velocity v, an insignificantly small difference of the angles φ' and φ (φ'≈ φ) is obtained, so k≈1 and the formula (2.2.2.1) is simplified to the approximate formula:

$$\Delta t_R = \gamma\Delta t_E \quad v' = v_R + v_E/\gamma \quad v' = v_0 + v_E(1-1/\gamma)$$

$$\gamma = 1+\frac{v_0\cos\varphi}{c_0-v_R\cos\varphi}=\frac{c_0+v_E\cos\varphi}{c_0-v_R\cos\varphi} \quad (2.2.2.1.1)$$

$v_E\cos\varphi$ is the vector projection of velocity v_E on the line ER and $v_R\cos\varphi$ is the vector projection of velocity v_R on the line ER, i.e. these are collinear vectors on the line ER so the expression (2.2.2.1.1) is simplified to (2.1.2.1):

$$\gamma = 1+\frac{v_L}{c_0-v_{PL}}=\frac{c_0+v_{EL}}{c_0-v_{RL}} \quad (2.2.2.1.1a)$$

where v_L, v_{EL} and v_{RL} are the components of the velocities v_0, v_E and v_R on the line of the light signal ER.

In the case when m_R is insignificantly small in relation to m_E, an approximate expression is obtained:

$$\begin{array}{l}\gamma = c_0/(c_0-v_0\cos\varphi), \Delta t_R = \Delta t_E\\ c_0/(c_0-v_0\cos\varphi), v = v_0\end{array} \quad (2.2.2.1.2)$$

In the case when m_E is insignificantly small in relation to m_R, an approximate expression is obtained:

$$\begin{array}{l}\gamma = (c_0+v_0\cos\varphi)/c_0, \Delta t_R = \Delta t_E,\\ (c_0+v_0\cos\varphi)/c_0, v = v_0c_0/(c_0+v_0\cos\varphi)\end{array} \quad (2.2.2.1.3)$$

a) intervals for φ = 0

For φ = 0, cos φ = 1 so the equation (2.2.2.1.1) becomes:

$$\begin{array}{l}\gamma = (c_0+v_E)/(c_0-v_R), \Delta t_R = \Delta t_E,\\ (c_0+v_E)/(c_0-v_R),\\ v = v_R + v_E(c_0-v_P)/(c_0+v_E).\end{array} \quad (2.2.2.1.4)$$

which is identical to the expression (2.1.2.1).

In the case when m_R is insignificantly small in relation to m_E, the expression (2.2.2.1.4) becomes:

$$\begin{array}{l}\gamma = c_0/(c_0-v_0), \Delta t_R = \Delta t_E,\\ c_0/(c_0-v_0), v = v_0\end{array} \quad (2.2.2.1.5)$$

which is identical to the expression (2.1.2.2).

In the case when m_E is insignificantly small in relation to m_R, the expression (2.2.2.1.3) becomes:

$$\begin{array}{l}\gamma = (c_0+v_0)/c_0, \Delta t_R = \Delta t_E,\\ (c_0+v_0)/c_0, v = v_0c_0/(c_0+v_0).\end{array} \quad (2.2.2.1.6)$$

which is identical to the expression (2.1.2.3).

b) the reception of the signal from Cosmos

When the Earth receives light signals from massive stars, the Earth's mass m_R is insignificantly small in relation to the mass of stars m_E, so the expressions (2.2.2.1.2) and (2.2.2.1.5) can be applied.

c) the intervals in the case of approaching bodies

The previous expressions have been derived for the situation of the bodies moving away from each other. As mentioned above, if the bodies approach each other, the sign in front of the velocity symbol should be changed in the previous expressions.

2.2.2.2. TIME INTERVALS FOR φ = π/2

For the angle φ near π/2, the formula (2.2.2.1) is used after the angle φ' has been calculated according to the formulae (2.2.2.2).

For the angle φ= π/2, tg(φ/2)= 1 so the expression (2.2.2.1) becomes:

$$k=\frac{v_R+\frac{v_0c_0\Delta t_E}{D_2}+\sqrt{\left[\left(v_R+\frac{v_0c_0\Delta t_E}{D_2}\right)^2+{c_0}^2-{v_R}^2\right]}}{(c_0+v_R)}$$

$$=\frac{v_R+\frac{v_0c_0}{D_2f_E}+\sqrt{\left(v_R+\frac{v_0c_0}{D_2f_E}\right)^2+{c_0}^2-{v_R}^2}}{(c_0+v_R)} \quad (2.2.2.2.1)$$

$$\tan\left(\frac{\varphi'}{2}\right)=k,\varphi'=2\text{atan}(k)$$

In the case when m_R is insignificantly small in relation to m_E, the expression (2.2.2.2.1) becomes:

$$k=v\frac{1+\frac{c_0\Delta t_E}{D_2}+\sqrt{\left(1+\frac{c_0\Delta t_E}{D_2}\right)^2+\frac{{c_0}^2}{{v_0}^2}-1}}{(c+v_0)}$$

$$=v\frac{1+\frac{v_0c_0}{D_2f_E}+\sqrt{\left(1+\frac{c_0}{D_2f_E}\right)^2+\frac{{c_0}^2}{{v_0}^2}-1}}{(c+v_0)} \quad (2.2.2.2.2)$$

$$\tan\left(\frac{\varphi'}{2}\right)=k,\varphi'=2\text{atan}(k)$$

In the case when m_E is insignificantly small in relation to m_R, the expression (2.2.2.2.1) becomes:

$$k=\frac{v_0\Delta t_E}{D_2}+\sqrt{\left(\frac{v_0\Delta t_E}{D_2}\right)^2+1}$$

$$=\frac{v_0}{D_2f_E}+\sqrt{\left(\frac{v_0}{D_2f_E}\right)^2+1} \quad (2.2.2.2.3)$$

$$\tan\left(\frac{\varphi'}{2}\right)=k,\varphi'=2\text{atan}(k)$$

When it comes to cosmic distances, the member $\frac{v_0c_0}{D_2f_E}$ can be disregarded, so for $\varphi=\pi/2$ we have k=1, γ=1.

The previous expressions have been derived for the situation of the bodies moving away from each other. As mentioned above, if the bodies approach each other, the sign in front of the velocity symbol should be changed in the previous expressions.

2.2.3. The Doppler Shift

The Doppler shift z is defined in the formula:

$$z=\Delta f/f_R=(f_E-f_R)/f_R=f_E/f_R-1$$

where:

f_E emitted frequency $f_E=1/\Delta t_E$

f_R observed frequency $f_p=1/\Delta t_R$

Δf the difference between the emitted and observed $\Delta f=f_R-f_E$

$$f_E/f_R=(1/\Delta t_E)/(1/\Delta t_R)=\Delta t_R/\Delta t_E=\gamma$$

$$z=\Delta t_R/\Delta t_E-1=\gamma-1 \quad (2.2.3)$$

Applying the expression (2.2.2.1.) to the formula (2.2.3), general formulae are obtained:

For E and R moving away from each other:

$$z=\frac{v_0\left(1-k\tan^2\frac{\varphi}{2}\right)}{c_0\left(1+k\tan^2\frac{\varphi}{2}\right)-v_R\left(1-k\tan^2\frac{\varphi}{2}\right)}$$

$$v_0=zc_0\frac{\left(1+k\tan^2\frac{\varphi}{2}\right)(m_E+m_R)}{\left(1-k\tan^2\frac{\varphi}{2}\right)\left[m_E(z+1)+m_R\right]} \quad (2.2.3.1)$$

For E and R approaching each other:

$$z=\frac{-v\left(1-k\tan^2\frac{\varphi}{2}\right)}{c_0\left(1+k\tan^2\frac{\varphi}{2}\right)+v_R\left(1-k\tan^2\frac{\varphi}{2}\right)}$$

$$v_0=-zc_0\frac{\left(1+k\tan^2\frac{\varphi}{2}\right)(m_E+m_R)}{\left(1-k\tan^2\frac{\varphi}{2}\right)\left[m_E(z+1)+m_R\right]} \quad (2.2.3.2)$$

2.2.3.1. Angle φ<< π/2

In the case of long distances for angle $\varphi<<\pi/2$ and small velocity v_0, an insignificantly small difference of the angles φ' and φ (φ'≈ φ) is obtained, so k≈1 and the formulae (2.2.3.1) and (2.2.3.2) are simplified to the approximate formulae:

For E and R moving away from each other:

$$z=\frac{v_0\cos\varphi}{c_0-v_R\cos\varphi}$$

$$v_0=\frac{zc_0}{\left(1+z\frac{m_E}{m_E+m_R}\right)\cos\varphi} \quad (2.2.3.1.1)$$

For E and R approaching each other:

$$z=\frac{-v_0\cos\varphi}{c_0+v_R\cos\varphi}$$

$$v_0=\frac{-zc_0}{\left(1+z\frac{m_E}{m_E+m_R}\right)\cos\varphi} \quad (2.2.3.1.2)$$

If m_R is insignificantly small in relation to m_E, then $v_R\approx v$ and $v_E\approx 0$, so the expressions (2.2.3.1.1) and (2.2.3.1.2) become:

For E and R moving away from each other:

$$z=v_0\cos\varphi/(c_0-v_0\cos\varphi)$$

$$v_0=zc_0/\left[(z+1)\cos\varphi\right] \quad (2.2.3.1.3)$$

For E and R approaching each other:

$$z=-v_0\cos\varphi/(c_0+v_0\cos\varphi)$$

$$v_0=-zc_0/\left[(z+1)\cos\varphi\right] \quad (2.2.3.1.4)$$

If m_E is insignificantly small in relation to m_R, then $v_E \approx v$ and $v_R \approx 0$, so the expressions (2.2.3.1.1) and (2.2.3.1.2) become:

For E and R moving away from each other:

$$z = v_0 \cos\varphi / c_0$$
$$v_0 = zc_0 / \cos\varphi \qquad (2.2.3.1.5)$$

For E and R approaching each other:

$$z = -v_0 \cos\varphi / c_0$$
$$v_0 = -zc_0 / \cos\varphi \qquad (2.2.3.1.6)$$

For φ = 0 (longitudinal Doppler shift) the equations (2.2.3.1.3) to (2.2.3.1.6) are simplified to the equations (2.1.3.2) and (2.1.3.3), that is (2.1.3.5) and (2.1.3.6).

2.2.3.2. Angle φ = π/2

For angle φ near π/2 the formula (2.2.3.1) is used after the angle φ' has been calculated according to the formula (2.2.2.2).

For the angle φ= π/2 the formula (2.2.3.1) is used after the angle φ' has been calculated according to the formula (2.2.2.2.1).

If one of the masses is insignificantly small in relation to the other mass and the angle φ=π/2 (transversal Doppler shift), the formulae (2.2.2.2.2) and (2.2.2.2.3) are used for calculating the angle φ'.

When it comes to cosmic distances, the member $\frac{v_0 c_0}{D_2 f_E}$ can be disregarded, so for φ= π/2 we have k=1, γ=1, z=0.

2.2.4. Exchange of Information with the Satellite

Let us consider the communication between the Earth and the satellite through a light signal.

Since the satellite's mass m_S is insignificant in relation to the Earth's mass m_E, the Earth can be considered to be at rest (v_E=0) while the satellite moves at the speed of $v_S=v_0$.

However, the communication with the satellite is not performed from the center of the Earth's mass but from the surface 6.400km distant from the center of the Earth's mass and the Earth rotates around its axis (tangential velocity on the equator around 0,465km/sec). Thus, in the communication with the satellite we should also take into account the rotational velocity of the point from which the communication is carried out, as well as the satellite's trajectory in relation to the direction of the Earth's rotation, i.e. the projection of the rotational velocity on the line of the satellite's movement during the communication.

The growth of the satellite's distance and the deviation of the signal's angle of π/2 in relation to the current direction of rotational velocity lead to the decrease of the influence of the Earth's rotation so it can be disregarded in the case of long distances and small angles of signals. Also, when the point from which the communication with the satellite is performed is in the vicinity of one of the Earth's poles (i.e. when the rotational velocity is $v_{rot} \approx 0$), the Earth's rotation can be disregarded.

This chapter will deal with the situation when the angle of the signal is φ<< π/2 and when the influence of the Earth's rotation can be disregarded.

Communication with the satellite includes sending the signal from the Earth towards the satellite and its returning to the Earth at specific intervals, according to Figure 2.2.4.1.

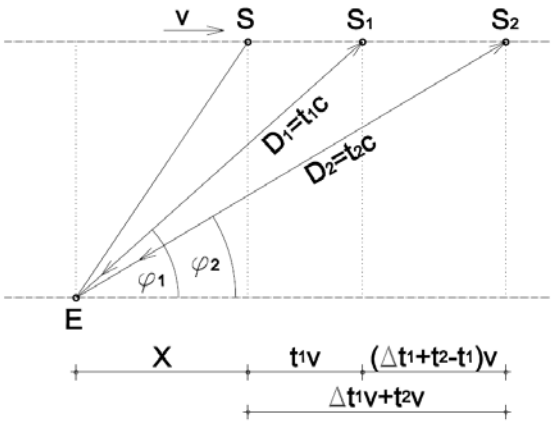

Figure 2.2.4.1.

We will observe two signals which, at the interval Δt_1, are emitted from the Earth (E) towards the satellite (S) and returned to the Earth.

While the first signal takes time t_1 to reach S from E moving at the speed of c_0, the satellite covers the additional distance of $\Delta X_1 = t_1 v_0$. Returning from S to E (having in mind that E is motionless), the return signal covers the same distance $t_1 c_0$ as the emitted signal.

After particular time Δt_1 the second signal is emitted. During the same time, S covers the additional distance of $\Delta X_2 = \Delta t_1 v_0$. While the second signal reaches E from S during the time t_2, the satellite covers the additional distance of $\Delta X_3 = t_2 v_0$. Returning from S to E (since E is motionless), the return signal covers the same distance $t_2 c_0$ as the emitted signal.

$$t_2 - t_1 = \Delta t_1 \frac{v_0\left(1 - k\tan^2\frac{\varphi_1}{2}\right)}{c_0\left(1 + k\tan^2\frac{\varphi_1}{2}\right)} \qquad (**)$$

Since the travel time of the first signal from E to S and back is $T_1 = 2t_1$ and the travel time of the second signal from E to S and back is $T_2 = 2t_2$, the time interval between the reception of the first signal and the second signal equals

$$\Delta t_2 = \Delta t_1 + 2\left(t_2 - t_1\right)$$

so we have:

$$\Delta t_P = \Delta t_1 \left[1 + 2\frac{v_0\left(1 - k\tan^2\frac{\varphi_1}{2}\right)}{c_0\left(1 + k\tan^2\frac{\varphi_1}{2}\right)}\right] \qquad (2.2.4.1)$$

Since the communication with satellites is performed at high frequencies (about 3GHz) and that the situation of long satellite distance and small velocity v_0 (in relation to the signal speed c_0) is being considered, the formula (2.2.4.1) for the signal angle $\varphi_1 << \pi/2$ is reduced to the approximate formula:

$$\Delta t_2 = \Delta t_1 \left[1 + 2v_0 \cos\varphi / c_0\right] \qquad (2.2.4.2)$$

Introducing the expression (2.2.4.2) in the formula (2.2.3), approximate formulae for the Doppler shift are obtained.

For E and S moving away from each other:

$$z = 2v_0 \cos\varphi / c_0$$
$$v_0 = zc_0 / 2\cos\varphi \qquad (2.2.4.3)$$

For E and S approaching each other:

$$z = -2v_0 \cos\varphi / c_0$$
$$v_0 = -zc_0 / 2\cos\varphi. \qquad (2.2.4.4)$$

2.2.4.1. Pioneer 10 Anomaly

Two spacecrafts, Pioneer 10 and 11, which were launched in 1972 and 1973, do not behave according to the calculations based on the relativistic formulae and on the basis of the measured Doppler shift [6].

Pioneer 10 should move at the speed of 12,2 km/sec. However, on the basis of the measured Doppler shift according to the relativistic calculations, the spacecraft moves at the increasingly slower speed so that each year it covers the distance which is smaller than expected by 8000 km.

Table 2.2.4.1 represents the difference of the Doppler shift calculated according to STR (special theory of relativity) and according to MSR (motion shapes reality). The calculation is performed for the leaving and returning (coming) signal on the basis of the approximate values of the signal angle (φ_1) in relation to the line of the spacecraft's movement.

The calculation according to MSR is carried out on the basis of the formula (2.2.4.3):

$$z = 2v_0 \cos\varphi / c_0.$$

STR is used as the basis for calculating the Doppler shift z':

$$z' = [(c + v*\cos\varphi)^2 / \left(c^2 - v^2\right)] - 1$$

Table 2.2.4.1.

v (km/sec) c (km/sec)	12,2 3,0E+05		The Doppler shift for Pioneer 10 leaving and coming signal				
Year	φ (°)	cos φ	According to STR (z')	According to MSR (z)	Δz=z-z'	Δv, km/sec	ΔD, km/year
1980	20,7	0,9354	7,6086E-05	7,6083E-05	-3,101E-09	-2,486E-04	-7.840
1982	17,6	0,9532	7,7529E-05	7,7526E-05	-3,156E-09	-2,484E-04	-7.832
1984	14,7	0,9673	7,8674E-05	7,8671E-05	-3,201E-09	-2,482E-04	-7.827
1986	12,5	0,9763	7,9409E-05	7,9405E-05	-3,230E-09	-2,481E-04	-7.825
1988	10,8	0,9823	7,9896E-05	7,9893E-05	-3,250E-09	-2,481E-04	-7.824
1990	9,6	0,9860	8,0198E-05	8,0194E-05	-3,262E-09	-2,481E-04	-7.824
	0	1,0000	8,1337E-05	8,1333E-05	-3,308E-09	-2,481E-04	-7.823

The table shows that, for the given speed, the Doppler shift calculated according to STR is bigger than the one calculated by MSR. The difference indicates the annual "lags" which extremely precisely correspond to the measured values. Thus, it is not an anomaly but the incorrect "relativistic" calculation.

2.3. On the Speed of Light

When talking about the speed of light, a difference should be made between the speed of light (photon) in relation to the body E emitting the light and the speed of light reaching the body R which moves in relation to the body E.

The speed of light is determined by the system of fixed emitters and receivers [7].

Thus, the postulate on the constant speed of light refers to the constant speed of the emitted light, independently of its frequency (the speed of the emitted light of any frequency is the same).

According to the analyses in chapter 2.2, when determining the speed of light reaching the body R in the system of two bodies E (light emitter) and R (light receiver) which are moving in relation to each other, the mutual motion of these two bodies should be taken into account.

When the photon moves from the body E at the speed of light c_0 towards the body R, this body R escapes from the photon at the speed v according to (2.2.1), (2.2.1a) and (2.2.1b). Thus, the speed of the photon reaching the body R is reduced by the escape speed of the body R, i.e. the speed of the photon (c) which has reached the body R, according to the classical law on velocity addition, amounts to:

$$c = c_0 - v,\ v = v_R + v_E / \gamma,\ v = v_0 - v_E(\gamma - 1)/\gamma \qquad (2.3.1)$$

where v_0, v_E, v_R and v are collinear components of the velocities on the line ER, according to (2.2.2.1.1) and (2.2.2.1.1a).

This change of the speed of light is recorded as the change of frequency (the speed of photon oscillation), i.e. as the Doppler shift.

Since the Doppler shift is z= γ-1, i.e. γ= z+1, by changing in (2.3.1) we have:

$$v = v_0 - v_E z / (z+1),\ c = c_0 - v_0 + v_E z / (z+1) \qquad (2.3.2)$$

The comments in chapter 2.2. illustrate that the difference of the velocities v_0 and v in the function of the relationship of the masses of the emitter m_E and the receiver m_R is:

$v_E = v_0 m_R/(m_E+m_R)$ $v_R = v_0 m_E/(m_E+m_R)$ $v_0 = v_E+v_R$ $v = v_0 - v_E z/(z+1)$

If m_R is insignificantly small in relation to m_E, then $v_R \approx v$ and $v_E \approx 0$, so the expressions (2.3.2) become:

$$v = v_0,\ c = c_0 - v_0 \qquad (2.3.3)$$

If m_E is insignificantly small in relation to m_R, then $v_E \approx v$ and $v_R \approx 0$, so the expressions (2.3.2) become:

$$v = v_0 / (z+1) = c_0 v_0 / (c_0 + v_0), \qquad c = c_0 - v_0 / (z+1) = c_0^2 / (c_0 + v_0) \tag{2.3.4}$$

References

[1] Einstein, Albert (1905), *"Zur Elektrodynamik bewegter Körper"*, Annalen der Physik 322 (10): 891-921.

[2] Feynman, R. P.; Leighton, R. B.; and Sands, M. "*The Feynman Lectures on Physics, Vol. 1.* Redwood City, CA: Addison-Wesley, pp. 10-1-10-9, 1989.

[3] Newton, Isaac. "*The Principia: Mathematical Principles of Natural Philosophy"*. University of California Press, (1999). 974 pp.

[4] Rosen, Joe; Gothard, Lisa Quinn (2009). "Encyclopedia of Physical Science". Infobase Publishing. p. 155.

[5] Landau, L.D.; Lifshitz, E.M. (2005). "*The Classical Theory of Fields. Course of Theoretical Physics: Volume 2*". Trans. Morton Hamermesh (Fourth revised English ed.). Elsevier Butterworth-Heinemann. pp. 1-3.

[6] Anderson et al, *"Study of the anomalous acceleration of Pioneer 10 and 11"*, Phys. Rev. D 65, 082004 (2002).

[7] Garner, C. L., Captain (retired) (April 1949). "*A Geodetic Measurement of Unusually High Accuracy*". U.S. Coast and Geodetic Survey Journal (Coast and Geodetic Survey): 68-74. Retrieved August 13, 2009.

International Journal of Physics, 2016, Vol. 4, No. 1, 21-25
Available online at http://pubs.sciepub.com/ijp/4/1/4

DOI:10.12691/ijp-4-1-4

Universe, a Spacetime Harmonic Oscillator

M. Khoshsima*

Department of Physics, Adelphi University, New York, USA
*Corresponding author: mkhoshsima@adelphi.edu

Abstract Energy field waves propagate in the fabric of spacetime. Interaction between spacetime field propagation and matter will generate physical photons. There are three regions of spacetime; (1) events in timelike region corresponding to the expanding universe, (2) events in lightlike region, the fabric of spacetime corresponding to spacetime with no expansion, (3) events in spacelike region corresponding to residual or evanescent universe. Universe is similar to a harmonic oscillator with two phase, right and left expansions. The equilibrium position for a two phase universe is the fabric of spacetime with surge of the stored energy in a singularity, expanding into the next phase of expansion. The evanescent universe is the spacelike event region where mass will decay. Expansion of universe and creation of matter is due to energy field propagation and superposition of energy fields in the fabric of spacetime.

Keywords: *lightlike event, energy fields, fabric of spacetime, timelike event, expanding universe, spacelike event, evanescent universe, universe as a harmonic oscillator, creation and annihilation of matter*

Cite This Article: M. Khoshsima, "Universe, a Spacetime Harmonic Oscillator." *International Journal of Physics*, vol. 4, no. 1 (2016): 21-25. doi: 10.12691/ijp-4-1-4.

1. Introduction

Although the energy propagations of sound or water waves require medium of propagation, in the theory of special relativity (SR) light/electromagnetic (EM) waves do not require any medium for propagation in the empty space (vacuum). However, according to the theory of relativity empty space is the four dimensional spacetime in which one can conceptually consider being the medium for the EM wave propagation. That is the reason why a medium such as ether is not required for light propagation. Therefore, it is possible to consider EM propagation being the actual oscillatory propagation of spacetime itself.

One can understand the characteristic of spacetime by analyzing the invariant interval given in the SR. There are three regions of spacetime corresponding to the three events happening in the SR. The "essence" or the "fabric" of spacetime which we refer to as "f-spacetime," is the actual spacetime prior to expansion. This will correspond to zero invariant interval where the events occur within the non-expanded spacetime. The distinguishing characteristic of this region is not only being the essence and "ground state" of spacetime, it is also the medium which "intrinsic" propagation velocity is equal to that speed of light. F-spacetime is void of space and time.

The timelike event corresponds to the expanding universe or the expanded spacetime where matter can exist. This is our observing universe. The spacelike event, on the other hand will correspond to the "residual" or "evanescent universe." If matter in timelike region gains a velocity greater than that of speed of light, it instantly will be decaying into evanescent universe by tunneling through the f-spacetime. Mass in the spacelike region will not only be decaying, it also will be imaginary.

Based on the above discussion, universe can considered being a two phase spacetime harmonic oscillator. That is, Universe expands from its equilibrium point which can be identified as f-spacetime to its maximum in the timelike region where it then will collapse to the singularity of f-spacetime with all the stored energy. Afterward it will instantly expand to the next phase opposite to that of the equilibrium where it becomes the next timelike region. The singularity of the universe is the instant moment in which there remain nothing but fabric of spacetime (f-spacetime) and the aggregation of all the stored energy. The stored energy in the singularity will force its way as propagating energy fields causing expansion of f-spacetime. The superposition of energy fields in the f-spacetime will also be the determining factor for the creation of particles and anti-particles in the expanding universe.

2. Propagation of Energy Fields

As we know, water is the medium for the propagation of energy in the form of water waves and similarly, air is the medium for the propagation of sound energy. As a consequence of propagation of energy in the form of waves, it was also assumed that light would propagate in a medium known as ether. However, according to the theory of SR light propagates in the empty space and does not require medium of propagation. On the other hand considering vacuum being identical to spacetime, one can assume light or EM waves propagate through the medium in which we can identify as the "fabric" of spacetime (f-spacetime). Spacetime is "everywhere" and such propagation can also happen everywhere in the universe. However, we do make a distinction between f-spacetime (fabric of spacetime with no expansion) and the expanded

spacetime which is the present universe, although we refer to both as spacetime. In what follows we shall intent to clarify this. Let us recall invariant interval in Cartesian coordinate system given in special relativity

$$ds^2 = c^2dt^2 - dx^2 - dy^2 - dz^2, \quad (1)$$

where we have chosen the Minkowski metric component to be of the form (1, -1, -1, -1). Eq. (1) describes the invariant interval between two events. The interval is due to the events that happen in the expanded spacetime (timelike event). In order to reach the fabric of spacetime without expansion (i.e. zero spacetime expansion), one should set the invariant interval ds^2 identically equal to zero. This off course will generate the equation

$$|\vec{v}| = c. \quad (2)$$

Eq. (2) is an expression for the characteristic velocity of propagation of spacetime that is equal to the speed of light. Light in the form of photon is the quanta of energy. Therefore, light in essence is spacetime energy wave (EM waves) propagation in the f- spacetime where the invariant interval is equal to zero. Quanta of energy or photon, is manifested when the spacetime field wave is scattered by matter. The transfer of momentum of spacetime wave to that of matter is that which generates the photon. Therefore, it is important to note that it is not the photon that propagates in the empty space rather it is the spacetime wave propagation having impact with matter that generates photon. The energy wave (field) propagation therefore, either can occur through matter such as energy of sound waves or through the f-spacetime oscillation.

3. Special Theory of Relativity and Boundaries of the Spacetime

The fabric of spacetime where v = c is the "criteria." We know that every observer in the expanding universe where ($ds^2 > 0$, timelike event), is subject to SR. It happens that as a consequence of SR, speed of light (c) is constant for all such observers. Reciprocally, in the inertia frame of c (f-spacetime), all other observers are at stand still, with zero velocity. One can thereby proclaim that the absolute observer is in the inertia frame of the fabric of spacetime where $ds^2 = 0$. It is this observer that measures spacetime at "stand still." According to the invariant interval in Eq. (1) there can only be three events, namely

$$ds \succ 0 \quad \text{timelike event,} \quad (3a)$$

$$ds = 0 \quad \text{lightlike event,} \quad (3b)$$

$$ds \prec 0 \quad \text{spacelike event.} \quad (3c)$$

We are "realistically" familiar with inequality (3a) and Eq. (3b). As we have mentioned before, Eq. (3b) is the criteria. It is because Eq. (3b) pertains to the actual fabric of spacetime and it is the absolute observer in the sense that it measures rest of the universe at rest. The inequality (3a) describes the events happening in the expanded universe where ds^2 is greater than zero. Schematically, this will correspond to an event not in the f-spacetime rather on the "boundary" of it (the expanding universe). In Figure 1. we have illustrated the events corresponding to relations (3a) and (3c) and Eq. (3b) in a flat spacetime.

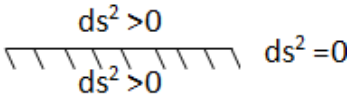

Figure 1. Straight line: Lightlike event corresponding to the "fabric" of spacetime where, $ds^2 = 0$. Boundary above the straight line: Timelike event corresponding to expanding universe where $ds^2 > 0$. Boundary below the straight line: Spacelike event corresponding to evanescent spacetime universe where $ds^2 < 0$

We need to understand the inequality (3c) where it corresponds to spacelike events. In special relativity it is a forbidden event where it corresponds to an imaginary spacetime invariant interval. This event is depicted below the fabric of spacetime in Figure 1. where it pertains to ($ds^2 < 0$) and can be explained by recalling the relativistic mass

$$m = \frac{m_0}{\sqrt{1-\frac{v^2}{c^2}}} = \gamma\, m_0, \quad (4a)$$

where γ is the relativistic constant. In the region $ds^2 > 0$, the expanding universe, mass is positive real and increase in magnitude with velocity v, as long as it is not equal or greater than c. At the fabric of spacetime where it has the characteristic of field propagation of v = c, a mass travelling with speed of light becomes infinite and therefore a singularity in spacetime. In other words, if mass gains a velocity of that speed of light it automatically inhibits the characteristic of f-spacetime where no massive particle are allowed. This region only allows energy wave propagation that eventually may manifest as particles. It is also interesting to note that according to the Eq. (4a) if mass acquires a velocity greater than speed of light it (mass) becomes imaginary and begins to decay with increasing velocity. The spacelike region where mass becomes imaginary is the analog of materials with imaginary propagation or dielectric constants where electromagnetic fields decay as evanescent waves

$$m \cong -i\frac{m_0}{\sqrt{\frac{v^2}{c^2}}} = -i\frac{m_0}{\sqrt{\frac{(\alpha c)^2}{c^2}}} = -i\frac{m_0}{\pm\alpha}, \quad (4b)$$

where $\alpha > 1$ is constant. In Figure 2. we have plotted relativistic mass versus velocity. Notice the particle at rest with mass m_0 in $ds^2 > 0$ region, an event in timelike expanding universe. As m_0 begins to move, its relativistic mass also begins to increase. There will be a pole (singularity) at v = c where mass cannot be tolerated in timelike event region. C is a property of fabric of spacetime only, velocity of intrinsic field oscillation. A massive particle with v = c cannot also be tolerated in lightlike event region. A particle therefore cannot have v = c anywhere in spacetime; It will be singularity in both f-spacetime and the expanding universe as shown in Fig. 2. It however, can leap through singularity and gain higher velocity than c into the evanescent region. Once the massive particle approaches speed v > c, it then will tunnel through the $ds^2 = 0$ region, into the $ds^2 < 0$ [Fig. 1.], where it will decay as shown in Figure 2.

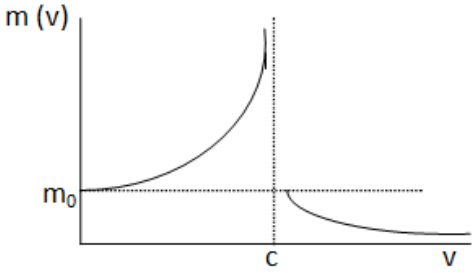

Figure 2. Relativistic mass vs. Velocity

4. Two Phase Universe, a harmonic Oscillator

The region in which we have identified as fabric of spacetime is simply spacetime in its essence, void of space and time (spacetime with no expansion). As an example consider a volume of mass-less little strings connected to one another while being at equilibrium. Let then apply an internal pulling force to the little strings which will cause their elongation. This would correspond to f-spacetime at equilibrium and the corresponding expanding universe. The difference however is that in reality f-spacetime contrary to the little strings is a conceptual object with zero mass and zero volume. The f-spacetime is therefore, a zero spacetime.

The internal energy does have a decisive rule in the expansion of spacetime and the creation of the particles. Consider a harmonic oscillator where due to its initial potential energy it will oscillate about its equilibrium position. The spring will expand from equilibrium to its maximum extension, it then contracts and expands to the other side of the equilibrium. Universe also due to its intrinsic potential energy behaves in the same manner. Universe by analogy to a harmonic oscillator has two major "components."The fabric of spacetime, analog to the mass-less string and the potential energy driving this fabric in the form of kinetic energy and expansion. The internal kinetic energy of the universe is independent from the fabric of spacetime. This energy not only is the cause for the accelerated expansion of the universe (similar to a harmonic oscillator), it also is responsible for the creation of matter; after all matter can consider being a "solidified" form of energy. As we know energy and matter are intrinsically related through the speed of light c, which we now know it is the characteristic propagation of f-spacetime

$$E = m_0\ c^2, E \propto m_0. \tag{5}$$

There are two phases of universe in which both phase will include the expansion and the evanescent region, i.e. $ds^2 > 0$ and $ds^2 < 0$ as well as fabric of spacetime $ds^2 = 0$. We will refer to these two phases as "right and left expansions." If we assume currently being at the right expansion then the right expansion will possess timelike events and consequently the left will be the residual or spacelike region, namely

$$ds_R^2 > 0 \text{ and } ds_L^2 < 0, \text{Right expansion}, \tag{6a}$$

and if be on the left expansion,

$$ds_L^2 > 0 \text{ and } ds_R^2 < 0, \text{Left expansion}. \tag{6b}$$

An example of two phase expansion of universe can be two empty balloons attached at the very ends. This corresponds to the fabric of spacetime empty of energy with no spacetime expansion. Now assume the right balloon being instantaneously bloated by air to its maximum. Then the air from the right balloon will enter to the left through the neck end. In this example there will be an equilibrium state where both balloons will be partially expanded. In two phase universe theory however, we have to assume one side completely being expanded and then complete contraction to the singularity into f-spacetime ($ds^2 = 0$) with then expansion into the other side. This requires a universe with initial condition similar to that of an ideal LC (inductor and capacitor) circuit where oscillation will be indefinite. From our point of view all that we observe is the universe expansion and contraction to singularity and the beginning of a new big bang. The right and left expansions become irrelevant.

5. Creation of Matter and Photon

The energy stored in the singularity ($ds^2 = 0$ region) after complete contraction of the universe will then cause the expansion of spacetime into second phase. As we have indicated, energy in the universe either propagates through the fabric of spacetime in the form of spacetime energy fields or propagation through matter. The energy propagations through matter are trivial. The energy propagation through spacetime will physically manifest only when spacetime vibrations having momentum impact with matter or through the superposition of the f-spacetime fields.

At the moment of big bang there will be tremendous amount of energy propagating in $ds^2 = 0$ that will lead to the expansion of fabric of spacetime. Similar to the expansion of matter (i.e. substance or gas) that is caused by the energy fields transferring kinetic energy to atoms and particles, energy field fields will also transfer kinetic energy to the f-spacetime in the form of expansion.

The propagating energy field waves in the $ds^2 = 0$ region will also interact with one another which will lead to generation of particles and anti-particles in the $ds^2 > 0$. This cannot happen prior to the expansion of spacetime into timelike region. In other words, creation of particles and anti-particles in the universe are the result of the f-spacetime energy waves' superposition while universe began expanding. Reciprocally, once matter and antimatter occupy same event in the $ds^2 > 0$ region, they immediately will annihilate into f-spacetime energy field waves. It is not the energy however, that causes the interaction, it rather is the transfer of relativistic momentum as shown in Eq. (7)

$$E = m_0\ c^2, \frac{E}{c} \Leftrightarrow\ \ m_0\ c. \tag{7}$$

Photons are therefore created in two ways, either through interaction of f-spacetime wave fields with matter in the form of momentum exchange or matter and antimatter annihilations. In any event, photon as a physical object will manifest only when f-spacetime energy waves interact as momentum exchange to that of matter. Matter

interactions in the particle level are such that it may generate new particles that are particular superposition of spacetime waves with some additional energy that will appear in f-spacetime. Additional energies remain until being manifested in the form of photons, or through superposition will later manifest as other forms of massive particles. We noticeably realize that particles are energy manifestation of lightlike or f-spacetime vibrations into a timelike spacetime. The contraction of universe to a singularity will eventually bring all particles and antiparticles into the same exact point of spacetime event that will lead to their annihilation into f-spacetime energy field waves. In Figure 3(a) and Figure 3(b) we have depicted the creation of particle and anti-particle through superposition into the expanding universe and decay of mass into evanescent spacetime for both right and left expansions.

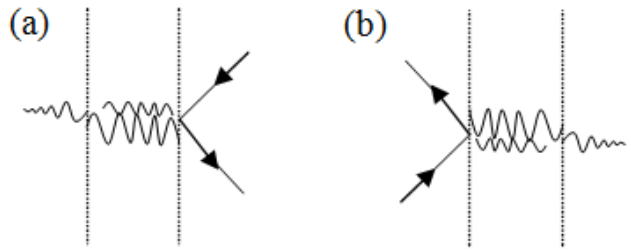

Figure 3. (a) Right expansion: superposition of energy waves creating particles and anti-particles in the expanding universe on the right, with imaginary matter decaying in the evanescent universe on the left. (b) Left expansion: superposition of energy waves creating particles and anti-particles in the expanding universe on the left, with imaginary matter decaying in the evanescent universe on the right

6. Quantum States of Matter and Anti-matter

Figure 3 shows the schematic for creation of particle and anti-particle pertain to the right and left expansions. The superposition of energy spacetime field waves in $ds^2 = 0$ will lead to the generation of particles and anti-particles into the expanded universe. This process can also happen in opposite directions. That is to say, matter and anti-matter may annihilate into propagation in f-spacetime. We can also expect the tunneling of matter through f-spacetime into the evanescent region. In this region as particle's velocity approaches infinity, the mass will decay to zero. It happens that once particle's speed reduces to $v < c$, according to Eq. (4a) the particle will no longer exist in the evanescent region, rather will tunnel back to $ds^2 > 0$ region and reappear once again in the expanding universe.

There are only a limited permitted amount of energy wave superposition that can leap through the interface and appear as types of particles and anti-particles which universe contains. Once particle appears in the timelike event, its mass will correspond to the half of the total energy of the superposition field waves

$$\frac{E}{c^2} = \frac{1}{2}m_0 + \frac{1}{2}\bar{m}_0, \tag{8}$$

where $\bar{m}_0$ is the mass of anti-particle. That which distinguishes a particle from its anti-particle partner is the charge it acquires. The anti-particle of a particle with charge q will have a charge of (-q). Namely,

$$\frac{E}{c^2} \Leftrightarrow \frac{1}{2}m_0(q) + \frac{1}{2}m_0(-q). \tag{9}$$

The Left hand side of Eq. (9) represents the superposition of energy waves in the f-spacetime. The right hand side of Eq. (9) expresses the creation of particle and anti-particle. If we assign a charge eigen-state to a massive particle, let say $|m(q)\rangle$, then the overlap of $\langle m(-q)|m(q)\rangle$ should lead to the annihilation of the masses and the release of energy in the form of f-spacetime field waves as is expressed in Eq. (9). A massive particle cannot be without a charge quantum state. A neutral particle such as neutron for example, is such that the superposition of total charge eigen-values within that particle is zero. A particle and anti-particle will come into existence (manifestation of energy in the form of matter in $ds^2 > 0$ region) in the general form of $m_0\ (\pm q)$ with also having other distinguished quantum numbers. However, it is the charge quantum number that will facilitate particle/anti-particle annihilation into f-energy field waves. The two universal attribute of particles pertain to spacetime discussion are therefore, rest mass and charge. Particle and anti-particle states in the form of matter will shatter into energy, once charge quantum states of the two interacting particle-anti-particle are vanished. We can therefore say charge is the "glue" that which localizes energy in the form of matter and if vanish, the energy no longer can be localized in timelike spacetime event in the form of matter, rather it will be energy propagating in lightlike f-spacetime. We should notice that in timelike spacetime energy is localized where as in lightlike spacetime energy is propagative.

Fundamental particles are the least number of possible superposition in f-spacetime fields whereas the composite particles (non-fundamental) are the consequence of additional superposition. Mass is the localized superposition of energy field states in the expanding spacetime. The localized field superposition carry charge quantum states that are responsible for localization of the energy fields in the form we know as matter.

7. Conclusion

Our universe is comprised of three events in special relativity i.e., timelike, lightlike and spacelike which correspond to the three regions of spacetime. The timelike region is the present expanding universe in which events are real and mass cannot acquire a speed equal or greater than speed of light. The lightlike region corresponds to the fabric of spacetime where its essential form is the universe prior to expansion and when it contains all the intrinsic potential energy, it will manifest instantly as big bang in a singularity. The spacelike region corresponds to the evanescent spacetime or the residual universe. It is the region where masses will manifest, however, if acquire a speed greater than speed of light and will be subject to decay.

The three regions of spacetime associated with expansion, singularity and evanescence will prompt us to

come to the logical conclusion that universe has a two phase or, the right and left expansions. This is indeed similar to a harmonic oscillator where each phase is the symmetric analog of other.

The fabric of spacetime is the medium in which all energy fields are contained while propagating with the characteristic speed, c. In the instant of the big bang the stored energy (propagating fields) in the lightlike region will flow in the form of expansion of fabric of spacetime. The fabric of spacetime in itself is physically void of space and time, however, instant surge of flow of super kinetic energy from the contraction of let say right universe will cause the expansion into next phase (left expansion). Energy can only be stored in the form of propagating fields that will cause the expansion of spacetime whereas their superposition will cause particle and anti-particle creation. In other words the propagation of energy fields will cause the expansion and their superposition will cause the creation of matter and anti-matter in the spacetime.

References

[1] D. Simpson, "A Mathematical Derivation of the General Relativistic Schwarzschild Metric," 2007

[2] S. Hawking, "A Brief History of Time," New York: Bantam Books, 1988.

[3] R.L. Faber, "Differential Geometry and Relativity Theory,": An Introduction. New York: Marcel Dekker, Inc., 1983.

[4] T. Marsh, "General Relativity," class notes, 2009

[5] "S. Chandrasekhar, "The Mathematical Theory of Black Holes". Clarendon Press (1983)

[6] C.W. Misner, K.S. Thorne, and J.A. Wheeler, "Gravitation". Freeman (1973).

[7] S. Weinberg, "Gravitation and Cosmology: Principles and Applications of the General Theory of Relativity". Wiley (1972)

[8] G. 't Hooft, " Introduction To General Relativity," Institute for Theoretical Physics; Utrecht University (2002)

[9] Poul Olesen, "General Relativity and Cosmology," The Niels Bohr Institute (2008).

[10] M. Kachelrieb, "Gravitation and Cosmology," Institute for fysikk; NTNU (2010).

[11] M. Khoshsima, "Black Hole Spacetime Equation in Special Relativity." International Journal of Astronomy, Astrophysics and Space Science; Vol. 2, No. 4, 2015, pp. 30-33.

International Journal of Physics, 2016, Vol. 4, No. 2, 26-31
Available online at http://pubs.sciepub.com/ijp/4/2/1

DOI:10.12691/ijp-4-2-1

The Model of Magnetic Field Based on the Concepts of Virtual Particles and Quantum Harmonic Oscillators Possessing Zero-Point Energy

Liudmila B. Boldyreva*

The State University of Management, Moscow, Russia
*Corresponding author: boldyrev-m@yandex.ru

Abstract The magnetic field model proposed in the paper is based on the two concepts of quantum mechanics: the creation of virtual particles pairs by quantum entities and the possibility of existence in the physical vacuum of quantum harmonic oscillators possessing zero-point energy. The characteristics of magnetism, i.e. the magnetic vector potential and magnetic induction, are shown to be associated with definite types of motion of quantum harmonic oscillators. The magnitude of magnetic vector potential is determined by the oscillation frequency of quantum harmonic oscillators. The magnetic induction is proportional to the speed of translational motion of quantum harmonic oscillators. The energy associated with these types of motion is analyzed. If in a certain region of physical vacuum there is no quantum harmonic oscillators, in particular this takes place in the motion of Cooper pairs of electrons in superconductors, no magnetic field may exist in the region, that is, there takes place the "expulsion" of magnetic field from the superconductor. It is shown that in the physical vacuum containing quantum harmonic oscillators there is a relationship, under definite conditions, between magnetic and electric fields.

Keywords: *zero-point energy, quantum harmonic oscillator, magnetic induction, magnetic vector potential, virtual particles,Meissner–Ochsenfeld effect, superconductivity*

Cite This Article: Liudmila B. Boldyreva, "The Model of Magnetic Field Based on the Concepts of Virtual Particles and Quantum Harmonic Oscillators Possessing Zero-Point Energy." *International Journal of Physics*, vol. 4, no. 2 (2016): 26-31. doi: 10.12691/ijp-4-2-1.

1. Introduction

The following magnetic field characteristics are considered in the paper: the magnetic induction, magnetic vector potential, relationship with electric field. The discussion of these characteristics is based on the following two concepts of quantum mechanics:

The 1st concept. In the physical vacuum a quantum entity may produce a pair of oppositely charged virtual particles having the following properties [1]:

1) A pair of virtual particles may be converted into a pair of real particles with the total spin equal to $\hbar$, the angular momentum being conserved.

2) A pair of virtual particles has a mass.

3) The electric properties of virtual particles are the same as those of real particles. Consequently, a pair of oppositely charged virtual particles is an electric dipole whose electric properties are the same as those of the electric dipole formed by a pair of oppositely charged real particles.

4) The virtual particle has spin with the same properties as the real particle spin, hence it follows that:

a) the spin of a pair of virtual particles has no definite direction, and by the magnitude of spin the magnitude of its projection onto a preferential direction is meant; this can be interpreted as a precession of the spin about the preferential direction; the precession is characterized by the precession phase, angle of deflection, and precession frequency;

b) spin correlations may take place between the spins of pairs of virtual particles.

The 2nd concept. In the physical vacuum there may exist quantum harmonic oscillators possessing zero-point energy. The concept of zero-point energy was developed in Germany by Albert Einstein and Otto Stern in 1913 [2]. According to this concept, it is the energy of the vacuum, which in quantum field theory is defined not as an empty space but as the ground state of the field whose features are as follows [3,4]:

1) the field consists of oscillators with oscillation frequency Ω (the oscillator is called at present "quantum harmonic oscillator", in this paper the abbreviation QHO is used);

2) the energy of such an oscillator is equal to $\hbar\Omega/2$, the energy is referred to as zero-point energy;

3) neighboring oscillators interact with each other.

The model of magnetic field developed in this paper gives reasons for the following:

- Virtual particles created in the physical vacuum by moving quantum entities produce in the physical vacuum, in their turn, the objects whose properties are similar to those of a QHO possessing zero-point energy.
- The magnetic induction is associated with the speed of motion of QHOs in the physical vacuum; the

specific energy of magnetic field is equal to the kinetic energy of the moving QHOs in a unit volume of the physical vacuum.

- The magnetic vector potential is determined by the oscillation frequency of QHO. The energy associated with the magnetic vector potential is equal to the energy associated with the oscillation.
- In the physical vacuum containing QHOs possessing zero-point energy, at certain conditions there is a relationship between magnetic and electric fields.

The equations derived in the paper provide explanation to experimentally established effect: the expulsion of magnetic field from a superconductor (in particular, the Meissner–Ochsenfeld effect) [5].

2. Propagation of Spin Precession in the Physical Vacuum

Every moving quantum entity produces a pair of oppositely charged virtual particles in the physical vacuum. According to the properties of virtual particles mentioned in Introduction, the pair has a precessing spin and a mass associated with it. In Fig. 1 are shown the following characteristics of a virtual particles pair: spin $\mathbf{S}_v$; precession frequency $\boldsymbol{\omega}_v$; precession angle (phase) α; angle of deflection θ; mass m_v performing a circular motion at speed $\boldsymbol{\upsilon}_v$ and having angular momentum $\mathbf{Z}_v$, $\mathbf{Z}_v \uparrow\uparrow \boldsymbol{\omega}_v$. The circulation of $\boldsymbol{\upsilon}_v$, $\boldsymbol{\Gamma}_v$, is determined as:

$$\boldsymbol{\Gamma}_v = \frac{2\pi \mathbf{Z}_v}{m_v} = \frac{2\pi Z_v}{m_v}\frac{\boldsymbol{\omega}_v}{\omega_v}. \quad (1)$$

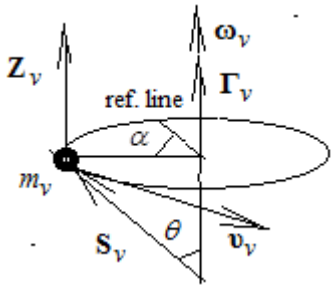

Figure 1. The characteristics of a pair of virtual particles: $\mathbf{S}_v$ is spin; m_v is the mass; $\boldsymbol{\omega}_v$ is the precession frequency; $\mathbf{Z}_v$ is the angular momentum of m_v; $\boldsymbol{\upsilon}_v$ is the speed of the circular motion of m_v; θ is the deflection angle; α is the precession angle (phase); $\boldsymbol{\Gamma}_v$ is circulation of $\boldsymbol{\upsilon}_v$; ref. line is the reference line

Energy U_S is associated with the precession of spin $\mathbf{S}_v$ and is a function of deflection angle θ [6]. The maximum value of U_S, $(U_S)_{\max}$, is defined as:

$$(U_S)_{\max} = S_v \omega_v. \quad (2)$$

The energy associated with the circular motion of m_v is defined [6] as:

$$U_m = Z_v \omega_v / 2. \quad (3)$$

According to the properties of pairs of virtual particles mentioned in Introduction, a pair of virtual particles may be converted into a pair of real particles with the total spin equal to $\hbar$, the angular momentum being conserved. Consequently, the total spin S_v of a virtual particles pair, at least while converting into real particles, must not be equal to zero. But a virtual particles pair may be created by the quantum entity whose spin equals $\hbar/2$ and while creating the virtual particles pair the quantum entity preserves this spin. Hence this may suggest that the physical vacuum has an intrinsic degree of freedom, i.e. spin, which manifests itself in the creation of virtual particles. That is, S_v is the total spin that determines the intrinsic degree of freedom of the physical vacuum in the region where the virtual particles pair is created.

According to the property 4b of pairs of virtual particles mentioned in Introduction, spin correlations may take place between the spins. Experiments conducted with superfluid ^{3}He-B showed that the spin correlations may be effected by spin supercurrent [7,8,9]. The spin supercurrent may emerge between the spins of the virtual particles pairs and the spins that determine the intrinsic degree of freedom of the physical vacuum. The spin supercurrent makes equal the respective characteristics of precessing spins (the deflection and precession angles), between which the spin supercurrent emerges, and thus the "propagation" of the spin precession of the virtual particles pairs may take place in the physical vacuum. Let us assume that the frequency $\boldsymbol{\omega}_v$ and frequency $\boldsymbol{\Omega}_v$, which arises as a result of the "propagation" of the spin precession are mutually related by the equation:

$$\boldsymbol{\Omega}_v = \boldsymbol{\omega}_v f(r), \quad (4)$$

where $f(r)$ is a function determining the dependence of Ω_v on distance r between the virtual particles pair with precession frequency $\boldsymbol{\omega}_v$ and the point where the spin precession with frequency $\boldsymbol{\Omega}_v$ arises.

The mass, mass angular momentum $\mathbf{Z}_{\Omega_v}$, energy W_m of circular motion of mass are associated with frequency Ω_v, as well as they are associated with frequency $\boldsymbol{\omega}_v$ (see Eq. (2)). Energy W_m is determined by the relation $W_m = Z_{\Omega_v} \cdot \Omega_v / 2$. If $Z_{\Omega_v} = \hbar$, then

$$W_m = \hbar \cdot \Omega_v / 2. \quad (5)$$

Equation (5) is the same as that determining the zero-point energy of a QHO. In addition to similarity in the equations determining the energy, the objects created in the physical vacuum due to the "propagation" of spin precession possess as well other properties of QHO that were given in Introduction: an oscillatory process (precession) with frequency Ω_v takes place, and neighboring objects can interact with each other (for example, by spin supercurrents). Because of the above-mentioned similarity, these objects can be referred to as QHO as well.

3. The Magnetic Induction

A pair of oppositely charged virtual particles is an electric dipole, $\mathbf{d}_v$. If the quantum entity that created a virtual particles pair has an electric charge, then the

entity's electric field, $\mathbf{E}_v$, exerts a moment $\mathbf{M}_v$ on the virtual particles pair as an electric dipole, $\mathbf{M}_v = \mathbf{d}_v \times \mathbf{E}_v$. Since the direction of electric dipole moment of virtual particles pair is associated with the orientation of $\boldsymbol{\omega}_v$ as $\mathbf{d}_v \uparrow\downarrow \boldsymbol{\omega}_v$ [10,11], the direction of precession frequency $\boldsymbol{\omega}_v$ depends on the direction of $\mathbf{E}_v$, that is on the sign of the moving quantum entities. It is shown in [10, 11] that the direction of precession frequency $\boldsymbol{\omega}_v$ of spin of virtual particles pair created by the charged quantum entity is determined as:

$$\boldsymbol{\omega}_v \uparrow\uparrow \mathbf{I}. \tag{6}$$

The electric current I may be looked upon as a flow of virtual particles pairs created by moving electrically charged quantum entities. Taking into account Eq. (6), that is, the same direction of spin precession frequencies of all virtual particles pairs created by the charged quantum entities that form the current, the total circulation $\boldsymbol{\Gamma}_I$ of the mass velocity of these virtual particles pairs is determined as $\boldsymbol{\Gamma}_I = z \cdot \boldsymbol{\Gamma}_v$, where z is the number of the quantum entities (having electric charge q) whose motion forms current I.

$$z = I / q. \tag{7}$$

Using Eqs. (1), (6) and (7) in the expression for $\boldsymbol{\Gamma}_I$ we obtain:

$$\boldsymbol{\Gamma}_I = \frac{2\pi Z_v \mathbf{I}}{m_v q} \tag{8}$$

It is shown in [6] that there is a complete analogy between the structures of formulas describing the magnetic interactions of current-carrying wires and the structures of formulas describing the interactions of vortices in an ideal incompressible liquid with positive density and negative pressure. The sign of the pressure p in a medium depends on the nature of internal stresses in it. If the internal stresses are like "omniradial tensions", the pressure will be negative [6]. The virtual particles pair is a pair of oppositely charged particles, thus there exists a repulsive force between the particles that compensates the electric attractive force between them. The existence of repulsive forces between virtual particles suggests that the medium consisting of virtual particles pairs has negative pressure, i.e. the following may be valid:

$$\rho u^2 / 2 - p = const, \tag{9}$$

where u and ρ are respectively the speed and density of the physical vacuum with QHO; ρ is positive because it is associated with the QHO mass. The dissipation free motion of celestial bodies, such as the planets of the solar system allows one to look upon the physical vacuum as a medium without shear (linear) viscosity.

We shall derive equations that establish a relationship between the characteristics of magnetic field and kinematic characteristic of the vortex line in the medium with the above mentioned properties (Eq. 9), assuming that the density ρ of the physical vacuum with QHO is constant.

Interaction of infinite vortex lines and interaction of two infinite current-carrying wires. The force acting on the unit length of either of the two infinite mutually parallel vortex lines having the same values of circulation $\boldsymbol{\Gamma}$ is $F = \rho\Gamma^2 / (2\pi r_w)$, where r_w is the distance between the vortex lines with circulation $\boldsymbol{\Gamma}$ [6]. The force on the unit length of either of the two infinite mutually parallel current-carrying wires (in the CGSE system of units): $F = 2I^2 / (r_w c^2)$, where I is the current, r_w is here the distance between the current-carrying wires, c is the speed of light [12]. By equating the above expressions for the forces and taking into account that the forces are attractive if the currents as well as velocity circulations around the vortex lines have the same direction, we obtain:

$$\boldsymbol{\Gamma} = \mathbf{I} 2\sqrt{\pi} / \left(c\sqrt{\rho}\right). \tag{10}$$

Note that using Eqs. (8) and (10) it is possible to relate density ρ to the characteristics of the virtual particles pair created by the quantum entity having electric charge q: $\rho = m_v^2 q^2 / (\pi c^2 Z_v^2)$.

The field of velocities generated by a closed vortex line and the magnetic induction around a current loop. The field of velocities $\mathbf{u}$ generated by a closed vortex line having circulation $\boldsymbol{\Gamma}$ along an arbitrary loop enclosing the vortex line is defined [6] as $\mathbf{u} = \frac{\Gamma}{4\pi}\int_{L'} \frac{d\mathbf{l} \times \mathbf{r}}{r^3}$, where $d\mathbf{l}$ is an infinitesimal vector element of the vortex line, L' is the length of the line, $\mathbf{r}$ is a radius vector from $d\mathbf{l}$ to the point of observation. Outside the vortex line, $curl\mathbf{u} = 0$. The structure of equation for $\mathbf{u}$ is the same as the structure of equation for the Biot-Savart law in the CGSE system of units, defining the magnetic induction $\mathbf{B}$ generated by a loop with current I: $\mathbf{B} = \frac{I}{c}\int_{L'} \frac{d\mathbf{l} \times \mathbf{r}}{r^3}$ (L' is the length of the loop, $d\mathbf{l}$ is the wire element) [12]. Having solved simultaneous equations for $\mathbf{B}$, $\mathbf{u}$ and Eq. (10), we obtain an equation relating the magnetic induction $\mathbf{B}$ to the velocity $\mathbf{u}$ of the medium:

$$\mathbf{B} = \mathbf{u} 2\sqrt{\pi\rho}. \tag{11}$$

The specific energy of the physical vacuum and the specific energy of magnetic field. The kinetic energy U_u of a unit volume of the medium moving at speed u is:

$$U_u = \rho u^2 / 2. \tag{12}$$

Taking into account Eq. (11), energy U_u in Eq. (12) can be represented in the form: $U_u = B^2 / (8\pi)$. This expression is the same as that for the specific energy of magnetic field B [12].

Notes:

1) The speed u of the motion of the physical vacuum with QHO specifying the magnetic induction in Eq. (11) is determined relative to the same frame as the speed of the charges, which determines the electric current I.

2) Equations determining the magnetic forces between the current-carrying wires and the magnetic induction

produced by electric current are written, first, for the vacuum whose permeability $\mu = 1$, and, secondly, they are written in the CGSE system of units in order to maintain the constant c in these equations to show a relation of magnetic field characteristics to the properties of the physical vacuum.

4. The Magnetic Vector Potential

In classical electrodynamics the magnetic field of strength **B** is determined by the equation [12] $\mathbf{B} = curl\mathbf{A}$, where **A** is a magnetic vector potential. The potential **A** created by element dy of a wire carrying current **I** is determined at the distance r from the wire (Figure 2), provided that $dy << r$, as [13]:

$$\mathbf{A} = \frac{\mathbf{I} \cdot dy}{4\pi r \cdot c}. \qquad (13)$$

There are a great number of experiments which suggest that magnetic vector potential has a physical meaning of its own [14]. In general, these experiments were as follows: the beam of quantum entities emitted by a source is split into two beams: one of them passes through the region where $\mathbf{B} = 0$ and $\mathbf{A} \neq 0$, the other through the region where $\mathbf{B} = 0$ and $\mathbf{A} = 0$; after that both beams arrive at an interferometer. The interference rings obtained suggest that there is a change in the wave function phase of quantum entities passing through the region where $\mathbf{B} = 0$ and $\mathbf{A} \neq 0$.

Let us analyze the physical process that could cause a change in the wave function phase of the quantum entities passing through the region of the physical vacuum where $\mathbf{A} \neq 0$. For this purpose let us consider the passage of a quantum entity through point P of the physical vacuum, which is located at a distance r from the wire carrying current I. Because of "propagation" of the precession of spin of virtual particles pairs created by the charges that form the current I (see Section 2) at point P, there is QHO with spin precession frequency $\mathbf{\Omega}_I$ determined as $\mathbf{\Omega}_I = z \cdot \mathbf{\Omega}_v$. Using (4) and (7) in the expression for $\mathbf{\Omega}_I$, we obtain:

$$\mathbf{\Omega}_I = \omega_v f(r)\mathbf{I}/q. \qquad (14)$$

The QHO spin precession (with frequency $\mathbf{\Omega}_I$) causes a change in the spin precession frequency $\boldsymbol{\omega}_q$ of the virtual particles pair created by the quantum entity at the point P. The nature of the change depends on the mutual orientation of $\boldsymbol{\omega}_q$ and $\mathbf{\Omega}_I$. If $\boldsymbol{\omega}_q \uparrow\uparrow \mathbf{\Omega}_I$ or $\boldsymbol{\omega}_q \uparrow\downarrow \mathbf{\Omega}_I$, the magnitude of spin precession frequency will change by:

$$\Delta\omega_q = \Omega_I. \qquad (15)$$

The change in the spin precession frequency will lead to a change in the spin precession phase. The value of change in spin precession phase $\Delta\alpha$ during time t is expressed as $\Delta\alpha = \Delta\omega_q \cdot t$, or in view of Eq. (15), as follows:

$$\Delta\alpha = \Omega_I \cdot t. \qquad (16)$$

Figure 2 shows as an example the relative direction of $\mathbf{\Omega}_I$ and $\boldsymbol{\omega}_q$, and also the change in the precession phase, $\Delta\alpha$, of spin $\mathbf{S}_q$ of the virtual particles pair created by a quantum entity ($\mathbf{S}_q'$ is the position of spin $\mathbf{S}_q$ after the action of vector potential).

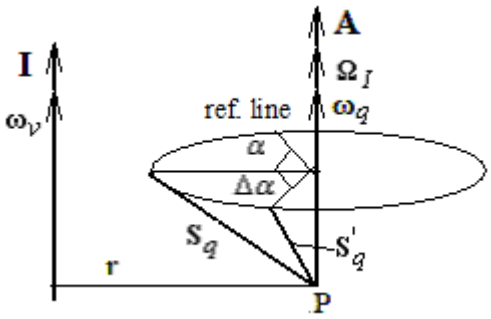

Figure 2. The characteristics of physical vacuum with QHO: $\mathbf{\Omega}_I$ is the QHO precession frequency; r is the distance between the wire and point P; **A** is the magnetic vector potential; $\boldsymbol{\omega}_v$ is the spin precession frequency of the virtual particles pair created by a charged quantum entity that is a constituent of current **I**; $\mathbf{S}_q$, $\boldsymbol{\omega}_q$ and α are respectively the spin, spin precession frequency and precession angle (phase) of the virtual particles pair created by the moving quantum entity; $\Delta\alpha$ is a change in spin precession phase α; $\mathbf{S}_q$ is the position of spin $\mathbf{S}_q$ after the action of vector potential; ref. line is a reference line

It is shown in [11,15] that the quantum entity wave function phase φ_ψ is essentially the precession angle (phase) of spin of the virtual particles pair created by a quantum entity in the physical vacuum; thus

$$\Delta\alpha = \Delta\varphi_\psi, \qquad (17)$$

where $\Delta\varphi_\psi$ is a change in the wave function phase φ_ψ. Taking into account Eq. (17), the quantity $\Delta\alpha$ as specified by Eq. (16) may determine the result of the above-described experiments with the two beams of quantum entities.

Therefore, the creation of QHO in the physical vacuum may be assumed to be the physical process that is responsible for the existence of magnetic vector potential. Using Eqs. (13) and (14), the magnitude of the magnetic vector potential **A** created by electric current **I** at the point P lying at distance r from the wire may be associated with the quantity $\mathbf{\Omega}_I$ at this point.

$$\mathbf{A} = \mathbf{\Omega}_I \frac{q \cdot dy}{4\pi \cdot c \cdot \omega_v \cdot r \cdot f(r)}. \qquad (18)$$

A change in the precession frequency of virtual particles pair spin results in a change of virtual particles pair energy and consequently in a change in the energy of the quantum entity that created this pair. The maximum change ΔU_q in the virtual particles pair energy associated with precessing spin S_q is determined according to Eq. (2) as follows: $\Delta U_q = S_q \cdot \Delta\omega_q$. Using Eqs. (15) and (18), we obtain for ΔU_q: $\Delta U_q = A \cdot 4\pi \cdot S_q \cdot c \cdot \omega_v r \cdot f(r)/(q \cdot dy)$.

A certain amount of energy is associated with frequency $\mathbf{\Omega}_I$. According to Eq. (2), the maximum value

of this energy, $(U_\Omega)_{\max}$, is determined by equation $(U_\Omega)_{\max} = S_{\Omega_I}\Omega_I$, where S_{Ω_I} is the value of QHO precessing spin at the point *P*. Using Eq. (18) in this expression we obtain:

$$(U_\Omega)_{\max} = A\frac{4\pi \cdot c \cdot \omega_v \cdot r \cdot f(r)}{q \cdot dy} S_{\Omega_I}. \qquad (19)$$

Note. The motion of a quantum entity in the physical vacuum with QHO is equivalent to the exposure of the entity to a magnetic field. Thus the quantum entities that in the above-described experiment pass through the region where $\mathbf{B} = 0$ in the laboratory frame, while $\mathbf{A} \neq 0$, are as well in a magnetic field in the *entities' frame*. The magnetic induction of this field, $\mathbf{B}_q$, according to Eq. (11), is determined by the relation $\mathbf{B}_q = -\boldsymbol{\upsilon}_q 2\sqrt{\pi\rho}$, where $\boldsymbol{\upsilon}_q$ is the quantum entity velocity. According to the Schrödinger equation, the exposure of a quantum entity to a magnetic field changes the wave function phase of the entity (we denote that change as $(\Delta\varphi_\psi)_{B_q}$). Therefore, the total change in the wave function phase $(\Delta\varphi_\psi)_\Sigma$ of a quantum entity, when it is moving in the region where $\mathbf{B} = 0$ in the laboratory frame and $\mathbf{A} \neq 0$, is determined as $(\Delta\varphi_\psi)_\Sigma = \Delta\varphi_\psi + (\Delta\varphi_\psi)_{B_q}$, where $\Delta\varphi_\psi$ is determined by Eqs. (15)-(18).

5. The Relationship of Magnetic Field and Electric Field

A pair of virtual particles may be converted into a pair of real particles, with the energy and total spin of virtual particles pair being equal respectively to the energy and total spin of the pair of real particles produced. Thus in the vacuum with QHO the laws of energy and angular momentum conservation are valid. The Einstein-de Haas effect [16] holds in such a medium: a change in the polarization of spin **S** of a volume of medium results in the rotation of the medium. That is the following is valid:

$$\partial\mathbf{S}/\partial t = -k_1 \cdot curl\mathbf{u}, \qquad (20)$$

where t is time, k_1 is a proportionality factor; $k_1 > 0$. Under the property 3 of virtual particles described in Introduction, a pair of oppositely charged virtual particles is an electric dipole, that is between the oppositely charged virtual particles there is electric field **E**. If to introduce a proportionality factor k_2: $\mathbf{E} = k_2\mathbf{S}$, then using Eqs. (11) and (20) we obtain:

$$\frac{\partial\mathbf{E}}{\partial t} = -\frac{k_1 k_2}{2\sqrt{\pi\rho}} curl\mathbf{B}.$$

The structure of this equation is the same as that of one of the Maxwell equations. Note that the dimension of factor $k_1k_2/(2\sqrt{\pi\rho})$ is the same as that of velocity.

6. The Expulsion of Magnetic Field from a Superconductor

This section provides an explanation to the fundamental property of superconductors: the so-called effect of expulsion of magnetic field from a superconductor. The effect takes place both in the case where the superconductor is exposed to an external magnetic field *B*, $B < B_c$, at $T < T_c$ (B_c is the critical value of magnetic induction at arbitrary *T*, T_c is the critical temperature) and in the case where the superconductor is exposed to magnetic field *B* at $T > T_c$, the superconductor being cooled down to the temperature of $T < T_c$ after that (the so-called Meissner–Ochsenfeld effect [5]). The effect shows that superconductivity cannot be treated as a mere loss of electric resistance by the conductor. If a regular conductor exposed to field *B* became superconducting at $T < T_c$, the magnetic field that was present in the conductor at the time of transition into the state of superconductivity would persist in the conductor.

In a superconducting substance, electrons form pairs (Cooper pairs). The momenta of the electrons in a pair are oppositely directed; thus according to Eq. (6) the precession frequencies of virtual particles pairs created by the electrons of a Cooper pair are directed oppositely to each other and consequently their sum is zero. Therefore, according to Eq. (4), in the vicinity of a Cooper pair no QHO will be produced in the physical vacuum. In such a physical vacuum without QHO the equation (9) is not valid, and no magnetic field will be formed there.

With QHO is associated the energy determined by Eq. (19). The absence of QHO implies that the motion of Cooper pairs will not be accompanied by energy losses due to formation of QHO.

Note. According to the properties of virtual particles pair (see Introduction), the pair has an electric dipole moment. The moment causes the interaction between the electrons due to dipole-dipole interaction between the virtual particles pairs created by the electrons. It is shown in [10,17] that the total electric dipole moment of a Cooper pair is equal to zero, which diminishes the interaction of the assembly of Cooper pair electrons in comparison with the interaction of a similar assembly of unpaired electrons.

Thus in the electric current formed by Cooper pairs there will be no energy losses of two types: energy losses due to creating QHO in the superconducting region and losses due to electric dipole-dipole interaction of virtual particles pairs produced by electrons of Cooper pairs. Superconductivity may be assumed to be caused by the absence of those two types of energy losses.

7. Discussion

The observation of the topological Aharonov-Casher phase shift by neutron interferometry.

Figure 3 presents a schematic diagram of the experiment that demonstrates the Aharonov-Casher topological phase shift [18]. Spin-polarized neutrons emitted by a source are divided into two beams. Neutrons of different beams pass on different sides of the line

charge and arrive at the interferometer entrances. The electric field strength in the region where the neutrons propagate is $\mathbf{E}_n$.

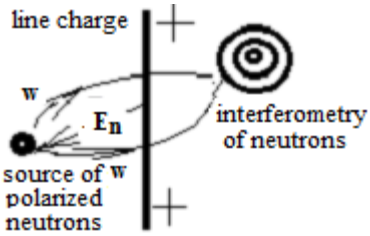

Figure 3. Diagram of the experiment that demonstrates the Aharonov-Casher topological effect. $\mathbf{E}_n$ is the electric field strength produced by the line charge in the region where the neutrons propagate; **w** is the neutron velocity

Interference fringes were observed in the experiment, which suggests that there is a difference in the wave function phases of the neutrons that passed on different sides of the line charge. The difference in the phases is such as if a magnetic field acted upon a neutron in the reference frame of the neutron, the magnetic induction $\mathbf{B}_n$ being equal to $(1/c)\mathbf{E}_n \times \mathbf{w}$. In the model developed in this paper, for the existence of magnetic field in the frame of neutron it is necessary that the physical vacuum in the region where neutrons propagate contained QHO in the same frame. However, the line charge, which is at rest (relative to the physical vacuum), does not create QHO in the physical vacuum. Therefore, in the model there is no magnetic field in the frame of reference of neutron.

To explain the topological Aharonov-Casher phase shift, let us consider the electric dipole moment $\mathbf{d}_v$ of virtual particles pair created by a neutron in the physical vacuum. In the electric field of the line charge, the moment $\mathbf{M}_n$ defined as $\mathbf{M}_n = \mathbf{d}_v \times \mathbf{E}_n$ will affect the characteristics of the precession of spin of virtual particles pair created by the neutron in the physical vacuum. These characteristics, according to [11,15], are essentially the characteristics of the neutron wave function. In more detail the effect of electric field on a quantum entity due to the existence of the electric dipole moment of the virtual particles pair created by a quantum entity in the physical vacuum is discussed in works [10,11].

8. Conclusion

According to the model advanced in this paper, magnetic field may exist in the physical vacuum containing quantum harmonic oscillators possessing zero-point energy. Such characteristics of magnetic field as the magnetic vector potential and magnetic induction are associated with definite types of motion of the quantum harmonic oscillators possessing zero-point energy. The magnitude of magnetic vector potential is determined by the oscillation frequency of quantum harmonic oscillators. The magnetic induction is proportional to the speed of translational motion of quantum harmonic oscillators. The kinetic energy of translational motion of quantum harmonic oscillators in a unit volume of the physical vacuum is equal to the specific energy of magnetic field.

Quantum harmonic oscillators are produced in the physical vacuum by moving quantum entities, in particular by quantum entities that form electric current. Energy is consumed for the maintenance of quantum harmonic oscillators in the physical vacuum. There may be a situation where in the motion of an assembly of quantum entities no quantum harmonic oscillators emerge. For example, this takes place in the motion of Cooper pair electrons in a superconductor. In this case, no energy of Cooper pair electrons is consumed for the maintenance of quantum harmonic oscillators and, besides, no magnetic field may exist in the region. The first property accounts for the phenomenon of superconductivity, the second one underlies the effect of expulsion of magnetic field from a superconductor.

In the physical vacuum containing quantum harmonic oscillators possessing zero-point energy, at certain conditions there is a relationship between magnetic and electric fields.

References

[1] Mandl, F., Shaw, G, *Quantum Field Theory*, John Wiley & Sons, Chichester UK, revised edition, 56, 176, 1984/2002.

[2] Einstein, A., Stern, O, "Einige Argumente für die Annahme einer molekularen Agitation beim absoluten Nullpunkt", *Annalen der Physik*, 40(3), 551, 1913.

[3] Puthoff, H.E, "On the Source of Vacuum Electromagnetic Zero-Point Energy", *Physical Review A*, 40, 4857-4862, 1989.

[4] Rugh, S.E., Zinkernagel, H, "The Quantum Vacuum and the Cosmological Constant Problem", *Studies in History and Philosophy of Modern Physics*, 33(4), 663-705, 2002.

[5] Meissner, W., Ochsenfeld, R, "Ein neuer Effekt bei Eintritt der Supraleitfähigkeit", *Naturwissenschaften*, 21(44), 787–788, 1933.

[6] Sedov, L.I, *A Course in Continuum Mechanics, vol. 1-4*, Wolters-Noordhoff, 1971-1972.

[7] Borovic-Romanov, A.S., Bunkov, Yu.M., Dmitriev, V.V., Mukharskii, Yu.M., Sergatskov, D.A, "Investigation of Spin Supercurrents in ^{3}He-*B*", *Physical Review Letters*, 62 (14), 1631, 1989.

[8] Dmitriev, V.V., Fomin, I.A, "Homogeneously precessing domain in ^{3}He-B: formation and properties", *Journal of Physics: Condensed Matter*, 21 (16), 164202, 2009.

[9] Bunkov, Yu.M, "Spin Superfluidity and Coherent Spin Precession", *Journal of Physics: Condensed Matter*, 21 (16), 164201 (6 pp), 2009.

[10] Boldyreva, L.B, *What does this give to physics: attributing the properties of superfluid ^{3}He-B to physical vacuum?* Moscow, KRASAND, 2012. ISBN 978-5-396-00407-8.

[11] Boldyreva L.B, "The Wave Properties of Matter: The Physical Aspect", *International Journal of Physics*, 2(6), 189-196, 2014, DOI: 10.12691/ijp-2-6-2.

[12] Purcell, E.M, *Electricity and Magnetism, Berkeley physics course, vol. 2*, McGraw-Hill Book company, 1965.

[13] Mende, F.F, "Physics of Magnetic Field and Vector Potential" *AASCIT Journal of Physics*, 1, No. 1, 19-27, 2015.

[14] Peshkin, M., Tonomura, A, *The Aharonov-Bohm effect. Springer-Verlag*, Berlin, 1989.

[15] Boldyreva, L.B, "Quantum correlations – Spin supercurrents", *International Journal of Quantum Information*, 12 (1), 1450007 (13 pages), 2014.

[16] Einstein, A., de Haas, W.J, "Proefondervindelijk bewijs voor bet hestaan der moleculaire stroomen van Ampere", *Amsterdam: Akad. Verl*., D 23. Biz. 1449-1464, 1915.

[17] Boldyreva, L.B, "The semiclassical model of superconductivity", *Physics Essays*, 21(3), 207, 2008.

[18] Cimmino, A., Opat, G.I., Klein, A.G, "Observation of the Topological Ahronov-Casher Phase Shift by Neutron Interferometry", *Phys. Rev. Lett*., 63, No. 4, 380-383, 1989.

[19] Registered with the IP Rights Office Copyright Registration Service. Ref: 4157649598.

International Journal of Physics, 2016, Vol. 4, No. 2, 32-36
Available online at http://pubs.sciepub.com/ijp/4/2/2

DOI:10.12691/ijp-4-2-2

Assessment of Natural Radioactivity of Soil Sample in Selected Locations of Basrah Governorate

Wejood. Tuama Saadon[1], Abdul R. H. Subber[2,*], Hussain. A. Hussain[1]

[1]Department of Physics College of Science, University of Basrah, Basrah, Iraq
[2]Department of Physics College of Education for Pure Sciences, University of Basrah, Basrah, Iraq
*Corresponding author: dabrhs@hotmail.com

Abstract The concentration levels of ^{226}Ra, ^{232}Th and ^{40}K in soil have a great concern in the recent decades, due to its effect on the human health. The radioactivity of some soil samples taken from selected locations in Basrah Governorate have been measured using a NaI(Tl) detector based on gamma ray spectroscopy. Radium equivalent activity, external and internal hazard indices associated with the natural radionuclide were calculated to assess the radiation hazard of the natural radioactivity on the occupiers. The present investigation shows that the level of natural radioactivity for ^{232}Th and ^{40}K in such soil is well below the acceptable limits, while ^{226}Ra is higher. From the analysing the results, it was found that soil in the area does not possess any health hazard to the inhabitant.

Keywords: *natural radioactivity, Basrah Governorate, NaI(Tl) detector, Radium equivalent activity*

Cite This Article: Wejood. Tuama Saadon, Abdul R. H. Subber, and Hussain. A. Hussain, "Assessment of Natural Radioactivity of Soil Sample in Selected Locations of Basrah Governorate." *International Journal of Physics*, vol. 4, no. 2 (2016): 32-36. doi: 10.12691/ijp-4-2-2.

1. Introduction

Humans are primarily exposed to radiation from the sun, cosmic rays and naturally-occurring radioactive elements (NORM) found in the earth's crust. Nearly in all nations, scientists probed since long time ago and are still probing the earth's crust and for a long time in the future to measure the radiation levels and quantify the hazards and doses affecting people, animals, plants and all kinds of life [1].

Human activities, such as a nuclear reactors and nuclear bomb testing are produced radionuclides and they called technical enhanced radioactive elements (TENORM). Some radionuclides, such as radium, uranium, thorium and potassium have existed since the formation of the earth. Natural environmental radioactivity and the associated external exposure due to gamma radiation depend primarily on the geological and geographical conditions. They appear at different levels in soil of each region in the world [2,3,4]. Since the distribution of radioactive nuclei in the environment is random, the knowledge of their distribution in soil plays an important role in radiation protection and measurements [5]. The main contributor of radiation exposure is the emanation of Radon gas from soil, the progeny of ^{226}Ra [6]. The sources of the radiations are terrestrial, extraterrestrial and anthropogenic. The radiation of terrestrial origin comes from various earthly materials which contain various amounts of 238U and 232Th and their decay products and ^{40}K. The level of radiation in any area depends on local geological conditions. Higher radiation levels are associated with igneous rocks, such as granite, granodiorites and syenites, and lower levels with sedimentary rocks with some exceptions where shales and phosphate rocks are a source of high radiation [7]. Assessment of radionuclides in soils and rocks in many parts of the world has been on the increase in the past two decades because of their hazard on the health of the populace . While this is the case, the research into natural radionuclide in the soils and rocks of Southern-Iraq is yet to receive the much needed attention compared to the rate of ordinary soil due to the increases of oil production in the area and processing being done in the region. As a contribution to focus on this area, a number of radiological indices were measured from on samples taken from oil field of Basrah.

The main objective of this study is to determine activity concentration of natural radionuclides in soil of selected area in Basrah Governorate. The radium equivalent, activity utilization indices and effective absorbed dose were calculated and compared with international available data.

2. Material and methods

2.1. Study Area

The area of study, shown in Figure 1, represent southern part of Basrah Governorate, which is considered as contaminated area due to the fallout ash during the Allies war on Iraq.

2.2. Sample Collection and Preparation

Soil were collected at each sampling location from different depth. About 500-600 gm of each sample was crushed into fine powder, and fine quality of the sample

was obtained using scientific sieve. Samples were heated in the oven at 110°C for 24h to remove moisture, put inside Marinalli beakers and then stored for 30 days to allow the equilibrium between ^{226}Ra and ^{222}Rn. The activity concentration of ^{226}Ra, ^{228}Ra, ^{238}U, ^{232}Th and ^{40}K was estimated from the gamma spectrum using Na(Tl) detector 3x3 inch with a 1024 channel computer analyzer USX supplied by Spectrum Technique Company. The detector was employed with lead shielding, 4 cm thickness, which reduced the background. The detector was calibrated using standard sources of ^{57}Co (peak 122 keV), ^{137}Cs (peak 662 keV) and ^{60}Co (peaks 1173, 1333 keV). The detector resolution is about 8% at 662 keV of ^{137}Cs. The efficiency calibration was achieved using eight standard sources include the calibration sources. The system was running freely, for 12 h live time, to evaluate the background spectrum. The Marinalli beaker contains sample was placed over the detector for counting.

Activity concentration A_i of any gamma-rays line taken to represent this parameter for the environmental radionuclides has been calculated using the relation [8]

$$A_i = \frac{Net\,count}{\varepsilon \times I_\gamma \times M \times t} \quad (1)$$

where ε is absolute gamma peak efficiency of the detector at this particular gamma-ray energy, I_γ decay intensity for the specific energy peak (including the decay branching ratio information), M the mass of the sample in kg and t is the counting time of the measurement in second.

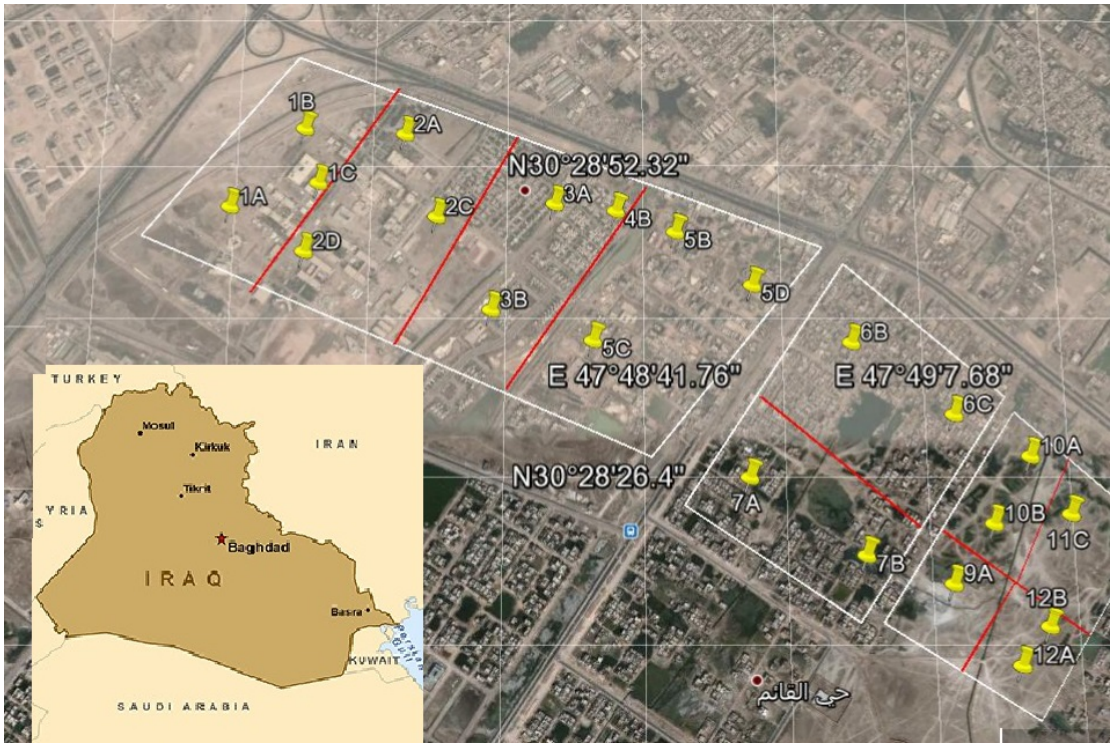

Figure 1. The studied area in Basrah governorate, southern part of Iraq

To evaluate activity concentrations of natural radionuclides, one has to recognized the belong city of each peak according to gamma decay of each isotope [9]. For ^{226}Ra we are looking for the gamma ray lines 295 keV(19.2%), 352 keV (37.1%), 609 keV (46.1%), 1120 keV (15%) and 1760 keV (15.4%). The peak of 186 keV assumed to be from ^{235}U since it has slight effect on the total concentration after subtracting the background, 42.8% for Ra and the rest for ^{235}U. The determination of existence of ^{232}Th was achieved by 338 keV (12%), 911 keV (29%), 964 keV (5.05%) and 969 keV (17%). The case of ^{238}U is recognized by 1001 keV (83%), 766 keV (29%) and 2204 keV (5%). For ^{40}K, this directly determined using 1460 keV (10%) peak.

3. Calculation of Activities, Hazard Indices and Dose Parameters

The exposure due to gamma- radiation is usually defined in term of radium equivalent activity (Ra_{eq}). Radium equivalent activity is used to assess the hazards associated with materials that contain ^{226}Ra, ^{232}Th and ^{40}K in Bq kg^{-1}, which is, determined by assuming that 370 Bq kg^{-1} of ^{226}Ra or 260 Bq kg^{-1} of ^{232}Th or 4810 Bq kg^{-1} of ^{40}K produce the same γ dose rate. The Ra_{eq} of a sample in (Bq kg^{-1}) can be achieved using the following relation [10];

$$Ra_{eq} = (A_{Ra}) + (A_{Th} \times 1.43) + (A_K \times 0.077) \quad (2)$$

The published maximal permissible Ra_{eq} is 370 Bq kg^{-1} [11].

The external and internal hazard indices are an evaluation of the hazard of the natural gamma radiation. The prime objective of this index is to limit the radiation dose to the admissible permissible dose equivalent limit around 1mSvy^{-1}. In order to evaluate this index, one can use the following relations [10]

$$H_{ex} = (A_{Ra}/370) + (A_{Th}/259) + (A_k/4810) \le 1 \quad (3)$$

$$H_{in} = (A_{Ra}/185) + (A_{Th}/259) + (A_k/4810) \le 1 \quad (4)$$

In order to estimate the annual effective dose rate in air, the conversion coefficient from absorbed dose in air to effective dose received by an adult must be considered. This value is published in UNSCEAR 2000 and UNSCEAR 1993, to be 0.7 $SvGy^{-1}$ for environmental exposure to gamma rays of moderate energy. The outdoor occupancy factor is about 0.2 [9]. The annual effective dose equivalent is given by the following equation [10];

$$E\left(mSv/y\right) = D(nGy/h)\times 8760(h/y) \times n\times 0.7(Sv/Gy)\times 10^{-6} \quad (5)$$

where

$$D\left(\frac{nGy}{h}\right) = 0.0417A_K + 0.462A_{Ra} + 0.606A_{Th} \quad (6)$$

and n=0.2 for outdoor and 0.8 for indoor.

The world average annual effective dose equivalent (E) from outdoor or indoor terrestrial gamma radiation only is 0.560 mSv/y [UNSCEAR].

4. Results and Discussions

The measured values of natural radioactivity concentration for ^{226}Ra, ^{232}Th, ^{238}U and ^{40}K for different location of southern part of Basrah Governorate, Iraq are given in Table 1. The worldwide average activity concentration for ^{226}Ra, ^{232}Th and ^{40}K reported by UNSCEAR are 50 Bq kg^{-1}, 27 Bq kg^{-1}, 400 Bq kg^{-1} respectively. From Table 1; the activity concentration of ^{226}Ra ranges from 8.0±2.9 Bq kg^{-1} to 197±16.8 Bq kg^{-1} with average value of 84.0±7.7Bq kg^{-1}, which is higher than the recommended limit of UNSCEAR. The specific activity of ^{232}Th ranged from 2.1±0.1Bq $kg^{-1}$to 12.0±0.5 Bq kg^{-1}, with average value of 8.2±1.0 Bq kg^{-1}. The range of activity for ^{40}K is from 57.0±2.9 Bq kg^{-1} to 635.0±18.3 Bq kg^{-1} and average value is 315±9 Bq kg^{-1}. Both average value for ^{232}Th and ^{40}K are below the recommended limit of UNSCEAR.

Table 1. The values ^{226}Ra, ^{232}Th and ^{40}K specific activity concentrations using gamma ray spectroscopy of soil samples from Basrah Governorate. The letters a, b, c and d are closed locations

S. ID	^{226}Ra Bq/kg	^{232}Th Bq/kg	^{40}K Bq/kg
1a	67.0±7.1	11.0±0.5	283.0±7.6
1b	156.0±7.0	9.9±0.4	295.0±0.3
1c	74.0±7.4	10.3±0.5	477.0±7.6
2a	38.0±0.3	5.7±0.1	181.7±7.2
2c	99.0±6.5	11.0±0.4	294.6±7.0
2d	30.0±2.7	5.1±0.5	48.0±8.3
3a	12.0±3.2	9.1±0.4	110.0±4.0
3b	103.0±16.0	7.3±1.1	254.0±15.9
4b	76.5±6.8	7.0±0.4	188.7±6.6
5b	112.8±14.1	6.8±0.9	331.0±14.8
5c	37.3±5.2	3.9±0.9	635.0±18.3
5d	54.0±14.3	7.9±0.9	486.0±18.0
6b	105.0±3.0	12.0±0.5	246.0±7.7
6c	99.3±3.8	10.2±0.4	262.0±7.9
7a	113.9±6.5	1.6±0.2	272.0±15.0
7b	68.6±16.2	10.4±0.1	583.0±19.1
9a	8.0±2.9	2.1±0.1	57.0±2.9
10a	98.0±8.0	9.6±0.5	370.0±9.3
10b	94.0±7.5	8.5±0.5	290.0±8.0
11c	123.0±7.8	12.0±0.5	433.0±9.3
12a	197±16.8	9.0±1.1	366.0±17.5
12b	82.0±17.0	10.5±1.1	415.0±18.0

From the table one can see that the maximum value of ^{226}Ra is 197±16.8 Bq/kg and minimum value is 8.0±2.9 Bq/kg with average value 88.9 Bq/kg. The maximum value of ^{232}Th is 12.0 Bq/kg and minimum is 1.6 Bq/kg with average value 8.4 Bq/kg. While in the case of ^{40}K the maximum value is 635.0±18.3 Bq/kg and minimum is 57.0±2.9 Bq/kg. All the results obtained were in the range of other workers in the same area, but in different locations [12,13,14]. No uniform trend in the variation of concentration of natural radionuclides found in the soil samples as can be seen from Figure 2. This figure shows no correlation between ^{226}Ra and ^{40}K and positive weak correlation between ^{226}Ra and ^{232}Th.

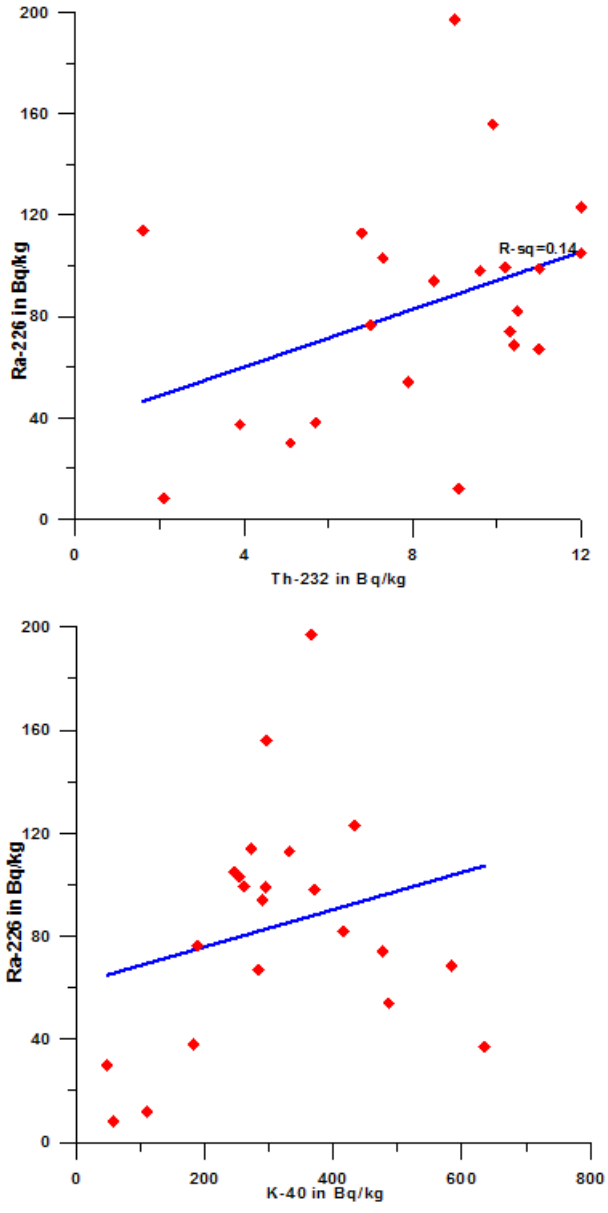

Figure 2. Correlation between ^{226}Ra and ^{232}Th and ^{40}K radionuclides

The radium equivalent activity (Ra_{eq}) of the soil samples tabulated in Table 2 ranges between 15 Bq kg^{-1} to 235 Bq kg^{-1} with average value 118 Bq kg^{-1}, which is lower than the recommended safe limit of ICRP, 370 Bq kg^{-1}. The air observed dose rate ranges between 15.3 nGy/h and 174.5 nGy/h with average value 93.0 nGy/h for outdoor. While for indoor; ranges between 29.0 nGy/h and 283.9 nGy/h with average value 167.4 nGy/h. The H_{ex} values are less than one in all samples, which is in

agreement with equation (3). However, in the case of H_{in} ; there are four sample exceeded unity with small amount in disagreement with equation (4). The annual effective outdoor and indoor gamma ray dose rates calculated in the study area ranges from 0.093 to 0.861 mSv/y and 0.142 to 1.300 mSv/y with respective mean values of 0.524 mSv/y and 0.823 mSv/y. These results are higher than the average worldwide value 0.56 mSv/y but still less than the action level of 3 - 10 mSv/y according to ICRP [15].

Table 2. Values of ^{226}Ra, ^{232}Th and ^{40}K hazard indices for soil samples of selected locations in Basrah Governorate

S.N.	Ra_{eq} Bq/kg	H_{ex}	D_{out} nGy/h	E_{out} mSv/y	H_{in}	D_{in} nGy/h	E_{in} mSv/y
1a	103	0.545	90.6	0.111	0.728	172.5	0.846
1b	191	0.759	127.6	0.157	1.180	246.9	1.200
1c	122	0.584	98.7	0.121	0.784	189.2	0.929
2a	59	0.300	50.2	0.062	0.404	95.8	0.470
2c	135	0.706	118.3	0.145	1.060	228.1	1.100
2d	41	0.301	49.7	0.061	0.450	95.2	0.467
3a	33	0.310	49.9	0.061	0.343	92.7	0.455
3b	131	0.536	174.5	0.856	0.900	111.0	0.816
4b	100	0.442	73.9	0.091	0.649	142.0	0.697
5b	146	0.564	95.7	0.117	0.869	185.7	0.911
5c	87	0.343	61.0	0.075	0.444	118.9	0.584
5d	99	0.467	79.7	0.098	0.613	153.0	0.751
6b	139	0.681	112.9	0.139	0.966	215.8	1.050
6c	132	0.605	101.0	0.124	0.874	193.8	0.951
7a	135	0.410	71.2	0.087	0.718	140.7	0.691
7b	124	0.595	101.3	0.124	0.781	194.3	0.953
9a	15	0.093	15.3	0.019	0.114	29.0	0.142
10a	138	0.611	102.9	0.126	0.878	198.0	0.971
10b	126	0.552	92..8	0.114	0.808	178.7	0.877
11c	170	0.759	127.5	0.156	1.090	245.2	1.200
12a	235	0.861	145.8	0.179	1.300	283.9	1.300
12b	126	0.601	101.2	0.124	0.825	193.9	0.951
Max	235	0.861	174.5	0.856	1.300	283.9	1.300
Min.	15	0.093	15.3	0.019	0.114	29.0	0.142
Average	118	0.524	93.0	0.168	0.758	167.4	0.823

5. Conclusion

The measured activity concentrations of ^{232}Th and ^{40}K in the soil samples of selected location in Basrah Governorate are lower than world level reported by UNSCEAR. However, the concentrations for ^{226}Ra are found to be higher than the worldwide mean value in small amount. This is may be related the effect of dust which contains some radioactive material fallout during the previous wars in the area. The results obtained from external hazard are less than unity, while in the indoor hazard there are some locations has value higher than unity. The annual effective doses for outdoor and indoor are less than the action level of ICRP. Week correlation has been found between ^{226}Ra and both ^{232}Th and ^{40}K, which indicates that one can't depends on the measurement of one parameter to determine the other.

Hence, the achievement of this work is that; soil taken from these locations in Basrah Governorate can be deal with and used as a construction material without posing any significant radiological threat to the occupiers.

Acknowledgments

The authors are very grateful for Prof. Laith A. Najam from Universityof Mosul for helping us in publishing the paper.

References

[1] Darwish D.A.E.,. Abul-Nasr K.T.M and El-Khayatt A.M., The assessment of natural radioactivity and its associated radiological hazards and dose parameters in granite samples from South Sinai, Egypt, Journal of Radiation Research and Applied Science, 2015, 8, 17-25.

[2] United Nation Scientific Committee on the Effect of Atomic Radiation. (2000). "Sources, effect and risks of ionization radiation, report to the general assembly, with Annexes, New York.

[3] Al-Jundi B. A., Abu-Rukah Y. and Shehadeh H. M., Natural Radioactivity Concentrations in Soil Samples along the Amman Aqaba Highway Jordan. Radiation Measurements, 2003, 36(1-6), 555-560.

[4] Jebur J.H. and Subber Abdul R. H., Natural radioactivity of some local and imported fertilizers in Basrah Governorate/Iraq, Scholars Research Library, Achieves of Physics Research, 2014, 5(50, 18-22.

[5] Khan H.M., Khan K., Atta M. A. and Jan F., Measurement of gamma activity of soil samples of Charsadda district of Pakistan. Journal of chemical society of Pakistan, 16,183-188, 1994.

[6] EPA (2007), Environmental Protection Agency, United State, Ionization Radiation fact book, Office of Radiation and indoor Air. EPA-402-F-06-061.

[7] Aziz Ahmed Qureshi1, Ishtiaq Ahmed Khan Jadoon, Ali Abbas Wajid, Ahsan Attique, Adil Masood, Muhammad Anees, Shahid Manzoor, and Aneela Tubassam, Study of Natural Radioactivity in mansehra granite, pakistan: environmental concerns, Radiation Protection Dosimetry , 2014, 158(4), 466–478.

[8] Amrani D and Tahtat M, Natural radioactivity in Algerian building materials. Applied Radiation and Isotopes, 54, 687-689, 2001.

[9] P. Papachristodoulou, C. A. Assimakopoulos, P.A, Paronis N E., and K. G. Loannides, , Use of HPGe γ-ray spectroscopy to assess the isotopic composition of uranium in soil., Journal of Environmental Radioactivity 64, 195-203.Journal of Environmental Radioactivity, 2003, 64, 195-203.

[10] Aziz Ahmed Qureshi, Ishtiaq Ahmed Khan Jadoon, Ali Abbas Wajid, Ahsan Attique, Adil Masood,Muhammad Anees, Shahid Manzoor, AbdulWaheed and Aneela Tubassam , Study of natural radioactivity in Mansehra granite, Pakistan: environmental concerns**,** Radiation Protection Dosimetry, 158(4), 466-478, (2014).

[11] UNSCEAR, United Nation scientific Committee on Effect of Atomic Radiation, VII (2008).

[12] Jabbar H. Jebur and Abdul Ridha H. Subber, Activity Concentration of ^{222}Rn Gas,^{226}Ra, ^{232}Th and ^{40}K in Crops and Soil Taken from Safwan Granges Using Active, Passive and Gamma Spectroscopy Techniques, British Journal of Applied Science & Technology, 2015, 11(6): 1-12.

[13] Munaf Qasim Jaber, Abdul. R. H. Subber and Noori H.N. Al-Hashmi, Natural radioactivity in marine sediment of Khor-Abdulla Northern west of the Arabian Gulf, Journal: JOURNAL OF ADVANCES IN PHYSICS, 2015, 9(1), 2340-2348.

[14] Jabbar H. Jebur and Abdul Ridha H. Subber, The Measurements of Natural Radioactivity, (Radon and Gamma concentrations), around the old fertilizer factory in Basrah/Iraq, Journal: JOURNAL OF ADVANCES IN PHYSICS, 2014, 7(1), 1324-1336

[15] ICRP, International Commission on Radiological Protection, by published by Elsevier, 2008.

International Journal of Physics, 2016, Vol. 4, No. 2, 37-42
Available online at http://pubs.sciepub.com/IJP/4/2/3

DOI:10.12691/ijp-4-2-3

Nuclide Spectra of Activities of Thorium, Uranium Series and Application in Gamma-spectrometry of Point Technogenic Samples

Pop O.M., Simulik V.M.*, Stets M.V.

Institute of Electron Physics of the National Academy of Sciences of Ukraine, Uzhgorod, Ukraine
*Corresponding author: vsimulik@gmail.com

Abstract The radioactive nuclei decay of the nuclides in the ^{232}Th, ^{235}U and ^{238}U series is under consideration. The Bateman-Rubinson system of differential equations is applied. The activity of any n-th nuclide of the series has been calculated. The standard nuclide spectra are found and are compared with experimental nuclide spectra of activities. The results of the measurements are the time parameters, which determine the event date. The examples of the measurement of the experimental nuclide spectra in the nuclear gamma spectrometry of the point technogenic samples have been considered.

Keywords: *^{232}Th, ^{235}U and ^{238}U series, standard sets of nuclides, technogenic samples, nuclear gamma spectrometry, experimental nuclide spectra, standard nuclide spectra of activities, decomposition*

Cite This Article: Pop O.M., Simulik V.M., and Stets M.V., "Nuclide Spectra of Activities of Thorium, Uranium Series and Application in Gamma-spectrometry of Point Technogenic Samples." *International Journal of Physics*, vol. 4, no. 2 (2016): 37-42. doi: 10.12691/ijp-4-2-3.

1. Introduction

Investigated samples can be considered as a chemical systems, i. e. as an ordered set of nuclides (chemical elements). Chemical systems are the generalization of the geochemical, biochemical and other nuclides systems in the samples. The sets of nuclides of the series ^{232}Th, ^{235}U and ^{238}U belong to such systems as well. For such systems the methods of the nuclear gamma spectrometry of environment with semiconductor detectors are used.

The gamma spectrometry of the sample results in the table of activities A of the gamma-active nuclides. It can be presented graphically in the form of the experimental nuclide spectrum of the nuclide activity A [1]. A comparative geochemical analysis on the basis of nuclides spectra, in which the nuclides ^{238}U, ^{234}U, ^{230}Th, ^{226}Ra (series ^{238}U); ^{232}Th, ^{228}Ra, ^{228}Ac (series ^{232}Th) for different samples are presented, is enough informative. Nevertheless, the nuclide spectra were not used for the dating and other time parameters determining.

The methods of nuclear chronometers (the method of uranium series) for the dating and samples age determining are used. Such methods are based on the application of the equation

$$t = -\frac{1}{\lambda_D}\ln\left[1-\frac{A_D}{A_P}\right]. \qquad (1)$$

Note that such methods are valid only for the closed chemical systems of nuclides.

These methods relate the activities of the parent A_P and the daughter A_D nuclides; λ_D is the decay constant. It is, e. g., a pair of long-lived nuclides A_D ^{234}U and A_P ^{238}U; A_D ^{230}Th and A_P ^{234}U; A_D ^{231}Pa and A_P ^{235}U. The equation (1) for the nuclide couple's activities calculations is found after a number of assumptions on the basis of the Bateman equations [2,3].

Note that a detail derivation of the equation (1) is presented in [4,5]. Its analysis and mathematical backgrounds are beyond this brief article. The examples and problems of the nuclear chronometers methods application are considered in many investigations, see, e. g., [1,4,5,6,7,8].

The evident increasing and complication of problems, e. g. the identification of the technogenic materials with the radioactive nuclides of the ^{232}Th, ^{235}U and ^{238}U series, puts forward new demands to the existing methods.

Our investigation is the search for further development of the gamma spectrometric variant of the nuclear chronometers method. This study is based on the measurement of the experimental nuclide spectra of activities of any nuclides of the series ^{232}Th, ^{235}U and ^{238}U. The results of its measurement, in particular, are the time parameters that determine the date of the event in the samples. The event here is the registered changes of the nuclide content of the ^{232}Th, ^{235}U and ^{238}U series [9].

2. The Solutions of the Bateman-Rubinson Equations. The Standard Set of Nuclides

Consider briefly the algorithm of the standard set method. The activity $A_n(T_e)$ of any n-th nuclide of the series can be presented by the generalized for the case of

branched chains expression, which is the solution of the Bateman-Rubinson system of differential equations [9,10,11,12,13], and has the form:

$$A_{nB}(T_e) = \lambda_n N_{nB}(T_e) = N_{10} \sum_j \left(\prod b_{ij} \right) \sum_i \lambda_i C_{ij} e^{-\lambda_i T_e}, \quad (2)$$

where A_{10} are the initial values of the parent nuclei activity; b_{ij} are the branching coefficients («internal» branching ratios, which values are the nuclear constants); $b_{ij} \leq 1$; C_{ij} are the coefficients, which depends on decay constants λ_{ij}, T_e is the proper time, which is present in the activities calculations.

The calculations are performed for:

- one mole of a substance: $N_{10} = N_A = 6{,}022 \cdot 10^{23}$ nuclei (Avogadro's number);

- the proper time T_e ^{232}Th (from 0 to $3{,}17 \cdot 10^{12}$ years); ^{235}U (from 0 to $3{,}17 \cdot 10^{12}$ years); ^{238}U (from 0 to $3{,}17 \cdot 10^{12}$ years).

The nuclear data are taken from [14]. Branching ratios b_i with the formation of clusters are not considered.

The following conditions are chosen for solving of the Bateman-Rubinson system of differential equations:

- the activities of all nuclides except parent (activity A_{10}) in the proper time moment T_e=0 are taken equal to zero;

- for an arbitrary time moment T_e any other possibilities of nuclei entrance and losses except the processes of decay and formation are absent.

A set of all these conditions, of the analytical expressions (2) and theirs solutions are called the standard conditions.

An ordered set of all radionuclides of one series, which activities $A(T_e)$ are determined by the expression (2), we call the standard set of this series. The standard nuclide set (SNS) is the ordered list of one series nuclides that are linked genetically by the mutual decay and formation [9]. The standard nuclide spectra of activities are the quantitative characteristic of the standard sets.

The result of event, as was indicated, is the registrated change of the nuclide content in the sample. It leads to the standard nuclide sets formation of the new daughter series [9]. We called these sets the standard daughter nuclide sets. The result of their formation will be the non-standard sets appearance. The non-standard set is the composition (sum) of two (and more) standard sets, which formation is caused by the event.

The experimental nuclide sets it is the nuclear gamma spectrometry registrated manifold of the parent and daughter ^{232}Th, ^{235}U and ^{238}U nuclide series in the samples. The standard and non-standard sets can be their models.

The experimental nuclide spectra of activities are the quantitative characteristics of the experimental nuclide sets. Indeed, the experimental nuclide spectra it is the ordered sequence of the experimental values of the gamma activities of the A nuclides of the ^{232}Th, ^{235}U and ^{238}U sets.

2.1. Tables of Standards

We have found the time dependence of the activities $A=f(T_e)$ for all nuclides of the ^{232}Th, ^{235}U and ^{238}U series. For these purposes the calculations of the values of the activities in (2) for the enough big number of points of the proper time T_e is applied. The table found is recalculated to the experimental values of the activities A. The table of standards is obtained as a result. Any row of this table is the standard nuclide spectrum of activities that is the standard for the concrete value of the proper time T_e. The values of activities for the corresponding nuclide series are given in the columns of the table.

2.2. The Measurement of the Experimental Nuclide Spectrum of Activities in the Table of Standards

The measurement is in comparison of the experimental nuclide spectrum ENS (T_m) with the corresponding standard that is the standard nuclide spectrum SNS (T_e):

$$\mathrm{ENS}(T_m) = \mathrm{SNS}(T_e). \quad (3)$$

The experimental nuclide spectrum corresponds to the standard conditions if the equality (3) is valid.

Measuring the gamma activities of scales we are working in the time scale T_m. It is the date (an ordinary calendar time). The calculations of the nuclide gamma activities are fulfilled in the scale of proper time T_e. The comparison (3) put into correspondence the proper time T_e to the date time T_m. The value of this proper time T_e is interpreted as the age (the duration of the existence) of the standard nuclide set, which is formed as a consequence of the event.

However, the nuclide activities, which form an experimental nuclide spectra, are the experimental values. These values are not determined in some sense. Moreover, the experimental set can be a nonstandard set. Therefore, the standard nuclide spectrum, which is equal exactly to the experimental nuclide spectrum, cannot be found. Thus, for the activity $A_n(T_m)$ of n–th nuclide the necessity of taking into account the uncertainties results in the inequality:

$$A(T_{e\min}) \leq A_n(T_m) \leq A(T_{e\max}), \quad (4)$$

where $A(T_{emin})$ belongs to the standard SNS $A(T_{emin})$; $A(T_{emax})$ belongs to the standard SNS $A(T_{emax})$; $A_n(T_m)$ belongs to the experimental nuclide spectrum ENS (T_m).

Since SNS $A(T_{emin})$ and SNS $A(T_{emax})$ are the standard spectra then the experimental nuclide spectrum ENS (T_m) satisfies the standard conditions as well.

By choosing the SNS $A(T_{emin})$ and the SNS $A(T_{emax})$ from the table of standards, we choose the meaning of the times T_{emin} and T_{emax}. Thereat, the time interval ΔT_e and its mean value ΔT_{mid}.

$$\Delta T_e = T_{e\max} - T_{e\min}, \quad (5)$$

$$\Delta T_{mid} = \frac{\left(T_{e\max} + T_{e\min} \right)}{2} \quad (6)$$

are determined. The value ΔT can be considered not only as an uncertainty of time T_e, but as some “interval of standardization” of the experimental nuclide spectrum ENS (T_m) as well. Inside this interval ΔT the experimental set is considered as the standard set.

2.3. Decomposition of the Experimental Nuclide Spectra

In order to determine the parent nuclide spectrum PNS or daughter nuclide spectrum DNS it is necessary to fulfill

the decomposition of the experimental nuclide spectrum ENS. The nuclide spectra peculiarity is as follows. It is the result of term by term subtraction of the corresponding eponymous activities of the experimental and standard spectra.

In this case one can write:

$$\text{ENS} = \text{PNS} + \text{DNS};$$
$$\text{PNS} = \text{ENS} - \text{DNS};$$
$$\text{DNS} = \text{ENS} - \text{PNS}.$$

Procedure of decomposition allows to find the standard sets on the basis of the experimental spectrum. Moreover, it allows to determine their standard nuclide spectra and theirs time coordinates T_e in the tables of standards. After the decomposition one of the known method of nuclear chronometers can be used for the determination of the proper time T_e.

Therefore, the pairs of nuclides, which are used in the methods of nuclear chronometers (1), contains in the standard set of all nuclides of the series. Thus, the standard nuclide set as a whole can be considered independently in the role of nuclear chronometer.

3. The Experimental Part

In this article the data for a few point technogenic samples are presented. These samples have a low but enhanced (in comparison with natural) activity. (The samples with higher, in comparison with natural, activity.) The radioactive source is called point if its size parameters (e. g. height h and radius r) are essentially lower (in 5-10 times) from the corresponding parameters of the detector (h = 60 mm; r = 50 mm). Such point-like conditions were used in the selection of the samples. Choosing the point samples we eliminated the problems of self-absorption, standard selection etc., during the samples gamma-spectroscopy.

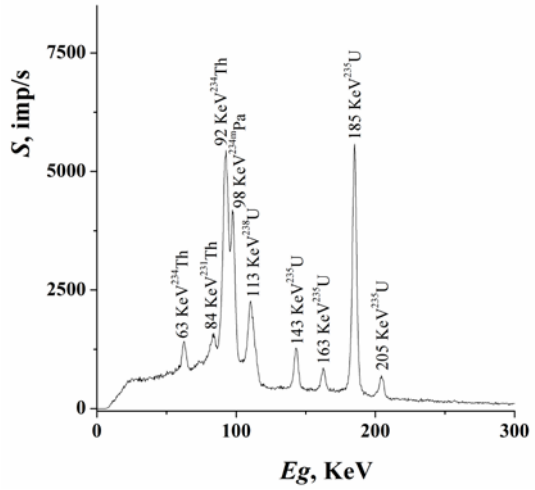

Figure 1. The characteristic apparatus gamma-spectrum of the technogenic sample

Apparatus gamma-spectra of technogenic samples found at HPGe-detector are 150 sm^3 (energy resolution – 2 KeV for the line 1332 KeV ^{60}Co), and at Ge(Li)-detector are 100 sm^3 (energy resolution – 3,9 KeV for the line 1332 KeV ^{60}Co). The passive multilayered low background detector defense is used. The samples are measured without any special preparation. The samples impermeability was guaranteed. The length of the measurement is 2–4 hours. The characteristic apparatus gamma-spectrum of the technogenic sample is given on the Figure 1.

4. Measurement Errors

Program package of SEG-40-Ge complex determines the absolute ($\Delta A(T_e)$) and the relative ($\delta_{\Delta A(Te)}$) measurement errors of the activities $A(T_e)$. The values of these errors are influenced at the determination of such important quantities as the time interval ΔT values errors and errors due to decomposition.

The appearance of the time interval ΔT and its value are the consequences of the different types measurement errors and uncertainties. The values T_{emin}, T_{emax} from the formula (2) cannot be determine analytically. Therefore, the assertion is accepted. For the monotonically increasing (decreasing) time dependences $A(T_e)$ the uncertainties of the times ΔT_{emin}, ΔT_{emax} are linearly proportional for the uncertainties $\Delta A(T_{emin})$, $\Delta A(T_{emax})$. Further, it is accepted that relative errors of the activities $A(T_{emin})$ and times T_e determination are equal, i. e. $\delta_{\Delta A(Te)} = \delta_{\Delta T}$. Therefore, if the relative errors $\delta A(T_{emin})$ and $\delta A(T_{emax})$ are known, then the absolute errors can be determined in terms of these relative errors:

$$\Delta A(T_{e\min}) = \delta A(T_{e\min}) \cdot A(T_{e\min});$$
$$\Delta A(T_{e\max}) = \delta A(T_{e\max}) \cdot A(T_{e\max}).$$

The relative error $\delta_{\Delta T}$ of the time interval ΔT value is given by

$$\delta_{\Delta T} = \begin{bmatrix} (\delta A(T_{emin}) \cdot A(T_{emin}))^2 \\ + (\delta A(T_{emax}) \cdot A(T_{emax}))^2 \end{bmatrix}^{1/2} / \begin{pmatrix} A(T_{e\max}) \\ -A(T_{e\min}) \end{pmatrix}.$$

The decomposition of spectra is the term by term subtraction of the experimental nuclide spectrum activities $A_n(T_m)$ from the eponymous activity of some standard $A_{ne}(T_m)$:

$$\Delta A_n(T_m) = A_n(T_m) - A_{ne}(T_m).$$

The value $A_n(T_m)$ is the experimental quantity. The value $A_{ne}(T_m)$ is the calculating quantity, which is determined on the basis of its parent nuclide activity. The relative error of the value $\Delta A_n(T_m)$ determination is given by

$$\delta\Delta A_{\text{n}}(T_{\text{m}}) = \begin{bmatrix} (\delta A_n(T_m) \cdot A(T_m))^2 \\ +(\delta A_{ne}(T_m) \cdot A_{ne}(T_m))^2 \end{bmatrix}^{1/2} / \begin{pmatrix} A_n(T_m) \\ -A_{ne}(T_m) \end{pmatrix}.$$

For the problems, where the decomposition is necessary, the found value of the relative error $\delta\Delta A_n(T_m)$ will be taken into account in the formulae for the error $\delta_{\Delta T}$ of time interval ΔT determination.

In the method of the nuclear chronometers the formula

$$\delta_t = \sqrt{\delta^2 \cdot \delta A_M + \delta^2 \cdot \delta A_D}$$

is used for the relative time error δ_t evaluation. Here δA_M, δA_D are the relative errors of the corresponding activities determination.

5. The Results of the Investigation

The standard sets determination includes the determination of the experimental nuclide spectra of activities ENS $A(T_m)$ in the table of standards. It finds a graphic mapping, respectively.

Figure 1 gives experimental nuclide spectrum ENS of A sample 1th and standards of comparison SNS $A(T_{emin})$ and SNS $A(T_{emax})$, which satisfy the condition (4). Experimental nuclide spectrum of the sample represents the standard nuclide set of the series ^{232}Th. Fig. 3 shows the positions of the experimental nuclide spectrum ENS A and the standards of comparison SNS $A(T_{emin})$ and SNS $A(T_{emax})$ at the nuclide activities time dependence of the series ^{232}Th. Imaginary they look like the points of intersection of the vertical line with these dependences and are presented as the rectangle. The width of «the rectangle» is given by the value of the time interval $\Delta T = T_{emax} - T_{emin}$. This interval represents the uncertainty of the position of the experimental nuclide spectrum ENS A given by the formula (4). The given measurement errors $\delta_{\Delta A(Te)}=\delta_{\Delta T}$ are found in condition that the activity determination error is equal to 5%.

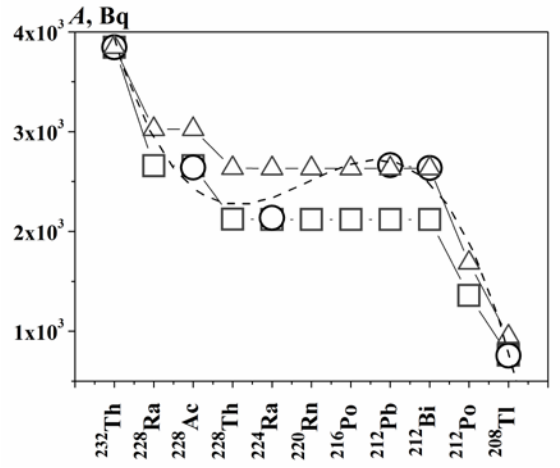

Figure 2. The experimental nuclide spectrum of activities of the sample 1th (circles – dashed line), and the standard spectra SNS $A(T_{emin})$ (four squares) and SNS $A(T_{emax})$ ^{232}Th

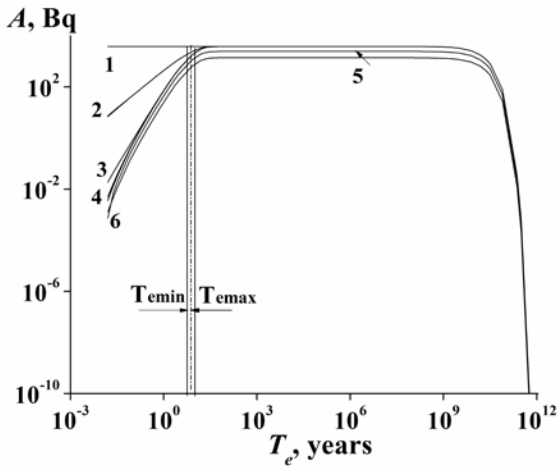

Figure 3. Time dependence of the activities of the standard nuclide set of the series ^{232}Th (1 – ^{232}Th, 2 – ^{228}Ra, ^{228}Ac, 3 – ^{228}Th, ^{224}Ra, 4 – ^{220}Rn, ^{216}Po, ^{212}Pb, ^{212}Bi, 5 – ^{212}Po, 6 – ^{208}Tl) of the sample 1th, time interval ΔT (in the form of the rectangle) and T_{mid} (dashed line in the rectangle)

Figure 4 shows experimental nuclide spectrum ENS A of the sample 10s and the comparison standards SNS $A(T_{emin})$ and SNS $A(T_{emax})$. Given sample contains the material, which contains the noticeable activities of the daughter nuclides ^{238}U – ^{230}Th, ^{226}Ra, ^{214}Pb, ^{214}Bi. Activities of the parent ^{238}U and daughter ^{234}Th are relatively smaller. Therefore, the sample contains a nonstandard set. It is a composition of two standard sets: the standard set ^{238}U and the standard set ^{230}Th. We fulfill the decomposition, by selecting at first the standard set ^{238}U, and after that the standard set ^{230}Th: DNS ^{230}Th = ENS $A(T_e)$ – PNS ^{238}U. The result after decomposition is given by the Figure 5.

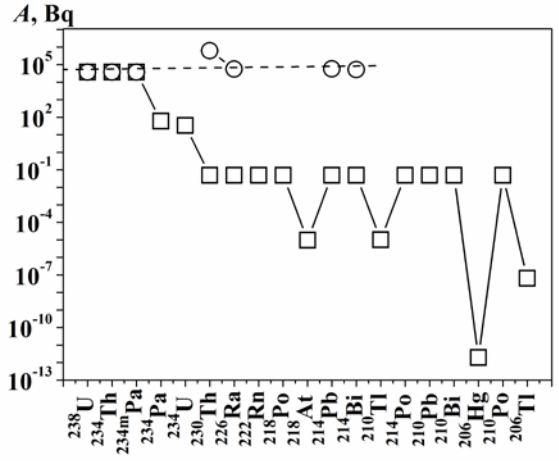

Figure 4. The experimental nuclide spectrum of activities of the sample 10s (circles – dashed line) and the standard spectrum SNS (four squares) ^{238}U before the decomposition

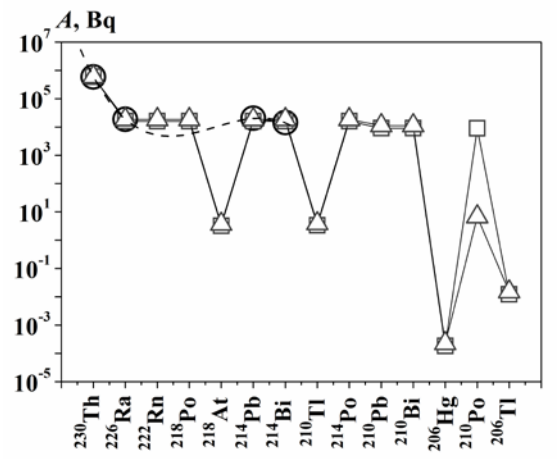

Figure 5. The experimental nuclide spectrum of activities of the sample 10s (circles – dashed line), and the standard spectrum SNS $A(T_{emin})$ (four squares) and SNS $A(T_{emax})$ (rectangles) ^{230}Th after the decomposition

The results of the measurement are given in the table. Moreover, the data for the nuclear chronometers method are given in the table as well. We determine, as it was already considered above, the time interval ΔT_{mid} (the formula (6)) of experimental set of the nuclides of the series. The time t (formula (1)) is determined in the method of nuclear chronometers. The conclusion about the satisfactory comparability between the values found with the help of two data methods can be suggested by the comparison of the values ΔT_{mid} and t.

The experimental nuclide spectra of the samples 1th, 2th satisfy the condition (4). It means that the main

component of their experimental sets are the standard sets ^{232}Th.

The experimental nuclide spectra of the samples 3u – 10u satisfy the condition (4). The standard sets method data and the nuclear chronometers data testify about the satisfactory comparability between each other. The standard sets of ^{238}U are the main parts of their experimental sets. Existence duration large values of the determined standard set of the ^{238}U (10^7 – 10^8 years) allowed to suggest that they were formed enough long ago (maybe in the epoch of the intensive geologic processes) and were not changed from these times.

The experimental nuclide spectra of the samples 10s – 13s do not satisfy the condition (4). After the decomposition of the experimental sets the standard sets and nuclear chronometers methods data are comparable within the errors. Therefore, the result of the decomposition demonstrates that the experimental nuclide set of the samples 10s – 13s can be represented as the composition of the standard set of ^{238}U and the standard nuclide set of ^{230}Th.

Relatively large values of the measurement errors can be localized by the decreasing of the measurement duration.

Table 1. Comparison of the Standard Sets and the Nuclear Chronometers Methods

№	Samples	Standard set (SS)	ΔT_{mid}, years	Error $\delta_{\Delta T}$, %	Nuclear chronometer	t, years	Error, δ_t, %
1	1th	^{232}Th	8	11	^{228}Th/^{232}Th	0,12	10
2	2th	^{232}Th	8	11	^{228}Th/^{232}Th	0,43	10
3	3u	^{238}U	$3\cdot10^7$	12	^{234}U/^{238}U	$3\cdot10^7$	14
4	4u	^{238}U	$3\cdot10^7$	14	^{234}U/^{238}U	$3\cdot10^7$	14
5	5u	^{238}U	$1{,}2\cdot10^7$	14	^{234}U/^{238}U	$1\cdot10^7$	16
6	6u	^{238}U	$2\cdot10^8$	18	^{234}U/^{238}U	$2\cdot10^8$	11
7	7u	^{238}U	$8\cdot10^7$	12	^{234}U/^{238}U	$8\cdot10^7$	12
8	8u	^{238}U	$5\cdot10^8$	10	^{234}U/^{238}U	$3{,}8\cdot10^8$	20
9	9u	^{238}U	$2{,}8\cdot10^8$	18	^{234}U/^{238}U	$2{,}8\cdot10^8$	19
10	10u	^{238}U	$1{,}2\cdot10^8$	21	^{234}U/^{238}U	$1{,}4\cdot10^8$	15
11	10s b*	^{238}U	$3{,}2\cdot10^8$	13	^{226}Ra/^{230}Th	117	14
	10s a*	^{230}Th	76	15	^{226}Ra/^{230}Th	74	14
12	11s b*	^{238}U	$1{,}6\cdot10^8$	17	^{226}Ra/^{230}Th	156	11
	11s a*	^{230}Th	73	14	^{226}Ra/^{230}Th	73	11
13	12s b*	^{238}U	$8\cdot10^8$	17	^{226}Ra/^{230}Th	209	12
	12s a*	^{230}Th	82	10	^{226}Ra/^{230}Th	85	12
14	13s b*	^{238}U	$2{,}4\cdot10^8$	20	^{226}Ra/^{230}Th	102	15
	13s a*	^{230}Th	71	23	^{226}Ra/^{230}Th	77	15

*b –before the decomposition
*a –after the decomposition
*c – a satisfactory pair of the nuclear chronometers is not found.

6. Conclusions

The standard nuclide spectra of the nuclide activities A of series ^{232}Th, ^{235}U, ^{238}U have been calculated. The table of standards by the nuclide activities A time dependence is created. Each spectrum from the table of standards is shown to be the standard itself. The experimental nuclide spectrum of activities A, by the way of its comparison with the standards of the standard nuclide spectrum A, has been measured. The measurement result is the time coordinate T_e, which is the position from the experimental nuclide spectrum of activities A in the table of standards. The found value can be interpreted as the duration of the standard set existence. Here the duration of the existence is considered as the time interval started from the moment of the event, in which this event appeared, and finished in the moment of the measurement.

Acknowledgement

The authors are much grateful to the director of the Institute of Electron Physics, full member of the Academy of Sciences of Ukraine O.B. Shpenik for the support of these investigations.

References

[1] Titaeva, N.A., *Nuclear geochemistry*, Taylor Francis Inc, United States, 1994, 304.

[2] Bateman, H., "Solution of a system of differential equations occurring in the theory of radioactive transformations," *Proc. Cambridge Phil. Soc.*, 15. 423-427. 1910.

[3] Rubinson, W., "The Equations of Radioactive Transformation in a Neutron," *Flux. J. Chem. Phys.*, 17 (6). 542-547. 1949.

[4] Faure, G., Principles of isotope geology, 2-nd ed, John Wiley & Sons, 1986, 589.

[5] Wagner, G. A., *Age Determination of Young Rocks and Artifacts: Physical and Chemical Clocks in Quaternary Geology and Archeology*, Springer Science & Business Media, 1998, 466.

[6] Choppin, G. R., Liljenzin, J. O., Rydberg, J., *Radiochemistry and Nuclear Chemistry*, Butterworth-Heinemann, Woburn, 2001, 858.

[7] Bourdon, B., Henderson, G. M., Lundstrom, C. C., and Turner, S. P., *Uranium-series geochemistry*, (Reviews in Mineralogy & Geochemistry, Vol. 52), Mineralogical Society of America, Washington, DC, 2003, 656.

[8] Vértes, A., Nagy, S., Klencsár, Z., Lovas, R. G., and Rösch, F., *Handbook of Nuclear Chemistry*, Springer Science & Business Media, 2010, 2444.

[9] Pop, O.M., Stets, M.V., "Models of evolution of the sets of radioactive $_{90}$Th^{232}, $_{92}$U^{235}, $_{92}$U^{238} nuclide series and their applications," *Reports of the National Academy of Sciences of Ukraine*, 4. 65-71. 2013. (in Ukrainian).

[10] Firestone, R.B., Shirley, V.S., Baglin, C.M., *Table of isotopes CD-ROM*. Eight Edition Version, 1, John Wiley & Sons, Inc., New York, 1996.

[11] Pressyanov, D. S., "Short solution of the radioactive decay chain equations," *Am. J. Phys.*, 70 (4). 444-445. 2002.

[12] Cetnar, J., "General solution of Bateman equations for nuclear transmutations," *Ann. Nucl. Energy*, 33. 640-645. 2006.

[13] Sun, Y., Buscheck, T. A., and Hao, Y., "An analytical method for modeling first-order decay networks," *Computers & Geosciences*, 39. 86-97. 2012.

[14] Thibes, R., and de Oliveira, S. L., "General solution to Bateman's differential equations with direct index notation," *International Journal of Pure and Applied Mathematics*, 93 (6). 879-883. 2014.

International Journal of Physics, 2016, Vol. 4, No. 2, 43-49
Available online at http://pubs.sciepub.com/ijp/4/2/4

DOI:10.12691/ijp-4-2-4

Anharmonicity and Impurity Effects on Infrared Absorption in High Temperature Superconductors

Hempal Singh, B. D. Indu*

Department of Physics, Indian Institute of Technology Roorkee, Roorkee-247667, India
*Corresponding author: drbdindu@gmail.com

Abstract Taking into account the effects of anharmonicities and point impurities the quantum dynamics of phonons for high temperature superconductors is developed using Green's function formalism via an almost complete Hamiltonian (without BCS Hamiltonian) which comprises the effects of (i) unperturbed electrons, (ii) unperturbed phonons, (iii) electron-phonon interactions, (iv) anharmonicities and (v) isotopic impurities. This is utilized to obtain the expressions for infrared absorption coefficient which can be resolved into diagonal and non-diagonal parts. Non-diagonal contribution arises only in impure crystals and vanishes in the case of pure crystal. The investigations are also made to study the dependence of infrared absorption coefficient on various parameters in the superconducting and normal regimes followed by numerical estimates for cuprate superconductor $YBa_2Cu_3O_{7-\delta}$. The temperature dependence of infrared absorption coefficients and automatic emergence of pairons appears as a special feature of the theory.

Keywords: *high temperature superconductors, green's function, infrared absorption coefficient*

Cite This Article: Hempal Singh, and B. D. Indu, "Anharmonicity and Impurity Effects on Infrared Absorption in High Temperature Superconductors." *International Journal of Physics*, vol. 4, no. 2 (2016): 43-49. doi: 10.12691/ijp-4-2-4.

1. Introduction

Due to the direct relation between the structure of the phonon spectrum in an impure crystal and the absorption line shape the problem of the optical absorption of impurity induced crystal in the infrared and far infrared, appears as a very interesting problem [1]. We have not come across the sufficient experimental results which has offered as much information about the vibrational spectra of crystals as have been endorsed by the infrared absorption experiments. As a result of interaction of radiation (photon) the light is absorbed by the crystal without any change in the electronic state but excites or de-excites one or two phonons. The appropriate selection rule for such interactions is that only modes whose wave vector **k** adds up to zero interact with the light incident on the crystal. The study of infrared properties of high temperature superconductors has equally attracted the theorists and experimentalists to establish the phenomenon and dynamical behavior. The far-infrared spectroscopy is used to explain the energy gap in BCS superconductors [2] as well. This interesting problem of infrared absorption with low impurity concentration using the method of Green's function of many body theory has been theoretically investigated by many authors [3-8]. The absorption coefficient of a harmonic crystal is temperature independent, while experimental evidences show that temperature plays an important role to study the absorption spectra. This arises only when nonlinear terms in the dipole moment or anharmonic terms in the potential energy are used [9]. The crystal structure is linked with absorption bands and these bands are often observed in the infrared spectra of crystalline solids [10]. If an ionic cubic diatomic crystal absorbs the infrared light, a single band coupled with optical mode of zero propagation constant will occur. As anharmonicity alone does not give any mechanism for absorption so the intrinsic lattice absorption can be explained on the basis of second order electric moment [11]. Czerny [12] and Barnes [13] make the observations on alkali halide crystals significantly provided the existence of side band (the short wavelength side) of the chief reflection or absorption band. Some authors tried to explain these side bands using the anharmonicity approach in which the potential energy (connected with lattice vibrations) contains the higher order terms like cubic and quartic [14,15,16]. An anharmonic quantum dynamical approached is used via double time temperature dependent Green's functions to develop the theory of infrared absorption for high temperature superconductors in the following sections of the present paper:

2. The Hamiltonian

To investigate the quantum dynamics of phonons let us consider almost complete crystal Hamiltonian in the form [17,18,19,20]

$$H = H_e + H_p + H_{ep} + H_A + H_D \tag{1}$$

$$H_e = \sum_q (\hbar\omega_{q\uparrow} b^*_{q\uparrow} b_{q\uparrow} + \hbar\omega_{q\downarrow} b^*_{q\downarrow} b_{q\downarrow} + \hbar\omega_{-q\uparrow} b^*_{-q\uparrow} b_{-q\uparrow} + \hbar\omega_{-q\downarrow} b^*_{-q\downarrow} b_{-q\downarrow}) \tag{1a}$$

$$H_p = \sum_k \frac{\hbar\omega_k}{4}[A_k^* A_k + B_k^* B_k] \tag{1b}$$

$$H_{ep} = \sum_{k,q}(g_k b_{Q\uparrow}^* b_{q\uparrow} + g_k^* b_{q\uparrow}^* b_{Q\uparrow} + g_k b_{Q\downarrow}^* b_{q\downarrow} + g_k^* b_{q\downarrow}^* b_{Q\downarrow})B_k \tag{1c}$$

$$H_A = \sum_{s\geq 3}\sum_{k_1,..,k_s} \hbar V_s(k_1,k_2,...,k_s)A_{k_1}A_{k_2}....A_{k_s} \tag{1d}$$

$$H_D = -\hbar\sum_{k_1,k_2}\left[C(k_1,k_2)B_{k_1}B_{k_2}\right] + \hbar\sum_{k_1,k_2}\left[D(k_1,k_2)A_{k_1}A_{k_2}\right] \tag{1e}$$

where H_e, H_p, H_{ep}, H_A and H_D, respectively are unperturbed electron-, unperturbed phonon-, electron-phonon-, anharmonic (upto quartic terms)-, and defect contributions to the Hamiltonian H. In the above equations $b_q^*(b_q)$ and A_k, B_k are the electron creation (annihilation) and phonon field and momentum operators, respectively. Also, $\uparrow(\downarrow)$ stand for spin up(down) and $\mathbf{Q}=\mathbf{k}+\mathbf{q}$ ($\mathbf{k}$ and $\mathbf{q}$ being phonon and electron wave vectors, respectively) and g_k stand for electron-phonon coupling coefficient. The symbols $V_s(k_1,k_2.....k_s)$, $C(k_1,k_2)$ and $D(k_1,k_2)$ stand for the anharmonic coupling coefficients, mass and force constant change parameters [17, 18, 19, 20].

3. The Phonon Green's functions

To obtain the phonon line spectrum, we evaluate the double time temperature dependent retarded phonon Green's function

$$G_{k,k'}(t-t') = -i\theta(t-t') < [A_k(t), A_{k'}^*(t')] > \tag{2}$$

where $\theta(t-t')$ is the Heaviside unit step function. Double differentiation of equation (2) with respect to t followed by the Fourier transformation yields

$$(\omega^2-\omega_k^2)G_{k,k'}(\omega) = \frac{\omega_k}{\pi}\left(\eta_{k,k'} + << F_k(t); A_{k'}^*(t') >>\right) \tag{3}$$

with

$$\eta_{k,k'} = \delta_{k,k'} + 4\omega_k^{-1}\sum_{k_1} C(k_1,-k)\delta_{k_1,k'} \tag{4}$$

Which, in turns, resolves the Green's function to be obtained in terms of phonon frequency shift $\Delta_k(\omega)$ and line width $\Gamma_k(\omega)$ as

$$G_{k,k'}(\omega) = \frac{\omega_k\eta_{k,k'}}{\pi[\omega^2-\tilde{\omega}_k^2-2\omega_k\{\Delta_k(\omega)-i\Gamma_k(\omega)\}]} \tag{5}$$

After appropriate algebraic simplification the Green's function takes the form

$$G_{k,k'}(\omega) = \frac{\omega_k\eta_{k,k'}}{\pi[\omega^2-\bar{\omega}_{kq}^2+2i\omega_k\Gamma_k(\omega)]} \tag{6}$$

$$\bar{\omega}_{kq}^2 = \tilde{\omega}_{kq}^2 + 2\omega_k\Delta_k(\omega) \tag{7}$$

$\tilde{\omega}_{kq}$ and $\bar{\omega}_{kq}$ are renormalized and perturbed mode frequencies.

4. The Phonon Frequency Width

The phonon line width enables one to investigate many dynamical properties of crystalline solids, e.g., life times, the phonon frequency (energy) spectrum and density of states which can be obtained in the following form [17,21]:

$$\Gamma_k(\omega) = \Gamma_k^D(\omega) + \Gamma_k^{3A}(\omega) + \Gamma_k^{3D}(\omega) + \Gamma_k^{ep}(\omega) \tag{8}$$

$$\Gamma_k^D(\omega) = \sum_{k_1}[\pi\varepsilon(\omega)R^D(k,k_1)\omega_{k_1}\delta(\omega^2-\tilde{\omega}_{k_1}^2) + 4\pi\omega_k^{-1}NR^{Dep}(k,k_1)|\tilde{\omega}|\delta(\omega^2-\tilde{\omega}_k^2)] \tag{8a}$$

$$\Gamma_k^{3A}(\omega) = 18\pi\varepsilon(\omega)\sum_{k_1,k_2}|V_3(k_1,k_2,-k)|^2\eta_1 A_\alpha \tag{8b}$$

$$\Gamma_k^{3D}(\omega) = 144\pi\varepsilon(\omega)\sum_{k_1,k_2}|V_3(k_1,k_2,-k)|^2 \times R^c(k,k_1)\omega_k^{-1}\eta_1 A_\alpha \tag{8c}$$

$$\begin{aligned}\Gamma_k^{ep}(\omega) = {} & \pi\omega_k^{-2}|g_k|^2\sum_q\Big[\bar{N}_{qQ\uparrow}\Omega_\uparrow\omega_{1q\uparrow}^c \times\delta(\omega-4\tilde{\omega}_{qQ_\uparrow}) + \bar{N}_{qQ\uparrow}\Omega_\uparrow\omega_{2q\uparrow}^c \times\delta(\omega-\tilde{\Omega}_\uparrow) + 3\bar{N}_{qQ\downarrow}\Omega_\downarrow\omega_{3q\downarrow}^c \times\delta(\omega-\tilde{\Omega}_\downarrow) + \bar{N}_{qQ\downarrow}\gamma_1\omega_{4Q\downarrow}^c \times\delta(\omega-\tilde{\Omega}_\downarrow)\Big] + 128\pi\sum_{k,q}\omega_k^{-2}|g_k|^4 \\ & \times\Big[\tilde{n}_k N(Q_\uparrow)\delta(\omega-\Omega_1) + \tilde{n}_k N(q_\uparrow) \times\delta(\omega-\Omega_2) + \tilde{n}_k N(Q_\downarrow)\delta(\omega-2\Omega_3) - 2\omega_k^{-1}\tilde{\omega}_k^2\hat{N}^2\varepsilon(\omega)\ \delta(\omega^2-\tilde{\omega}_k^2)\Big]\end{aligned} \tag{8d}$$

various symbols are well defined in the references elsewhere [17,21].

5. The Infrared Absorption Coefficients

The optical absorption coefficient which is related to Green's function can be given by [5],

$$\alpha(\omega) = \frac{4\pi\omega}{\eta c}\mathrm{Im}\left[\sum_{\alpha,\beta}\sum_{l,l'}e_i(l)e_j(l')t_\alpha t_\beta(2\pi/\hbar) << U_{i\alpha}(l,t);U_{j\beta}(l',O) >>_\omega\right] \tag{9}$$

In the above equation $<<.....>>_\omega$ is the Fourier transform of phonon Green's function, t_α is the

polarization vector of incident radiation, c is the speed of electromagnetic radiation, η is the refractive index and $e_i(l)$ is the charge on the *i*-th atom in the *l*-th unit cell. For diatomic crystal and $\mu_\alpha^{-1} = M_1M_2(M_1+M_2)^{-1}$ is the reduced mass. Eq. (9) can be written in the form [22]

$$\alpha(\omega) = \left(\frac{4\pi \mathrm{N}e^2}{\eta c}\right)\left(\frac{\pi\mu\omega}{\omega_0}\right)\mathrm{Im}\,G_{k,k'}(\omega) \tag{10}$$

Using Eq. (6) in (10) the absorption coefficient can be obtained in the following form

$$\alpha(\omega) = \left(\frac{8\pi \mathrm{N}e^2\mu}{\eta c}\right)\frac{\omega_k \eta_{kk'}\Gamma_k(\omega)}{[(\omega^2-\bar{\omega}_k^2)^2+4\omega_k^2\Gamma_k^2(\omega)]} \tag{11}$$

The Absorption coefficient given in Eq. (11) can be separated into diagonal and non-diagonal contributions, namely;

$$\left[\alpha(\omega) = \alpha_d(\omega) + \alpha_{nd}(\omega)\right]$$

$$\alpha_d(\omega) = \frac{P_c\omega_k\Gamma_k(\omega)}{[(\omega^2-\bar{\omega}_k^2)^2+4\omega_k^2\Gamma_k^2(\omega)]} \tag{12}$$

$$\alpha_{nd}(\omega) = \frac{P_c C(-k,k')\Gamma_k(\omega)}{[(\omega^2-\bar{\omega}_k^2)^2+4\omega_k^2\Gamma_k^2(\omega)]} \tag{13}$$

where $P_c = 8\pi \mathrm{N}e^2\mu/\eta c$. For $k \neq k'$ the non-diagonal contribution arises and it chiefly depends on the mass change parameter $C(-k,k')$. This contribution is momentous only for impurity induced crystal and vanishes for a pure crystal. Now making use of Eq. (8) in Eq. (12) and after some algebra we can derived the expression for diagonal contribution in the following form

$$\begin{aligned}\alpha_d^D(\omega) = P_c\omega_k A_D(\omega)\Big[&1-4\omega_k^2A(\omega)\\ &\times\left(\Gamma_k^{3A}(\omega)+\Gamma_k^{3D}(\omega)+\Gamma_k^{ep}(\omega)\right)^2\\ &+2\Gamma_k^D(\omega)\left(\Gamma_k^{3A}(\omega)+\Gamma_k^{3D}(\omega)+\Gamma_k^{ep}(\omega)\right)\\ &\times\left\{1-4\omega_k^2A(\omega)[\Gamma_k^D(\omega)]^2\right\}\Big]\end{aligned} \tag{14}$$

$$\begin{aligned}\alpha_d^{3A}(\omega) = P_c\omega_k A_{3A}(\omega)\Big[&1-4\omega_k^2A(\omega)\\ &\times\left(\Gamma_k^{D}(\omega)+\Gamma_k^{3D}(\omega)+\Gamma_k^{ep}(\omega)\right)^2\\ &+2\Gamma_k^{3A}(\omega)\left(\Gamma_k^{D}(\omega)+\Gamma_k^{3D}(\omega)+\Gamma_k^{ep}(\omega)\right)\\ &\times\left\{1-4\omega_k^2A(\omega)[\Gamma_k^{3A}(\omega)]^2\right\}\Big]\end{aligned} \tag{15}$$

$$\begin{aligned}\alpha_d^{3D}(\omega) = P_c\omega_k A_{3D}(\omega)\Big[&1-4\omega_k^2A(\omega)\\ &\times\left(\Gamma_k^{D}(\omega)+\Gamma_k^{3A}(\omega)+\Gamma_k^{ep}(\omega)\right)^2\\ &+2\Gamma_k^{3D}(\omega)\left(\Gamma_k^{D}(\omega)+\Gamma_k^{3A}(\omega)+\Gamma_k^{ep}(\omega)\right)\\ &\times\left\{1-4\omega_k^2A(\omega)[\Gamma_k^{3D}(\omega)]^2\right\}\Big]\end{aligned} \tag{16}$$

$$\begin{aligned}\alpha_d^{ep}(\omega) = P_c\omega_k A_{ep}(\omega)\Big[&1-4\omega_k^2A(\omega)\\ &\times\left(\Gamma_k^{D}(\omega)+\Gamma_k^{3A}(\omega)+\Gamma_k^{3D}(\omega)\right)^2\\ &+2\Gamma_k^{ep}(\omega)\left(\Gamma_k^{D}(\omega)+\Gamma_k^{3A}(\omega)+\Gamma_k^{3D}(\omega)\right)\\ &\times\left\{1-4\omega_k^2A(\omega)[\Gamma_k^{ep}(\omega)]^2\right\}\Big]\end{aligned} \tag{17}$$

Where

$$A_D(\omega) = \frac{\Gamma_k^D(\omega)}{[(\omega^2-\bar{\omega}_k^2)^2+4\omega_k^2[\Gamma_k^D(\omega)]^2]}\ ;$$

$$A_{3A}(\omega) = \frac{\Gamma_k^{3A}(\omega)}{[(\omega^2-\bar{\omega}_k^2)^2+4\omega_k^2[\Gamma_k^{3A}(\omega)]^2]}\ ;$$

$$A(\omega) = \frac{1}{[(\omega^2-\bar{\omega}_k^2)^2]}\ ;$$

$$A_{3D}(\omega) = \frac{\Gamma_k^{3D}(\omega)}{[(\omega^2-\bar{\omega}_k^2)^2+4\omega_k^2[\Gamma_k^{3D}(\omega)]^2]}\ ;$$

$$A_{ep}(\omega) = \frac{\Gamma_k^{ep}(\omega)}{[(\omega^2-\bar{\omega}_k^2)^2+4\omega_k^2[\Gamma_k^{ep}(\omega)]^2]}$$

The terms in the square brackets of Eqs. (14) to (17) can be further simplified to give

$$\begin{aligned}\alpha_d^D(\omega) = P_c\omega_k A_D(\omega)\Big[&1-8\omega_k^2A(\omega)\Gamma_k^D(\omega)\\ &\times\left\{\left(\Gamma_k^{3A}(\omega)+\Gamma_k^{3D}(\omega)+\Gamma_k^{ep}(\omega)\right)^2\right\}\\ &\times\left\{1-4\omega_k^2A(\omega)[\Gamma_k^D(\omega)]^2\right\}\Big]\end{aligned} \tag{18}$$

$$\begin{aligned}\alpha_d^{3A}(\omega) = P_c\omega_k A_{3A}(\omega)\Big[&1-8\omega_k^2A(\omega)\Gamma_k^D(\omega)\\ &\times\left\{\left(\Gamma_k^{3A}(\omega)+\Gamma_k^{3D}(\omega)+\Gamma_k^{ep}(\omega)\right)^2\right\}\\ &\times\left\{1-4\omega_k^2A(\omega)[\Gamma_k^D(\omega)]^2\right\}\Big]\end{aligned} \tag{19}$$

$$\begin{aligned}\alpha_d^{3D}(\omega) = P_c\omega_k A_{3D}(\omega)\Big[&1-8\omega_k^2A(\omega)\Gamma_k^{3D}(\omega)\\ &\times\left\{\left(\Gamma_k^{D}(\omega)+\Gamma_k^{3A}(\omega)+\Gamma_k^{ep}(\omega)\right)^2\right\}\\ &\times\left\{1-4\omega_k^2A(\omega)[\Gamma_k^{3D}(\omega)]^2\right\}\Big]\end{aligned} \tag{20}$$

$$\begin{aligned}\alpha_d^{ep}(\omega) = P_c\omega_k A_{ep}(\omega)\Big[&1-8\omega_k^2A(\omega)\Gamma_k^{ep}(\omega)\\ &\times\left\{\left(\Gamma_k^{D}(\omega)+\Gamma_k^{3A}(\omega)+\Gamma_k^{3D}(\omega)\right)^2\right\}\\ &\times\left\{1-4\omega_k^2A(\omega)[\Gamma_k^{ep}(\omega)]^2\right\}\Big]\end{aligned} \tag{21}$$

Which after further simplification yield,

$$\alpha_d^D(\omega) = P_c\omega_k A_D(\omega)\Big[1-\Big\{4\omega_k^2 A(\omega)[\Gamma_k^D(\omega)]^2\Big\} -8\omega_k^2 A(\omega)\Gamma_k^D(\omega) \times\Big\{\Big(\Gamma_k^{3A}(\omega)+\Gamma_k^{3D}(\omega)+\Gamma_k^{ep}(\omega)\Big)\Big\} +32\omega_k^4 A(\omega)[\Gamma_k^D(\omega)]^3 \times\Big\{\Big(\Gamma_k^{3A}(\omega)+\Gamma_k^{3D}(\omega)+\Gamma_k^{ep}(\omega)\Big)\Big\}\Big] \quad (22)$$

$$\alpha_d^{3A}(\omega) = P_c\omega_k A_{3A}(\omega)\Big[1-\Big\{4\omega_k^2 A(\omega)[\Gamma_k^{3A}(\omega)]^2\Big\} -8\omega_k^2 A(\omega)\Gamma_k^{3A}(\omega) \times\Big\{\Big(\Gamma_k^{D}(\omega)+\Gamma_k^{3D}(\omega)+\Gamma_k^{ep}(\omega)\Big)\Big\} +32\omega_k^4 A(\omega)[\Gamma_k^{3A}(\omega)]^3 \times\Big\{\Big(\Gamma_k^{D}(\omega)+\Gamma_k^{3D}(\omega)+\Gamma_k^{ep}(\omega)\Big)\Big\}\Big] \quad (23)$$

$$\alpha_d^{3D}(\omega) = P_c\omega_k A_{3D}(\omega)\Big[1-\Big\{4\omega_k^2 A(\omega)[\Gamma_k^{3D}(\omega)]^2\Big\} -8\omega_k^2 A(\omega)\Gamma_k^{3D}(\omega) \times\Big\{\Big(\Gamma_k^{D}(\omega)+\Gamma_k^{3A}(\omega)+\Gamma_k^{ep}(\omega)\Big)\Big\} +32\omega_k^4 A(\omega)[\Gamma_k^{3D}(\omega)]^3 \times\Big\{\Big(\Gamma_k^{D}(\omega)+\Gamma_k^{3A}(\omega)+\Gamma_k^{ep}(\omega)\Big)\Big\}\Big] \quad (24)$$

$$\alpha_d^{ep}(\omega) = P_c\omega_k A_{ep}(\omega)\Big[1-\Big\{4\omega_k^2 A(\omega)[\Gamma_k^{ep}(\omega)]^2\Big\} -8\omega_k^2 A(\omega)\Gamma_k^{ep}(\omega) \times\Big\{\Big(\Gamma_k^{D}(\omega)+\Gamma_k^{3A}(\omega)+\Gamma_k^{3D}(\omega)\Big)\Big\} +32\omega_k^4 A(\omega)[\Gamma_k^{ep}(\omega)]^3 \times\Big\{\Big(\Gamma_k^{D}(\omega)+\Gamma_k^{3A}(\omega)+\Gamma_k^{3D}(\omega)\Big)\Big\}\Big] \quad (25)$$

The higher order terms with cubic and higher powers add negligibly small contribution [7,19,20] and can be dropped from above Eqs. (22) to (25). Thus making use of substantial contributions only the Eqs. (22) to (25) can be further simplified to give

$$\alpha_d^D(\omega) = P_c\omega_k A_D(\omega)\Big[1-4\omega_k^2 A(\omega)\Gamma_k^D(\omega) \times\Big\{\Gamma_k^D(\omega)+2\Gamma_k^{3A}(\omega)+2\Gamma_k^{ep}(\omega)\Big\}\Big] \quad (26)$$

$$\alpha_d^{3A}(\omega) = P_c\omega_k A_{3A}(\omega)\Big[1-4\omega_k^2 A(\omega)\Gamma_k^{3A}(\omega) \times\Big\{\Gamma_k^{3A}(\omega)+2\Gamma_k^{D}(\omega)+2\Gamma_k^{ep}(\omega)\Big\}\Big] \quad (27)$$

$$\alpha_d^{3D}(\omega) = P_c\omega_k A_{3D}(\omega)\Big[1-4\omega_k^2 A(\omega)\Gamma_k^{3D}(\omega) \times\Big\{\Gamma_k^{3D}(\omega)+2\Gamma_k^{D}(\omega)+2\Gamma_k^{ep}(\omega)\Big\}\Big] \quad (28)$$

$$\alpha_d^{ep}(\omega) = P_c\omega_k A_{ep}(\omega)\Big[1-4\omega_k^2 A(\omega)\Gamma_k^{ep}(\omega) \times\Big\{\Gamma_k^{ep}(\omega)+2\Gamma_k^{D}(\omega)+2\Gamma_k^{3A}(\omega)\Big\}\Big]. \quad (29)$$

Thus the final form of absorption coefficients can be obtained as

$$\alpha_d^D(\omega) = P_c\omega_k\sum_{k_1}\Big[\pi R^D(k,k_1)\omega_{k_1}(2\tilde{\omega}_{k_1})^{-1} +8\pi\omega_k^{-1}NR^{Dep}(k,k_1)\Big]A_D^{k_1}(\omega) \quad (30)$$

$$\alpha_d^{3A}(\omega) = 18\pi P_c\omega_k\sum_{k_1,k_2}\left|V_3(k_1,k_2,-k)\right|^2\eta_1 \times\Big[S_{+\alpha}\omega_{+\alpha}A_{3A}^{+\alpha}(\omega)+S_{-\alpha}\omega_{-\alpha}A_{3A}^{-\alpha}(\omega)\Big] \quad (31)$$

$$\alpha_d^{3D}(\omega) = 144\pi P_c\omega_k\sum_{k_1,k_2}\left|V_3(k_1,k_2,-k)\right|^2 \times R^c(k,k_1)\omega_k^{-1}\eta_1\times\begin{bmatrix}S_{+\alpha}\omega_{+\alpha}A_{3D}^{+\alpha}(\omega)\\ +S_{-\alpha}\omega_{-\alpha}A_{3D}^{-\alpha}(\omega)\end{bmatrix} \quad (32)$$

$$\begin{aligned}\alpha_d^{ep}(\omega) &= P_c\pi\omega_k^{-1}\left|g_k\right|^2 \sum_q\Bigg[\frac{\bar{N}_{qQ\uparrow}(3\omega_{qQ\uparrow}+\omega_{qQ}^c)\omega_{1q\uparrow}^c}{[(16\tilde{\omega}_{qQ\uparrow}^2-\bar{\omega}_k^2)^2+4\omega_k^2[\Gamma_k^{ep}(\omega)]^2]} +\frac{\bar{N}_{qQ\uparrow}(3\omega_{qQ\uparrow}+\omega_{qQ}^c)\omega_{2q\uparrow}^c}{[\{(3\tilde{\omega}_{qQ\uparrow}+\tilde{\omega}_{qQ}^c)^2-\bar{\omega}_k^2\}^2+4\omega_k^2[\Gamma_k^{ep}(\omega)]^2]} \\ &+\frac{3\bar{N}_{qQ\downarrow}(3\omega_{qQ\downarrow}+\omega_{qQ}^c)\omega_{3q\downarrow}^c}{[\{(3\tilde{\omega}_{qQ\downarrow}+\tilde{\omega}_{qQ}^c)^2-\bar{\omega}_k^2\}^2+4\omega_k^2[\Gamma_k^{ep}(\omega)]^2]} +\frac{\bar{N}_{qQ\downarrow}(4\omega_{q\downarrow}+2\omega_{Q\downarrow}+\omega_{qQ\downarrow}^c)\omega_{4Q\downarrow}^c}{[\{(3\tilde{\omega}_{qQ\downarrow}+\tilde{\omega}_{qQ}^c)^2-\bar{\omega}_k^2\}^2+4\omega_k^2[\Gamma_k^{ep}(\omega)]^2]}\Bigg] \\ &+128P_c\pi\omega_k\sum_{k,q}\left|g_k\right|^4\omega_k^{-2} \times\Bigg[\frac{\tilde{n}_k N(Q_\uparrow)}{[\{(7\tilde{\omega}_{Q\uparrow}+\tilde{\omega}_Q^c)^2-\bar{\omega}_k^2\}^2+4\omega_k^2[\Gamma_k^{ep}(\omega)]^2]} +\frac{\tilde{n}_k N(q_\uparrow)}{[\{(7\tilde{\omega}_{q\uparrow}+\tilde{\omega}_q^c)^2-\bar{\omega}_k^2\}^2+4\omega_k^2[\Gamma_k^{ep}(\omega)]^2]} \\ &+\frac{\tilde{n}_k N(Q_\downarrow)}{[\{(6\tilde{\omega}_{Q\downarrow}+2\tilde{\omega}_Q^c)^2-\bar{\omega}_k^2\}^2+4\omega_k^2[\Gamma_k^{ep}(\omega)]^2]} +\frac{\tilde{n}_k N(q_\downarrow)}{[\{(6\tilde{\omega}_{Q\downarrow}+2\tilde{\omega}_Q^c)^2-\bar{\omega}_k^2\}^2+4\omega_k^2[\Gamma_k^{ep}(\omega)]^2]} \\ &-\frac{2\omega_k^{-1}\tilde{\omega}_k^2\hat{N}^2(2\tilde{\omega}_k)^{-1}}{[\{(6\tilde{\omega}_{Q\downarrow}+2\tilde{\omega}_Q^c)^2-\bar{\omega}_k^2\}^2+4\omega_k^2[\Gamma_k^{ep}(\omega)]^2]}\Bigg]\end{aligned} \quad (33)$$

And similarly the non-diagonal contribution can be obtained as

$$\alpha_{nd}^{D}(\omega) = P_c\omega_k\ C(-k,k')\sum_{k_1}\Big[\pi R^{D}(k,k_1)\omega_{k_1}(2\tilde{\omega}_{k_1})^{-1} + 8\pi\omega_k^{-1}NR^{Dep}(k,k_1)\Big]A_D^{k_1}(\omega) \quad (34)$$

$$\alpha_{nd}^{3A}(\omega) = 18\pi P_c\omega_k\ C(-k,k')\sum_{k_1,k_2}\left|V_3(k_1,k_2,-k)\right|^2\eta_1 \times\Big[S_{+\alpha}\omega_{+\alpha}A_{3A}^{+\alpha}(\omega) + S_{-\alpha}\omega_{-\alpha}A_{3A}^{-\alpha}(\omega)\Big] \quad (35)$$

$$\alpha_{nd}^{3D}(\omega) = 144\pi P_c\omega_k\ C(-k,k')\sum_{k_1,k_2}\left|V_3(k_1,k_2,-k)\right|^2 \times R^{c}(k,k_1)\omega_k^{-1}\eta_1 \times\Big[S_{+\alpha}\omega_{+\alpha}A_{3D}^{+\alpha}(\omega) + S_{-\alpha}\omega_{-\alpha}A_{3D}^{-\alpha}(\omega)\Big] \quad (36)$$

$$\begin{aligned}\alpha_{nd}^{ep}(\omega) = {} & P_c\pi\omega_k^{-1}\left|g_k\right|^2\ C(-k,k')\\ & \sum_q\Bigg[\frac{\bar{N}_{qQ\uparrow}(3\omega_{qQ\uparrow}+\omega_{qQ}^{c})\omega_{1q\uparrow}^{c}}{[(16\tilde{\omega}_{qQ\uparrow}^{2}-\bar{\omega}_k^{2})^2+4\omega_k^{2}[\Gamma_k^{ep}(\omega)]^2]}\\ & +\frac{\bar{N}_{qQ\uparrow}(3\omega_{qQ\uparrow}+\omega_{qQ}^{c})\omega_{2q\uparrow}^{c}}{[\{(3\tilde{\omega}_{qQ\uparrow}+\tilde{\omega}_{qQ}^{c})^2-\bar{\omega}_k^{2}\}^2+4\omega_k^{2}[\Gamma_k^{ep}(\omega)]^2]}\\ & +\frac{3\bar{N}_{qQ\downarrow}(3\omega_{qQ\downarrow}+\omega_{qQ}^{c})\omega_{3q\downarrow}^{c}}{[\{(3\tilde{\omega}_{qQ\downarrow}+\tilde{\omega}_{qQ}^{c})^2-\bar{\omega}_k^{2}\}^2+4\omega_k^{2}[\Gamma_k^{ep}(\omega)]^2]}\\ & +\frac{\bar{N}_{qQ\downarrow}(4\omega_{q\downarrow}+2\omega_{Q\downarrow}+\omega_{qQ\downarrow}^{c})\omega_{4Q\downarrow}^{c}}{[\{(3\tilde{\omega}_{qQ\downarrow}+\tilde{\omega}_{qQ}^{c})^2-\bar{\omega}_k^{2}\}^2+4\omega_k^{2}[\Gamma_k^{ep}(\omega)]^2]}\Bigg]\\ & +128P_c\pi\omega_k\ C(-k,k')\sum_{k,q}\left|g_k\right|^4\omega_k^{-2}\\ & \times\Bigg[\frac{\tilde{n}_k N(Q_\uparrow)}{[\{(7\tilde{\omega}_{Q\uparrow}+\tilde{\omega}_{Q}^{c})^2-\bar{\omega}_k^{2}\}^2+4\omega_k^{2}[\Gamma_k^{ep}(\omega)]^2]}\\ & +\frac{\tilde{n}_k N(q_\uparrow)}{[\{(7\tilde{\omega}_{q\uparrow}+\tilde{\omega}_{q}^{c})^2-\bar{\omega}_k^{2}\}^2+4\omega_k^{2}[\Gamma_k^{ep}(\omega)]^2]}\\ & +\frac{\tilde{n}_k N(Q_\downarrow)}{[\{(6\tilde{\omega}_{Q\downarrow}+2\tilde{\omega}_{Q}^{c})^2-\bar{\omega}_k^{2}\}^2+4\omega_k^{2}[\Gamma_k^{ep}(\omega)]^2]}\\ & +\frac{\tilde{n}_k N(q_\downarrow)}{[\{(6\tilde{\omega}_{Q\downarrow}+2\tilde{\omega}_{Q}^{c})^2-\bar{\omega}_k^{2}\}^2+4\omega_k^{2}[\Gamma_k^{ep}(\omega)]^2]}\\ & -\frac{2\omega_k^{-1}\tilde{\omega}_k^{2}\hat{N}^2(2\tilde{\omega}_k)^{-1}}{[\{(6\tilde{\omega}_{Q\downarrow}+2\tilde{\omega}_{Q}^{c})^2-\bar{\omega}_k^{2}\}^2+4\omega_k^{2}[\Gamma_k^{ep}(\omega)]^2]}\Bigg]\end{aligned} \quad (37)$$

Where

$$A_D^{k_1}(\omega) = \frac{1}{\Big[(\tilde{\omega}_{k_1}^{2}-\bar{\omega}_k^{2})^2+4\omega_k^{2}[\Gamma_k^{D}(\omega)]^2\Big]}\ ;$$

$$A_{3A}^{+\alpha}(\omega) = \frac{\left(\left|2\tilde{\omega}_{+\alpha}\right|\right)^{-1}}{\Big[(\tilde{\omega}_{+\alpha}^{2}-\bar{\omega}_k^{2})^2+4\omega_k^{2}[\Gamma_k^{3A}(\omega)]^2\Big]}\ ;$$

$$A_{3A}^{-\alpha}(\omega) = \frac{\left(\left|2\tilde{\omega}_{-\alpha}\right|\right)^{-1}}{\Big[(\tilde{\omega}_{-\alpha}^{2}-\bar{\omega}_k^{2})^2+4\omega_k^{2}[\Gamma_k^{3A}(\omega)]^2\Big]}\ ;$$

$$A_{3D}^{+\alpha}(\omega) = \frac{\left(\left|2\tilde{\omega}_{+\alpha}\right|\right)^{-1}}{\Big[(\tilde{\omega}_{+\alpha}^{2}-\bar{\omega}_k^{2})^2+4\omega_k^{2}[\Gamma_k^{3D}(\omega)]^2\Big]}\ ;$$

$$A_{3D}^{-\alpha}(\omega) = \frac{\left(\left|2\tilde{\omega}_{-\alpha}\right|\right)^{-1}}{\Big[(\tilde{\omega}_{-\alpha}^{2}-\bar{\omega}_k^{2})^2+4\omega_k^{2}[\Gamma_k^{3D}(\omega)]^2\Big]}$$

6. Results and Discussions

The results thus obtained can be analyzed for a model cuprate crystal $YBa_2Cu_3O_{7-\delta}$. For the purpose of numerical estimation following physical constants have been used:

$a = 3.8\times10^{-8}\ cm,\ b = 3.9\times10^{-8}\ cm,\ c = 11.60\times10^{-8}\ cm,$

$g_k = 0.5,\ \eta = 1,\ f = 0.05263,$ Mass of $Y = 147.58\times10^{-24}\ gm,$

$\hbar = 1.05\times10^{-27}\ cm^2\ gm\sec^{-1},\qquad \mu = 3.57\times10^{-23}\ gm,$

$k_B = 1.3807\times10^{-16}\ cm^2\ gm\sec^{-2}\ K,$

$\phi^{II}(r) = 1.13\times10^{6}\ erg\sec^{-2},$

$\phi^{III}(r) = -1.14\times10^{14}\ erg\sec^{-3}.$

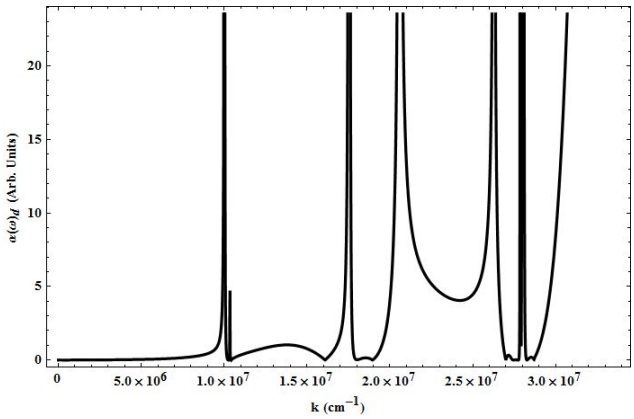

Figure 1. Nature of $\alpha(\omega)_d$ for $YBa_2Cu_3O_{7-\delta}$ in superconducting region

A careful investigation reveals that the diagonal contribution to infrared absorption coefficient exhibits 11 peaks corresponding to the energies 19.85 meV, 20.51 meV, 27.37 meV, 34.80 meV, 40.79 meV, 52.01 meV, 53.78 meV, 55.17 meV, 55.56 meV, 56.36 meV and 60.75 meV in the superconducting region which is depicted in Figure 1.

Correspondingly, the contribution due to various individual processes is shown in Figure 2, which confirms that the contribution due to anharmonic processes and impurities is extremely sensitive as compared to others. The emergence of several peaks at various k-values with different magnitudes due to individual processes is self-explanatory. The three dimensional behaviour of

absorption coefficient with varying temperature and phonon wave vector is depicted in Figure 3.

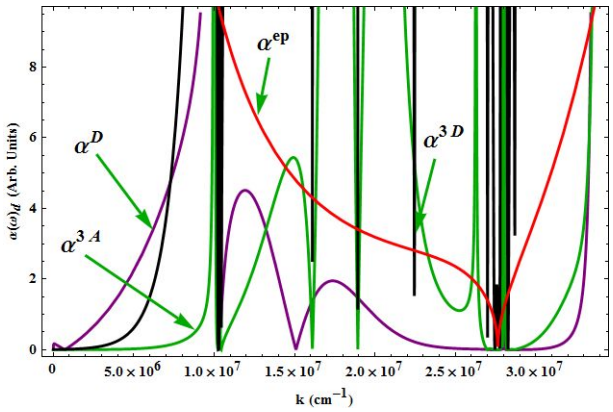

Figure 2. Various contributions to $\alpha(\omega)_d$ for $YBa_2Cu_3O_{7-\delta}$ in superconducting region

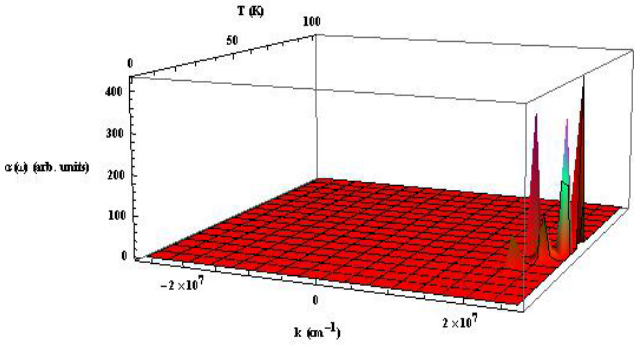

Figure 3. 3D depiction of $\alpha(\omega)$ for $YBa_2Cu_3O_{7-\delta}$ with k and T in superconducting region

Below transition temperature this graphics clearly exhibits sharp five absorption peaks of variable heights at different temperatures appearing at higher side of the phonon wave vector. Similarly, Figure 4 portrays the typical 3-D behaviour of $\alpha(\omega)$ with ω_q and phonon wave vector at the higher end of k.

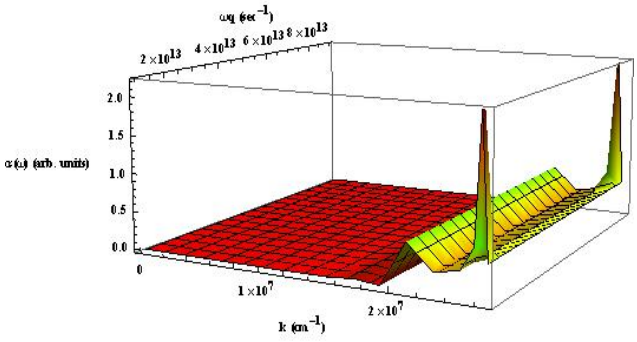

Figure 4. 3D depiction of $\alpha(\omega)$ for $YBa_2Cu_3O_{7-\delta}$ with ω_q and k in superconducting region

Further, the three dimensional variation of $\alpha(\omega)$ has been depicted with ω_q and temperature in Figure 5 where one can see large number of peaks with different heights and nature. The appearance of large number of peaks, however have not been observed through any experiment but one may observe and confirm them with the help of high resolution experiments in future.

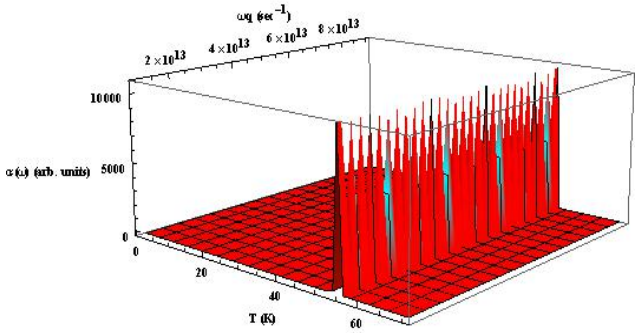

Figure 5. 3D Nature of $\alpha(\omega)$ for $YBa_2Cu_3O_{7-\delta}$ with ω_q and T in superconducting region

After a careful inspection of diagonal contribution it can be plotted to observe its significance which is portrayed as Figure 6. The infrared absorption coefficient shows 8 various peaks at 18.69 meV, 21.28 meV, 27.88 meV, 40.7 meV, 52.01 meV, 55.73 meV, 56.55 meV and 62.09 meV normal region.

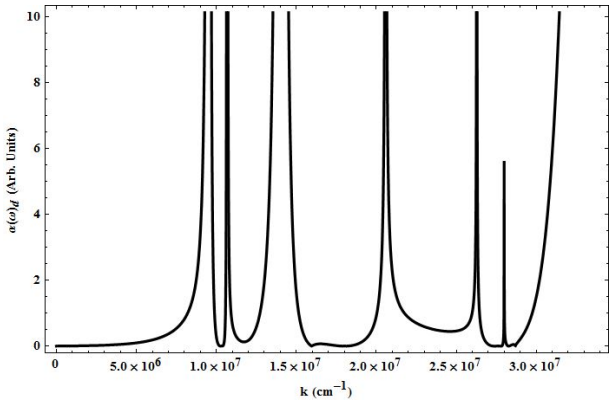

Figure 6. Behaviour of $\alpha(\omega)_d$ for $YBa_2Cu_3O_{7-\delta}$ in normal region

Comparatively this contribution is of lower magnitude as compared to the diagonal part, but the sensitivity is of similar intensity.

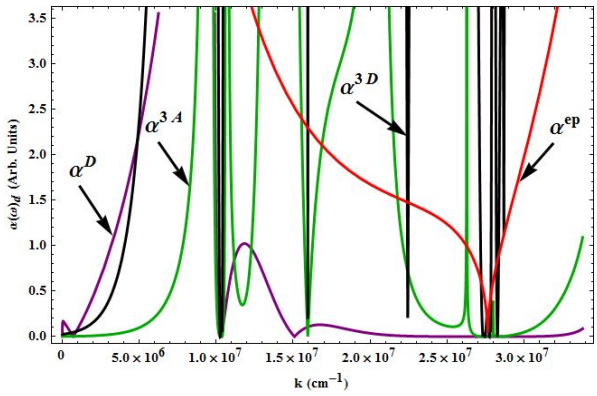

Figure 7. Various contributions to $\alpha(\omega)_d$ for $YBa_2Cu_3O_{7-\delta}$ in normal region

Figure 7 also shows the various contributions for diagonal infrared absorption coefficient in normal region with various peaks.

7. Conclusions

Taking into account the anharmonicities, impurity and electron-phonon effects, the infrared absorption coefficient

has been derived in terms of diagonal and non-diagonal contributions. The various components of infrared absorption coefficient depend upon electron-phonon coupling, temperature and concentration. As we go from superconducting to normal region the nature of curves change sharply with substantial modifications in the phonon spectra. It has been confirmed that infrared absorption coefficient not only depends upon defect concentration but also on temperature, renormalized mode and pairons frequencies which emerges as a new feature of present theory. This theory which is very unique and complex, gives a very good treatment of high temperature superconductors and is applicable for other systems also. The peculiar feature of the theory is the auto-emergence of pairons during the quantum dynamical developments where no use of BCS Hamiltonian has been made. It emerges from the present study that the optical absorption (infrared absorption) for high temperature superconductors can be made successfully with the help of present theory in both superconducting and normal regions.

Acknowledgement

One of the author Hempal Singh is thankful to MHRD for financial support to carry out this research work.

References

[1] K. Patnaik and J. Mahanty, Infrared Absorption due to Substitutional Impurity in Cubic Crystals, *Phys. Rev*., 155, 987, 1967.

[2] T. Timusk, D. A. Bonn, J. E. Greedan, C. V. Satger, J. D. Garrett, A. H. O'Reilly, M. Reedyk, K. Kamaras, C. D. Porter, S. L. Herr and D. B. Tanner, Infrared properties of $YBa_2Cu_3O_{t-\delta}$, *Phys. C*, 153, 1744, 1988.

[3] Maradudin, A. A, In astrophysics and the many-body problem. Benjamin, New York, 1963.

[4] G. Benedek and G. F. Nardelli, Lattice response functions of imperfect crystals: Effects due to a local change of mass and short-range interaction, *Phys. Rev.*, 155, 1004, 1967.

[5] R. J. Elliott and D. W. Taylor, Vibrations of random dilute alloys. *Proc. R. Soc. London A*, 296, 161, 1967.

[6] Martin, T. P, Impurity-induced infrared absorption in a monatomic fcc lattice, Phys. Rev., 160, 686, 1967.

[7] Maradudin, A. A, Advances in research and applications, solid state physics. vols. 18 and 19. edited by F. Seitz and D. Turnbull (Academic Press, New York) 1966.

[8] Genzel, L, Optical properties of solids. edited by S Nudelman and S S Mitra, 1969.

[9] Semwal, B. S. and Sharma, P. K, Dielectric susceptibility and infrared absorption in an anharmonic crystals, *Prog. Theo. Phy.*, 51, 639, 1974.

[10] Florence H. Forziati and Rowen, John W, Effect of changes in crystalline structure on the infrared absorption spectrum of cellulose, *J. Res. Nat. Bur. Stand*., 46, 38, 1951.

[11] Lax,M. and Burstein, E, Infrared lattice absorption in ionic and homopolar crystals, *Phys. Rev*., 97, 39, 1955.

[12] Czerny, M, Measurement on the rock salt in ultra red for testing the theory of dispersion. *Z. Physik*, 65, 600, 1930.

[13] Barnes, R. B. and Czerny, M, Messungen am NaCl und KCl im Sprktrabereic inher ultraroten Eigenschwingungen. *Z. Physik*, 72, 447, 1931.

[14] Born, M. and Blackman, M, Uber die feinstruktur der reststrahlen. *Z. Physik*, 82, 551, 1933.

[15] Blackman, M, Die feinstruktur der reststrahlen. *Z. Physik*, 86, 421, 1933.

[16] Robert Brattain, R., Barnes, R. B. and Seitz, F, On the structure and interpretation of the infrared absorption spectra of crystals. *Phys. Rev.*, 48, 582, 1935.

[17] Ashokan, Vinod, Indu,B. D, and Dimri, A. Kr, Signature of electron-phonon interactions in high temperature superconductors, *AIP Advances*, 1, Article ID:032101, 2011.

[18] K. N. Pathak, Theory of anharmonic crystals., *Phys. Rev.*, 139, 1569, 1965.

[19] Indu, B. D, Theory of lattice specific heat of an isotopically disordered anharmonic crystal, *Int. J. Mod. Phys. B*, 4, 1379, 1990.

[20] Indu, B. D, Enhanced phonon density of states in impure anharmonic crystals, *Mod. Phys. Lett. B*, 6, 1665, 1992.

[21] Singh, Hempal, Singh, Anu, Ashokan, Vinod and Indu,B. D, Signature of anharmonicities in high temperature superconductors, *Ind. J. Appl. Res.*, 3, 35, 2013.

[22] Painuli, C. P, Jagdish Chandra, and Indu, B. D, Infrared absorption in defect induced anharmonic solids, *Pramana. J. Phys.*, 40, 345, 1993.

International Journal of Physics, 2016, Vol. 4, No. 3, 50-54
Available online at http://pubs.sciepub.com/ijp/4/3/1

DOI:10.12691/ijp-4-3-1

Natural Radioactivity and Associated Dose Rates in Soil Samples in the Destroyed Fuel Fabrication Facility, Iraq

Abdulla Ahmad Rasheed[1], Nada Farhan Kadhum[1], Nadhim Khaleel Ibrahim[2,*]

[1]Department of Physics, College of Science, AL-Mustansiriya University, Iraq
[2]Ministry of Science and Technology, Iraq
*Corresponding author: nawi1980@yahoo.com

Abstract The activity concentrations of naturally occurring radionuclides ^{226}Ra, ^{232}Th and ^{40}K in soil samples collected from Fuel Fabrication Facility in Al-Tuwaitha nuclear site were measured by using a high resolution gamma spectrometry system via High Purity Germanium (HPGe) Detector with a relative efficiency of (>40%) and resolution (<1.8keV) at energy of (1.33MeV) for ^{60}Co. The average activity concentrations of ^{226}Ra, ^{232}Th and ^{40}K in soil samples were found to be 15.78±1.16, 14.09±1.33 and 306.42±18.1 Bqkg^{-1}, respectively. The results obtained for the corresponding radionuclides are lower than the worldwide average values of 35, 30, and 400 Bqkg^{-1}, respectively. The average absorbed dose rate in air (Dγ), the average radium equivalent activity (Ra_{eq}) and the average external hazard index (H_{ex}) were determined as 28.90±2.12 nGyh^{-1}, 59.52±4.45 Bqkg^{-1} and 0.16±0.012, respectively, which are below the permissible limit.

Keywords: *activity concentration, gamma spectrometry, radium equivalent activity, hazard indices*

Cite This Article: Abdulla Ahmad Rasheed, Nada Farhan Kadhum, and Nadhim Khaleel Ibrahim, "Natural Radioactivity and Associated Dose Rates in Soil Samples in the Destroyed Fuel Fabrication Facility, Iraq." *International Journal of Physics*, vol. 4, no. 3 (2016): 50-54. doi: 10.12691/ijp-4-3-1.

1. Introduction

Exposure to ionizing radiation from natural sources is a continuous and unavoidable feature of life. Human beings are exposed to natural background radiation every day from the ground, building materials, air, food, outer space, and even elements in their own bodies. Gamma radiation emitted from primordial radionuclides and their progenies are ones of the main external sources of radiation exposure to the humans [1].

There are many activities increasing the radioactive exposure from natural sources of radiation, such as, mining and use of ores containing naturally radioactive materials, the radioactive residues resulting from nuclear weapons testing, the use of radioactive materials in industry and medicine, and operation and decommissioning of the nuclear power plants and other nuclear facilities [2].

The natural radioactivity in the environment is the main source of radiation exposure for human body. Natural radionuclide in soil contributes a significant amount of background radiation exposure to the population through inhalation and ingestion. The main contributors of radionuclides are ^{226}Ra, ^{232}Th and ^{40}K. Since these radionuclides in soils are not uniformly distributed and vary from region to another [3].

2. Materials and Methods

2.1. Study Area

The Fuel Fabrication Facility (FFF) is one of many facilities in Al-Tuwaitha site. Al-Tuwaitha Nuclear Research Center (ATNRC) is the principal nuclear site in Iraq and covers an area about 1.3 km^2 and is located approximately 1 km east of the Tigris River 18 km south of Baghdad. This site is fortified by large earthen berms around the facilities which cover over one km^2 [4,5]. Figure 1 shows Al-Tuwaitha site map location and the building layouts within Al Tuwaitha and the associated sector names. Al-Tuwaitha site was heavily bombed during the Gulf War of 1991, and most of the facilities were extensively damaged [6].

2.2. Samples Collection

Ten (10) soil samples were collected from different location inside the Fuel Fabrication Facility at 5 to 10 cm depth from the top surface soil layer to make approximately 1 kg weight per sample, each soil sample is filled into secure polyethylene bag to prevent cross contamination and sent to the laboratory.

2.3. Samples Preparation

Sample preparation is carried out by placing each soil sample in an oven for drying at a temperature of 80°C for 2h, thus ensuring complete removal of any residual moisture. The dried samples were pulverized into a fine powder. To obtain uniform particle sizes, a 500 µm mesh is then used to sieve the samples which are transferred to 500 ml labeled Marinelli beakers and weighed, sealed and labeled. The samples are stored for at least one month in order to maintain secular equilibrium between ^{238}U, ^{226}Ra, and ^{232}Th and their short-lived progeny. The samples were each counted on a High Purity Germanium Detector for one hour (3600s).

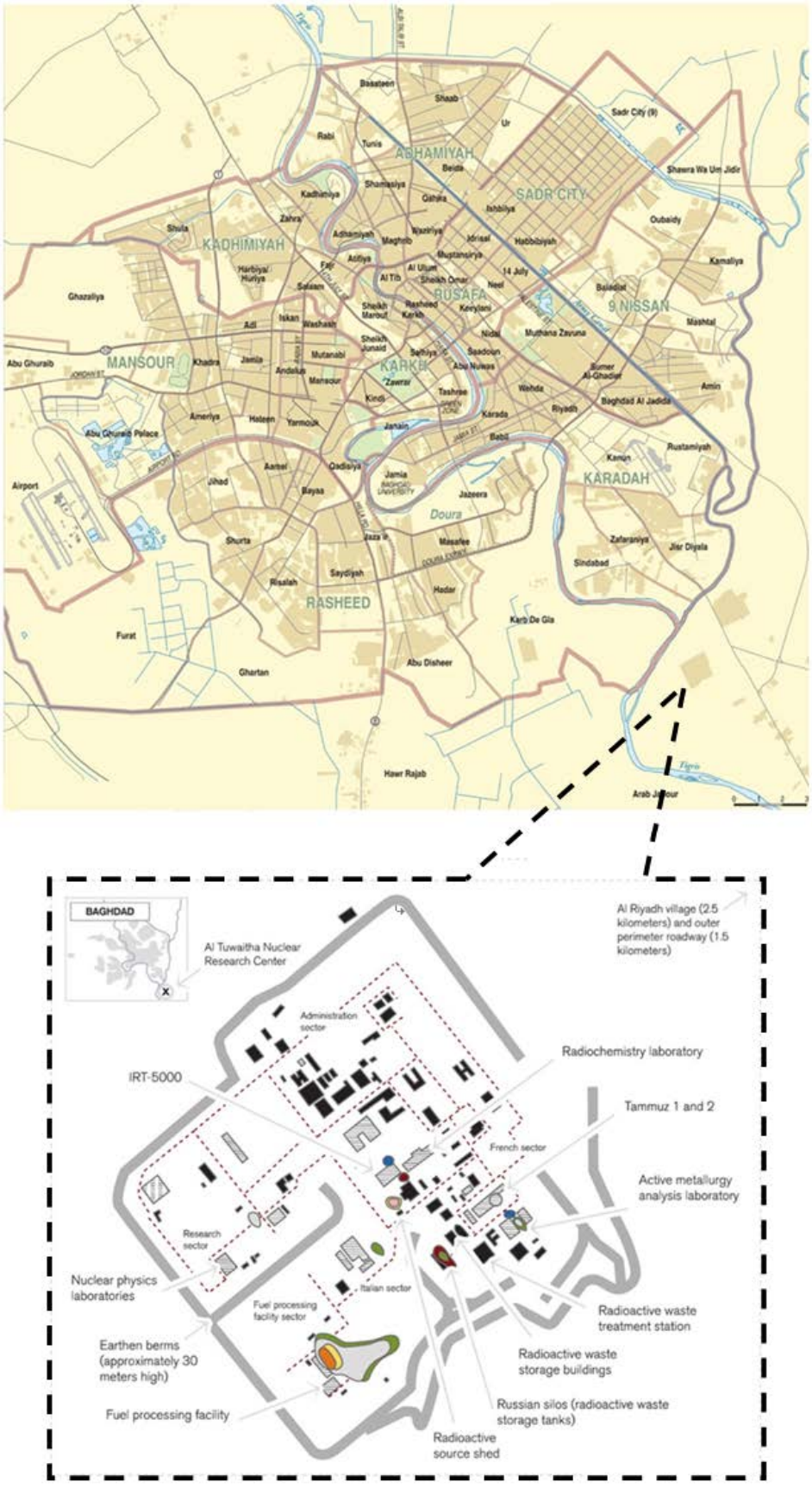

Figure 1. Al-Tuwaitha site map location, Baghdad, Iraq

2.4. Gamma Spectroscopy System

In this work, gamma spectroscopy technique has been used for measuring the specific activity concentration of radionuclides. For certain radionuclides that cannot be effectively measured directly in the field, soil samples of the area under investigation should be collected and then analyzed to determine the radionuclide concentration with a laboratory-based procedure. All processes in this work have been performed in Central Laboratory Directorate

(CLD) at Ministry of Science and Technology (MoST) of Iraq.

2.4.1. High Purity Germanium (HPGe) Detector

A pure germanium closed end-coaxial P-type detector manufactured by CANBERRA Company (model GC4018) with a relative efficiency of (>40%) and resolution (<1.8keV) at energy of (1.33MeV) for 60Co. It contains a HPGe crystal has a diameter of 62mm, a length of 60mm and a distance from window 4.67mm. It is surrounded with lead shielding 10cm thickness to reduce the background radiation from various natural radiation sources and to isolate from other radiation sources used in nearby surroundings.

2.4.2. Calibration of the Gamma Spectrometry System

In order to obtain any meaningful results from a gamma spectrometry system, such as isotope identification, qualitative and quantitative analysis, the system must be calibrated both in terms of energy as well as efficiency. Normally calibration is done with standard sources and reference material of known activity.

The energy calibration related channel number of the spectrometer to the energy of the standard reference material. The calibration was performed by matching principal gamma rays in the spectrum of the standard to the channel numbers.

A standard source of multi-gamma energy has been used to calibrate the efficiency of the detector. Figure 2 shows the efficiency calibration curve for the (HPGe) detector using mixed standard source in the 500 ml Marinelli beaker by acquiring spectrum for one hour (3600s) with different energy ranges from 59.5 keV for ^{241}Am to 1836.06 keV for ^{88}Y.

The net count rate was determined at photopeaks for all energies used for determining the efficiency. The efficiency is related to the count rate of standard [7] as:

$$\varepsilon\left(E_\gamma\right)=\frac{N}{AI_\gamma\left(E_\gamma\right)t}\times 100\% \quad (1)$$

Where:

$\varepsilon(E_\gamma)$ is the detection efficiency at energy E_γ.

N is the net peak area under the specific peak corrected for the background at energy E_γ.

A is the activity in (Bq) of standard source at the measured time.

$I_\gamma(E_\gamma)$ is the abundance at energy E_γ.

t is the time of measurement (3600sec).

The efficiency of the detector is related to energy by the expression:

$$\begin{aligned} ln\varepsilon &= 5.576e1-1.14e2*ln(E) \\ &+5.855e1*ln(E)\wedge 2-1.286e1*ln(E)\wedge 3 \\ &+1.296*ln(E)\wedge 4-4.949e-2*ln(E)\wedge 5 \end{aligned} \quad (2)$$

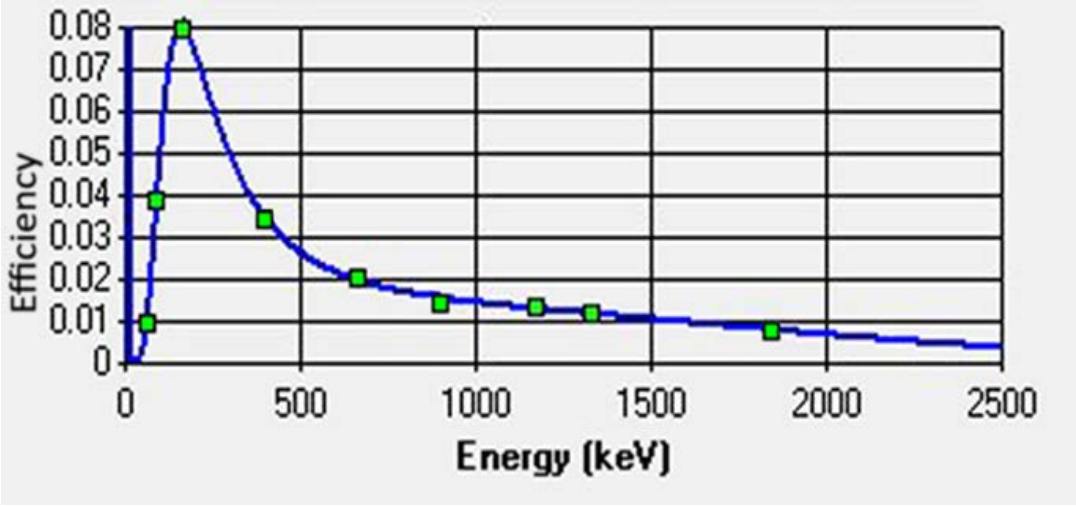

Figure 2. The efficiency calibration curve for the (HPGe) detector

2.5. Specific Activity Calculation:

Some radionuclides of the natural decay chains (e.g. ^{238}U, ^{232}Th, and ^{226}Ra) cannot be determined directly by gamma spectrometry but only by measuring their daughter radionuclides. In these cases, it is necessary to ensure that there is equilibrium between the parent radionuclide and the daughter radionuclides being measured.

Several transitions from decays of shorter-lived radionuclides in the ^{238}U decay chain, such as ^{226}Ra, ^{214}Pb and ^{214}Bi (which can be thought of as ^{226}Ra indicators), were used to estimate the weighted mean of activity concentration of ^{226}Ra. The activity concentration of ^{232}Th is determined using gamma-ray transitions associated with the decay of ^{228}Ac. The gamma-ray peaks associated with decays from ^{40}K at 1461 keV, are used to determine the activity concentrations for these nuclei. The lines suitable for evaluation have been compiled In Table 1.

Table 1. Selected gamma lines for the determination of natural radionuclides [8]

Radionuclide determined	Radionuclide measured	Energy E_γ keV	Emission probability I_E %
^{226}Ra	^{226}Ra	186.10	3.51
	^{214}Bi	609.31 1120.29 1238.11 1764.49	44.6 14.70 5.94 15.10
^{232}Th	^{228}Ac	209.25 338.32 911.60 968.97	3.89 11.27 25.80 15.8
^{40}K	^{40}K	1460.83	10.67

The specific activity, in terms of the activity concentration, is defined as the activity per unit mass of the sample. The specific activity of individual radionuclides in soil samples is given by the following equation [4]:

$$A(Bq/kg) = \frac{N}{\varepsilon(E_\gamma) I(E_\gamma) t_c m} \quad (3)$$

Where
N = the corrected net peak area of the corresponding full-energy peak

$$N = N_S - N_B \quad (4)$$

N_S = the net peak area in the sample spectrum,
N_B = the corresponding net peak area in the background spectrum,
$\varepsilon(E_\gamma)$ = the counting efficiency of the specific nuclide's energy,
$I(E_\gamma)$ = the absolute transition probability by gamma decay through the selected energy (E_γ),
t_c = the counting live-time of the sample spectrum collection in seconds,
m = the mass (kg) of the measured sample.

2.6. Absorbed Dose Rate

The absorbed dose rate (D_γ) due to gamma radiation of naturally occurring radionuclides ^{238}U, ^{232}Th and ^{40}K, were calculated on guidelines provided by UNSCEAR [2].

$$D_\gamma\,(\text{nGy/h}) = 0.462A_{Ra} + 0.621A_{Th} + 0.042A_K \quad (5)$$

Where the factors (0.462, 0.621 and 0.042) are the conversion factors for naturally occurring radionuclides ^{226}Ra, ^{232}Th and ^{40}K, respectively. The average of (D_γ) in air (1m) from terrestrial sources of gamma radiation in soil is estimated as (55 nGy/h) [9].

2.7. Radium Equivalent Activity (Ra_{eq})

Due to the non-uniformity in the distribution of natural radionuclides in the soil samples, the actual activity level of ^{238}U, ^{232}Th and ^{40}K in the samples can be evaluated by means of a common radiological index named the radium equivalent activity (Ra_{eq}). Radium equivalent activity (Ra_{eq}) is used to assess the hazards associated with materials that contain ^{226}Ra, ^{232}Th and ^{40}K in Bq/kg [2], which is determined by assuming that 370 Bq/kg of ^{226}Ra or 260 Bq/kg of ^{232}Th or 4810 Bq/kg of ^{40}K produce the same γ dose rate [7,10]. The Ra_{eq} of a sample in (Bq/kg) can be achieved using the following relation [7]:

$$Ra_{eq}\,(\text{Bq/kg}) = A_{Ra} + 1.43A_{Th} + 0.077A_K \quad (6)$$

Where, A_{Ra}, A_{Th} and A_K are the specific activities concentrations (Bq/kg) of ^{226}Ra, ^{232}Th and ^{40}K, respectively. The published maximal admissible (permissible) Ra_{eq} is 370 Bq/kg [2]. Which corresponds to an effective dose of 1 mSv for the general public [11].

2.8. External Hazard Index

The external hazard index is an evaluation of the hazard of the natural gamma radiation [12]. The prime objective of this index is to limit the radiation dose to the permissible dose equivalent limit of $1mSvy^{-1}$ [13,14]. In order to evaluate this index, a model proposed by Beretka and Mathew in 1985 [10]. This assumes the following relation:

$$H_{ex} = \left(\frac{A_{Ra226}}{370}\right) + \left(\frac{A_{Th232}}{259}\right) + \left(\frac{A_{K40}}{4810}\right) \le 1. \quad (7)$$

This model takes into account that the external hazard which is caused by gamma-rays corresponds to a maximum radium-equivalent activity of 370 Bq/kg for the material [7,15]. In order to keep the radiation hazard insignificant, the value of external hazard index must not exceed the limit of unity [6].

3. Results and Discussion

The results can be summarized as:
(i) Activity concentrations, and (ii) Radiological indices.

3.1. Activity Concentrations

Activity concentrations of ^{226}Ra, ^{232}Th, and ^{40}K radionuclides in the Fuel Fabrication Facility soil samples were determined by equation (3) and the results have been shown in Table 2. The activity concentration of ^{226}Ra in the soil ranged from 4.7±0.5 (IFFF-8) to 25.1±1.6 (IFFF-2) $Bq.kg^{-1}$ with mean 15.78±1.16 $Bq.kg^{-1}$, ^{232}Th ranged from 3.1±0.6 (IFFF-8) to 22.9±1.2 (IFFF-5) $Bq.kg^{-1}$ with mean 14.09±1.33 $Bq.kg^{-1}$, and ^{40}K ranged from 75.7±7.2 (IFFF-8) to 475.5±25.8 (IFFF-2) $Bq.kg^{-1}$ with mean 306.42±18.1 $Bq.kg^{-1}$, respectively. The average activity concentrations of terrestrial radionuclides ^{226}Ra, ^{232}Th and ^{40}K are within the world wide average concentrations of these radionuclides reported by UNSCEAR (2000) as 35, 30 and 370 Bq kg^{-1}, respectively.

Table 2. The activity concentrations values for different soil samples

Sample code	^{226}Ra (Bq/kg)	^{232}Th (Bq/kg)	^{40}K (Bq/kg)
IFFF-1	18.3±1.2	19.7±1.2	380.9±21.9
IFFF-2	25.1±1.6	18.9±2	475.5±25.8
IFFF-3	21.8±1.6	20.2±2.4	383.7±22.7
IFFF-4	12.5±0.8	13±0.9	270.1±15.7
IFFF-5	19.6±0.9	22.9±1.2	306.6±16.5
IFFF-6	11.7±1.1	19.8±2.3	303.6±19.9
IFFF-7	12.4±0.7	10±0.8	262.4±14.3
IFFF-8	4.7±0.5	3.1±0.6	75.7±7.2
IFFF-9	16.3±1.5	13.3±1.9	304.9±17.8
IFFF-10	15.4±1.7	<MDA	300.8±19.2
Min.	4.7±0.5	3.1±0.6	75.7±7.2
Max.	25.1±1.6	22.9±1.2	475.5±25.8
Average	15.78±1.16	14.09±1.33	306.42±18.1
World mean value	35	30	370

3.2. Radiological Indices

In order to assess the health effects, the radiation hazards such as absorbed dose rate (Dγ), radium equivalent activity (Ra_{eq}), and external hazard index (H_{ex}) have been calculated from the activity of ^{226}Ra, ^{232}Th, and ^{40}K radionuclides using the equations (5), (6) and (7), respectively and the values have shown in Table 3.

The Table 2 shows that the absorbed dose rate in air due to terrestrial gamma rays at 1m above the ground were calculated for ^{226}Ra, ^{332}Th and ^{40}K and ranged from 7.28±0.91 to 43.3±3.06 nGyh^{-1} with mean of 28.90±2.12 nGyh^{-1} which is lower than the world average value of 55 nGyh^{-1} [9].

Table 3. Absorbed dose rate, Radium equivalent activity and External hazard index

Sample code	Absorbed dose rate (D_γ) (nGy/h)	Radium equivalent activity (Ra_{eq}) (Bq.kg^{-1})	External hazard index (H_{ex})
IFFF-1	36.59±2.4	75.6±5	0.2±0.01
IFFF-2	43.3±3.06	88.74±6.45	0.24±0.02
IFFF-3	38.73±3.18	80.23±6.78	0.22±0.02
IFFF-4	25.19±1.59	51.89±3.3	0.14±0.01
IFFF-5	36.16±1.85	75.97±3.89	0.21± 0.01
IFFF-6	30.45±2.77	63.39±5.92	0.17±0.02
IFFF-7	22.96±1.42	46.9±2.95	0.13±0.01
IFFF-8	7.28±0.91	14.96±1.91	0.04±0.01
IFFF-9	28.6±2.62	58.8±5.59	0.16±0.02
IFFF-10	19.75±1.59	38.56±3.18	0.1±0.01
Min.	7.28±0.91	14.96±1.91	0.04±0.01
Max.	43.3±3.06	88.74±6.45	0.24±0.02
Average	28.90±2.12	59.52±4.45	0.16±0.012
Global limit	55	370	≤ 1

4. Conclusions

This study shows that the average activity concentrations of ^{226}Ra, ^{232}Th and ^{40}K in soil samples were found to be 15.78±1.16, 14.09±1.33 and 306.42±18.1 Bqkg^{-1}, respectively. The results obtained for the corresponding radionuclides are below the worldwide average values of 35, 30, and 400 Bqkg^{-1}, respectively. The average absorbed dose rate in air (Dγ), the average radium equivalent activity (Ra_{eq}) and the average external hazard index (H_{ex}) were determined as 28.90±2.12 nGyh^{-1}, 59.52±4.45 Bqkg^{-1} and 0.16±0.012, respectively, which are below the permissible limit. However, this data may provide a general background level for the area studied and may also serve as a guideline and a baseline data for future measurement and assessment of possible radiological risks to human health in Al-Tuwaitha site.

Acknowledgments

The authors are very grateful for Prof. Laith A. Najam from University of Mosul for helping us in publishing the paper.

References

[1] United Nations Scientific Committee on the Effects of Atomic Radiation (UNSCEAR), Sources, Effects, and Risks of Ionizing Radiation (1993).

[2] United Nations Scientific Committee on the Effects of Atomic Radiation (UNSCEAR), Report to the General Assembly, United Nations, New York (2000).

[3] Bozkurt, A., Yorulmaz, N., Kam, E., Karahan, G. and Osmanlioglu, A.E. "*Assessment of environmental radioactivity for Sanliurfa region of southeastern Turkey*". Rodiat, Meas.

[4] Chesser R. K., Rodgers B. E., Bondarkov M., Shubber E. and Phillips C. J., "*Piecing together Iraq's nuclear legacy*", Bulletin of the Atomic Scientists, May/June, vol. 65, no. 3, pp. 19-33, (2009).

[5] Cochran J. R. and Danneels J. J., "*Support of the Iraq Nuclear Facility Dismantlement and Disposal Program*" Sandia National Laboratories report, SAND2009-1732 (2009).

[6] International Atomic Energy Agency (IAEA), "*The Iraq Decommissioning Project – Eight Years of Accomplishments*", 18 September, Vienna, Austria (2013).

[7] United Nations Scientific Committee on the Effect of Atomic Radiation (UNSCEAR), "*Ionising Radiation: Sources, and Biological Effect*", New York: United Nations. ISBN: 9211422426 (1982).

[8] Authority of the Standards Policy and Strategy Committee, "Measurement of radioactivity in the environment - Soil", British Standard, ISO 18589-1(2005).

[9] Bou-Rabee, F., Bem, H., "*Natural radioactivity in building materials utilized in the State of Kuwait*", Journal of Radioanalytical and Nuclear Chemistry, 213(2): p. 143-149 (1996).

[10] Beretka J. and Mathew P. J., "*Natural Radioactivity of Australian Building Materials, Industrial Wastes and by Products*", Health Physics, 48: 87-95 (1985).

[11] Ajayi, O. S., "*Measurement of Activity Concnetrations of ^{40}K, ^{226}Ra and ^{232}Th for Assessment of Radiation Hazards from Soils of the Southwestern Region of Nigeria*", Radiation and Environmental Biophysics 48, 323-332 (2009).

[12] Ibrahim N., "*Natural activities of ^{238}U, ^{232}Th and ^{40}K in building materials*". Journal of Environmental Radioactivity, 43(3): p. 255-258 (1999).

[13] International Commission on Radiological Protection (ICRP), "*Recommendations of the International Commission on Radiological Protection 60*", in ICRP Publication 60, Pergamon Press Annals of the ICRP, Oxford, UK (1990).

[14] Al-Hamarneh I. F. and Awadallah M. I., "*Soil radioactivity levels and radiation hazard assessment in the highlands of northern Jordan*". Radiation Measurements, 44(1): p. 102-110 (2009).

[15] Amrani, D., Tahtat, M., "*Natural radioactivity in Algerian building materials*", Applied Radiation and Isotopes, 54(4): p. 687-689 (2001).

International Journal of Physics, 2016, Vol. 4, No. 3, 55-58
Available online at http://pubs.sciepub.com/ijp/4/3/2

DOI:10.12691/ijp-4-3-2

Measurement of Radon 222 Concentrations in the Basements of the New Engineering Building from the Pontificia Universidad Católica del Perú

Rojas Jhonny, Bertín Perez, Patrizia Pereyra*, María Elena Lopez, Luis Vilcapoma

Sección Física, Pontificia Universidad Católica del Perú, Lima-Perú
*Corresponding author: ppereyr@pucp.edu.pe

Abstract Historical data of 222 Radon concentrations were collected in the building of Engineering PUCP recently built with eleven levels (eight on grades and three basements). The measurements were made in the three basement levels of the building. The first results of the history of 222 Radon concentrations in the basements of this building used as a parking lot are shown. The monitoring started the first week it was opened to the public. As nuclear track detectors we use the polymer cellulose nitrate (LR115 - Type 2). Changes in the concentration of 222 Radon registered, are linked into account aspects such as the use of exhaust extractors, increase in the number of vehicles, construction time and seasonal parameters. The results show adequate levels of 222 Radon concentration in all basements, the highest value is 97, 41 Bq/ m^3 at the deepest level, the third.

Keywords: *radon, new building, basements, LR-115-Type 2*

Cite This Article: Rojas Jhonny, Bertín Perez, Patrizia Pereyra, María Elena Lopez, and Luis Vilcapoma, "Measurement of Radon 222 Concentrations in the Basements of the New Engineering Building from the Pontificia Universidad Católica del Perú." *International Journal of Physics*, vol. 4, no. 3 (2016): 55-58. doi: 10.12691/ijp-4-3-2.

1. Introduction

The Pontifical Catholic University from Peru (PUCP), in the context of preparations to celebrate its first centenary has recently completed the construction of a classroom building of eleven levels (eight floors and three basements) within its university campus. Taking advantage of this new construction, it is intended to obtain historical data regarding the evolution of 222 Radon concentrations in the recent building taking into account environmental and other factors that affect it, the measurements have been made in the three basements levels of the building.

Nearly all naturally occurring radioisotopes belong to one of three radioactive series in the soil, thorium, actinium and uranium [1]. Radon isotopes, belonging to these radioactive series, are colorless and odorless. 222 Rn is the most stable isotopes of radon with an average half-life of 3.826 days, which is universally known as radon or radon gas; part of the uranium series radioactive and is an immediate relative of 226 Ra, with an average half-life of 1602 years; radon thus formed by the decay of radium in the soil and rocks entering homes, buildings, basements, tunnels, mines and accumulates particularly in enclosed areas [2].

Radon is the most important source of naturally occurring radiation and the largest contributor to the dose of ionizing radiation received by living organisms. This is mainly due to exposure to radon and its decay products in the air in confined areas; radon is the second leading cause of lung cancer in the general population after the tobacco; epidemiological studies have shown the relationship between exposure to indoor radon and lung cancer. The World Health Organization (WHO), showed the health effects due to exposure in homes (1979) [3], through a European work group in the study of indoor air quality. Later, radon was classified as a human carcinogen by the IARC (International Agency for Research on Cancer) in 1988, the specialized agency in cancer research of the WHO [3]; also, several studies conducted by the ICRP (International Commission on Radiation Protection) show cancer risk associated with exposure to radon and its decay products [4]. Finding a direct relationship of increased lung cancer, in 2005, two studies showed definitive evidence between residential radon exposure and lung cancer [5,6].

According to the above, several organizations in Europe and the United States have made recommendations and have established limits on the concentration of radon in interiors. In USA the maximum recommended limit is 4 pCi/l (150 Bq/m^3). In England, the limit is 200 Bq/m^3 (5.4 pCi/l). The European community recommends not exceeding 400 Bq/m^3 in existing housing and 200 Bq/m^3 in new buildings in accordance with the recommendations given by the Environment Committee of the European Community on February 21st, 1990. The Environmental Protection Agency (EPA) recommends that if levels exceed 200 pCi/l (7400 Bq/m^3) actions should be taken to reduce levels within several weeks. For levels between 740 and 7400 Bq/m^3 a reduction below 4 pCi/l should be

achieved within several months. For levels between 4 and 20 pCi/l these should be reduced below 150 Bq/m^3 over a period of several years. And in the case of levels below 150 Bq/m^3, although this level of exposure is of lower risk, reduction of such low levels is sometimes difficult to achieve [7].

So, measuring the concentration of radon and its decay products becomes important because they affect health. For this purpose, different measuring methods are used; including nuclear tracks solid state detectors. The use of this type of detector is justified by the fact that a heavy charged particle causes a great ionization as it passes through a medium. An alpha particle ionizes molecules that are close to its path. The primary ionization process creates a chemically unstable area near the path of the particle that contains free radicals; this area is known as a latent track [8]. The material containing the latent track is exposed to a chemical solution, which becomes more intense (the etch rate is higher) in the latent track area; the solutions commonly used are NaOH or KOH. The effect caused by this chemical attack is that it etches the tracks on the detector's surface, and it can be observed that the etch rate in the damaged area will be higher. Thus the particle tracks are etched or formed, and can be seen under a microscope or by use of the spark counting method or some other method such like image processing.

Using a suitable calibration factor, which depends on several parameters such as the shape of the container where the detector was calibrated, energy of the alpha particles related with the radioisotope, the parameters of the etching and counting process, etc. They are determined in a laboratory under controlled environmental conditions. The following relation is used [12]:

$$r = kCt \quad (1)$$

Where ρ is the density of tracks in (tr.cm^{-2}), k the calibration factor (tr. cm^{-2} /t Bq.m^{-3}), C the concentration in (Bq.m^{-3}) and t is the exposure time (in days).

2. Experimental Procedures

The effect of the tracks left by the particles occurs in many materials such as cellulose nitrate particles or different polycarbonates, these materials, are also used to detect radon. This track forming effect is only seen in dielectric materials; in semiconductors by recombination processes the latent tracks are unstable and disappear [9].

The most common commercial detectors used for this purpose are the CR39 and the LR115; these detectors have certain differences, the first and most important is the active layer´s thickness, which is 12 microns for LR115 type II and 0.5 mm for CR39, also the tracks formed in them are different, in the case of LR115 they are little holes. The LR115 is based on nitro cellulose while the CR39 is based on polycarbonates, due to these characteristics there are differences in their parameters, which are compared in [10].

Concentration on a specific location based on the solid state detector is derived from the density of tracks observed in the SSNTD.

This work has been focused on determining the concentration levels of 222 Radon in the basements of a new building at the PUCP (Figure 1), opened in mid-2014. A few days after opened, the places were selected to measurement radon 222; each of places had to be checked to make a survey representative the concentration of radon 222 so every week students and professor were reviewed the experimental procedure because of in previous measurements (other places) the detectors were lost and the data could not be retrieved.

Figure 1. (a) New engineering building of the PUCP (b) Panoramic view of the basements

For this purpose, the LR115 detector with the above-mentioned characteristics was used. As the construction of the new building had just ended, the PUCP's Nuclear Tracks research group decided to monitor the concentration of Radon 222 in this new building, particularly in the basement where staff work 8 hours a day with the relevant labor turnover. For measurements, critical places such as corners were selected as these are placed far away enough from the existing exhaust fans. Places near the exhaust fans were also considered.

2.1. Materials

The materials used were: LR115 - type 2 detectors, etching 2.5 N NaOH thermostatic baths, and an optical microscope including a computer interface. (Figure 2). Each of these materials were used the better way so the LR115 – type 2 due to is very sensitive are stored as manufacturer recommends so these detectors have a very low background, the thermostatic baths are controlled by a thermocouple type k through temperature controller also distilled water was used to stop the etching this to neutralize the NaOH then the optical microscope were used for displaying the tracks are white holes, this holes are counted and related to the radon concentration. Also we used radon monitor to measurement radon concentration outside of the basement.

Figure 2. Equipment used for counting nuclear tracks associated to 222 Radon concentrations

2.2. Experimental Setup

The LR115 detectors were placed in the three basements of the new building of Engineering PUCP. Ten detectors are installed in every basement; four pairs in each corner and a couple stood on the stairs, all were placed at a height of approximately 1.5 m above the floor. In total thirty detectors were placed at all three levels like show in the Table 1.

Exposure time of the detectors was thirty days each period, this was repeated five times (periods 1 to 5), after that, the detectors were etched under the above mentioned conditions and recording time of 90 minutes. Subsequently the respective counting was made using a microscope; during the counting five fields of the detector were taken, since track distribution is random, with 10X magnification with a 3mm radius field approximately. Equation 1 was used to quantify Radon concentration with calibration factors of 20,41Bq m^{-3} corresponding to 100 tracks per cm^2 [11], both recording and counting were brought to standard conditions in the experimental physics laboratory of the PUCP.

Table 1. Positions of 222 Radon detectors in the basement of the PUCP Engineering building, where P1 is the first basement, P2 the second basement and P3 the third basement

DETECTORS (2 detectors by position)	POSITION (Defined by the number of parking lots in each basement)
P1-1,2	Near parking lot 03
P1-3,4	Near parking lot 53
P1-5,6	Between the exit symbol and an electric box
P1-7,8	Wall near the driveway to the parking lot
P1-9,10	Emergency stairs (near the elevators) between the basement 1 and the surface
P2-1,2	Near parking lot158
P2-3,4	Near parking lot 132
P2-5,6	Near parking lot 98
P2-7,8	Extinguisher case near the elevators
P2-9,10	Emergency stairs (near the elevators) between basements 2 and 1
P3-1,2	Near parking lot 216
P3-3,4	Near parking lot 182
P3-5,6	Near parking lot 162
P3-7,8	Near parking lot 242
P3-9,10	Emergency stairs (near the elevators) between basements 3 and 2

3. Results

This report presents the measurements of 222 Radon in the basement of the new building of Engineering PUCP, made during the winter and spring of 2014 (southern hemisphere), for five consecutive periods, from August to December, every thirty days on average. The value of this study lies in the fact of verifying whether there is compliance with the standards of radon indoor concentration. Natural radon levels are determined for the first time in such workplaces in the PUCP, thus helping the relevant authorities to establish an appropriate healthy working environment. The results are shown in the following tables 2, 3, 4 and figures 3, 4, 5. Also there are measurements which were done outside of the basements near of the new building through digital radon monitor Canary® to compare outdoor and indoor radon concentration.

Table 2. Results of monitoring 222 Radon in the first basement of the PUCP Engineering Building

Detector	Mean value (Bq m^{-3})	Minimum (Bq m^{-3})	Maximum (Bq m^{-3})
P1-1	37.82 ± 23.45	11.54	74.50
P1-2	21.19 ± 15.40	9.75	47.22
P1-3	24.92 ± 22.73	5.42	62.96
P1-4	23.62 ± 5.69	18.43	32.53
P1-5	27.01 ± 8.81	16.92	38.47
P1-6	23.19 ± 11.13	12.31	37.77
P1-7	25.91 ± 3.43	20.60	29.38
P1-8	38.31 ± 18.14	22.77	67.33
P1-9	26.17 ± 11.26	15.18	41.97
P1-10	27.17 ± 14.25	6.15	41.55

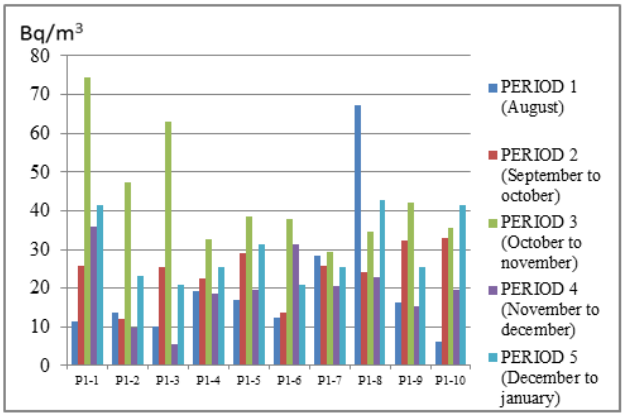

Figure 3. Histogram of the results of Radon 222 measurements in the first basement of the PUCP Engineering building, indicating the concentration in Bqm^{-3} for each period

Table 3. Results of monitoring 222 Radon in the second basement of the PUCP Engineering Building

Detector	Mean value (Bq m^{-3})	Minimum (Bq m^{-3})	Maximum (Bq m^{-3})
P2-1	34.83±9.08	19.23	42.28
P2-2	29.10±14.32	7.69	47.22
P2-3	21.63±8.99	10.00	31.16
P2-4	19.91±6.44	11.54	27.28
P2-5	23.75±13.09	12.31	45.12
P2-6	20.02±3.98	14.62	24.13
P2-7	28.97±7.62	22.77	41.97
P2-8	30.03±8.43	17.69	39.04
P2-9	32.87±30.52	9.75	86.18
P2-10	23.58±7.87	10.84	32.53

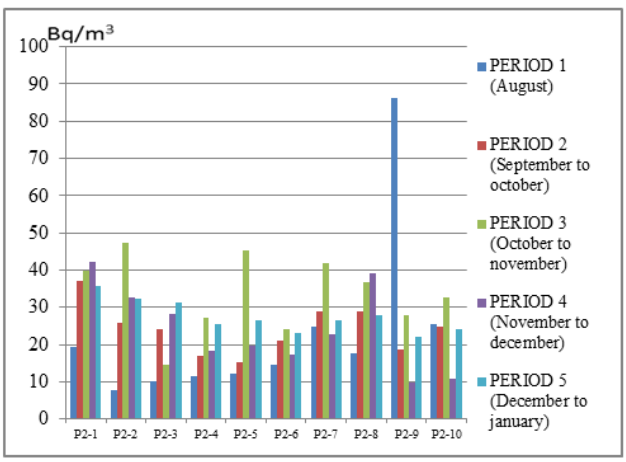

Figure 4. Results of Radon 222 monitoring in the second basement

Table 4. Results of Radon 222 measurements in the third basement of the PUCP Engineering building

Detector	Mean value (Bq m^{-3})	Minimum (Bq m^{-3})	Maximum (Bq m^{-3})
P3-1	34.15 ± 18.52	14.48	64.01
P3-2	38.01 ± 28.57	16.09	82.89
P3-3	41.92 ± 18.87	13.85	59.81
P3-4	50.81 ± 32.72	23.09	97.59
P3-5	22.30 ± 4.917	17.69	30.01
P3-6	17.84 ± 14.21	6.92	41.55
P3-7	34.64 ± 10.82	25.74	52.46
P3-8	28.53 ± 12.27	17.69	47.22
P3-9	21.91 ± 8.88	8.84	30.43
P3-10	18.21 ± 6.57	11.26	25.18

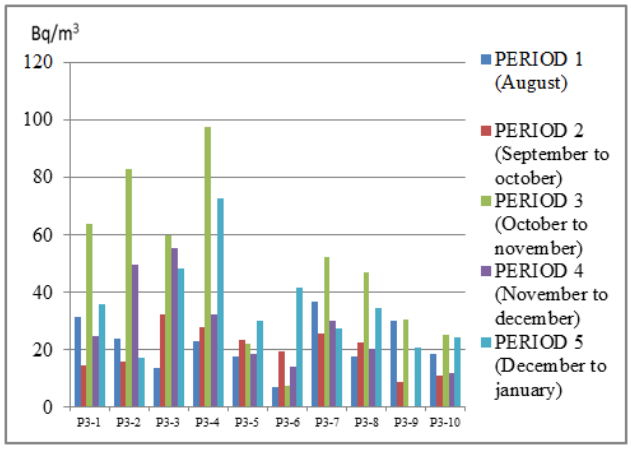

Figure 5. Results of Radon 222 monitoring in the third basement

Table 5. Results of monitoring 222 Radon in outside of the basements of the PUCP Engineering Building

Outdoor measurement near of new building (Bq m-3)	Indoor measurement in a multipurpose classroom (Bq m-3)
5±1	11±2

4. Conclusions

This work has enabled taking measurements in a newly constructed building with different materials among which cement predominates and the particularity of walls kept unpainted and large basements with relatively poor ventilation. The results of the measurements in the basements show the presence of Radon 222 in such environments Table 2, Table 3 and Table 4. However, the levels found in different measurement periods in each of the places measured, are below the maximum allowable levels recommended by different organization like EPA and European community mentioned above. It is noteworthy that the highest measurement was found in the deepest basement, the third. The concentration level found was 97.59 Bq/m^3, Table 4. It could be related with the deepness and also less ventilation factors. In all the cases, however, the results indicate that for the moment no corrective action is necessary. Also measurements outside of the basements in Table 5 are shown encountering low values of radon concentration than inside of basements, so we can conclude that there is a major presence of radon in closed places than open spaces. It is planned to check in the future the possible presence of Radon 222 in other environments of the building and continue monitoring the basements where staff remains 24 hours a day in labor turnover periods.

References

[1] F. Goded, V. Serradell., "Teoría de Reactores y Elementos de Ingeniería Nuclear", Tomo I, 3° Edición, 1975.

[2] World Health Organization, "SELECTED POLLUTANTS", 2010.

[3] World Health Organization, "WHO HANDBOOK ON INDOOR RADON", 2009.

[4] ICRP, 1987. Lung Cancer Risk from Exposures to Radon Daughters. ICRP Publication 50.

[5] S Darby, D Hill, A Auvinen, J M Barros-Dios, H Baysson, F Bochicchio, et al., "A Radon in Homes and Risk of Lung Cancer: Collaborative Analysis of Individual Data from 13 European Case-control Studies", British Medical Journal, 2005 January 29, 330 (7485): 223.

[6] D Krewski, JH Lubin, JM Zeilinski, M Alavanja, VS Catalan, RW Field, et al.,"A Residential Radon and Risk of Lung Cancer: A Combined Analysis of 7 North American Case-control Studies"., Epidemiology, 2005 March; 16 (2):137-45.

[7] "Radon Risk If You've Never Smoked", http://www.epa.gov/radon/healthrisks.html. 1999-2001.

[8] Espinosa, G., "Trazas Nucleares en Sólidos", UNAM. México, 1994.

[9] R.L. Fleischer, P.B. Price, R.M. Walker, Nuclear Tracks in Solids, University of California Press, Berkley, 1975.

[10] D. Nikezic 1, K.N. Yu., "Profiles and parameters of tracks in the LR115 detector irradiated with alpha particles", Nuclear Instruments and Methods in Physics Research B 196 (2002) 105-112.

[11] Pereyra P., "Aplicación de la técnica de huellas nucleares en dosimetría de partículas alfa", Tesis de bachiller de la Pontificia Universidad Católica del Perú., 1991.

[12] KP Eappen and YS Mayya Calibration factors for lr-115 (type-ii) based radon thoron discrimination dosimeter. Radiation Measurements, 38(1):5-17, 2004.

International Journal of Physics, 2016, Vol. 4, No. 3, 59-63
Available online at http://pubs.sciepub.com/ijp/4/3/3

DOI:10.12691/ijp-4-3-3

Effect of Annealing by CO2 Laser on Structural and Optical Properties of CuO Thin Films Prepared by Sol – Gel Method

Khalil Ibrahim Mohammed[1,*], Awatif Sabir Jasim[2], Sahar Naji Rashid[2]

[1]Department of Physics, College of Science, Kirkuk University Kirkuk, Iraq
[2]Department of Physics, College of Science, Tikrit University, Tikri, Iraq
*Corresponding author: khalil69math@yahoo.com

Abstract Laser heat treatment is one of the important industrial applications of laser and being studied at the present time as a substitute for conventional thermal annealing. In this research (CuO) thin films have been deposition on a glass by (Sol - Gel / Spin Coating) technique and annealed by two ways, the first one using a convection oven, where they were annealing with three temperatures (400 °C, 500 °C, 600 °C) for one hour, and the second way using a continuous (CO2) laser with (10.6 μm) wavelength and (10 W) power and three intervals (10 min, 15 min, 20 min), were studied structural and optical properties of membranes prepared by both ways to determine the effect of laser annealing on them, and the results of (XRD) tests showed that these membranes with the structural of multi-crystalline monoclinic type and increase the degree of oven annealing temperature, as well as increasing the duration of the laser annealing lead to increased volumes of granular membranes rates. The results of the (AFM) tests to the topography of the surfaces of the membranes to be of crystalline uniformity and homogeneity superficially good, especially for laser annealed membranes. The results of optical examinations of these membranes showed that they having high permeability, especially in the regions of the visible spectrum and the near-infrared and increased with increase the degree of oven annealing temperature and the duration of laser annealing, and less energy gap of these membranes values with increase the temperature degree of annealing or increase of laser annealing time. In addition to this, the optical properties studied in this research included absorbance, reflectivity, refractive index, coefficients of absorption and extinction, and real and imaginary dielectric constants.

Keywords: *Annealing, Co2 Laser, CuO thin films*

Cite This Article: Khalil Ibrahim Mohammed, Awatif Sabir Jasim, and Sahar Naji Rashid, "Effect of Annealing by CO2 Laser on Structural and Optical Properties of CuO Thin Films Prepared by Sol – Gel Method." *International Journal of Physics*, vol. 4, no. 3 (2016): 59-63. doi: 10.12691/ijp-4-3-3.

1. Introduction

Laser is one of the most important inventions of the twentieth century and continues to evolve in various fields and applications [1], since the first laser system manufacturing in the early sixties and the areas of the 2 use of laser is on the rise [2], and among the various applications is laser materials treatment, such as laser annealing process [3]. The oven heat treatment is using for annealing and production of nano-crystals, and laser annealing technique is promising technology for this purpose, where used several types of lasers different in wavelengths including carbon dioxide laser (CO2 laser) [4] which is characterized by a small amount of power with the good quality of consumption came out suitable for annealing [5]. Laser annealing has become one of the topics that have attracted the attention of researchers at the present time [6]. Copper oxide (CuO) semiconductor material is called scientifically (tenorite) or (cupric), one of the stable oxides, is characterized as a brown powder near to black odorless [7] no dissolving in water or bases [8], also features owning non-toxic nature, the possibility of availability, low cost of production [9,10], the quality of electrical and optical properties [10], is one of the most important materials used in optoelectric applications, when it is material known as (TCO) [9], has a wide variety in photoelectric devices applications [7], in the energy sources and diodes link (pn-junction) etc. [11]. Thin film technology has contributed significantly to the study of semiconductors and gave a clear idea of many of the physical properties as well as chemical [12]. To study the characteristics of the semiconductor it became necessary to make a thin film does not exceed the thickness of a few microns [13], and in this paper adoption of carbon dioxide laser in addition to the convection oven for anneal (CuO) thin films prepared rotational by spin coating which is one of (sol - gel) technique methods, and study the structural and optical properties of them.

2. Experimental

In this paper glass bases were used to precipitate membranes on them, they have been cleaned to be free of

impurities or plankton by washing the samples with plain water and then cleaned with nitric acid diluted (HNO3) and washed with distilled water lukewarm with put them on magnetic stirrer for (10 min) and then put them in acetone after that they dried and placed in ethanol for (10 min) and dried to be ready to the deposition on them. Copper acetate dehydrate high purity have been used for the preparation of (CuO) thin films, were prepared from the solution concentration (0.2 M) dissolving (1.597 g) of copper acetate in (30 ml) of ethanol (purity of 99.99%), were mixing the solution using magnetic 3 stirrer device for an hour at (60°C) to complete the melting process, and in the meantime added to this mixture component of a solution of (0.84 g) of (diethanolamine) dissolved in (10 ml) of ethanol and operates as installed, has added drip and after this product is covered solution in the volumetric vial was developed and leave it for a period of (24 hour) to obtain a homogeneous solution, then deposited membranes copper oxide on the glass bases by placing the samples to spin coating device basis by using the rotational speed (3000 rpm) for a period of (30 sec), drying temperature was (100°C) for (10 min) and then submitted to the (150°C) for (10 min) and other, were obtained on a number of thin-film layers precipitated by six layers where this deposition process repeated for each layer of them, all membranes have been annealed in two ways:

1- Conventional Thermal Annealing: by useing thermal oven to anneal thin films at three temperatures (400°C, 500°C, 600°C) for one hour.

2- Rapid Thermal Annealing: by useing CW-CO2 laser device of type (engraving machine) with (50 W) power and (10.6 μm) wavelength, which can be increased by the energy resulting from control by changing the power inside tube laser, the power annealing (10 W) in three interval (10 min, 15 min, 20 min), where installed the current index in the device at (5 mA) to reach the power (10 W), and the distance is measured between the laser source and the sample is equal to (48.5 cm), the laser spot of the sample was (0.5 cm).

Thickness measuring of the thin films was by microscope using pro axel program where the sample was set in a certain way so that its edge was under the microscope, and using suitable lens magnification power to observe membrane layer formed on the glass base by the computer screen, with using the computer program it had been identified by two points opposite on the edges of the membrane by the index and install the reading taken pixels unit, which represents the difference between the desired membrane thickness, and repeating the process three or more times at different distances from the edge of the membrane and taking the rate we got approximate thickness membrane unit pixel which can be converted to the nanometer unit using the following relationship:

$$1\mu\text{m} = \text{pixel} / 50.205 \qquad (1)$$

Where (1 μm = 1000 nm). After completion of the annealing process, was chosen best membranes that have been obtained to conduct structural 4 and optical tests on it to see the effect of the conditions used in the preparation of this research by using synthetic tests two techniques:

1- X–Ray Diffraction (XRD): to study crystal structure of annealed thin films by study x-ray pattern, used)XRD-6000(device type.

2- Atomic Force Microscope (AFM): to study topographic of thin films surfaces, used (AA 3000 SPM) device type.

Optical tests had been done by (UV spectrophotometer) which included absorbance and transition at (190–1100 nm) wavelength range.

3. Results and Discussion

a- Structural Results

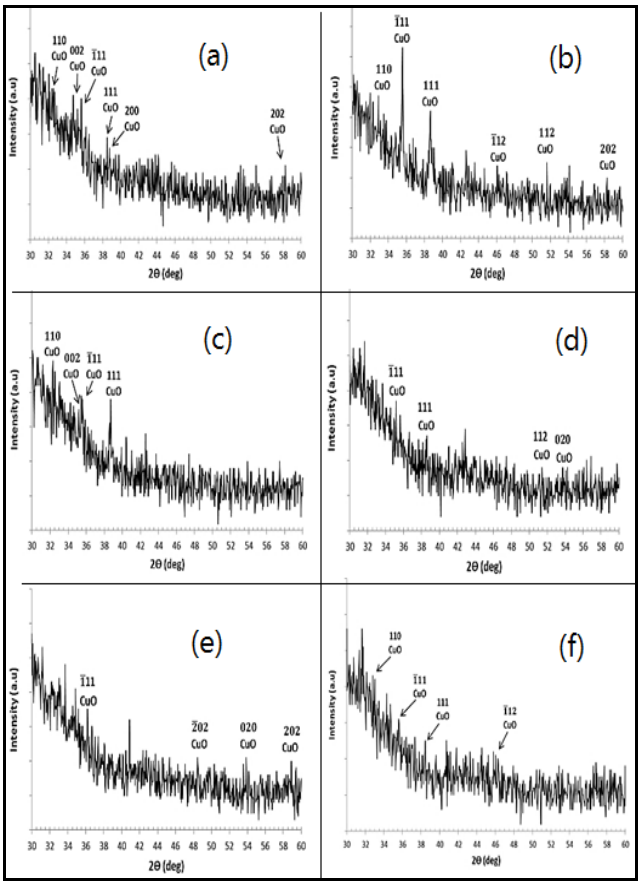

Figure 1. X-ray diffraction scheme of the copper oxide thin films which annealed:(a) by oven at (400 °C), (b) by oven at (500 °C), (c) by oven at (600 °C), (d) by laser for (10 min), (e) by laser for (15 min), (f) by laser for (20 min)

XRD results showed the multi crystalline monoclinic type of CuO thin films which had annealed by oven or by laser, agree with previous researches, and approximately corresponding with American standard for testing materials card (ASTM), card number (05-0661). In the furnace annealing case as in the Figure (1- (a, b, c)) there is emergence of peaks diffraction in both preference directions ($\bar{1}11$) and (111) in addition to the levels (110), (002), (200), ($\bar{1}12$), (112) and (202) with differentiation in membranes where different appearance and disappearance of some of them in grades annealing used for heat, while in laser annealing case as in the figures (1-(d, e, f)), there is no certain preferential direction, but there are different diffraction peaks which their appearance and isappearance depends on the duration of laser annealing, they are ($\bar{1}11$), (111), (112), (020), ($\bar{2}02$), (202), (110) and ($\bar{1}12$) as well as the emergence

of some of peaks at a number of angles that do not belong to the installation of crystalline material used because of laser high energy laser, this means that the high energy of laser led to formation of effective dispersion centers which have been working to create a sniper levels at grain boundaries working on the sniper charge carriers and freeze in place, especially since annealing was in the air and thus affect the structural properties of the membrane.

Increase in the degree of furnace annealing temperature led to increase particle size, as well as increasing the duration of laser annealing led to similar results in terms of improving the degree of crystallization of the material and narrow diffraction peaks and increase the granular size, since the increase of time annealing with high energy lead to increased temperature and thus increasing the particle size membranes. It noted some of the shapes in the above, we find in spite of the appearance of the material diffraction peaks but they look like random and this means that they have acquired the crystalline state in part of annealing process, the reason for this may be that the preparatory conditions have not had the opportunity to part of the atoms of the material to arrange themselves should also be to get to the case of long-term arrangement for all parts of the article.

The obtained results for the topography of the surface membranes also showed (CuO) that the membrane surfaces of uniformity crystalline and homogeneity superficial good as in the Figure 2- (a, b, c, d, c, e, f)), has resulted in increased oven annealing temperature to reduce distractions resulting in membranes within the preparation conditions in this research, while these deviations did not appear in the case of laser annealing where the surfaces of the membranes form more regularly.

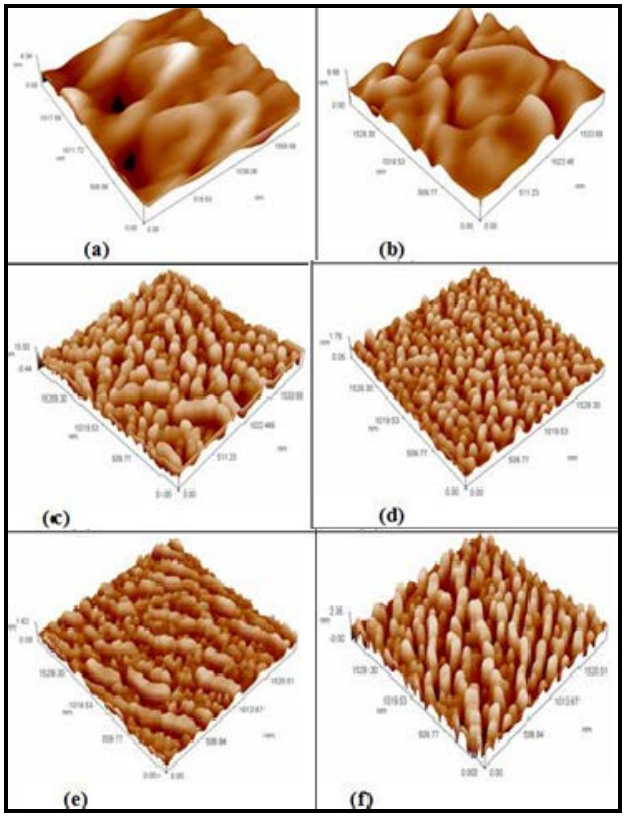

Figure 2. AFM image of copper oxide thin films which annealed: (a) by oven at (400 °C), (b) by oven at (500 °C), (c) by oven at (600 °C), (d) by laser for (10 min), (e) by laser for (15 min), (f) by laser for (20 min)

b- Optical Results

The results showed that the transition of CuO thin films increases with the degree of oven annealing temperature, this is consistent with the results of previous research where up to high levels in the visual areas and infrared, note that the values less when annealing at (500 °C) especially in the visible region, due to the deviation in these membranes at this annealing degree according to (AFM) results. As well as the effect of increasing the duration of laser annealing is similar to the effect of increasing the degree of annealing temperature on the spectrum transition, and an increase in the duration laser annealing led to the improvement of crystallized material, as in Figure 3-a,b, and show a strong response to the many types of solar cells as well as many applications as a result of high transition, and exhibits the spectrum absorbance behavior opposite to the transition spectrum as in Figure 4-a,b.

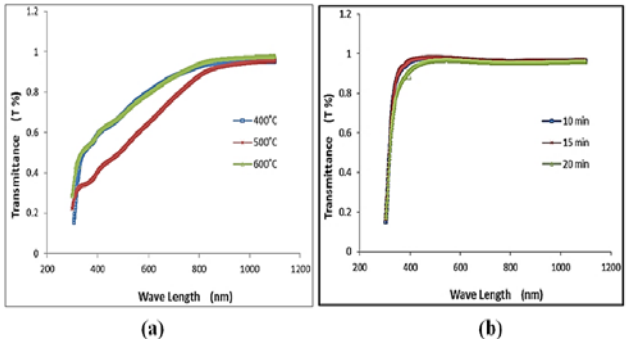

Figure 3. Transition spectrum of CuO thin films: (a) furnace annealing (b) laser annealing

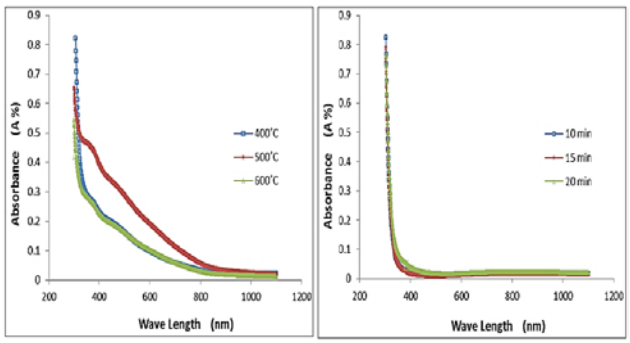

Figure 4. Absorbance spectrum of CuO thin films: (a) furnace annealing (b) laser annealing

In figure 5-a,b we find the increased reflectivity for a particular range of wavelengths as a result of a decrease of transition, then the curve begins to decrease at higher wavelengths with the observation that the rates decrease with increasing degree of annealing temperature, it may be due simplex in the form of curves difference to the different nature of the surfaces, we also find that the effect of laser annealing is similar to the effect of furnace on reflectivity spectrum, noting that the decline curve, up wavelength faster than in the case annealing oven may be due to the high power laser led to the irregular surfaces of the membranes, which led to the similarity of the behavior of the curve for all the times of annealing. In general, the reflectivity be few at energies least of (Eg) and peak appearance in the reflectivity curve is when the value of the wavelength corresponding to the value of the energy

gap. We find a slowly increase of absorption coefficient (equation 2) with photon energy increase and then there is a rapid increase at the absorption edge for a certain extent of energies, and laser annealing led to increase the value of a simple than in the case of oven annealing as shown in Figure 6-a,b.

$$\alpha = 2.303A/t \qquad (2)$$

Where (A) represents the absorbance and (t) the thickness of thin film.

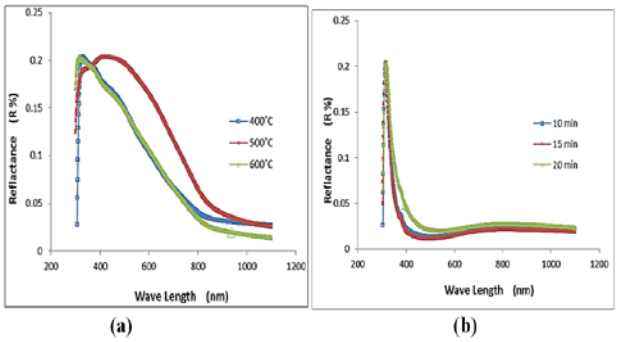

Figure 5. Reflectance curve of CuO thin films: (a) furnace annealing (b) laser annealing

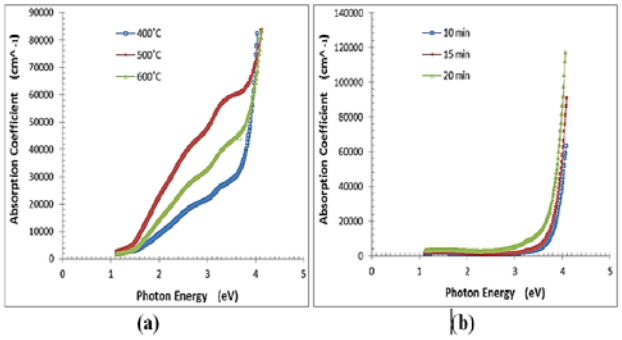

Figure 6. Absorption coefficient as a function of photon energy of CuO thin films:(a) furnace annealing (b) laser annealing

The results showed that the electronic transition is allowed direct type and that the energy gap slightly decreases with increasing oven temperature annealing and values range between (3.75 eV - 3.5 eV) where its value at (500 °C) is at less value because the absorbance at this degree is high. As well as an increase for laser annealing range values between (3.9 eV - 3.8 eV) as shown in Figure 7-A,B.

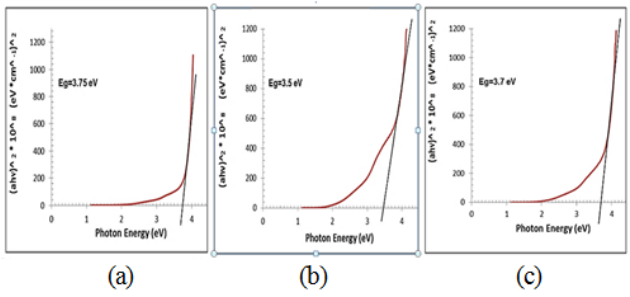

Figure 7A. Allowed direct energy band gap of CuO thin films furnace annealed at: (a) 400°C, (b) 500°C, (c)600°C

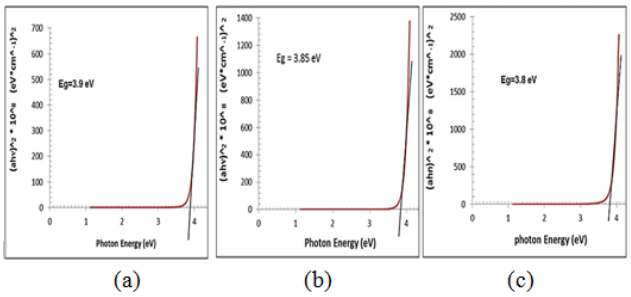

Figure 7B. Allowed direct energy band gap of CuO thin films laser annealed at: (a) 10 min, (b) 15 min, (c) 20 min

The results also showed, as shown in Figures (8-a,b) the change in the refractive index (equation 3) is similar to the (R) change, where little value is at few energies (high wavelengths) and then rise to larger value 9 of its at energy which equal to (Eg) and decreases then, and at all temperature annealing noting the emergence of meanders in curves due to the different nature of the surfaces of membranes, we find that the laser annealing leads to the same results with a note almost meanders curved disappearance has been attributed to high-energy of laser that led to the increase smoothness and irregular surfaces of the membranes.

$$n = \left(\frac{1+R}{1-R}\right) + \sqrt{\frac{(1+R)^2}{(1-R)^2} - \left(k^2+1\right)} \qquad (3)$$

Where (R) represents reflectivity and (K) coefficient of extinction. From figures (9-a,b) we find that the extinction coefficient curve (equation 4) is similar to the (α) curve, and the value be larger in the case of laser annealing than its in the case of oven annealing with note irregular shape of the curves in the laser annealing case.

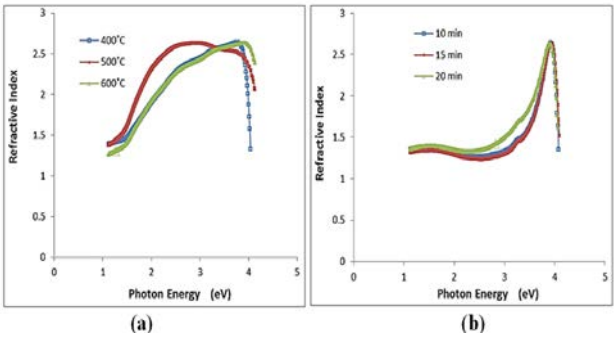

Figure 8. Refractive index as a function of photon energy of CuO thin films: (a) furnace annealing (b) laser annealing

$$k = \frac{\alpha\lambda}{4\pi} \qquad (4)$$

Where (λ) represents wavelength. And from figures (10-a,b) we find that the real dielectric constant change (equation 5) is similar to the change of (n), where (εr) can be calculated from the refractive index, while the change of dielectric imaginary constant (equation 6) is similar to the change of (α) with a decrease in the values of (εi) at the end of the curve at high energies and this behavior is more pronounced in the case of laser annealing with the observation that increasing the duration of laser annealing led to increased values as shown in Figure 11-a,b.

$$\varepsilon_r = n^2 - k^2 \quad (5)$$

$$\varepsilon_i = 2nk \quad (6)$$

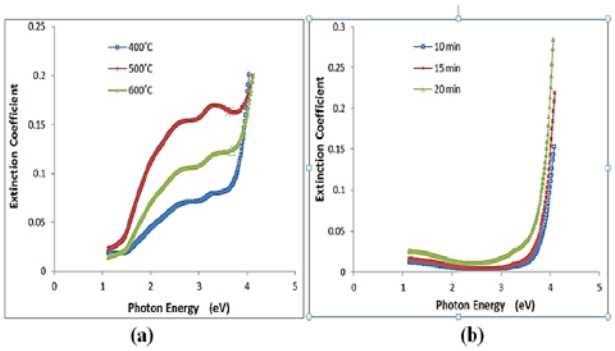

Figure 9. Extinction coefficient as a function of photon energy of CuO thin films:(a) furnace annealing (b) laser annealing

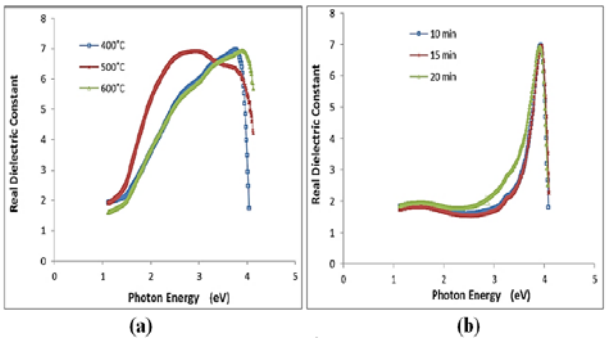

Figure 10. Real dielectric constant as a function of photon energy of CuO thin films:(a) furnace annealing (b) laser annealing

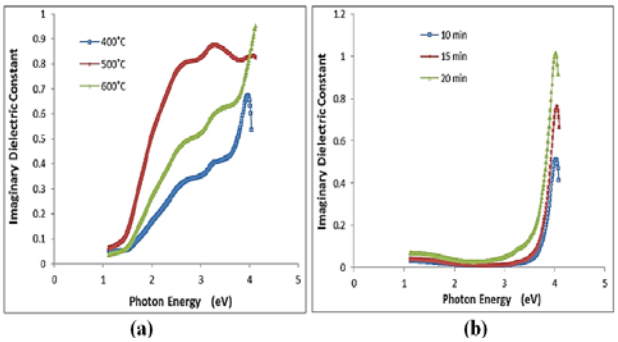

Figure 11. Imaginary dielectric constant as a function of photon energy of CuO thin films:(a) furnace annealing (b) laser annealing

In general by observed the figures that represent the optical parameters of (CuO) membranes furnace annealed, find little difference in form of curves as a result of simple deviation indicated by the results of (AFM), while laser annealing shows homogeneity and irregular forms of curves.

4. Conclusions

1. We can use CO2 laser for annealing and get an approximately similar results to those which obtained by furnace annealing, at the prepared conditions of this paper, in relative little time.
2. Structural results showed that CuO thin films are multi crystalline monoclinic type, and the increase of degree of furnace annealing temperature, as well as laser annealing interval time, lead to enhancing crystallization. Results also showed that the homogenously of membranes surfaces is increasing with increase of furnace annealing temperature, as well as laser annealing interval time.
3. Optical results showed that these thin films have direct electronic transition, where they have just allowed direct energy gaps at the prepared conditions of this paper, and the values of energy gap decrease at increase of furnace annealing temperature, as well as laser annealing interval time, when the thin films defects will decrease and the transition will increase.

References

[1] J. Dutta Majumdar and I. Manna, "Laser processing of materials", Sadhana, Vol.28, parts 3&4, India, (2003).

[2] Muslim F. and Hiba S., *"Study the optical properties of Copper oxide thin films prepared by laser deposition"*, Journal of Nahrin university, V. 4, No. 12, (2009).

[3] BreckHitz, J.J. Ewing and Jeff Hecht, "Introduction to laser technology", third edition, IEEE press, America, (2001).

[4] Clara G., Maurizio F., Cristina A., Alessandro C., Yoann J., Giancarlo C. R., Faruk F. and Efrain S., *"CO_2 laser annealing on erbium-activated glass–ceramic waveguides for photonics"*, optical materials31, published by Elsevier B.V., (2009).

[5] Anthony J. D., Thomas V. H. and Jr., *"The CO_2 laser: the workhorse of the laser material processing industry"*, SPIE professional magazine, (2010).

[6] Ian W. B., *"Laser processing of thin films and microstructures oxidation, deposition and etching of insulators"*, edited by Aram Mooradian, Springer sense in materials science, (1987).

[7] SuraMejbel A., Dr. Nadir F. and Dr. Hayfa G. R., *"The Effect of Thickness on The Optical and Structural Properties of Copper Oxide The Nano- Grain Size"*, M.Sc. thesis, Education College, AL-Mustansiriyah University, (2010).

[8] Mazin H. H., *"Study The Structural and Optical Properties Of Copper Oxide Thin Films ImpureBy Indium"*, M.Sc. thesis, Education College, AL-Mustansiriyah University, (2005).

[9] Samir H. A. and Riyam I. J., *"Study the optical properties of copper oxide thin film deposited by cold spray"*, AL-Qadisiya journal for engineering sciences, Vol.6, No.4, (2013).

[10] Hayder M. A., Shatha S. Batros J., Ashwaq A. J. and Elham H. N., *"The effect of annealing on the structural and optical properties of copper oxide thin films prepared by SILAR method"*, J. Baghdad for sci., Vol.11(2), (2014).

[11] Kadhim A. A., Ali A. K.. and Mohammed R. A., *"Effect of annealing temperature and laser pulse energy on the optical properties of CuO films prepared by pulsed laser deposition"*, Iraqi journal of physics, Vol.12, No.23, (2014).

[12] Rudainah S. A., Dr. Nabeel A. B. and Dr. Ziad T. K., *"Study of Structural and Optical Properties of $Ni_{(1-x)}Zn_xO$ Thin Films Prepared By Chemical Spray Pyrolysis Method"*, M.Sc. thesis, Science College, DiyalaUniversity, (2013).

[13] Majed H. H., Khudhaier A. and Fatima H., *" The study of optical and electrical of CuO and silver Oxide doped CuO thin films prepared by Spray pyrolysis Technique"*, M.Sc. thesis, Education College, AL-Mustansiriyah University, (2003).

International Journal of Physics, 2016, Vol. 4, No. 3, 64-68
Available online at http://pubs.sciepub.com/ijp/4/3/4

DOI:10.12691/ijp-4-3-4

A 3D Brans-Dicke Theory Model

T. G. do Prado*, E. F. Reis, M. C. Vergès, V. Piccirillo, J. R. Ciappina

Federal University of Technology-Paraná, Departament of Mathematics 84016-210, Ponta Grossa, PR, Brasil
*Corresponding author: thiagogilbertodoprado@gmail.com

Abstract The evidence of an accelerated universe and the gap of 70 percent in the total energy, collected by WMAP, are problems that cannot be solved by standard models based on General relativity. Therefore the search for an alternative theory that solves the open questions in General Relativity became an important research field in the past few years. A particular alternative is the Brans-Dicke theory, which has been broadly studied as concerned to k-essence type fields in 4D. However, this theory is almost unexplored in the context of the dimensional reduction in 3D. In the present work, we study the Brans-Dicke Theory in a dimensional reduction context. In order to do this, we consider the Brans-Dicke theory in the vacuum, and in the presence of matter fields.

Keywords: *cosmology, dimensional reduction, general relativity, lower dimensional gravitation*

Cite This Article: T. G. do Prado, E. F. Reis, M. C. Vergès, V. Piccirillo, and J. R. Ciappina, "A 3D Brans-Dicke Theory Model." *International Journal of Physics*, vol. 4, no. 3 (2016): 64-68. doi: 10.12691/ijp-4-3-4.

1. Introduction

The evidence of an accelerated expansion of the universe, observed by WMAP [3], opened the discussion of the general relativity eventual limits. There are many options for alternative theories of gravity, and among them we can cite scalar-tensor theories like supergravity, Kaluza-Klein theories, dual string theories, M-Theory, etc [1,2,4,5,14]. One particular kind of scalar-tensor theory to describe an accelerate expansion of the universe, called Brans-Dicke theory [6,7], was proposed in the early sixties . This theory uses the principle of Mach and the hypothesis of Dirac [8], considering an eventual variation in time of the Newton's gravitational constant, thus ensuring the universality of free fall (equivalence principle) [20, 22, 23].

Most of the works which have been published in this theory up to now consider four flat dimensions, and some of them have tried to associate the scalar field of the Brans-Dicke theory as quintessence field [9], $\Lambda C\ DM$ models [19] and as a type of K-essence field [10,18]. Others have tried to find a solution for the observed accelerated expansion using a dimensional reduction of the 5*D* Brans-Dicke theory without matter [11,12].

Concerning three dimensions, a broad study has been done in gravitational theories since the publication of [13], motivated by the fact that 3*D* theories avoid some complications found in higher dimensions [15,16]. However, there are not as many results about 3D scalartensor theories, and it would be interesting to find some results in this subject, more specifically in 3*D* Brans-Dicke theory. For instance, we can see some problems like the association of the scalar field of the Brans-Dicke theory to K-essence fields which models the dark energy, as done in [10]. The goal in this paper is to construct and then analyze the behavior of a 3*D* Brans-Dicke model. For this we consider a Brans-Dicke scalar field which depends only on the cosmic time.

2. The 3D Brans-Dicke Theory

The action of Brans-Dicke theory in 3*D* will be described by [5]

$$S=\frac{1}{16}\int d^3x\sqrt{\left|g^{(3)}\right|}\left[\phi R^{(3)}-\frac{\omega}{\phi}g^{(3)}_{ab}\nabla^a\phi\nabla^b\phi\right]+\int d^3x\sqrt{\left|g^{(3)}\right|}\mathcal{L}^{(3)}_M, \tag{1}$$

where R is the scalar curvature associated to the 3*D* metric $g^{(3)}_{ab}$, ϕ is the scalar FIeld of the Brans-Dicke theory, ω is a theory dimensionless parameter, and $\mathcal{L}_M$ represents the lagrangian of the matter. The matter FIelds do not depend on the scalar field ϕ (this is necessary in order to preserve the weak equivalence principle [5]). Note that, in 3*D*, the field ϕ has dimensions of inverse length.

The equations for the gravitational field derived from (1), can be written in the following form

$$G_{ab}=\frac{8\pi}{\phi}T^{(3)}_{ab}+\frac{\omega}{\phi^2}\left[\nabla_a\phi(\nabla_b\phi)-\frac{1}{2}g^{(3)}_{ab}(\nabla_c\phi)(\nabla^c\phi)\right]+\frac{1}{\phi}\left(\nabla_a\nabla_b\phi-g^{(3)}_{ab}\nabla^2\phi\right), \tag{2}$$

where $\nabla^2=\nabla^a\nabla_a$, and $T^{(3)}_{ab}$ is the energy momentum tensor associated with the matter fields for 3*D*. From the equation (1) it is possible to find that the field equation for the scalar field ϕ is given by

$$\nabla^c\nabla_c\phi=\frac{8\pi}{\omega+2}T^{(3)}, \tag{3}$$

where $T^{(3)} = g^{ab}T_{ab}$ is the trace of energy momentum tensor. In the context of a perfect fluid approximation, it can be seen from the second term in the equation (2) as the energy momentum tensor associated with the BD scalar field ϕ, and write

$$8\pi T_{ab}^{BD} = \frac{\omega}{\phi^2}\left[(\nabla_a\phi)(\nabla_b\phi) - \frac{1}{2}g_{ab}(\nabla_c\phi)(\nabla^c\phi)\right] + \frac{1}{\phi}\left(\nabla_a\nabla_b\phi - g_{ab}\nabla^2\phi\right). \quad (4)$$

We consider a perfect fluid approximation for the matter fields. Then the energy momentum tensor associated with matter field will be given by

$$T_{ab} = g_{ab}p + (\rho + p)u_a u_b, \quad (5)$$

where p and ρ represent the pressure and energy density associated with the matter-fluid and u_a is the velocity vector. The pressure and energy density are related by the state equation $p = \sigma\rho$, where σ is a parameter of proportionality. Comparing this relation with equation (3) we see that the BD scalar field and this matter-fluid are related by

$$\nabla^c\nabla_c\phi = \frac{8\pi}{\omega+2}(2\rho - p). \quad (6)$$

As the BD scalar field ϕ has non-minimal coupling with gravity, it is impossible to write an expression similar to the equation (5), relating the associated pressure p_{BD} and energy density ρ_{BD} for the field ϕ, these quantities being identified as the spatial and temporal components of the energy momentum tensor associated with the BD scalar field, given by the equation (4). However, they are related by the equation of state

$$p_{BD} = \sigma_{BD}\rho_{BD}.$$

3. 3D Brans-Dicke Cosmology in the Absence of Matter

Let the spacetime be described by the 3D FRLW metric, that is given by [5]

$$ds^2 = g_{ab}dx^a dx^b = dt^2 - a^2(t)\left[\frac{dr^2}{1-kr^2} + r^2 d\varphi^2\right], \quad (7)$$

where $a(t)$ is a dimensionless cosmic scale factor, and k is a parameter which can assume only one of three values: −1 (open universe), 0 (at universe) and +1 (closed universe). The observations done by WMAP, show that for 4*D* standard model the universe is about at. Then following this tendency, we will consider only the at case for the 3*D* model. Replacing (7) and $\phi = \phi(t)$ in (2); we find that the pressure p_{BD} and the energy density ρ_{BD} associated with the BD scalar field are given by

$$\rho_{BD} = \frac{1}{8\pi}\left[\frac{\omega}{2}\left(\frac{\dot\phi}{\phi}\right)^2 - 2\frac{\dot a}{a}\frac{\dot\phi}{\phi}\right], \quad (8)$$

$$p_{BD} = \frac{1}{8\pi}\left[\frac{\omega}{2}\left(\frac{\dot\phi}{\phi}\right)^2 - 2\frac{\dot a}{a}\frac{\dot\phi}{\phi} + \frac{\ddot\phi}{\phi}\right]. \quad (9)$$

If the BD scalar field is assumed as a perfect fluid, then the equations (8) and (9) are complemented by the equation of state [5,24,25]

$$\dot\rho_{BD} + 2\frac{\dot a}{a}(\rho_{BD} + p_{BD}) = 0. \quad (10)$$

Considering the at metric from (7) in the equations (2) and (6) we find

$$\left(\frac{\dot a}{a}\right)^2 = 8\pi\rho_{BD}, \ddot\phi + 2\frac{\dot a}{a}\dot\phi = 0. \quad (11)$$

In order to solve this system of coupled equations, we consider the ansatz

$$\phi(t) = \frac{1}{G_0}a^n(t), a(t) = a_0\left(1 + \frac{\beta}{\sqrt{G_0}}t\right)^\alpha, \quad (12)$$

where G_0 denotes the present value for the Newton's gravitational constant and β is a dimensionless parameter. Using the equation (12) in (11) we get a condition that relates the α to n parameters, namely

$$\alpha = \frac{1}{n+2}. \quad (13)$$

Now, substitution of the ansatz in (10) results

$$\omega = -1,$$

that implies in two possibilities for the parameter n

$$n = 0 \ \ or \ \ n = -2.$$

The only acceptable possibility for the n parameter is $n = 0$, resulting in $\alpha = \frac{1}{2}$, because the value $n = -2$ results in a divergent parameter α, without a physical meaning. For this value of α, the Brans-Dicke scalar field is given by $\phi(t) = \frac{1}{G_0}$, and the scale factor, has the form

$$a(t) = a_0\left(1 + \frac{\beta}{\sqrt{G_0}}t\right)^{\frac{1}{2}}. \quad (14)$$

Thus, when we consider ϕ depending only on time, the 3*D* Brans-Dicke model reduces exactly to the results of the 3*D* general relativity model. Therefore for a massless universe, the 3*D* Brans-Dicke theory does not have any K-essence behavior.

4. 3D Brans-Dicke Cosmology in the Presence of Matter

In this section we address the cosmology problem derived from the 3*D* Brans-Dicke theory in the presence of matter for a at background. As can be seen in Section II, the matter will be modeled like a perfect fluid with

associated energy density ρ and pressure p. Substituting the FRLW metric (7) in the field equations (2), we see that the resulting Friedmann equations, in this case, are given by

$$\left(\frac{\dot{a}}{a}\right)^2 = \frac{8\pi}{\phi}\rho + 8\pi\rho_{BD}, \tag{15}$$

$$\ddot{\phi} + 2\left(\frac{\dot{a}}{a}\right)\phi = \frac{8\pi}{(\omega+2)}(\rho - 2p). \tag{16}$$

The energy density ρ and the pressure p are related by

$$p = \sigma\rho.$$

Thus the equation (16) can be rewritten as

$$\ddot{\phi} + 2\left(\frac{\dot{a}}{a}\right)\phi = \frac{8\pi(1-2\sigma)}{(\omega+2)}\rho. \tag{17}$$

If we require the conservation of the energy momentum tensor, then we see that the equations of state for the matter fields and for the BD scalar field ϕ are given by

$$\dot{\rho} + 2\left(\frac{\dot{a}}{a}\right)(1+\sigma)\rho = 0, \tag{18}$$

$$\dot{\rho}_{BD} + 2\left(\frac{\dot{a}}{a}\right)(\rho_{BD} + p_{BD}) = \frac{\dot{\phi}}{\phi^2}\rho. \tag{19}$$

The non-minimal coupling between the BD scalar field ϕ and gravity in the equation (1) amounts to a mixed term in the equation of state for ϕ involving the matter density ρ, which makes its solution a non-trivial one. Also, we see that, since the BD scalar field ϕ is massless and does not interact with matter, the equation (18) preserves the weak equivalence principle. And, by integrating equation (18), we obtain that the energy density ρ is related to the scale factor $a(t)$ by means of

$$\rho = \left(\frac{a(t)}{a(0)}\right)^{-2(1+\sigma)}.$$

As in the previous section, now we propose the ansatz

$$\phi(t) = \frac{1}{G_0}(1+\chi t)^{\gamma}, a(t) = a_0(1+\chi t)^{\beta}, \tag{20}$$

as solutions for the equations (15) and (17), where χ is a constant. Replacing this ansatz in the coupled field equations (15) and (17) gives us the results

$$\beta = \frac{\omega+2}{2\omega+4\sigma+2}, \gamma = \pm\beta\sqrt{\frac{2(1-2\sigma)}{2(\omega+2)+\omega(1-2\sigma)}}. \tag{21}$$

Unlike the scalar-vaccum configuration, now it is not possible to determine the parameter ω; since the state equation (19) is coupled. The equation (21) shows that there are two possibilities for γ, but for small values of ω the positive value of γ allows a negative value for the energy density, which is forbidden by the strong energy condition [17]. Therefore the negative choice is the only possibility for γ.

If we replace the ansatz (20) in the general equations (8) and (9) we find that the equations for the energy density and pressure associated with the BD scalar field are given by

$$\rho_{BD} = \frac{1}{8\pi}\gamma\left(\frac{\omega\gamma}{2} - 2\beta\right)\frac{\chi^2}{(1+\chi t)^2}, \tag{22}$$

$$p_{BD} = \frac{1}{8\pi}\left[2\beta\gamma + \frac{\omega\gamma^2}{2} + \gamma(\gamma-1)\right]\frac{\chi^2}{(1+\chi t)^2}, \tag{23}$$

and the Brans-Dicke energy density and pressure are related by

$$p_{BD} = \sigma_{BD}\rho_{BD}.$$

If the strong energy condition [17] is considered, we find that the deceleration parameter for the *3D* model constructed with the Brans-Dicke theory, is given by

$$q = \frac{\Omega(1-\sigma)}{\phi(t)} + \Omega_{BD}(1-\sigma_{BD}), \tag{24}$$

where

$$\Omega = \frac{8\pi}{H(t)^2}\rho \text{ and } \Omega_{BD} = \frac{8\pi}{H(t)^2}\rho_{BD},$$

and H is the Hubble parameter. We observe that the first term in the right side is related to the matter fields, while the second term is related to the BD scalar field.

The behavior of the 3*D* Brans-Dicke model as a Kessence theory, depends on the possible values for the dimensionless parameter ω of theory, parameter σ_{BD} that relates the Brans-Dicke energy density and pressure, and the parameter σ that relates the energy density and pressure of matter fields. For this last parameter, there are two possibilities: $\sigma = 0$ that describes a Matter Dominate Era (**MDE**); $\sigma = \frac{1}{2}$ Radiation Dominate Era (**RDE**).

For the **RDE**, the 3*D* Brans Dicke theory recovers the cosmological standard model results. For the **MDE** the behavior of the parameter σ_{BD} is described by Figure 1.

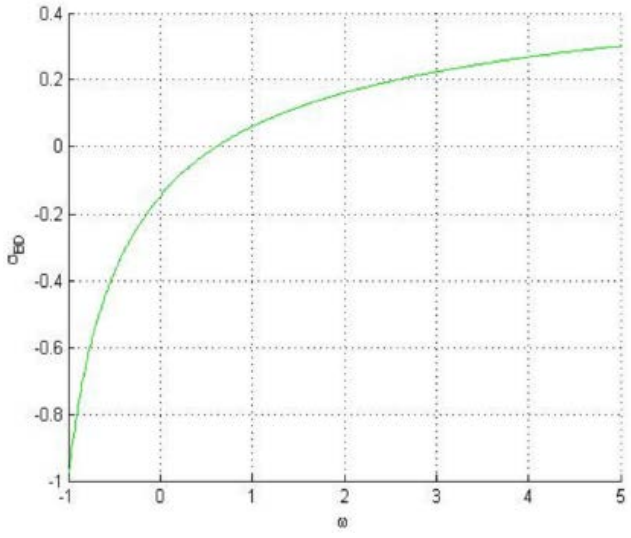

Figure 1. σ_{BD} parameter in terms of dimensionless parameter of theory ω

Analyzing Figure 1, we found that σ_{BD} has negative values for $-1.32 < \omega < 0.61$. However, the Brans-Dicke Theory is inconsistent for small values of the dimensionless parameter ω in a solar system level, this consistence is restored only for larger values of ω [5]. For large values of $\omega(\omega \geq 50.000)$, σ_{BD} does not assume positive values, which is inconsistent with the description of an accelerated expansion of a 3D universe.

A comparison between the scale factors of the 3*D* and 4*D* Brans-Dicke models is shown in Figure 2. As expected, the models have a different behavior as presented in [10]. Figure 2 shows that there is a value of time that the two models converge to the same result, diverging again shortly thereafter.

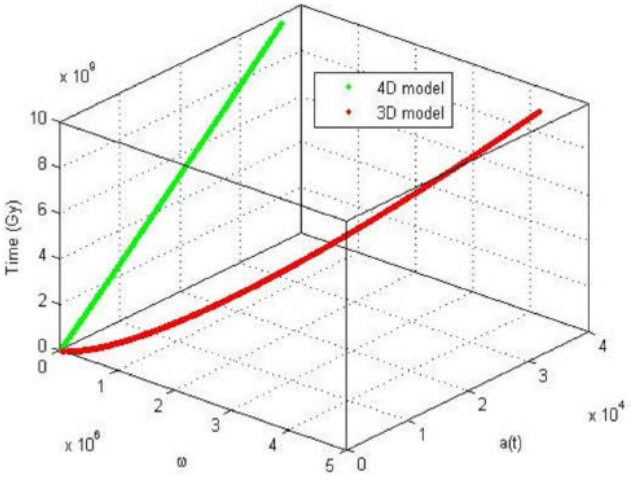

Figure 2. Comparison between scale factor $a(t)$ behavior for vacuum of 3*D* (red) and 4*D* (green) models

For the MDE, the energy density of Brans-Dicke scalar field is non null. This is expected because the Brans-Dicke scalar field is generated by matter fields (3). The analysis of Figure 1 shows that the Brans-Dicke model can only describe a K-essence field $(\sigma_{BD} < 0)$ for some values of the dimensionless parameter $\omega(-1.32 < \omega < 0.61)$. However for the consistency of the theory, only larger values of ω are allowed in a solar system level $(\omega \geq 50.000)$ [5,21]; and for $\omega > 0.61$, the 3*D* theory no describe a K-essence model $(\sigma_{BD} > 0)$. In the RDE the 3*D* and 4*D* models has the same behaviour. The 3*D* Brans-Dicke model restores the General Relativity results when $\omega \to \infty$.

Table 1. 3*D* and 4*D* Brans-Dicke models

Era model	3*D* BD	3*D* BD
vacuum	$a(t) \sim t^{\frac{1}{2}}$	$a(t) \sim t^m m > 1$
RDE	$a(t) \sim t^{\frac{1}{2}}$	$a(t) \sim t^{\frac{1}{2}}$
MDE	$a(t) \sim t^{\frac{\omega+2}{2(\omega+1)}}$	$a(t) \sim t^{\frac{2(\omega+1)}{\omega+4}}$
BD	*DNE*	$a(t) \sim t$

Table 1 shows a comparation between the scale factor behavior of 3*D* and 4*D* Brans-Dicke models for the different evolution eras. An interesting result is that there is no difference between vacuum Era and **RDE** in the 3*D* Brans-Dicke model. Therefore, the 3*D* model has only two distinct evolution Eras, while the 4*D* Brans-Dicke model has four distinct Eras (see Table 1) [10]. This comparison shows that for the scalar tensor theories like Brans-Dicke theory, the choice of spatial dimension is a very important factor for the theory behavior.

5. Conclusions

In the absence of matter fields (vacuum), the energy density of the Brans-Dicke scalar field vanishes, i.e. $\rho_{BD} = 0$, and the 3*D* Brans-Dicke theory recovers the 3*D* General Relativity results. This result is expected since the Brans-Dicke scalar field is generated by matter fields (3). However the 4*D* Brans-Dicke model does not reduce to the 4*D* General Relativity model when the matter fields vanish [10], and a new Era of scalar field emerges in the 4*D* Brans-Dicke model. This new Era in the 4*D* model is due to K-essence behavior of Brans-Dicke scalar field in 4D model, which does not happen in the 3*D* model.

In the presence of matter fields, the energy density of the 3*D* scalar fields is non-null. However, even in the presence of matter fields, the 3*D* Brans-Dick model does not have a K-essence behavior like found in the 4*D* model [10]. Another important information is that 3*D* Brans-Dicke model has only two distinct evolution Eras, the vacuum and RDE Eras are the same and the MDE Era. In this sense we conclude that the difference of scale factor behavior between 3*D* and 4*D* Brans-Dicke models is mainly due to the dimensional factor of the field equations.

Acknowledgments

The authors thank CNPq and CAPES for financial support and the Professor Rodrigo Frehse Pereira for the support with the text editor.

References

[1] E. Berti. Astrophysical Black Holes as Natural Laboratories for Fundamental Physics and Strong-Field Gravity. Braz. J. Phys., 43:341-350, 2013.

[2] J. C. Fabris, F. T. Falciano, J. Marto, N. Pinto-Neto, P. Vargas Moniz. Dilaton Quantum Cosmology with a Schrdinger-like Equation. Braz. J. Phys., 42:475-481, 2012.

[3] D. N. Spergel et al. First year Wilkinson microwave anisotropy probe (WMAP) observations: determination of cosmological parameters. Astrophys. J., 148:175, 2003. (arXiv:astro-ph/0302209).

[4] P. Jordan. Schwerkraft undWeltall. Friedrich Vieweg und Sohn, Braunschweig, 1955.

[5] Y. Fujii, K. Maeda. The scalar-tensor theory of gravitation. Cambridge University Press, Cambridge, 2004.

[6] C. Brans, R. H. Dicke. Mach's principle and a relativistic theory of gravitation. Phys. Rev., 124:925, 1961.

[7] R. H. Dicke. Mach's principle and invariance under transformation of units. Phys. Rev., 125:2163, 1962.

[8] P. A. M. Dirac. New basis for cosmology. Proc. Roy. Soc., A165:199, 1938.

[9] N. Banerjee, D. Pavon. A Quintessence scalar field in Brans-Dicke theory. Class. Quant. Grav., 18:593, 2001.

[10] H. Kim. Brans-Dicke scalar field as a unique k-essence. Phys. Lett., B606:223, 2005.

[11] L. Qiang, Y. Ma, M. Han, D. Yu. Five-dimensional Brans-Dicke theory and cosmic acceleration. Phys. Rev., D71:061501, 2005.

[12] J. Ponce de Leon. Late time cosmic acceleration from vacuum Dicke theory in 5D. Class. Quantum Grav., 27:095002, 2010.

[13] M. Ba~nados, C. Teitelboim, J. Zanelli. Black hole in three-dimensional spacetime. Phys. Rev. Lett., 69:1849, 1992.

[14] O. Aharony, S. S. Gubser, J. Maldacena, H. Ooguri, Y. Oz. Large N Field Theories, String Theory and Gravity. Phys. Reports, 323:183, 2000.

[15] A. Maloney, W. Song, A. Strominger. Chiral gravity, log gravity and extremal CFT. Phys. Rev., D81:064007, 2010.

[16] A. A. Bytsenko and M. E. X. Guimarães. Truncated heat kernel and one-loop determinants for the BTZ geometry. Eur. Phys. J. C., 58:511, 2008.

[17] S. W. Hawking, G. F. R. Ellis. The large structure of space-time. Cambridge University Press, Cambridge, 1973.

[18] E. Nabulsi, A. Rami. Effective cosmology a la Brans-Dicke with a non-minimally coupling massive inaton field interacting with minimally coupling massless field. Braz. J. Phys., 40(3):273, 2010.

[19] D. A. Tretyakova, A. A. Shatskiy, I. D. Novikov, S. Alexeyev. Nonsingular Brans-Dicke ∧ cosmology. Phys. Rev., D85:124059, 2012.

[20] S. V. Sushkov, S. M. Kozyrev. Composite vacuum Brans-Dicke wormholes. Phys. Rev., D84:124026, 2011.

[21] K. H. Saaidi, A. Mohammadi, H. Sheikhahmadi. parameter and Solar System constraint in chameleon-Brans-Dicke theory. Phys. Rev., D83:104019, 2011.

[22] Feng-Quan Wu and Xuelei Chen. Cosmic microwave background with Brans-Dicke gravity. II. Constraints with the WMAP and SDSS data. Phys. Rev., D82:083003, 2010.

[23] Feng-QuanWu, Li-e Qiang, XinWang, Xuelei Chen. Cosmic microwave background with Brans-Dicke gravity. I. Covariant Formulation. Phys. Rev., D82:083002, 2010.

[24] S. Weinberg. Gravitation and Cosmology. Wiley, Barbacena, 1972.

[25] C. W. Misner, K. S. Thorne, J. A. Wheeler. Gravitation. W. H. Freeman and Company, 1973.

International Journal of Physics, 2016, Vol. 4, No. 3, 69-73
Available online at http://pubs.sciepub.com/ijp/4/3/5

DOI:10.12691/ijp-4-3-5

A 5 Year Retrospective Study of 131I Therapy for Thyroid Cancer Practice in King Abdulaziz University Hospital

Mawya A. Khafaji[1], Majdi R. ALnowaimi[2,*]

[1]Department of Radiology, Faculty of Medicine Kind Abdulaziz University, Jeddah, Saudi Arabia
[2]Department of Nuclear engineering, faculty of Engineering Kind Abdulaziz University, Jeddah, Saudi Arabia
*Corresponding author: malnowaimi@kau.edu.sa

Abstract Since 1940s, intake of Iodine 131 is a deeprooted postoperative therapy for malignant thyroid. However, clinical practice does differ significantly between hospitals. This paper presents a retrospective study of a clinical practice for patients diagnosed with thyroid cancer at King Abdulaziz University Hospital (KAUH). The aim of this study was to benchmark KAUH practice patterns against international guidelines. A total of 100 patients with thyroid cancer were included, 70% females and 30% males with median age of 42.5 and 43.5 years respectively. Cases were patients, diagnosed with thyroid cancer and treated with radioactive iodine at KAUH in Saudi Arabia between 2005 and 2011. Some additional patient's data were excluded from the study because of missing information or lost to follow-up. Medical records included patient's gender, age, clinical diagnoses, iodine dose, and the recurrence. Where, thirty-three percent (33%) of the patients had papillary carcinoma, (3%) had follicular carcinoma and (1%) had Hurtle cell tumors. All patients had their total/partial thyroidectomy at KAUH. Dose administered ranged from (50 to 300) mCi with the 61% receiving a dose of 100mCi. A statistical test, Chisquare test, were used to allow us to test for deviations of observed frequencies from expected frequencies. The medical record showed that 3% of the patient had died and 4% had a recurrence that was successfully treated by the time of the study. Moreover, the 5-year survival rates for patients with thyroid cancers was 93%. The thyroid cancer incidence and the I-131 practice in KAUH is consistent with international data and standards.

Keywords: *radioactive iodine, thyroid cancer, nuclear medicine*

Cite This Article: Mawya A. Khafaji, and Majdi R. ALnowaimi, "A 5 Year Retrospective Study of 131I Therapy for Thyroid Cancer Practice in King Abdulaziz University Hospital." *International Journal of Physics*, vol. 4, no. 3 (2016): 69-73. doi: 10.12691/ijp-4-3-5.

1. Introduction

Therapeutic Nuclear Medicine is a medical imaging branch that involves the usage of small amounts of radioactive material to treat many diseases; including cancer. Radioactive Iodine 131 is a β-emitting radionuclide with a physical half-life of 8.1 d; a principal γ-ray of 364 KeV; and a principal β-particle with a maximum energy of 0.61 MeV, an average energy of 0.192 MeV, and a range in tissue of 0.8 mm. It is an isotope of iodine used in the treatment of residual of thyroid after a complete or a partial thyroidectomy [1]. The purpose of the treatment is usually to distort the normal and cancerous thyroid tissue. Oral administration of I-131 has been a commonly accepted procedure for treatment of conditions of the thyroid since the 1940s [1].

Thyroid malignancies vary in incidence worldwide with a rising trend over the last 20 years. According to the Saudi Cancer Registry report of 2007, thyroid cancer comprised 9.9% of female malignancies ranking second to breast. Males, however, had a lower incidence at 6.4% making it the 4th most common cancer. Regarding age, thyroid cancer ranked the 1st among patients aged 15-29. The mean age for diagnosis was 43 years among males and 37 years among females [2].

Types of thyroid cancer are classified according to cell of origin into follicular and para-follicular. Follicular malignancies include papillary (which is the most common) followed by follicular and anaplastic cancers. Para-follicular malignancies include medullary thyroid cancer, which is a rare subtype [3].

The most widely used modality for treatment of differentiated thyroid cancers, include subtotal thyroidectomy followed by radioactive ablation of the gland remnants or any metastatic foci [4,5].

The 1st published use of radioactive iodine was in 1948, and since then, it has been increasing dramatically. However, there are no clear guidelines pertaining to the optimum dose used for treatment [6].

Selection of doses can be either empirically or by dosimetry [7,8]. The efficacy of therapy is directly related to tumor uptake, which depends on cell differentiation and inversely related to tumor stage and grade [9].

Activities between 50 mCi- 200 mCi are the most commonly used [7]. However, a meta-analysis revealed that the dose does not change efficacy on the condition

that the tumor cells are well differentiated, making a lower dose more favorable to decrease toxicity [10].

Activity of the radioactive iodine dose administrated varies; the common method is according to the estimated size of the thyroid gland and the result of the radioactive iodine uptake RAIU. The purpose of the treatment also plays a role in the selection of the activity of radioiodine administrated; for the postoperative ablation of thyroid 75-150 mCi are typically used, for the treatment of presumed thyroid cancer in the neck or mediastinal lymph nodes activity of 150-200 mCi is administrated, for the treatment of distant metastasis administration of radioactive iodine of activity more than 200 mCi [1].

This paper audits the records of 100 cases with histologically proven thyroid cancer during 2005-2010 at King Abdulaziz University Hospital (KAUH) Jeddah. Age, sex, and referring department have also been presented. We also report the doses of radioactive Iodine used for the treatment and relate it to the type of thyroid cancer.

2. Methodology

The medical records of patients diagnosed with thyroid cancer in king Abdulaziz university hospital between January 2005 and December 2010 were reviewed retrospectively. All in-patients were included in the study. One hundred (100) cases were admitted during this time period. Data comprised of type of thyroid cancer along with age, gender, referring department and dose of RAI received to patients. Data analysis was done using SPSS version 20.0. Chi-square test was applied for categorical data represented as frequencies and percentages. P-value < 0.05 was used as a significance level.

3. Results

One hundred (100) medical records were reviewed. Of these, 70% patients were females and 30% were males with a female to male ratio of 2.3:1. Median age for the females was 42.5 years, and for males 43.5 years. Thirty-three (33%) patients had a papillary carcinoma, three (3%) had follicular carcinoma, (1%) had Hurtle cell tumors, twenty-five (25%) patients had tumors with non-specified histology, 22 (22%) patients had other types, as medullary thyroid carcinoma and lymphoma, and 16 (16%) patients had undifferentiated neoplasms. The pediatric age group comprised 5% of the sample population.

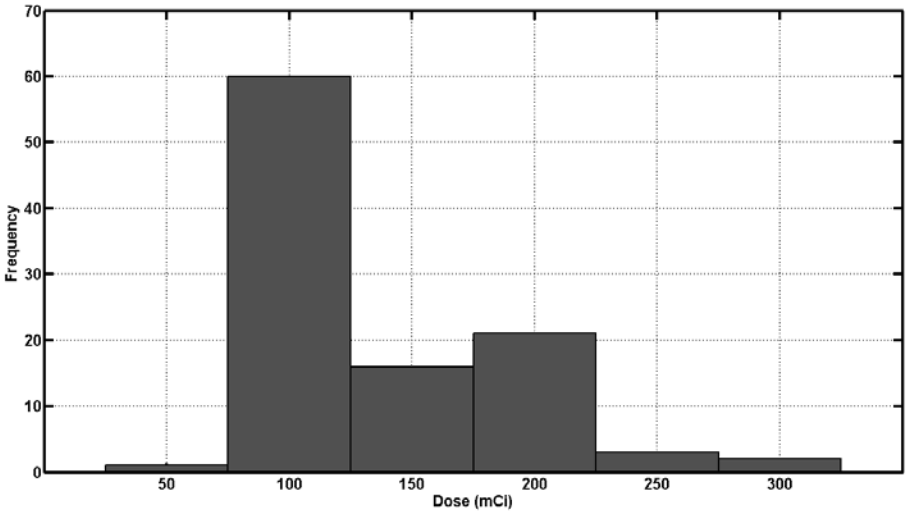

Figure 1. Activity range used

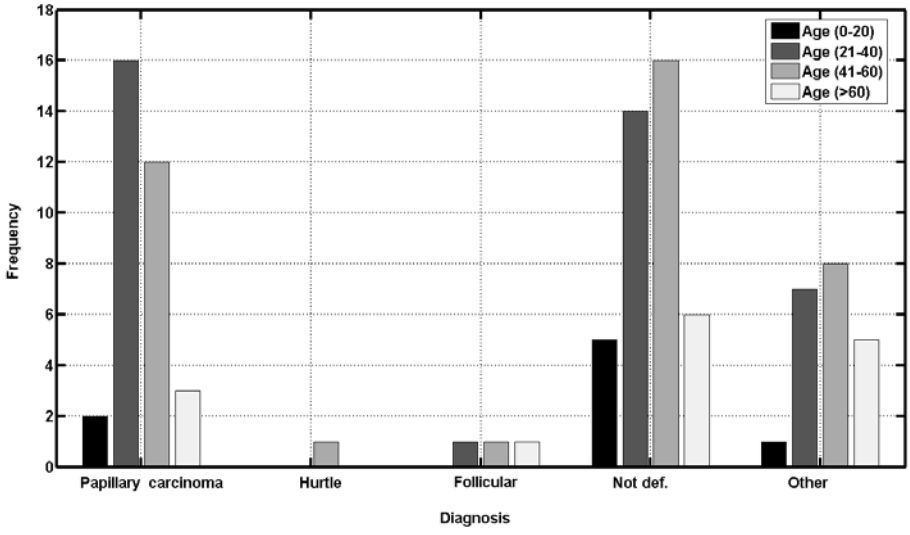

Figure 2. Diagnosis according to age

Activities administered ranged from 50 to 300 mCi with the majority (61%) receiving a dose of 100 (Figure 1) regardless of their age group, gender, or diagnosis. A dose of 300 was only used in papillary cancers. For follicular and hurtle cell tumors, only a dose of 100 was administered. Patients less than 20 years did not receive doses that exceeded 200, and patients aged 60 years and older were more likely to receive a dose of 200 than their younger counterparts.

Papillary carcinoma occurred most frequently between the ages 21-40 (Figure 2). It was also the commonest in both males and females (Figure 3).

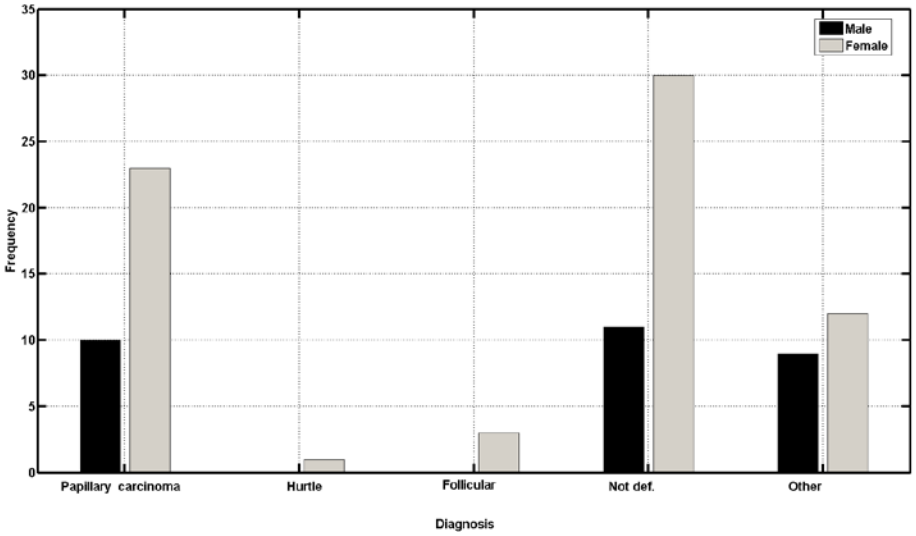

Figure 3. Diagnosis according to gender

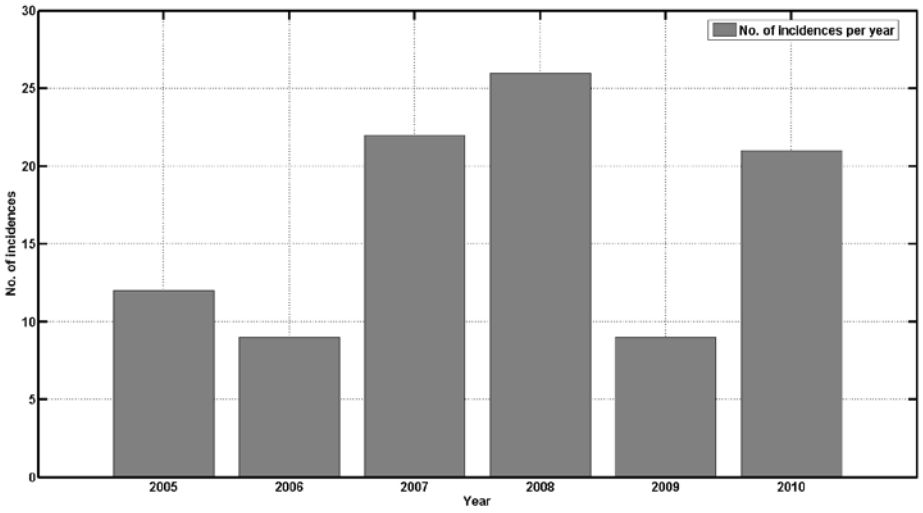

Figure 4. Disease incidences 2005-2010

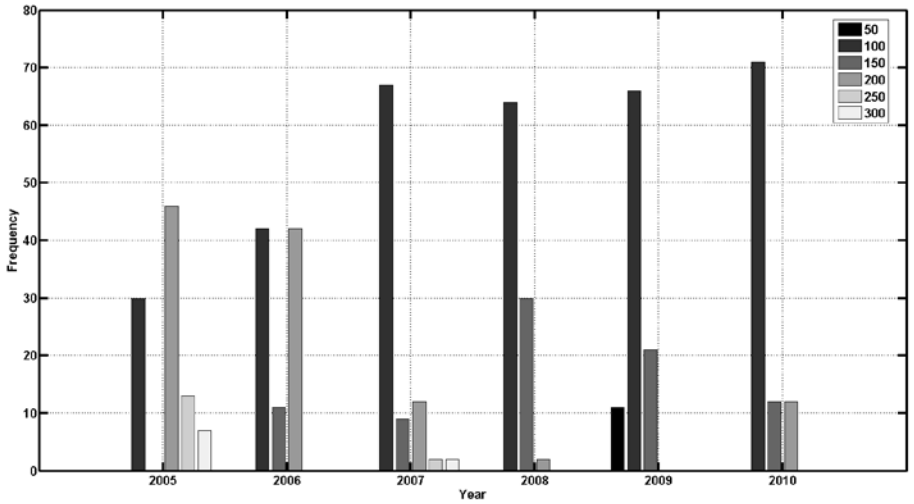

Figure 5. Activities throughout the years 2005-2010

The patterns of thyroid cancers throughout the five years of study shows that the incidence did not change drastically except for the years 2007 and 2009 (Figure 4).

During those years only 9 patients were diagnosed. Doses of 250 and more were not used beyond the year of 2007 (Figure 5).

The outcome of the treatment was that 3% of patients died, 4% had a recurrence, and 93% were alive and well. Those who died were all females with neoplasms of non-specified histology and no recurrence. All patients that died received a dose of 200. Their tumor type was not specified. All were females and none were recurrences.

Those who had a recurrence were also all females with papillary tumors. All were successfully treated by the time of the study with a second dose of RAI that exceeded their first by 50 mCi.

4. Discussion

Our study population demographics coincide with the expected distribution of thyroid malignancies; Being more common in females with a median age of 42.5 in females and 43.5 in males [11,12,13,14]. Our male: female ratio was 1:2.3 in concordance with other populations. However, male: female ratios as high as 1:7 has been reported [11]. In addition, a peak of 60-70 years for the incidence of these malignancies has been reported in male patients [15]. Studies that related gender and age to prognosis report that males tend to have a worse prognosis than women and that the pediatric age group tend to have recurrent cancers but better long-term survival [15,16]. In contrast, our study revealed that all patients who died as well as all those who had a recurrence were adult females. Similar to other populations, papillary carcinoma was the most common type with no variation with regard to age and sex (Figure 2 and Figure 3) [11,12,13,14]. Some of our patients had anaplastic tumors and still received RAI. The American Thyroid Association (ATA) does not recommend the unnecessary use of RAI in anaplastic tumors [17]. There is insufficient data that explains the use of RAI in our hospital for this type of tumor.

Activities administered were mostly 100 mCi, commonly used in other countries, with a range of 50-300 mCi (Figure 1) [4,5,9,11,12,13,14]. It has been suggested that for low risk malignancies, no or low doses of RAI are sufficient as it does not affect overall survival with the benefit of having lower or no toxicity [9,18-24]. In fact, doses as low as 30 mCi have been shown to be as effective as doses of 100mCi [25]. There is a trend towards lower doses and even outpatient use with regimens consisting of two 20-mCi doses [26]. In our hospital, doses of 250 and more were not used beyond the year of 2007. (Figure 5)

It has been proposed that success of treatment depends on adequate surgical removal and thyroid hormone suppression rather than RAI dose [20,21,22,23,24].

Our study did not reveal any change of dose in relation to age as reported elsewhere which can be attributed to the scarcity of studies relating the younger age groups to doses higher than 100 mCi due to ethical considerations [27]. Thyroid malignancies in the pediatric age group are in general better differentiated. The ATA recommends that doses given be adjusted to weight or surface area [25].

In conclusion our study did not reveal major changes in thyroid cancer incidence through 2005-2010 (Figure 4). Other studies have shown an increase incidence of thyroid cancers. It has been suggested that this is not a true increase but rather an increase in the discovery of asymptomatic papillary thyroid cancers due to better access to health care systems [28].

References

[1] Meier DA, Brill DR, Becker DV, Clarke SE, Silberstein EB, Royal HD, BalonHR. (2002). Procedure guideline for therapy of thyroid disease with (131)iodine. Journal of Nuclear Medicine.43(6):851-61

[2] Kingdom of Saudi Arabia Ministry of Health National Cancer Registry. Cancer incidence and survival report Saudi Arabia (2007). Available at: http://www.scr.org.sa/reports/SCR2007.pdf.

[3] Parthasarathy, KL, Crawford ES. (2002). Treatment of Thyroid Carcinoma: Emphasis on High-Dose 131I Outpatient Therapy. Journal of Nuclear Medicine Technology.30(4):165-71.

[4] Pacini F, Castanga MG, Brilli L, Pentheroudakis G. (2010). Thyroid cancer: ESMO Clinical Practice Guidelines for diagnosis, treatment and follow-up. Annals of Oncology. 21(5): v214-19.

[5] Hoelzer S, Steiner D, Bauer R, Reiners C, Farahati J, Hundahl SA, Dudeck J. (2000). Current practice of radioiodine treatment in the management of differentiated thyroid cancer in Germany. Europian Journal of Nuclear Medicine. 27(10):1465-72.

[6] Seidlin SM, Oshry E, Yalow AA 1948 Spontaneous and experimentally induced uptake of radioactive iodine in metastases from thyroid carcinoma; a preliminary report. TheJournal of Clinical Endocrinology & Metabolism.8:423-432.

[7] Nostrand, DV, Wartofsky L. (2007). Radioiodine in the Treatment of Thyroid Cancer.Endocrinology and Metabolism Clinics of North America.36(3):807-22.

[8] Dorn R, Kopp J, Vogt H, Heidenreich P, Caroll RG, Gulec SA. (2003). Dosimetry-Guided Radioactive Iodine Treatment in Patients with Metastatic Differentiated Thyroid Cancer: Largest Safe Dose Using a Risk-Adapted Approach. The Journal of Nuclear Medicine. 44(3): 451-56.

[9] Carballo M, Quiros RM. (2012). Review Article: To Treat or Not to Treat: The Role of Adjuvant Radioiodine Therapy in Thyroid Cancer Patients. Journal of Oncology.(2012):1-11.

[10] Valachis A, Nearchou A. (2012).High versus low radioiodine activity in patients with differentiated thyroid cancer: A meta-analysis. ActaOncologica. 0(0):1-8.

[11] Ogbera, AO. (2010). A two-year audit of thyroid disorders in an urban hospital in Nigeria.Nigerian Quarterly Journal of Hospital Medicine. 20(2): 81-5.

[12] Abdullah M. (2002). Thyroid cancer: The Kuala Lumpur experience. The New Zealand Journal of Surgery.72(9):660-4.

[13] Gkountouvas A, Nikas M, Chatjimarkou F, Thomas D, Georgiadis P, Kaldrimidis P. (2010). Thyroid cancer in Greece.A tertiary center experience. Journal of Balkan Union of Oncology. 15(4):674-8.

[14] Shields JA, Farringer JL Jr. (1977). Thyroid cancer. Twenty-three years' experience at Baptist and St. Thomas Hospitals. The American Journal of Surgery. 133(2): 211-5.

[15] Hsieh SH, Chen ST, Hsueh C, Chao TC, Lin JD. (2012). Gender-Specific Variation in the prognosis of papillary thyroid cancer TNM stages II to IV. International Journal of Endocrinology. 2012 (2012): Article ID 379097, 5 pages.

[16] Jonklaas J, Nogueras-Gonzalez G, Munsell M, Litofsky D, Ain KB, Bigos ST, Brierley JD, Cooper DS, Haugen BR, Ladenson PW, Magner J, Robbins J, Ross DS, Skarulis MC, Steward DL, Maxon HR, Sherman SI; National Thyroid Cancer Treatment Cooperative Study Group. (2012). The impact of age and gender on papillary thyroid cancer survival. The Journal of Clinical Endocrinology & Metabolism. 97(6):E878-87.

[17] Smallridge RC, Ain KB, Asa SL, Bible KC, Brierley JD, Burman KD, Kebebew E, Lee NY, Nikiforov YE, Rosenthal MS, Shah MH, Shaha AR, Tuttle RM. (2012). American Thyroid Association Guidelines for Management of Patients with Anaplastic Thyroid Cancer. Thyroid. 22(11); 1104-1139.

[18] Haymart DG, Stewart AK, Griggs JJ, Banerjee M. (2013). Disease Severity and Radioactive Iodine Use for Thyroid Cancer. The Journal of Clinical Endocrinology & Metabolism. 98(2): 678-686.

[19] Grünwald F, Ruhlmann J, Ammari B, Knopp R, Hotze A, Biersack HJ. (1988). Experience with a high-dose therapy concept in metastatic differentiated thyroid cancer. Nuklearmedizin. 27(6):266-71.

[20] Schvartz C, Bonnetain F, Dabakuyo S, Gauthier M, Cueff A, Fieffé S, Pochart JM, Cochet I, Crevisy E, Dalac A, Papathanassiou D, Toubeau M. (2012). Impact on overall survival of radioactive iodine in low-risk differentiated thyroid cancer patients.The Journal of Clinical Endocrinology & Metabolism. 97(5): 1526-35.

[21] Sacks W, Fung CH, Chang JT, Waxman A, Braunstein GD. (2010). The effectiveness of radioactive iodine for treatment of low-risk thyroid cancer: a systematic analysis of the peer-reviewed literature from 1966 to April 2008. Thyroid. 20(11):1235-45.

[22] Barbesino G, Goldfarb M, Parangi S, Yang J, Ross DD, Daniels GH. (2012). Lobe ablation with radioactive iodine as an alternative to completion thyroidectomy after hemithyroidectomy in patients with follicular thyroid cancer: long-term follow-up. Thyroid. 22(4):369-76.

[23] Ibrahimpasic T, Nixon IJ, Palmer FL, Whitcher MM, Tuttle RM, Shaha A, Patel SG, Shah JP, Ganly I. (2012). Undetectable thyroglobulin after total thyroidectomy in patients with low- and intermediate-risk papillary thyroid cancer--is there a need for radioactive iodine therapy?.Surgery. 152(6):1096-105.

[24] Afroz S, Ahmed K, Yasmeen S, Ahmed F, Nisa L. (1992). Role of radioiodine in management of thyroid cancer: experience with 70 cases. Bangladesh Medical Research Council Bulletin. 18(2): 68-71.

[25] Cooper DS, Doherty GM, Haugen BR, Kloos RT, Lee SL, Mandel SJ, Mazzaferri EL, McIver B, Pacini E, Schlumberger M, Sherman SI, Steward DL, Tuttle RM. (2009). Revised American Thyroid Association Management Guidelines for Patients with Thyroid Nodules and Differentiated Thyroid Cancer. Thyroid. 19(11); 1167-1214.

[26] Clerc J. Bienvenu-perrard M. Pichard de Malleray C. Dagousset F. Delbot T. Dreyfuss M. Groussin L. Marlowe RJ, Leger FA. Chevalier A. (2012) Outpatient thyroid remnant ablation using repeated low I131 iodine activites (740 MBq/20mCi * 2) in patients with low-risk differentiated thyroid cancer. Journal of Clinical Endocrinology and Metabolism. 97:871-80

[27] Van Nostrand D, Atkins F. (2011).Pediatric Differentiated Thyroid Cancer: Can the Prescribed Activity of I-131 Be Increased? The Journal of Clinical Endocrinology & Metabolism. 96(8):2401-2403

[28] Morris LGT, Sikora AG, Tosteson TD, Davies L. (2013). The Increasing Incidence of Thyroid Cancer: The Influence of Access to Care. Thyroid. 23(7); 885-891.

International Journal of Physics, 2016, Vol. 4, No. 4, 74-77
Available online at http://pubs.sciepub.com/ijp/4/4/1

DOI:10.12691/ijp-4-4-1

A Theoretical Study of the Atomic Properties for Subshells of N^+ and O^{+2} Using Hartree-Fock Approximation

Hayder Ali Abd Alabas*, Qassim Shamkhi AL-Khafaji, Abbas Hassan Raheem

Department of physics, Faculty of Sciences, Kufa University, Iraq
*Corresponding author: hydar40@yahoo.com

Abstract In this research, we calculated the atomic properties of systems have been studied (N^+ and O^{+2}) for intra-shells (1s, 2s and 2p) using Hartree-Fock wave function. These properties included, one-particle radial density function, one-particle and inter-particle expectation values, inter-particle density function and expectation values of energies. All these atomic properties increase with atomic number, have highest values in 1s shell and lowest values in 2p shell. All results are obtained numerically by using the computer program (MathCad 14) because it able to calculation and plot functions. All atomic properties are calculated in atomic units.

Keywords: *Hamiltonian operator $\hat{H}$, wave function ψ, Approximation methods, multi-electron systems and Hund's rules*

Cite This Article: Hayder Ali Abd Alabas, Qassim Shamkhi AL-Khafaji, and Abbas Hassan Raheem, "A Theoretical Study of the Atomic Properties for Subshells of N^+ and O^{+2} Using Hartree-Fock Approximation." *International Journal of Physics*, vol. 4, no. 4 (2016): 74-77. doi: 10.12691/ijp-4-4-1.

1. Introduction

The Hartree-Fock Self-Consistent Field approximation (HF-SCF), it is a good approximation to many-electron systems, which is described by wave function. The essence of HF-SCF approximation is to replace the complicated many-electron problem by a one-electron problem in which electron-electron repulsion is treated in an average way [1]. The approximation is based on two grounds, first, each electron moves in the potential field of the nucleus plus the N-1 other electrons (central field approximation) that mean the electrons move independently [2]. The second must on initial wave function consistent with final it when inter in the calculation. The wave functions $\psi(x_i)$ where x_i spin orbitals included four quantum number (n, l, m_l, m_s), using in the calculation obey on Pauli exclusion principle, so consequently the wave function antisymmetric when two electrons exchange their locations.

2. Theory

In order to wave function satisfy the antisymmetric principle have to have written as slater determinant which named after John C. Slater [3].

$$\Psi_{HF}(x_1, x_2, ..., x_N) = (N!)^{-\frac{1}{2}} \begin{vmatrix} \varphi_i(x_1) & \cdots & \varphi_j(x_1) \\ \vdots & \ddots & \vdots \\ \varphi_i(x_N) & \cdots & \varphi_j(x_N) \end{vmatrix}. \quad (1)$$

Slater created such a basis set of functions known as the slater-type orbitals (STO's), which written [4].

$$\gamma_{nlm}(r, \theta, \varnothing) = R_{nl}(r) Y_{l,ml}(\theta, \varnothing) \quad (2)$$

Where $R_{nl}(r)$ represented radial part of the wave function and its given as [5].

$$R_{nl}(r) = N_{nlm_l} S_{nl}(r) \quad (3)$$

N_{nlm_l} Normalized constant and written as

$$N = \frac{(2\xi)^{n+\frac{1}{2}}}{((2n)!)^{\frac{1}{2}}} \quad (4)$$

$$S_{nl}(r) = r^{n-1} \exp(-\xi r) \quad (5)$$

Where n principle quantum number, r is the distance of the electron from the atomic nucleus, $Y_{l,ml}$ is spherical harmonic, (ξ) the orbital exponent.

The Hartree-Fock spin orbitals can be described as a linear combination of slater orbitals from the function called basis functions written as [6].

$$\varphi_{HF} = \sum_{i=0}^{k} c_i \gamma_i \quad (6)$$

Where c_i represent the constant coefficient and γ_i is the slater orbitals.

The two-particle density $\Gamma(x_m, x_n)$ contains all of the information necessary to calculate the energy and many properties of the atom or ion [7]. Written as

$$\varphi_{HF} = \sum_{i=0}^{k} c_i \gamma_i$$

$$\Gamma_{HF}(x_m, x_n) = \frac{N(N-1)}{N} \iiint |\psi_{(x_m, x_n, x_p, \ldots x_q)}|^2 \, dx_p \ldots dx_q \quad (7)$$

Where x_n represents the combined space and spin coordinate of electron n and $dx_p \ldots dx_q$ indicates integration summation over all N-electron except m and n.

The two-particle radial density function $D(r_1, r_2)$ it is probability density of finding the electron 1 at r_1 and electron 2 at r_2 from nucleus simultaneously written as [8]

$$D(r_1, r_2) = \iint \Gamma(r_1, r_2) r_1^2 r_2^2 d\Omega_1 d\Omega_2 d\sigma_1 d\sigma_2 \quad (8)$$

The one-particle radial density function $D(r_1)$ it is the probability density function of finding an electron at a distance r_1 and $r_1 + dr_1$ from the coordinate origin (i.e. nucleus) written as [9].

$$D(r_1) = \int_0^\infty D(r_1, r_2) dr_2. \quad (9)$$

The one-particle expectation value $\langle r_1^n \rangle$ can be calculated from the following equation [10].

$$r_1^n = \int_0^\infty r_1^n D(r_1) dr_1. \quad (10)$$

Standard deviation Δr_1 it is spead out or difference in the expectation value written as [11]

$$\Delta r_1 = \left[\left\langle r_1^2 \right\rangle - \left\langle r_1^2 \right\rangle \right]^{1/2}. \quad (11)$$

The inter-particle distribution function $f(r_{12})$ it is the probability density function of finding the electron 1 and electron 2 at the distance between r_{12} and $r_{12} + dr_{12}$ written as [12]

$$f(r_{12}) = \int \Gamma(r_1, r_2) dr_2 dr_1 \quad (12)$$

The inter–particle expectation value $\langle r_{12}^n \rangle$ It is given by [13]

$$\left\langle r_{12}^n \right\rangle = \int_0^\infty r_{12}^n f_{(r_{12})} dr_{12} \quad (13)$$

Standard deviation Δr_{12} it is defined as [14].

$$\Delta r_{12} = \left[r_{12}^2 - {r_{12}}^2 \right]^{1/2} \quad (14)$$

The expectation value of total energy for the system written by equation

$$E = \left\langle \hat{H} \right\rangle = -\langle T \rangle + -\langle V_{en} \rangle + \langle V_{ee} \rangle \quad (15)$$

Where T kinetic energy, V_{en} electron-nucleus attraction energy and V_{ee} electron-electron repulsion energy.

$$\langle V_{en} \rangle = -Z \left\langle r_1^{-1} \right\rangle \quad (16)$$

$$\langle V_{ee} \rangle = \left\langle r_{12}^{-1} \right\rangle \quad (17)$$

From condition of the virial theorem [15]. The energy expectation value of total energy is related to expectation value of potential energy.

$$\langle E_T \rangle = \frac{1}{2} \langle V_T \rangle = -\langle T \rangle. \quad (18)$$

3. Results and Discussion

Table 1 and Table 2 have contained the results of one-particle distribution function $D(r_1)$ and the inter- particle distribution function $f(r_{12})$ respectively. $D(r_1)$ and $f(r_{12})$ increases when atomic number Z increase because the distance between electrons and nucleus in 1s shell is smallest as well as the distance between electrons as a Figure 1, Figure 2. The greatest value of $D(r_1)$ in 1s shell and smallest value in 2p shell. From Figure 1 when r_1=0 or ∞, $D(r_1)$=0, that means the probability of finding the electron inside the nucleus or far away from it equal zero. We noted two peaks of $D(r_1)$ for 2s shell, the first peak represented the probability of finding the electron in 1s shell due to penetration phenomenon and the second peak represented the probability of finding the electron in 2s shell. The largest value of $f(r_{12})$ in 1s shell for each system as a Figure 2. From Figure 2 when r_{12}=0 or ∞, $f(r_{12})$ =0 that means the probability of finding two electrons in the same position or too far away from each other equal zero.

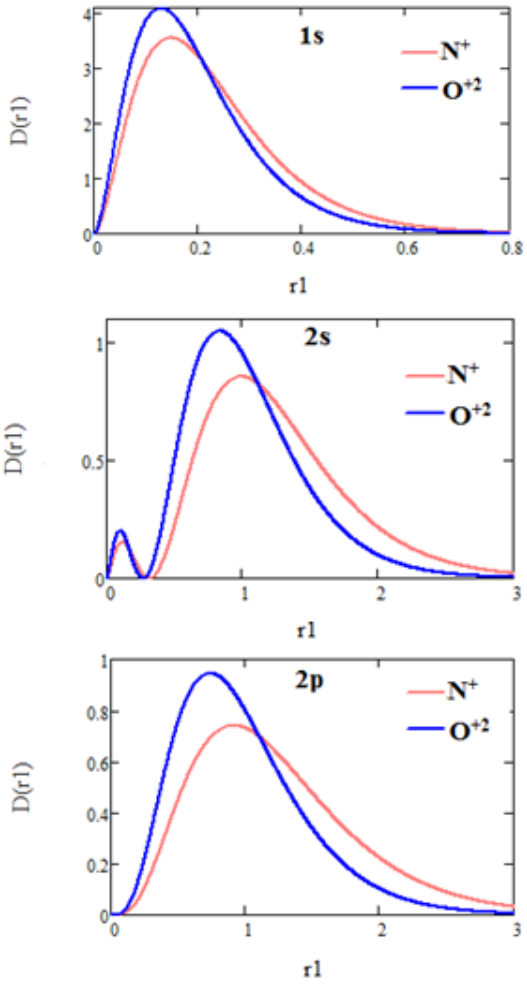

Figure 1. The relation between one-particle radial density distribution function and location for each system

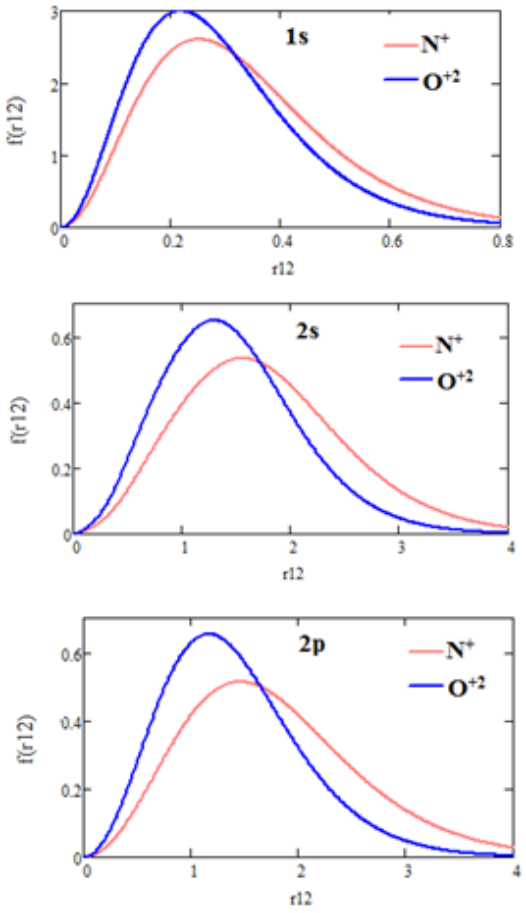

Figure 2. The relation between inter-particle distribution function and location for each system

Table 1. The maximum values of the one-particle distribution function and corresponding location r_1 for each system

Shell	N^+		O^{+2}	
	r_1	$D(r_1)$	r_1	$D(r_1)$
1s	0.149	3.5506	0.1295	4.0873
2s	0.995	0.85549	0.8383	1.0493
2p	0.9184	0.74078	0.7397	0.94572

Table 2. The maximum values of the inter-particle distribution function and corresponding location for each system

Shell	N^+		O^{+2}	
	r_{12}	$f(r_{12})$	r_{12}	$f(r_{12})$
1s	0.2515	2.6028	0.2179	2.9971
2s	1.5496	0.53358	1.2904	0.64889
2p	1.4508	0.51315	1.1614	0.65307

Table 3. The one-particle expectation values $\langle r_1^n \rangle$ where (n=-1,1,2) and standard deviation for each system

Shell		N^+	O^{+2}
1s	$\langle r_1^{-1} \rangle$	6.65657	7.65037
	$\langle r_1^{1} \rangle$	0.22808	0.19821
	$\langle r_1^{2} \rangle$	0.07009	0.05289
	Δr_1	0.13442	0.11661
2s	$\langle r_1^{-1} \rangle$	1.14084	1.38855
	$\langle r_1^{1} \rangle$	1.25284	1.03371
	$\langle r_1^{2} \rangle$	1.87455	1.26794
	Δr_1	0.55221	0.44653
2p	$\langle r_1^{-1} \rangle$	1.05597	1.31909
	$\langle r_1^{1} \rangle$	1.24366	0.98447
	$\langle r_1^{2} \rangle$	1.93255	1.19954
	Δr_1	0.62118	0.47996

Table 3 and Table 4 have contained the one-particle $\langle r_1^n \rangle$ and inter-particle $\langle r_{12}^n \rangle$ expectation values and standard deviation. When $n = -1$ the expectation values increase when the atomic number increase and the highest value of $\langle r_1^{-1} \rangle$ in 1s shell and lowest value in 2p shell. When $n = 1,2$ the expectation values decrease when Z increase. The highest value in 2s shell and lowest value in 1s shell.

Table 4. the inter-particle expectation values $\langle r_{12}^n \rangle$ where (n=-1,1, 2) and standard deviation for each system

Shell		N^+	O^{+2}
1s	$\langle r_{12}^{-1} \rangle$	4.12789	4.74807
	$\langle r_{12}^{1} \rangle$	0.33334	0.28964
	$\langle r_{12}^{2} \rangle$	0.14018	0.10577
	Δr_{12}	0.17047	0.14793
2s	$\langle r_{12}^{-1} \rangle$	0.72448	0.87655
	$\langle r_{12}^{1} \rangle$	1.7744	1.46203
	$\langle r_{12}^{2} \rangle$	3.74909	2.53585
	Δr_{12}	0.77499	0.63112
2p	$\langle r_{12}^{-1} \rangle$	0.73785	0.92953
	$\langle r_{12}^{1} \rangle$	1.78177	1.40714
	$\langle r_{12}^{2} \rangle$	3.86509	2.39905
	Δr_{12}	0.83088	0.64731

The standard deviation Δr_1 and Δr_{12} decrease when atomic number increase because decrease the distance between electrons and between electrons and nucleus. in addition, the largest value of Δr_1 in 2p shell and smallest value in 1s shell for each system.

Table 5. The expectation values for all attraction, repulsion, kinetic and total energies of intra-shells for each system.

Shell		N^+	O^{+2}
1s	$-\langle V_{en} \rangle$	79.87884	91.80444
	$\langle V_{ee} \rangle$	4.12789	4.74807
	$-\langle V_T \rangle$	75.75095	87.05637
	$\langle T \rangle$	37.87548	43.52819
	$-\langle E_T \rangle$	37.87548	43.52819
2s	$-\langle V_{en} \rangle$	13.69008	16.6626
	$\langle V_{ee} \rangle$	0.72448	0.87655
	$-\langle V_T \rangle$	12.9656	15.78605
	$\langle T \rangle$	6.4828	7.89302
	$-\langle E_T \rangle$	6.4828	7.89302
2p	$-\langle V_{en} \rangle$	12.67164	15.82908
	$\langle V_{ee} \rangle$	0.73785	0.92953
	$-\langle V_T \rangle$	11.93379	14.89955
	$\langle T \rangle$	5.9669	7.44978
	$-\langle E_T \rangle$	5.9669	7.44978

Table 5 contained the results of expectation of energies which increase when atomic number increase. They have highest value in 1s shell and lowest value in 2p shell.

4. Conclusions

When to increase the atomic number, the one-particle distribution function, the inter-particle distribution function and the expectation values of energies are increased. These properties have highest values in 1s shell and lowest values in 2p shell. When r_1=0 or ∞ and r_{12}=0 or ∞ , D (r_1)=0 and $f(r_{12})$=0 respectively. For expectation values $\langle r_1^n \rangle$, $\langle r_{12}^n \rangle$, where $n = -1$ increase when Z increase and the highest of $\langle r_1^{-1} \rangle$ in 1s shell. While when

$n = 1,2$ the expectation values decrease when Z increase and lowest value in 1s shell.

References

[1] Szabo and N.S. Ostlund, "Modern Quantum Chemistry Introduction to Advanced Electronic Structure Theory", Dover Publications, INC., New York, 1989.

[2] I. N. Levine, "Quantum chemistry", *Prentice-Hall, Inc. New Jersey*. 2000.

[3] J. c. Slater, "Quantum theory of atomic structure." McGRAW-HILL BOOK COMPANY, INC., New York, 1960.

[4] Q. S. Alkafaji, S. K. AL-Shebly, H. H. Bilal, and N. H. Ali, *J. Adv. Phys.*, Vol. 5, pp. 1-4, 2016.

[5] B. H.Al-Asaad, S. A.Hasson and K. H.Al-Bayati, *J. Um-Salama Sceience* Vol. 4, No. 3, pp. 393-396, 2007.

[6] K.H.AL-bayati, K. A. Mohammed and K.O.AL-baiti, *J.Um-Salama Sceience*, Vol. 2, No. 2, pp. 317-326, 2005.

[7] R. J. Dosh, *J. Kufa of Physics*, Vol. 6, No. 1, pp. 107-111, 2014.

[8] H. Matsuyama and T. Koga, *Theor. Chem. Acc.*, Vol. 118, pp. 643-647, 2007.

[9] T. Oyamada, K. Hongo, Y. Kawazoe, and H. Yasuhara (2010) J. of Chem. Phys., Vol. 133.

[10] Koga et al. (1999) J. Chem. Phys., Vol. 110, No. 12, pp. 5763-5771.

[11] K. H. AL-bayati, A.K. Ahmed and N.CH.AL-Tamimei, *J.Um-Salama Sceience*, Vol. 3, No. 2, pp. 246-253, 2006.

[12] C. A. Coulson and A. H. Neilson, *Proc. Phys. Soc.*, Vol. 78, pp. 831-837, 1961.

[13] R. J. Boyd and C. A. Coulson, *J. Phys. B At. Mol. Phys.*, Vol. 6, pp. 782-793, 1973.

[14] R. J.Dosh and Q. S. AL-Kafaji, *J. Kufa of Physics*, Vol. 5, No. 1, pp. 91-102, 2013.

[15] C. L. Ladera and E. Alomá, *Lat. Am. J. Phys. Educ.*, Vol. 4, No. 2, pp. 260-266, 2010.

International Journal of Physics, 2016, Vol. 4, No. 4, 78-84
Available online at http://pubs.sciepub.com/ijp/4/4/2

DOI:10.12691/ijp-4-4-2

Stability of Dissipative Optical Solitons in the 2D Complex Swift-Hohenberg Equation

P. Yoboue[1], A. Diby[2], O. Asseu[1,3,*], A. Kamagate[1]

[1]Ecole Supérieure Africaine des Technologies d'Information et de Communication (ESATIC), Abidjan, Côte d'Ivoire
[2]Université Félix Houphouët Boigny, Abidjan, Côte d'Ivoire
[3]Institut National Polytechnique Félix Houphouët Boigny (INP-HB), Yamoussoukro, Côte d'Ivoire
*Corresponding author: oasseu@yahoo.fr

Abstract This article deals with stationary localized solutions of the (2D) two-dimensional complex Swift-Hohenberg equation (CSHE). Our approach is based on the semi-analytical method of collective coordinate approach. According to the parameters of the equation and a suitable choice of ansatz, the stationary dissipative solitons of the 2D CSHE equation are mapped. This approach allows to describe the influence of the parameters of the equation on the various physical parameters of the pulse and their dynamics. Finally, the major impact of spectral filtering terms on the dynamic of the solitons is demonstrated.

Keywords: *dissipative soliton, spatio-temporal, collective coordinate approach, Ginzburg-Landau equation, complex Swift-Hohenberg equation, spectral filtering*

Cite This Article: P. Yoboue, A. Diby, O. Asseu, and A. Kamagate, "Stability of Dissipative Optical Solitons in the 2D Complex Swift-Hohenberg Equation." *International Journal of Physics*, vol. 4, no. 4 (2016): 78-84. doi: 10.12691/ijp-4-4-2.

1. Introduction

Since several years, the stability domain of the spatio-temporal dissipative soliton self-confined in the temporal and spatial dimensions remains a serious issue of nonlinear optics [1]. The choice of relevant nonlinearity for such self-confinement and ensure a stable solution are thorny. Furthermore, the relation between the dimensionality and nonlinear effect used is especially essential.

It should be specified that dissipative systems in nonlinear optics admit stable solitons in one, two, and three dimensions [2]. These solitons can also be purely temporal, spatial or spatio-temporal. Dissipative soliton has been widely studied in nonlinear dissipative optics, from fundamental point of view and due to the clear physical meaning in particular application. Important applications are passively mode-locked laser systems and optical transmission lines.

Indeed, the formation of this dissipative structure is much more complex than that of conservative systems, because in addition to the right balance between the dispersion and the nonlinearity, dissipative solitons exchange energy and (or) matter with an external source. They exist only when there is a continuous energy supply to the system. Whenever the energy supply is stopped, soliton "stops living." Their shape, amplitude, velocity are all fixed and defined by the parameters of the system [3] rather than by the initial condition.

The properties and conditions of their existence have been studied extensively [4,5]. The theoretical study of these soliton has recently received a boost during the past decade leading to an impressive number of works in several fields of nonlinear science [4,6,7,8]. However most of these stable soliton solutions studies use purely numerical approaches [9,10]. Solving numerically the equation for a given set of parameters and a given initial condition is an extremely lengthy and costly procedure, which can take up to several days in a standard PC.

Alternative variational semi-analytical methods can overcome this difficulty [11]. These theoretical tools can perceive soliton solutions more efficiently and envisage their domains of existence with relative flexibility [12,13,14].

Recently, it has been demonstrated in our previous works that the collective variable approach [15] is a useful tool and reduces significantly the computation time for predicting approximately the domains of existence of stable light bullets in the parameter space of the (3D) complex cubic-quintic Ginzburg-Landau equation [13].

This present work provides evidence for the stationary solutions of the (2D) complex Swift-Hohenberg equation, which, to our knowledge has not been enough reported in the literature. This equation is useful in the description of the dynamics of dissipative solitons in laser cavity in experimental situations.

2. Materials and Methods

2.1. Theory of dissipative Soliton in Swift-Hohenberg System

One of the main properties of wave is that they tend to spread out as they evolve. The principal cause for this is that distinct frequency; that are superposed to create the wave packet, propagate with different velocities and (or)

in different directions. It knows that generally the nonlinear effects accelerate the spreading of the wave. Nevertheless, under certain conditions, nonlinearity may compensate the linear effects. The resulting balanced localized pulse or beam of light, which propagates without decay, is generally known as soliton. Therefore, optical solitons are localized waves that propagate stably in nonlinear media with dispersion, diffraction or both.

Originally, the terminology soliton was reserved for conservative systems and particular set of integrable solutions existing as a result of the delicate balance between dispersion (diffraction) and nonlinearity.

However, similar classes of stable self-sustained structures can be found for a wide range of physical systems far from equilibrium. The term dissipative system has been used by Nicolis and Prigogine [16] to describe these systems far from equilibrium. As a new paradigm of nonlinear waves, solitons in real dissipative environments are known as dissipative soliton [4]. The dissipative soliton has different characteristics than those of conservative systems. They are attracting a significant surge of research activities on their spatial (temporal) complexity during the last years, particularly for systems modelled by the cubic quintic complex Ginzburg-Landau equations [4,5]. Apart from the balance between dispersion (diffraction) and nonlinearity, the separate balance between gain and loss is essential for the pattern formation of the dissipative soliton. This second balance is very crucial, and gives the dissipative soliton a markedly different dynamic from that of conservative solitons. The shape, amplitude and widths of the dissipative soliton are fixed, depend drastically on the system parameters [17] and may evolve stationary, periodically, or even chaotically [10,18,19]. One of the generic equations describing the dynamics of dissipative solitons and that we have intensely studied is the complex Cubic-quintic Ginzburg-Landau equation model [4,20,21]. This equation could be applied to the modeling of a wide-aperture laser cavity with a saturable absorber in the short pulse regime of operation. The model includes the effects of two-dimensional transverse diffraction of the beam, longitudinal dispersion of the pulse, and its evolution along the cavity. The spectral filter of this model is restricted to the term of second order and can only describe a spectral response with a single maximum.

However, experiences indicate that the gain spectrum is usually wide and can have multiple peaks.

To be more realist we need to add others terms of higher-order spectral filtering to the complex Cubic-quintic Ginzburg-Landau equation (CGLE), this lead to the complex Swift-Hohenberg equation (CSHE).

The complex Swift-Hohenberg equation is useful to describe soliton propagation in optical systems with linear and nonlinear gain and spectral filtering such as communication links with lumped fast saturable absorbers or fiber lasers with additive-pulse mode-locking or nonlinear polarization rotation. It is clear that the higher order of the spectral filter is extremely essential to analyze the generation of more complex impulse.

According to this equation, we will investigate the steady state of the 2D stationary solutions. It describes as well quantitatively as qualitatively many nonlinear effects which occur during the propagation and can be read in this normalized form [4,22]:

$$\psi_z - i\frac{D}{2}\psi_{tt} - i\frac{1}{2}\psi_{rr} - i\gamma|\psi|^2\psi - i\nu|\psi|^4\psi = \delta\psi + \varepsilon|\psi|^2\psi + \beta\psi_{tt} + \mu|\psi|^4\psi + \gamma_2\psi_{ttt} \quad (1)$$

where $\mu, \delta, \beta, D, \nu, \gamma, \gamma_2$and ε are real constants. Without the additive term $\gamma_2\psi_{ttt}$ this equation is the same as the CGLE one. The physical meaning of each term depends on the real problem which must be examined. In optics, this equation describes the laser systems [23,24], optical regeneration for optical fibre transmission systems with soliton signals [25], nonlinear cavities with an external pump [26] and the parametric Oscillator [27]. When applied to the propagation of the pulses in a laser system, as is the case in our study $\psi = \psi(r,t,z)$ represents the normalized optical envelope and is function of three real variables. With t the retarded time in the frame moving with the pulse, z is the propagation distance or the cavity round-trip number. And finally $\mathrm{r}\left(\mathrm{r} = \sqrt{\mathrm{x}^2 + \mathrm{y}^2}\right)$ represents the transverse coordinate, taking account of the spatial diffraction effects.

The left-hand side contains the conservative terms: namely, $D = +1(-1)$ which is for the anomalous (normal) dispersion propagation regime and ν which represents, if negative, the saturation coefficient of the Kerr nonlinearity. In the following, the dispersion is anomalous, and ν is kept relatively small. The right-hand-side of equation (1) includes all dissipative terms: $\delta, \varepsilon, \beta$ and μ are the coefficients for linear loss (if negative), nonlinear gain (if positive), spectral filtering (if positive) and saturation of the nonlinear gain (if negative), respectively. And finally γ_2 represents the higher-order spectral filter term, which is very important in this present study.

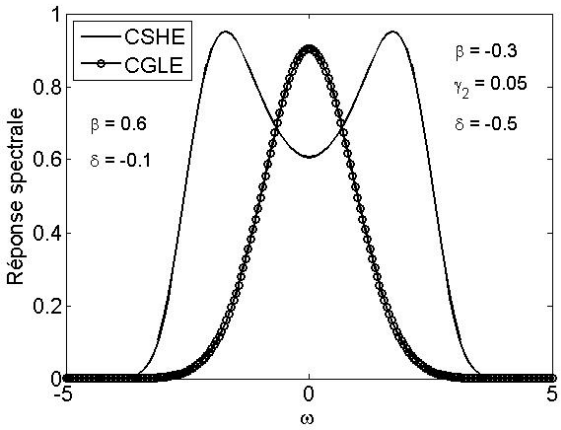

Figure 1. Evolution of the spectral response in the case of the complex Cubic-quintic Ginzburg-Landau equation (in circle) and of the complex Swift-Hohenberg equation (in solid curve). The other parameters appear inside the figure

In order to have stable pulses in the frequency domain, γ_2 must be positive and β can have both sign (positive or negative) contrary to the case of the CGLE equation where β must be strictly positive. If β is greater than zero, we obtain a spectral response with a single maximum, on the other hand (β less than zero) we have now two maxima. To support this comments, the effect of the spectral filter is shown in Figure 1. It is described by the following transfer function:

$$T(\omega) = exp\left(\delta - \beta\omega^2 - \gamma_2\omega^4\right). \quad (2)$$

The circle curve shows the spectral response in the case of the complex Cubic-quintic Ginzburg-Landau equation CGLE (with $\gamma_2 = 0$), it is a Gaussian curve with amplitude δ and width β. This curve has a single maximum. In the case of the complex Swift-Hohenberg equation (CSHE), the response of spectral filter is much affected and depends on three parameters with γ_2 positive. This situation gives a spectral response with two distinct maximums. In this work we will carefully investigate this situation where γ_2 is nonzero.

The parameter values are chosen according to that the width and height of the two spectral responses are not too different. However, as the spectral response is different, it goes without saying that the (2D) two-dimensional dissipative soliton in both case are different profiles for the same value of the cubic gain ε.

2.2. Stability Study

Our study, really, is to examine the stationary soliton of the 2D complex Swift-Hohenberg equation by semi-analytical approach, as far as we knew this has not been done previously. More specifically, our major goal is to provide an approximate mapping of the regions of existence of stable and unstable solutions in the parameter space of the equation (1), as we have done previously with the 3D complex Cubic-quintic Ginzburg-Landau equation one [13].

To achieve this goal, we use the collective variable approach, which helps to simplify the characterization of the pulse by use of a low dimensional equivalent mechanical system based on a finite number of degrees of freedom. Each degree of freedom can then be described by means of a coordinate called the *collective variable*. Indeed, the propagation of the pulse describes not only the pulse as a collective entity (localized in time and space) but also all other localized or non-localized excitations, such as noise or radiation, which are always more or less present in the real system. For a better understanding of these dynamic processes, it is important to develop analytical approaches to help to bring the dynamics of the pulse to that of a simple mechanical system with only a small number of degree of freedom.

The mean idea in the collective variable approach is to associate collective variables with the pulse's parameters of interest for which equations of motion may be derived. One may introduce N collective variables, z dependent; say X_i with$i = 1, 2, .., N$, in a way such that each of them can correctly describe a fundamental parameter of the pulse (amplitude, width, chirp …) [15,28]. To this end, one can decompose the field $\psi(x, y, t, z)$ in the following way:

$$\psi(r,t,z) = f(x_1, x_2, \ldots x_n, t) + q(z,t) \qquad (3)$$

where f the ansatz function is a function of the collective variables and is chosen to draw, at best, the configuration of the pulse. And $q(z,t)$ is a residual field that represents all other excitations in the system (noise, radiation, dressing field, etc.) [15]. The choice of the trial function that introduces the collective variables in the theory is important for the success of the technique. After choosing the ansatz function one can pursue the process of characterization of the pulse by neglecting the residual field. This approximation is called *the bare approximation* [15]. In this way one can consider the fact that the pulse propagation can be completely characterized that the ansatz function.

By neglecting the residual field ($q = 0$) *the bare approximation*, as is the case in most practical studies [10], we chose a Gaussian function as ansatz function that is given by the following:

$$f = A\exp\left(-\frac{t^2}{w_t^2} - \frac{r^2}{w_r^2} + \frac{i}{2}c_t t^2 + \frac{i}{2}c_r r^2 + ip\right). \qquad (4)$$

So, here we are assuming that all the pulses are purely Gaussian with spatial and temporal chirp and do not consider other forms of pulses.

In such case, the field is necessarily $\psi(r,t,z) = f$, with t, r the spatial and temporal variables along t and r axis respectively. A, w_t, w_r, c_t, c_r, and p represents the collective variables. Stands for soliton amplitude, $\sqrt{2ln2}\,w_t$ and $\sqrt{2ln2}\,w_r$ represent the temporal and spatial widths respectively. $c_t/(2\pi)$ is the parameter of the chirp along t axis, $c_r/(2\pi)$ the parameter of the spatial chirp and p is the global phase that evolves along with propagation. When a stationary regime is reached, the phase becomes a linear function of the propagation distance z.

After this choice of the ansatz function, variational analysis could be carried out by neglecting the residual field (*the bare approximation).* Applying the bare approximation to the 2D CSHE, consists in substituting the field $\boldsymbol{\psi}$ by the given trial function $\boldsymbol{f}$ ($\boldsymbol{\psi} = \boldsymbol{f}$) and projecting the resulting equations in the following direction:

$$\frac{\partial \boldsymbol{f}^*}{\partial \boldsymbol{X}}\left(X = \boldsymbol{A}, \boldsymbol{w_t}, \boldsymbol{w_r}, \boldsymbol{c_t}, \boldsymbol{c_r}, \boldsymbol{p}\right).$$

A jet of six differential equations which govern the evolution of the optical pulse parameters propagating in space and time is obtained:

$$\begin{aligned}
\dot{A} &= A\delta + \frac{3}{4}A^3\varepsilon - \frac{2}{w_t^2}A\beta + \frac{5}{9}A^5\mu - Ac_tD \\
&\quad - 2Ac_r + 3\left(2c_t^2 - w_t^2c_t^4 + \frac{3}{w_t^4}\right)A\gamma_2, \\
\dot{w}_t &= 2w_tc_tD - \frac{1}{4}w_tA^2\varepsilon - \frac{2}{9}A^4w_t\mu \\
&\quad + \left(1 - w_t^4c_t^2\right)\frac{2\beta}{w_t} + \left(w_t^8c_t^4 - 1\right)\frac{12}{w_t^3}\gamma_2, \\
\dot{w}_r &= 4w_rc_r - \frac{1}{4}w_rA^2\varepsilon - \frac{2}{9}A^4w_r\mu, \\
\dot{c}_t &= 2\left(\frac{1}{w_t^4} - c_t^2\right)D - \frac{8}{w_t^2}c_t\beta - \frac{1}{2w_t^2}A^2\gamma \\
&\quad - \frac{4}{9w_t^2}A^4\nu + 48c_t\left(\frac{1}{w_t^4} + c_t^2\right)\gamma_2, \\
\dot{c}_r &= -4c_r^2 - \frac{1}{2w_r^2}A^2\gamma + \frac{4}{w_r^4} - \frac{4}{9w_r^2}A^4\nu, \\
\dot{p} &= 2\beta c_t + \frac{3}{4}A^2\gamma - \frac{D}{w_t^2} - \frac{2}{w_r^2} + \frac{5}{9}A^4\nu \\
&\quad - 12c_t\left(\frac{1}{w_t^2}2 - w_t^2c_t^2\right)\gamma_2.
\end{aligned} \qquad (5)$$

It is important to point out that these equations give no explicit information with regard to the different solutions of the equation CSHE (1) and their stability. Thereby, they give us the first idea on the dynamic of the light pulse. They simply reveal in detail the influence of each equation CSHE (1) parameters on the various physical parameters of the soliton.

Thus, one's can clearly see that spectral filter coefficients (β and γ_2) affect the amplitude of the pulse, its temporal width, temporal chirp and the global phase. However, these parameters have no formal effect on the spatial variables. The temporal (w_t) and spatial widths (w_r) also depend on the nonlinear gain (ε) and its saturation (μ). As expected, the terms of spectral filtering coefficients (β and γ_2) and dispersion term (D) affect the temporal width and have no action on the radial component.

Similarly, the spatial c_r and temporal c_t chirp parameters are influenced in the same way by the Kerr term saturation of the optical nonlinearity (ν), but the temporal term is also affected by the terms of spectral filtering coefficients (β and γ_2) and dispersion term (D). Finally, not any parameters of the soliton are influenced by (p), the global phase, but are governed by the second order spectral filter term (γ_2).

In this way, the equation of propagation of the optical wave is transformed into a system of differential equations, describing the evolution of the physical parameters of the pulse (amplitude, width...) during the propagation.

This approach provides the basic parameters of the fixed points, and a mapping of different types of solutions, thereby reducing by several orders of magnitude the volume of calculation required usually.

The fixed points (FPs) of the system are found by imposing the left-hand side of equation (5) to be zero ($\dot{X} = 0$ with $X = A, w_t, w_r, c_t, c_r, p$). The threshold of existence of FPs can be estimated by the relation $\varepsilon_s \approx 2\sqrt{\delta\mu}$. If $\varepsilon > \varepsilon_s$, we have in general both stable and unstable fixed points.

The stability of FPs is determined by the analysis of the eigenvalues λ_j ($j = A, w_t, w_r, c_t, c_r, p$) of the matrix $M_{ij} = \partial\dot{x}_i/\partial x_j$.

The stability criterion is as follows: if the real part of at least one of the eigenvalues is positive, the corresponding FP is unstable. Hence, to have stable FP, the real parts of all the eigenvalues of the matrix M_{ij} must be negative.

The stable fixed points correspond to stationary solutions of the 2D complex Swift-Hohenberg equation (1).

In addition, the fundamental parameter which helps to control the state of the solution and study its stability is the total energy Q given by the following equation:

$$Q(z) = \int_{-\infty}^{+\infty}\int_{0}^{+\infty} 2\pi r \left|\psi(r,t,z)\right|^2 dr dt \cdot \qquad (6)$$

For the dissipative system, the total energy gives us the main information about the soliton dynamics. It's not conserved but evolves in accordance with the so-called balance equation. When a stationary solution is reached, the total energy converges to a constant value. However, the soliton, is a pulsating one, the total energy is an oscillating function of *z*. And finally, when we have unstable solutions, energy tends to infinity.

2.3. (2D) CSHE Stationary Dissipative Soliton

The stationary solutions of the 2D complex Swift-Hohenberg equation exist in finite regions in the parameter space. Nevertheless, it would be extremely difficult to map in extensor these regions in the all dimensional parameter in which we operate. For this raison, we restrict ourselves to fix all the parameters except for two which vary. By setting key parameters and by individually varying the nonlinear gain (ε) and the Kerr term saturation of the optical nonlinearity (ν), we have revealed in the (ν, ε) plane, the stationary solution of the 2D complex Swift-Hohenberg equation. By investigating the parameter regions situated in the neighbourhood of the parameters $D = \gamma = 1$, $\beta = -0.3$, $\delta = -0.5$, $\mu = -0.1$ and $\gamma_2 = 0.05$, with an initial pulse

$$\psi(r,t,0) = 2.86 exp\left(-\frac{t^2}{0.7} - \frac{r^2}{1.36}\right) \qquad (7)$$

and by individually varying $\boldsymbol{\nu}$ from -0.3 to -0.16 and $\boldsymbol{\varepsilon}$ from 0.49 to 0.57, so for each value pair ($\boldsymbol{\nu}, \boldsymbol{\varepsilon}$) the Newton-Raphson allows to look for the fixed point and we study its stability. Thus one's can easily realize the cartography of the solution of the equation (1). Figure 1 shows the mapping of the solutions for the range of selected values. The dotted lines correspond to the fixed points which represent the stationary solution of the 2D complex Swift-Hohenberg equation. It can be noticed that this stability area is very narrow with low value of the nonlinear gain($\boldsymbol{\varepsilon}$), therefore highly sensitive. That implies that a small change $\boldsymbol{\varepsilon}$ of can have a real impact on the system. Thus, all the solitons parameters (amplitude, width, chirp...) stay stationary throughout propagation. The total energy of the system also has the same dynamic which does not change at all, during propagation for these values considered. Besides the stationary domain, we have instable fixed points which can be dived in two categories: the limit-cycle attractor and the instable solutions. Here, our main interest is to study the dynamic of the pulse in the dotted line domain.

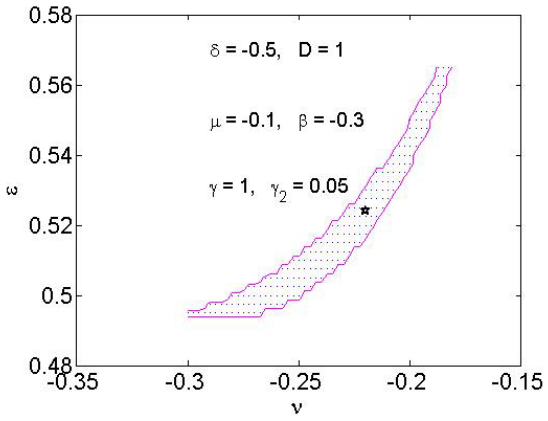

Figure 2. cartography of the solutions of the 2D complex Swift-Hohenberg equation in the ($\boldsymbol{\nu}, \boldsymbol{\varepsilon}$) plane. The stable fixed points regions in dotted lines represents the domain of stationary solitons of the equation. Other CSHE parameters appear inside the figure

This first analysis shows that the 2D complex Swift-Hohenberg equation stationary solutions exist in the space of selected parameters. In this way, it is more revealing to map the area of stability in space of the spectral filters

namely in the (β, γ_2) plane. For this, the star point (see Figure 2) in the stability domain of the Figure 2 corresponding to $\nu = -0.22$ and $\varepsilon = 0.524$ is considered. From this point, the stable solutions in (β, γ_2) plane for the selected values $\nu, \delta, \gamma, D, \mu$ and ε are maped.

The Figure 3 summarizes this result. The dotted lines represent the stationary solutions. As will be seen from this cartography, the stationary solutions of the 2D complex Swift-Hohenberg equation exist for both positive and negative values of γ_2; the same holds true for β. This stability domain is wide with sensitive value of γ_2.

This first interesting results illustrate that the stationary dissipative solutions of the 2D complex Swift-Hohenberg equation can be found for any signs of the parameters β and γ_2. Based on those results, the dynamics of the dissipative soliton depending on the signs of spectral filter and its high-order term (same signs or opposite signs) are carefully examined.

Accordingly, four points marked with a star, a circle, a square and a triangle are chosen (Figure 3).

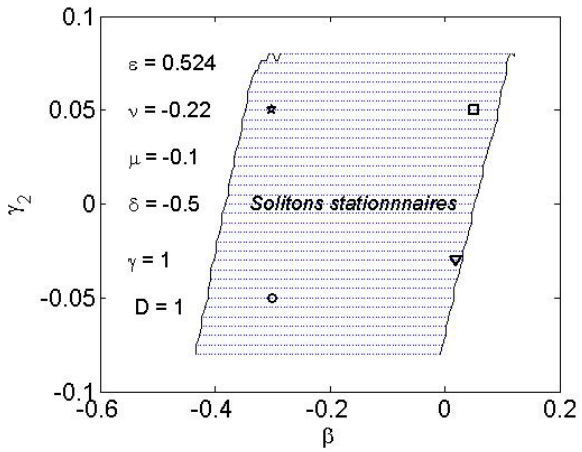

Figure 3. cartography of the solutions of the 2D complex Swift-Hohenberg equation in the $(\boldsymbol{\beta}, \boldsymbol{\gamma_2})$ plane. The stable fixed points regions in dotted lines represents the domain of stationary solitons of the equation. Other CSHE parameters appear inside the figure

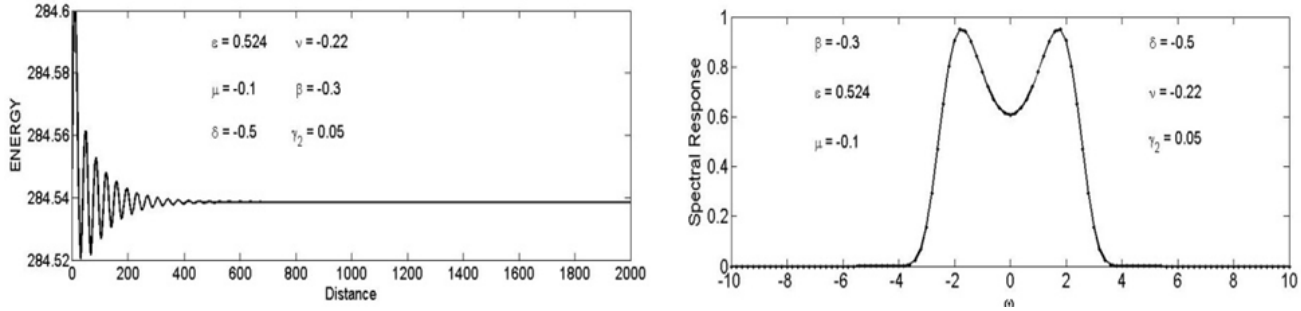

Figure 4. (up) evolution of the total pulse energy of the stationary dissipative soliton, and (below) the spectral filter response in case $\boldsymbol{\beta} < 0$ and $\boldsymbol{\gamma_2} > 0$

The star in the figure corresponds to the case where these parameters are of opposite signs [$\beta = -0.3$ (negative) and $\gamma_2 = 0.05$ (positive)]. The characteristics of such a pulse are represented by the Figure 4. The transfer function of the spectral filtering of that stationary soliton with β positive and γ_2 negative has two maxima. The total energy of that soliton after a short oscillation remains constant over long distances. This dynamic characterizes a stationary solution.

When the spectral filtering and its high-order term are of the same negative signs [$\beta = -0.3$ (negative) and $\gamma_2 = -0.05$ (positive)] represented by a circle in Figure 3, the transfer function also has two maxima at its ends but with no central pulse. So these solutions do not have the same profile and features as in the situation described previously. The solution is still stationary as shown by the evolution of the total energy, but has less energy than the previous one due to the value of γ_2. This situation is well summarized in Figure 5.

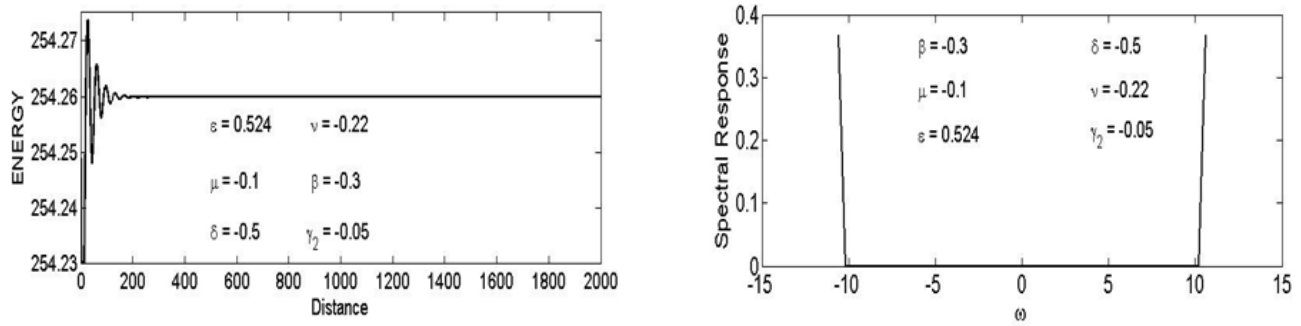

Figure 5. (up) evolution of the total pulse energy of the stationary dissipative soliton, and (below) the spectral filter response in case $\boldsymbol{\beta} < 0$ and $\boldsymbol{\gamma_2} < 0$

In case where the spectral filtering and its high-order term are of the same positive signs [$\beta = 0.05$ (positive) and $\gamma_2 = 0.05$ (positive)] represented by a square in Figure 3 the transfer function has only a single maximum. The soliton dynamic is not changed; it is still stationary but has energy much lower than that of the first two cases treated. The Figure 6 draws these behaviours.

The last case studied corresponds to the scenario where the spectral filtering and its high-order term are of opposite signs [$\beta = 0.02$ (positive) and $\gamma_2 = -0.03$ (negative)] represented by a triangle in Figure 3. Here, the transfer function of the spectral filtering of the pulse shown in Figure 7 has the same behaviour as that of the

circle. The optical soliton has the same dynamic as the previous case, but with even lower energy.

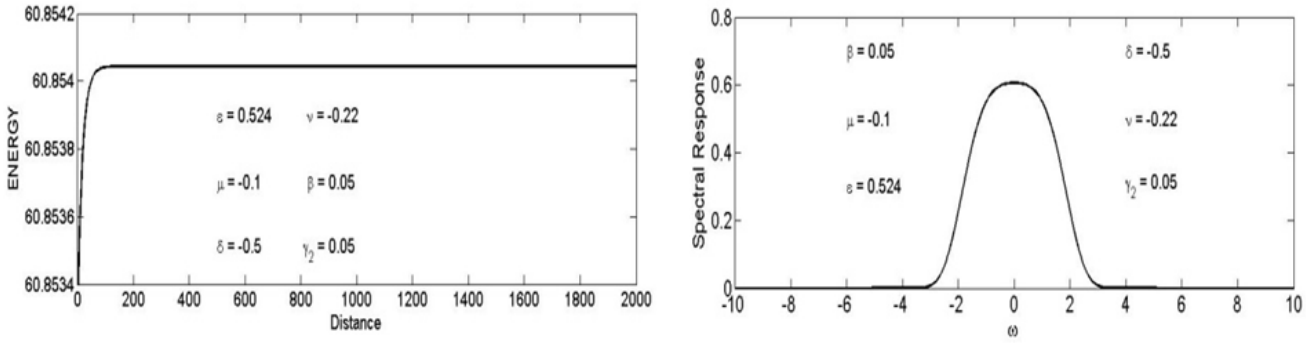

Figure 6. (up) evolution of the total pulse energy of the stationary dissipative soliton, and (below) the spectral filter response in case $\boldsymbol{\beta} > 0$ and $\boldsymbol{\gamma_2} > 0$

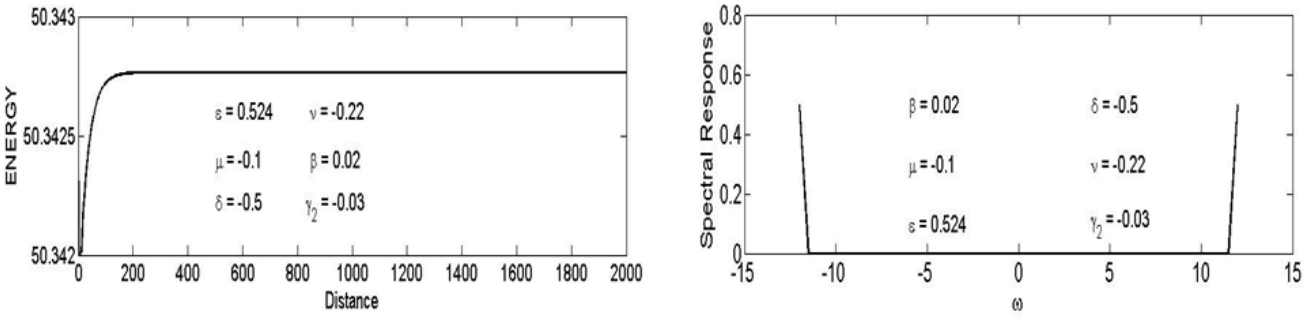

Figure 7. (up) evolution of the total pulse energy of the stationary dissipative soliton, and (below) the spectral filter response in case $\boldsymbol{\beta} > 0$ and $\boldsymbol{\gamma_2} < 0$

It appears from the different scenarios studied that the spectral filtering and its high-order term parameters (β and γ_2) have a great influence on the dynamics of the spectral response. It is certainly true that if stationary solutions regardless the signs of β and γ_2 are obtained, they have a real impact on the spectral response of the pulse.

So when the high-order term is greater than zero ($\gamma_2 > 0$) and no matter the sign of the spectral filtering, the spectral response has one or two distinct maxima.

However, in the scenario where the high-order term is less than zero ($\gamma_2 < 0$) the spectral response has the same behavior with zero central pulse for any signs of β.

These results clearly show that in the cases of experimental; the choices of the spectral filtering and its high-order term (β and γ_2) are very crucial according to the shape of the spectrum.

3. Conclusion

At the end of our study, we have demonstrated, for the first time to our knowledge, the stationary dissipative solutions of the 2D complex Swift-Hohenberg equation with our collective variable approach. Particularly, the regions of existence of stationary dissipative soliton in the (ν, ε) and (β, γ_2) planes are shown. It has been also shown that the validity of these studies is based on a careful selection of the ansatz function.

Our results reveal the essential character of the spectral filtering and its high-order term parameters (β and γ_2). Our study shows that it is possible to observe the stationary dissipative solutions of the 2D complex Swift-Hohenberg equation, whatever the signs of β and γ_2. It has been also shown that theses parameters have a real impact on the spectral response.

The collective variable approach is very efficient to obtain stable stationary solutions when a suitable trial function is chosen. This technique is incomparably quicker than direct numerical computations.

This work can be extensive and we are confident that these applications will numerous in the fields of physics, chemistry and biology as described by the complex Swift-Hohenberg equation.

References

[1] Y. Silberberg, Collapse of optical pulses, Optics Letters 15 (1990), 1282-1284.

[2] N. N. Rosanov, Spatial hysteresis and optical patterns, Springer Berlin, 2002.

[3] N. Akhmediev and A. Ankiewicz, Solitons Around Us: Integrable, Hamiltonian and Dissipative Systems, Lecture Notes in Physics, Springer, Heidelberg, 2003.

[4] N. Akhmediev and A. Ankiewicz, Dissipative solitons. Ed. Springer, Heidelberg, 2005.

[5] N. Akhmediev and A. Ankiewicz, Dissipative solitons: from optics to biology and medicine, Springer, Heidelberg, 2008.

[6] Q. Zhou, Y. Zhong, M. Mirzazadeh, A.H. Bhrawy, E. Zerrad and A. Biswas, Thirring combo solitions with cubic nonlinearity and spatio-temporal dispersion, Waves in Random and Complex Media. Vol. 26 (2016), Issue 2, 204-210.

[7] Q. Zhou, M. Mirzazadeh, E. Zerrad, A. Biswas and M. Belic, Bright, dark and singular solitons in optical fibers with spatio-temporal dispersion and spatially-dependent coefficients, Journal of Modern Optics. Vol. 63 (2016), Number 10, 950-954.

[8] M. Mirzazadeh, M. Eslami, M. Savescu, A. H. Bhrawy, A. A. Alshaery, E. M. Hilal and A. Biswas, Optical solitons in dwdmsystem with spatio-temporal dispersion, Journal of Nonlinear Optical Physics and Materials. Vol. 24 (2015), Issue 1, 1550006.

[9] J.M. Soto Crespo, Ph. Grelu and N. Akhmediev, Optical bullets and "rockets" in nonlinear dissipative systems and their transformations and interactions, *Optics Express* 14 (2006), 4013-4025.

[10] J.M. Soto Crespo, N. Akhmediev and Ph. Grelu, Spatiotemporal optical solitons in nonlinear dissipative media: From stationary light bullets to pulsating complexes, *CHAOS* 17 (2007), 037112.

[11] A. H. Arnous, M. Mirzazadeh, S. Moshokoa, S. Medhekar, Q. Zhou, M. F. Mahmood, A. Biswas and M. Belic, Solitons in optical metamaterials with trial solution approach and backlund transform of riccati equation, Journal and Computational and Theoretical Nanoscience. Vol. 12 (2015), Number 12, 5940-5948.

[12] V. Skarla and N. Aleksic, Stability Criterion for Dissipative Soliton Solutions of the One-, Two-, and Three-Dimensional Complex Cubic-Quintic Ginzburg-Landau Equations, Phys. Rev. Lett. 96 (2006), 013903.

[13] A. Kamagaté, Ph. Grelu, P. Tchofo-Dinda, J.M. Soto-Crespo, N. Akhmediev, Stationary and pulsating dissipative light bullets from a collective variable approach. Phys. Rev. E, 2009, 79, 026609.

[14] M. Mirzazadeh, M. F. Mahmood, F. B. Majid, A. Biswas and M. Belic, Optical solitons in birefringent fibers with riccati equation method, Optoelectronics and Advanced Materials - Rapid Communications. Vol. 9 (2015), Numbers7-8, 1032-1036.

[15] P. Tchofo-Dinda, A.B. Moubissi, K. Nakkeeran, Collective variable theory for optical solitons in fibers. Phys Rev. E, 64 (2001), 016608.

[16] G. Nicolis and I. Prigogine, Self-organization in nonequilibrium systems - From dissipative structures to order through fluctuations, John Wiley \& sons, New York,1977.

[17] W.V. Saarlos and P.C. Hhenberg, Fronts, pulse, sources and sinks in generalized Ginzburg-Landau. Physica D, 56 (1992), 303-367.

[18] N. Bekki and K. Nozaki, Formations of spatial patterns and holes in the generalized Ginzburg-Landau equation, Phys. Lett., 110 (1985), 133-135.

[19] N. Akhmediev and V.V. Afanasjev, Novel arbitrary-amplitude soliton solutions of cubic-quintic complex Ginzburg-Landau equation, Phys. Rev. Lett., 75 (1995), 2320-2323.

[20] Y. Kuramoto, Chemical Oscillations, Waves and Turbulence Dissipative Solitons, Springer-Verglag, Berlin, 1984.

[21] C. Normand, Y. Pomeau, M.G. Velarde, Convective instability: A physicist's approach, Rev. Mod. Phys., 49 (1977), 581-624.

[22] N. Akhmediev and A. Ankiewicz, Solitons of the Complex Ginzburg-Landau equation, Springer, Berlin, 2001.

[23] P.A. Belanger, Coupled-cavity mode-locking: a nonlinear model, J. Opt. Soc. Am. B, 8 (1991), 2077-2082.

[24] J.D. Moores, On the Ginzburg-Landau laser mode-locking model with fifth-oder saturable absorber term, Opt. commun., 96 (1993), 65-70.

[25] L.F. Mollenauer, J.P. Gordon and S.G. Evangelides, The sliding-frequency guiding: an improved from soliton jitter control, Opt. Lett., 1992, vol.17 (1992), 1575-1577.

[26] W.J. Firth and A.J. Scroggie, Optical bullet holes: Robust controllable localized states of a nonlinear cavity, Phys. Rev. Lett., 76 (1996), 1623-1626.

[27] P.S. Jian, W.E. Torruellas, M. Haelterman, U. Peschel and F. Lederer, Solitons of singly resonant optical parametric oscillators, Opt. Lett, 24 (1994), 400-402.

[28] M. Mirzazadeh, A. H. Arnous, M. F. Mahmood, E. Zerrad and A. Biswas, Solitons solutions to resonant nonlinear Schrodinger's equation with time dependent coefficients by trial solution approach, Nonlinear Dynamics. Vol. 81 (2015), Issue 1-2. 277-282.

International Journal of Physics, 2016, Vol. 4, No. 4, 85-105
Available online at http://pubs.sciepub.com/ijp/4/4/3

DOI:10.12691/ijp-4-4-3

On the Origin of Magnetism and Gravitation and on the Nature of Electricity and Matter

Hans-Joerg Hochecker*

Donaustr. 22, 30519 Hannover, Germany
*Corresponding author: physics@hochecker.eu

Abstract This is a significantly improved resumption of my previous paper on gravitation [40]. I can show in a improved way that gravitation is an electric effect. To this, it is necessary to better understand the qualities of the electric charges and their forces. I start by showing that the magnetic field can be represented as an angled electric field. To this, the electric field must have two qualities: the dependence of the electric force on the velocity, and the electric anti-field. All previous cognitions on electrodynamics stay with it untouched. Then, I apply these two new qualities to gravitation, and it turns out that gravitation is an electric effect if a third quality applies to the electric field: the quantization of the energy transfer of the electric field. These three new qualities complete our picture of electrodynamics. Finally, I go to the origins of the three new qualities with the help of the early quantum mechanics. This turns out well by representing the electric charge as a space time wave, in which its frequency corresponds to its mass.

Keywords: *gravitation, magnetism, electric fields, special relativity, quantum-mechanics*

Cite This Article: Hans-Joerg Hochecker, "On the Origin of Magnetism and Gravitation and on the Nature of Electricity and Matter." *International Journal of Physics*, vol. 4, no. 4 (2016): 85-105. doi: 10.12691/ijp-4-4-3.

1. Preface

It has always been my desire to better understand gravitation. And ever since (that is always) the similarities but also the differences between the gravitation and the electric force were clear to me. Now, after many years of hard work it turns out that gravitation is an electric effect. It appears that the task was to better understand the qualities of the electric charges and their forces.

It all started with a more exact analysis of magnetism. It turns out that the magnetic field can be represented as an angled electric field if the electric force is velocity-dependent and if, in addition, the electric anti-field exists. These two prerequisites can be regarded as two new qualities of the electric field (which I will describe in this work here in detail). All previous cognitions on electrodynamics stay untouched with it, which explains why these two qualities haven't stood out yet. However, due to these two new qualities we get new insights on electrodynamics, such as on the origin of magnetism. Therefore, they complete our picture of the electrodynamics.

At next, I have applied the two new qualities to gravitation and it turns out that gravitation is an electric effect if the energy transfer of the electric field to an electric charge is quantized. This last-named prerequisite is another quality of the electric field which fits in without problems and which further completes our picture.

Then, I wanted to go to the origins of the three new qualities of the electric field, which took me to the early quantum mechanics. It turns out that the electric charge can be represented as a spacetime wave, in which its frequency corresponds to its mass. From this representation of the electric charge the three new qualities of the electric field can wonderfully be derived and used. For example, the deBroglie wavelength can be calculated very simply with the help of the anti-field.

About the sectioning: This work consists of three parts: 1. On magnetism, 2. On gravitation, and 3. On quantization. Every part contains an introduction of its own and a closing remark of its own. In addition, there also is a general preface (this is this here), and, quite near to the end, a general conclusion.

2. Part 1: Magnetism as an Electric Angle-effect

2.1. Introduction to Part 1 / Motivation

The magnetic force really is fascinating: Whenever an electric charge has a velocity, a magnetic field arises, which is both perpendicular to this velocity and perpendicular to the electric field of this charge. And whenever a charged particle has a velocity perpendicular to a magnetic field, a magnetic force arises, which is both perpendicular to this velocity and perpendicular to the magnetic field.

Both the source of the magnetic field and the charged particle on which the magnetic field exerts the force have to be in motion. And the magnetic force is *always* perpendicular to the velocity of the charge on which the magnetic field has an effect.

This law on magnetism had been discovered soon, and as soon as that a problem was discovered: by changing into a reference system in which the source *or* the receiver (that is the charged particle on which the magnetic field has an effect) doesn't move the magnetic force disappears, of course. But a force cannot simply disappear. Einstein finally could solve the problem in a brilliant way by showing that not only the magnetic force but also the electric force depends on the reference system [1]. In his solution he famously postulated that the speed of light is equal for all inertial observers, or reference systems, which means that space and time are relative.

So, it was understood *when* a magnetic force arises - that is, whenever an electric charge is moving (both the one which produces the magnetic field and the one on which the magnetic field has an effect). But, *how* is the magnetic force actually being created? How is this phenomenon created? In which way does a magnetic force arise, when an electric charge is moving? This is still unknown. Einstein also had regarded the magnetic force simply as given.

Well, I think, I can explain, how the magnetic force is being created.

To be able to show how the magnetic force arises I will define two new qualities for the electric field. As the first quality, I will introduce the velocity-dependence of the electric force. This quality is valid exclusively under consideration of the second quality: the anti-field. Therefore, I then introduce the anti-field as the second quality. Finally, I show how the magnetic force results and can be calculated from these two qualities.

2.2. Velocity-Dependence of the Electric Force

I will now describe the first of the two qualities of the electric field: the velocity-dependence of the electric force which is, as said already, valid exclusively under consideration of the second quality (the anti-field).

The electric field *always* propagates (in a classical vacuum) with the speed of light $\vec{c}$. And while the electric field propagates with the speed of light, it exerts an electric force on electric charges. So, one can come to the assumption that the electric force is directly connected to the velocity with which the electric field moves relative to an electric charge. The relative velocity between an electric field and the electric charge on which the field exerts a force (I call this charge receiver) corresponds to the vector addition of the speed of light $\vec{c}$ with the velocity $\overrightarrow{v_R}$ of this charge. Therefore, the force of an electric field on a charge changes by the velocity of this charge. But, though, the force shall be all the grater the grater the velocity of the charge is relative to the field. Therefore the velocity of the receiver $\overrightarrow{v_R}$ must be subtracted from the speed of light $\vec{c}$ of the field. Therefore, the force arises by $(\vec{c} - \overrightarrow{v_R})$.

So, the force of an electric field on a charge (a receiver) changes by the velocity $\overrightarrow{v_R}$ of this charge (this receiver). This means that an *additional* force, which is proportional to the velocity $\overrightarrow{v_R}$ of the receiver, arises. This becomes particularly clear if the $\overrightarrow{v_R}$ is perpendicular to the speed of light $\vec{c}$ of the field.

In an analogous way the force of the field also changes if the source of the field has the velocity $\overrightarrow{v_S}$.

The field of a motionless charge also moves with the speed of light relative to its source,of course. If the source has the velocity $\overrightarrow{v_S}$, then the force of the field results by the vector addition of $\overrightarrow{v_S}$ and $\vec{c}$. But differently as at the $\overrightarrow{v_R}$, here the strength of the field shall be all the grater the smaller the velocity $\overrightarrow{v_S}$ of the source is relative to the field.

The $\overrightarrow{v_S}$, too, can be perpendicular to the speed of light $\vec{c}$of its field. So, an arbitrary $\overrightarrow{v_S}$ can be decomposed into one component parallel to the speed of light of the field (this is $\overrightarrow{v_{S\parallel}}$), and one component perpendicular to the speed of light of the field (this is $\overrightarrow{v_{S\perp}}$). The $\overrightarrow{v_{S\parallel}}$ must be added to $\vec{c}$ so that the strength of the field is all the grater the smaller $\overrightarrow{v_S}$ is. Whereas for the $\overrightarrow{v_{S\perp}}$ it is as for the $\overrightarrow{v_R}$, which means that the $\overrightarrow{v_{S\perp}}$ is to be subtracted from the $\vec{c}$. So, the correct and complete change of the strength of the field, which yields by the $\overrightarrow{v_S}$, corresponds to the vector: $(\vec{c} + (\overrightarrow{v_{S\parallel}} - \overrightarrow{v_{S\perp}}))$.

It is as if the $\overrightarrow{v_S}$ would be mirrored. Therefore, instead of the $\overrightarrow{v_S}$ the mirrored $\overrightarrow{v_S}$ is used for the calculation of the strength of the field, that is the $|\overrightarrow{v_S} = \overrightarrow{v_{S\parallel}} - \overrightarrow{v_{S\perp}}$.

Therefore, the strength of the field arises from the vector $(\vec{c}+|\overrightarrow{v_S})$.

Of course, the velocity with which the field propagates doesn't change due to $|\overrightarrow{v_S}$. But the strength of the field changes. In addition, the direction of the force of the field also changes, *without* changing the direction in which the field propagates. This means that the $|\overrightarrow{v_S}$ causes an angle φ between the direction in which the field propagates and the direction of the force of the field. This angle is calculated by: $\tan(\varphi) = \frac{-v_{S\perp}}{|\vec{c}+\overrightarrow{v_{S\parallel}}|}$ (see Figure 2.1).

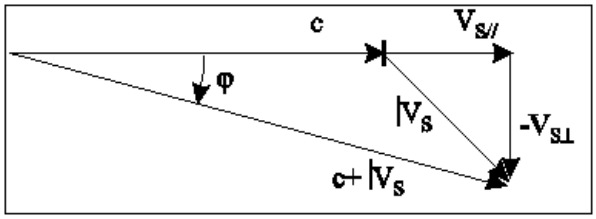

Figure 2.1.

If the strength and direction of the field change by the velocity $|\overrightarrow{v_S}$ of the source, then, naturally, the strength of the force, which results by $\overrightarrow{v_R}$, will also change in a proportional way.

The change of the strength of the field arises from $|\overrightarrow{v_S}$. However, the field still propagates with the speed of light $(\vec{c})$. This means that the force which arises from $\overrightarrow{v_R}$ regarding the speed of light $\vec{c}$ of the field will be proportional to that force, which arises by $\overrightarrow{v_R}$ regarding the $|\overrightarrow{v_S}$. From this proportionality we can derive, how grate the influence of the $|\overrightarrow{v_S}$ is on the force. If we name the part, which the $|\overrightarrow{v_S}$ has on the force which arises by $\overrightarrow{v_R}$, $\overrightarrow{v_{SR}}$ then we get: $\frac{v_{SR}}{|v_S} = \frac{-v_R}{c}$ (see Figure 2.2).

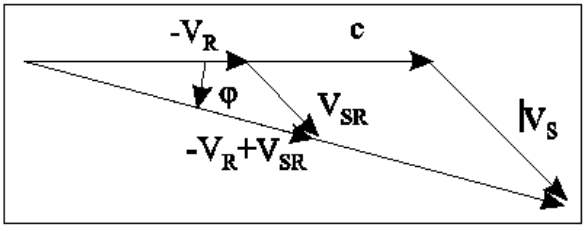

Figure 2.2.

We recognize here, in addition, that the force which arises from a $\overrightarrow{v_R}$ is turned by the angle φ in respect to $-\overrightarrow{v_R}$. This is always that way, because the $\overrightarrow{v_R}$ always produces its own force, which, independently of the direction of the $\overrightarrow{v_R}$ relative to the field, is always proportional to the strength of the field. The force which arises from $\overrightarrow{v_R}$ is: $-\overrightarrow{v_R} + \overrightarrow{v_{SR}}$, as it can be seen at Figure 2.2.

Before I come to the calculations of the forces it is necessary to introduce the second quality of the electric field, that is the anti-field, because without taking the anti-field into account the velocity-dependence of the electric force doesn't make sense.

2.3. The Anti-field

A velocity-dependence of the electric force, as I have described in the previous chapter, has *never* been observed in any experiment. This is due to the second quality which I would like to introduce here for the electric field: the anti-field. Due to the anti-field, all the electric qualities, known from the experiments, remain valid, while at the same time the combination of the velocity-dependence of the electric force with the anti-field automatically yields the magnetic force.

So, what is the anti-field? The anti-field is a field which always appears then when a field exerts a force on a charge. It resembles a reflection; this shall mean that the anti-field always propagates exactly in the opposite direction to the field. The anti-field always appears only when the field interacts with a charge. But, taken exactly, the field, too, can bee observed only when it interacts with a charge. Of the field one assumes in principle that it always exists. I make the same acceptance for the anti-field now. The anti-field shall always exist, too. In this sense one then cannot regard the anti-field as a reflection either. Here, the anti-field would rather be a field of its own which always appears together with the field. The anti-field is, just as the field, a quality of space. Both qualities, the one of the field and the one of the anti-field, always appear together. I am sure that there is a connection between the anti-field and the anti-particles or the anti-matter [2]. However, the exact connections on this are still not quite clear to me - but, though, an interesting connection on this yields in part 3 of this work.

In any case, the anti-field is just as real as the field. This means that it exerts an electric force on an electric charge, exactly as the field does. So, the electric force on a charge *always* consists of the force of the field plus the force of the anti-field. And although the anti-field always propagates exactly in the opposite direction to the field, the force of the anti-field (on a charge) still *always has the same sign as the force of the field* (on the same charge). Therefore, if the force, which arises from the speed of light of the field $\vec{c}^+$ (I mark the speed of light of the field with a high-ranking "+"), is positive, then the force, which arises from the speed of light of the anti-field $-\vec{c}^-$ (I mark the speed of light of the anti-field with a high-ranking "-"), must be positive, too. But since it always is $\vec{c}^+ = -\vec{c}^-$, the force of the anti-field must be multiplied with -1.

One can say that the anti-field behaves exactly oppositely to the field.

At the force of the field the velocity of the source $|\overrightarrow{v_S}$ must be taken into account. At the anti-field this is exactly the same. But, however, at the anti-field the force must be multiplied with -1, therefore the strength of the anti-field arises from the vector: $-(\vec{c}^- + |\overrightarrow{v_S}) = (\vec{c}^+ - |\overrightarrow{v_S})$ (see Figure 2.3).

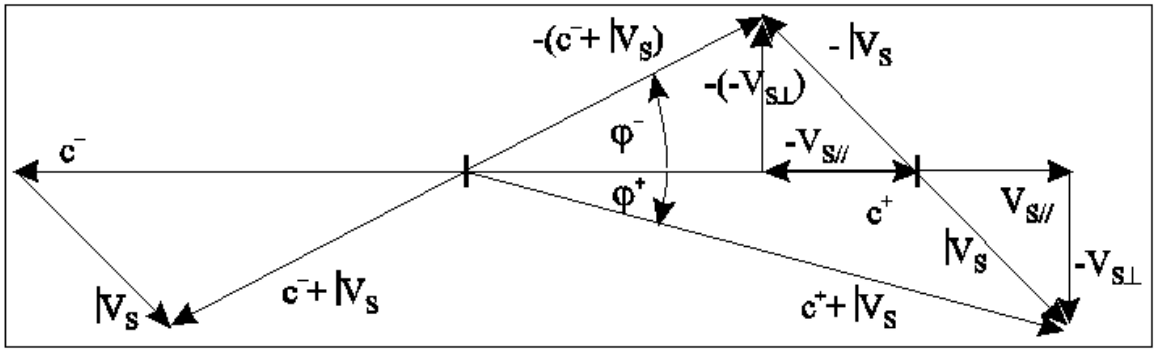

Figure 2.3.

So we see, that the anti-field changes by $-|\overrightarrow{v_S}$ (while the field changes by $+|\overrightarrow{v_S}$).

The angle φ^- which results from $|\overrightarrow{v_S}$ between the direction in which the anti-field propagates and the direction of the force of the anti-field is calculated by: $\tan(\varphi^-) = \frac{-(-v_{S\perp})}{|\vec{c}+(-\overrightarrow{v_{S\parallel}})|}$ (in Figure 2.3 the angle for the field is correspondingly: φ^+).

If the strength and direction of the anti-field change by the velocity $|\overrightarrow{v_S}$ of the source, then the strength of the force, which arises from $\overrightarrow{v_R}$ regarding the anti-field, will also change in a proportional way, of course.

The $\overrightarrow{v_R}$ produces a force at the-anti field which is opposite to the force which it produces at the field. At the same time, however, the anti-field propagates in the opposite direction to the field. This then would turn back the direction of the force which arises by $\overrightarrow{v_R}$. But since, in addition, it must be multiplied with -1, the force of the $\overrightarrow{v_R}$ which arises from the anti-field remains exactly opposite to the force which arises from the field.

The part which the $|\overrightarrow{v_S}$ has of the force, which arises at the anti-field by the $\overrightarrow{v_R}$, results from the $-|\overrightarrow{v_S}$, of course. The $-\overrightarrow{v_{S\parallel}}$ (of the $-|\overrightarrow{v_S}$) is opposite to $+\overrightarrow{v_{S\parallel}}$. This would mean that the force which arises from the $\overrightarrow{v_R}$ in the direction of the $\overrightarrow{v_{S\parallel}}$ at the anti-field is turned back, so that it would have the same direction as the force at the field. But, here too, it must be multiplied with -1 again, so that the force which arises by the $\overrightarrow{v_R}$ in the direction of the $\overrightarrow{v_{S\parallel}}$ at the anti-field is opposite to the force at the field. For the force, which arises by the $\overrightarrow{v_R}$ in the direction of the $-(-\overrightarrow{v_{S\perp}})$ (of the $-|\overrightarrow{v_S}$), the $-(-\overrightarrow{v_{S\perp}})$ must be multiplied with -1.

If we name the part which the $|\overrightarrow{v_S}$ has on the force, which arises from $\overrightarrow{v_R}$ regarding the anti-field, $\vec{v}^{-}{}_{SR}$ (and that one of the field then correspondingly $\vec{v}^{\mp}{}_{SR}$), then the force which arises from $\overrightarrow{v_R}$ at the anti-field is: $+\overrightarrow{v_R} + \vec{v}^{-}{}_{SR}$. Therefore, at the anti-field the force arises by the $+\overrightarrow{v_R}$, while at the field it arises by the $-\overrightarrow{v_R}$. This also can be recognized because of $\vec{c}^{+} = -\vec{c}^{-}$. Formulated differently: by the $\overrightarrow{v_R}$ the force of the anti-field (which arises from $-(\vec{c}^{-}+|\overrightarrow{v_S})$) changes in an exactly opposite way to the force of the field (which arises from $(\vec{c}^{+}+|\overrightarrow{v_S})$, see Figure 2.3).

As in the case of the field, the force at the anti-field, which arises from $\overrightarrow{v_R}$ regarding the speed of light $\vec{c}^{-}$ of the anti-field, also is proportional to the force which arises by the $\overrightarrow{v_R}$ regarding the $|\overrightarrow{v_S}$. Here we have to paid attention particularly to the signs. So the proportionality which is valid is: $\frac{v^{-}{}_{SR}}{|-\overrightarrow{v_{S\parallel}}-\overrightarrow{v_{S\perp}}|} = \frac{v_R}{c^{-}}$ (see Figure 2.4).

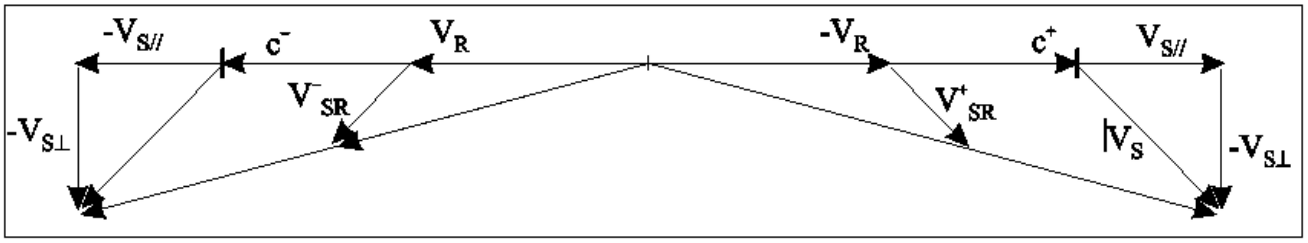

Figure 2.4.

The force which an arbitrary $\overrightarrow{v_R}$ produces at the anti-field always has the angle $\tan(\varphi) = \frac{-v_{S\perp}}{|\vec{c}^{-}+(-\overrightarrow{v_{S\parallel}})|}$ to $+\overrightarrow{v_R}$. This corresponds to the magnitude of the angle φ^{+}.

I think, that it has got clear what the anti-field is. Somehow difficult maybe here the idea that the anti-field always propagates *towards* its source. This has always to be taken into account in all considerations. It is easier to understand this connection if one considers that, in the end, both the electric field and the electric anti-field are qualities of the spacetime. This will get even clearer in part 3 of this work.

I think, that the anti-field is more than only a theoretical construct. I think, that the anti-field is exactly as real as the electric field. But, though, since both always appear together, it will be hard to observe them separated - I will say more about that in part 2 of this work, in which I treat gravitation. Both fields - the field and the anti-field - always act together and yield in the sum the forces which we know as electric and magnetic forces.

I cannot prove the existence of the anti-field. But I think that the results, which I show in this work, speak for themselves. Particularly in part 3 of this work, where I carry out the quantum mechanical considerations to part 1 and part 2, there are strong indications in favour of the existence of the anti-field.

2.4. Calculation of the Magnetic Force

Now, with the help of the two qualities of the electric force just described, I will derive the magnetic force.

To simplify the representations in the further course, it is helpful to look at the electrostatic case: The electrostatic force between two charges is calculated by Coulombs law: $F_S = \frac{q_1 \cdot q_2}{r^2 \cdot \varepsilon_0 \cdot 4 \cdot \pi}$ in which q_1 and q_2 are the electric charges, r is the distance between them, and ε_0 is the electric constant in the vacuum [3].

Now the electric force shall be dependent on the relative velocity between the field or the anti-field and the charge. In the electrostatic case ($\overrightarrow{v_S} = \overrightarrow{v_R} = 0$), the relative velocity between the field or the anti-field and the charge is always the speed of light, these are $\vec{c}^{+}$ and $\vec{c}^{-}$. Thus, the electrostatic force for the field can be represented as: $\overrightarrow{F_E} = \frac{1}{2} \cdot \frac{q_1 \cdot q_2}{r^2 \cdot \varepsilon_0 \cdot 4 \cdot \pi} \cdot \frac{\vec{c}^{+}}{|\vec{c}|} = F_c \cdot \vec{c}^{+}$ with $F_c = \frac{1}{2} \cdot \frac{q_1 \cdot q_2}{r^2 \cdot \varepsilon_0 \cdot 4 \cdot \pi \cdot |\vec{c}|}$. The factor ½ arises because the actual (real) electric force results respectively half from the field and half from the anti-field. And for the anti-field it is: $\overrightarrow{F_E} = -F_c \cdot \vec{c}^{-}$. Thus, the sum of the field and anti-field is: $\overrightarrow{F_E} = F_c \cdot \vec{c}^{+} - F_c \cdot \vec{c}^{-} = 2 \cdot F_c \cdot \vec{c}^{+}$.

So, for the calculation of the strength of the field one uses for the electric force F_S: $\overrightarrow{F_S} = F_c \cdot (\vec{c}^{+}+|\overrightarrow{v_S}) - F_c \cdot (\vec{c}^{-}+|\overrightarrow{v_S}) = 2 \cdot F_c \cdot \vec{c}^{+}$, with $F_c = \frac{1}{2} \cdot \frac{q_S \cdot q_P}{r^2 \cdot \varepsilon_0 \cdot 4 \cdot \pi \cdot |\vec{c}|}$, where q_P is a small test charge (probe) and q_S is the charge of the source.

For the force of the field or anti-field on a motionless receiver ($\overrightarrow{v_R} = 0$) one simply would replace the test charge (q_P) by the charge of the receiver (q_R).

One recognises here very well that the sum of the forces of the field and the anti-field on a motionless receiver ($\overrightarrow{v_R} = 0$) is independent from $|\overrightarrow{v_S}$.

If the receiver moves with the velocity $\overrightarrow{v_R} \neq 0$, then there is, in addition to the force which is exerted on the motionless receiver, the force from the $\overrightarrow{v_R}$.

The additional force which results from the $\overrightarrow{v_R}$ by the field plus the anti-field is: $\overrightarrow{F_R} = F_c \cdot \overrightarrow{v_R} - F_c \cdot \overrightarrow{v_R} = 0$. Plus the part which the $|\overrightarrow{v_S}$ has on the force which results from the $\overrightarrow{v_R}$ by the field plus the anti-field. This part is for the field: $F_c \cdot \vec{v}^{+}_{SR} = F_c \cdot [\frac{-v_R}{c^{+}} \cdot (+\overrightarrow{v_{S\parallel}}) + \frac{-v_R}{c^{+}} \cdot (-\overrightarrow{v_{S\perp}})]$. And for the anti-field: $F_c \cdot \vec{v}^{-}_{SR} = F_c \cdot [\frac{v_R}{c^{-}} \cdot (-\overrightarrow{v_{S\parallel}}) + \frac{v_R}{c^{-}} \cdot (-\overrightarrow{v_{S\perp}})]$. And the sum from the field and the anti-field yields in a parallel direction to $\overrightarrow{v_R}$: $F_c \cdot [\frac{-v_R}{c^{+}} \cdot (+\overrightarrow{v_{S\parallel}}) + \frac{v_R}{c^{-}} \cdot (-\overrightarrow{v_{S\parallel}})] = F_c \cdot [\frac{-v_R}{c^{+}} \cdot (\overrightarrow{v_{S\parallel}}) + \frac{v_R}{c^{+}} \cdot (\overrightarrow{v_{S\parallel}})] = 0$. And the sum from the field and the anti-field yields in a perpendicular direction to $\overrightarrow{v_R}$: $F_c \cdot (\frac{-v_R}{c^{+}} \cdot (-\overrightarrow{v_{S\perp}}) + \frac{v_R}{c^{-}} \cdot (-\overrightarrow{v_{S\perp}})) = F_c \cdot (\frac{v_R}{c^{+}} \cdot \overrightarrow{v_{S\perp}} + \frac{v_R}{c^{+}} \cdot \overrightarrow{v_{S\perp}}) = 2 \cdot F_c \cdot \frac{v_R}{c^{+}} \cdot \overrightarrow{v_{S\perp}}$.

We notice, that by the $\overrightarrow{v_R}$ here there is a resultant force which is perpendicular to $\overrightarrow{v_R}$. This force meets exactly the conditions of the magnetic force ($\overrightarrow{F_M}$). So we can write: $\overrightarrow{F_M} = 2 \cdot F_c \cdot \frac{v_R}{c^{+}} \cdot \overrightarrow{v_{S\perp}}$.

The direction of the $\overrightarrow{F_M}$ results from the direction of the $\overrightarrow{v_{S\perp}}$ and the sign of the F_c. The F_c is positive at same charges and negative at opposite charges.

I think, that no doubt can be: by the introduction of the velocity-dependence of the electric force and by the

introduction of the anti-field the magnetic force can quite obviously be derived from the electric force.

2.5. Remarks on the Magnetic Force

So we see that the F_M corresponds to the magnetic force.

And the angles φ^+ and φ^- of the electric field and anti-field correspond to the idea of the magnetic field. Now, one doesn't have to speak any more about the magnetic field, which is regarded as given, but one can speak about the angles φ^+ and φ^-, whose way of emergence is known.

On relativity:

We know that the magnetic force depends on the relative velocities. This means that the magnitude of the magnetic force depends on the reference system. And this means that the magnitude of the angles φ^+ and φ^- must also dependent on the reference system.

I have described that the angles φ^+ and φ^- result by the addition of the vector | $\overrightarrow{v_S}$ of the velocity of the source and the vector $\vec{c}^+$ or $\vec{c}^-$ of the speed of light. We know from the SRT that the speed of light is equally in magnitude for all observers. Of course, the velocity of the source $\overrightarrow{v_S}$ depends on the reference system. So, while $\overrightarrow{v_S}$ changes, the speed of light remains constant; this means: the angles φ^+ and φ^- change (in dependence of the reference system).

This is actually fascinating: the magnitudes of the angles φ^+ and φ^- depend on the observer. The angles φ^+ and φ^- aren't an abstract construct. The angles φ^+ and φ^- are really existing angles. They are the angles between the propagation direction of the field or anti-field (respectively with $\vec{c}^+$ and $\vec{c}^-$) and the direction of the force of the field or anti-field. But still, different observers will observe different angles. Well, we know such phenomena from the SRT. There, e.g., space and time also depend very really on the observer.

Of course, the transformations between inertial reference systems are carried out quite normally according to the SRT. Not only the angles φ^+ and φ^- but also the electric force changes, so that the sum of both forces yields the right acceleration.

On the magnetic force:

So, I have described the magnetic force as a result of the angles φ^+ and φ^- of the electric field. Therefore, it makes sense to want to express the magnetic force by means of the electric force.

The magnitude of the electrostatic force ($\overrightarrow{F_E}$) is (as described already): $F_E = 2 \cdot F_c \cdot c$. Hence, the magnitude of the magnetic force ($\overrightarrow{F_M}$) is: $F_M = F_E \cdot \frac{v_R \cdot v_{S\perp}}{c^2}$.

So we see, that we can calculate the magnetic force directly through the electrostatic force. We neither must calculate a magnetic field, nor the cross product from $\overrightarrow{v_R}$ and the magnetic field.

Therefore, to calculate e.g. the magnetic force of a current that flows through a straight homogeneously charged conductor on a charge (which can be considered a point charge), we proceed similarly as in the case of the calculation of the electric field, while we still must, in addition, take into account the term $\frac{v_R \cdot v_{S\perp}}{c^2}$. The $v_{S\perp}$ can be expressed in dependence of v_S, and if L is the plumb line from the charge to the conductor, and λ is the linear charge density of the conductor, and q_R is the point charge, then the integration yields: $F_M = q_R \cdot \frac{v_R \cdot v_S}{c^2} \cdot \frac{\lambda}{8 \cdot \varepsilon_0 \cdot L}$.

In the case that $v_R = v_{S\perp} = c$, it is: $F_M = F_E$. At the speed of light the magnetic force is equally in magnitude to the electric force. In the case that the source and the receiver move together parallel with the speed of light the magnetic and electric force cancel each other out mutually. This means: if charges could move with the speed of light, then they wouldn't exert any forces on each other. So such charges could move together as a group. Their mass, though, could only exist as energy, as in the case of the photons. These connections will get even more understandable in part 3. One then understands there, too, that electric charges can never be faster than their field.

On the electrodynamics:

The central statement of the electrodynamics [4] is: A changing electric field produces a magnetic field, and vice versa. This principle of the electrodynamics is very useful. However, it only represents a simplification of the actual events.

Let us consider e.g. the oscillating circuit: according to the electrodynamics a growing magnetic field builds up in the spool of the oscillating circuit due to the permanently faster decreasing current from the capacitor, and the energy of this magnetic field then keeps the current flowing due to the decreasing magnetic field. At a more exact consideration we see that attractive magnetic forces which are vertical to the direction of the current have an effect on the free charges, which produce the current, and which move parallel in the parallel windings of the spool. These magnetic forces move the free charges towards the middle of the spool, from what a magnetic force results, which slows down the current. As the current decreases, the free charges move back again, they move therefore in the opposite direction, which means, that they then drive the current. This system builds-up to the frequency of the oscillating circuit.

Let us consider as the next example the electromagnetic waves (EMW): here, too, the electrodynamics says that an ever faster decreasing electric field produces an ever faster growing magnetic field, which is the reason for the phase displacement of 90°. At a more exact consideration we see that at the emergence of the EMW the angles φ^+ and φ^-, which have been already described in detail, arise in the electric field or anti-field. An EMW arises, if an electric dipole oscillates. When the charges are removed from each other furthest, the directions of their motions change, while they stop for a moment. At this moment the angles are $\varphi^+ = \varphi^- = 0$, while the electric field is at its maximum. When they pass each other at the transit point then the electric field is (almost) zero for a moment, while φ^+ and φ^- are at their maximum (perpendicular to the direction of the motion), since the velocities of the charges $v_S$are at their maximum at this moment. In this way the alternating electric and magnetic field arises. So one could assume that the electric field and the magnetic field *don't* produce each other but that they spread alternating into space due to the way of their creation.

So one can consider the emergence of the angles φ^+ and φ^- as an additional insight on the electrodynamics.

Regarding the exact nature of the energy quanta of the EMW, the photons, I will say some more in part 3 of this work.

2.6. Closing Remark to Part 1

I think, that I have been able to describe the emergence of the magnetic force much more exactly than this was the

case till now. By the two new qualities of the electric field - the velocity-dependence of the electric force and the electric anti-field - new connections arise, which don´t create any contradictions to known experimental facts, but which help us to understand the nature of the electric field and the emergence of its forces much better.

I could particularly show that the magnetic field isn't a field of its own but that it is only an angled electric field. - While, of course, taken exactly, I have shown that the field has the angle φ^+ and the anti-field the angle φ^-.

3. Part 2: Gravitation as an Electric Effect

3.1. Introduction to Part 2 / Motivation

The electric forces [5,6] are immensely great compared with gravitation. At Bohr's atom model, e.g., the gravitational forces of the masses of the electric charges can be neglected. The difference of the forces is immense. At the hydrogen atom, e.g., which consists of a proton and an electron the ratio of the electric force to the gravitational force is: $\approx 2{,}41 \cdot 10^{39}$. This is a gigantic number. These facts are already known for a long time and so they seem trivial; nevertheless, I would like to show an example here to elucidate them: If the gravitational force of the protons were approximately as great as its electrical force, then the earth would need to have only a diameter of about $\approx 18\text{m}$ to exert the same forces on us as it does, and the moon would have only a diameter of about $\approx 4\text{m}$. A man then would only have a mass of: $\approx 8{,}35 \cdot 10^{-14} g$.

So, the electric forces of ordinary matter are gigantically great compared with the gravitational forces of everyday live. However, we notice nothing of these immense electric forces since ordinary matter always consists of as many protons as electrons so that their electric fields cancel each other. And although it is very clear that the resulting electric field is zero, still, the thought sticks that gravitation could be a result of these immense electric forces. Some kind of residual or side effect. Something remains.

I have thought about this problem very, very often, again and again, but it never worked out completely. At all considerations the problem was that repulsion and attraction have always cancelled each other out exactly. For any effect, which could somehow be derived from the electric charges and their fields, there always were the corresponding counter-forces, due to which the overall effect became zero.

Also by applying the velocity-dependence of the electric force the problems couldn't be overcome.

At all considerations, I always assumed that the fields of the positive and negative charges exert their forces at the same time. Until I understood that the transfer of the energy of the electric field to a charge takes place in quanta. This means that always only the fields of the positive *or* negative charges exert their forces respectively. So the electric fields of the positive and negative charges transfer their energy quanta not at the same time but after each other.

By the quantization of the energy transfer of the electric field to an electric charge gravitation can now be represented easily as an electric effect with the help of the velocity-dependence of the electric force.

I will show this gradually in the following.

3.2. Basic Idea

The basic idea with which everything started is amazingly simple. We know: same charges repel and opposite charges attract. If, now, the repulsion were a little weaker than the attraction, or the attraction were a little stronger than the repulsion, then, in the result, one would have an attraction which could correspond to gravitation.

But what can weaken the repulsion and strengthen the attraction?

Well, this is actually simple: we find exactly this sought-after connection in the velocity-dependence of the electric force.

The electric force of an electric field on an electric charge (the receiver) depends on the velocity $\overrightarrow{v_R}$ of this charge. The force is strengthened if the receiver moves towards the field (that is, he moves in the opposite direction to the field), and weakened if the receiver moves away from the field (that is, he moves in the same direction as the field).

Now, we know that there is the anti-field. Due to the anti-field the additional forces which arise from the $\overrightarrow{v_R}$ at the field and at the anti-field cancel each other exactly, so that only the electric and magnetic forces remain.

So, how can there be a gravitational effect here, at which the attraction is strengthened and the repulsion is weakened?

Well, this results automatically from the quantization of the energy transfer of the electric field to an electric charge, as I will show in the following.

3.3. The Quantization of the Energy Transfer of the Electric Field to an Electric Charge

In this chapter, I will describe the quantization of the energy transfer of the electric field to an electric charge.

Usually we ignore the electric fields of the protons and electrons if these cancel each other by superposition. But even if the forces of fields cancel each other, these fields still exist. And since these fields still exist, they still can exert their forces, therefore, transfer energy. But, they don't make this continuous and simultaneous but in quanta and after each other. In combination with the velocity-dependence of the electric force, a small residual effect results: gravitation.

Here, it is decisive to distinguish between the field and the anti-field. Till now, it has sufficed to assume that the field and the anti-field exert their forces simultaneously. At the quantization instead the field and the anti-field have to be distinguished, exactly as the positive and negative charges. So there are 4 combinations: positive field, positive anti-field, negative field, and negative anti-field. The quantization means that always only one of the fields can exert a force on a charge. If the fields of many charges superimpose, then the forces of the same fields add themselves up. This means, in the end, that a charge (as a receiver) has 4 different states between which it alters. As soon as a certain energy quantity is reached, the charge changes its state. I will say some more about this energy quantity in part 3 of this work.

The force of a field produces a velocity $\overrightarrow{v_{(t)}}$ (t is the time). The fields of the positive and negative charges exert their forces on a charge, seen statistically, in a balanced way after each other (at electrically neutral matter), so that this charge moves around a centre to and fro.

In addition to the kind of the charge, it also must be distinguished between the field and the anti-field. Here, it is that the field and the anti-field of one kind of a charge always - not only seen statistically - exert their forces after each other.

In part 1, on magnetism, we have seen that the forces which arise by a constant velocity ($\overrightarrow{v_R}$) from the field and the anti-field cancel each other. This, of course, is also valid when the field and the anti-field exert their forces after each other, since the $\overrightarrow{v_R}$ is equal in magnitude for the field and the anti-field.

Both the field and the anti-field of one type of a charge produce by their forces velocities in the *same* direction. But, though, due to the quantization the forces are not exerted simultaneously but after each other. And this means inevitably that the velocity relative to the field is different from the velocity relative to the anti-field! This, of course, concerns only the velocities which result from the forces of the field and the anti-field for one type of a charge after each other. Already existing, constant velocities are equal in magnitude for all fields, as said already.

So: The force of the field and the one of the anti-field on a charge produce velocities by which the forces of the field and the anti-field on this charge change, since the electric forces are velocity-dependent. And since the field and the anti-field exert their forces after each other, the velocity of the charge relative to the field is different from its velocity relative to the anti-field, which means that the force of the field and the one of the anti-field change in a different way. This difference is finally the gravitation. I will carry out the necessary calculations in the following chapter.

The described quantization may seem strange, on the other hand, there are numerous quantum phenomena [12] at subatomic particles - so, why should the electric charges not behave quantized when it is about the energy which they get from the electric fields?

3.4. On the Calculation of Gravitation

If the quantization shall produce gravitation, then the electric repulsion must be weakened and the electric attraction strengthened. This is *always* the case when *first* the anti-field and *then* the field exerts its force: at the repulsion (of same charges) the force of the anti-field produces a velocity in the opposite direction to the direction into which the anti-field propagates, which results in a strengthening of the force of the anti-field. Then the force of the field produces a velocity in the same direction in which the field propagates, which results in a weakening of the force of the field. The velocity produced before by the anti-field also has the same direction as the field, which causes an additional weakening of the field. So the weakening of the field is greater than the strengthening of the anti-field. Thus, altogether the weakening of the repulsion is greater than the strengthening of the repulsion. At the attraction (of opposite charges) it is analogous.

Let us now do the calculations:

The force of the field and the one of the anti-field each cause at a charge a velocity $\overrightarrow{v_{(t)}}$, in the direction of the respective force. As we have seen in part 1 of this work, the velocity $\overrightarrow{v_{(t)}}$ corresponds to a force (in part 1 that was the velocity $\overrightarrow{v_R}$ of the receiver) which also can contain a magnetic component. I will regard the magnetic component later on. Therefore, for the moment, we consider only the component of the $\overrightarrow{v_{(t)}}$ which is parallel to the speed of light $\vec{c}$ of the field or anti-field.

Since we want to integrate, it is easier to only work with the magnitudes. If the $\overrightarrow{v_{(t)}}$ has the same direction as the $\vec{c}$, then:

$$N \cdot F_c \cdot (c - v_{(t)}) = m_R \cdot \frac{dv}{dt}, \tag{3.1}$$

where F_c is known from part 1: $F_c = \frac{2 \cdot q_S \cdot q_R}{r^2 \cdot \varepsilon_0 \cdot 4 \cdot \pi \cdot |\vec{c}|}$ - here, we are primarily interested in the forces of the fields and the anti-fields on *one* elementary charge unit, this is the q_R (the R stands for "receiver" again). The q_S (the S stands for "source" again) is an elementary charge unit which produces a field and an anti-field, which exert their forces on q_R. The N is the number of the sources, that is the number of the elementary charge units which exert their forces with their fields and anti-fields on q_R. And m_R is, of course, the mass of q_R.

The N stands for those charges (of the sources) which are at the same place. At a spatial distribution of these charges an integration must be done over the corresponding volume. About, e.g., a homogeneous spherical distribution we know that it can be assumed that all charges are in the centre.

In part 1, the F_c still was multiplied with the factor ½ since the electric force results half from the field and half from the anti-field. Since we have learned now that the field and the anti-field exert their forces not at the same time but after each other, the factor ½ is not to be used. Instead, the field and the anti-field each exert their forces only for the half of the time. Furthermore, the charges of every *type* of charge only exert their forces for approximately the half of the time, too. Thus, the force must be multiplied with the factor 2. This factor 2 can formally be assigned to the field constant ε_0.

The $\overrightarrow{v_{(t)}}$ produces a force in addition to the force which arises from the $\vec{c}$ of the field or anti-field. If we want to know how big this additional force is, then we must know how big the $\overrightarrow{v_{(t)}}$ is in the course of time. From (3.1) we get:

$$\frac{N \cdot F_c}{m_R} \cdot dt = \frac{dv}{(c - v_{(t)})} \Rightarrow \frac{N \cdot F_c}{m_R} \cdot \int_{t_0}^{t} dt = \int_{v_0}^{v} \frac{dv}{(c - v_{(t)})} \tag{3.2}$$

$$\Rightarrow v_{(t)} = c - (c - v_0) \cdot e^{-t \cdot Q}$$

with $t_0 = 0$ and $Q = \frac{N \cdot |F_c|}{m_R}$. Since the q_S and the q_R have signs of their own, here, the absolute value of F_c is used, since the signs are already inserted according to the respective case. The v_0 is, of course, the initial velocity; that is the velocity which the receiver already has before a field or anti-field exerts its force. At the v_0, as at the $v_{(t)}$, we also consider, for the moment, only the component

which is parallel to c, while, of course, the v_0 can have the same or the opposite sign as the c.

If the $\overrightarrow{v_{(t)}}$ has the opposite direction as the $\vec{c}$, then we get:

$$N \cdot F_c \cdot (c + v_{(t)}) = m_R \cdot \frac{dv}{dt}. \tag{3.3}$$

Integrating yields:

$$v_{(t)} = -c + (c + v_0) \cdot e^{t \cdot Q}. \tag{3.4}$$

Now we can calculate the force of the fields and anti-fields of the sources on a charge, the receiver, in the course of time (that is $F_{(t)}$).

We start with the attraction (between opposite charges). At attraction, of course, the sources have the opposite sign as the receiver. The *anti-fields* of the sources exert their forces *first*. At attraction, the anti-fields of the sources have the same direction as the forces which they exert on the receiver. So it is: $F^-_{(t)} = N \cdot F_c \cdot (c - v_{(t)})$ (the high-ranking "-" indicates the anti-field). Here, we use (3.2) for the $v_{(t)}$. Thus we get: $F^-_{(t)} = N \cdot F_c \cdot (c - v_0) \cdot e^{-t \cdot Q}$, in which v_0 is the velocity which the receiver already had before the anti-fields have exerted their forces. *Then* the *fields* of the sources exert their forces. At attraction, the fields of the sources have the opposite direction as the forces which they exert on the receiver. So it is: $F^+_{(t)} = N \cdot F_c \cdot (c + v_{(t)})$ (the high-ranking "+" indicates the field). Here, we use (3.4) for the $v_{(t)}$. Thus we get: $F^+_{(t)} = N \cdot F_c \cdot (c + v_0) \cdot e^{t \cdot Q}$. For the v_0, here, we must use the velocity which the receiver has after the anti-fields have exerted their forces. (This means, that we must take into account the velocity which the anti-fields have produced.) If we assume that the anti-fields have exerted their forces for the time period T, we get the velocity: $v_{(T)} = c - (c - v_0) \cdot e^{-T \cdot Q}$. Therefore: $F^+_{(t)} = N \cdot F_c \cdot (c + (c - (c - v_0) \cdot e^{-T \cdot Q})) \cdot e^{t \cdot Q}$.

For the moment, we assume that the anti-field and the field exert their forces equally for the same time period, therefore, that the anti-field and the field each exert their forces the half of the time. It is not quite clear if that is to be always this way. Whether it also can be different and which implications this would have, must be cleared in further, following works.

So, the total time for the field and the anti-field is $2 \cdot T$. So we can determine the average force from the field and the anti-field over the time. And then this average force shall correspond to the sum of the electrostatic force plus the gravitational force (F_G). Or said differently: We set the sum of the momenta which result by the anti-field and the field each in the time T equal to the momentum which results from the resultant force from the electrostatic force and the gravitational force in the time $2 \cdot T$. So it is:

$$\begin{aligned} &\frac{\int_0^T F^-_{(t)} \cdot dt + \int_0^T F^+_{(t)} \cdot dt}{2 \cdot T} = N \cdot (F_c \cdot c + F_G) \\ &\Rightarrow \frac{F_c \cdot 2 \cdot c \cdot (e^{T \cdot Q} - 1)}{2 \cdot T \cdot Q} = F_c \cdot c \cdot (1 + \frac{F_G}{F_c \cdot c}) \\ &\Rightarrow e^{T \cdot Q} = 1 + T \cdot Q \cdot (1 + K), \end{aligned} \tag{3.5}$$

with $K = \frac{F_G}{F_c \cdot c}$.

From (3.5), the time T can be calculated at which the velocity-dependence of the electric force produces, at attraction, exactly the gravitational force.

At repulsion (between same charges) we proceed analogously: The anti-fields of the sources exert their forces first. At repulsion, the anti-fields of the sources have the opposite direction as the forces which they exert on the receiver. So it is: $F^-_{(t)} = N \cdot F_c \cdot (c + v_{(t)})$. Here we use (3.4) for the $v_{(t)}$. Thus we get: $F^-_{(t)} = N \cdot F_c \cdot (c + v_0) \cdot e^{t \cdot Q}$. Then the fields of the sources exert their forces. At repulsion, the fields of the sources have the same direction as the forces which they exert on the receiver. So it is: $F^+_{(t)} = N \cdot F_c \cdot (c - v_{(t)})$. Here we use (3.2) for the $v_{(t)}$. Thus we get: $F^+_{(t)} = N \cdot F_c \cdot (c - v_0) \cdot e^{-t \cdot Q}$. For the v_0, here, too, we must use the velocity which the receiver has after the anti-fields have exerted their forces. If we assume that the anti-fields have exerted their forces for the time-period T, we get the velocity: $v_{(T)} = -c + (c + v_0) \cdot e^{T \cdot Q}$. Therefore: $F^+_{(t)} = N \cdot F_c \cdot (c - (-c + (c + v_0) \cdot e^{T \cdot Q})) \cdot e^{-t \cdot Q}$. To get the average force, we integrate as in the case of the attraction and we finally get:

$$\Rightarrow e^{-T \cdot Q} = 1 - T \cdot Q \cdot (1 - K). \tag{3.6}$$

From (3.6), the time T can be calculated at which the velocity-dependence of the electric force produces, at repulsion, exactly the gravitational force.

Unfortunately, the equations (3.5) and (3.6) can not be solved exactly for T. So there must be used approximation procedures which are not quite trivial.

For the attraction, that is (3.5), we get: $T_+ = \frac{-W\left(-\frac{e^{-\frac{1}{K+1}}}{K+1}\right) \cdot (K+1) - 1}{(K+1) \cdot Q}$, were $W\left(-\frac{e^{-\frac{1}{K+1}}}{K+1}\right)$ is the Lambert-W function, and the subscript "+" at the T indicates the attraction.

For the repulsion, that is (3.6), we get: $T_- = \frac{W\left(\frac{e^{\frac{1}{K-1}}}{K-1}\right) \cdot (K-1) - 1}{(K-1) \cdot Q}$, were the subscript "-" at the T indicates the repulsion.

3.5. Discussion on the Calculations

The first, that we notice, is that (3.5) and (3.6), therefore T_+ and T_-, are independent from the initial velocity (v_0). The v_0 is the velocity which the receiver has before the anti-field of a source exerts its force, that is, before any source exerts a force on the receiver at all. When the time during which the anti-field exerts its force is exactly as long as that one of the field (that is T for each), the v_0 is correctly cancelled.

At next, we see that T_+ and T_- depend on K. And $K = \frac{m_R \cdot m_S \cdot G \cdot \varepsilon_0 \cdot 4 \cdot \pi}{2 \cdot q_S \cdot q_R}$, were G is the gravitational constant. I must go into more detail on m_S: At equation

(3.5), F_G is the gravitational force by whose amount the electric force changes. Due to the quantization always only one type of a charge (positive or negative) of the sources exert their forces on the receiver. But for the gravitational force, the masses of both types of a charge must be taken into account. In addition, the mass of the neutrons also must be taken into account (I will say more on that later). So, for electrically neutral matter, $m_S$always is the sum of the mass of the proton (m_{p^+}), the electron (m_{e^-}), and the neutron (m_n), so that $m_S = m_{e^-} + m_{p^+} + m_n$. (The number of the sources (that is N) doesn't appear in K.) So, for electrons and protons *as receivers*, there are two different values for K, at electrically neutral matter. Therefore, the value of T_+ or T_-depends on $m_S \cdot m_R$, but this had to be expected since the magnitude of gravitation is determined here. In the chapter "Gravitational and inert mass", I analyse the connection between m_S and T_+ and T_-more detailed.

Furthermore, we recognise that both T_+ and T_- are proportional to $1/Q$. And since $Q = \frac{N \cdot F_c}{m_R}$, we get, quite generally, for T the proportionality: $T \propto \frac{r^2 \cdot m_R}{N}$. We know that, due to the quantization of the electric force, a charge moves to and fro in the direction of the force. Therefore, the $1/T$ is the frequency with which a charge, with the mass m_R, oscillates within a gravitational field, while, of course, we know now that the gravitational field results from the sum of the electric fields of the positive and negative charges. The frequency of this electric gravitational oscillation is reversed proportional to m_R, and, because of K, it depends on $m_S \cdot m_R$. In addition, the frequency of the electric gravitational oscillation decreases with a growing distance from the source of the gravitational field, and it increases with a growing gravitational field since N is the number of the sources.

The grater N is, all the smaller T is. For an object, such as the earth, N is inconceivably great. Nearby the earth, T is correspondingly small. The electric gravitational oscillation seems more like a trembling than like a clear motion here. On the other hand, one can consider electric charges as being approximately dot-like in the first place (I will go into more detail on that in part 3 of this work), so that there is sufficient space even for the smallest motions.

It also is astonishing that $T \propto r^2$. Without a gravitational field it is $T = 0$, what also could apply to a Lagrange point. Automatically, the question comes up, which further consequences the electric gravitational oscillation could have, except, of course, that it produces gravitation. It could have effects on the processes in an atom, influence the interaction behaviour of the electric charges, or influence even the life expectancy of electric particles - or it may not.

At next, to better understand T, we regard the hypothetical case that the mass of the receiver is equal in magnitude at both at the positive and at the negative charges, that, therefore, K is always the same. We are interested in knowing whether in this case the T_+ of the attraction and the T_- of the repulsion are also equal in magnitude. Thus, we want to know, whether their difference is zero. Inserting yields: $\Delta T = T_- - T_+ = W_- + W_+ + \frac{2}{1-K^2}$, were W_- and W_+ are the Lambert-W functions for the repulsion and the attraction respectively. In our case it is: $K \ll 1$, which means that both W_- and W_+ are very near to -1. So it is: $W_- + W_+ \approx -2$. In addition it is: $\frac{2}{1-K^2} \approx 2$. And this means that $\Delta T \approx 0$, which means that the process of repulsion and the process of attraction are nearly identical. A more exact calculation shows that $\Delta T > 0$. Therefore: $T_- > T_+$, which means that even at always equal masses the T_+ and the T_- are not exactly the same. But this seems quite plausible since, overall, the force is weakened at the repulsion while it is strengthened at the attraction. The difference, though, is very small. It can be seen at the graphic 3.1 (which can be found a little below) in the difference of the slopes of the exponential functions for the forces in the course of the time.

After we have calculated T, we also can calculate $v_{(T)}$.

The first that we notice if we insert T into $v_{(T)}$ is that Q is cancelled. Thus, the $v_{(T)}$ is independent from N and from r^2. So the $v_{(T)}$ is independent from the magnitude of the source of the gravitational field, and from the position within the gravitational field, which means: the $v_{(T)}$ is independent from the strength of the gravitational field.

Since the K is not cancelled, the $v_{(T)}$ depends on $m_S \cdot m_R$. In addition, it must be distinguished whether the $v_{(T)}$ has the same or the opposite direction as the $c$of the field or anti-field. For electrons and protons, this results in six different values for $v_{(T)}$, which characterize the respective type of the interaction. In this sense, the $v_{(T)}$ is a quantum quantity for electric charges.

After we have calculated $v_{(T)}$, we also can calculate easily the change of the energy, which results by the force of the anti-field or field: $E = 1/2 \cdot m_R \cdot (v_{(T)}^2 - v_0^2)$. At small velocities we can calculate non-relativistically. We also could have calculated $E = F_c \cdot \int_0^T (c \pm v_{(t)}) \cdot ds = F_c \cdot \int_0^T (c \pm v_{(t)}) \cdot v_{(t)} \cdot dt$, but one doesn't get any handy equations here.

The energy, calculated here, consists of energy quanta whose magnitude results from the way of the respective interaction, which, therefore, depends on $m_S \cdot m_R$. So, there are energy quanta of different magnitude. And so we see that, at the quantization of the energy transfer of the electric field to an electric charge, the field *isn't* subdivided into quanta, as at first one could assume. The quantization rather arises from the quantum levels of the receiver.

Once again, we come back now to our hypothetical case at which the masses of the elementary charge units are equal in magnitude. We have seen that $T_- > T_+$, while, at the same time, the force at the repulsion altogether is smaller than at the attraction ($F_- < F_+$). This could compensate each other so that in the two cases the same amount of energy would be transferred, which, of course, may not be, since more energy is transferred at the attraction than at the repulsion. To check this, we calculate the $v_{(T)}$ for the attraction by adding the $v_{(T)}$ of the anti-field to the one of the field, in which, of course, the T of the anti-field is equal in magnitude as the one of the field. We get: $2c \cdot (e^{T_+} - 1) + v_0$. And for the repulsion we get: $2c \cdot (1 - e^{-T_-}) + v_0$. The difference $\Delta v = 2c \cdot ((e^{T_+} + e^{-T_-}) - 2)$ must be bigger than zero. Therefore it must be

$(e^{T_+} + e^{-T_-}) > 2$. If we call $d$the difference between T_+ and T_-, than : $T_- = T_+ + d$. And therefore: $(e^{T_+} + e^{-(T_+ + d)}) > 2$. Or more general: $(e^{T} + e^{-(T+d)}) > 2$. Conversion yields: $2 \cdot e^{T} - e^{2 \cdot T + d} < 1$. This inequality is valid, because for $T = 0$it is $2 \cdot e^{0} = 2$ and $e^{2 \cdot 0 + d} \approx 1 + d$, and for $T > 0$the $e^{2 \cdot T + d}$ increases faster than the $2 \cdot e^{T}$. And therefore it is $\Delta v > 0$, as demanded.

Although we get the correct results it seems strange that we get differently grate quanta even if the masses are all the same. This shows us that the magnitude of the quanta cannot only depend on the masses. The magnitude of the quanta rather depends also on the velocity $v_{(t)}$ of the receiver. I will go into that ingrater detail in part 3 of this work.

So we see, that $T_- > T_+$. However, the difference is negligible small, and, of course, it must be very small, because the fact that the repulsion lasts longer than the attraction means a weakening of the gravitation, which, of course, is an attraction.

I want to go into that in a little more detail now: Since T_+ or T_- are very small, the exponential function, with which we calculate $F_{(t)}$, can be regarded, in sufficient precision, as being straight. For each, for the attraction as for the repulsion, we get one such straight for the field and one for the anti-field. The slopes of these 4 straights differ only very little from each other. These differences correspond to the difference between $c$and $c \pm v_{(T)}$ (and we know that $v_{(T)} \ll c$). From the differences of the slopes, $T_- > T_+$ arises. Approximately, $\Delta T (\approx 0)$ can be neglected. If one must know it more precisely, then, from the momentum *calculated* for the gravitation, the momentum $N \cdot (F_c \cdot c + F_G) \cdot \Delta T$ must be subtracted, to get the momentum of the actual gravitation.

At $T_- > T_+$ we also recognize that the repulsion of a *net* charge of the sources (which means that the source is *not* electrically neutral) is greater than the attraction, but, though, the difference is smaller than the gravitational force of these net charges, so it might hardly be measurable.

Alternatively, we could have set $T_- = T_+ = T$ in the first place, and then calculate T by $N \cdot (\int_0^T F_+^+ + \int_0^T F_+^- + \int_0^T F_-^+ + \int_0^T F_-^-) = N \cdot (F_c \cdot c - F_G)$. For the T calculated in this way, we then expect: $T_- > T > T_+$. But, though, in this case, too, the repulsion of a net charge of the sources is a little (very little) greater than the attraction. One can clarify himself these connections very well at the graphic which I show below and which shows the force in the course of the time, because there the areas correspond to the momenta.

Altogether, it remains to say that it still could get quite thrilling to evaluate the actual values for T_+^+, T_+^-, T_-^+, and T_-^-- particularly by experiments.

I illustrate in graphic 3.1 the force in the course of the time for the attraction, while, to make it better recognizable, the values are exaggerated hopelessly: $v_0 = 0$, $c = 10$, and $T_+ = 0.2$. The fat line shows that the force decreases exponentially until $T_+ = 0.2$, then it jumps, and then it increases exponentially until $T_+ = 0.4$, in which the slope is smaller when the force decreases than when it increases. From this a tiny difference already arises between the electrostatic force and the average force which results from the field and the anti-field. Therefore, regarding the areas B and D it is: D>B. The areas represent the respective change of momentum. The area A represents the change of momentum which is caused by the electrostatic force. But, what we primarily see in the graphic, is, that the difference between the average force and the electrostatic force is represented mainly by the area C. The area C results due to the jump of the force at the change from the anti-field to the field. From this, a simplified representation can be derived for the emergence of gravitation, which I will show in chapter after the next chapter briefly.

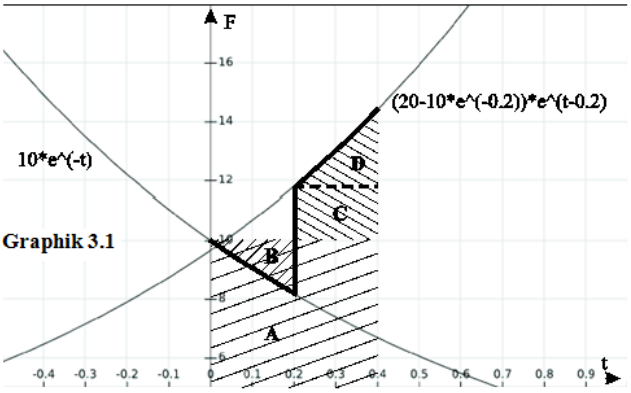

Graphik 3.1

Graphik 3.1.

At the end of this chapter, I would like to say something about the neutrons briefly:

I, in principle, assume that the neutrons also participate in gravitation. But, gravitation is an electric effect. Therefore the neutrons must consist of positive and negative electric charges equal in magnitude. Because the neutron has a similar mass as the proton, I assume that the neutron consists of *one* positive and *one* negative elementary charge unit.

Alternatively, it is also possible to assume that the neutron is alternately positive and negative. This possibility results from the qualities of the field and the anti-field, as I will show in part 3 of this work. In any case, the neutron takes part in gravitation according to its mass.

3.6. Gravitational Mass and Inertial Mass

At the calculation of the $v_{(T)}$ (through the equation (3.1)) I have assumed that m_R is the inertial mass. For the calculation of the gravitational force (through the equations (3.5) or (3.6)) I have assumed that m_R is the gravitational mass. So, I haven't distinguished between inertial and gravitational mass.

Now it is, that, because of the quantization of the transfer of the electric energy, always only *either* the positive *or* the negative charges of the sources exert their forces on a receiver. This would mean that, for the time T, too, always only *either* the masses of the positive *or* of the negative charges of the sources are taken into account for gravitation. And, in turn, this would mean that, in the end, the gravitational acceleration of the protons would be greater than the one of the electrons. But, there isn't any single experiment, that would ever have shown such a result.

For that reason, for the mass m_S of the source both the masses of the positive and those of the negative sources are taken into account, so that $m_S = m_{e^-} + m_{p^+} + m_n$

(while the number of the sources still results by the multiplicationwith N).

In the first moment, this seems a little strange. Why should the masses, whose charges don't exert forces, should be taken into account? Let us remember, what the T is. The time $T$is the time-period of a quantum level of a receiver. Actually, it is not very clear, how the magnitude of T results. I just calculate how great T must be, so that gravitation results. Here now we recognize that the T_+ of the attraction and the T_- of the repulsion are not independent of each other.

We know that the electric fields of the positive and negative sources still exist, although they cancel each other, at electrically neutral matter. They exert equally strong attractive as repulsive forces on a receiver. One can regard these attractive and repulsive forces also as a state of tension.

From this way of looking at the state of the receiver, the following connection (which I will explain in grater detail in part 3 of this work) can be derived: A charge, which isn't exposed to any fields, is in the state of equilibrium. As soon as the field of a source exerts its force on a receiver, a velocity ($v_{(t)}$) which disturbs the state of equilibrium arises. As soon as the perturbation exceeds a certain extent, the receiver changes his quantum level. The velocity $v_{(T)}$ at which the receiver changes his quantum level depends both on the masses of the sources whose fields cause the state of tension and on the mass of the receiver.

In the end, a receiver can never be in the state of equilibrium even if he is within the fields of electrically neutral matter. Instead, he will move to and fro, in dependence of the strength of the state of tension, while the anti-fields and fields of the positive and negative charges exert their forces alternately.

So one can say that the changes of the quantum level of the receiver are caused by the anti-fields and fields of the sources, while T_+ and T_- yield from the state of tension. The state of tension for its part obeys $\frac{N}{r^2}$, as it shall be.

3.7. Simplified (alternative) Representation

To check in a simple way whether the velocity-dependence of the electric force and the quantization of the energy transfer produce gravitation, I had started with a very simple representation. Since this simplified representation contains some interesting aspects, I would like to describe it briefly here.

Essentially, I had assumed that an electric charge (with mass) doesn't get its velocity (that was in the previous chapter the $v_{(t)}$) continuously by an acceleration but that the velocity occurs spontaneously for every quantum (that was in the previous chapter the $v_{(T)}$). The energy for this spontaneous $v_{(T)}$ comes temporarily from the mass of the charge, while the relativistic change of the mass can be neglected since the $v_{(T)}$ is very small. Then the force of the field or anti-field acts on the charge and transfers exactly that amount of energy to the charge which corresponds to $v_{(T)}$. But, though, this amount of energy isn't seen in a change of the velocity of the charge, instead the mass of the charge increases until it has reached its original magnitude again. Meanwhile, the charge has been moving with the velocity $v_{(T)}$ (for the time-period T), of course. Here, I assume again that for the anti-field and for the field $T^+ = T^- = T$, since, e.g., there otherwise may be problems with the magnetic force.

Under the prerequisites mentioned, here, the $v_{(T)}$ can be calculated very easily by equating the average force from the field and the anti-field with the resultant from the electrostatic force and the gravitational force, again, as in the previous chapter, which means that we equate the momenta caused by the forces:

$$\frac{T \cdot N \cdot F_c (c \mp v_{(T)}^-) + T \cdot N \cdot F_c (c \pm (v_{(T)}^- + v_{(T)}^+))}{2 \cdot T} = N \cdot (F_c \cdot c \pm F_G),$$

were $v_{(T)}^-$ is the velocity of the anti-field and $v_{(T)}^+$ the one of the field; and at $\pm$ and $\mp$ the upper signs correspond to the attraction and the lower to the repulsion. The N is the number of the sources, as in the previous chapter. Doing the multiplications yields: $v_{(T)}^+ = 2 \cdot \frac{F_G}{F_c}$. Since the $v_{(T)}^-$ doesn't appear in the result (it cancels itself) its value can be chosen freely. I choose (more or less arbitrarily): $v_{(T)}^- = v_{(T)}^+ = v_{(T)}$.

Now, it is easy to calculate the $T$for the mass m_R of a charge (a receiver) since the average force of the field and the anti-field shall cause the change of the velocity $2 \cdot v_{(T)}$ in the time $2 \cdot T$:

$$\frac{T \cdot N \cdot F_c \cdot (c \mp v_{(T)}) + T \cdot N \cdot F_c \cdot (c \pm 2 \cdot v_{(T)})}{2 \cdot T} = m_R \cdot \frac{2 \cdot v_{(T)}}{2 \cdot T}.$$

Doing the multiplications yields:

$$T = \frac{m_R}{N \cdot F_c \cdot \left(\frac{c}{v_{(T)}} \pm \frac{1}{2} \right)} = \frac{m_R \cdot v_{(T)}}{N \cdot F_c \cdot c},$$

where $\pm\frac{1}{2}$ is negligibly small compared with $\frac{c}{v_{(T)}}$.

We immediately recognise that, e.g., at the attraction the force of the anti-field $F_c \cdot (c - v_{(T)})$ can by no means transfer the same amount of energy as the force of the field $F_c \cdot (c + 2 \cdot v_{(T)})$ in the same time T. This means that the anti-field transfers less energy than necessary for the production of $v_{(T)}$, and the field transfers correspondingly more energy, so that the energy balance is compensated at the end (at the repulsion it is analogous).

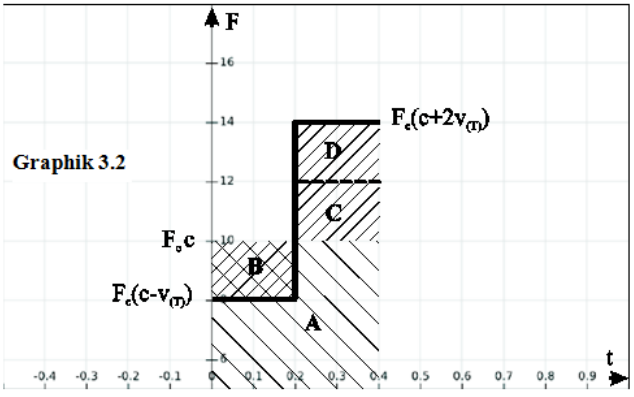

Graphik 3.2.

In graphic 3.2 I illustrate, again, the force in the course of time for the attraction, while, to make it better recognizable, the values are, again, exaggerated hopelessly: $v_0 = 0$, $c = 10$, and $T = 0.2$. The fat line shows from $T = 0$ till $T = 0.2$ the constant force of the anti-field, then the force jumps, and then we see the constant force of the field until $T = 0.4$. The area A represents again the change of the momentum which is caused by the electrostatic force. The areas B and D are equal in size, so that the difference between the electrostatic force and the average force of the field and the anti-field is represented exactly by the area C.

At the end of this chapter we want to see now how big $v_{(T)}$ is. For a proton within the gravitational field of electrically neutral matter we get $v_{(T)p+} \approx 8.8 \cdot 10^{-28} ms^{-1}$. It is inconceivable to see, how small $v_{(T)}$is. And T isn't less small either. For a proton we get: $T_{p+} \approx \frac{r^2}{N} \cdot 456 \cdot 10^{-28} s$. For a proton on the earth's surface, $r$is the radius of the earth, and N is the number of the positive or negative charges of the earth.

I think that in this chapter the character of the quantization gets recognizable very well.

3.8. The Magnetic Part of Gravitation

At first, we shall regard the initial velocity v_0. It corresponds to the velocity v_R of the receiver from part 1 of this work where we have calculated the magnetic force. We had found out that, at motionless sources, the forces of the field and the anti-field which arise by the v_R cancel each other exactly. This is still valid on temporal average, when the fields and anti-fields exert their forces not at the same time but after each other.

If the sources move, therefore, if the fields and the anti-fields have an angle, then a magnetic force arises by the v_R (which is here now the v_0). But, since the fields and the anti-fields of the positive and negative charges alternate exactly at electrically neutral matter, no magnetic force will arise on temporal average here either. (Except of some very small effects which can arise by changes of the directions, which I will not treat further here.)

Now, we shall regard $v_{(T)}$. If the sources move (with v_S), as, e.g., the electrons in the atoms do, then there are angles between the forces of their fields and anti-fields and the directions in which their fields and anti-fields propagate. The $v_{(T)}$ for its part has the same direction as the force from which it arises.

We want to find out now which consequences the change of the direction of the force has. This time, as example, we regard the repulsion. We know that when $v_S = 0$ at repulsion always $v^-_{(T)} > v^+_{(T)}$, since for the field the $v^-_{(T)}$ is added to the initial velocity, so that it is weakened more than the anti-field is strengthened by the emergence of the $v^-_{(T)}$. In Figure 3.1 the case $v_S \neq 0$ is represented, while only one possible v_S is represented. The Figure 3.1 corresponds to the Figure 2.3 from part 1 of this work. The $v^-_{(T)}$ and the $v^+_{(T)}$ for $v_S = 0$ are represented as $v^-_{(T0)}$ and $v^+_{(T0)}$ (and they are represented far too great, so that they will be recognisable better, because in reality $v^-_{(T0)}$ and $v^+_{(T0)}$ are negligible small compared with c^+). In Figure 3.1 we can see that $v^-_{(T)}$ gets smaller in the direction of c^+ (therefore also in the direction of c^-) due to the angle φ^-. But exclusively the component of the $v^-_{(T)}$ which is parallel to c^+ is responsible for the weakening of the field, which, of course, exerts its force after the anti-field. Therefore, the weakening of the field is weakened (for $v_S \neq 0$ compared with $v_S = 0$), which means that the repulsion altogether is weakened less, so that gravitation is also weakened.

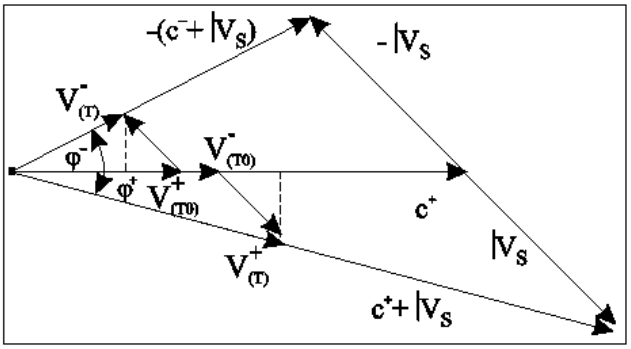

Figure 3.1.

But, of course, we know that, in the end, gravitation isn't weakened all in all; the explanation for that is that the v_S is, e.g., the velocity of the electrons in the atom. And in Figure 3.1 only one possible direction is represented for the v_S. At its motion within the atom the electron will move also in exactly the opposite direction, and there then gravitation is strengthened (by the same amount as it is weakened in the opposite direction).

This then is the conclusion of this chapter: In the end, at electrically neutral matter, with no net-currents flowing, the magnetic forces of the fields and anti-fields of the positive and negative charges compensate each other exactly. That is: there is no resultant magnetic force at gravitation. More detailed considerations, which are surely necessary here, will follow in further works.

However, one already recognizes how easily the equilibrium of the forces can be disturbed. E.g., one only would need to assume that the electron doesn't always move continuously within the atom, but, that it executes something like "quantum jumps". The equilibrium could already be disturbed. It isn't clear either yet, how accelerations have an effect.

At the end of this chapter, I still would like to draw our attention to such an equilibrium of forces to avoid irritations since the connection doesn't immediately discloses itself:

The $v_{(T)}$ always has the same direction as the force. This means that if the sign of the force changes then the direction of the $v_{(T)}$ changes, too, so that the magnetic force has the same direction both for the attraction and for the repulsion.

So, here, one could come to the incorrect assumption that a resultant magnetic force arises if a charge (a receiver) moves to and fro due to the positive and negative fields and anti-fields of an electrically neutral object (which represents the sources).

But actually, one must consider that a receiver isn't accelerated only positively but that he must also be accelerated negatively (therefore slowed down) so that he can move at all to and fro. And while the receiver slows down he continuous to move in the same direction as

when he was accelerated, but here now the force has the opposite sign, and this means that the magnetic force has the opposite direction when slowing down as when accelerating, so that *no* resultant magnetic force arises.

So, although gravitation results from the quantization for the transfer of the electric energy, there don't seem to occur any considerable magnetic effects.

I nevertheless think that the magnetic part of gravitation is most likely to show deviations from classic gravitation - if there are any at all. Also a technical influence on gravitation seems here more possible then elsewhere - I remind the somehow strange results regarding the super-conductive, rotating plates [33,34,35,36]. In any case, the magnetic part of gravitation must urgently be analysed more exactly.

3.9. On General Relativity

I don't treat general relativity (GR) [7,8,9] here. However, I don't see any contradictions any way.

In GR the principles of special relativity (SR) are applied to the gravitational acceleration. The result is the description of the gravitational field as curved spacetime. The great advantage of this consideration is that the changes of spacetime, which arise in accordance with SR, can be taken into account here. So, in this way, e.g., the planetary orbits [16] are calculated more correctly than only by Newton's laws since the conditions of SR, which are to be regarded as valid, are applied to gravitation.

Since we know now that gravitation isn't a force of its own, since gravitation is an electric effect, it is necessary to apply the conditions of SR to the electric fields and anti-fields, or to their forces and accelerations. Here, the quantization of the transfer of the electric energy, as it is described in this work, is to be taken into account. The result of such an procedure must be GR here again, too.

We can regard the curvatures of spacetime of GR as some sort of resultant field. If we look more exactly, then we see the electric fields and anti-fields and the quantum levels of the electric charges to whose accelerations SR is applied. In turn the electric forces yield in their sum the conditions of GR. It principally is about two different ways of looking at the same thing, and both ways yield the same results.

GR is more general (of course). It describes gravitation without going the detour via the electric force. But, though, I cannot derive GR from the electric forces yet. This is a task for coming works.

The question, whether the curved spacetime actually exists, cannot be answered here either. I merely show that in reality the gravitational field reveals to consist of electric fields and anti-fields at a more exact consideration. For this reason I also can not make any helpful statements on the gravitational waves here, although one can suspect that the gravitational effects, from which the gravitational waves arise, exist quite independently from the existence of the curved spacetime.

3.10. Closing Remark to Part 2

I think that I could show clearly that gravitation is an electric effect. Therefore, a gravitational force of its own, without electric forces, cannot exist.

Apart from the velocity-dependence of the electric force, which is known from part 1, I only have assumed that electric charges can change between different quantum levels if their energy state changes. From this then gravitation can be calculated as an electric effect. A relativistic calculation of this electric effect then would yield GR.

Being able to present the connection between the gravitation and the electric force opens numerous new cognitions, particularly regarding the behaviour of electric charges. New approaches arise for experiments, and also new technical applications will appear hopefully soon, particularly regarding the magnetic part of gravitation.

A new, exciting world opens up, with thrilling challenges.

4. Part 3: On Quantization and on Electricity as Alternating Spacetime

4.1. Introduction to Part 3 / Motivation

We have seen that gravitation is an electric effect between electric charges. And although the electric charges exert exclusively electric forces on each other, the gravitational force is nevertheless proportional to the product of the interacting masses. This means that the electric field of a charge and also the charge itself must have a quality in which the mass of the charge is disclosed. From this quality, the quantization of the transfer of the electric energy arises, from which then the $v_{(T)}$ results, and therefore gravitation.

I will show that the mass of the electric charge is substantiated in the fact that the electric charge is a spacetime wave. Further interesting connections then arise apart from the quantization of the transfer of the electric energy. Not least, the emergence of the electric force can be understood better here, too.

4.2. The Electric Charge as a Spacetime Wave

Already deBroglie had used the equation $\frac{m_0}{\sqrt{1-\frac{v^2}{c^2}}}\cdot c^2 = h\cdot f$ at his derivation of the matter waves, were m_0 is the rest mass, v the velocity, f the frequency, and hPlanck´s constant.

The term before the equality sign can be developed: $\frac{m_0}{\sqrt{1-\frac{v^2}{c^2}}}\cdot c^2 = m_0\cdot c^2 + \frac{1}{2}\cdot m_0\cdot v^2 + \ldots .$

The first term after the equality sign (that is $m_0\cdot c^2$) was ignored by deBroglie since it is constant and deBroglie was only interested in the velocity of the mass-particle.

But exactly this first term is particularly interesting for us here.

Because we can write:

$$m_0\cdot c^2 = h\cdot f_{m0} \Rightarrow f_{m0} = \frac{m_0\cdot c^2}{h}. \qquad (4.1)$$

Here, the frequency f_{m0} is assigned to a particle with the rest-mass m_0. One generally assumes that there cannot be an electric charge without mass. I additionally state that, in principle, mass without charge cannot be, either, while I always assign two opposite charges equal in magnitude to every electrically neutral mass (such as the neutron). So, if the frequency f_{m0} is assigned to a mass m_0, then this frequency is assigned to an electric charge with the mass m_0.

Here, an electric charge reveals to be an oscillation whose frequency is proportional to its mass. This is exactly the quality of an electric charge, we were looking for: the mass of an electric charge is represented in the frequency of the electric charge.

Therefore, it cannot be distinguished between the mass and the electric charge. In this sense, it doesn't make sense to distinguish between the electric charge and its field either. Much more, the electric charge is the oscillation of its field. I will describe this oscillation more exactly now.

In the first part of this work, I show that the magnetic field is an angled electric field, which means that there isn't a magnetic field of its own. In the second part of this work, I show that gravitation is an electric effect, which means that there isn't a gravitational field of its own. It almost seems as if the electric field were the most basic of all fields. And now we see that the electric field appears to be oscillation.

A field represents a spatial quality. And the most basic element of space is space itself. If the electric field is the most basic of all fields, then it seems almost compelling that the oscillation of the electric field is the oscillation of space itself. Of course, space still has, in addition, the quality of time. An electric charge is, therefore, oscillating spacetime.

We know from GR, and the gravitational waves derived from it, that oscillating spacetime contains energy. In a similar way also the oscillating spacetime of the electric charges contains energy. This energy can be transferred to charges and cause changes of the velocity, according to the forces of the electric charges.

I cannot say much about the exact composition of the spacetime and its oscillations of electric charges yet. But, I can name some qualities of these oscillations and show, at least, in principle, how they cause changes of velocity. This is carried out in the coming chapters.

4.3. Energy / Beat (interference)

The electric force is proportional to r^{-2} and arises, according to the previous chapter, from an oscillation of spacetime. If we assume that the force is proportional to the amplitude of the oscillation of spacetime, then the amplitude of the oscillation of spacetime is proportional to r^{-2}, too. This implies that the charge has a centre towards which the amplitude of the oscillation of spacetime increaseswith r^{-2}.

Since the electric force (of a motionless charge) is equal in all directions, we have to assume, for symmetric reasons, that the oscillation of spacetime of an electric charge is a spherical oscillation - which corresponds to a longitudinal oscillation. This oscillation spreads, starting out from the centre, into infinity, with an amplitude proportional to r^{-2}.

As we know by now, an electric charge consist of a field and an anti-field. All electric qualities applied similarly to the field as to the anti-field till now. Thus, I assume that the f_m applies both to the field and to the anti-field. For a motionless charge the f_{m0} of the field shall be equal to that of the anti-field. The field and the anti-field propagate with the speed of light in opposite directions. If two waves of the same frequency and opposite directions superimpose, then a *standing wave* is made. So, a motionless electric charge is a standing spherical wave whose amplitude increases towards the centre with r^{-2}, while the field moves away from the centre, and the anti-field moves towards the centre.

If an electric charge with the mass $m$moves with the velocity v_m, then the f_m changes according to the velocity, and to be more precise both the f_m of the field and that of the anti-field change. For the wave, which propagates in the same direction as the charge, the frequency increases, and for the wave, which propagates in the opposite direction as the charge, the frequency decreases. If the frequencies of two waves (which superimpose) are different, then *beat* arises.

For beat there are two frequencies: the carrier frequency and the frequency of the beat.

We first regard the carrier frequency. The carrier frequency is the average frequency of the frequencies, which superimpose. Under consideration of the relativistic time-dilatation, which arises for a charge which moves with the velocity v_m, the carrier frequency of the charge is:

$$f_m = \frac{f_{m0}}{\sqrt{1-\frac{v_m^2}{c^2}}}, \qquad (4.2)$$

were f_{m0} is the frequency of the standing wave. We begun with assigning the frequency f_{m0} to the rest mass m_0. Now we see that by the introduction of the anti-field the carrier frequency corresponds exactly to the relativistic mass. Inserting (4.1) into (4.2) yields: $f_m = \frac{m \cdot c^2}{h}$. So we can retain: The entire energy of the mass is located in the carrier frequency.

The wavelength of the carrier frequency also changes according to the relativistic length-contraction and is: $\lambda_m = \lambda_{m0} \cdot \sqrt{1-\frac{v_m^2}{c^2}}$, were λ_{m0} is the wavelength of a rest mass.

Now, we regard the frequency of the beat (f_b). The frequency of the beat is the difference of the frequencies of the waves, which superimpose. Under consideration of the relativistic time-dilatation, which arises for a charge which moves with the velocity v_m, the frequency of the beat of the charge is: $f_b = f_{m0} \cdot \frac{2 \cdot v_m}{c} \cdot \frac{1}{\sqrt{1-\frac{v_m^2}{c^2}}}$. If the velocity of the mass is considerably smaller than the speed of the light (that is $v_m \ll c$), then the root term is approximately 1, so that

$$f_b = \frac{f_{m0} \cdot 2 \cdot v_m}{c} \qquad (4.3)$$

is a good approximation. The beat propagates with the speed of light. So, if λ_b is the wavelength of the beat then:

$$c = f_b \cdot \lambda_b. \tag{4.4}$$

Inserting (4.1) and (4.4) into (4.3) finally yields: $\lambda_b = \frac{h}{m_0 \cdot 2 \cdot v_m}$. This corresponds exactly to the deBroglie wavelength which deBroglie calculated for the matter-waves of the masses (which are confirmed, e.g., by double split-experiments [11]). The $2 \cdot v_m$ is the difference of velocity, which results for the mass between the field and the anti-field.

It is really remarkable: By introducing the anti-field, the deBroglie wavelength can be represented very simply as a beat, which arises between the spacetime wave of the field and the anti-field if the mass moves with the velocity v_m.

I regard this as an excellent confirmation (no proof) for the existence of the anti-field. I think that the anti-field is not a theoretical construct but it is physical reality.

So, the mass of an electric charge isn't a small object in the centre of the charge, as it may has been imagined classically. The mass rather corresponds to the frequency with which the charge oscillates and can not be distinguished from the charge. But, due to r^{-2}, the amplitude increases very fast towards the centre, so that, at a collision, the intensity of the interaction increases very fast as the centres approach, from what a radius can be derived for the interaction, which then is likely to be assigned to the mass.

The velocity of a mass corresponds to the motion of the centre of an electric charge and arises from the difference of the frequencies of the field and the anti-field. So, an electric charge has not a mass which is struck but the frequencies of the field and the anti-field which alternate.

4.4. On the Emergence of the Electric Force

The space-time wave of the anti-field propagates with the speed of light towards the centre, while the amplitude increases with r^{-2}. The increase of the amplitude can be represented geometrically: while the anti-field propagates towards the centre a spherical surface of this anti-field decreases with r^{-2}, and the density of the points on this sphere increases correspondingly. In this sense, the space of the anti-field becomes compressed on its way towards the centre. The space compressed into the centre then leaves the centre as a field. But, though, the anti-field isn't reflected at the centre; instead it goes through the centre.

So, on its way through the centre the anti-field becomes a field. Both move in the same direction. It seems, as if they could be one and the same wave, but the field and the anti-field have different spacetime parameters. When the anti-field goes through the centre its spacetime parameters alternate, so that it becomes a field. We can call the combination of the wave of the anti-field which becomes the wave of the field the continuous wave. Thus, there are two continuous waves for every straight that goes through the centre which propagate in opposite directions. So, if a receiver moves with a velocity ($\overrightarrow{v_R}$), then the wavelengths of the continuous waves are different in the direction of the $\overrightarrow{v_R}$.

The electric force of a field and an anti-field of an electric charge, which I call source, on a receiver corresponds to the acceleration - that is the change of the velocity - of the receiver. This means that the frequencies of the continuous waves of the receiver change in the direction of the change of the velocity. And this means, formulated quite generally, that the frequency of the field of the receiver, that is f_R^+, changes in relation to that one of the anti-field, which is f_R^-. The change of f_R^+ and f_R^- is caused by the field and the anti-field of the source. Since I show in this work here that gravitation is an electric effect, it is clear that, in the first place, the force of the electric field is independent of the mass of the charge of the source. Thus, it is clear that the force of the field and the anti-field of the source is independent of the respective wavelength (these are λ_S^+ and λ_S^-). It is an important component of this work that the electric force is velocity-dependent (as it is in part 1 of this work). So we can assign to *each wave* of the field or anti-field of the source (which, of course, propagate with the speed of light) a certain change of the frequency of the field or anti-field of the receiver, which then is δf_R^+ or δf_R^-, were then, of course, δf_R^+ or δf_R^- are directly proportional to λ_S^+ or λ_S^-. In addition, we know that the electric force is proportional to r^{-2}. From that we have derived that the amplitude of the spacetime wave of the field or anti field of the source (this is A_S^+ or A_S^-) is also proportional to r^{-2}. Here this means that δf_R^+ or δf_R^- is proportional to A_S^+ or A_S^-.

The actual acceleration of the receiver is inverse proportional to its inert mass. But, in this representation of the connections there isn't a mass as such, neither inertly norgravitationally. Here, the inertia corresponds to the time-period Δt which is necessary for a δf_R^+ or δf_R^-. This time-period corresponds to the time which one wave of the source needs to move along the centre of the receiver, by which a δf_R^+ or δf_R^- arises. Of course, it isn't necessary to always consider a whole wave of the source; a fraction of one wave of the source causes a correspondingly smaller change of the frequency of the receiver. The δf_R^+ or δf_R^- cause a beat which in turn corresponds to a velocity of the receiver (including his centre). The frequency of the beat is the difference of the frequencies, and here, that is δf_R^+ or δf_R^-. So, regarding equation (4.3) it is $f_b = \delta f_R^+$ or $f_b = \delta f_R^-$. The mass of the receiver corresponds to the frequency f_{m0} and the velocity v_m corresponds to the change of the velocity of the receiver (this then is v_R). Since the waves of the source produce, in the same period Δt, always equally grate δf_R^+ or δf_R^-, we see in equation (4.3) that the change of the velocity of the receiver is exactly inverse proportional to his mass - because then $f_{m0} \cdot v_R$ is constant. So, the quality of the inertial mass (that is inertia) results quite automatically if the changes of the frequency which the waves of the source produce on the receiver are independently of the mass of the receiver (which corresponds to f_{m0}).

Here, now it becomes clear how the velocity-dependence of the electric force arises: due to a velocity $\overrightarrow{v_R}$ of the receiver the velocity with which the waves of the source move along the centre of the receiver changes, so that the time-period Δt for a δf_R^+ or δf_R^- changes, too.

If we say, independently of whether it is a field or an anti-field, that every wave of the source (this then is λ_S) causes a certain change of the frequency of the receiver

(this then is δf_R), then it is: $\frac{\delta f_R}{\lambda_S} = K_R$, were K_R is a constant still to be defined. In addition, it is: $\lambda_S = \Delta t \cdot (c \pm v_{R(t)})$, were $v_{R(t)}$ is the magnitude of the component of $\overrightarrow{v_R}$, that is parallel to the speed of light c of the waves of the source. By inserting (4.3) and for $\Delta t \to 0$ we finally have: $\frac{dv_R}{dt} = \frac{(c \pm v_{R(t)}) \cdot K_R \cdot c}{2 \cdot f_{m0}}$, were, in this case, f_{m0} is the frequency of the rest mass of the receiver. This corresponds exactly to the equations (3.1) or (3.3) from part 2 of this work. Therefore, by considering (4.1) it is: $K_R = \frac{2 \cdot F_c \cdot c}{h}$.

The velocity-dependence of the electric force arises from the relative velocity between the waves of the source and the receiver. By the component of $\overrightarrow{v_R}$ that is perpendicular to the $c$of the waves of the source, the angle $\tan(\varphi_r) = \frac{v_{R\perp}}{c}$ results between the waves of the source and the receiver. Due to φ_r the δf_R^+ or δf_R^- also have a corresponding angle so that the beat also has the angle φ_r. And this means that the change of the velocity of the receiver also has the angle φ_r, what corresponds to an additional force which is proportional to the $v_{R\perp}$.

So we see that the velocity-dependence of the electric force, as I have represented it in part 1 of this work, and which means there that the $\overrightarrow{v_R}$ produces an additional force of its own, can be very well derived from the representation of the electric charge as a spacetime wave.

One important characteristic of electric charges is the duality: there are two different types of charges in which same charges repel and opposite charges attract each other. This duality is mirrored in the duality of the field and the anti-field. This duality of the electric charges results when the field of the one type of a charge corresponds to the anti-field of the other type of a charge, and vice versa. In this way, one receives changes of the velocity which correspond to the direction of the force. Here, it is decisive that there always is only one type of an interaction between the source and the receiver: either always only the fields interact with the fields and the anti-fields with the anti-fields or always only the fields interact with the anti-fields. For purely practical reasons, I decide that always only the field of the source interacts with the field of the receiver and the anti-field of the source with the anti-field of the receiver. Another difference in the interaction arises from the relative direction of the motion: when the receiver and the waves of the source move towards each other, then they produce exactly the opposite δf_R as when they move in the same direction.

We first consider the repulsion between same charges. The field of the source (λ_S^+) interacts with the field of the receiver (f_R^+). At repulsion the frequency of the wave of the receiver becomes grater when the wave moves towards the source (I then call his frequency f_{R1}^+), and it becomes smaller, when the wave moves away from the source (I then call his frequency f_{R2}^+). (I draw the connections symbolically in Figure 4.1. To not overload the Figure I *don't* represent the amplitude of the waves with r^{-2}, instead I draw it just "flat". M_S and M_R are the centres of the source and the receiver respectively, while the source is in a grate distance from the receiver.) So, if the fields of the source and of the receiver move towards each other then f_R^+ gets greater, and vice versa. If, on the other hand, the anti-fields of the source and of the receiver move towards each other, then exactly the inverse happens: then f_R^- gets smaller, and vice versa. So, the frequency of the continuous wave which moves towards the source gets greater, and the frequency of the continuous wave which moves away from the source gets smaller, what corresponds to a repulsion.

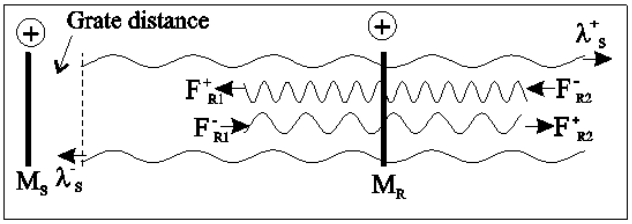

Figure 4.1.

We now consider the attraction between opposite charges. Here, the field of the one charge is the anti-field of the other charge. Thus, the field of the source (λ_S^+) interacts with the anti-field of the receiver (therefore with f_{R1}^- and f_{R2}^-). So, the field of the source corresponds to the anti-field of the receiver. Since λ_S^+ moves towards f_{R2}^-, the f_{R2}^- becomes smaller and the f_{R1}^- becomes correspondingly greater - very analogous to the anti-fields at the repulsion. The λ_S^-, in turn, corresponds to the field of the receiver so that f_{R1}^+ becomes smaller and f_{R2}^+ greater. So, the frequency of the continuous wave which moves towards the source gets smaller, and the frequency of the continuous wave which moves away from the source gets grater, what corresponds to a attraction.

As we know, the field and the anti-field of the source don't exert their forces at the same time but after each other. Therefore, the frequencies of the two continuous waves always change only on one side, in which these changes of the frequencies spread from the centre of the receiver with the speed of light.

The changes of the frequencies of the receiver arise because the wave of the field or anti-field of the source causes an oscillation (that is a spacetime wave) in the centre of the receiver which spreads from the centre and which superimposes the wave of the field or anti-field of the receiver. The changed frequencies of the receiver correspond to a velocity and yield the beat which corresponds to the matter-waves.

According to this logic, we can assume for the anti-particles [32] that the field and the anti-field of an anti-particle are switched compared with a normal particle.

About the vacuum one can say that it is filled densely with the spacetime waves of the positive and negative electric charges - only the centres of charges (that are particles) are rare there. [13]

Perhaps it hasn't got as clear by the descriptions up to now, but it is remarkable: Electric charges consist exclusively of spacetime. The mass corresponds to their frequency, and the forces, which they exert on each other, result from the changes of their spacetime waves. So, in the end, all matter we know only consists of spacetime.

4.5. On the Emergence of the Electric Quantization

The quantization of the transfer of the electric energy (which I call shorter "electric quantization") leads to gravitation. I will show now, how this quantization results.

The electric quantization means that the receiver can only be in certain quantum levels, in which always only the fields *or* the anti-fields of *one* type of a charge of the sources can cause changes of the frequency of the receiver. The beat arising in this process corresponds to the velocity $v_{R(t)}$. The electric quantization then results by the fact that the receiver changes his quantum level as soon as the changes of the frequency (and therefore also the $v_{R(t)}$) have reached a certain magnitude. If we call the time-period of a quantum level generalized T, then the quantum levels change each time when $v_{R(T)}$ is reached.

The beat is calculated from the difference of the frequencies of the field and the anti-field of the receiver. In an analogous way we also can calculate the difference of the wavelengths of the field and the anti-field of the receiver. Generalized (that is, for the moment, without distinguishing between the field and the anti-field, and between the positive and negative charges), this difference is for each quantum level:

$$\delta\lambda_R = \frac{2 \cdot v_{R(T)}}{f_{R0}}, \tag{4.5}$$

were f_{R0} is the frequency of the rest mass of the receiver. (To avoid mistakes: the $\delta\lambda_R$ *isn't* the wavelength of the beat).

In part 2 of this work we have seen that $v_{R(T)}$ is a somehow complicated exponential function of T, in which T depends on $K = \frac{m_R \cdot m_S \cdot G \cdot \varepsilon_0 \cdot 4 \cdot \pi}{q_S \cdot q_R}$. But, we know that K and therefore also T is very small and for values near zero the slope of the exponential function is ≈ 1. So we can say, in good approximation, that $v_{R(T)}$ is proportional to $m_R \cdot m_S$ and therefore also to $f_{R0} \cdot f_{S0}$ (in which the f_{S0} represents the frequencies of the rest masses of the sources.) This means that $\delta\lambda_R$ is roughly independent of f_{R0}, and approximately proportional to f_{S0}. This means that $\delta\lambda_R$ results almost exclusively from the frequencies of the waves of the *sources*. The electric quantization then arises by the fact that the magnitude of the $\delta\lambda_R$ at which the quantum level of the receiver changes each time is proportional to the frequencies of the waves of the sources. Or formulated a little differently: the magnitude of the changes of the wavelength of the receiver is, for every quantum level, proportional to the frequencies of the waves of the sources.

Here now it may be interesting to realize the magnitudes of the quantization: in part 2 of this work, I have assessed the time-period of a quantum level of a proton on the earth's surface in strongly simplified terms. It is: $T_{p+} \approx \frac{r^2}{N} \cdot 456 \cdot 10^{-28} s$. The number N of the positive or negative charges of the earth is $N \approx 3.57 \cdot 10^{51}$, and for the radius of the earth it is $r^2 \approx 3.969 \cdot 10^{13}$, so that $T_{p+} \approx 5 \cdot 10^{-64} s$. On the other hand, the time-period of the frequency of the mass of a proton is: $T_{mp+} \approx 4.5 \cdot 10^{-24}$. Here we see, despite the only very rough estimation, how unbelievably small the change is, which a quantum causes at a charge. The reason for that could be the condensation of the space in the centre.

Now, I want to try to find a descriptive interpretation for the connections on the electric quantization. We know that the fields and the anti-fields of the sources don't exert their forces at the same time but after each other, with the consequence that the frequencies of the continuous waves always change only on one side of the receiver, with respect to the centre. From that, the the following interpretation arises: the imbalance between the frequencies on the one and the other side of the centre cannot exceed a certain magnitude, just as if a difference in pressure would arise. As soon as the imbalance has reached a certain magnitude, the charge alters its quantum level. The imbalance corresponds to a difference in the wavelengths between the two sides (with respect to the centre) of a continuous wave, and this imbalance is proportional to the frequencies of the waves of the sources, so that, therefore, it can be all the bigger, the bigger the frequencies of the waves of the sources are.

But, in addition, we also know that although always only the fields or anti-fields of one type of a charge can exert their forces, nevertheless the masses of the respective other type of a charge have to be taken into account for gravitation, too. For this, there is the following interpretation: we know that the field of the one type of a charge corresponds to the anti-field of the other type of a charge, and we know that always only the ones of the same kind interact with each other. So, if, therefore, the fields of the one type of a charge of the sources interact with the field of the receiver, then the anti-fields of the other type of a charge of the sources counteract, but this *without* being able to actually exert their forces. Instead, these anti-fields of the other type of a charge of the sources will support the receiver, so that the difference of the wavelength, which the fields of the sources, that interact with the receiver, can cause, gets appropriately grater.

This interpretation is, of course, still very vague, and the reason for that is that it still isn't clear at all which spacetime parameters the waves of the electric charges have. It also isn't clear at all, in which way different spacetime waves influence each other. On this topic, I have made some general considerations in my work "Theory of objects of space" [39]. This work here represents a first specification of my considerations then. But, there is still a long way to go. However, we already receive important notes. So, e.g., we can assume that the spacetime parameters of the waves of the electric charges must overall fulfil, for gravitation, the parameters of GR.

4.6. Effects on Gravitation

In part 2 of this work, we have calculated $v_{R(T)}$ or T only for small, *non-relativistic* velocities, and we can make here exactly the same. But, though, these non-relativistic velocities are not always to be neglected, since, as we can see, $\delta\lambda_{R(T)}$ is proportional to the frequencies of the waves of the sources and these frequencies are directly proportional to the velocities of the sources and the receivers, and this, of course, is also relevant for

non-relativistic velocities. This means, in the end, that there is a *velocity-dependence* for *gravitation, too* (just as for the electric force). And as in the case of the electric force, also at gravitation, the changes of the field and the anti-field cancel each other. And this means that, at gravitation, too, we get a force which corresponds to the magnetic force [15,26-31]. From this then, among other things, the gravitational waves arise! [37,38]

For grater, relativistic velocities the increase of the mass has to be taken into account, of course. Since the average frequency from the field plus the anti-field of a source changes, not only the inertial mass of a source changes but in the same way the gravitational mass changes, too. I still cannot say here exactly which consequences this has on gravitation since I cannot know yet whether I know all the relevant factors. However, for the moment, it seems as if the gravitational force of a mass increases by its velocity *in the direction* of the velocity.

Perpendicular to the velocity of a source the frequencies of the field and the anti-field of the source change exactly in the same way (so there isn't any beat). Due to the relativistic time-dilatation, the average frequency perpendicular to the velocity v_S of a source becomes: $f_S^+ = f_S^- = f_{S0} \cdot \sqrt{1-\frac{v_S^2}{c^2}}$. For the moment, this means that the gravitational force gets *smaller* perpendicular to v_S. If this is correct, then, e.g., the velocities of the electrons within the atom shells must be taken into account, and also the atomic nuclei could have relevant velocities, e.g., inside the sun.

A horizontally rotating mass on the earth's surface also should get lighter - but, though, so insignificantly, that it would hardly be measurable. There have already been corresponding experiments [33,34,35,36] with superconductive rotating plates. The results achieved there are considerably bigger than the relativistic changes let expect, though. If the results would be confirmed, one would need to look for other causes. The superconductivity could be relevant. As we know by now, electric charges are spacetime waves. Some of these spacetime waves could develop resonances at superconductivity so that the frequencies and amplitudes of the spacetime waves of the charges the rotating plate consists of change, so that the weight of the plate changes. One could go even so far to assume that the resonant spacetime waves of the charges of the plate change the spacetime waves, which come from the earth, and go through the plate, in such a way that gravitation changes above the rotating plate. But all this is very very speculative. As far as it concerns the meaning of the rotation of the plate, I would suspect that not the rotation itself but the cause for the rotation (that is the drive) has meaning.

In this work here, we have already seen multiple times that there seem to be different factors which have the potential to be able to influence gravitation, and although it will need much effort, I believe that a more exact look will be worthwhile, because we finally want to better understand gravitation, to see how we can use it.

4.7. The Electromagnetic Waves

The electromagnetic waves (EMW) [17,18,19,20] transfer their energy by energy quanta, the photons [10]. We know that photons are influenced by gravitation, and since we have understood now that gravitation is an electric phenomenon, photons must therefore have electric qualities. In addition, we know that photons are *not* influenced by electric fields, therefore, photons must be electrically neutral. But photons always move with the speed of light, therefore, they cannot consist of opposite electric charges equal in magnitude, since beat isn't possible for the speed of light. We know that photons can collide, similar to mass particles. Therefore, a momentum is assigned to the photons, which arises from the speed of light multiplied with the mass which corresponds to the frequency of the photons. Photons cannot have a rest mass since they always move with the speed of light.

I will design a construct, now, that corresponds to all these qualities of a photon, in the hope, that it is as similar to the actual photons as possible.

It finally turns out that a photon resembles very much to an electric charge: it is a *spherical* spacetime wave whose amplitude increases towards the centre, and it consists of a field and an anti-field. The essential difference compared with an electric charge is that the field and the anti-field of a photon *don't* move relatively to the centre, while the centre moves with the speed of light. The magnetic part of the photon is represented by the angle φ of the electric field, as I have described in part 1 of this work.

At a particle with mass, the kinetic energy is the increase of its relativistic mass. This increase of the mass corresponds to an increase of the average (carrier-) frequency of the field plus the anti-field of this mass (see equation 4.2). The frequency of a photon corresponds exactly to this additional frequency which a particle with mass has due to its kinetic energy. The frequency of the photon corresponds to a mass, and so this mass corresponds to the kinetic energy of the photon. So, if a photon looses its complete kinetic energy at an interaction, no rest mass is left. The kinetic energy of the photon is: $E_{kinP} = m_P \cdot c^2 = f_P \cdot h$, were m_P is the mass and f_P the frequency of the photon. And the momentum of the photon is: $P_P = m_P \cdot c = \frac{f_P \cdot h}{c}$.

EMW, such as radio waves, consist in dependence of the amplitude of many photons. The individual photons of an EMW are, similar as in the case of a laser, in resonance.

I will describe now, how it happens that photons are effected by a gravitational field but not by an electric (net) field.

At an electric charge, the field and the anti-field propagate with the speed of light in opposite directions and the differences of their frequencies cause beat, which corresponds to a velocity of the electric charge. At a photon instead, the field and the anti-field *don't* propagate relative to each other, they are static to each other. Correspondingly, at a photon, the beat also will be static. This static beat doesn't change the velocity of the centre of the photon. So we recognize that changes of the frequency of the field and the anti-field of a photon don't cause any changes of the velocity at the photon.

As in the case of an electric charge at a photon, too, always only the frequency of the field *or* the anti-field changes, according to its quantum level, in which, each time, the frequency on one side of the centre changes in an opposite way as on the other side. And, of course, positive

and negative charges will cause exactly opposite changes of the frequencies at a photon.

So, the fields and anti-fields of the sources cause a static beat at a photon as a receiver. This static beat doesn't produce a velocity at the photon. But, we know that photons are influenced by gravitation, which means that the velocity-dependence of the electric force must be valid for photons. We achieve this by saying that the velocity which corresponds to the static beat of a photon has to be taken into account so at the velocity-dependence of the electric force as if it were an actual velocity. This can be justified by the fact that the (interaction-) behaviour of the photon changes due to the static beat, even if its velocity doesn't change.

For the frequency of a photon, only the average frequency from its field plus its anti-field is relevant, while the static beat only has meaning for the velocity-dependence of the electric force. The average frequency changes both for positive and for negative charges of the sources always by the amount which corresponds to gravitation. The static beat instead changes for positive and negative charges of the sources exactly oppositely, so that it is zero on average.

Therefore, for a photon, that propagates parallel to the gravitational field, the frequency (and therefore the *energy*) of the photon changes according to gravitation.

At a photon that propagates perpendicular to the gravitational field the average frequency changes perpendicular to the direction in which the photon propagates. According to our assumption, a photon shall fall according to gravitation. This means that, for a photon that propagates perpendicular to the gravitational field, the *direction* in which it propagates changes. This change of the direction results from the change of the average frequency (perpendicular to the direction in which this photon propagates) and not from the appropriate static beat - thus, a resultant average frequency arises in the new direction. The fields and anti-fields of *one* type of a charge of the sources always change the average frequency of a photon only by the amount which corresponds to gravitation (since, as described, the field and the anti-field of the photonchange oppositely). Therefore, if a photon propagates perpendicular to the electric field of a net charge, then its direction will change only by the amount which corresponds to the gravitational force of the *net charge*, which will be negligibly small, at least in laboratories. But, in addition, the trajectory of the photon is shifted parallel, due to the net charges; I still must calculate whether this is measurable under laboratory conditions.

Of course, the magnitude of the change of the direction in which the photon moves is proportional to the component of the speed of light of the photon which is perpendicular to the gravitational field.

At an electric charge as a receiver, the changes of the frequency spread with the speed of light, starting from the centre. At a photon as a receiver, this isn't possible since it already moves with the speed of light. At an electric charge as a receiver, the changes of the frequencies arise from the superposition with an oscillation which is produced by the fields and anti-fields of the sources in the centre of the receiver and which spreads from there with the speed of light. The changes of the frequencies of a photon also arise from the superposition with an oscillation which is produced by the fields and anti-fields of the sources, but this oscillation, which I call superposition-oscillation, does not have to arise in the centre of the photon. The superposition-oscillation can rather appear in the whole area of the photon *at the same time*. The reason for that is, that the fields and anti-fields of the sources, which cause the superposition-oscillation, already exist in the whole area of the photon, and they just cause a change of the photon when the photon is in the corresponding quantum level. But, of course, just because the photon has the ability to change as a whole at the same time, this *doesn't* have to happen. Instead, every interaction with a photon must be analysed carefully, to find out the temporal and spatial sequence in accordance with which the frequencies of the photon change. I will not do this in this work here, though. This is a task for future works.

Independently of the temporal and spatial sequence in accordance with which the frequencies of the photon change, even if the whole photon changes at the same time, the centre of the photon always moves with the speed of light, of course.

We recognize, here, a striking similarity to the entanglement: on the one hand, events can take place simultaneously, on the other hand, the centres still move with the speed of light. Actually, I wouldn't have taken the possibility of the simultaneity into consideration at all if I didn't know that entanglement exists [24,25]. Thanks to the unbelievable phenomenon of entanglement, now it is easy to understand, how it is possible that photons are influenced by the fields and anti-fields of the sources although they move with the speed of light. But, though, I am still far away from being able to convey the simultaneity at the change of a photon to the entanglement of two photons. My first thought about entangled photons would be that they are parts of the same system which can always change only at the same time, while, of course, they always keep the speed of light - I cannot say much more here yet. But it seems very obvious, though, that this simultaneity can, if it is possible for photons, happen also at electric charges, which, of course, are very similar to the photons.

In principle, the entanglement must be coupled to some time phenomenon, perhaps similar as in my description in my "Theory of objects of space" [39]. This could mean that the field and the anti-field are also connected by a time phenomenon - but, really, this is an other building site.

A photon consists, exactly as an electric charge, of a field and an anti-field. At the photon, though, the field and the anti-field are static to each other. If, now, two identical photons meet exactly centrically with exactly opposite velocities then this corresponds to the origin of two couples, of which each consists of one field and one anti-field, and which move in opposite directions (with the speed of light). And this corresponds, in the end, to the creation of two opposite electric charges - but they are at the same place, of course, so that they recombine immediately again. But, if the two photons, which produce the couple of charges, don't have exactly identical frequencies, then beat can arise, with the consequence that the electric charges have opposite velocities, in which, of course, here, it is necessary to consider the conservation of momentum and energy, particularly regarding the masses.

In addition, there are experiments [21,22] particularly with strong magnetic fields [23] which indicate that a couple of charges, that may exist for a short moment, can also arise from only *one* photon. I don't know yet, how this happens. But, it seems, in principle, to be possible that the field and the anti-field of a photon become part of an electric charge again.

4.8. Remarks on Particle Physics

Although electric charges are spacetime waves, they also have, due to the fast increase of their amplitude towards the centre, particle character, because the intensity of their interactions increases very fast when the distance decreases.

If the distance between two protons becomes very small, e.g., inside a sun, their frequencies can get into a kind of resonance so that they don't repel any more, and they form a unit, an atomic nucleus. At this, the neutrons seem to serve as a connection. One can imagine an atomic nucleus as a complex assembly of oscillations. To merge a proton and an electron seems to be more difficult (then the creation of an atomic nucleus), otherwise this would happen also inside a sun. The reason for that could be the great difference of the frequencies between the proton and the electron. Instead, the electrons form the atom shell. At this, it is interesting that the deBroglie wavelengths, which arise from the velocities which are assigned to the electrons in the atom shell, correspond approximately to the diameter of the atom shell. Therefore, we can imagine that the waves of the beat of the electrons form the atom shell. Here, complex superposition patterns arise, from which the atomic orbitals of the electrons may result.

We recognize the strong interaction in these considerations. I still can say nothing to the weak interaction here.

Of course, we know that electric charges consist of quarks [14]. This could mean that the frequencies of the electric charges have sub-structures which correspond to the quarks. On the other hand, the existence of the quarks is observable only at particle collisions so that it cannot be said, whether they exist already before the collision. It is very well possible that the quarks arise only at the collision. Two particles, which collide with each other, don't simply move at straight trajectories with steady velocities towards each other. The particles will rather oscillate, specially when the distances become very small, and they will leave their straight trajectories, while, of course, their waves superimpose. At such a process complex superposition patterns can arise. A complex assembly of oscillating spacetime arises, from which all possible particles can result. For reasons, which I don't know, many of these particles seem to exist only for a very short time. Among others, the quarks also arise. The fact, that the elementary particles can be assembled of quarks, shows us that the superposition of the waves obeys to fixed rules, at the collisions of particles.

A remark on the Higgs-Boson: In this work here, I have defined the mass as a spacetime wave, while the inertia results from the time which is necessary for a change of the frequency. On the other hand, it makes sense, in the context of particle physics, to define the Higgs-Boson. Therefore, it is necessary to find out, what corresponds to the Higgs-Boson if the mass is understood as a spacetime wave. In the end, the Higgs-Boson must be connected directly with the frequency of the mass, as it is defined in equation (4.1). And at collisions, the Higgs-Boson always arises in a way which is connected directly to the frequency of the mass.

A remark on the frequency of the gravitational oscillation: we have seen that the electric charges oscillate due to gravitation with extremely high frequencies. The question is, now: which meaning has this gravitational frequency at collisions? Well, I don´t know yet; but, since the gravitational frequency is proportional to the mass of the electric charge, there could be a connection to the Higgs-Boson here, too.

The graviton, which is mentioned occasionally, is, as I would think, most likely to be connected to the quantization of the transfer of the electric energy, since this, after all, is responsible for gravitation.

These short remarks on particle physics shall show that particle physics is very well compatible with the idea that particles are spacetime waves.

4.9. Closing Remark to Part 3

We have seen, here, in part 3, that it makes sense to regard the electric charge as a spacetime wave whose amplitude increases towards the centre with r^{-2}, because, regarding the charge as a spacetime wave, allows us to better understand the qualities of the electric charges and their forces. So it turns out that the quality of the relativistic mass of an electric charge corresponds to the *frequency* of its spacetime wave, while the deBroglie wavelength of the matter-waves turns out to be the *beat* (interference) of the frequencies of the field and the anti-field of the spacetime waves of an electric charge. The velocity-dependence of the electric force, and the quantization of the transfer of the electric energy, due to which gravitation results, also result to be qualities of the spacetime waves of the electric charges, while electromagnetic waves are a special manifestation of these spacetime waves.

We finally recognise that, perhaps, even almost all forces can be explained by the forces between the spacetime waves of which the electric charges consist, and which also yield the electric forces. This seems obvious if we consider that space and time are the most basic quantities of physics.

But, the cognition that, in the end, all matter, that we know, consists of oscillating spacetime is particularly fascinating, here.

4.10. Conclusion

In this work, we have learned more about the qualities of the electric charges and their forces, which helps us to better understand magnetism, and to recognize gravitation as an electric effect.

Essentially, it is about three qualities: the velocity-dependence of the electric force, the electric anti-field, and the quantization of the transfer of the electric energy.

In part 1, I show that the magnetic field isn't a field of its own, but that it is only an angled electric field, in which the angle of the electric field has to be regarded relativistically.

In part 2, I show that gravitation is an electric effect, which means that there cannot be a gravitational force of

its own without electric forces. Overall, of course, the electric forces, which produce gravitation, yield the conditions of GR.

In part 3, I finally describe the electric charge to be a spacetime wave, whose amplitude increases towards the centre with r^{-2}, from what then the mentioned qualities of the electric charges and their forces can be derived. The relativistic mass corresponds to the frequency of this spacetime wave.

Besides a better understanding of the electric charges and their forces, and a better understanding of gravitation, which will hopefully lead to new experiments and applications soon (which I point out in this work occasionally) I would like to highlight that a new field has entered the stage of physics: the electric anti-field.

Particularly interesting is the cognition, because it has not only physical but perhaps also philosophical meaning, that, in the end, all matter, that we know, consists of oscillating spacetime.

References

[1] A. Einstein, Zur Elektrodynamik bewegter Körper Annalen der Physik 17, 891-921 (1905).

[2] PAM Dirac: The Quantum Theory of the Electron. In: Proceedings of the Royal Society of London. Series A, Containing Papers of a Mathematical and Physical Character. A, Nr.778, 1928, S.610-624.

[3] Dieter Meschede: Gerthsen Physik. 23. Auflage, Springer, Berlin/Heidelberg/New York 2006, ISBN 3-540-25421-8.

[4] James Clerk Maxwell, A Dynamical Theory of the Electromagnetic Field, Royal Society Transactions 155, 1865, Seiten 459-512.

[5] Introduction to Electrodynamics (3rd Edition), D.J. Griffiths, Pearson Education, Dorling Kindersley, 2007.

[6] Electromagnetism (2nd Edition), I.S. Grant, W.R. Phillips, Manchester Physics, John Wiley & Sons, 2008.

[7] Dirac, Paul (1996), General Theory of Relativity, Princeton University Press.

[8] Einstein, Albert (1916), "Die Grundlage der allgemeinen Relativitätstheorie", Annalen der Physik 49.

[9] Hartle, James B. (2003), Gravity: an Introduction to Einstein's General Relativity, San Francisco: Addison-Wesley.

[10] M. Planck: Zur Theorie des Gesetzes der Energieverteilung im Normalspectrum. In: Verhandlungen der Deutschen physikalischen Gesellschaft. 2, Nr. 17, 1900, S. 245, Berlin (vorgetragen am 14. Dezember 1900).

[11] Roger Bach, Damian Pope, Sy-Hwang Liou, Herman Batelaan Controlled double-slit electron diffraction In: New Journal of Physics, Roger Bach et al 2013 New J. Phys.15 033018.

[12] JoernBleck-Neuhaus: ElementareTeilchen. Von den Atomenüber das Standard-Modell biszum Higgs-Boson. 2., überarbeitete Auflage. Springer, Berlin Heidelberg 2013.

[13] J. Baez. What´s the energy density of the vacuum?, 2006.

[14] M. Gell-Mann: A Schematic Model of Baryons and Mesons in Phys. Lett. 8, 1964, 214-215.

[15] Moshe Carmeli, John G. Hartnett, Firmin J. Oliveira On the anomalous acceleration of Pioneer spacecraft Int.J.Theor.Phys. 45 (2006) 1074-1078.

[16] Albert Einstein: Erklärung der Perihelbewegung des Merkur aus der allgemeinen Relativitätstheorie. In: Sitzungsberichte der Preußischen Akademie der Wissenschaften.

[17] Chandrasekhar Roychoudhuri, Rajarshi Roy: The nature of light: What is a photon? In: Optics and Photonics News. 14, Nr. 10, 2003, ISSN 1047-6938, Supplement, S. 49-82.

[18] Harry Paul: Photonen: Eine Einführung in die Quantenoptik. 2. Auflage. Teubner, Stuttgart 1999, ISBN 3-519-13222-2. (Teubner-Studienbücher Physik).

[19] Klaus Hentschel: Einstein und die Lichtquantenhypothese. In: Naturwissenschaftliche Rundschau. 58(6), 2005, ISSN 0028-1050, S. 311-319.

[20] Liang-Cheng Tu, Jun Luo, George T. Gillies: The mass of the photon. In: Reports on Progress in Physics. 68, Nr. 1, 2005, S. 77-130.

[21] J D Franson Apparent correction to the speed of light in a gravitational potential In: New Journal of Physics, J D Franson 2014 New J. Phys.16 065008.

[22] Berestetskii V B, Lifshitz E M and Pitaevskii L P 1980 Quantum Electrodynamics (Oxford: Pergamon).

[23] H. Grote: On the possibility of vacuum QED measurements with gravitational wave detectors In: Phys. Rev. D 91, 0220022 - 7 January 2015.

[24] Max Born, Albert Einstein: Albert Einstein, Max Born. Briefwechsel 1916-1955. München (Nymphenburger) 1955, S. 210.

[25] Simon Gröblacher, Tomasz Paterek, Rainer Kaltenbaek, Caslav Brukner, Marek Zukowski, Markus Aspelmeyer, Anton Zeilinger: An experimental test of non-local realism. In: Nature. 446, 2007, S. 871-875. (Abstract).

[26] Jacob Biemond The MagneticFfield of Pulsars and the Gravito-Magnetic Theory Trends in Pulsar Research (Ed. Lowry, J. A.), Nova Science Publishers, New York, Chapter 2 (2007).

[27] Shervgi S. Shahverdiyev Unification of Electromagnetism and Gravitation in the Framework of General Geometry Proceedings of the workshop in "Fizika" N 12, 2004.

[28] Friedrich W. Hehl An Assesment of Evans´Uunified Field Theory Foundations of Physics 38 (2008) 7-37.

[29] Bahram Mashhoon, Frank Gronwald and Herbert I.M. Lichtenegger Gravitomagnetism and the Clock Effect Lect.Notes Phys. 562 (2001) 83-108.

[30] Sumana Bhadra Electromagnetic Mass Models in General Theory of Relativity Ph.D. thesis, Sambalpur University, Jyoti Vihar, Burla – 768019, Orissa, India (2007).

[31] J.H. Field Forces Between Electric Charges in Motion: Rutherford Scattering, Circular Keplerian Orbits, Action-at-a-Distance and Newton's Third Law in Relativistic Classical Electrodynamics arXiv:physics/0507150v3 (2007).

[32] Weinberg, S. (1995). The Quantum Theory of Fields, Volume 1: Foundations. Cambridge University Press.

[33] M. Tajmar and C. J. de Matos Extended Analysis of Gravitomagnetic Fields in Rotating Superconductors and Superfluids ARC Seibersdorf research GmbH, A-2444 Seibersdorf, Austria and ESA-HQ, European Space Agency, 8-10 rue Mario Nikis, 75015 Paris, France.

[34] M. Tajmar, F. Plesecu, B. Seifert and K. Marhold Measurement of Gravitomagnetic and Acceleration Fields Around Rotating Superconducters AIP Conf. Proc. 880, 1071 (2007).

[35] Martin Tajmar, Florin Plesescu, Klaus Marhold and Clovis J. Matos Experimental Detection of the Gravitomagnetic London Moment Space Propulsion, ARC Seibersdorf research GmbH, A-2444 Seibersdorf, Austria and ESA-HQ, European Space Agency, 8-10 rue Mario Nikis, 75015 Paris, France (2006).

[36] V.V. Roschin and S. M. Godin Experimental Research of the Magnetic-Gravity Effects Institute for High Temperatures, Russian Academy of Science.

[37] Misner, C. W.; Thorne, K. S.; Wheeler, J. A. (1973). Gravitation. W. H. Freeman.

[38] Einstein, A (1918). "Ueber Gravitationswellen". Sitzungsberichte der Königlich Preussischen Akademie der Wissenschaften Berlin. part 1: 154-167.

[39] H.-J. Hochecker Theory of Objects of Space At: http://www.hochecker.eu.

[40] Hans-Joerg Hochecker Magnetism as an Electric Angle-effect and Gravitation as an Electric Effect International Journal of Physics Vol. 3, No. 4, 2015, pp 175-201.

International Journal of Physics, 2016, Vol. 4, No. 4, 106-112
Available online at http://pubs.sciepub.com/ijp/4/4/4

DOI:10.12691/ijp-4-4-4

Scattering Events and Heat Conductivity of Layered $La_{2-x}Sr_xCuO_4$ Superconductors

Rakhi Sharma[1], B. D. Indu[2,*], Pawan Kumar[1]

[1]Department of Physics, Gurukula Kangari Vishwavidyalaya, Haridwar-249401, India
[2]Department of Physics, Indian Institute of Technology Roorkee, Roorkee-247667, India
*Corresponding author: drbdindu@gmail.com

Abstract The problem of heat conduction in layered $La_{2-x}Sr_xCuO_4$ superconductor has been investigated in a new frame work of in-plane and cross-plane concepts with the help of modified Callaway model of thermal conductivity based on relaxation time approximation. Using the many body quantum dynamical theory of the expressions for thermal conductivity in context of in-plane and cross plane have been obtained and results are found in excellent agreement with experimental observations for layered $La_{2-x}Sr_xCuO_4$ cuprate superconductors. The theory explores the possibility of device fabrication cold in one direction and hot in the other.

Keywords: *relaxation times, in-plane and Cross- plane thermal conductivity, scattering process*

Cite This Article: Rakhi Sharma, B. D. Indu, and Pawan Kumar, "Scattering Events and Heat Conductivity of Layered $La_{2-x}Sr_xCuO_4$ Superconductors." *International Journal of Physics*, vol. 4, no. 4 (2016): 106-112. doi: 10.12691/ijp-4-4-4.

1. Introduction

A detailed understanding of thermal transport and management in layered systems is increasingly emerging as thrust area in the modern efficient energy technology and theorists are interestingly involved to explain this phenomenon. The study of heat transport in conventional and high temperature superconductors (HTS) emerged as an important tool to understand the scenario of phonon and electron energy spectrum along with various collision events. The thermal conductivity κ was understood in such systems contributed both by electrons and phonons in the form of electronic thermal conductivity κ_e [1] and phonon conductivity κ_{ph} [2] related by $\kappa = \kappa_e + \kappa_{ph}$. At fairly low temperatures the Widemann-Franz law often breaks down severely and the metallic behavior of solids which become superconducting suggests that the electronic thermal conductivity starts to disappear and one can take $\kappa_e \to 0$ negligibly small with $\kappa \simeq \kappa_{ph}$ instead of the concept of isolated channels [3,4,5]. The layered high temperature superconductor structures are highly anisotropic in character and thus the in-plane and cross-plane thermal transport becomes more and more important. Some investigations reveal [6,7] that scattering of electrons from phonons, impurities and interfacial roughness can be used to determine in-plane electron transport and resonant tunneling effects and the in plane scattering can be used to determine cross-plane transport [8,9,10] and this is further supported by the different phonon velocities in different directions [9]. Lattice vibrations can couple to each other and strongly couple with any structural defect, surface boundaries, dislocations or point defects [2,4,11,12,13,14,15].

The thermal conductivity of layered structures based on Boltzmann transport equation approach has studied by many theorists [16,17,18] using the method of relaxation time approximation (RTA). The validity of RTA, however, suffers from many adequacies because of its derivation for low frequency phonons at low temperatures, additivity of lifetimes of individual scattering events and its incompatibility to explain inelastic phonon scattering processes [18-24]. Adopting the quantum mechanical approach these inadequacies have been successfully removed from the phenomenological theories of thermal conductivity [18,20,21]. The discrepancies involved due to the phonon dispersion relation and violation of Matthiessen's rule of additivity of inverse relaxation time have been removed by introducing the equivalence between relaxation times and line widths [20,21]. The electron-phonon and the resonance scattering events are found to be highly sensitive in microstructures also, which successfully explain the abnormal behavior (dip and rise) of thermal conductivity curve at and above the critical temperature T_c. In this region an utmost care has to be taken as the thermal transport takes place in the presence of pairons in HTS which do not contribute to thermal conductivity.

In the present work we have investigated the role of various scattering processes based on many body quantum dynamics and the thermal conductivity is resolved into in-plane and cross-plane contributions which addresses the possibility of restricting the heat flow in a particular direction and allowing it in the another which can be exploited to the development of exotic technological HTS crystals for industrial use. In the present case in-plane

thermal conductivity is observed greater than cross-plane thermal conductivity.

2. Formulation of the Problem

The anisotropic considerations suggest that the thermal conductivity of a layered crystal can be resolved as a contribution of in-plane thermal conductivity $\kappa_{\parallel}$ and cross -plane thermal conductivity $\kappa_{\perp}$ as

$$\kappa = \kappa_{\parallel} + \kappa_{\perp} \tag{1}$$

where $\kappa_{\parallel}$ and $\kappa_{\perp}$ can be obtained from Callaway expression [2] using relaxation time approximation in the following form

$$\kappa_{\parallel} = \left(\frac{k_B}{2\pi^2 v}\right)\left(\beta^2\hbar^2\right)\int_0^{\omega_D} \tau_{k\parallel} \frac{\omega_{\parallel}^4 e^{\beta\hbar\omega_{\parallel}}}{\left(e^{\beta\hbar\omega_{\parallel}} - 1\right)^2} d\omega_{\parallel} \quad (1a)$$

$$\kappa_{\perp} = \left(\frac{k_B}{2\pi^2 v}\right)\left(\beta^2\hbar^2\right)\int_0^{\omega_D} \tau_{k\perp} \frac{\omega_{\perp}^4 e^{\beta\hbar\omega_{\perp}}}{\left(e^{\beta\hbar\omega_{\perp}} - 1\right)^2} d\omega_{\perp} \quad (1b)$$

where ω_D is the Debye Frequency, $\beta = (k_B T)^{-1}$ and in order to get rid of the inadequacies involved due to Matthiessen's rule the relaxation times $\tau_{k\parallel}^{-1}(\omega)$ and $\tau_{k\perp}^{-1}(\omega)$ are along in-plane and cross-plane directions which can be replaced by phonon line widths $\Gamma_{k_{\parallel}}(\omega)$ and $\Gamma_{k_{\perp}}(\omega)$ [18,20,21]. The evolution of $\Gamma_{k_{\parallel}}(\omega)$ and $\Gamma_{k_{\perp}}(\omega)$ can be obtained with the help of quantum dynamics of phonons [20,21,25,26,27,28].

3. The Collision Processes

In order to investigate the many body quantum dynamics to explore the various scattering mechanism, let us consider the Hamiltonian for a HTS in the form

$$H = H_p + H_A + H_e + H_{ep} + H_D \tag{2}$$

where,

$$H_p = \sum_k \frac{\hbar\omega_k}{4}[A_k^* A_k + B_k^* B_k] \tag{2a}$$

$$H_A = \sum_{s\geq 3}\sum_{k_1,..,k_s} \hbar V_s(k_1,k_2,...,k_s) A_{k_1} A_{k_2} .... A_{k_s} \tag{2b}$$

$$H_e = \sum_q \begin{pmatrix} \hbar\omega_{q\uparrow} b_{q\uparrow}^* b_{q\uparrow} + \hbar\omega_{q\downarrow} b_{q\downarrow}^* b_{q\downarrow} \\ +\hbar\omega_{-q\uparrow} b_{-q\uparrow}^* b_{-q\uparrow} + \hbar\omega_{-q\downarrow} b_{-q\downarrow}^* b_{-q\downarrow} \end{pmatrix} \tag{2c}$$

$$H_{ep} = \sum_{k,q} \begin{pmatrix} g_k b_{Q\uparrow}^* b_{q\uparrow} + g_k^* b_{q\uparrow}^* b_{Q\uparrow} \\ +g_k b_{Q\downarrow}^* b_{q\downarrow} + g_k^* b_{q\downarrow}^* b_{Q\downarrow} \end{pmatrix} B_k \tag{2d}$$

$$\begin{aligned} H_D = &-\hbar \sum_{k_1,k_2} \left[C(k_1,k_2) B_{k_1} B_{k_2} \right] \\ &+\hbar \sum_{k_1,k_2} \left[D(k_1,k_2) A_{k_1} A_{k_2} \right]. \end{aligned} \tag{2e}$$

In the above equations the symbols H_p, H_A, H_e, H_{ep} and H_D respectively stand for harmonic phonon- [25], anharmonic phonon- [26,27,28], electron-[29,30], electron-phonon coupling- [29,30,31] and Defect-Hamiltonian [26,28,29,30,31]. This Hamiltonian can be used to evaluate the double time temperature dependent phonon Green's function

$$\begin{aligned} G_{kk'}(t-t') &= \langle\langle A_k(t); A^*_{k'}(t')\rangle\rangle \\ &= -i\theta(t-t')\langle A_k(t), A^*_{k'}(t')\rangle. \end{aligned} \tag{3}$$

in the form

$$G_{kk'}(\omega) = \frac{\omega_k \eta_{kk'}}{\pi[\omega^2 - \tilde{\omega}_k^{\,2} - 2\omega_k \tilde{P}(k,k',\omega)]} \tag{4}$$

here $\tilde{\omega}_k$ is the renormalized phonon frequency and $\tilde{P}(k,k',\omega)$ is the self-energy operator or response function

$$\tilde{P}(k,k',\omega) = Lim_{\varepsilon\to 0^+} \Delta_k(\omega) - i\Gamma_k(\omega) \tag{5}$$

Where $\Delta_k(\omega)$ (real part of $\tilde{P}(k,k',\omega)$) is shift in the phonon frequency and the imaginary part is the phonon frequency line width at the half maximum of the phonon frequency peak and can be written in the form

$$\Gamma_k(\omega) = \Gamma_k^A(\omega) + \Gamma_k^{ep}(\omega) + \Gamma_k^D(\omega) + \Gamma_k^{AD}(\omega) \tag{6}$$

Here $\Gamma_k^D(\omega)$, $\Gamma_k^A(\omega)$, $\Gamma_k^{AD}(\omega)$ and $\Gamma_k^{ep}(\omega)$ are the individual contributions of line widths (life times) due to point defect scattering, phonon-phonon scattering, interference scattering and electron-phonon scattering, respectively, more details of every term are available in the references elsewhere [26,27,28,31] and will be discussed in the rest of the paper.

The relaxation time as per Callaway formalism is given by $\tau^{-1} = \sum_i \tau_i^{-1}$ for i type of scattering processes not interacting with each other which in general is never found in a real system and addresses the wrong application of Matthiessen's rule. The i type of collision events may be described in terms of boundary scattering τ_{CB}^{-1}, impurity scattering $\tau_D^{-1}(\omega)$, phonon-phonon collision $\tau_{ph}^{-1}(\omega)$, interference scattering $\tau_{AD}^{-1}(\omega)$, electron-phonon $\tau_{e-p}^{-1}(\omega)$, resonance scattering $\tau_R^{-1}(\omega)$ events, etc. The problem of use of adequate dispersion relations and the inverse additivity of relaxation times can be resolved by taking the concept of renormalized and perturbed mode frequencies [18,31] and $\tau^{-1} = \Gamma_k(\omega)$ [18,20,21,31] which in accordance with Eq. (1) can be resolved in the form

$$\tau^{-1} = \tau_{k_{\parallel}}^{-1} + \tau_{k_{\perp}}^{-1} = \Gamma_{k_{\parallel}}(\omega) + \Gamma_{k_{\perp}}(\omega) = \Gamma_k(\omega) \tag{7}$$

where

$$\tau_{k_{\|}}(\omega)=\tau_{\|CB}{}^{-1}+\Gamma_{k_{\|}}^{A}(\omega)+\Gamma_{k_{\|}}^{AD}(\omega)+\Gamma_{k_{\|}}^{ep}(\omega)+\Gamma_{k_{\|}}^{D}(\omega)+\tau_{\|R}{}^{-1} \quad (8a)$$

$$\tau_{k_{\perp}}(\omega)=\tau_{\perp CB}{}^{-1}+\Gamma_{k_{\perp}}^{A}(\omega)+\Gamma_{k_{\perp}}^{AD}(\omega)+\Gamma_{k_{\perp}}^{ep}(\omega)+\Gamma_{k_{\perp}}^{D}(\omega)+\tau_{\perp R}{}^{-1}. \quad (8b)$$

Despite of several serious objections in the numerically amenable Callaway model established wide acceptability to successfully analyze thermal conductivity by the use of the concept of the relaxation times which has convoluted dependence on frequency, temperature and various distribution functions in a large number of scattering processes involved and resorts it as a very sensitive quantity. However, this model was greatly modified by a large number of authors to shape it up in a physically justifiable format [1,4,19,20,21,22,23,35]. A brief account of these events for the layered systems is described as follows:

3.1. Combined Boundary Scattering

The concept of boundary scattering phenomenon [15,16,17,18,20,21,31,32] is based on the assumption that at low temperatures the long wavelength phonons of low frequency get excited and scatters from the crystal boundaries at the relaxation rate of $\tau_B{}^{-1}=v/L$ where $L=1.22(l_1l_2)^{1/2}$ is the Casimir length [15] and l_1, l_2 are cross sectional area of the specimen. Some limitations of Casimir theory which enforced to use L as a parameter in most of the work on thermal conductivity and this was modified by considering the involvement of crystal micro boundaries due to micro scale fluctuations in the internal boundaries of the crystal [32] in the form of $\tau_{CB}^{-1}=v_p/L_B$, L_B being the modified Casimir length. Here the term τ_{CB}^{-1} can be modified for the layered systems as $\tau_{CB}^{-1}=\tau_{\|CB}^{-1}+\tau_{\perp CB}^{-1}$, where $\tau_{\|CB}^{-1}=v_{p\|}/L_{\|}(B)$ and $\tau_{\perp CB}^{-1}=v_{p\perp}/L_{\perp}(B)$. These microscale fluctuations incorporated in L_B offer significant resistance for longer wavelengths and strong phonon-boundary scattering is indeed the reason for increased thermoelectric performance of nanostructures and silicon nanowires in particular [33].

3.2. Impurity Scattering

The contribution of scattering from defect events starts as the temperature starts rising and higher frequency phonons begin to excite with shorter wavelengths. Phonons get localized around the impurity sites and interact with impurities offering much thermal resistance. However, the point impurity scattering was described by Klemens [4] for mass change parameter but when one develops the same problem with the help of many body quantum dynamical theory the lifetime can be obtained in the following forms [16-21]

$$\Gamma_k^D(\omega)=8\pi\varepsilon(\omega)\sum_{k1}R(-k,k_1)R^*(-k,k_1)\omega_{k_1}\delta\left(\omega^2-\tilde{\omega}_k{}^2\right) \quad (9)$$
$$\approx A\omega^4+A_1\omega^2$$

It is noteworthy here that apart from the Klemens expression there arises force constant change term depending on square of frequency which of course is highly sensitive in the description of heat capacity. This result can further be obtained for a layered crystal in the form

$$\Gamma_k^D(\omega)=\Gamma_{k_{\|}}^D(\omega)+\Gamma_{k_{\perp}}^D(\omega) \approx A_{m_{\|}}\omega_{\|}{}^4+A_{m_{\perp}}\omega_{\perp}{}^4+A_{1\|}\omega_{\|}{}^2+A_{1\perp}\omega_{\perp}{}^2 \quad (10)$$

$A_j(j=\|,\ \perp)$ being layered system constants. The variation of defect scattering rates with temperature and reduced frequency for in plane and cross plane cases is shown in Figure 1 dissimilar trend for both the cases, i.e., for cross plane defects contribute dominatingly as compared to in plane scenario heralding that the cross plane heat conduction can be limited significantly.

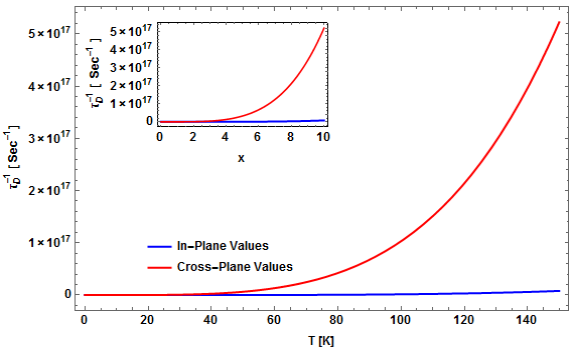

Figure 1. Behavior of τ_D^{-1} vs T [inset τ_D^{-1} vs x] for in-plane and cross-plane references.

3.3. Phonon-Phonon Processes

With further rise in temperature more and more phonons with higher frequencies get excited and start interacting with the cubic and quartic phonon fields of each other giving rise to phonon-phonon scattering. In HTS the quartic phonon scattering does not take place as it is a phenomenon generally operative at high temperatures and one can restrict to $\Gamma_k^A(\omega)=\Gamma_k^{3A}(\omega)$. In the earlier work the phonon-phonon scattering relaxation time was mostly taken to vary arbitrarily with the powers of frequency and temperature and their multiplier coefficients which couldn't justify the physics of the problem. This problem was systematically undertaken to study quantum dynamically [18,20,21,31] and revealed the following exact frequency and temperature dependence:

$$\Gamma_k^{3A}(\omega)=18\pi\varepsilon(\omega)\sum_{k_1,k_2}|V_3(k_1,k_2,-k)|^2\,\eta_1[S_{+\alpha}\omega_{+\alpha}\times\delta(\omega^2-\omega_{+\alpha}{}^2)-S_{-\alpha}\omega_{-\alpha}\delta(\omega^2-\omega_{-\alpha}{}^2)] \quad (11)$$
$$\approx B\omega^2T$$
$$\approx\Gamma_{\|k}^{3A}(\omega)+\Gamma_{\perp k}^{3A}(\omega)\approx B_{\|}\omega_{\|}{}^2T+B_{\perp}\omega_{\perp}{}^2T.$$

Where $B_j\,(j=\|,\ \perp)$ are constants for a layered system.

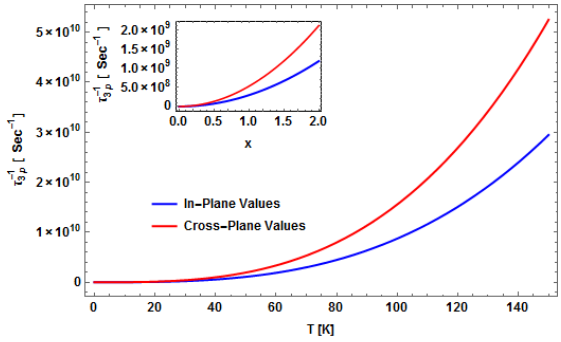

Figure 2. Behavior of τ_{3p}^{-1} vs T [inset τ_{3p}^{-1} vs x] for in-plane and cross-plane references

Figure 2 depicts the variation of phonon-phonon life times in plane and cross plane references with T and x. Apart from defects this scattering infers that the trend for in plane and cross plane cases is similar but the thermal resistance offered by cross planes is certainly higher and may enable one to technological exploitation of the idea that in cross plane direction the system is cold and in the in plane scene it is hot giving way for heat transport.

3.4. Interference Scattering

At elevated temperatures the phonons of localized fields start interacting with those of anharmonic fields giving rise to impurity-anharmonicity interaction modes and interference scattering [18,20,21,31]. Taking these interactions with cubic anharmonicity only the related line width takes the form

$$\begin{aligned}&\Gamma_k^{AD}(\omega)=\Gamma_k^{3D}(\omega)\\&=144\pi\varepsilon(\omega)\sum_{k_1,k_2,k_3}|V_3(k_1,k_2,-k)|^2\ R(k_1,k_2)\omega_k{}^{-1}\eta_1\\&\times[S_{+\alpha}\omega_{+\alpha}\delta(\omega^2-\omega_{+\alpha}{}^2)-S_{-\alpha}\omega_{-\alpha}\delta(\omega^2-\omega_{-\alpha}{}^2)]\\&\approx D\omega^4\approx D_{\|}\omega_{\|}{}^4T+D_{\perp}\omega_{\perp}{}^4T.\end{aligned}\tag{12}$$

This interaction is portrayed in Figure 3 and well prophesied that the cross plane behavior of thermal resistance is much more dominant above the transition temperature as compared to the in-plane heat transport.

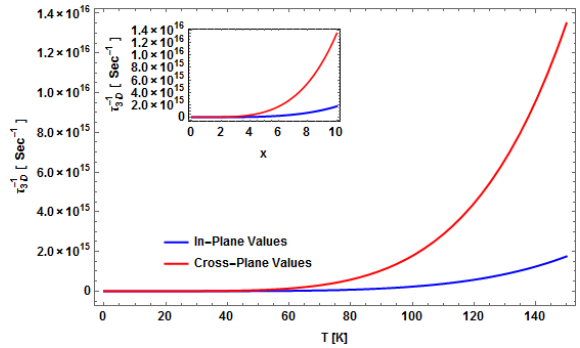

Figure 3. Behavior of τ_{3D}^{-1} vs T [inset τ_{3D}^{-1} vs x] for in-plane and cross-plane references

3.5. Electron-phonon Scattering

Ziman [13] successfully explored the problem of heat transport by electrons which was developed later quantum mechanically [31] and found it a highly sensitive quantity by describing the electron energy line width in the form

$$\begin{aligned}&\Gamma_k^{ep}(\omega)=g^2\omega^2\left[-A_{1e}\left(e^{x/2}+1\right)^{-1}+A_{2e}\coth\left(3x/2\right)\right]\\&\approx g^2\omega_{\|}{}^2\left[-A_{\|1e}\left(e^{x_{\|}/2}+1\right)^{-1}+A_{\|2e}\coth\left(3x_{\|}/2\right)\right]\\&+g^2\omega_{\perp}{}^2\left[-A_{\perp1e}\left(e^{x_{\perp}/2}+1\right)^{-1}+A_{\perp2e}\coth\left(3x_{\perp}/2\right)\right]\end{aligned}\tag{13}$$

with $x=\hbar\omega/k_BT,\ x_j=\hbar\omega_j/k_BT;\ (j=\|,\perp)$. The details of various symbols appearing in the above equations are well described in the references elsewhere [16,17,18,19,20,28,30,32] and needs no reproduction. Electron-phonon interaction events are highly sensitive to the frequency variations and helps in understanding the fact that the pairons or cooper pairs do not contribute to the thermal transport and this typical behavior of electron-phonon events is shown in Figure 3.

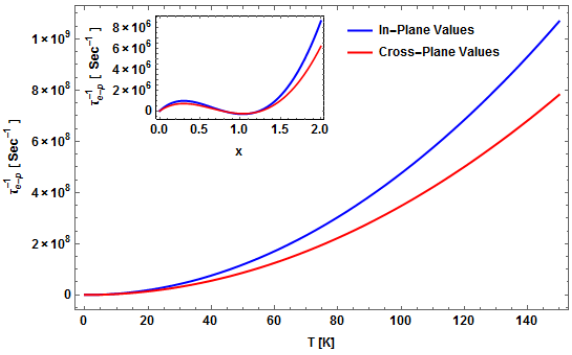

Figure 4. Behavior of τ_{e-p}^{-1} vs T [inset τ_{e-p}^{-1} vs x] for in-plane and cross-plane references

3.6. Resonance Scattering

Pohl [33] associated the dip just above the maximum peak of thermal conductivity with impurity and resonance scattering and the related relaxation rate was described by him is given by

$$\tau_R^{-1}=R\omega^2T^n\left[\left(\omega_0{}^2-\omega^2\right)+\left(\Omega/\pi\right)^2\omega_0{}^2\omega^2\right]^{-1}\tag{14}$$

which gives its form for layered systems as follows:

$$\begin{aligned}&\tau_R^{-1}=R_{\|}\omega_{\|}{}^2T^n\left[\left(\omega_{\|0}{}^2-\omega_{\|}{}^2\right)+\left(\Omega/\pi\right)^2\omega_{\|0}{}^2\omega_{\|}{}^2\right]^{-1}\\&+R_{\perp}\omega_{\perp}{}^2T^n\times\left[\left(\omega_{\perp0}{}^2-\omega_{\perp}{}^2\right)+\left(\Omega/\pi\right)^2\omega_{\perp0}{}^2\omega_{\perp}{}^2\right]^{-1}\end{aligned}\tag{15}$$

where $R_{\|}$, $R_{\perp}$ are the in-plane and cross-plane proportionality constants related to the impurity concentration. $\omega_{0\|}$ and $\omega_{0\perp}$ are respective resonance frequencies and Ω is the damping constant.

4. Analysis of Thermal Conductivity

In order to justify the outcome of the above findings we have taken up the numerical analysis of thermal conductivity of high temperature oxide superconductor La-Sr-Cu-O samples. The experimental results of Uher [5]

for the samples La_2SrCuO_4, $La_{1.8}Sr_{0.2}CuO_4$, and $La_{1.85}Sr_{0.15}CuO_4$ have been taken for the purpose of analysis for different temperature ranges $0-70K$, $0-100K$ and $0-140K$, respectively. The values of various constants and parameters used in the analysis of in-plane and cross-plane thermal conductivity are furnished in Table 1, separately for each sample. The numerical estimation has been carried out in the light of Eqs. (1), (1a) and (1b) have been portrayed in Figure 5 through 7, which reveal excellent agreements between theory and experimental observations throughout all the temperature ranges. The phonon velocity can be replaced by the group velocity $v_p \approx v_g$ which can be further resolved via simplest dispersion relation of the form $\omega^2 = \omega_{\|}^2 + \omega_{\perp}^2 = v_{g_{\|}}^2 k_{\|}^2 + v_{g_{\perp}}^2 k_{\perp}^2$ with $k^2 = k_{\|}^2 + k_{\|}^2$, $k_{\|}^2 = k_x^2 + k_y^2$ and $k_{\perp} = k_z$ in the Debye approximation [18]. This concept is well supported by Holland's two mode analysis [35]. During the numerical computation it is observed that the contribution of combined boundary and impurity scattering events is highly effective at low temperatures but their significance gradually diminishes with the rise of temperature and these processes are eventually replaced by the phonon-phonon scattering and interference processes. The findings of Kristoffel *et al* that the impurities play a very essential role in the cuprate superconductors [36] is well supported in the present work.

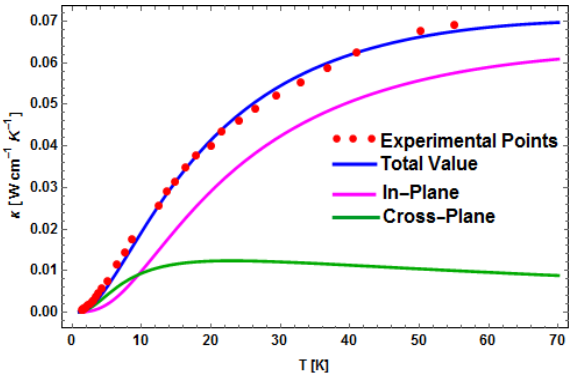

Figure 5. Analysis of thermal conductivity of La_2SrCuO_4 sample

The phonon-phonon interactions and higher order collision events certainly take place in the system when the temperature is continuously elevated resulting in the excitation of higher and higher frequency phonons with considerably smaller wavelength enabling the collisions at smaller distances and the thermal resistance continuously becomes more and more severe. Obviously,

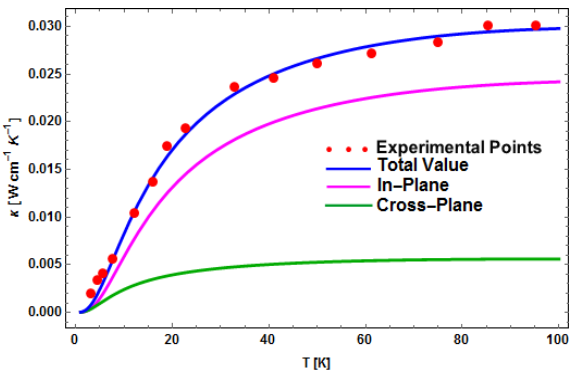

Figure 6. Analysis of thermal conductivity of $La_{1.8}Sr_{0.2}$ CuO_4 sample

The situation becomes so intense that the phonons of anharmonic phonon fields start interacting with the phonons of localized fields giving rise to the interference interactions with higher magnitude of thermal resistance. The varied frequency and temperature dependence for phonon processes by earlier worker at their choice thus gets proper justification through phonon-phonon and interference processes and work at and above the thermal conductivity maxima.

Table 1. Constants and parameters used in the analysis of thermal conductivity of high temperature superconductor $La_{2x}S_xCuO_4$ samples

Sample	La_2SrCuO_4	$La_{1.8}Sr_{0.2}CuO_4$	$La_{1.85}Sr_{0.15}CuO_4$
Tc (K)	37	37	37
θ (K)	410	400	410
$g_{\|}$	0.7	0.7	0.7
$g_{\perp}$	1.6	0.6	0.6
$L_{\|}$(B)$(\times10^{-3}\ cm)$	0.155	0.153	0.155
$L_{\perp}$ (B)$(\times10^{-3}\ cm)$	0.275	0.145	0.145
$A_{m\|}$ $(\times10^{-43}\ s^3)$	17.9197	83.6587	53.6597
$A_{m\perp}(\times10^{-43}\ s^3)$	20.0659	70.6197	350.6197
$B_{\|}$ $(\times10^{-22}\ sK^{-1})$	20.8982	20.8972	50.8982
$B_{\perp}$ $(\times10^{-22}\ sK^{-1})$	218.6982	20.6972	90.6982
$D_{\|}$ $(\times10^{-45}\ s^3K^{-1})$	7.14134	7.14134	7.84134
$D_{\perp}(\times10^{-45}\ s^3K^{-1})$	110.4134	7.41344	60.4134
$v_{\|}$ $(\times10^{5}\ cms^{-1})$	6.2	6.4	7.5
$v_{\perp}$ $(\times10^{5}\ cms^{-1})$	4.0	6.1	7.5
$A_{\|1e}(\times10^{2}erg^{-2}K^{-2})$	9.89	9.89	9.89
$A_{\perp1e}(\times10^{2}erg^{-2}K^{-2})$	19.89	2.091	9.89
$A_{\|2e}(\times10^{2}erg^{-2}K^{-2})$	9.8909	9.89	9.89
$A_{\perp2e}(\times10^{2}erg^{-2}K^{-2})$	19.85	2.07	9.85
$R_{\|}$ $(\times10^{32}s^3)$	-	-	0.80
$R_{\perp}$ $(\times10^{32}s^3)$	-	-	1.41
$\omega_{\|0}$ $(\times10^{12}s^{-1})$	-	-	3.11
$\omega_{\perp0}$ $(\times10^{12}s^{-1})$	-	-	3.05

The electron-phonon interactions primarily participate in the thermal transport above the conductivity maximum in the case of high temperature superconductors where conductivity curve shows a cusp like trend near the transition temperature. This cusp is more and more pronounced in case of YBaCuO superconductors [5,31,37].

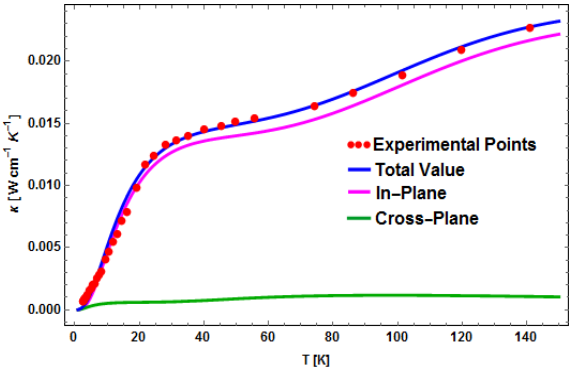

Figure 7. Analysis of thermal conductivity of $La_{1.85}Sr_{0.15}CuO_4$ sample

Since the pairons are generated as a result of phonon mediated effects of electrons and never contribute in the

thermal transport and may be attributed to negative thermal resistance (Figure 4 inset) in this region giving cusp like behavior.

Coming to the case of in plane and cross plane thermal transport the various parameters used in computation show that in plane values are always smaller than those of cross plane values. Before going into further details let us define the thermal conductivity functions for in-plane $\zeta_{\|}$ and cross-plane $\zeta_{\perp}$ contributions as

$$\zeta_{\|} = \frac{k_B \beta^2 \hbar^2 \omega_{\|}{}^4 e^{\beta\hbar\omega_{\|}}}{2\pi^2 v_{\|}\, \Gamma_k(\omega_{\|}, T)\left(e^{\beta\hbar\omega_{\|}} - 1\right)^2} \tag{16a}$$

$$\zeta_{\perp} = \frac{k_B \beta^2 \hbar^2 \omega_{\perp}{}^4 e^{\beta\hbar\omega_{\perp}}}{2\pi^2 v_{\perp}\, \Gamma_k(\omega_{\perp}, T)\left(e^{\beta\hbar\omega_{\perp}} - 1\right)^2}. \tag{16b}$$

The variation of conductivity function for in-plane and cross plane have been portrayed with $x_{\|}$, T is depicted in Figure 8 and Figure 9.

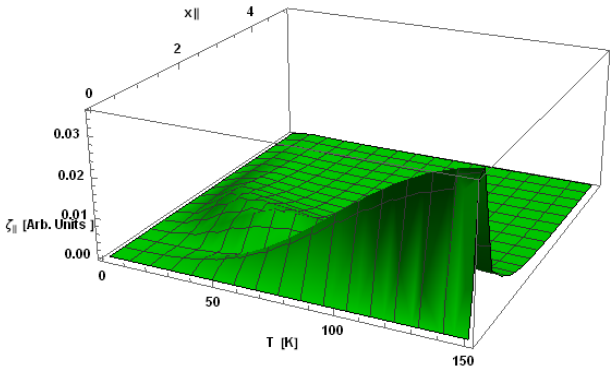

Figure 8. Variation of in-plane thermal conductivity function $\zeta_{\|}(x_{\|}, T)$ versus $x_{\|}$ and T for all collision process

For reduced frequencies between $x_j < 1$ the thermal conductivity function shows sharp peak and the behavior becomes more pronounced at higher temperatures and as is clear from contour lines at the frequencies $x_j > 1$ the contribution remains almost constant, notably the curve flattens very rapidly in case of cross plane reference.

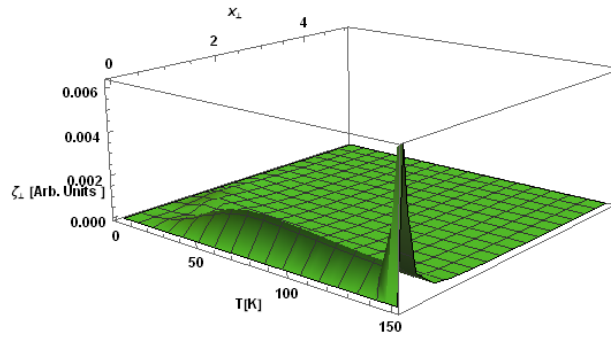

Figure 9. Variation of cross-plane thermal conductivity function $\zeta_{\perp}(x_{\perp}, T)$ versus $x_{\perp}$ and T for all collision process

The curves in Figure 5 – Figure 7 show that the nature of $\kappa_{\|}$ almost follows the nature of experimental curves but the behavior of $\kappa_{\perp}$ is completely different and slightly rising trend at initial low temperatures but immediately becomes constant for elevated temperatures inferring that it becomes least temperature sensitive.

5. Conclusions

Present investigations successfully describe the behavior of thermal conductivity of cuprate superconductors and is applicable to the all types of high temperatures superconductors. Further, the present study supports that the thermal conductivity in both directions i.e. parallel to the layers and perpendicular to the layers is always smaller than that of bulk materials. It is also inferred that the thermal transport is quite efficient parallel to the layers and along the growth axis or in the cross-plane direction is found quite small compared to the in-plane direction of $La_{2-x}Sr_xCuO_4$ superconductors. This idea can be technologically exploited in fabrication/design of the devices in which the system should not respond to temperature in a particular direction whereas shows maximum response to temperature in the rest of the directions. In other words, the theory concludes that it is possible to develop the devices which is hot in the in plane direction but cold in the cross plane direction.

References

[1] Bardeen, J., Rickayazen G. and Tewordt L., Theory of the thermal conductivity of superconductors, *Phys. Rev. B*, 113, 982-994, 1959.

[2] Callaway, J., Model for lattice thermal conductivity at low temperatures, *Phys. Rev*., 113, 1046-1051, 1959.

[3] Parrott, J. E. and Stukes, A. D., *Thermal conductivity of solids*, Pion Limited, London, 1975.

[4] Klemens, P. G., Thermal conductivity and lattice vibrational modes, *Sol. Stat. Phys*., 7, 1-98, 1958.

[5] Uher, C., Thermal conductivity of High T_c Superconductors, *J. Superconductivity*, 3, 337-389, 1990.

[6] Cahill, D. G., Goodson, K., and Majumdar, A., Thermometry and Thermal Transport in Micro/ Nanoscale Solid-State Devices and Structures, *J. Heat Trans.*, 124, 223-241, 2002.

[7] Cahill, D. G., Ford, W. K., Goodson, K.E., Mahan, G. D., Majumdar, A., Maris H. J., Merlin, R., and Phillpot, S. R., Nanoscale Thermal Transport, *J. Appl. Phys.*, 93, 793-818, 2003.

[8] Mahan, G.D., *Thermal Conductivity*, edited by Terry M. Trit, Kluwer Academic/Plenum Publishers, New York, 1-285, 2004.

[9] Narayanamurti, V., Stormer, H. L., Chin, M. A., Gossard, A.C., and Wiegmann, W., Selective Transmission of High-Frequency Phonons by a Superlattice: The dielectric Phonon Filter, *Phys. Rev. Lett.*, 43, 2012-2016, 1979.

[10] Varshney, D., Chaudhry, K. K. and Singh, R. K., Analysis of in-plane thermal conductivity anomalies in $YBa_2Cu_3O_{7-\delta}$ cuprate Superconductors, *New J. Phys.*, 5, 72.1-72.17, 2003.

[11] Klemens, P. G., The scattering of low-frequency lattice waves by static imperfections, *Proc. Phys. Soc. A*, 68, 1113-1128, 1955.

[12] Carruthers, P., Theory of thermal conductivity of solids at low temperatures, *Rev. Mod. Phys*., 33, 92-138, 1961.

[13] Ziman, J. M., *Electrons and Phonons*, Clarendon Press, Oxford, U. K., 1962.

[14] De Hass, W. J., Biermasz, T., Thermal conductivity in diamond and potassium chloride, *Physica* 5 , 47-53, 1938.

[15] Casimir, H. B. G., Note on the Conduction of Heat in Crystals, *Physica*, 5, 495-500, 1938.

[16] Hyldgaard, P., and Mahan, G. D., Phonon Superlattice Transport, *Phys. Rev. B*, 56, 10754-10757, 1997.

[17] Chen, G., Size and Interface Effects on Thermal Conductivity of Superlattices and Periodic Thin-Film Structures, *J. Heat Trans*., 119, 220-229 1997.

[18] Saini Richa, Ashokan Vinod, Indu, B.D., Phonon conduction in superlattices, *Superlattices and Microstructures*, 82, 574-583, 2015.

[19] Erdos, P., and Halley, S. B., Low-Temperature Thermal Cond--uctivity of Impure Insulators, *Phys. Rev.*,184 , 951-967, 1969.

[20] Gairola, R. P., Low-Temperature Lattice Thermal Conductivity of Nonmetallic Solids with Isotopic Impurities, *Phys. State Solidi B*, 125, 65-74, 1984.

[21] Bahuguna, B.P., Painuli, C. P. , and Indu, B. D., Phonon Heat Con-ductivity of Garnets Containing Rare Earth Ions, *Acta Phys. Pol. A*, 80, 527-554, 1991.

[22] Ward, A., and Broido, D. A., Intrinsic lattice thermal conductivity of Si/Ge and GaAs/AlAs superlattice, *Phys. Rev.* B, 77, 245328-1-7, 2008.

[23] Broido, D. A., Ward, A. and Mingo, N., Lattice thermal conductivity of silicon from empirical interatomic potentials, *Phys. Rev.* B, 72 , 014308-1-8, 2005.

[24] Ward, A., Ab initio theory of the lattice thermal conductivity in diamond, *Phys. Rev.* B, 80, 125203-1-8, 2009.

[25] Pathak, K. N., Theory of anharmonic crystals., *Phys. Rev.*, 139, A1569-A1580, 1965.

[26] Sharma, P.K., and Bahadur, R., Thermal Conductivity for Phonon Scattering by Substitutional Defects in Crystals, *Phys. Rev. B*, 12, 1522-1530, 1975.

[27] Indu, B. D, Theory of lattice specific heat of an isotopically disordered anharmonic crystal, *Int. J. Mod. Phys. B*, 4, 1379-1393, 1990.

[28] Indu, B. D, Enhanced phonon density of states in impure anharmonic crystals, *Mod. Phys. Lett. B*, 6, 1665-1672, 1992.

[29] Frohlich, H., *New perspective in modern physics*, edited by R. E. Marshak , John Wiley, New York, 1966.

[30] Fan, H. Y., *Elements of solid state physics*, John Wiley, New York, 1987.

[31] Ashokan, V., Indu, B. D. and A. Kr. Dimri, Signature of electron phonon interaction in high temperature superconductors, *AIP Advances*, 1, 032101-1-032101-16, 2011.

[32] Indu, B. D., Low temperature lattice thermal conductivity of Mg_2 Sn, Mg_2Si, and Mg_2Ge, Nuovo *Cimento* B, 58, 345-350, 1980.

[33] Hochbaum, A., Chen, R., Delgado, R., W., Liang, Garnett, E., Najarian, M., Majumdar, A., and Yang, P., "Enhanced Thermoelectric Performance of Rough Silicon Nanowires", *Nature*, 451, 163-167, 2008.

[34] Pohl, R. O., Thermal Conductivity and Phonon Resonance Scattering, *Phys. Rev. Lett*., 8, 481-483, 1962.

[35] Holland, M.G., Analysis of thermal conductivity, *Phys. Rev.*, 132, 2461-2471, 1963.

[36] Kristoffel, N. and Rubin, P., Localized electron levels of cuo2 planes perturbed by detects in high-Tc superconductors, *Rev. Solid State Sci.*, 5, 449-460,1991.

[37] Ashokan, V. and Indu, B.D., Theory of thermal conductivity of high temperature superconductors: a new approach, *Mod. Phys. Letters B*, 25, 663-678, 2011.

International Journal of Physics, 2016, Vol. 4, No. 4, 113-118
Available online at http://pubs.sciepub.com/ijp/4/4/5

DOI:10.12691/ijp-4-4-5

Effects of Magnetic Flux Density on the Population of *Escherichia coli* in River Njoro Water

Thirika Anne[1,*], Ndiritu Francis[1], Kiruki Silas[2]

[1]Department of Physics, Faculty of Science, Egerton University, P.O. BOX 536 Njoro, Kenya
[2]Department of Physical Sciences, Chuka University, P.O. BOX 109 Chuka, Kenya
*Corresponding author: annethirika@gmail.com

Abstract In this study, the experimental results of the concentration of *Escherichia coli* in water exposed to magnetic flux density are presented. Water samples were collected from River Njoro, Nakuru County, Kenya. The initial *Escherichia coli (E.coli)* counts for the samples were obtained using Membrane Filtration techniques. The samples were then exposed to different magnetic flux densities (2mT, 6mT and 10mT) at time intervals of 6 hours and 18 hours for each magnetic flux. Membrane filtration was also done after magnetic treatment of the samples. The data obtained was photographed and presented in tables and bar graphs. The maximum disinfection efficiency was 82.2% for bacteria exposed to a magnetic flux of 10 mT for 6 hours. This study proved that magnetic field can be used as inhibitory factor against the *E.coli*.

Keywords: *Magnetic Flux Density (MFD), Colony Forming Units (CFU), Escherichia Coli (E. coli)*

Cite This Article: Thirika Anne, Ndiritu Francis, and Kiruki Silas, "Effects of Magnetic Flux Density on the Population of *Escherichia coli* in River Njoro Water." *International Journal of Physics*, vol. 4, no. 4 (2016): 113-118. doi: 10.12691/ijp-4-4-5.

1. Introduction

Many rivers are reportedly prone to high bacterial contamination due to heightened ecological activities and may be unsuitable for human consumption when untreated [1]. Previous studies have indicated that the microbial quality of the River Njoro water sources is poor and unacceptable for human consumption due to consistent increase in total and fecal coliforms, and also due to pathogenic loading downstream [2]. This water is contaminated with pathogens which lead to widespread of acute and chronic illnesses, which are major causes of death and misery among the residents of Njoro. A recent report indicates that about 3.41 million people die each year from water, sanitation and hygiene-related causes [3]. Water and sanitation crisis claim more lives through related diseases than wars claim [4,5]. Pathogenic microorganism, especially *Escherichia coli*, was chosen to be an experimental model in this study: it is widely distributed in the environment such as soil, water and air; it causes several diseases such as urinary tract infection, wound infection, traveler's diarrhea, sepsis and meningitis; the presence of *E.coli* in water also indicates recent fecal contamination and the possible presence of disease-causing pathogens, such as bacteria, viruses, and parasites.

One of the key cornerstones of public health is access to safe water, however, water purification is an expensive process and this has hindered the government effort of providing majority of the population with treated water despite this being one of the requirements of the millennium development goals. Moreover, most common water purification methods have been shown to have serious negative impact to health and the environment. Chlorination for instance, which is one of the most widely used disinfectants [6] produce chemical compounds known as disinfection by-products (DBPs). Of these, Trihalomethanes (THMs) and Halo acetic acids (HAAs) found in the highest concentrations in chlorine treated drinking water are linked to high risks of cancer [7]. There has been growing concern over the health effects of boiling water as a purification method. This is because boiling tends to concentrate harmful inorganic contaminants, hence reducing water portability [8]. Again in developing countries, the major source of energy for cooking and boiling water is firewood which is expensive and environmentally unfriendly. Helping people gain access to safe drinking water is one of the most important health-related infrastructure programs in the world hence in the new millennium, there is a growing concern for the need to balance the risks of the need to disinfect the water to reduce the threat of disease from microorganisms against the potential health risks from disinfection byproducts that are formed as a result of adding a disinfectant. This study therefore intended to address this dilemma by establishing a water purification strategy that circumvents the health risks associated with the classical purification procedures.

It has been realized that the advantages of using water exposed to magnetic field as compared to normal water are enormous. Magnetic waste water treatment is a process that has been introduced to chemical industries to remove heavy metals and organic pollutants from waste water [17]. Stimulation of both animal and plant growth with magnetic field as a way to increase the quality and quantity of yield has caught the interest of many scientists

worldwide [16]. For instance, it has been established that magnetic treatment of irrigation water can improve primary productivity of water resulting to an increased crop production, a decrease in plant disease rate and an improved taste of agricultural products [16]. It is not clearly known how this is achieved but it could be attributed to the ability of such water to retain and highly dissolve the essential minerals [15].

In latest years, several studies have been performed to verify direct effects exerted by extremely low-frequency (ELF) electromagnetic fields (EMFs) on cell functions. In particular, it has been demonstrated that ELF-EMF can negatively [14] or positively [18] affect functional parameters (cell growth and viability) of a cell. The effects of magnetic fields on cells are thus not fully understood since some of the results have been inconsistent and have in other cases contradicted each other. The aim of this study was thus to evaluate the effect of magnetic flux density on the population of *E.coli* in River Njoro water.

2. Materials and Methods

2.1. Study Area

Njoro River is located within the Kenyan Rift Valley in Nakuru County and is approximately 60 kilometers (km) in length [9]. It has its source on the eastern slopes of the Mau Escarpment and its mouth in Lake Nakuru [9]. It is the main source of water to people and animals living in Njoro area.

2.2. Experimental Design

The voltage amount required was controlled by a variable transformer with low voltage power unit 022.317: 0–25 V, 8.5A rms max. This device is manufactured by Dexing magnet tech. Co.,Ltd, Fujian, China and distributed by UNILAB, Kenya. Magnetic field strength for the Helmholtz coils was set at 2 mT with the aid of a magnetic flux density unit (PHWE 612.002) and by varying the current in the coil. Petri dish 2mT was placed in between the two pairs of Helmholtz coils. The specifications of Helmholtz coil used are model PHWE 06990.10; 320 turns, diameter 14 cm. This coil is manufactured by San Electrical industries, Mumbai, India. For the next 6 hours, water in Petri dish 2mT was exposed to the Helmholtz field set at 2 mT. The Petri dish C served as a control under the same conditions except for the fact that it was not exposed to a magnetic field. The Bacterial count was done before and after exposure of the water samples to the magnetic flux. The magnetic field strength was increased from 2mT to 6 mT and finally 10 mT and the above procedure was repeated for each case. Exposure time was varied from 6 and 18 hours for each set magnetic field. The experiments were repeated three times. The Magnetic flux density was measured using a magnetic flux density unit (manufactured by Seatrend tech and development Company Ltd, Chongqing, China) connected to a multimeter model ALDAAVD830B, manufactured by Salicon Nano Technology Private Limited in Delhi, India.

2.3. Bacteriological Analysis

Membrane filtration was done according to American Public Health Association [10]. Appropriate dilutions of the water samples were done using distilled water. 100ml of the sample or its dilution was aseptically filtered through a membrane filter (47mm diameter, 0.45µm pore size) on a filtration unit. The filter was then taken off using a pair of sterilized forceps and placed on the surface of the corresponding culture media. Colony forming units (CFU) per 100 ml of the sample or its dilution were calculated as described in the United States Department of Agriculture, Food Safety and Inspection Services manual [11]. Filters were placed on Chromocult agar (merck) plates (manufactured by Henan Boom Gelatin Co., Ltd, Henan, China) and incubated at 37^0C for 18-24 hours. Typical colonies appearing blue were counted as *E.coli* and expressed as CFU's /100ml.

2.4. Statistical Analysis

All experiments were repeated three times and data was presented in tables and graphs. Statistical significance of each difference observed among the mean values was determined by standard error analysis. All mean data were statistically analyzed with a general linear model procedure of statistical analysis system. The Statistical analysis was done using the Statistical Package for Social Sciences (SPSS) software (Version 17.5). Pearson correlation analysis was carried out to determine the relationship between magnetic field intensity and bacterial count. One-way ANOVA with 95% confidence level was done to compare the effect of the magnetic field intensities with the bacterial count.

3. Results and Discussion

Different trends on the densities of *E. coli* at different levels of treatment were noted and results obtained indicated in Table 1 and Figure 3, Figure 4, Figure 5 and Figure 6. Presence of *E.coli* was characterized by development of blue colonies on the surface of the Chromocult culture medium. Figure 1 and Figure 2 (a, b, c, d) show *E.coli* density without B-field exposure (control), under a B-field exposure of 2mT, of 6 mT and of 10 mT for 6 and 18 hours respectively.

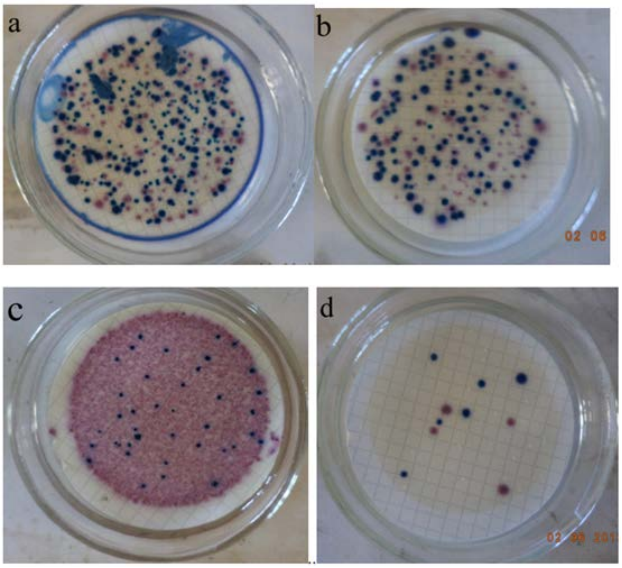

Figure 1. Shows plates a, b, c, d with *E.coli* Densities (blue colonies) after 6 Hours of Exposure: a) Without Magnetic Field; b) Magnetic Field of 2mT; c) Magnetic Field of 6 mT; d) Magnetic Field of 10 mT.

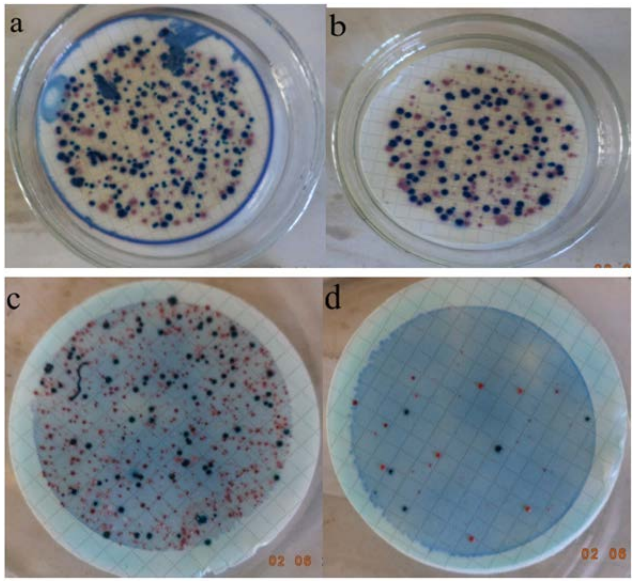

Figure 2. Shows plates a, b, c, d with *E.coli* Densities (blue colonies) after 18 Hours of Exposure: a) Without Magnetic Field; b) Magnetic Field of 2mT; c) Magnetic Field of 6 mT; d) Magnetic Field of 10 mT

It was observed that the control recorded the highest number of CFUs for both 6 and 18hours. Increasing the magnitude of magnetic field led to a significant decrease in the numbers of *E. coli* with the least number of CFUs given by the highest magnetic flux density. MFD was able to decrease *E. coli* concentration in River Njoro water significantly and hence proved to be a possible small scale cost-effective method of disinfecting water for domestic consumption and reducing incidences of waterborne diseases. More time of exposure to radiation for disinfection was required for low magnetic fields. This is similar to [12] who studied the effect of pulsed magnetic field intensity on bactericidal property in sterilization fresh watermelon juice and showed that the overall bactericidal effect was strengthened as the magnetic field intensity increased.

Table 1. Effect of Different Magnetic Flux Densities on *E. coli* Numbers (CFU/100ml) after 6Hrs and 18Hrs of Exposure (average ± standard deviation)

Time of exposure	MFD	Mean± Std. Dev
6hrs	control	687.5± 172.31
	2 mT	337.5± 95.35
	6mT	237.5± 102.1
	10 mT	122.5± 42.72
18hrs	control	680±176.3
	2 mT	542.5± 153.3
	6mT	225±68.56
	10 mT	125±51.96

Results in Table 1 showed that, the highest means of *E. coli* were recorded with the control. The *E. coli* numbers decreased proportionally with the increase in the magnetic intensity. The least magnetic intensity of 2mT at 6hrs gave a mean number of 337.5 CFU/100ml but after 18hrs the number increased to 542.5 CFU/100ml. The magnetic intensity of 6mT had more inhibitory effects on *E. coli* at both 6hrs and 18hrs of magnetic treatment, where bacteria counts were 225 CFU/100ml and 237.5 CFU/100ml respectively. This study showed that the highest magnetic intensity of 10mT gave the least mean numbers of *E. coli* as122.5 CFU/100ml and 125CFU/100ml after 6hrs and 18hrs of exposure respectively.

The acceptable level of *E.coli* in any drinking water is 0 – 100 CFU /100 ml (WHO, 2006). In this study, the highest MFD gave a disinfection level of 122.5 CFU/ 100ml of water which is very close to the WHO maximum acceptable contamination level of *E. coli* in drinking water. Looking at the trend of the results obtained in this study, this level could be reached by increasing the strength of MFD slightly since as the MFD is increased the number of CFUs are decreased significantly.

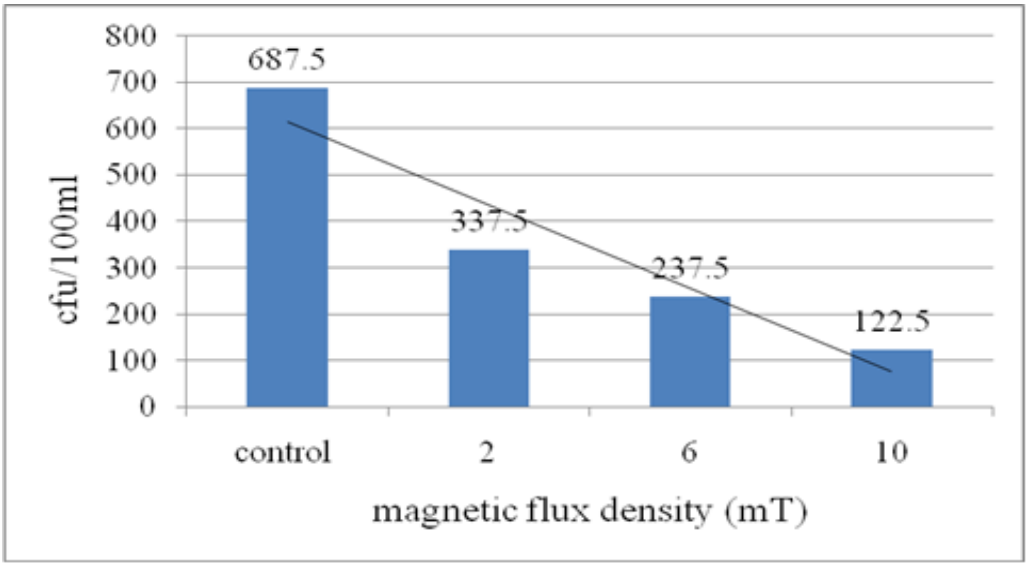

Figure 3. Mean Densities of *E. coli* (cfu/100ml) Due to Different Strengths of MFD after 6 Hours of Exposure

Figure 3 and Figure 4 show a strong inverse relationship between magnetic flux density and mean numbers of *E.coli*. It is clear that with increasing strength of magnetic field, the mean numbers of *E.coli* decreased significantly. The application of electromagnetic pulses evidently causes a lethal effect on *E. coli* cells [13].

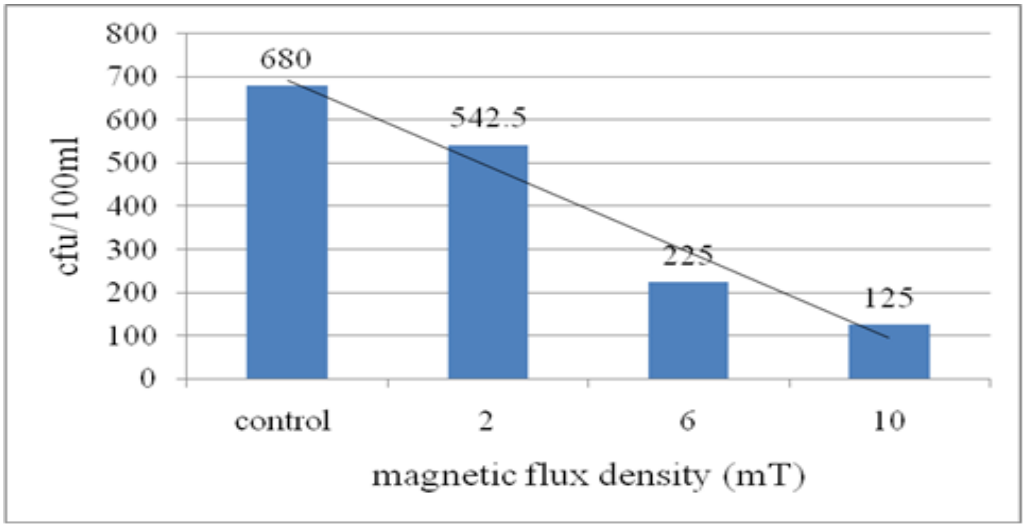

Figure 4. Mean Densities of *E.coli* (cfu/100ml) Due to Different Strengths of MFD after 18 Hours of Exposure

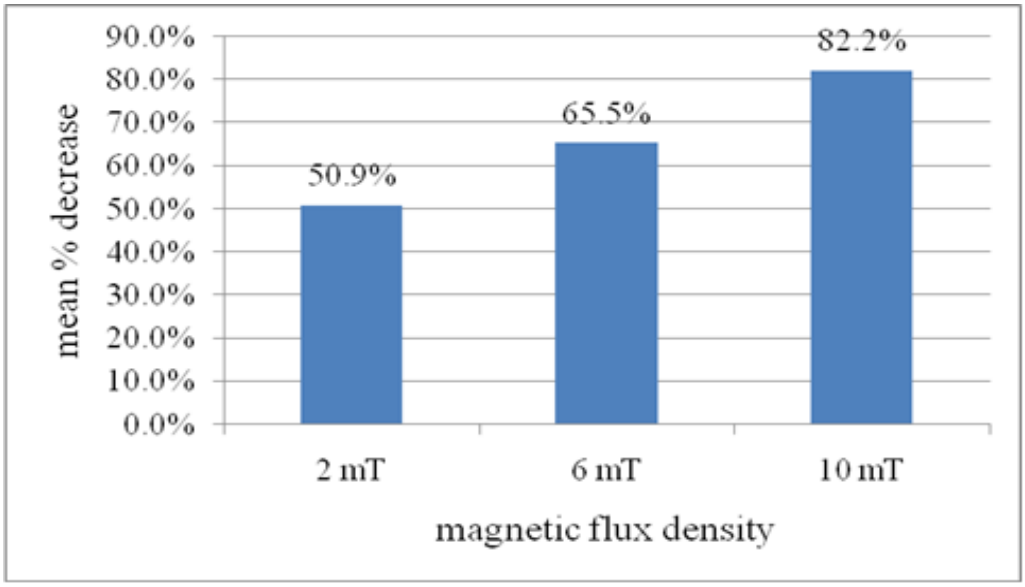

Figure 5. Percentage Decrease in the Mean Number of *E.coli* in Water after 6 Hours of Exposure to Different Intensities of MFD (2mT, 6mT and 10mT)

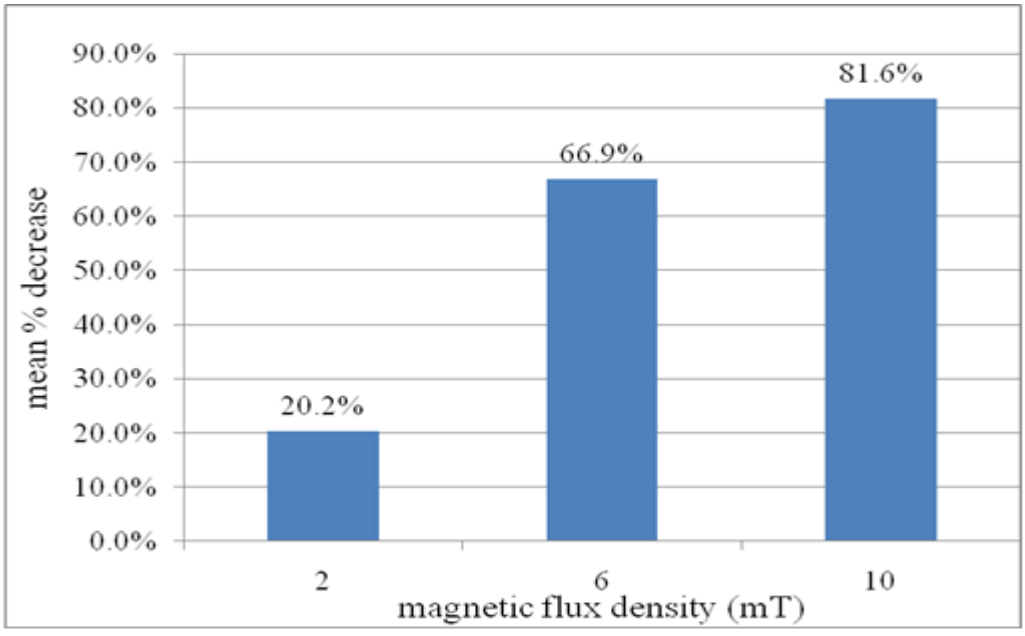

Figure 6. Percentage Decrease in the Mean Number of *E.coli* in Water after 18 Hours of Exposure to Different Intensities of MFD (2mT, 6mT and 10mT)

This study indicates that treatment of water with constant magnetic fields always gives rise to a disinfection effect. The magnitude of this effect depends on the strength of magnetic flux density used as well as the time of exposure. Fields of 2mT, 6mT and 10mT caused percentage decrease of 50.9, 65.5 and 82.2 respectively in the number of *E.coli* as compared to the control after 6 hours of exposure (Figure 5) and a percentage decrease of 20.2, 66.9 and 81.6 respectively after 18 hours of exposure (Figure 6).

The maximum disinfection level for *E.coli* attained in this study was 82.2% with increasing strength of the magnetic flux and period of exposure. This could possibly imply that with a slight increase in both the MFD and time of exposure, the disinfection level could get to at least 99%. The main damaging role of the magnetic fields might be on the cellular membrane that strongly affects, not only the cellular physiological functions, but also the cell-to-cell communications of the bacteria [14].

Table 2. Correlation between MFD (mT) and Mean Number of *E.coli* (cfu/100ml) after 6 Hours of Exposure

		MFD	MEAN
MFD	Pearson Correlation	1	-.999(*)
	Sig. (2-tailed)	.	.026
	N	3	3
MEAN	Pearson Correlation	-.999(*)	1
	Sig. (2-tailed)	.026	.
	N	3	3

* Correlation is significant at the 0.05 level (2-tailed).

Table 3. Correlation between MFD (mT) and Mean Number of *E.coli* (cfu/100ml) after 18 Hours of Exposure

		MFD	MEAN
MFD	Pearson Correlation	1	-.976(*)
	Sig. (2-tailed)	.	.024
	N	4	4
MEAN	Pearson Correlation	-.976(*)	1
	Sig. (2-tailed)	.024	.
	N	4	4

* Correlation is significant at the 0.05 level (2-tailed).

An inhibitory effect of EMF on the growth of *E.coli* may be due to the interaction between electric charges induced by EMF and that of the cytoplasm membrane resulting in partial abolishment of electric potential of the cytoplasm membrane with a subsequent decrease in the macromolecular biosynthesis. Also EMF may cause damage of bacterial DNA and inhibition of its replication. The cellular membrane of the microorganism could also have been affected by the external magnetic field, resulting to a disturbance in their metabolic activity and, consequently, a change in their cell division. Correlation analysis demonstrated that MFD was negatively significantly correlated with mean number of CFU ($r = -.999$, $p<0.05$) and ($r = -976$, $p<0.05$) for 6hours and 18hours of exposure respectively as shown in Table 2 and Table 3.

4. Conclusion

The findings of this study have met the initial aim of this research which was to investigate the effect of magnetic field on the concentration of *E.coli* in River Njoro water. The ANOVA significance test ($p < 0.05$) showed that magnetic field has a significant effect on the microbiological aspect of river Njoro water. The maximum disinfection efficiency was recorded as 82.2% for *E.coli* exposed to 10mT magnetic flux density for a period of 6 hours. This proves to be a promising method of disinfecting water.

Arising from the findings of this study, we propose that further research on the following areas concerns need to be done:

- A study to show how long the inhibitory effects of magnetic field lasts in the treated water after withdrawing the field;
- A study to show effect of magnetic field treatment on other strains of bacteria.

References

[1] World Water Assessment Program, "Kenya National Water Development Report. Case study", UNESCO VOL.12, pp 1-244, 2006.

[2] Kiruki, S, Mageto, OK, Ncene, WB and Gikuru, SK. "Prevalence of multidrug resistant enteropathogenic bacteria causing diarrhea in Kibera community in Nairobi, Kenya", Journal of Tropical Microbiology and Biotechnology, VOL 2: 24-30, 2006.

[3] World Health Organization. *The World Health Report*. World health Organization, 2012.

[4] World Health Organization. *The World Health Statistics*. World health Organization, 2011.

[5] Abel, PD. *Water Pollution Biology*. Taylor and Francis, pp.179-184, 2002.

[6] Vesilind PA, Peirce, JJ and Weiner, RF. *Environmental Pollution and Control*. 3rd ed. Butter WorthHeinmann, Bosten, pp. 77-83, 1990.

[7] United States Environmental Protection Agency, Current Drinking Water Standards. United States Environmental Protection Agency: Washington, DC, May, 2016.

[8] Rubenowitz-Lundin, E and Hiscock, K. *Water hardness and health effects*. Essential of Medical Geology, Elsevier Academic Press, pp. 331-345, 2005.

[9] Jenkins, MW and Lelo, FK and Chiuri, W and Shivoga, WA and Miller, SN, "World Water and Environmental Resources Congress: Community Perceptions and Priorities for Managing Water and Environmental Resources in the River Njoro Watershed in Kenya", Environmental Resources Congress, Salt Lake City, Utah, June 27-July 1, 2004.

[10] America Public Health Association. *Standard Methods for the Examination of water and Wastewater*. American Public Health Association/American Water Works Association/Food safety and Inspection Services: Washington, DC, 2008.

[11] United States Department of Agriculture Food Safety and Inspection Service. Most probable number procedures and tables: Laboratory Guide Book. pp. 5-8, United States Department of Agriculture Food Safety and Inspection Service, Washington, June 2014.

[12] Ma, H, Zhongli, P, Mengxiang, G and Lin, L. "Efficacy in Microbial Sterilization of Pulsed Magnetic Field Treatment" International Journal of Food Engineering, Berkeley Electronic Press, Vol. 4 2008.

[13] Li, M, Qu, J and Peng, Y. "Sterilization of Escherichia coli cells by the application of pulsed magnetic field". Journal of Environmental Science, VOL 16, pp. 348-352, 2004.

[14] Molouk, MKA and Amna, ANS. "The effect of magnetic field on the physical, chemical and microbiological properties of the lake water in Saudi Arabia". .Journal of Evolutionary Biology Research, VOL **2**, pp. 7-14, 2010.

[15] Johan, S, Fadil, O and Zularisham, A. Effect of Magnetic Fields on Suspended Particles in Sewage. Malaysian Journal of Science, 23: 141-148, 2004.

[16] Maheshwari, BL and Grewal, HS. Magnetic treatment of irrigation water: its effects on vegetable crop yield and water productivity. Agriculture and Water Management, 96: 1229-1236, 2009.

[17] Tomska, A, Wolny, L. Enhancement of biological wastewater treatment by magnetic field exposure. Desalination 222, 368-373, 2007.

[18] Smothers KW, Curtiss CD, Gard BT, Strauss RH and Hock VF. Magnetic Water Treatment Public Works Technical Bulletin, 420:34-449, 2001.

International Journal of Physics, 2016, Vol. 4, No. 5, 119-122
Available online at http://pubs.sciepub.com/ijp/4/5/1

DOI:10.12691/ijp-4-5-1

Measurement of Radon Gas Concentration in Tap Water Samples in Wassit Governorate by Using Nuclear Track Detector (CR-39)

Laith Ahmed Najam[1,*], Mahmood Salim Karim[2], Taghreed Khalid Hameed[2]

[1]Department of Physics, College of Science, University of Mosul, Mosul, Iraq
[2]Department of Physics, College of Education, Al-Mustansiriyah University, Baghdad, Iraq
*Corresponding author: prof.lai2014@gmail.com

Abstract In the present work, we have measured the radon gas concentration in environmental water sample of selected regions in Wassit governorate by using alpha-emitters registrations which are emitted from radon gas in (CR-39) nuclear track detector. The results of measurements indicate that the highest average radon gas concentrations in tap water samples were found in Nuamaniya region, which was equal to (0.820±0.04 Bq/L), while the lowest average radon gas concentration was found in Jassan region, which was equal to (0.325±0.02 Bq/L), with an average value of (0.563±0.12Bq/L). The highest value of annual effective dose (AED) in tap water samples was found in Nuamaniya region, which was equal to (0.08 μSv/y), while the lowest value of annual effective dose (AED) was found in Jassan region, which was equal to (0.03μSv /y), with an average value of (0.05±0.01 μSv/y), the tap water in Wassit governorate is safe as far as radon concentration is concerned.

Keywords: *water sample, tap water, radon concentration, CR-39 detector*

Cite This Article: Laith Ahmed Najam, Mahmood Salim Karim, and Taghreed Khalid Hameed, "Measurement of Radon Gas Concentration in Tap Water Samples in Wassit Governorate by Using Nuclear Track Detector (CR-39)." *International Journal of Physics*, vol. 4, no. 5 (2016): 119-122. doi: 10.12691/ijp-4-5-1.

1. Introduction

Radon (^{222}Rn) is a radioactive gas with a half- life of about (3.825 day) and decay constant of about (0.1812 day^{-1}). It is produced by the decay of naturally occurring radionuclide (radium) (^{226}Ra), which is in turn a decay product in the (^{238}U) series [1].

Thoron gas (^{220}Rn), which is a decay product in the (^{232}Th) series. The half- life is about (55.6 s) which is much shorter than that of radon. Because of such a short half-life of ^{220}Rn, its emanation from building materials such as (soil, brick, gravel,sand, etc…) as well as, its infiltration from the ground. Among the other radon isotopes, is the actinon (^{219}Rn) which is part of the (^{235}U) series, which does not contribute significantly to human radiation exposures due to both low natural abundance of the (^{235}U) precursor and of its very short half-life of about (3.96 s). [2].

Radon gas can enter the dwellings through water systems. In big cities, in many areas, ground water is used as the main water supply for homes and communities. Small public water works and private domestic wells often have closed systems and short transit times that do not remove radon from the water or permit it to decay. This radon escapes from the water to the indoor air as people take showers, wash clothes or dishes, or otherwise use of water [3].

2. Experimental Setup

A- Description of Study Area

Wassit city is located in eastern Iraq, on the border with Iran. Wassit shares internal boundaries with the city of Diyala, Babil, Baghdad, Thi-Qar, Qadissiya and Missan as shown in Figure 1. Wassit is intersected by the Tigris River, along which a ribbon of irrigated farmland runs, giving way to a dry desert landscape to the northeast. Wassit has a dry, desert climate, with temperatures easily exceeding 40°C in summer. Rainfall is scarce and concentrated in the winter months [4].

B- The Detector

The CR-39 plastic detector used in the present study is sensitive to alpha particles of energy up to 40 MeV. It was used as integrating detector of α-particles from ^{222}Rn and daughters nuclei.

When an α-particle penetrates the detector, the particle causes damage along its path, the damage is then made visible by chemical etching. The etching produces a hole in the detector along the path of the particle. The hole can be easily observed in a light transmission microscope with moderate magnification [5].

C- The Exposure

The samples of water were collected (1/4 litter) volume of samples of tap water were also collected from the same sites in Wassit governorate. The tap water obtained from the water networks in sites houses and the detector area (1×1 cm^2) as shown in Figure 2.

Figure 1. Map showing locations of the studied sites in Wassit city

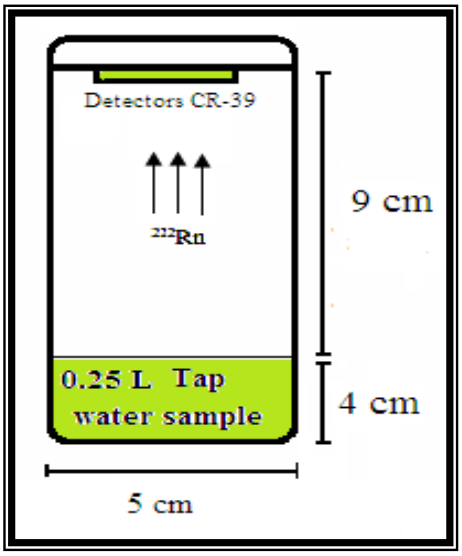

Figure 2. Sealed-cup technique in water sample

After one month of exposure the detectors were etched chemically in NaOH solution for 6.25 N at temperature 60°C for 6 hours, then with distilled water and finally with a 50% water/alcohol solution. After a few minutes of drying in the air, the detector was ready for track counting. The tracks were counted using an optical microscope having a magnification of 400X.

3. Radon Concentration Measurement

The radon gas concentration in the tap water samples was obtained by using the relation [6]:

$$\text{Tracks density}\,(\rho) = \frac{\text{Average number of total pits (track)}}{\text{Area of field view}}. \quad (1)$$

The standard water sample which was as shown in fig. (3), using the relation [7]:

$$C_X = \rho_X (C_S / \rho_S) \quad (2)$$

Where:
C_X : alpha particles concentration in the unknown sample.
C_S : alpha particles concentration in the standard sample.
ρ_X : track density of the unknown sample (track/mm^2).
ρ_S : track density of the standard sample (track/mm^2).

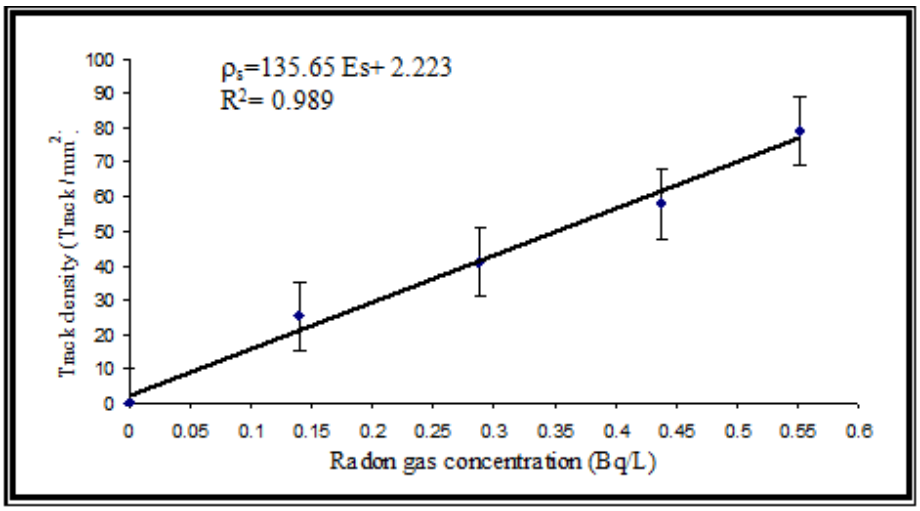

Figure 3. the relation between (C_{Rn}) and track density in water standard samples

3.1. The Annual Effective dose in Water

The annual effective dose of an individual consumer due to intake of radon from tap water is evaluated using the relationship [8]

$$AED_w = C_w C_{Rw} D_{cw} \quad (3)$$

Where AED_w is the annual effective dose (Sv/y) due to ingestion of radionuclide from the consumption of water.
C_w is the concentration of radon in the ingested tap water (Bq/L).
C_{Rw} is the annual intake of tap water (L/y)
D_{cw} is the ingested dose conversion factor for radon (Sv/Bq). As an example:

$$C_w = 19.5\ \text{Bq/L}, C_{Rw} = 730\ \text{L/y}, D_{cw} = 5\times10^{-9}\ \text{Sv/Bq}.$$

3.2. Radon Exhalation Rate (RER)

The radon exhalation rate (RER) in units $Bq.m^{-2}.h^{-1}$ can be calculated by [9]:

$$RER = \frac{CV\lambda}{A[T + \lambda^{-1}(e^{-\lambda T} - 1)]} \quad (4)$$

Where:
C: is the integrated Radon exposure($Bq.m^{-3}$).
V: is the volume of air in the cup (m^3)
λ :is the decay constant for ^{222}Rn (h^{-1}) = 0.1812 day^{-1} =0.00755 h^{-1}
A: is the surface area of the sample (m^2)
T: is the exposure time (h) = 30 day =720 h

3.3. Calculation of Dissolved Radon Concentration

The dissolved radon concentration tap water in terms of (Bq/L) units was obtained using the relation [10].

$$C_d(\text{Bq/L}) = C_w \lambda h T / L \quad (5)$$

Where:
C_w = the integrated radon exposure ($Bq.L^{-1}$)
λ = Decay constant for ^{222}Rn (h^{-1}) = 0.1812 day^{-1} = 0.00755 h^{-1}
h = the distance from the surface of water to detector (m) = 0.09 m
T = the exposure time (h) =30 day = 720 h
L = the depth of the sample (m) = 0.04m.

4. Results and Discussion

This study was to measure the radon concentration (C_{Rn}) in water sampling, the water samples were taken directly from tap water (tap water) in sites houses was carried 10 samples in Wassit governorate by using the sealed-cup technique.

Table 1 present C_{Rn} the water samples from different regions in Wassit governorate. It can be noticed that, the highest average C_{Rn} in tap water samples was found in Nuamaniya region which was equal to (0.820±0.04 Bq/L), while the lowest average C_{Rn} was found in Jassan region which was equal to (0.325±0.02 Bq/L), as shown in Figure 4, with an average value of (0.563±0.12 Bq/L). The highest value of (AED) in tap water samples was found in Nuamaniya which was equal to (0.08 μSv/y), while the lowest value of (AED) was found in Jassan region which was equal to (0.03 μSv/y), with an average value of (0.05±0.01 μSv/y), the highest value of (RER) in tap water samples was found in Nuamaniya region which was equal to (0.95 μBq/m^2h), while the lowest (RER) in tap water samples was found in Jassan which was equal to (0.38 μBq/m^2h), with an average value of (0.65 ±0.14 μBq/m^2h), the highest value of (C_d) in tap water was found in Nuamaniya region which was equal to (10.03 Bq/L), while the lowest (C_d) in tap water samples was found in Jassan which was equal to (3.98 Bq/L), with an average value of (6.89±1.4 Bq/L). The present results in Wassit governorate show that the radon gas concentration in tap water samples is below the allowed limit from (EPA, 2000) which was equal to (11 Bq/L) [11], while the (AED) in all samples study is below the normal limits of world which was equal to (1 mSv/y) [12], therefore the tap water in Wassit governorate is safe as far as radon concentration is concerned.

Table 1. Regions studied, radon gas concentration C_{Rn} ($Bq.L^{-1}$), annual effective dose (AED), radon exhalation rate (RER), radon concentration dissolved in water (C_d), for tap water samples in Wassit governorate

Regions Studied	C_{Rn} ($Bq.L^{-1}$)				Mean of C_{Rn} ($Bq.L^{-1}$)	(AED) (μSv/y)	(RER) (μBq/m^2h)	Cd ($Bq.L^{-1}$)
	1	2	3	4				
Kut	0.43	0.48	0.39	0.36	0.415±0.04	0.04	0.48	5.08
Al-Hai	0.42	0.44	0.38	0.47	0.427±0.03	0.04	0.49	5.23
Badra	0.65	0.72	0.66	0.69	0.680±0.03	0.07	0.79	8.32
Jassan	0.34	0.33	0.28	0.35	0.325±0.02	0.03	0.38	3.98
Sheek Saad	0.53	0.51	0.55	0.47	0.515±0.03	0.05	0.6	6.30
Zorbatya	0.66	0.57	0.63	0.59	0.612±0.03	0.06	0.71	7.49
Al-Suwira	0.75	0.68	0.77	0.73	0.732±0.03	0.07	0.85	8.96
Al-Azezia	0.47	0.52	0.55	0.57	0.527±0.03	0.05	0.61	6.45
Nuamaniya	0.87	0.77	0.79	0.85	0.820±0.04	0.08	0.95	10.03
Al-Wahda	0.54	0.63	0.58	0.57	0.580±0.03	0.06	0.67	7.09
	Average				**0.563±0.12**	**0.05±0.01**	**0.65 ±0.14**	**6.89±1.4**

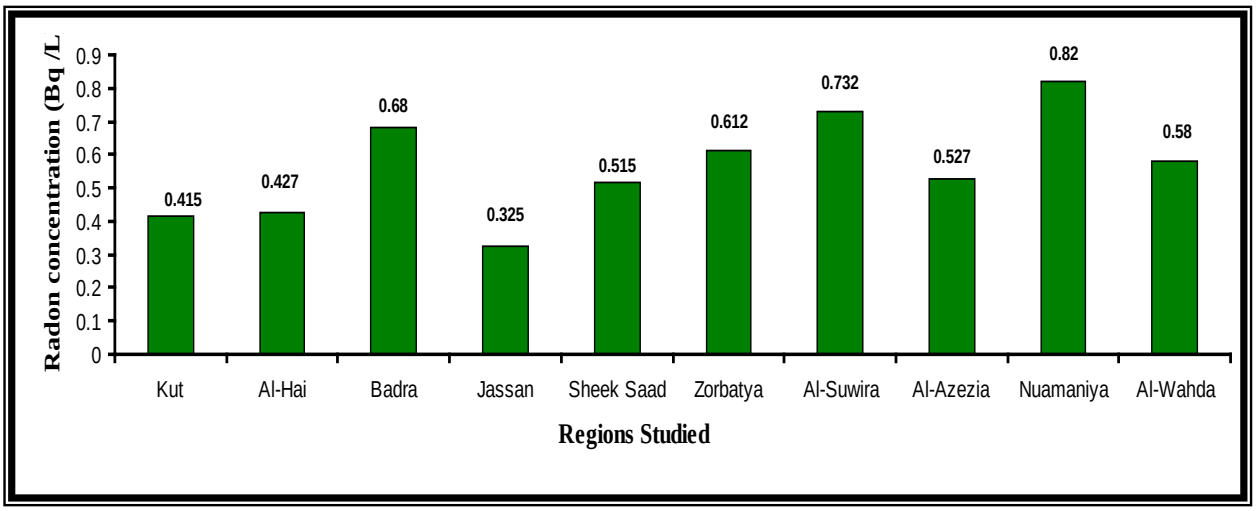

Figure 4. Histogram illustrating the change in (C_{Rn}) in tap water samples in all regions studied in Wassit governorate

5. Conclusions

The tap water samples in all regions in Wassit governorate is lower than the recommended value of (11 Bq/L) reported by the (EPA), so that the tap water was safe for consumption and does not constitute a danger or hazard to the citizens

References

[1] NRC, "Health Effects of Exposure to Radon", National research council, biological effects of ionizing radiation (BEIR), VI Report, (1999).

[2] Harb S., El-Kamel A. H., Zahran A. M., Abbady A., and Ahmed F.A. "Assessment of natural radioactivity in soil and water samples from Aden governorate south of Yemen region" International Journal of recent research in Physics and Chemical Sciences, 1, pp.1-7, (2014).

[3] Shashikumar. T.S, Chandrashekara. M.S, Paramesh. L. "Studies on Radon in soil gas and Natural radionuclides in soil, rock and ground water samples around Mysore city" International Journal of Environmental Sciences, 1,No.5, pp.787-797, (2011).

[4] Gazprom Neft produces first oil at Badra oilfield, Iraq (09/01/2014), http://www.gazprom-neft.com/press-center/news/1096837.

[5] Khan AJ, Varshney AK, Prasad R, Tyagi RK, Ramachandran T.V. "Calibration of a CR-39 plastic track detector for the measurement of radon and its daughters in dwellings" Nucl Tracks Radiat Meas, 17, pp.497-502, (1990).

[6] Amalds O., Custball N.H. & Nielsen G.A. "Cs^{137} in Montarq Soils", Health Physics, 57 No.6, pp. 955-958, (1989).

[7] Durrani S.A. and Bull R.K., "Solid State Nuclear Track Detection: Principles, Methods and Applications", Pergammon Press, U.K., (1987).

[8] Alam M. N., Chowdhry M. I., Kamal M., Ghose S., Islam M. N. & Awaruddin M., "Radiological assessment of tap water of the Chittagong region of Bangladesh", Radiat. Prot. Dosim., 82, pp.207–214, (1999).

[9] Ferreira A.O., Pecequilo B.R. and Aquino R.R., "Application of a Sealed Can Technique and CR-39 detectors for measuring radon emanation from undamaged granitic ornamental building materials", Radioprotection Journal, 46, No.6, pp.49-54, (2011).

[10] Kant K., Upadhyay S.B. and Chakarvarti S.K. "Alpha activity in Indian thermal springs" Iran. J. Radiat. Res. 2, No. 4, pp.197-204, (2005).

[11] Najem H, AL-Khalifa I.J and Salman H.B, " Determination of radon concentration in soil of Basrah governorate by using solid state nuclear track detectors " Basrah Science Journal, 26, No.1, pp.38-48, (2012).

[12] Environmental Protection Agency (EPA) regulations, Final Rule for Non-Radon Radionuclides in Tap Water, Technical Fact Sheet, EPA, 815-F-00-013, (2000).

International Journal of Physics, 2016, Vol. 4, No. 5, 123-129
Available online at http://pubs.sciepub.com/ijp/4/5/2

DOI:10.12691/ijp-4-5-2

A New Equivalent Theory with Special Relativity Theory, Particle Wave in 5-dimensional Space-time

Xiao Lin Li*

Chongqing, China
*Corresponding author: hidebrain@hotmail.com

Abstract There exist a new physics model. Real physical world is 5-dimensional space-time. Human world is 4-dimensional space-time. Human world just is the projection of real physics world. Particle wave is present in 5-dimensional space-time. So we can derive out Mass-energy equation. So we can derive out all results of Special Relativity Theory. In 5-dimensional space-time, speed of all particles is the light speed c. It is reason that the light speed c is very special. Coordinates transformation in 5-dimensional space-time, can derive out Lorentz transformation. The new physics model theory is a equivalent theory with Special Relativity Theory. In 5-dimensional space-time, there only exist space expansion or space contraction. In 5-dimensional space-time, there not exist time expansion or time contraction, time is absolute. In 5-dimensional space-time, particle rest mass only is particle movement portions at 4th dimensional space. The new 5-dimensional space-time theory, is consistent with space-time system of Special Relativity Theory, and it can transition to space-time system in Lorentz symmetry breaking smoonthly. The new 5-dimensional space-time theory has more wide range adaptation than Special Relativity Theory.

Keywords: *de Broglie wave, particle wave, Special Relativity Theory, mass-energy equation, 5th dimension, 4th dimensional space, 5-dimensional space-time, the Light speed, Particularity of the light speed, The source of particle rest mass, Lorentz symmetry, coordinates transformation, Lorentz transformation, Lorentz symmetry breaking, equivalent theory with Special Relativity Theory*

Cite This Article: Xiao Lin Li, "A New Equivalent Theory with Special Relativity Theory, Particle Wave in 5-dimensional Space-time." *International Journal of Physics*, vol. 4, no. 5 (2016): 123-129. doi: 10.12691/ijp-4-5-2.

1. Introduction

We know. There exist de Broglie wave,or particle wave,in Quantum Mechanics. To particle wave,there exist two formula, de Broglie formula.

$$E = h\nu$$

$$P = \frac{h}{\lambda}$$

The particle wave concept, is a basic concept in Quantum Mechanics. The de Broglie formula is a basic principle in Quantum Mechanics. De Broglie formula can not be derive out from Quantum Mechanics. De Broglie formula can not be derive out from Special Relativity Theory also. It is a independent and basic principle in current physics theory. It is correct or wrong, only the physical experiment can do the judgement.

In physical history, many scientists, include de Broglie, want to find the relationship between de Broglie formula and Special Relativity Theory. But not success.

We know. Special Relativity Theory is rely on light speed c strictly. In Special Relativity Theory, space and time is symmetry strictly. Once the light speed c is not invariant, Special Relativity Theory will be no longer valid. In Quantum Field Mechanics, many scientists take out the possibility of Lorentz symmetry breaking. So, once the Lorentz symmetry breaking evidence has been found by experiment, Special Relativity Theory will be incorrect, so space and time is not symmetry again, new space-time theory will be necessary. So we need to try to study any new model about space-time.

After continuous exploration, author find a very interesting result. If we extend the particle wave and the de Broglie formula to 5-dimensional space-time, we can simply derive out all results of Special Relativity Theory. Author have found the relationship between de Broglie wave and Special Relativity Theory successfully. By this way, author put forward a new 5-dimensional space-time theory. The new theory is a equivalent theory with Special Relativity Theory.

At next chapter, author will explain this new theory in detail.

2. Derive out Energy-mass Equation from de Broglie Formula

In the quantum mechanics, the particle wave group velocity V_g is equal with particle velocity V. That is V_g =V.

The phase velocity $V_p = \frac{c^2}{V}$

So we obtain, $V_g V_p = V \cdot \frac{c^2}{V} = c^2$

So we obtain a equation,

$$V_g V_p = c^2. \quad (2.1)$$

The equation (2.1) is derived. But we think from the other side. We suppose this equation is exist at first, not be derived out. The physics source will be explained at the next chapter. Start from this equation, do some logical reasoning, we can obtain very meaningful results.

From de.Broglie equation, we obtain a equation,

$$V_g = \frac{d\varpi}{d\kappa} = \frac{d(\hbar\varpi)}{d(\hbar\kappa)} = \frac{dE}{dP} \quad (2.2)$$

Please pay attention to the equation, $V_g = \frac{dE}{dP}$.

From de.Broglie equation, we can derive out, the phase velocity,

$$V_p = \lambda\nu = \frac{h}{P}\frac{E}{h} = \frac{E}{P}. \quad (2.3)$$

Take (2.3) and (2.2) into (2.1),we obtain,

$$V_g V_p = \frac{E}{P}\frac{dE}{dP} = \frac{dE^2}{dP^2} = c^2$$

So we obtain a equation,

$$\frac{dE^2}{dP^2} = c^2 \quad (2.4)$$

So we obtain, $dE^2 = dP^2 \cdot c^2$.

So, we obtain,

$$E^2 = P^2c^2 + cons\tan t \quad (2.5)$$

This equation is so familiar. It's more like energy-momentum equation in Special Relativity Theory. The constant is wait solving. Now we start to solve the constant value.

The group velocity V_g is equal with particle velocity V. That is V_g =V.

Exist equation,

$$\mathrm{P} = \mathrm{mV}. \quad (2.6)$$

So,

$$\mathrm{V} = V_g = \mathrm{P}/\mathrm{m}. \quad (2.7)$$

Take (2.3) and (2.7) into (2.1), get,

$$V_g V_p = \frac{E}{P}\cdot\frac{P}{m} = \frac{E}{m} = c^2$$

So obtain,

$$E = mc^2. \quad (2.8)$$

Equation (2.8) is the energy-mass equation in Special Relativity Theory.

Take (2.8) into (2.5), obtain,

$$m^2c^4 = P^2c^2 + cons\tan t$$

So we can set the constant is value when P=0.

We set $m^2c^2 = m_o^2c^2$ when P=0.So,

$$E^2 = m^2c^4 = P^2c^2 + m_o^2c^4. \quad (2.9)$$

This is the energy-mass equation in Special Relativity Theory.

Derive out equation (2.9), so we can derive out all results in Special Relativity Theory. From equation (2.9), we can derive out this result that the light speed c is the maximum speed.

Summarize the reasoning steps above again. We suppose exist the equation $V_g V_p = c^2$ at first. Then we use de.Broglie formula. Then we obtain equation $\frac{dE^2}{dP^2} = c^2$. Then use the equation P=mV. So we can derive out equation (2.9), and can energy-mass equation.

We can discover, the equation, $V_g V_p = c^2$ ($\frac{dE^2}{dP^2} = c^2$), is so much important. But why it is exist? It will be explained at the next chapter.

In fact, the equation, P=mV. It's usage is that take mass concept into this theory. This mass is momentum mass. Momentum mass have another name, inertial mass. This mass is not gravitational mass.

From the reasoning steps above, we can see this. Before use equation P=mV, from (2.1) to (2.5), reasoning don't have relationship with mass concept.

Use equation (2.6), we take mass concept into this theory. Then we can derive out equation (2.9). (2.9) is the energy-mass equation.

Why V_g =V? In Classical mechanics, dP=Fdt, dE=Fds.So, dE/dP=Fds/Fdt=ds/dt=V. From de.Broglie equation, can obtain (2.2), Vg=dE/dP. So we obtain V_g =V.

Reasoning steps above seems only formal changes, it is not substantive changes. But, if our thinking is no longer been limited by Special Relativity Theory. Then we can get new thinking.

In fact, the $\frac{dE^2}{dP^2} = c^2$, only is a special case. The wide case is

$$\frac{dE^2}{dP^2} = f(P)c^2 \quad (2.10)$$

When f(P) =constant, we can get $\frac{dE^2}{dP^2} = c^2$, so we can derice out energy-mass equation, so we can derive out all results in Special Relativity Theory. This means that the new thinking theory is equivalent with Special Relativity Theory.

If we change f(P). f(P) is other form. This will lead to many Lorentz-Violating Extension case. To f(P),there exist many other form. The (2.10) formula is a theory pattern. We can consider that Special Relativity Theory is one type of this pattern. About this theory pattern, it is a topic worthy of further study.

3. New Physics Model, Particle Wave in 5-dimensional Space-time

In above chapter, this equation, $V_g V_p = c^2$, is a hypothesis. So, what is its physical meaning? Thoughts two years, author finally found its physics significance. This equation's physical model, will bring a new view of physics.

This equation means that the particle wave is present in 5-dimensional space-time. The physical process of human perception, just is the spatio-temporal projection on the 4-dimensional space-time. Real physical process happen in 5-dimensional space-time.

The physical world of human perception, is in a 4-dimensional space-time. One dimension is time. Three dimension is space. Now we assume that a real physical world is in 5-dimensional space-time. There exist 5 dimensions. One dimension is time. Four dimension is space. Real physical world is in 4-dimensional space. Humans live in 3-dimensional space. The physical process of human perception, is only the projection on the 3-dimensional space.

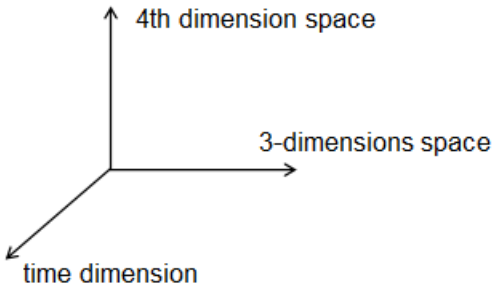

The new 4th dimension space, and 3-dimensional space, forming orthogonal relationships. Total of 4-dimensional space is a Hilbert space. This like 3-dimensional space also. The vector operations in 4-dimensional space, follow the standard vector arithmetic rules also.

Because there add a new dimension. And velocity and momentum is vectors, not scalars. In the new 4-dimensional space, particle movement and particle wave movement, has very different property, compare with movement property in 3-dimensional space.

However, mass, energy, wavelength, frequency. To these physical quantity, because it is a scalar, then there not have difference.

Now, we assume that, in new 4-dimensional,the wave particle duality still holds, De.Broglie equation still holds.

$$\begin{aligned} E &= h\nu \\ P &= \frac{h}{\lambda} \end{aligned} \tag{3.1}$$

Please notice that the frequency and wavelength, are in 4-dimensional space, not just in 3-dimensional space. Energy and momentum are in 4-dimensional space, not just in 3-dimensional space. The velocity of the particle, particle-wave phase velocity and group velocity, is a 4-dimensional vector, not a 3-dimensional vector.

To energy and frequency, in 4-dimensional space, and in 3-dimensional space, its value are same. Because it is a scalar.

To momentum and velocity, in 4-dimensional space, and in 3-dimensional space, it is not the same. Because it is a vector.

To wavelength, it is a length quantity, is closely related with dimensions. It is not a scalar or vector. In 4-dimensional space, and in 3-dimensional space, it is also not the same.

In the following statements, please reader distinguish each physical quantity carefully. It is in 4-dimensional space, or it is in 3-dimensional space.

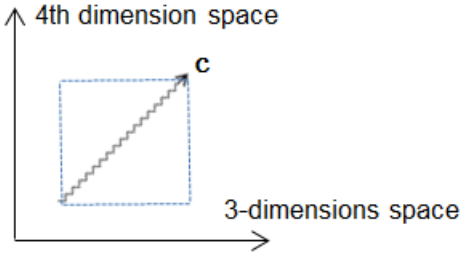

Now, we assume that, in the new 4-dimensional space, particle-wave phase velocity and the Group velocity is the same, and its numeric value is the speed of light c. And, in the new 4-dimensional space, all particles, all particle wave, movement speed is light speed c. In 4-dimensional space, there not exist static particle, and not exist static particle wave. As long as the particle exist, it is in movement at the speed of light c necessarily, inevitably accompanied by the particle-wave. And, in the new 4-dimensional space, the Group velocity of the particle-wave, and particle velocity of the particle-wave , have same value, V_g =V.

So, obtain,

$$\begin{aligned} V_g &= c. \\ V_p &= c \end{aligned} \tag{3.2}$$

So, we obtain this equation,

$$V_g V_p = c^2. \tag{3.3}$$

Please notice that distinction, the phase velocity and the Group velocity, is in new 4-dimensional space, is not only in 3-dimensional space.

We can see that, the vast majority of cases, to the Group velocity of the particle-wave, its projection speed in 3-dimensional space, is no more than a numerical vector which in the 4-dimensional space. So, in 3-dimensional space, particle velocity, which is the Group velocity of projection speed, do not exceed the speed of light c. Only in extreme cases, the particle velocity completely only have the component in 3-dimensional space. In the 4th dimension, its velocity component is zero. The projection speed in 3-dimensional space, is entirely the vector itself values. The particle speed is the speed of light c in 3-dimensional space. Photon are examples of this status.

Then, there exist another special case. Particle-wave group velocities, complete only have the component in 4th dimension. In 3-dimensional space, its projection components, completely to zero. This is a what? In fact, in this case, is the static object in 3-dimensional space.

In 3-dimensional space, the particle is static, not move, it was just an illusion. In new 4-dimensional space, the particle movement is at the speed of light c. Therefore, the particle has energy. Energy is a scalar, not a vector, its physical effects in each dimension will show effect. This is the physical source that particle have rest mass in the 3-dimensional space. But the particle velocity and momentum is a vector, orthogonal component is zero in 3-dimensional space, the projection is zero, so it will not show effects. This is a proper physical explanation about particle rest mass. Why particle-wave have frequency and wavelength when particle is static in 3-dimensional space? This is its physical explanation.

To phase velocity, because it involves the wavelength, than the Group velocity, is more complex. Obviously, lengths is closely associated with dimensions. The length in 4-dimensional space, the projection length in 3-dimensional space, they have what kind of relationship, it is not sure. Wavelength in 4-dimensional space, and projection of the wavelength in 3-dimensional space, is clearly not a simple vector orthogonal relationships. The relationships is not clear also. It is still a problem that requires careful study.

Exist a equation:

$$P = mV. \tag{3.4}$$

Its usage is that take mass concept into theory. This mass is momentum mass. Momentum mass have another name, inertial mass. This mass is not gravitational mass. But please notice that the momentum here, is the momentum in 4-dimensional space. Here the velocity V, is in 4-dimensional space also. But the mass quality is a scalar, so in 4-dimensional space, and in 3-dimensional space, is same, have same numeric value.

Because in 4-dimensional space, the particle speed V is the speed of light c. And V_g =V. So, (3.4) equation is equivalent to this:

$$P = mV = mc. \tag{3.5}$$

But it is correct only in 4-dimensional space. In 3-dimensional space, it is incorrect.

The momentum in 4-dimensional space, have an orthogonal component in 3-dimensional space. Mark the orthogonal component in 3-dimensional space with lowercase p. There exist p=mv. Here, p is the 3-dimensional momentum, v is a 3-dimensional velocity. m is a scalar.

In 4-dimensional space, from (3.1) and (3.2), can obtain:

$$V_p = \lambda\nu = \frac{h}{P}\frac{E}{h} = \frac{E}{P} = c.$$

And (3.5), so obtain:

$$E = Pc = mcc = mc^2. \tag{3.6}$$

We assume, in 5-dimensional space-time (4-dimensional space,1-dimensional time),have V=Vg also. So obtain,

$$V = V_g = c \tag{3.7}$$

To the momentum P in 4-dimensional space, have an orthogonal component in 3-dimensional space (mark with P1), and have an orthogonal component in new 4th dimension(mark with P2). There exist, $P^2 = P_1^2 + P_2^2$. And (3.6), so obtain:

$$P^2c^2 = P_1^2c^2 + P_2^2c^2 = E^2 = m^2c^4.$$

When particle is static in 3-dimensional space, P1=0, P=P2. Named this mass with rest mass. Mark this mass with m_0 .So obtain:

$$P_2c = m_0cc = E_0 = m_0c^2. \tag{3.8}$$

So obtain:

$$E^2 = m^2c^4 = p^2c^2 + m_0^2c^4. \tag{3.9}$$

Here, p=P1, is the momentum component in 3-dimensional space. Therefore, the energy-mass equation in Special Relativity Theory, is a simple result of this new physical view. In the new view, the result of energy-mass equation is very direct, not exist complex reasoning process in Special Relativity Theory.

Why the mass-energy equation shows a strict right angle triangle relationship, which is a very strange phenomenon. This is many people's doubts. On this issue, the new physical view, can give a very direct answer. Indeed, mass-energy equation, is a vector orthogonal relationship performance.

As can be seen, the momentum of the particle in the 4th dimension component values, is a variable that will always remain the same. This is the particle rest mass in 3-dimensional space. Why it is not chang? It need further study.

In 4-dimensional space, there is no static particle. But judging from the macroscopic physical, in 3-dimensional space, there exist static object. Why? It need further study.

From the above discussion, we can see that particle mass is a human artificial concept. Mass concept is taked into physics is by a equation, P=mV. Mass seems to not have real physical meaning. Energy, momentum, speed, frequency, wavelength, these concepts, have a real physical meaning. Therefore, the real physical meaning of mass quality, need further study.

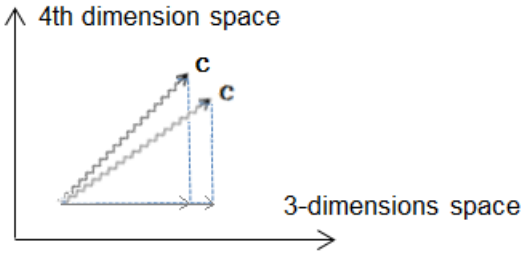

From the diagram above, we can see also, the energy-momentum of the particle increases, showed speed in 3-dimensional space projection component mounting. In 4-dimensional space, the real is the rotation of the particle velocity vector in the 4th dimension. Greater energy-momentum particle movement and 3-dimensional orthogonal angle is smaller, and the 4th dimension orthogonal angles greater. There only exist rotation of velocity vector. The value of velocity vector is invariant.

The photon is the most exceptional circumstances, only have motion components in 3-dimensional space completely, not have moving components in the 4th

dimension, so the photon rest mass is zero, so the photon speed is equal to the light speed c in 3-dimensional space.

In 5-dimensional space-time, all particles, including photons, its movement speed is the speed of light, is c. This is the essence of Lorentz symmetry. Photons are no longer in a special place in physics. Ignore particle charge, spin, etc property. Only study on kinematics, not inspect on kinetics, all particles is same. Particle rest mass in the 3-dimensional space is different, only because particle's moving components in the 4th dimension space is different. This means that, there exist a new particle symmetry in 5-dimensional space-time.

In this new model, the 1-dimensional time, and the 4-dimensional space, is not symmetry again. The time dimension will return back to absolute time dimension in Newtonian mechanics. The time dimension in every coordinates is synchronous. But, in this new model, the space dimensions, is not same with space dimension in Newtonian mechanics. In this new model, space dimensions will be expanding or contracted when coordinates transformation. This will be discussed in detail at next chapter.

This new physics model, have a equivalent relation with Special Relativity Theory. Coordinates transformation in Special Relativity Theory is a physics equivalent effect in the new 5-dimensional space time theory. This will be discussed in detail at next chapter.

4. Coordinates Transformation in 5-dimensional Space-time

In 5-dimensional space-time model, particle wave speed value is invariant. This speed value is light speed c always. So, coordinates transformation of different observer, is only a rotate transform of the velocity vector in 4-dimensional sapce. The value of velocity vector is invariant. The transformation effect is that change direction of motion. This effect is that rotate the velocity vector only, not change the value of velocity vector.

Imitate Special Relativity Theory, we take next derivation.

In A coordinates, particle coordinates values is x_1, x_2, x_3, and x_4. Start from coordinates origin.There exist this formula.

$$(x_1)^2+(x_2)^2+(x_3)^2+(x_4)^2=c^2t^2. \tag{4.1}$$

In B coordinates, particle coordinates values is $x_1^{'}$, $x_2^{'}$, $x_3^{'}$, and $x_4^{'}$. Start from coordinates origin also.There exist this formula.

$$(x_1^{'})^2+(x_2^{'})^2+(x_3^{'})^2+(x_4^{'})^2=c^2(t^{'})^2. \tag{4.2}$$

In two coordinates, the time dimension is absolute time. Two time value is equal. So exist.

$$t=t^{'}. \tag{4.3}$$

Imitate Special Relativity Theory, change style, can get two formula.

$$(x_1)^2+(x_2)^2+(x_3)^2+(x_4)^2-c^2t^2=0. \tag{4.4}$$

$$(x_1^{'})^2+(x_2^{'})^2+(x_3^{'})^2+(x_4^{'})^2-c^2(t^{'})^2=0. \tag{4.5}$$

So can get.

$$\begin{aligned}&(x_1)^2+(x_2)^2+(x_3)^2+(x_4)^2-c^2t^2\\&=(x_1^{'})^2+(x_2^{'})^2+(x_3^{'})^2+(x_4^{'})^2-c^2(t^{'})^2\end{aligned} \tag{4.6}$$

The (4.6) formula, is coordinates transformation formula in 5-dimensional space-time model.

Because the time dimension is absolute, its same in all coordinates, so exist (4.3) formula. So can simplify (4.6), get (4.7).

$$\begin{aligned}&(x_1)^2+(x_2)^2+(x_3)^2+(x_4)^2\\&=(x_1^{'})^2+(x_2^{'})^2+(x_3^{'})^2+(x_4^{'})^2\end{aligned} \tag{4.7}$$

(4.7) is a rotate transform of the velocity vector in 4-dimensional space. The value of velocity vector is invariant. The transformation effect is that change direction of motion. This effect is that rotate the velocity vector only, not change the value of velocity vector. This result is very obvious. In different coordinates, will observing space expansion or space contraction.

From (4.6), we can derive out coordinates transformation formula of Special Relativity Theory.

Formula (4.6) is coordinates transformation formula in 5-dimensional space-time. But human live in 4-dimensional space-time. Human only can sense the 3-dimensional space. Human can not sense the 4th dimension space. So, to human, in (4.6) formula, there don't exist x_4 and $x_4^{'}$. But human can't change the fact physics process. The (4.6) formula is the fact physics process. How to solve this problem? Key is the time dimension.

Human can't sense the 4th dimension space . So human consider that not exist x_4 and $x_4^{'}$. So human remove x_4 and $x_4^{'}$ from (4.6) formula. So human get (4.8) formula.

$$\begin{aligned}&(x_1)^2+(x_2)^2+(x_3)^2-c^2t^2\\&=(x_1^{'})^2+(x_2^{'})^2+(x_3^{'})^2-c^2(t^{'})^2.\end{aligned} \tag{4.8}$$

But in (4.8) formula, the time dimension, t and $t^{'}$, is not equal again.

(4.8) formula, is the coordinates transformation formula of Special Relativity Theory.

To human, the 4th dimension space expansion or contraction, is replaced by time dimension expansion or contraction. This is the mystery of Special Relativity Theory. Human observing time dimension expansion or contraction, this is only a observation effects. This is not the fact physics process. But human can't distinguish the difference between observation effects and fact physics process, because human can't sense the 4th dimension space. Human consider that time dimension expansion or contraction is fact physics truth. Human consider that space and time is symmetry.

So, from above description, we can get this derivation. The coordinates transformation in 5-dimensional space-time contains the coordinates transformation of Special Relativity Theory.

If there exist another intelligent biology in universe, which can sense the 4th dimension space. To this

intelligent biology, they observing physics process, they will take the (4.6) formula, not take the (4.8) formula.

This likes the observation question in quantum mechanics. Human observing physics process, is equal to the fact physics process? To space-time, human observing space-time, is equal to the fact physics space-time? Human observing results, 100% is equal to fact physics process?

Human can't distinguish the difference between Special Relativity Theory and 5-dimensional space-time theory. So, to physics, what significance can take out by the new 5-dimensional space-time model? The new 5-dimensional space-time model is only a duplicate theory with Special Relativity Theory? No. the significance taked out by the new 5-dimensional space-time theory is that transform to Lorentz symmetry breaking smoothly.

The new 5-dimensional space-time model, is integration between particle wave and space-time theory. The new model can derive out results of Special Relativity Theory also. To the new model, the most important is that time and space is separate. The new model contains that space and time symmetry in 4-dimensional space-time. And the new model contains that space and time is not symmetry 5-dimensional space-time also. The new model not only is consistent with space-time system of Special Relativity Theory, but also can transition to space-time system in Lorentz symmetry breaking smoonthly. The new model has more wide range adaptation than Special Relativity Theory.

Special Relativity Theory is rely on light speed c strictly. In Special Relativity Theory, space and time is symmetry strictly. Once the Lorentz symmetry breaking evidence has been found by experiment, Special Relativity Theory will be incorrect, so space and time is not symmetry again. New space-time theory will be necessary. In the new 5-dimensional space-time theory, space and time is not symmetry. So the new model can transition to Lorentz symmetry breaking smoonthly.

The new 5-dimensional space-time theory can explain physics process when space and time is symmetry. The new 5-dimensional space-time theory can explain physics process when space and time is not symmetry also. This is value of the new model.

The new 5-dimensional space-time theory can explain three physics process that Special Relativity Theory can not explain.

1. The source of particle rest mass. In current theory, particle rest mass is a property by human set and measuring. But human can't explain the source of rest mass. In new 5-dimensional space-time theory, particle rest mass just is particle movement portions at 4th dimensional space. When observing in 5-dimensional space-time, particle don't have rest mass. All particles, include photon, have same movement property. Obviously, in 5-dimensional space-time model, particle will have a new symmetry. This new symmetry will take out what influence, this topic is worth studying.
2. In Quantum Mechanics, when particle is static, particle have wave movement also. At this time, particle wave has limited frequency, but has unlimited wavelength. This is a confusing question. This is not easy to understand. In fact, this is a theory weakness. In new 5-dimensional space-time model, this question has been explained reasonably. When particle is static in 4-dimensional space-time system, but particle is moving in 5-dimensional space-time system. The particle wave is in 5-dimensional space-time. So particle has limited frequency and limited wavelength. The unlimited wavelength is a semblance, not the fact.
3. Space is relative, time is absolute. This can bring logical consistency of theory. Time expansion or contraction in Special Relativity Theory, it's truth is frequency and wavelength change of particle wave. This only is transform effect, not the physics fact. In Quantum Mechanics, all physics process is particle wave process. When coordinates transformation, all particle wave frequency and wavelength will change. So all physics process frequency will change. This is truth of Time expansion or contraction in Special Relativity Theory. But humen live in 4-dimensional space-time system, can't distinguish the difference between time change and frequency change. Human measuring time, must use equipment. Measuring time, fact is measuring equipment's frequency. Human explain these measuring results, it is frequency change, or it is time change, human can't distinguish it.

If the new 5-dimensional space-time theory is correct, there exist three question need to be study.

1. Human live in 4-dimensional space-time system. But human how to observing the 4th dimensional space in 5-dimensional space-time system? Human how to break the dimensional limit?
2. In new 5-dimensional space-time model, all particle's movement speed is light speed c, not change. This is a strong constraint conditions. But why? What power bring this constraint conditions?
3. In new 5-dimensional space-time model, all particle movement speed is light speed c, not change. So there not exist acceleration. There not exist accelerated process. So the equivalence principle in General Relativity Theory, is no longer valid. In new 5-dimensional space-time system, what changes will be occur to General Relativity Theory? In fact, there exist this conflict between General Relativity Theory and Quantum Field Mechanics also. In Quantum Field Mechanics, there not exist particle acceleration also. So, this conflict is not a proof that the new 5-dimensional space-time theory is wrong. Because the new 5-dimensional space-time theory is extended from particle wave. The de Broglie wave, or particle wave, is a basic principle in Quantum Mechanics. So the new 5-dimensional space-time theory is a quantum theory. So this conflict is exist in this new theory also. But in new 5-dimensional space-time theory, this conflict is very obvious, because all particle movement speed is light speed c. Particle speed is same always, not change.

In Quantum Mechanics, particle wave and de Broglie formula are basic principle. So the new model, also is a

new thinking about the relationship between Quantum Mechanics and Special Relativity Theory.

5. Conclusion

From a new perspectives, author take a new thinking, about Special Relativity Theory. The author put forward a new theory model. Particle wave is present in 5-dimensional space-time. In 5-dimensional space-time, speed of all particles is the light speed c. In this new model, we can derive out all results of Special Relativity Theory. This new model is a equivalent theory with Special Relativity Theory. The current physics experiments, could not deny the new physics model. This prove one result. There exist other theory model that can explain these physical phenomena. Special Relativity Theory is not the only theory that can explain these physical phenomena. This take out a new thinking. Does there exist a new equivalent model with General Relativity Theory? The new equivalent model can be integrated with Quantum Mechanics. So we can solve the Quantum gravity problem.

The new 5-dimensional space-time theory, is a self-consistent theory. There not exist logical contradiction from current physics theory. The new 5-dimensional space-time theory, meet current physical experiment results, and can explain current physical experiment results. So the 5-dimensional space-time, no longer appears only in science fiction. To 5-dimensional space-time, human need to think seriously about it.

References

[1] Broglie, Louis de, The wave nature of the electron, Nobel Lecture, December 12, 1929.

[2] "The Feynman Lectures on Physics(Volume I,II,III)",R. P. Feynman,R. B. Leighton,M. Sands.

[3] D. Colladay and V.A. Kostelecký, Lorentz-Violating Extension of the Standard Model, Phys. Rev. D 58, 116002 (1998).

International Journal of Physics, 2016, Vol. 4, No. 5, 130-134
Available online at http://pubs.sciepub.com/ijp/4/5/3

DOI:10.12691/ijp-4-5-3

Effect of the Geometrical Shape of the Magnetic Poles and the Distance between Them on the Focal Properties of the Condenser Magnetic Lens in the Scanning Electron Microscope (SEM)

Mohammed A. Hussein*

Department of Mechanization and Agricultural Equipment, University of Kirkuk, College of Agriculture / Hawija
*Corresponding author: mohdphy@yahoo.com

Abstract The research aims to study the effect of changing the geometric shape of the poles and the distance between them on the focal properties in the condenser magnetic lens and thus the efficiency of the scanning electron microscope through its impact on the amount of miniaturization in the electronic beam passers-through optical column system lenses as well as the amount of aberrations that contribute to reducing the clarity and precision in the resulting image for the sample to be tested. We used six condenser lenses equal in the internal and external geometry and the length of the lens as well as for the coil area and vary the poles and the distance between them to get out the best model.

Keywords: *condenser lens, scanning electron microscope, thermionic emission scanning electron microscope, ray tracing*

Cite This Article: Mohammed A. Hussein, "Effect of the Geometrical Shape of the Magnetic Poles and the Distance between Them on the Focal Properties of the Condenser Magnetic Lens in the Scanning Electron Microscope (SEM)." *International Journal of Physics*, vol. 4, no. 5 (2016): 130-134. doi: 10.12691/ijp-4-5-3.

1. Introduction

The scanning electron microscope is one of the most common instruments for measurement and analysis of micro structures with a high degree of accuracy through the use source of electron beam with short wavelength less than 1nm [1].

Classifies scanning electron microscope depending on the type electron gun into two types, namely scanning electron microscope with a thermal emission and scanning electron microscope with field emission, high analysis capability prefers to use a electron microscope field emission, but because of the high cost and the fact that requires a high degree of vacuum up to Torr10 -10 [2,3]. As well as high precision in the alignment so it preferred to use a thermal emission, which is still Aoudad high share in the markets because of the relatively few cost as well as being does not require a high degree of vacuum up to 10-7 Torr.

Currently, it has a scanning electron microscope with a thermal emission actually analyzed 50 times larger than the boundary theory as a result of irregularities in the electron source size, aberrations and energy dispersive through the optical column and the adoption of precision in magnetic lenses and other defects manufacturing and engineering industry, so manufacturers have focused electron microscopes modern development source the electron beam for the degree of high brightness, system lenses low aberration and scattering a few energy.

Using scanning electron microscope, accelerated electron beam with a very short wavelength less than 0.01nm, so to enhance resolving power compared with optical microscope, which depends on the visible light source wavelength extent with range between 300-700nm.

To facilitate the design of the electron lens system and reduce the time and the loss resulting from the manufacture of these lenses and thus proving its failure has applied numerical simulation software widely as suggested Munro [3] finite element method from first order to analysis of the electron lenses. while developed Renou et, al. [4] analysis programs for electron gun based on the boundary element method. from another side applied [5] Zhu and Munro finite element method of the second order for the analysis of different kinds of electron guns. As display Grella et, al. [6] method of Monte Carlo to calculate the scattered electrons. use each Khursheed and Osterberg [7] finite element method in the design spectroscopy scanning electron microscope.

2. The Theoretical Side

Magnetic lens consists generally of a circular coil is made of copper wire insulated electrically, coil contains (N) of turns When passes a continuous electrical current amount (I) in the coil, it generates a magnetic field symmetry axially(Bz) along an axis (Z) acts on deviation

electrons passers through it towards the coil center according to ampers law. [8].

$$\int_{z_o}^{z_i} B_z dz = \mu_o NI$$

$$\mu_0 = 4\pi * 10^{-7}\, H.m^{-1}.$$

Vacuum permeability
Bz Axial magnetic flux density.

To study the effect of the shape of the poles and the distance between them in the condenser magnetic lens on the optical performance have to create a small image of the first real image composed within the thermal gun, which ranges in diameter dG of (20-100) μm were six models of condenser magnetic lenses equal in geometrical dimensions, internal and external diameter and area of the coil but different in shape of the poles and the distance between them (Figure 1) shows the illustrate of the six designs of the condenser magnetic lens.

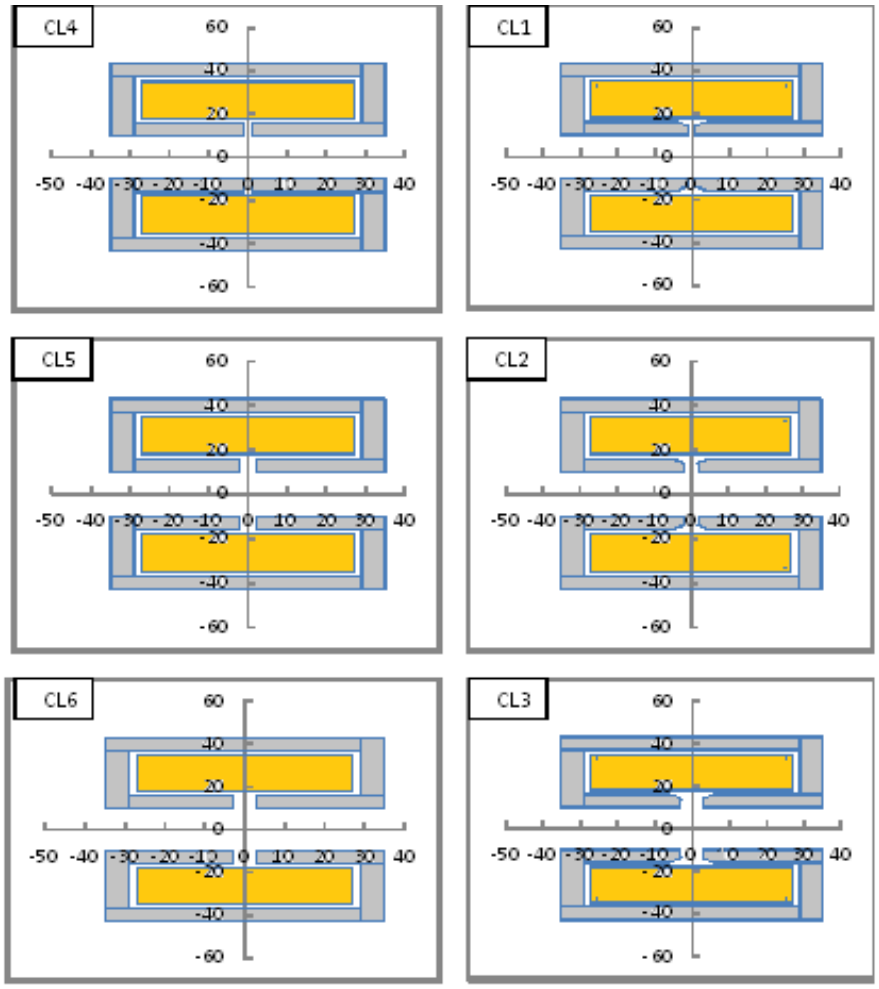

Figure 1. shows the condenser magnetic lenses CL1, CL2, CL3, CL4, CL5, CL6

It is also necessary to study the distribution of the trajectory of magnetic flux lines inside the lens to see the flux leakage in its structure (Figure 2) shows the trajectory of magnetic flux lines within six magnetic lenses, which are parallel and regular on the optical axis.

As has been the distribution of the density of magnetic flux axial Bz for condenser magnetic lenses described in figure (1) When excitation NI = 1000A.t using a program [9] AMAG which is based on the finite element method to know the properties of the focus of (focal length f, and image position Zi, and the number of times demagnification dM ... etc). Figure 3 shows the distribution of magnetic flux density Bz along the Z axis.

Table 1. Bmax values and positions, values of the refraction of the beam Zp, location of the intersection of the beam with the optical axis or the focus positions Zf, and the focal length f

Sample	Location Bmax(mm)	Maximum value of magnetic flux density B_{max} (T)	location of refraction beam Zp (mm)	Location of focus Zf (mm)	Focal length f(mm)
CL1	0	.08677712	-1.72	8.5	8.19
CL2	0	.08444092	-1.84	8.617	8.34
CL3	0	.08181226	-1.97	8.88	8.60
CL4	0	.08619454	-1.71	8.614	8.26
CL5	0	.08424169	-1.83	8.671	8.37
CL6	0	.08193578	-1.96	8.905	8.61

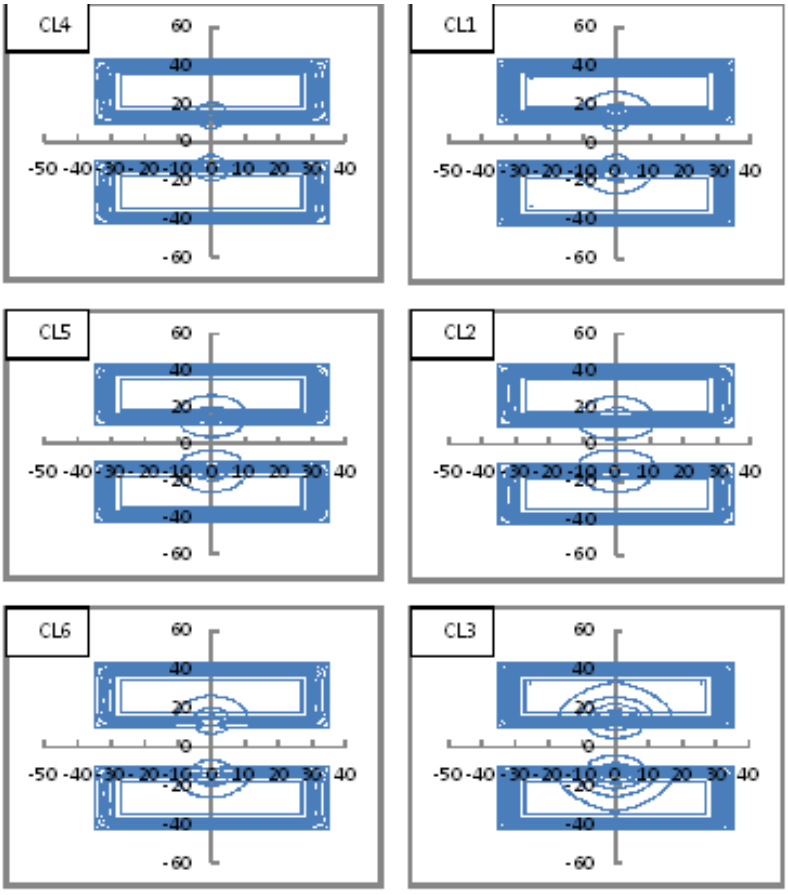

Figure 2. trajectory of magnetic flux lines within the magnetic lenses CL1, CL2, CL3, CL4, CL5, CL6

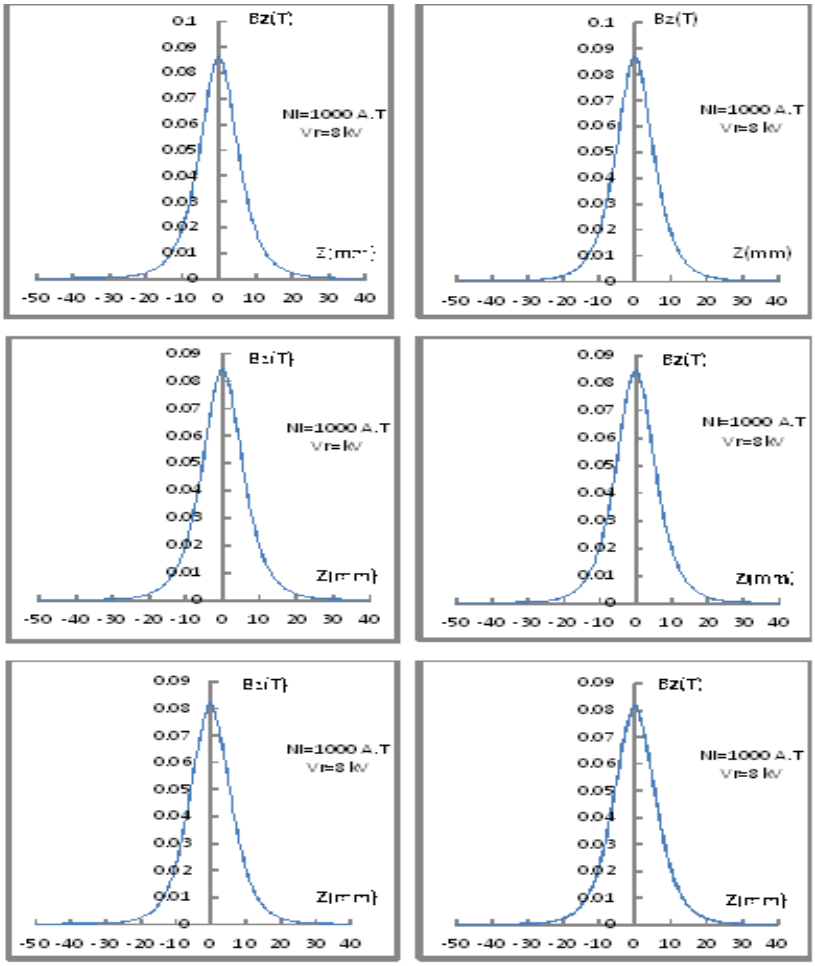

Figure 3. shows the distribution of magnetic flux density Bz along the axis Z

The electron beam trajectory is calculated by solving the axial Ray equation numerically using the method of (Rang-Kutta) from fourth order Figure 4 shows trajectory of the accelerated electron beam by voltage Vr = 8kV when excitation NI = 1000A.t starting from the point of intersection of the electron gun at (Zo = -40) to the position of the image plan formed by the condenser lens Table 1 shows the values and positions Bmax and values of refraction of the electron beam position Zp and the location of the intersection of the electron beam with the optical axis or focus position Zf and focal length of the condenser magnetic lens six.

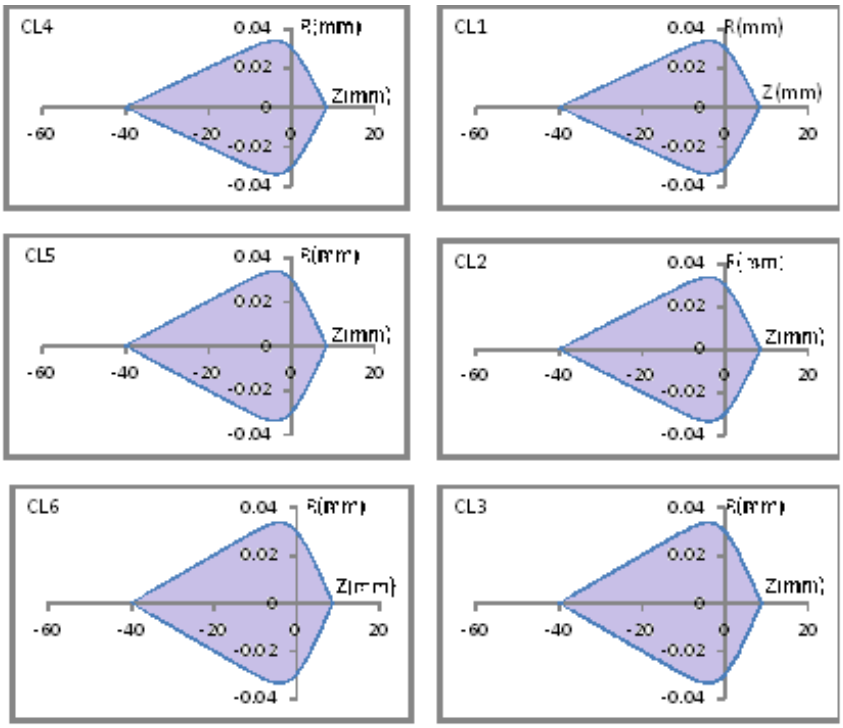

Figure 4. Ray tracing of electron beam accelerated by voltage Vr = 8kV when excitation, NI = 1000A.t

It was awarded a number of times demagnification and beam diameter emerging from condenser magnetic lenses d1 on the assumption that dG = 50μm [10] as well as the calculate of Spherical aberration coefficient, chromatic aberration coefficient and the focal length Table 2 shows the demagnification, beam diameter, Spherical aberration and chromatic aberration.

Table 2. demagnification values, electron beam diameter, spherical and chromatic aberration

Sample	Value of demagnification dM	Beam diameter d1(nm)	Spherical aberration Cs(mm)	Chromatic aberration Cc(mm)
CL1	4.05	12345	7.46	6.32
CL2	3.96	12626	7.43	6.42
CL3	3.83	13054	7.48	6.60
CL4	4	12500	7.60	6.38
CL5	3.95	12658	7.49	6.45
CL6	3.81	13123	7.50	6.61

3. Conclusion

Showing from changes that made on the geometrical shape of the magnetic poles and the distance between them, its affecting on the focus properties of the condenser magnetic lens and electron beam diameter required downed on the objective lens that acts in its role on increasing demagnification in electron beam diameter and bring it down to the desired sample surface study of the surface to get a clear image and free of defects and deformities.

Explained the results that we have obtained from the study of the six models of magnetic lenses that CL1 model has the best focal properties of spherical Cs and chromatic Cc aberrations, the magnetic flux intensity Bz, the focal length f, as well as the smaller electron beam diameter d1, therefore be adopted as the best condenser magnetic lens from the six models.

References

[1] A. Khursheed, Magnetic axial field measurements on a high resolution miniature scanning electron microscope,Rev. Sci. Instrum. 71 (4) (2000) 1712-1715.

[2] J.I. Goldstein, D.E. Newbury, P. Echlin, D.C. Joy, C. Fiori, E. Lifshin, Scanning Electron Microscopy and X-Ray Microanalysis, Plenum Press, New York, 1981.

[3] E. Munro, Image Processing and Computer Aided Design in Electron Optics, P. W. Hawkes Ed., Academic Press, London (1973) 284.

[4] A. Renau, F.H. Read, J.N.H. Brunt, J. Phys. E 15 (1982) 347.

[5] X. Zhu, E. Munro, J. Vac. Sci. Technol. B 7 (1989) 1862.

[6] L. Grella, G. Lorusso, T. Niemi, D.L. Adler, Nucl. Instr. and Meth.A 519 (2004) 242.

[7] A. Khursheed, M. Osterberg, Nucl. Instr. and Meth.A 556 (2006) 437.

[8] Hawkes, P. W. and Kasper, E. (1996), "Principle of Electron Optics", Academic Press, London.

[9] Lencovà, B. (1986), “Program AMAG for computation of vector potential in rotationally symmetric magnetic electron lenses by FEM”, Inst. Sci. Instrum., Czech. Acad. Sci., Brno, Czechoslovakia, pp. 1-58.

[10] Ayache, J., Beaunier, L., Boumendil, J.,Ehret, G. and Laub, D., (2010), "Sample Preparation Handbook for Transmission Electron Microscopy", Methodology Springer Science+Business Media.

International Journal of Physics, 2016, Vol. 4, No. 5, 135-139
Available online at http://pubs.sciepub.com/ijp/4/5/4

DOI:10.12691/ijp-4-5-4

Quantization of the Scalar, Electromagnetic and Dirac Fields in Gravity and the Theory of the Gravitational Gauge Field

M. Khoshsima*

Department of Physics, Adelphi University, New York, USA
*Corresponding author: mkhoshsima@adelphi.edu

Abstract Real scalar field, EM field and Dirac field can be quantized in gravity. The equation of motion in each field will contain a "gravitational" covariant derivative that will produce new energy-momentum dispersion relation. The dispersion relation in each case preserves the old energy accompanied with a perturbed term. The mathematics of the field quantization will remain unchanged with additional energy perturbation due to interaction with spacetime curvature. The correction of Dirac Lagrangian due to gravitational covariant derivative will lead to the probable existence of the gravitational gauge field, an analog to the EM gauge field.

Keywords: *Lagrangian with gravitational covariant derivative, Equation of Motion, Energy-momentum dispersion relation, Perturbation in energy, gravitational symmetry, Gravitational gauge field*

Cite This Article: M. Khoshsima, "Quantization of the Scalar, Electromagnetic and Dirac Fields in Gravity and the Theory of the Gravitational Gauge Field." *International Journal of Physics*, vol. 4, no. 5 (2016): 135-139. doi: 10.12691/ijp-4-5-4.

1. Introduction

In quantum field theory scalar field, EM field and Dirac field are successfully quantized. However, such quantization neglects gravity. In order to include the effect of gravity in quantization one is required to express Lagrangian and equation of motion (EOM) in (gravitational) covariant form. Consequently, equation of motion will include an additional perturbation term that is due to particle field experiencing spacetime curvature (gravity). One can show that the gravitational covariant form of EOM will lead to the change in energy-momentum dispersion of the particle field, although the mathematics of quantization will remain unchanged.

As we shall see, Lagrangian for real scalar field and EM field remain invariant under gravitational covariant derivative however Dirac Lagrangian will have an addition term that can be corrected by introducing gravitational gauge field. This is "gravitation symmetry" that will make the Dirac Lagrangian invariant under gravitational covariant derivative requirement. In this endeavor the second degree gravitational tensor behavior will not be an obstacle for interactional gauge theory. We shall find out that the gravitation gauge and EM gauge fields are vector analog of one another.

2. Quantization of Real Scalar Field in Gravity

Let us recall the free Lagrangian density for the real scalar field, $\phi(\mathrm{x})$

$$L=\frac{1}{2}\partial_{\mu}\phi(\mathrm{x})\ \partial^{\mu}\phi(\mathrm{x})-\frac{1}{2}\mathrm{m}^{2}\phi^{2}(\mathrm{x}), \tag{1}$$

where, m is the mass. Using Euler-Lagrange equation, the equation of motion (EOM) for the above Lagrangian will be

$$\left(\partial_{\mu}\ \partial^{\mu}+\mathrm{m}^{2}\right)\ \phi(\mathrm{x})=0, \tag{2}$$

which is known as Klein-Gordon equation. The EOM for a real scalar field in curved spacetime will require the replacement of 4-derivative into "gravitational covariant derivative," $\mathrm{D}_{g\mu}$

$$\left(\mathrm{D}_{g\mu}\ \mathrm{D}_{g}^{\mu}+\mathrm{m}^{2}\right)\ \phi(\mathrm{x})=0. \tag{3}$$

The gravitational covariant derivative in equation (3) can be expanded in the form of

$$\left(\partial_{\mu}\ \partial^{\mu}+\mathrm{m}^{2}-\mathrm{g}^{\mu\nu}\ \Gamma_{\mu\nu}^{\rho}\ \partial_{\rho}\right)\ \phi(\mathrm{x})=0, \tag{4}$$

which does preserve the original Lagrangian along with the additional term, $\Gamma_{\mu\nu}^{\rho}$ being the affine connection . In order to solve Equation (4), we shall express $\phi(\mathrm{x})$ in terms of its Fourier transform

$$\phi(\mathrm{x})=\int\frac{\mathrm{d}^{4}\mathrm{k}}{(2\pi)^{4}}\ \phi(\mathrm{k})\ \mathrm{e}^{-\mathrm{ik}_{\mu}\ \mathrm{x}^{\mu}}. \tag{5}$$

Equations (4) and (5) will give us energy-momentum dispersion relation for a real scalar field in gravity

$$K_0^2 = \vec{K}^2 + m^2 + i\, g^{\mu\nu}\Gamma^{\rho}_{\mu\nu}\, K_\rho. \quad (6a)$$

In the equation above, K_0 is the energy of the particle field, $\vec{K}$ is the momentum and K_ρ is the 4-momentum. Next, we expand the mass in Equation (6a) in terms of 4-momentum

$$K_0^2 = \vec{K}^2 + g^{\mu\nu}K_\mu K_\nu + i\, g^{\mu\nu}\Gamma^{\rho}_{\mu\nu}\, K_\rho. \quad (6b)$$

The last two terms in equation (6b) are tensors and can be combined together into an "effective mass"

$$m^2{}_{eff} = g^{\mu\nu}\left(K_\mu K_\nu + i\,\Gamma^{\rho}_{\mu\nu}\, K_\rho\right). \quad (7)$$

Assuming the gravitation contribution manifesting as a perturbation in mass, therefore

$$m_{eff} \approx m + i\,\frac{g^{\mu\nu}\,\Gamma^{\rho}_{\mu\nu}\, K_\rho}{2\,m}. \quad (8)$$

Notice that, $\left[g^{\mu\nu}\,\Gamma^{\rho}_{\mu\nu}\, K_\rho\right] = \left[K^{\rho}_{g} K_\rho\right] = [m]^2$, where $K^{\rho}_{g} = g^{\mu\nu}\,\Gamma^{\rho}_{\mu\nu}$ is the equivalence of gravitational 4-momentum. One can then express the energy of the particle field

$$K_0 = \sqrt{\vec{K}^2 + m^2_{eff}} = \omega'_k. \quad (9)$$

We can interpret Equations (8) and (9) such that a scalar field particle in gravity will experience perturbation in its mass and energy. Perturbation being imaginary is perhaps an indication of the decaying nature of particle energy in the gravitational field. Therefore, a scalar field in gravitational field will experience perturbation in mass and energy, with modified energy spectrum of $\omega_k \rightarrow \omega'_k$

$$\phi(x) = \int \frac{d^3k}{(2\pi)^{3/2}\sqrt{2\omega'_k}} \begin{pmatrix} \hat{a}\,(\vec{k})e^{-i\,(\omega'_k\, x^0 - \vec{k}.\vec{x}} \\ +\hat{a}^+(\vec{k})e^{i\,(\omega'_k\, x^0 - \vec{k}.\vec{x}} \end{pmatrix}. \quad (10a)$$

Consequently, the energy operator will be

$$\hat{H} = \int d^3k\,\omega_k \left(a^+(\vec{k})\, a\,(\vec{k})\right) \rightarrow \int d^3k\ \omega'_k \left(a^+(\vec{k})\, a\,(\vec{k})\right). \quad (10b)$$

We note that the real scalar field quantization in gravity will remain similar to that of the situation where gravity is absent however the Hamiltonian will change due to perturbation in energy. The particle-gravitational interaction contribution, $g^{\mu\nu}\Gamma^{\rho}_{\mu\nu}\, K_\rho$, can further be simplified by expanding the affine connection

$$g^{\mu\nu}\Gamma^{\rho}_{\mu\nu}\, K_\rho = g^{\mu\rho}{}_{,\,\mu}\, k_\rho. \quad (11)$$

According to Equation (11) the gravitational 4-momentum can now be expressed in terms of derivative of metric tensor, $k^{\rho}_{g} = g^{\mu\rho}{}_{,\,\mu}$. Once we know the metric, $g^{\mu\nu}$ the energy perturbation due to gravity can easily be determined. K_ρ, also is the 4-momentum of the field particle. So perturbation in energy in terms of virtual (imaginary) invariant mass is the product of particle field 4-momentum with gravitational field 4-momentum. Now we can express energy-momentum spectrum in terms of the metric

$$K_0^2 = \vec{K}^2 + m^2 + i\, g^{\mu\nu}{}_{,\,\mu}\, K_\nu. \quad (12)$$

Here, the magnitude of the perturbed energy will be inversely proportional to the magnitude of the unperturbed energy of the scalar field particle

$$\left|K_{0perturbed}\right| \approx \frac{g^{\mu\rho}{}_{,\,\mu}\, K_\rho}{2\omega_k}, \quad (13)$$

where, $\omega_k = \sqrt{\vec{K}^2 + m^2}$.

3. Gravitational Symmetry of the Scalar Field

The real scalar field Lagrangian for a free particle (Eqn.(1)) with mass m has a non-continuous symmetry under

$$\phi(x) \rightarrow -\phi(x). \quad (14)$$

Once the interaction term $\sim -\lambda\,\phi^4(x)$ is added to the Lagrangian, it is possible to proceed with symmetry breaking. However, we may introduce a new symmetry of different sort regarding the interaction with gravity; "gravitational symmetry." If Lagrangian remains constant under gravitational covariant requirement, it then will have gravitational symmetry; otherwise physics will require correction by introducing gravitational gauge. Let us take the gravitational covariant derivative form of Equation (1)

$$L = \frac{1}{2} D_{g\mu}\phi(x)\ D^{\mu}_{g}\phi(x) - \frac{1}{2} m^2\phi^2(x). \quad (15a)$$

For a scalar field, $D_{g\mu}\phi(x) = \partial_\mu\phi(x)$. Therefore, real scalar field Lagrangian already has symmetry under gravity

$$L \overset{g}{\rightarrow} L_g = L. \quad (15b)$$

One can say gravitation gauge correction will not be required for real scalar field Lagrangian. We also will not elaborate on complex scalar field because the physics will remain the same as the real scalar field and therefore redundant.

4. Canonical Quantization of the Electromagnetic Field

In order to quantize the EM field in gravity, likewise we need to start with the gravitational covariant of the EM Lagrangian

$$L = -\frac{1}{4} F^{\mu\nu}\ F_{\mu\nu}. \quad (16a)$$

It is interesting to notice that the gravitational covariant form of the EM tensor will also remain invariant under covariant derivative

$$F_{\mu\nu} = \partial_\mu A_\nu - \partial_\nu A_\mu \overset{g}{\rightarrow}$$
$$D_{g\mu} A_\nu - D_{g\nu} A_\mu \quad (16b)$$
$$= (\partial_\mu A_\nu - \Gamma^\rho_{\mu\nu} A_\rho) - (\partial_\nu A_\mu - \Gamma^\rho_{\mu\nu} A_\rho) = F_{\mu\nu}.$$

One can conclude, EM Lagrangian also has symmetry in regards to the gravitational requirement. Once more

$$L \overset{g}{\rightarrow} L_g = L. \quad (16c)$$

Now, without any further elaboration, we recall the gravitational covariant EOM for EM field

$$D_{g\mu}\ D^\mu_g\ A^\sigma(x) = 0. \quad (17a)$$

After expansion of the covariant derivative and simplification

$$\left[\partial_\mu\ \partial^\mu + g^{\mu\nu} \begin{pmatrix} \Gamma^\sigma_{\mu\sigma,\nu} - i\,\Gamma^\sigma_{\mu\sigma} K_\nu \\ -i\,\Gamma^\sigma_{\nu\sigma} K_\mu + i\,\Gamma^\sigma_{\mu\nu}\ K_\sigma \end{pmatrix}\right] A^\rho(x) = 0. \quad (17b)$$

Once again, the new EOM does preserve the original form with an addition term (in the parenthesis) pertain to gravitational contribution. The energy-momentum spectrum for the above Lagrangian will be

$$K_0^2 = \vec{K}^2\ + g^{\mu\nu} \begin{pmatrix} \Gamma^\sigma_{\mu\sigma,\nu} - i\,\Gamma^\sigma_{\mu\sigma} K_\nu \\ -i\,\Gamma^\sigma_{\nu\sigma} K_\mu + i\,\Gamma^\sigma_{\mu\nu}\ K_\sigma \end{pmatrix}. \quad (18)$$

The gravitational contribution in equation (18) can actually be further simplified and expressed in terms metric. As it is expected since we are dealing with a vector filed, the spectrum is gravitationally more complicated, although there is no mass. The perturbation does not manifest in mass-energy, rather, in momentum-energy as should be expect for a photon. The quantization of EM field particle in gravity will remain unchanged although the photon particle field energy will be perturbed by the terms that include affine connection.

5. Quantization of Dirac Field

Due to the fact that spinors are not vectors, Dirac field can be more subtle to quantize in gravitational field. Let us express Lagrangian density for a Dirac field in its gravitational covariant derivative form

$$L = \bar{\Psi}\left(i\,\gamma^\mu\ D_{g\mu} - m\right)\Psi. \quad (19a)$$

Notice that the above Lagrangian, unlike real scalar and EM field is not invariant under gravitational covariant derivative as shown below

$$L = \bar{\Psi}\left(i\,\gamma^\mu\ \partial_\mu - m\right)\Psi + \bar{\Psi}\ \left(i\,\gamma^\mu\ \Gamma^{\nu\ 1/2}_{\mu\rho}\ \Psi\right)^\rho{}_\nu. \quad (19b)$$

Instead of spinor in the second term of equation (19b), if we encountered a second degree tensor the analysis would have then been easier. Also note that because there is little "affinity" between tensor and the spinor in the second term of the above equation, we rather change the tensor operation into an invariant scalar, as it will make sense later on. Accordingly one has to take the square root of the affine connection in order to choose proper units (this will also be clear later on)

We have already seen the real scalar field being passive under first gravitational covariant derivative, namely

$$D_{g\mu}\phi(x)\ = \partial_\mu \phi(x). \quad (20a)$$

On the other hand EM vector field can easily be acted on by a covariant derivative whereas a spinor field is neither scalar nor a vector field and has subtle affinity with tensors. The key is that the Lagrangian has to be a Lorentz scalar otherwise it will not be a valid Lagrangian. In order to resolve this issue we shall contract the last term of Equation (19b) by a (1/1) tensor so that the Lagrangian will remain invariant under Lorentz transformation. Now, not only the Lagrangian is Lorentz invariant, the Dirac field will also be multiplied by scalars only

$$L = \bar{\Psi}\left(i\,\gamma^\mu\ \partial_\mu - m\right)\Psi + \bar{\Psi}\ \left(i\,\gamma^\mu\ \left(\Gamma^\nu_{\mu\rho}\ T^\rho_\nu\right)^{1/2}\Psi\right). \quad (21)$$

Again, the half power in the second term is due to unit corrections. In order to proceed with quantization, let us express EOM for Dirac fields in the expanded gravitational covariant form

$$i\,\gamma^\mu\ \partial_\mu \Psi - m\,\Psi + i\left(\gamma^\mu\ \Gamma^{\nu\ 1/2}_{\mu\rho}\ \Psi\right)^\rho{}_\nu = 0, \quad (22a)$$

$$i\,\gamma^\mu\ \partial_\mu \bar{\Psi} + m\,\bar{\Psi} + i\left(\gamma^\mu\ \Gamma^{\nu\ 1/2}_{\mu\rho}\ \bar{\Psi}\right)^\rho{}_\nu = 0. \quad (22b)$$

As far as perturbation is concerned, Equations (22a) and (22b) are similar. We would concentrate on Ψ only. To make Equation (22a) completely Lorentz invariant we likewise introduce a (1/1) tensor T^ρ_ν in the last term

$$i\,\gamma^\mu\ \partial_\mu \Psi + i\,\gamma^\mu\ \left(\Gamma^\nu_{\mu\rho}\ T^\rho_\nu\right)^{1/2}\ \Psi - m\,\Psi = 0. \quad (23)$$

Similarly, the half power is due to unit correction as it shall be clear later on. As for scalar and EM fields, the above EOM for the Dirac field does contain a perturbed term. One way of being able to analyze this equation is to express the tensor T^ρ_ν in terms of Dirac field 4-momentum, by analogy to real scalar and EM fields. Let

$$T^{\rho\ 1/2}_\nu = \left(K^\rho K_\nu\right)^{1/2}. \quad (24)$$

This is a fair assumption because for real scalar and EM fields it was the 4-momentum of the field that accompanied the affine connection. Simply put, it is the 4-momentums that interact with one another. It happens that for a spinor as compared to a vector, tensor operation is null. After all the perturbation term should include interaction between gravity (affine connection) and the 4-momentum (of the particle field). Naturally we can combine the first two terms in Equation (23)

$$\left(i\,\gamma^\mu\ \left(\partial_\mu + \ \left(\Gamma^\nu_{\mu\rho} K^\rho K_\nu\right)^{1/2}\right) - m\right)\Psi = 0. \quad (25a)$$

We now can retrieve modified form of Dirac equation in gravity

$$\left(\mathrm{i}\,\gamma^{\mu}\ \nabla'_{g\mu}-\mathrm{m}\right)\Psi=0, \tag{25b}$$

where, $\nabla'_{g\mu}=\partial_{\mu}+\left(\Gamma^{\nu}_{\mu\rho}\ \mathrm{K}^{\rho}\mathrm{K}_{\nu}\right)^{1/2}$. Let us proceed with solving the above equation. We should note that the perturbed component of the equation is due to the Dirac field interacting with gravity. At this point we will express Equations (25) in terms of 4-momentum and we can see why parenthesis in the second term is in half power

$$\left(\gamma^{\mu}\ \mathrm{K}_{\mu}+\mathrm{i}\,\gamma^{\mu}\ \left(\Gamma^{\nu}_{\mu\rho}\mathrm{K}^{\rho}\ \mathrm{K}_{\nu}\right)^{1/2}-\mathrm{m}\right)\Psi=0. \tag{26}$$

Let us then proceed by expanding the matrices

$$\left[\begin{bmatrix}\mathrm{E}\text{-}\mathrm{m} & -\vec{\sigma}.\,\vec{\mathrm{k}}\\ \vec{\sigma}.\,\vec{\mathrm{k}} & -(\mathrm{E}+\mathrm{m})\end{bmatrix}+\begin{bmatrix}\left(\Gamma^{\nu}_{0\rho}\mathrm{K}^{\rho}\mathrm{K}_{\nu}\right)^{1/2} & \vec{\sigma}.\left(\Gamma^{\nu}_{i\rho}\mathrm{K}^{\rho}\mathrm{K}_{\nu}\right)^{1/2}\\ -\vec{\sigma}.\left(\Gamma^{\nu}_{i\rho}\mathrm{K}^{\rho}\mathrm{K}_{\nu}\right)^{1/2} & \left(\Gamma^{\nu}_{0\rho}\mathrm{K}^{\rho}\mathrm{K}_{\nu}\right)^{1/2}\end{bmatrix}\right]\begin{bmatrix}\Psi^{+}_{1}\\ \Psi^{+}_{2}\end{bmatrix}=0. \tag{27a}$$

Where, we have used Dirac matrices in the above equation. Notice that the second matrix is the perturbation due to interaction with gravity. Combining the two matrices

$$\begin{bmatrix}\mathrm{E}+\left(\Gamma^{\nu}_{0\rho}\mathrm{K}^{\rho}\mathrm{K}_{\nu}\right)^{1/2}\text{-}\mathrm{m} & -\vec{\sigma}.\left(\vec{\mathrm{k}}\text{-}\left(\Gamma^{\nu}_{i\rho}\mathrm{K}^{\rho}\mathrm{K}_{\nu}\right)^{1/2}\right)\\ \vec{\sigma}.\left(\vec{\mathrm{k}}\text{-}\left(\Gamma^{\nu}_{i\rho}\mathrm{K}^{\rho}\mathrm{K}_{\nu}\right)^{1/2}\right) & -(\mathrm{E}+\left(\Gamma^{\nu}_{0\rho}\mathrm{K}^{\rho}\mathrm{K}_{\nu}\right)^{1/2}+\mathrm{m})\end{bmatrix} \tag{27b}$$
$$\times\begin{bmatrix}\Psi^{+}_{1}\\ \Psi^{+}_{2}\end{bmatrix}=0.$$

Equations (27) clearly show the perturbation in spinor energy while experiencing gravitational field. We therefore conclude that the Dirac field quantization in gravity similar to that of scalar and EM fields does remain unchanged, likewise, with having a perturbation in energy spectrum. As a simple example we shall consider a slow moving particle field where $\tau=\mathrm{t}$, and therefore $\Gamma^{\nu}_{0\rho}=\Gamma^{\mathrm{i}}_{00}$. The perturbation term in non-relativistic limit will be

$$\begin{aligned}\Gamma^{\nu}_{0\rho}\mathrm{K}^{\rho}\mathrm{K}_{\nu}\ &=\ \Gamma^{\mathrm{i}}_{00}\mathrm{K}^{0}\mathrm{K}_{\mathrm{i}}=(-\tfrac{1}{2})\,\mathrm{h}_{00,}{}^{\mathrm{i}}\mathrm{K}^{0}\mathrm{K}_{\mathrm{i}}\\ &=\left(\nabla_{\mathrm{i}}\ \varphi\right)\mathrm{K}^{0}\mathrm{K}_{\mathrm{i}}\\ &\approx \mathrm{m}\frac{\partial\phi}{\partial\,\mathrm{x}^{\mathrm{i}}}\frac{\partial\,\mathrm{x}^{\mathrm{i}}}{\partial\,\mathrm{t}}\mathrm{E}\cong\frac{\partial\mathrm{E}^{2}}{\partial\,\mathrm{t}}.\end{aligned} \tag{28a}$$

So the overall perturbation is in the units of classical non-relativistic energy transition. Notice that there can't be any $\Gamma^{\nu}_{0\mathrm{i}}$ component of the affine connection. Inserting the above term in Equation (27b) will give

$$\begin{bmatrix}\mathrm{E}+\sqrt{\left(\nabla_{\mathrm{i}}\ \varphi\right)\ \mathrm{K}^{0}\mathrm{K}_{\mathrm{i}}}\text{-}\mathrm{m} & -\vec{\sigma}.\,\vec{\mathrm{k}}\\ \vec{\sigma}.\,\vec{\mathrm{k}} & -(\mathrm{E}+\sqrt{\left(\nabla_{\mathrm{i}}\ \varphi\right)\ \mathrm{K}^{0}\mathrm{K}_{\mathrm{i}}}+\mathrm{m})\end{bmatrix} \tag{29}$$
$$\times\begin{bmatrix}\Psi^{+}_{1}\\ \Psi^{+}_{2}\end{bmatrix}=0.$$

Equation (29) is the solution to the original Dirac equation plus the perturbation term.

6. Gravitational Gauge Field

Let us recall Dirac Lagrangian in gravity, Equation (21)

$$L=\bar{\Psi}\left(\mathrm{i}\,\gamma^{\mu}\ \partial_{\mu}-\mathrm{m}\right)\Psi+\bar{\Psi}\left(\mathrm{i}\,\gamma^{\mu}\ \Gamma^{\nu\ 1/2}_{\mu\rho}\ \Psi\right)^{\rho}_{\nu}. \tag{30a}$$

In order to correct the perturbation term in the above Lagrangian we shall introduce a new term that will include, $\mathrm{A}_{g\mu}$ the proposed gravitational gauge field with $\mathrm{g}_{g'}$ being a constant

$$\begin{aligned}L=\bar{\Psi}\ &\left(\mathrm{i}\,\gamma^{\mu}\ \partial_{\mu}-\mathrm{m}\right)\Psi+\ \bar{\Psi}\ \left(\mathrm{i}\,\gamma^{\mu}\ \Gamma^{\nu\ 1/2}_{\mu\rho}\ \Psi\right)^{\rho}_{\nu}\\ &+\bar{\Psi}\left(\ \mathrm{g}_{g'}\ \gamma^{\mu}\mathrm{T}^{\upsilon 1/2}_{\rho}\mathrm{A}_{g\mu}\Psi\right)^{\rho}_{\upsilon}.\end{aligned} \tag{30b}$$

Combining the last two terms

$$\begin{aligned}L=\bar{\Psi}\ &\left(\mathrm{i}\,\gamma^{\mu}\ \partial_{\mu}-\mathrm{m}\right)\Psi\\ &+\mathrm{g}_{g'}\bar{\Psi}\,\gamma^{\mu}\left(\left(\mathrm{T}^{\nu 1/2}_{\rho}\mathrm{A}_{g\mu}+\mathrm{i}\frac{1}{\mathrm{g}_{g'}}\Gamma^{\nu\ 1/2}_{\mu\rho}\right)\Psi\right)^{\rho}_{\upsilon}.\end{aligned} \tag{30c}$$

At this point we also let the gauge transformation

$$\mathrm{T}^{\nu 1/2}_{\rho}\mathrm{A}_{g\mu}\rightarrow\ \mathrm{T}^{\nu 1/2}_{\rho}\mathrm{A}_{g\mu}-\mathrm{i}\frac{1}{\mathrm{g}_{g'}}\ \Gamma^{\nu\ 1/2}_{\mu\rho}, \tag{31a}$$

and multiplying the transformation by $\mathrm{T}^{\rho 1/2}_{\nu}$ from the right hand side

$$\mathrm{T}^{\nu 1/2}_{\rho}\mathrm{A}_{g\mu}\mathrm{T}^{\rho 1/2}_{\nu}\rightarrow\mathrm{T}^{\nu 1/2}_{\rho}\mathrm{A}_{g\mu}\mathrm{T}^{\rho 1/2}_{\nu}-\mathrm{i}\frac{1}{\mathrm{g}_{g'}}\left(\Gamma^{\nu}_{\mu\rho}\mathrm{T}^{\rho}_{\nu}\right)^{1/2}. \tag{31b}$$

The Lorentz-gravitational invariant Lagrangian then becomes

$$L=\bar{\Psi}\left(\mathrm{i}\,\gamma^{\mu}\left(\partial_{\mu}-\mathrm{i}\,\mathrm{g}_{g'}\left(\mathrm{T}^{\nu}_{\rho}\ \mathrm{A}^{2}{}_{g\mu}\ \mathrm{T}^{\rho}_{\nu}\right)^{1/2}\right)-\mathrm{m}\right)\Psi. \tag{32a}$$

The product of the two tensors $\mathrm{T}^{\nu}_{\rho}\ \mathrm{T}^{\rho}_{\nu}$ is an invariant constant which can be absorbed into, $\mathrm{g}_{g}=\mathrm{g}_{g'}\sqrt{\mathrm{T}^{\nu}_{\rho}\ \mathrm{T}^{\rho}_{\nu}}$. However, according to Equation (24)

$$\mathrm{g}_{g}=\mathrm{g}_{g'}\sqrt{\mathrm{K}^{\rho}\ \mathrm{K}_{\rho}\ \mathrm{K}^{\nu}\ \mathrm{K}_{\nu}}=\mathrm{g}_{g'}\mathrm{m}_{a}\mathrm{m}_{b}. \tag{32b}$$

Where, g_{g}, can be defined as the product of strength of the gravitational interaction with the invariant masses of the two Dirac field. Consequently the Lagrangian will become

$$\begin{aligned}L&=\bar{\Psi}\ \left(\mathrm{i}\,\gamma^{\mu}\left(\partial_{\mu}-\ \mathrm{i}\,\mathrm{g}_{g}\ \mathrm{A}_{g\mu}\right)-\mathrm{m}\right)\ \Psi\\ &=\bar{\Psi}\ \left(\mathrm{i}\,\gamma^{\mu}\nabla_{g\mu}-\mathrm{m}\right)\ \Psi.\end{aligned} \tag{32c}$$

$\nabla_{g\mu}$ is the proposed gravitational gauge covariant derivative for the above Lagrangian. In order to express the current in the Lagrangian

$$L = \bar{\Psi}\left(i\,\gamma^{\mu}\,\partial_{\mu} - m\right)\Psi + \bar{\Psi}\left(g_g\,\gamma^{\mu}A_{g\mu}\right)\Psi = \bar{\Psi}\left(i\,\gamma^{\mu}\,\partial_{\mu} - m\right)\Psi + g_g j^{\mu}A_{g\mu}, \quad (33)$$

with Dirac current $j^{\mu} = \bar{\Psi}\,\gamma^{\mu}\,\Psi$ and the interaction strength, g_g. Finally, gravitation gauge transformation requirement will be as follows

$$A'_{g\mu} = A_{g\mu} - i\frac{1}{g_g}\left(\Gamma^{\nu}_{\mu\rho}\,K^{\rho}K_{\nu}\right)^{1/2}, \quad (34a)$$

$$\nabla_{g\mu} = \partial_{\mu} - i\,g_g\,A_{g\mu}. \quad (34b)$$

Equations (34) are analog of local gauge symmetry in QED with EM gauge vector field A_{μ}. However, here we have introduced gravitational symmetry to generate gravitational gauge vector field $A_{g\mu}$. It is also interesting to note that we were successful to generate a gravitational vector field very similar to that of its analog, EM gauge vector field. The key determining factor in this case is the affine connection due to gravity (caused by particles' mass) interacting with 4-momentum of the particle field. As in electro-dynamics where charge e appears in the interaction so do masses of the two particles in gravitational dynamics between the two particles.

7. Conclusion

The quantization of the particle filed in gravity remains unchanged however the energy-momentum dispersion relation of the particle does change. This change or perturbation in energy can be due to interaction of particle filed with the gravitational field. Dirac free particle Lagrangian will require correction due to additional term in Lagrangian caused by external gravity or the gravity of the massive fields. This symmetry of gravity will generate gravitational gauge field which is an analog to that of the EM gauge field.

References

[1] M. Schwartz, "Quantum Field Theory and the Standard Model" Cambridge University Press, 4th Printing 2015.

[2] S. Hawking, "A Brief History of Time," New York: Bantam Books, 1988.

[3] R.L. Faber, "Differential Geometry and Relativity Theory," An Introduction. New York: Marcel Dekker, Inc., 1983.

[4] T. Marsh, "General Relativity," class notes, 2009.

[5] "S. Chandrasekhar, "The Mathematical Theory of Black Holes". Clarendon Press (1983).

[6] C.W. Misner, K.S. Thorne, and J.A. Wheeler, "Gravitation". Freeman (1973).

[7] S. Weinberg, "Gravitation and Cosmology: Principles and Applications of the General Theory of Relativity". Wiley (1972).

[8] G. 't Hooft, " Introduction To General Relativity," Institute for Theoretical Physics; Utrecht University (2002).

[9] Poul Olesen, "General Relativity and Cosmology," The Niels Bohr Institute (2008).

[10] M. Kachelrieb, "Gravitation and Cosmology," Institute for fysikk; NTNU (2010).

[11] M. Khoshsima, "Black Hole Spacetime Equation in Special Relativity." International Journal of Astronomy, Astrophysics and Space Science; Vol. 2, No. 4, 2015, pp. 30-33.

[12] M. Khoshsima, "Universe, a Spacetime Harmonic Oscillator." International Journal of Physics, Vol. 4, no. 1(2016): 21-25.

International Journal of Physics, 2016, Vol. 4, No. 5, 140-145
Available online at http://pubs.sciepub.com/ijp/4/5/5

DOI:10.12691/ijp-4-5-5

Replacement of Einstein's Relativity Theory with a New One: Why the Second Postulate is Superfluous?

Mamaev A. V.*

Candidate of engineering sciences, Bureau Chief, JSC "Lianozovo Electromechanical Plant Research and Production Corporation", Russia
*Corresponding author: gromoboy1942@mail.ru

Abstract My purpose consisted in creation of a new relativistic space-time theory instead of Einstein's Relativity Theory, but basing upon only one postulate. This could become feasible only if a law of light propagation in a moving inertial reference frame could be made a consequence of the relativity postulate. It was made a reality by P.M. Rapier's discovery of a quadratic dependence of the light speed upon the light source speed. Considering various ways of making the second postulate superfluous the most short of them was through introducing into the theory of a new concept "light speed in a moving inertial reference frame" by means of usage of the known four-dimensional Minkovski's formalism. This new light speed was defined as equal to a fourth component of a four-dimensional speed of any moving particle. Then using this newly introduced concept the time-measurement unit was calculated for a moving light clock that occurred to be equal to the time measurement unit of a stationary light clock. And as a very happy event the time dilation effect was deleted from the theory.

Keywords: *special relativity theory, light speed in a moving inertial reference frame, Galilean speed or velocity, Lorentz speed or velocity, proper time, light clock, time measurement unit*

Cite This Article: Mamaev A. V., "Replacement of Einstein's Relativity Theory with a New One: Why the Second Postulate is Superfluous?" *International Journal of Physics*, vol. 4, no. 5 (2016): 140-145. doi: 10.12691/ijp-4-5-5.

1. Foreword

The history shows that all theories and sciences evolve in such a way, that realness of phenomena visible by eyes are gradually changed by realness of phenomena perceived mentally. For example, movement of the Sun and far stars and immovability of the Earth visible to Ptolemy's eyes after some time were replaced by movement of the Earth around the Sun and with respect to far stars perceptible by Copernicus's brain.

The first stage of any theory or any science therefore is based upon seeing any phenomenon by means of eyes. And the eye sees only the light – electromagnetic radiation with wavelengths between 380 nm (violet color) and 780 nm (red color). What else do we know about the light? We know that the light propagates in vacuum having the velocity equal to 299 792 458 m/s. At that this value is measured in the stationary inertial reference frame (IRF). At what speed the light propagates in any moving IRF we can only guess. In order to answer this question we, first of all, should form a concept "light speed (or velocity) in vacuum of a moving IRF". Why we must perform this task?

We must perform this task due to todays situation when we know only speed of light in a stationary IRF. Because it has happened in such a way, that in 1905 Albert Einstein [1] defined only speed of light in a stationary IRF and introduced two postulates:

1. A relativity postulate: "The laws, by which the states of physical systems undergo change, are not affected, whether these changes of state be referred to the one or the other of two systems of co-ordinates in uniform translatory motion".

2. A postulate of light speed independence on the speed of a light source: "Any ray of light moves in the "stationary" system of co-ordinates with the determined velocity c_0, whether the ray be emitted by a stationary or by a moving body".

Keeping in mind that any of two IRF, moving each with respect the other at some specific speed V, may be called as a stationary one (at that the other one should be considered as a moving one), from these two Einstein's postulates it was concluded, that the speed of light in vacuum of all IRF (irrespective of whether each of these IRF is considered to be a stationary one or a moving one) is equal to the same value $c_0 = 299\,792\,458$ m/s.

Such erroneous conclusion was used by Einstein himself when he derived Lorentz's transformation of coordinates from one IRF to another IRF, namely he wrote: "…*Light (as required by the principle of the constancy of the velocity of light, in combination with the principle of relativity) is also propagated with velocity* c_0 *when measured in the moving system*".

But neither Einstein in 1905, nor his numerous admirers in the past did not take into their minds, that an assumption about equality of light speed in a moving IRF to the light speed in a stationary IRF results in

contradiction between the effect of time dilation in Einstein's special relativity theory (SRT) and the relativity principle.

Indeed, it is well known that a light clock (consisting of two parallel mirrors, a photoelectric sensor on one of mirrors, a pulse counter connected to the output of the photoelectric sensor and a light pulse circulating between mirrors) is a physical system, which must comply with the relativity principle.

Because the relativity principle with respect to such physical system as the light clock must read:

The laws, by which the indications of light clock undergo change, are not affected, whether these changes of indications be referred to the one or the other of two systems of co-ordinates in uniform translatory motion.

That means that time dilation effect existing in the SRT according to the relativity principle should be absent. Indeed, if we consider that distance between mirrors of a stationary light clock is equal to L_0, then the time measurement unit for a stationary light clock is equal to the value

$$T_0 = 2 \cdot L_0 / c_0. \quad (1)$$

And the time measurement unit for the same light clock, moving at the speed V in a direction perpendicular to planes of light clock mirrors, in case of an assumption that light speed in a moving light clock also is equal to c_0 will be equal to the value

$$T = \frac{L}{c_0 - V} + \frac{L}{c_0 + V} = \gamma \cdot T_0, \quad (2)$$

where $L = \frac{L_0}{\gamma} = L_0 \sqrt{1 - V^2/c_0^2}$ is the distance (according to the SRT) between light clock mirrors, moving at the speed V.

Thus, the assumption that the light speed in a moving IRF is also equal to the same value c_0, leading to the existence of time dilation effect in the SRT, leads to a contradiction with the relativity principle (indications of a light clock depend on what IRF these indications are referred to). Therefore it is expedient to consider what value of the light speed in a moving IRF will not lead to a contradiction with the relativity principle that is to consider what value of light speed in a moving IRF will result in equality of time measurement units for stationary and moving light clocks of the precisely similar design.

2. Introduction of a New Physical Concept

First of all let us form a new concept "light speed in vacuum of a moving IRF". It is unlikely that this concept has been considered as having some positive sense up until todays time. As opposed to this concept the concept "light speed in vacuum of a stationary IRF" was widely known because it was included into the Einstein's second postulate (see above) [1].

How can we practically perform measurement of the "light speed in vacuum of a moving IRF"? We can perform such measuring in accordance with Figure 1.

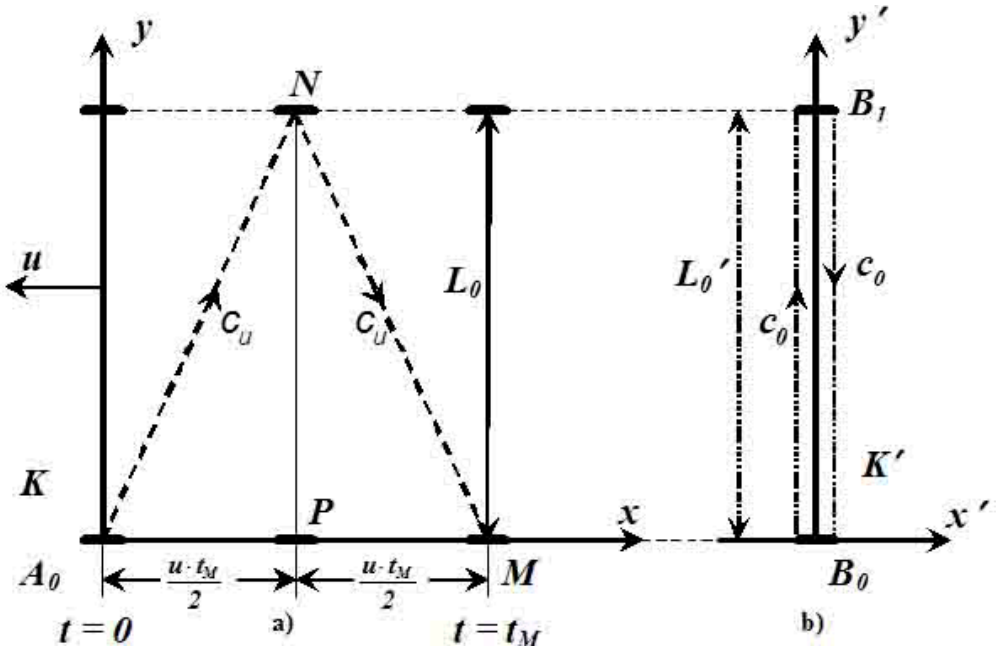

Figure 1. Propagation of light in a light clock in two IRF moving each with respect the other

a) propagation of light in a "moving" IRF K from a point of view of an observer resting in this "moving" IRF K, where light propagates along straight lines **A_0N, NM** at the light speed c_u;

b) propagation of light in a "stationary" IRF K' from a point of view of an observer resting in this "stationary" IRF K', where light propagates at the speed c_0.

Let us consider two IRF $\mathbf{K}'(x', y')$ and K (x, y) moving each with respect to another one at the velocity u (see Figure 1). In all points of the unprimed IRF K named with letters (points ***A_0, N, M***) there are clocks that are synchronized (show the same time at any time moment of the IRF *K*). The primed IRF $\mathbf{K}'$ in Figure 1 is a stationary

IRF. That means that an arbitrary light clock with stationary mirrors in points B_0 and B_1 of the primed IRF $\mathbf{K}'$ is at rest in this primed IRF $\mathbf{K}'$ and the moving unprimed IRF K is moving in a direction, that is parallel to planes of mirrors B_0 and B_1.

At the zero time moment $\mathbf{t_0} = \mathbf{t_0}' = \mathbf{0}$ of the both systems, when a point $\mathbf{B_0}$ of the IRF $\mathbf{K}'$ coincides with the point $\mathbf{A_0}$ of the IRF **K**, two light sources in the point $\mathbf{B_0}$ radiate simultaneously two light pulses, one of which propagates from the point $\mathbf{B_0}$ to a point $\mathbf{B_1}$ of the IRF $\mathbf{K}'$ and the second pulse propagates from the point $\mathbf{B_0}$ to the point $\mathbf{A_0}$, where a spot on the X axis of the unprimed coordinate system **K** is marked. When the light pulse radiated in the point $\mathbf{B_0}$ arrives to the point $\mathbf{B_1}$, a light source in the point $\mathbf{B_1}$ radiates a light pulse that puts a spot mark in a point **N** of the IRF **K.** Simultaneously a pulse arrived from the point $\mathbf{B_0}$ is reflected by the mirror in the point $\mathbf{B_1}$ and moves back to the point $\mathbf{B_0}$. When the pulse reflected from the point $\mathbf{B_1}$ arrives back to the point $\mathbf{B_0}$ a light source in the point $\mathbf{B_0}$ puts a spot mark in the point **M** of the IRF **K** and stops a clock situated in the point **M** (at a time moment $\mathbf{t_M}$).

Then an observer being at rest in the "moving" IRF ***K*** measures the optical length of light ray path $\boldsymbol{S = A_0N + NM}$ in the moving IRF ***K*** and makes read out of the indication $\boldsymbol{t_M}$ of the clock being at rest in the point ***M*** of the IRF ***K*** and being stopped at a moment, when the light pulse in the IRF $\mathbf{K}'$ returns back to the point $\boldsymbol{B_0}$ after reflection from the mirror in the point $\boldsymbol{B_1}$. Then the "light speed in vacuum of the moving IRF" may be calculated using the formula

$$c_u = \frac{S}{t_M}. \tag{3}$$

So the value "light speed in vacuum of the moving IRF" can be rather simply measured and calculated in the experiment, if the light in Figure 1 propagates in vacuum.

By the way, as the time moment t_M of the light pulse arriving to the point *M* of the IRF *K* coincides with a time moment of the light pulse returning back to the point B_0 in the IRF $\mathbf{K}'$, and the optical length of light pulse path $S = A_0N + NM$ in the IRF *K* is greater than optical length of the light pulse path $S' = 2L_0$ in the stationary IRF $\mathbf{K}'$, the value of "light speed in a moving IRF" c_u exceeds the value of "light speed in the stationary IRF" $c_0 = \frac{S'}{t_M}$, that means that $c_u > \boldsymbol{c_0}$. Thus, during the time travel of the light pulse from the point $\boldsymbol{B_0}$ to the point $\boldsymbol{B_1}$ and back from the point $\boldsymbol{B_1}$ to the point $\boldsymbol{B_0}$ at the speed c_0 in the stationary IRF $\mathbf{K}'$ the same light pulse performs in the moving IRF ***K*** a travel from the point $\boldsymbol{A_0}$ through the point ***N*** to the point ***M*** at the greater speed c_u. So, considering a rectangular triangle $\boldsymbol{A_0NP}$ in the Figure 1, we have

$$c_u^2 = c_0^2 + u^2 \tag{4}$$

or

$$c_u = \sqrt{c_0^2 + u^2}. \tag{5}$$

Now let us consider the same situation from the point of view of the SRT in Minkovski's four-dimensional world [[2], p. 12].

3. Real Physical Sense of the New Concept

Terletskiy [[3], p. 53] said "From a point of view of the four-dimensional geometry of space-time the real physical sense can be ascribed only to four-dimensionally covariant values. In mechanics of a particle such values are a four-dimensional scalar known as a proper mass ***m***, as well as four-dimensional vectors of the velocity $\vec{U}_k$, the acceleration $d(\vec{U}_k)/d(t)$ and the momentum $\vec{P}_k$".

First of all we shall consider now a four-dimensional vector of the velocity $\vec{U}_k$.

Formation of a four-dimensional vector (4-vector) of the velocity is introduced in the SRT similarly to a three-dimensional vector in the three-dimensional space, where position of a particle is specified by a three-dimensional radius-vector $\vec{r}$ and a three-dimensional vector of the velocity $\vec{v}$ is defined as a derivative from the three-dimensional radius-vector $\vec{V} = d\vec{r}/dt$.

To define a 4-vector of the velocity as a time derivative (Newton's fluxion) of the 4-vector $\vec{R}$ is prohibited in the SRT. We require a 4-vector of velocity therefore we may divide the increment $d\vec{R}$ of a four-dimensional radius $\vec{R}$ only by a scalar. In the SRT neither the time, nor its differential are invariants of the Lorentz's transformation. Therefore in the SRT we can take as an invariant value depending upon time either the four-dimensional interval

$$ds^2 = c_0^2dt^2 - dx^2 - dy^2 - dz^2 = c_0^2dt'^2, \tag{6}$$

or the proper time

$$d\tau = \frac{ds}{c_0} = dt\sqrt{1-V^2/c_0^2} = \frac{dt}{\gamma}, \tag{7}$$

where $\gamma = \frac{1}{\sqrt{1-V^2/c_0^2}}$ is the relativistic factor and ***V*** is the velocity of a particle.

So, let us introduce a 4-vector of a particle velocity

$$\vec{U} = \frac{d\vec{R}}{d\tau}. \tag{8}$$

In the coordinate representation this 4-vector of the velocity $\vec{U}$ can be written in the following way

$$u_i = \frac{dR_i}{d\tau}, \tag{9}$$

where i = 1, 2, 3, 4.

It is well known that three first derivatives in the formula (9) can be written as

$$u_\alpha = \frac{dx_\alpha}{d\tau} = \gamma\frac{dx_\alpha}{dt} = \gamma V_\alpha, \tag{10}$$

where α = 1, 2, 3; $V_\alpha = dx_\alpha / dt$ are projections of the 3-vector $\vec{V}$ onto the respective coordinate axes (***x, y, z***).

The values, defined by equalities (10), are the first three components of 4-dimensional Galilean vector $\vec{U}$ changing from zero to infinity (hereinafter the velocity, changing from zero to infinity we can name as Galilean velocity and designate it with a letter ***u***, in order to distinguish it from the Lorentz's velocity, changing from zero to the velocity of light in vacuum of the stationary IRF c_0, that we hereinafter will designate using a latter ***V***. At that relation between Lorentz's and Galilean velocities are defined by means of equalities [4]

$$u = \frac{V}{\sqrt{1 - V^2/c_0^2}}, V = \frac{u}{\sqrt{1 + u^2/c_0^2}}. \quad (11)$$

Taking into account that in the SRT $R_4 = c_0 t$, as well as the equation (7), let us find the fourth component of the 4-velocity. We obtain

$$u_4 = \frac{dR_4}{d\tau} = \gamma \frac{d(c_0 t)}{dt} = \gamma c_0. \quad (12)$$

As from equalities (7), (11) and (12) it follows that

$$\gamma = \frac{1}{\sqrt{1 - V^2/c_0^2}} = \sqrt{1 + u^2/c_0^2}, \quad (13)$$

then in the moving IRF (if $V \neq 0$, $\gamma \neq 1$) we obtain $u_4 = \gamma c_0$.

Consequently, the value

$$u_4 = \gamma c_0 = c_u = \frac{c_0}{\sqrt{1 - V^2/c_0^2}} = c_0 \sqrt{1 + u^2/c_0^2}, \quad (14)$$

which is the fourth component of the 4-velocity of a particle in vacuum of a moving IRF, we define as the light speed in vacuum of a moving IRF.

Physically the light speed c_u in vacuum of a moving IRF can be in the SRT not equal to the value c_0 because of change of the longitudinal (along direction of movement) size of moving vacuum volumes in the result of which the values of the dielectric permittivity and magnetic permittivity of vacuum volumes can also be changed.

4. New Calculation of a Time Measurement Unit of a Moving Light Clock

Now (**after introduction of the definition for the 4-velocity of light in vacuum of a moving IRF**) let us take a light clock (two parallel mirrors at a distance each from another equal to L_0, in the very *IRF*, where this light clock is at rest, between which, alternatively reflecting, a light pulse is circulating, on one of mirrors a source of light pulse, photo diode and pulse counter are situated).

The unit of time measurement of this light clock, stationary in an immovable IRF, is determined by equality (1).

Now let this light clock move so that planes of the both mirrors of this light clock are perpendicular to the light clock direction of movement.

As we have determined earlier, see equality (14), the light in vacuum of a moving IRF propagates at the speed

$$c_u = \gamma c_0, \quad (15)$$

where c_0 is the speed of light in vacuum of a stationary IRF; γ is the relativistic factor determined by expressions (13).

Then after radiation of the light by a source, situated on the backward mirror of the light clock, the velocity of light closing with the foremost mirror of the light clock will be equal to $(c_u - u)$, and the velocity of light closing with the backward mirror after light reflection from the foremost mirror will be equal to $(c_u + u)$, where c_u is the velocity of light in vacuum of a moving IRF, ***u*** is the Galilean velocity of light clock. Therefore the unit of time measurement by the moving light clock will be determined by the formula:

$$E = \frac{L}{(c_u - u)} + \frac{L}{(c_u + u)}, \quad (16)$$

where $L = \frac{L_0}{\gamma}$ is the distance between mirrors of the moving light clock, measured in the IRF, with respect to which this light clock moves at the speed ***u***.

Having substituted into the formula (16) the values $L = \frac{L_0}{\gamma}$, $c_u = \gamma c_0$ and $\gamma = \sqrt{1 + u^2/c_0^2}$, we shall obtain that

$$E = \frac{2L_0}{c_0}. \quad (17)$$

Thus, using the above stated new physical concept the time measurement unit of the moving light clock becomes equal to time measurement unit of the stationary clock (the right part of the formula (17) coincides with the right part of the formula (1)).

Now let us return to a case, shown in Figure 1, when the light clock is situated so that planes of its parallel mirrors are parallel to the direction of light clock movement.

A time interval between radiation of a light pulse from the point B_0 and its return to the same point B_0 in the stationary IRF $\mathbf{K}'$ after reflection from the mirror in the point B_1 is equal to

$$\Delta t' = \frac{2 \cdot L_0}{c_0}. \quad (18)$$

If we designate with symbols Δt a time interval in the moving IRF ***K*** between radiation of the same light pulse from the point A_0 and a moment of its arrival to the point ***M,*** then the path passed by this light pulse in the moving IRF K can be determined using the Pythagorean theorem

$$S = 2\sqrt{L_0^2 + \left(\frac{u\Delta t}{2}\right)^2}. \quad (19)$$

But the IRF *K* moves with respect the stationary IRF $\mathbf{K}'$ at the speed ***u*** (Galilean speed). Therefore we must consider, that speed of propagation of this light signal in the moving IRF *K* along straight lines A_0N and ***NM*** is determined according to the expression (15) (this means that it is equal to the speed of light in vacuum of the

moving IRF). As a consequence the time interval $\Delta t = t_M - t_0$ (where t_0 is a time moment of light pulse emission in point A_0) can be determined by dividing the light path S, determined by the equation (19), by the speed of light in the moving IRF K, determined by the expression (15). We shall obtain

$$\Delta t = \frac{2 \cdot \sqrt{L_0^2 + \left(\frac{u\Delta t}{2}\right)^2}}{c_0 \gamma}. \quad (20)$$

Solving the equation (20) with respect to the value Δt, we have

$$\Delta t = \frac{2 \cdot L_0}{[c_0 \sqrt{\gamma^2 - (u/c_0)^2}]}. \quad (21)$$

Taking into account the equality (13), the expression (21) takes the form

$$\Delta t = \frac{2 \cdot L_0}{c_0}. \quad (22)$$

The formulas (18) and (22) mean that the time interval between some two events in the moving IRF ***K*** connected with propagation of light is equal to the time interval between the same events in the stationary IRF $\mathbf{K}'$.

Consequently, introduction of the concept "**the speed of light in vacuum of a moving IRF**" excludes from the space-time theory such an effect as time dilation in the moving IRF and converts into the unscientific space opera the statement about possibility of journey in the future of the Earth by means of long traveling in space at large speeds (close to the speed of light).

5. New Space-time Theory and the Velocity Addition Laws

Introduction of the concept "**the speed of light in vacuum of a moving IRF**" excludes from the space-time theory such an effect as time dilation in the moving IRF and the so called Einstein's SRT needs to be replaced by a new space-time theory, based upon only one relativity postulate. Such a theory was developed and published in [5]. Main content of the paper [5] is as follows: A new relativistic space-time theory (NRSTT) based upon a single principle of relativity is considered. A new concept of "speed of light in vacuum of a moving inertial reference frame" (IRF) is introduced, depending upon speed of the IRF motion according to a quadratic formula. This dependence provides introduction of a new and uniform understanding of such astronomical phenomena as microwave background radiation, red shift of far star spectrums becoming more shifted as the distance to a star increases, novae and supernovae, pulsars, object SS-433 etc. These astronomical phenomena are considered from a point of view of NRSTT with more details in [6].

Coordinates and time transformations of the NRSTT have the form

$$c_u t = \gamma(c_0 t' + \beta x'), x = \gamma(x' + \beta c_o t'), y = y', z = z', \quad (23)$$

$$c_0 t' = \gamma(c_u t - \beta x), x' = \gamma(x - \beta c_u t), y' = y, z' = z, \quad (24)$$

where $c_u = \gamma c_0$, $\gamma = \frac{1}{\sqrt{1-\beta^2}}$, $\beta = \frac{u}{c_u}$, x, y, z, t and x', y', z', t' are coordinates and time of any event in the unprimed and primed IRF, respectively, u is the speed of one IRF with respect to another one.

These transformations provide invariance of the four-dimensional interval and give a possibility to detect real properties of moving bodies: contraction of their longitudinal sizes without time dilation, without prohibition of superlight speeds, without dependence of mass upon the speed, but with dependence of particles electrical charge values upon their speeds. A solution of the muon-electron universality problem is given and an approach to the merchantable method of cold nuclear fusion is discussed.

In the NRSTT there is its own law of speeds addition. It can be written in two forms: 1) the first one is

$$w = v\,\gamma_s + s\,\gamma_v, \quad (25)$$

where $\gamma_s = \sqrt{1 + \frac{s^2}{c_0^2}}$; $\gamma_v = \sqrt{1 + \frac{v^2}{c_0^2}}$; v, s are the summands; w is a sum of two summands, w is a sum of two speeds (*v, s, w are Galilean speeds*) and the second form is

$$\beta_w = \frac{\beta_u + \beta_s}{1 + \beta_u \beta_s}, \quad (26)$$

where $\beta_u = \frac{u}{c_0\,\gamma_u}$; $\beta_s = \frac{s}{c_0\,\gamma_s}$; $\beta_w = \frac{w}{c_0\,\gamma_w}$; u, s, w are Galilean speeds (they can vary from zero to infinity).

6. Conclusion

The latest and most advanced (simplest) considerations of the NRSTT issues are made in a report for the Congress-2016 "Fundamental problems of natural sciences and engineering" in Saint-Petersburg [7].

The report [7] considers self-contradictoriness of Einstein's SRT and a new relativistic space-time theory based upon the only relativity principle, without ban of superlight speed, without lag of a moving light clock with respect to a stationary light clock (without time dilation) and with dependence of a particle electrical charge upon its speed of motion. A new concept "light speed in a moving inertial frame of reference" is considered, which provides equality of time measurement units in a moving light clock and in a stationary light clock. It is shown in the report that experiments on particle accelerators do not contradict the new theory, if the known experiment by Neddermeyer S.H. and Anderson C.D., earlier considered to be experimental confirmation of existence in nature of particles with a mass intermediate between the mass of a proton and the mass of an electron, is interpreted in favor of experimental detection of charge dependence upon speed and superlight speeds.

The content of the report [7] is given below (numbers of pages are given in accordance with [7]):

- Introduction (p. 91),

1. Self-contradictoriness of Einstein's SRT (p. 92),

2. Derivation of coordinates and time transformations of the NRSTT (p. 95),

3. Absence of prohibition for superlight speeds of motion (p. 99),

4. Transformation of electromagnetic field parameters in the NRSTT (p. 100),

5. New relativistic particle dynamics (p. 103-116),

6. Alternative interpretation of the experiment by Anderson and Neddermeyer in 1938 (p. 117),

- References (17 items) (p.p. 119-120),

- Translation into Russian of the paper by Neddermeyer S.H., Anderson C.D. “Cosmic-ray particles of intermediate mass” (p.p. 120-122).

So, the answer to a question put in the title of this article (why the second postulate is superfluous) is the following: Einstein’s second postulate is superfluous because it is wrong, the law of light propagation in a moving inertial reference frame is a consequence of the relativity postulate and the space-time theory can be constructed basing upon not two, but only one postulate – principle of relativity (according to Occam’s razor principle). It is important to underline that the constancy of light speed is not necessary now because it is wrong, and prohibition of superlight speeds is also wrong. Both light and particles are allowed to move at any speed whatever great it could be. And Einstein’s second postulate is wrong for the reason that the time measurement unit for a moving light clock is not equal to the time measurement unit of a stationary light clock if the second postulate is true. But they should be equal in order to prevent determination which of two IRF moving each with respect the other uniformly and rectilinearly is at rest by measuring a value of the time measurement unit.

Acknowledgments

I am grateful to reviewers for their contributions to improve the paper.

References

[1] Einstein A. On Electrodynamics of moving bodies, June 30, 1905, [url]http://www.fourmilab.ch/etexts/einstein/specrel/www/[/url].

[2] Minkovski G. Space and time. In book. “Principle of Relativity”, M., Atomizdat, 1973, p.167 (in Russian).

[3] Terletsky Y.P. Paradoxes of Special Relativity, M. Nauka, 1966, p. 53 (in Russian).

[4] Rapier P.M. A recent application of detection and estimation practices in radio and radar astronomy. Spectroscopy Letters, 4 (9), 303-311 (1971).

[5] Mamaev A.V. New Relativistic Space-Time Theory. “The Way of Science”/ 2014. No.1 (1), p.p. 10-84. (In Russian). [url]http://scienceway.ru/d/706321/d/the-way-of-science--1-%281%29-march.pdf[/url]

[6] Mamaev A.V. “Astronomical phenomena disprove Einstein’s Special Relativity Theory, “The Way of Science”/ 2014. No.5 (5). p.p. (10-19).

[7] Mamaev A.V. New Relativistic Space-Time Theory. International Congress-2016 “Fundamental Problems of Natural Sciences and Engineering”, Saint Petersburg. July 25-30 2016. In a book Congress-2016 Proceedings “Fundamental problems of natural sciences and engineering”. Issue 37-2, p.p. 91-122 (In Russian).

International Journal of Physics, 2016, Vol. 4, No. 6, 146-151
Available online at http://pubs.sciepub.com/ijp/4/6/1

DOI:10.12691/ijp-4-6-1

Measurement of Radon Exhalation Rate from Destroyed Building Material in the Gaza Strip

M.O. El-Ghossain*

Department of Physics, The Islamic University of Gaza, Gaza, Palestine
*Corresponding author: ghossain@iugaza.edu.ps

Abstract Building materials are one of the potential sources of indoor radioactivity because of the naturally occurring radionuclides in them. Radon exhalation rate is one of the most important factors for evaluation of the environmental radon level. Radon contributes more than half of the total ionizing radiation dose Indoor radon has been recognized as one of the health hazards for mankind because long-term exposure to radon increases the risk of developing lung cancer. This study aims at assessing the contribution of destroyed building materials in war 2014 towards the total indoor radon exposure to the inhabitants of in Gaza. 40 Samples have been collected from common destroyed building materials in Jabalia district. The closed-can technique has been employed in this study using solid state nuclear track detectors (CR-39). After 124 days of exposure to radon, CR-39 detectors were etched chemically by (6 N) NaOH solution at 75°C for three months and then counted under an optical microscope. Results obtained from the current study show that radon exhalation rates from concrete and asbestos have relatively high values as compared to other building materials while glass, marble and a red brick contribute less to radon exhalation rate. The average radon exhalation rate in term of area in the studied samples ranged from (86.506) $mBq.m^{-2}.h^{-1}$ for glass samples to (469.017) $mBq.m^{-2}.h^{-1}$ for Concrete samples. In general, the annual effective doses from the investigated building materials are low and under the global value (from 1 to 5 mSv/y) except for Concrete and asbestos samples with average values (9.464) and (9.3528) mSv/y, respectively.

Keywords: *radon, CR39, calibration, building materials*

Cite This Article: M.O. El-Ghossain, "Measurement of Radon Exhalation Rate from Destroyed Building Material in the Gaza Strip." *International Journal of Physics*, vol. 4, no. 6 (2016): 146-151. doi: 10.12691/ijp-4-6-1.

1. Introduction

All building materials contain various amounts of main natural radionuclides of the uranium (^{238}U) and thorium (^{232}Th) series, and since those radionuclides are sources of Radon gas then the knowledge of the natural radioactivity of building materials is important for the determination of population exposure to radiations. For the aforementioned reasons we intend to study the concentration of Radon and the exhalation rate from destroyed building materials in the 2014 war used in the districts of Jabalia in the northern Gaza Strip [1,2,3,4,5]. It will then be compared to results obtained with the results of previous studies. Then we will study the health risks of radon gas.

In this study, we present our data concerning measurement of the radon exhalation rate from destroyed building material samples collected from Jabalia district in the Gaza strip in Palestine using close vessel technique. The location of this district is shown in Figure 1. Houses in this district are mainly constructed from soil, bricks, cement, sand, granite and marble. This district is located in the northern part of the Gaza strip of Palestine.

This study was done during the month of March to July 2015, which includes the following main stages, where the samples are collected from destroyed building materials.

The purpose of this study is to measure the Radon exhalation rates from destroyed building materials during 2014 war against Gaza, Palestine. Our study will include samples of a red brick, marble, ceramic, concrete, tiles, asbestos, glass and building stones from different origins used in the mentioned area of study.

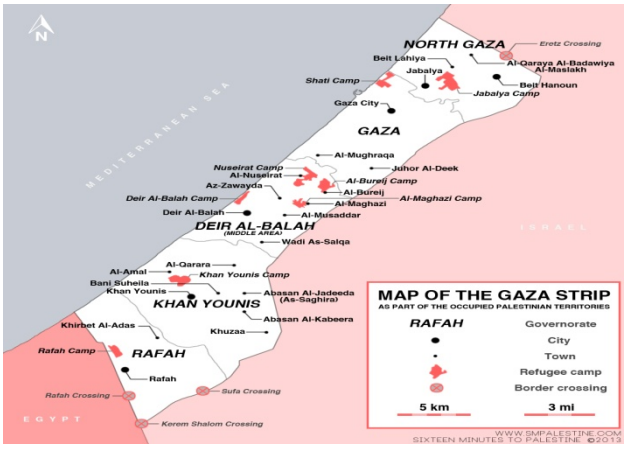

Figure 1. The figure shows the map of the Gaza strip

In a previous studies, in Egypt, a study on ^{222}Rn exhalation rate from Egyptian building materials was performed in 2009 and found that the radon exhalation rate in the studied samples ranged from (2.2 x 104 ± 7.2 x102) μBq m^{-2} s^{-1}, for granite sample, to (3.4x101 ± 9.0x100) μBqm^{-2} s^{-1}, for portland cement with an average value (1.8x103 ± 6.5x101) μBq m^{-2} s^{-1} [6]. In Nablus

district, Palestine, They measured Radon exhalation rates from granite and marble have relatively high values as compared to other building materials followed- in order- by cement, ceramic, concrete, building stones, and porcelain, while gypsum, sand, gravel and bricks contribute less to radon exhalation rate which was found to range from (55.37 ± 15.01) mBq/m^2h for gypsum samples to (589.54 ± 73.24) mBq/m^2h for granite samples, with a total average value of (268.56 ± 166.21) mBq/m^2h. The corresponding radon concentration, effective radium content, and annual effective dose average values were (148.49 ± 91.13) Bq/m^3, (1.93 ± 1.20) Bq/Kg and (3.74 ± 2.30) mSv/y [7].

2. Materials and Experimental Methods

Different samples of destroyed building materials after the 2014 war against Gaza were collected randomly from different destroyed buildings, like, houses, commercial companies, and factories, all around the area of study during the month of March to July. Samples were a red brick, marble, ceramic, concrete, tiles asbestos, glass and building stones, samples were from different origins, used in construction of building in Jabalia district, Gaza Strip, Palestine. Samples were then identified and given a number and an identifying symbol which identify the location of the samples, as in Table 1. 5 kg from each sample were collected and dried in a temperature controlled furnace (oven) at a temperature100°C for two hours to ensure that moisture was completely removed. And then the samples were crushed to a fine powder and sieved through a small mesh size to remove the larger grains size and render them more homogenous. The respective net weights of the samples ready for measurement were recorded.

Table 1. List of numbers and codes for samples studied in this research

Sample NO.	Sample code	Type	Sample NO.	Sample code	Type
1	G1	ceramic	21	A1	building stones
2	G2	ceramic	22	A2	building stones
3	G3	ceramic	23	A3	building stones
4	G4	ceramic	24	A4	building stones
5	G5	ceramic	25	A5	building
6	F1	red brick	26	D1	marble
7	F2	red brick	27	D2	marble
8	F3	red brick	28	D3	marble
9	F4	red brick	29	D4	marble
10	F5	red brick	30	D5	marble
11	B1	concrete	31	H1	asbestos
12	B2	concrete	32	H2	asbestos
13	B3	concrete	33	H3	asbestos
14	B4	concrete	34	H4	asbestos
15	B5	concrete	35	H5	asbestos
16	E1	tiles	36	C1	glass
17	E2	tiles	37	C2	glass
18	E3	tiles	38	C3	glass
19	E4	tiles	39	C4	glass
20	E5	tiles	40	C5	glass

The close vessel technique was used in this study “can technique” or we call them “Dosimeters”. Dosimeters are plastic cylindrical vessels of volume (7.93×10^{-4}) m^3 with cross sectional area of (5.02×10^{-3} m^2) as shown in figure 2. The destroyed building material samples were put at the bottom of these vessels. About 200 g of each sample was placed in a plastic can of dimensions15.8 cm in height and 8 cm in diameter.

The use of plastic solid-state nuclear track detectors, SSNTDs of type CR-39, which were cut into small pieces, 2cm×2cm and fixed on the top of inner surface of the can, in such a way that its sensitive surface always facing the sample. The can was sealed air tight with adhesive tape and kept for assessment of radon exhalation for exposure evaluation over four months. During the exposure period (one hundred and twenty four days), the detector was exposed freely to the emergent radon from the sample in the can so that it could record alpha particles resulting from the decay of radon in the remaining volume of the can [3,4,5,6,7,8].

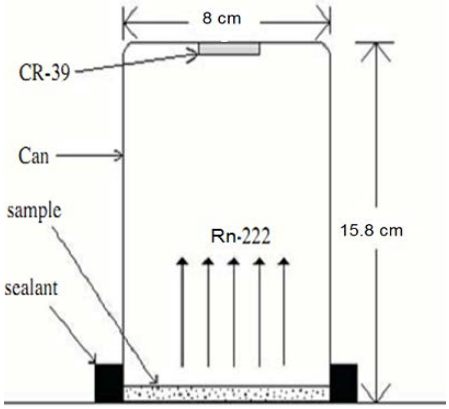

Figure 2. CR-39 set up for Radon Detection

After the mentioned period, forty detectors were taken out of the dosimeters. The detectors were then chemically etched in 6 N-solution of Sodium Hydroxide (Na OH) at a temperature of 70 C for four hours and one third of an

hour. The etching process was performed at chemistry Laboratories at An-Islamic University using the setup. In addition, the function of the condenser is to keep the concentration of the Na OH solution constant, and the function of the thermometer is to make sure that the temperature is constant during the whole period of the etching process. After four hours and one third of an hour detectors were washed by running and distilled water and then dried to remove any remaining amount of the etchant from the surface of the detectors. By now alpha tracks formed on the detectors were ready for scanning and counting.

A digital optical microscope with 400 times magnification was used to count the number of tracks per field of view; about ten fields of view were scanned randomly for each detector. Tracks of alpha particles emitted by radon in a CR-39 detector were scanned by the microscope as shown in Figure 3. The area of the field of view was calculated by the digital microscope and found to be equal about 5.3×10^{-3} cm^2 ; the average number of tracks per field of view was used to calculate the track density. The calculated track density was converted into radon concentrations in Bq/m^3 using the calibration factor (k) obtained by the standard manufacturer, where every track per cm^2 per day on the CR-39 detectors corresponds to an exposure of 12.5 Bq/m^3 for the activity of radon gas and its daughters and we use previous calibrations [6,7,8].

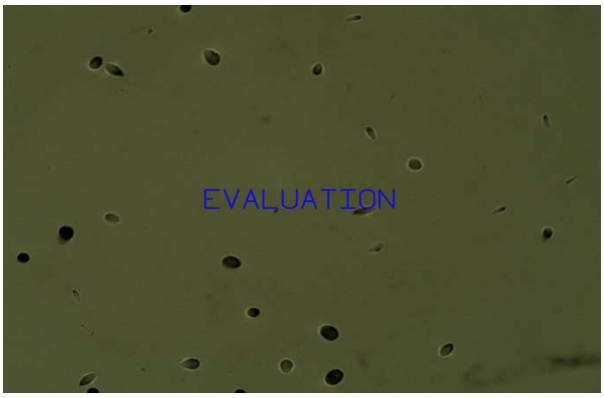

Figure 3. Tracks of alpha particles emitted by radon in a CR-39 detector. One viewing field from the microscope has the area of about 0.53 mm^2

Calculations:

The radon concentrations, radon exhalation rate were calculated using the experimental measured average track densities according to the following relations from previous studies [7,8,9,10].

2.1. Determination Radon Concentration:

$$C_{Rn} = k\frac{\rho}{T_{eff}} \qquad (1)$$

C_{Rn}: is the radon concentration (Bq/m^3)
K: is the calibration factor = 12.5 Bqm^{-3}/tracks $cm^{-2}h^{-1}$.
ρ : Is the track density (tracks/ cm^2)
T_{eff}: effective time = $[t + (e^{-\lambda t} - 1)/\lambda]$
t: exposure time

2.2. Determination Radon Exhalation Rate in Area

The radon exhalation rate (Ex) of any sample is defined as the flux of radon released from the surface of material. The surface exhalation rate in the building material samples was calculated using equation (2), the radon exhalation rate in terms of area (surface exhalation rate) in units of $Bq\cdot m^{-2}\cdot h^{-1}$ can be obtained by as [8,9,10,11,12].

$$E_x = \frac{CV\lambda}{A[t + (e^{-\lambda t} - 1)/\lambda]} \qquad (2)$$

Where:
C: is the integrated radon exposure ($Bq\cdot m^{-3}\cdot h$);
V: is the volume of air in the cup (m^3) = $7.942\times10^{-4}m^3$
λ: is the decay constant for Rn^{222} (h^{-1}) = $7.56\times10^{-3}h^{-1}$
A: is the surface area of the sample (m^2) = $5.0265\times10^{-3}m^2$
t: is the exposure time (h) = 124 days = 2976h

2.3. Determination Radon Exhalation Rate in Mass

The mass exhalation rate ($Bqkg^{-1}\cdot h^{-1}$) in the building material samples is calculated using the following formula 3:

$$E_M = \frac{CV\lambda}{M[t + (e^{-\lambda t} - 1)/\lambda]} \qquad (3)$$

Where E_M is the mass exhalation rate in ($Bqkg^{-1}\cdot h^{-1}$) and M is the mass of sample (kg) [8-15].

2.4. Determination the Annual Effective Dose

The following equation was used to calculate the annual effective dose as in equation 4:

$$\text{Dose} = \epsilon f_{Rn} T_y C_{Rn} \qquad (4)$$

Where:
f_{Rn}: is the conversion factor = 9 nSv / (Bq h m-3).
T_y: is the time spent indoors per year = 7000 hours
□ is the equilibrium factor (= 0.4)
C_{Rn} : is the radon concentration.

Substituting the previous parameters in equation (4) we can evaluate the annual effective dose simply according to the following relation 5 [16,17,18].

$$\text{Dose}(\text{mSv/y}) = 0.0252\text{x}C_{Rn}. \qquad (5)$$

3. Results and Discussion

Results and discussion for radon concentrations, radon exhalation rate in terms of area E_x, and radon exhalation rate in term of mass E_m for destroyed building material samples used in Jabalia city are given in this chapter. Equations 1, 2, 3 and 5 respectively were used for calculating radon concentrations, radon exhalation rate in term of area, E_x, radon exhalation rate in terms of mass, E_m, and Annual Dose for destroyed building material samples used in this study which include a red brick, marble, ceramic, concrete, tiles, asbestos, glass, and building stones. The results of Radon concentration only is shown in Table 2 for all building materials.

But radon exhalation rate in terms of area E_x, and radon exhalation rate in term of mass E_m, and annual effective dose for Ceramic is shown in Table 3.

The radon exhalation rate in terms of area E_x, and radon exhalation rate in term of mass E_m, and annual effective dose for each individual sample collected from Jabalia area are summarized in Table 3.

Table 2. Radon concentration only is shown in Table 2 for all building materials

NO.	code	Type	C_{Rn} Bq/m^3	NO.	code	Type	C_{Rn} Bq/m^3
1	G1	Ceramic	64.19	21	A1	stones	90.34
2	G2	Ceramic	80.83	22	A2	stones	145.82
3	G3	Ceramic	114.12	23	A3	stones	128.38
4	G4	Ceramic	205.41	24	A4	stones	209.22
5	G5	Ceramic	73.70	25	A5	stones	186.40
Average 107.65				**Average 152.03**			
6	F1	red brick	104.61	26	D1	marble	39.78
7	F2	red brick	114.12	27	D2	marble	77.98
8	F3	red brick	99.85	28	D3	marble	76.08
9	F4	red brick	66.57	29	D4	marble	124.49
10	F5	red brick	38.04	30	D5	marble	102.23
Average 84.63				**Average 84.11**			
11	B1	Concrete	337.60	31	H1	asbestos	267.86
12	B2	Concrete	274.20	32	H2	asbestos	395.96
13	B3	Concrete	383.57	33	H3	asbestos	408.93
14	B4	Concrete	422.24	34	H4	asbestos	492.93
15	B5	Concrete	460.28	35	H5	asbestos	290.05
Average 375.58				**Average 371.14**			
16	E1	Tiles	133.14	36	C1	glass	49.92
17	E2	Tiles	177.52	37	C2	glass	48.90
18	E3	Tiles	190.20	38	C3	glass	114.12
19	E4	Tiles	180.69	39	C4	glass	98.90
20	E5	Tiles	134.87	40	C5	glass	34.23
Average 163.28				**Average 69.21**			

Table 3. Summary of results of the average radon exhalation rate in terms of area Ex, radon concentration, radon exhalation rate in terms of mass Em and the annual effective dose from all destroyed building materials used in Jabalia district using standard calibration [6,7,8,9,10]

Sample Type	C_{Rn} (Bq/m^3)	E_x (mBq.m^{-2}.h^{-1})	E_m (mBq.Kg^{-1}.h^{-1})	Dose (mSv.y^{-1})
Concrete	375.58	469.017	11.799	9.464
asbestos	371.14	463.895	11.659	9.3528
Tiles	163.28	204.087	5.129	4.1144
building stones	152.03	190.025	4.776	3.831
Ceramic	107.65	133.92	3.57	2.7126
red brick	84.63	105.945	2.658	2.1324
Marble	84.11	105.130	2.642	2.1194
glass	69.21	86.506	2.174	1.744
Aver.	175.95	219.815	5.550	4.433

The data listed in Table 1 clearly show that concrete, tiles, building stones and asbestos are have high radon exhalation rate in terms of area E_x, radon concentration, radon exhalation rate in terms of mass E_m and the annual effective dose. But the glass have low radon exhalation rate in terms of area E_x, radon concentration, radon exhalation rate in terms of mass E_m and the annual effective dose.

The Figure 4 shows the comparison between destroyed building materials in terms of the average radon exhalation rates in term of area where the concrete have the highest value with 469.017 mBq.m^{-2}.h^{-1} then asbestos with 463.895 mBq.m^{-2}.h^{-1} then (tiles, building stones, ceramic, a red brick, marble and glass) with (204.087, 190.025, 133.92, 105.945, 105.130 and 86.506) mBq.m^{-2}.h^{-1} respectively. Note that the glass have the lowest value of the materials studied.

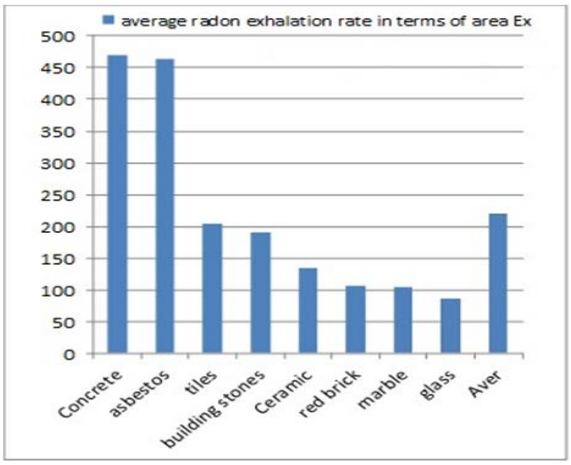

Figure 4. This figure shows the Comparing histogram for the average radon exhalation rates in term of area.

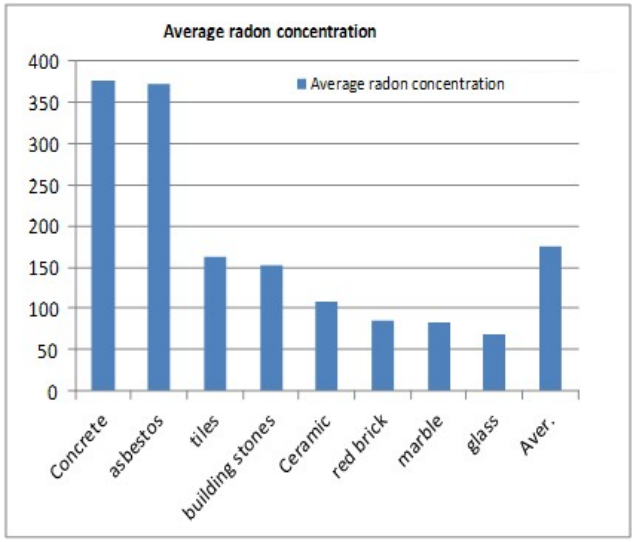

Figure 5. This figure shows the Comparing histogram for the average radon concentration rates

The Figure 5 shows the comparison between destroyed building materials in terms of the average radon concentration rates where the concrete have the highest value with 375.580 By/m^3 then asbestos with 371.140 By/m^3 then (tiles, building stones, ceramic, a red brick, marble and glass) with(163.280, 152.030, 107.650, 84.630, 84.110 and 69.210) respectively. Note that the glass has the lowest value of the materials studied.

The Figure 6 shows the comparison between destroyed building materials in terms of the average radon exhalation rates in term of mass where the concrete have the highest value with 11.799 mBq.kg^{-1}.h^{-1} then asbestos with 11.659 mBq.kg^{-1}.h^{-1} then (tiles, building stones, ceramic, a red brick, marble and glass) with (5.129, 4.776, 3.570, 2.658, 2.642 and 2.174) mBq.kg^{-1}.h^{-1} respectively. Note that the glass has the lowest value of the materials studied.

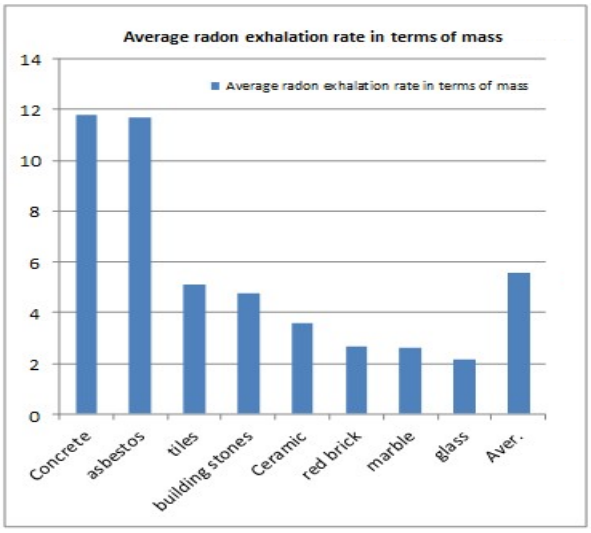

Figure 6. This figure shows the Comparing histogram for the average radon exhalation rates in term of mass

The Figure 7 shows the comparison between destroyed building materials in terms of the average annual effective dose for radon gas where the concrete have the highest value with 9.464 msv.y^{-1} then asbestos with 9.352 msv.y^{-1} then (tiles, building stones, ceramic, a red brick, marble and Glass) with (4.114, 3.831, 2.712, 2.132, 2.119 and 1.744) msv.y^{-1} respectively. Note that the glass has the lowest value of the materials studied.

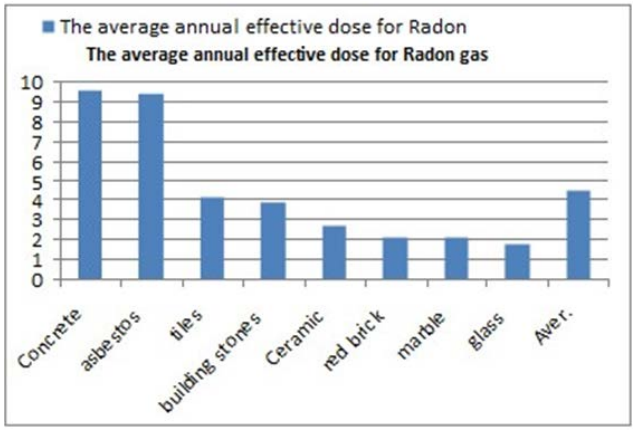

Figure 7. This figure shows the Comparing histogram for the average annual effective dose for radon gas

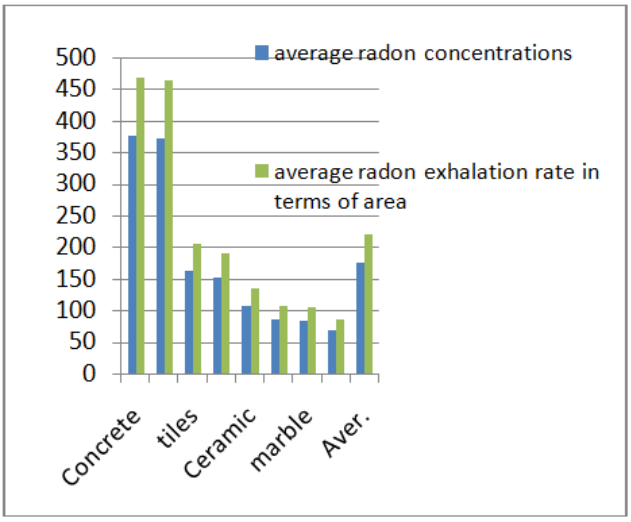

Figure 8. This figure shows the Comparing histogram for the average radon concentrations (C_{Rn} Ave.) and exhalation rates (E_x Ave.) from building materials used in Jabalia district

In Figure 8 We notice that, the concrete have the highest value of the average radon concentration and the average radon exhalation rate in term of area E_x, then (asbestos, tiles, building stones, ceramic, a red brick, marble and glass) respectively.

4. Conclusion

Using the closed can technique and the solid state nuclear track detectors (CR-39), we measured the radon exhalation rate from building material samples used in Jabalia in order to assess the contribution of individual material (e.g. red brick, marble, ceramic, concrete, tiles, asbestos, glass, and building stones) to the total indoor radon exposure of the inhabitants of Jabalia district. The corresponding radon concentration, and the annual effective dose were determined and compared with the effective dose limit values recommended by the National Council on Radiation Protection which (from 1 to 5 mSv/y). Results obtained from the current study show that the radon exhalation rates from asbestos and concrete have

relatively high values as compared to other building material samples followed red brick, marble, ceramic, tiles, glass, and building stones contribute less to the indoor radon. From the results of our study we can conclude that the Concrete have the maximum values of radon concentrations 375.58Bq/m^3, radon exhalation rate in term of area469.017mBq.m^{-2}.h^{-1}, radon exhalation in term of mass 11.799 mBq.Kg^{-1}.h^{-1} and the annual effective dose 9.464 mSv.y^{-1},also asbestos have maximum values of radon concentrations 371.14 Bq/m^3, radon exhalation rate in term of area 463.895 mBq.m^{-2}.h^{-1}, radon exhalation rate in term of mass 11.659 mBq.Kg^{-1}.h^{-1} and the annual effective dose 9.3528 mSv.y^{-1}. But the glass have the minimum values radon concentrations 69.21 Bq/m^3, radon exhalation rate in term of area 86.506 mBq.m^{-2}.h^{-1}, radon exhalation rate in term of mass 2.174 mBq.Kg^{-1}.$h^{-1}$and the annual effective dose 1.744 mSv.y^{-1}. In comparison with the annual effective dose of Radon by NCRP, we found that concrete and asbestos are 9.46 and 9.35 mSv/y, are much higher than the proposed limit which is 1 to 5 mSv/y, and all other material are below the limit. There are many researchers studied radon gas for building materials, comparison with previous studies will be shown in following tables, the results obtained in Sudan are in Table 4 [19]:

Table 4. Results from Sudan (Elzain) [19]

Sample Type	CRn (Bq/m^3)	Ex (mBq.m^{-2}.h^{-1})	Em (mBq.Kg^{-1}.h^{-1})	Dose (mSv.y^{-1})
Ceramics	128	240	2.84	3.59
Red brick	190	355	4.21	5.32
Block	197	369	4.37	5.52
Ispistos	214	402	4.76	6.01

The results obtained in Palestine are in Table 5 [7]:

Table 5. Results from Palestine (Shoqwara) [7]:

Sample Type	CRn (Bq/m^3)	Ex (mBq.m^{-2}.h^{-1})	Em (mBq.Kg^{-1}.h^{-1})	Dose (mSv.y^{-1})
marble	240.55	438.79	3.01	6.06
ceramic	193.71	347.42	2.59	4.88
concrete	179.37	325.38	2.46	4.52
building stones	147.00	268.59	1.95	3.70

All these results are close to the values we have for the building materials we studied.

References

[1] Maher O. El-Ghossain, Abedalqader A. Abu Shammala, "Radioactivity measurements in tap water in Gaza Strip (Al-Naser Area)" Journal of the Association of Arab Universities for Basic and Applied Sciences (2012) 11, 21-26.

[2] El-Ghossain, M.O., Abusaleh, Raed M., 2007. Measurement of radiation concentration in soil at middle of Gaza Strip using different type of detectors. The Islamic University Journal 15 (1), 23-37.

[3] Raed.M.Abusaleh, "Measurement of Radiation concentration in Soil at middle Gaza strip", Islamic University of Gaza, 2005.

[4] Mahmoud Rasas. Measurement of Radon and its Daughter's Concentration Indoor and Outdoor throughout Gaza Strip, thesis, Islamic University of Gaza, 2003.

[5] Nabil Hamed, Measurement of Radon Concentration in Soil at North Gaza, thesis, Islamic University of Gaza, 2005.

[6] Nabil M. H., Masahiro H., Tetsuo I., Shinji T., Masahiro F., Abdel Fattah H. and Emad K., ^{222}Rn exhalation rate from Egyptian building materials using active and passive methods, *Jpn. J. Health Physics*, 44(1): 106-111, 2009.

[7] Measurement of Radon Exhalation Rate from Building Materials F. Shoqwara, N. Dwaikat, G. Saffarini, Research & Reviews: Journal of Physics Volume 2, Issue 1, ISSN: 2278-2265.

[8] Measurement of Radon-222 concentration levels in water samples in Sudan Abd-Elmoniem A. Elzain1, Department of Physics, University of Kassala, Kassala, Sudan, Pelagia Research Library, Advances in Applied Science Research, 2014, 5(2):229-234.

[9] Krewski, D., J.H. Lubin, J.M. Zielinski et al. Residential radon and risk of lung cancer: a combined analysis of 7 North American case -control studies. Epidemiology, 16(2): 137-145, 2005.

[10] El-Zain, A.-E.A. A Study of Indoor Radon Levels and Radon Effective Dose in Dwelling of Some Cities of Gezira State in Sudan. Journal of Nuclear Technology and Radiation Protection, 29, 307-312, 2014.

[11] Darby, S., Hill, D., Auvinen, A. et al. Radon in homes and risk of lung cancer: collaborative analysis of individual data from 13 European case-control studies. BMJ, 330: 223, 2005.

[12] Markkanen M. Radiation Dose Assessments for Materials with Elevated Natural Radioactivity. Report STUK-B-STO 32, Radiation and Nuclear Safety Authority – STUK, 1995.

[13] NCRP, National Council on Radiation Protection and Measurements, Recent applications of the NCRP public dose limit recommendation for ionizing radiation, NCRP Statement No. 10, December, 2004.

[14] Karim, M.S., Abdullah, M.H. and Abass, W.H. Measurement of Radon Gas Concentration in Cement Samples by Using Nuclear Track Detector (CR-39). Diyala Journal for Pure Sciences, 8, 2222-8373, 2012.

[15] Saad, A.F., Abdalla, Y.K., Hussein, N.A. and Elyaseery, I.S. Radon Exhalation Rate from Building Materials Used on the Garyounis University Campus, Benghazi, Libya. Turkish Journal of Engineering Environmental Sciences, 34, 67-74, 2010.

[16] Measurement of Radium Content and Radon Exhalation Rates in Building Material Samples using Passive and Active Detecting Techniques published by Zakariya A. Hussein, Mohamad S. Jaafar and Asaad H. Ismail, Medical Physics, Physics Department, Education College, Salahaddin University -Erbil, 44002, Iraqi Kurdistan, IRAQ, published on September-2013.

[17] Hesham A. Yousef, A. H. El-Farrash, A. Abu Ela, Q. Merza Measurement of Radon Exhalation Rate in Some Building Materials Using Nuclear Track Detectors World Journal of Nuclear Science and Technology, 2015, 5, 141-148.

[18] Radon Concentration in Some Building Materials in Iraq Using CR-39 Track Detector International journal of Physics, Vol.1, No, 3, 2013, 73-76.

[19] Radon exhalation rates from some building materials used in Sudan published by Abd-Elmoniem A. Elzain, Indoor and Built Environment 2015, Vol. 24(6) 852-860 published on 5 June 2014.

International Journal of Physics, 2016, Vol. 4, No. 6, 152-157
Available online at http://pubs.sciepub.com/ijp/4/6/2

DOI:10.12691/ijp-4-6-2

Theoretical Approach of VTSM to Lattice Dynamical Study of Indium Antimonide (InSb)

Pandey Suresh Chandra[1], Dubey Jay Prakash[2,*], Upadhyaya Kripa Shankar[3]

[1]Department of Physics, Mahatma Ghandhi Gramodaya Vishwavidyalaya, Chitrakoot, Satna M. P., India
[2]Department of Physics, Dr. K. N. Modi University, Newai, Rajasthan, India
[3]Department of Physics, Nehru Gram Bharati University, Allahabad, U. P., India
*Corresponding author: jpdubebl@yahoo.com

Abstract A theoretical study of InSb based on the effect of van der Waal's interactions (VDWI) and three-body interactions (TBI) into the rigid shell model (RSM) of zinc blende structure (ZBS). The van der Waal's three body shell model (VTSM) is performed to analyze the phonon dispersion curves, Debye temperatures variation, combined density of states (CDS) curves, two-phonon Raman and anharmonic elastic properties, where the short range interactions are operative upto the second neighbours. Our results are reasonably good agreement observed between theoretical and experimental data.

Keywords: *phonons, van der Waal's interactions, debye temperature variation, combined density of states curve, phonon dispersion curves, lattice dynamics*

Cite This Article: Pandey Suresh Chandra, Dubey Jay Prakash, and Upadhyaya Kripa Shankar, "Theoretical Approach of VTSM to Lattice Dynamical Study of Indium Antimonide (InSb)." *International Journal of Physics*, vol. 4, no. 6 (2016): 152-157. doi: 10.12691/ijp-4-6-2.

1. Introduction

Structurally, the most semiconductors consist of a network of covalent bonds leading to an open crystal structure. The general theory of lattice dynamical model [1,2] and in the specific case discussed for phonon dispersion curves for various II- VI and III-V compounds [3,4,5] exhibit tetrahedral coordination under ambient conditions. It gives rise to more dramatic changes in the physical properties of semiconductors than can be attained through temperature variation alone, including band gap closure and metallization. The InSb is a narrow band gap (0.18eV) semiconductor material transition. The molecular lattice dynamical simulation is the choice of the inter-atomic potential, which determines the failure or success of a simulation. In consequence InSb is widely used in infra-red (IR) detectors, lasers and filters etc. The phenomenological models which have been used to calculate the frequencies of ZB crystals classified into two categories (i) rigid-ion model (RIM) [6,7,8] and (ii) rigid-shell model (RSM) [9,10]. The RIM involves the ion rigidity hypothesis; whereas the shell model takes into account the long-range coulomb interaction and also ionic polarizability consideration. The same remarkable theory of Kucher and researcher [11,12] in which the previously developed polarizable atom method [13] is used to calculate the spectrum of diamond type crystals. In constructing a model for a lattice with covalent bonding there is fundamental difficulty related to the introduction of non-central forces [14]. In this usual definition of a non-central interaction [15] the corresponding force parameters are two-centre parameters, while actuality non-central forces cannot be due to rotation of one atom about another, but must be due to a change in the configuration of the atoms or bonds. Hence these force parameters must take into account at least two coordination spheres. The rigid ion model and its various ramifications [16,17,18,19] have been widely used to explain several lattice dynamics properties of perfect and imperfect Z-B type crystals. These model, although economical in force parameters, ignore completely the non-central interaction in the lattice. The valance force field model (VFFM) as used by Price et al. [20] incorporates bond bending, bond-stretching and point coulombic interactions. Later on the original 14 parameter VFFM was modified on the lines of shell model by Vegelatos et al. [5] and Feldkamp et al. [21]. In addition to lattice dynamics by Garg et al. [22], have investigated the mechanical properties of zinc-blende semiconductor by using three body force shell model [TSM] and derive the expressions for the third order elastic constants (TOEC) and pressure derivatives of second order elastic constants (SOEC) on the way of Singh and Verma [23,24]. Analysis of these models RIM [6,7,8]; RSM [9,10]; VFFM [20]; TSM [22,23,24]; BCM [25]; DDM [26] and ECM [27] reveal that the crystal dynamics study of zinc-blende crystals is still not well understood. The present model, known as van der Waals three body force shell model (VTSM), has 14 parameter computed for each crystal with the same input data (physical properties) and VWI has been added to short-range repulsive interactions operative up to second nieghbour. So, it is obvious that along with the TBI, VWI must be taken into consideration in any discussion of lattice dynamics of these crystals. This new

model, VTSM, co-operate VWI along with long range coulomb interactions, TBI and short range second neighbor interactions in the framework of RSM. The effect of TBI and VWI is quite significant and plays a very important role in the description of the lattice dynamics of Indium pnictides (InP, InSb, InAs).

In this communication, we have mainly discussed a theoretical approach of lattice dynamical study of InSb. The experimental data of InSb for phonon dispersion curves [20], harmonic and anharmonic elastic constants [28], Debye temperature variation [16,29,30,31,32], two phonon IR spectra [33,34] are available. The second order IR spectra of InSb, provides additional information of phonon mode frequencies at critical points near the edge of the first Brillion zone. The formalism of our model VTSM has been given by Pandey et al. [35] and also from Dubey et al [36,37,38].

The proposed investigations have been carried out by adopting a simple method to determine a consistent set of 14 parameters (i.e. four TBI parameters b, ρ, $f(r_0)$, $r_0f''(r_0)$; two nearest neighbor short-range repulsive interaction parameter parameters A_{12} and B_{12}; four second-nearest-neighbour short-range repulsive interaction parameters A_{11}, B_{11}, A_{22}, B_{22}; distortion polarizabilities of negative and positive ions d_1 and d_2 and shell charges of the negative and positive ions Y_1 and Y_2, respectively) of VTSM. The broad outlines about the theoretical framework of present model for calculations have been classified in section 2.

2. Method of Calculation

The values of the input data Price et al. [20], Banerjee and Varshni [16], Slutsky and Garland [39], Kunc et al. [40], Hass and Henvis [41] and calculated VTSM model parameters have been shown in Table 1. The values of A_i, B_i, C_i calculated from the knowledge of b, ρ; the values of various order of derivatives of $f(r_0)$ and van der Waal's coupling coefficients. The values of VDW coefficients used by us in the present study have been determined using SKV method [42] as suggested by Singh and Singh [43] and reported by Sharma and Verma [44]. Thus our model parameters are [b, ρ, $f(r_0)$, $r_0f'(r_0)$, A_{12}, A_{11}, A_{22}, B_{12}, B_{11}, B_{22}, d_1, d_2, Y_1 and Y_2]. The values of the VDW coefficients are shown in Table 2. Our model parameters of VTSM used to compute the phonon spectra of InSb for allowed 48 non-equivalent wave vectors in the first Brillouin zone. The frequencies along the high symmetry directions [q00], [qq0] and [qqq] were plotted against the wave vector to obtain the phonon dispersion curves (PDCs). These curves were compared with measured by coherent inelastic neutron scattering technique [45] especially TA modes are very much different not only from ours but from BCM calculations of Rajput and Browne [45] alongwith in Figure 1. Since the neutron scattering experiments provide us very few data for the symmetry directions, we have also computed CDS and the Debye temperature variation for the complete description of the frequencies for the Brillouin zone.

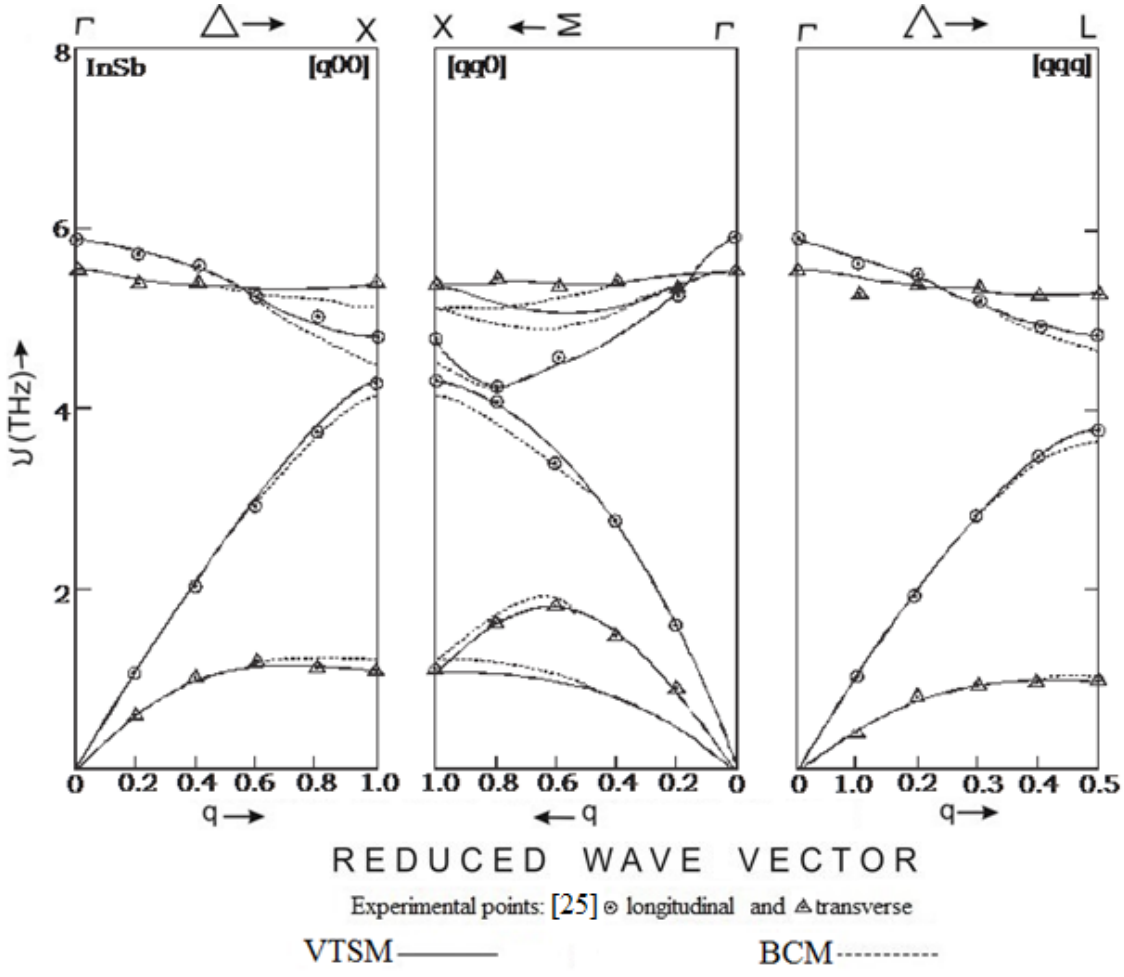

Figure 1. Phonon dispersion curves for InSb

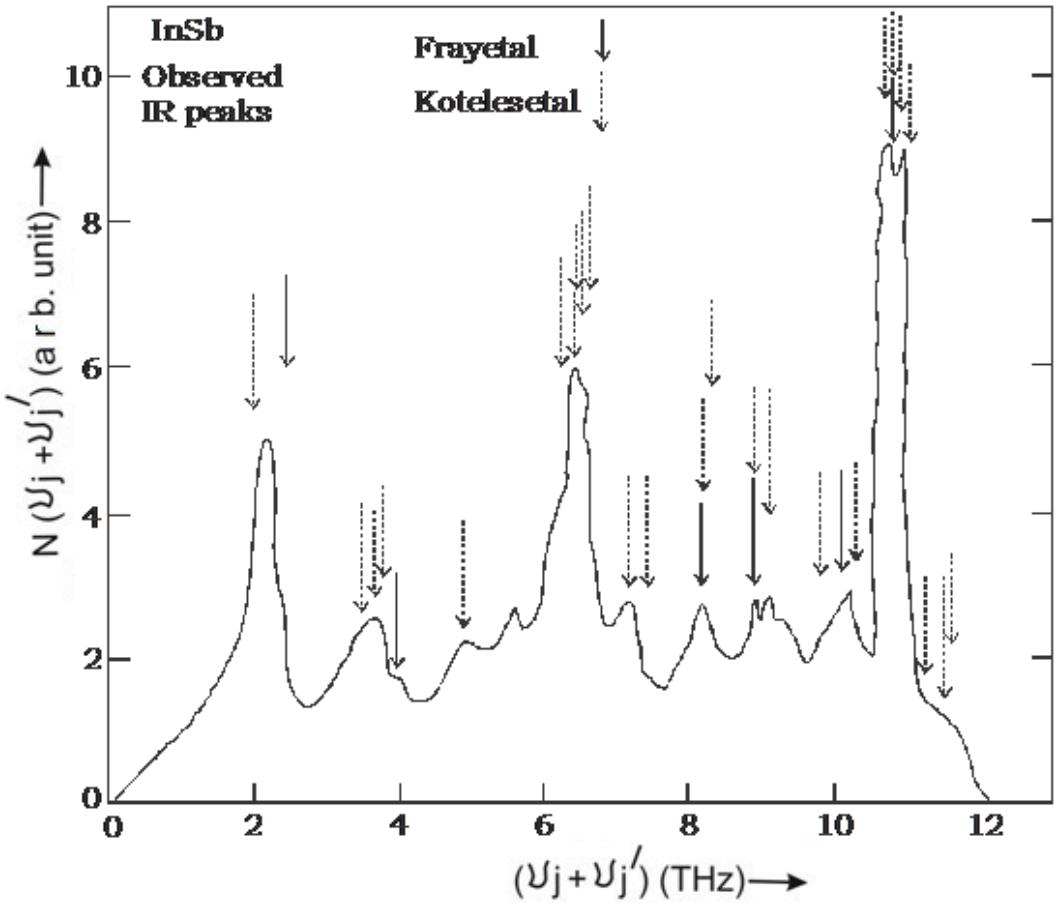

Figure 2. Combined density of states curve for InSb

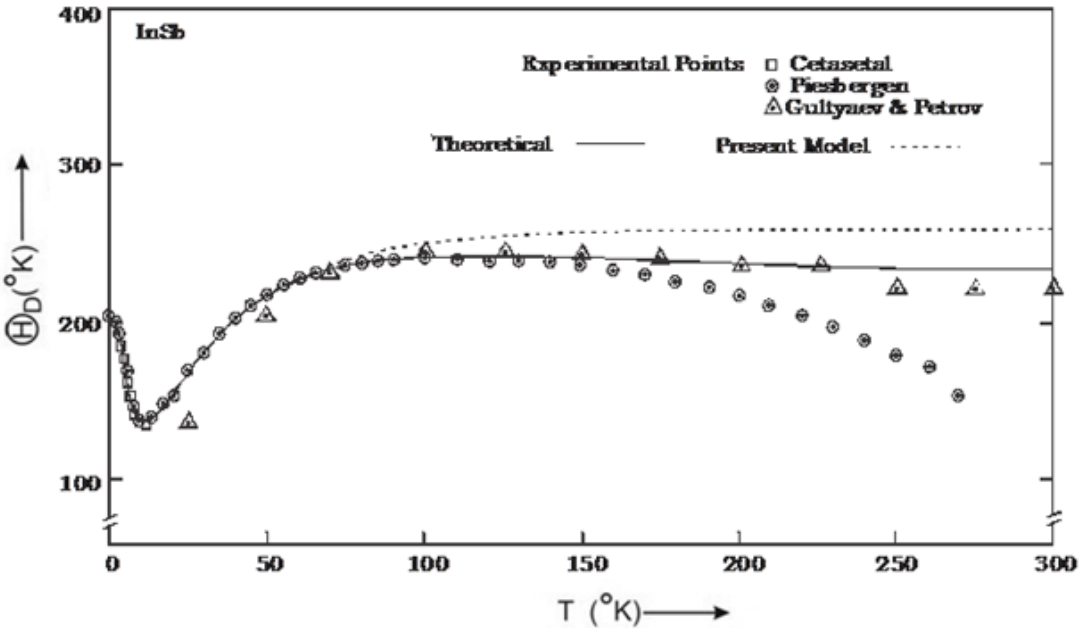

Figure 3. Debye characteristics temperatures Θ_D (°K) as a function of temperature T for InSb

The complete phonon spectra were used to compute the combined density of states CDS, $N(\upsilon_j+\upsilon_j)$ corresponding to the sum modes $(\upsilon_j+\upsilon_j)$ following procedure of Smart et al. [46]. A histogram between $N(\upsilon_j+\upsilon_j)$ and $(\upsilon_j+\upsilon_j)$ has been plotted and smoothed out as shown in Figure 2. These curves show well defined peaks which correspond to two-phonon IR spectra. These CDS peaks have been compared with the assignments calculated and shown in Table 3. The Debye temperature variation for InSb measured from [16,29,30,31,32] and those calculated by us using VTSM has been compared in Figure 3. The measured values of TOEC by Sadao [28] shown in Table 4. The measured values of pressure derivatives of SOEC by Peresada [47] have also been calculated us compared with these calculated by Ford et al. [48] in Table 5.

3. Results and Discussion

3.1. Phonon Dispersion Curves

From Figure 1, our phonon dispersion curves for InSb agree well with measured data reported by Price et al. [20]. It is evident from PDC that our predictions using present model VTSM are better than those by using BCM [25]. Our model has successfully explained the dispersion of phonons along the three high symmetry directions. From Figure 1 and Table 6, it is clear that: there are deviations of 5.26% along LO(X), 2.98% along TO(X), 1.16% along LA(X), 5.36% along TA(X), 1.87% along LO(L), zero% along TO(L), 3.94% along LA(L), 5.10% along TA(L) and 0.57% along LO(Δ), 1.72% along LA(Δ), zero% along TA(Δ) from experimental results. From BCM, deviations are 5.26% along LO(X), 4.27% along TO(X), 1.16% along LA(X), 7.14% along TA(X), 2.49% along LO(L), 0.19% along TO(L), 4.20% along LA(L), 7.14% along TA(L) and 0.95% along LO(Δ), 1.72% along LA(Δ), zero% along TA(Δ). From Table 6 it is clear that VTSM has very small deviation from experimental data. Our model, VTSM has 5.26% along LO(X), 5.36% along TA(X) and 5.10% along TA(L) improvement over BCM due to inclusion of TBI and VDWI coefficients. Thus, our VTSM model has better agreement with experimental data over BCM [25].

3.2. Combined Density of States

The present model is capable to predict the two phonon IR spectra [33,34]. The results of these investigations for CDS peaks have been presented in Figure 2. The theoretical peaks are in good agreement with both observed IR spectra for InSb. The assignments made by the critical point analysis have been shown in Table 3. The interpretation of IR spectra achieved from both CDS approach and critical point analysis is quite satisfactory. This explains that there is an excellent agreement between experimental data and our theoretical results.

Table 1. Input data and model parameters for InSb [C_{ij} and B (in 10^{11} dyne/cm^2), υ (in THz), r_0 (in 10^{-8} cm),α_i (in 10^{-24} cm^3), b (in 10^{-12} erg), ρ (in 10^{-8} cm)]

Input Data		Model Parameters	
Properties	Values	Parameters	Values
C_{11}	6.67[a]	b	1.790
C_{12}	3.65[a]	ρ	0.576
C_{44}	3.02[a]	$f(r_0)$	-0.260
B	4.51[b]	$r_0 f'(r_0)$	1.263
r_0	2.80[b]	A_{12}	15.199
υ_{LO} (Γ)	5.90[c]	B_{12}	-8.052
υ_{TO} (Γ)	5.54[c]	A_{11}	50.731
υ_{TO} (X)	5.38[c]	B_{11}	-12.341
υ_{TA} (X)	1.12[c]	A_{22}	–8.434
υ_{LO} (L)	4.82[c]	B_{22}	–42.125
υ_{LA} (L)	3.81[c]	d_1	0.219
α_1	0.22[d]	d_2	3.843
α_2	13.25[d]	Y_1	–0.476
ε_0	17.88[e]	Y_2	–1.633

[a]-(Slutsky [39]); [b]- (Banerjee [16]); [c]- (Price [20]); [d]- (Kunc et al. [40])]); [e]- (Hass [41])

Table 2. van der Waal's Interaction Coefficients for InSb (C_{ij} and C in units of 10^{-60} erg cm^6 and d_{ij} and D in units of 10^{-76} erg cm^8)

Parameters	Numerical Values
C_{+-}	956
C_{++}	431
C_{--}	2286
d_{+-}	748
d_{++}	227
d_{--}	2067
C	5200
D	3341

Table 3. Assignments for the observed peak positions in Combined Density of States in terms of selected phonon frequencies at Γ, X and L critical points for InSb

CDS Peaks (cm^{-1})	I.R Active			
	Observed I. R. Peaks		Present Study	
	Exp. [33]	[34]	Values (cm^{-1})	Assignments
73	83	-	80	2TA (Δ)
87	84-87	86	80	2TA (Δ)
-	115	-	-	-
-	117	-	-	-
134	124	134	137	LA + TA (Δ)
-	127	-	-	-
163	161	-	-	-
190	-	-	193	2LA(Δ)
205	208	-	-	-
212	211	-	-	-
-	214	-	213	TO + TA (L)
-	214	-	213	TO + TA (Δ)
218	219	-	217	LO + TA (L)
-	220	-	-	-
-	225	-	-	-
240	240	-	-	-
-	246	-	-	-
-	-	-	267	TO + LA (L)
270	-	-	270	TO + LA (Δ)
-	-	-	-	LO + LA (L)
-	273	274	273	LO + LA (Δ)
-	278	-	-	-
296	299	297	-	-
301	305	-	-	-
-	320	-	-	-
-	322	-	-	-
-	326	-	-	-
338	-	336	-	-
-	345	-	346	2TO (Δ)
-	349	-	350	LO + TO (Δ)
357	356	-	353	2LO (Δ)
-	359	361	-	-
-	363	-	-	-
-	367	-	-	-
-	370	-	-	-
-	375	-	-	-
-	384-388	-	-	-

Table 4. Third Order Elastic Constants (in the unit of 10^{11}dyne/cm^2) for InSb

Property	Present Study	Experimental Results [28]
C_{111}	−3.79	−3.56
C_{112}	−2.54	−2.66
C_{123}	−0.92	−1.00
C_{144}	+0.12	+0.16
C_{166}	−1.24	−1.39
C_{456}	−0.015	−0.004

Table 5. Values of pressure derivatives of SOEC (in dimensionless) for InSb

Properties	Values		
	Present Study	Experimental [47]	Other [48]
dK'/dP	3.94	4.58	4.19
dS'/dP	0.53	0.47	1.23
dC'$_{44}$/dP	0.42	0.47	1.23

Table 6. Comparison of frequencies from various sources (X and L points) for InSb

Expt. [20] (THz)	BCM [25]			VTSM (Present Study)			% Improvement Over BCM (a ~ b)
	Value (THz)	(±) Deviation	% (a)	Value (THz)	(±) Deviation	% (b)	
4.75	4.50	0.25	5.26	4.75	0.00	0.00	5.26
5.38	5.15	0.23	4.27	5.30	0.08	1.49	2.98
4.30	4.25	0.05	1.16	4.30	0.00	0.00	1.16
1.12	1.20	0.08	7.14	1.10	0.02	1.78	5.36

3.3. Third Order Elastic Constants (TOEC), Pressure Derivatives of Second Order Elastic Constants (SOEC)

Our calculations on TOEC are reported in Table 4 and compared with measured data of Sadao [28] on TOEC of InSb. Further, pressure derivatives of SOEC for InSb have also been compared with the calculated results of Ford et al. [48] and measured data of Peresada [47] as shown in Table 5. The results are in good agreement.

3.4. Debye Temperature Variation

From Figure 3, our study shows a better agreement with the measured data of Banerjee, Gultyaev, Cetas, Piesbergen and Passler [16,29,30,31,32] and the theoretical results reported by Rajput and Browne [45] using BCM. To conclude, we can say that our present model gives a better interpretation of the Debye temperatures variation for InSb.

4. Conclusion

The inclusion of VDWI with TBI has influenced both the optical branches and the acoustic branches. Another striking feature of present model is the excellent reproduction of almost all branches. Hence the prediction of PDC for InSb using VTSM may be considered more satisfactory than from other models BCM [45]. The basic aim of the study of two phonon IR spectra is to correlate the neutron scattering and optical measured data of InSb. In this paper, we have systematically reported phonon dispersion curves, combined density of states, Debye temperature variation and a part of harmonic and anharmonic properties of InSb. On the basis of overall discussion, it is concluded that our VTSM is adequately capable of describing the crystal dynamics of InSb. This model has also been applied equally well to study the crystal dynamics of other compound of this group InP and InAs.

Acknowledgements

The author One of us J. P. Dubey is very grateful to Dr. Pramod Kumar Pandey, Professor in department of Physics, Pt. S. N. S. Govt. P. G. College (Auto.), Shahdol (M.P.), India for many useful discussions and the computer center, B. H. U., Varanasi, for providing computational assistance and also thankful to Dr. Devendra Pathak, Vice chancellor, Dr. K. N. Modi University Newai, Rajasthan, India for encouragement.

References

[1] Born M. and Huang K., Dynamical Theory of Crystal Lattices, Oxford University Press 1954.
[2] Maradudin A. A., Montroll E. and Weiss J., Theory of Lattice Dynamics in the Harmonic Approximation, Supplement 3, Solid State Physics, Academic Press, New York 1963-1964.
[3] Henion B., Moussa F., Pepy G. and Kunc K., Phys. Lett., 36 A, 376, 1971.
[4] Farr M. K., Traylor J.G. and Sinha S. K., Lattice dynamics of GaSb, Phys. Rev B, 11pp 1587-1594, 1975.
[5] Vegelatos N., Wehe D. and King J. S., J. Chem. Phys. 60, 3613, 1974.
[6] Vetelinos J. F., and Mitra S. S., Phys. Rev. 178, 1349, 1959.
[7] Vetelino J. F., Mitra S.S. and Namjoshi K.V., Phys. Rev., B2, 967, 1970.
[8] Vetelino J. F., Mitra S. S., Brafman O. and Damen T. C., Solid State Comm., 7, 1809, 1969.
[9] Dick B. G. and Overhauser A.W., Phys. Rev., 112, 90, 1958.
[10] Cochran W., Proc. Roy. Soc. (London), A253, 260, 1959; Adv. Phys., 9, 387, 1960.
[11] Kuncher T. I. and Tolpygo K. B., Sov. Phys. Solid State, 4, 729, 1962; 8, 261, 1966.
[12] Kuncher T. I., Sov. Phys. Semicond., 2, 98, 1968.
[13] Tolpygo K. B., Sov. Phys. Solid State, 3, 98, 1961.
[14] Oskot-Skii V. S. and Efros A. L., Sov. Phys. Solid Stae, 3, 448, 1961.
[15] Kittel C., Introduction to Solid State Physics, John Willey and Sons, New York, Chap. 3, 1968.
[16] Banerjee R. and Varshni Y. P., Canad. J. Phys., 47, 451, 1969.
[17] Banerjee R. and Varshni Y. P., J. Phys. Soc. of Japan, 30, 1015, 1971.
[18] Talwar D. N. and Agrawal B. K., Phy. Rev. B8, 693, 1972.
[19] Talwar D. N. and Agrawal B. K., Solid State Comm., 11, 1691, 1972.
[20] Price D. L., Rowe J. M. and Nicolow R. M., Phys. Rev., B3, 1268, 1971.
[21] Feldkamp L. A., Steiman D. K., Vegalatos N., King J. S. and Venkataraman G. J., J. Phys. Chem. Solids 32, 1573, 1971.
[22] Garg V. K., Puriand D.S. and Verma M. P., Phys. Stat. Sol. (b) 87, 401, 1978.
[23] Singh R. K., and Verma M. P., Phys. Stat. Sol. 36, 335, 1969; 38, 851, 1970.

[24] Singh R. K., Many body interactions in binary ionic solids. Physics Report (Netherlands) 85, 259, 1982.
[25] Weber W., Phys. Rev. Lett. 33, 371, 1974.
[26] Hardy J. R., Phil. Mag. 4, 1278, 1959.
[27] Weber W., Phys. Rev. Lett. 33, 371, 1974.
[28] Sadao adachi semiconductor wiley in materiala for electronic and opto electronic application department of electronic engineering Gunma University, Japan 1965.
[29] Gultyaev P. V. and Petrov A. V., Sov. Phys. Sol. Stat. 1, 330, 1959.
[30] Cetas T. C., Tilford C. R. and Swenson C. A., Phys. Rev. 174, 835, 1968.
[31] Piesbergen U., semiconductor and Semimetals 2, 49, 1966.
[32] Passler S. R., AIP Advances 3, 082108, 2013.
[33] Koteles E. S. and Datars W. R., Phys. Rev. B 9, 572, 1974.
[34] Fray S. J., Johnson F. A. and Jones R. Proc. Phys. Soc. London, 76, 939, 1960.
[35] Pandey S. C., Dubey J. P. and Upadhyaya K. S., Jour. of Appl. Phys. 8, 01, 2016.
[36] Dubey, J. P., Tiwari, R. K., Upadhaya, K. S. and Pandey P. K., Turk. J. Phys. 39, 242 2015.
[37] Dubey J. P., Tiwari R. K., Upadhaya, K. S. and Pandey, P. K., Jour. of Appl. Phys. 7, 67 2015.
[38] Dubey J. P., Tiwari R. K., Upadhaya K. S. and Pandey P. K., Turk. J. Phys. in press 2016.
[39] Slutsky J. and. Garland, C. W Phys. Rev. 113, 167, 1959.
[40] Kunc K., Balkanski M. and Nusimovici, M. A. Phys. Stat. Sol. (b) 79, 229, 1975.
[41] Hass M. and Henvis B. W. J. Phys. Chem. Sol. 23, 1099, 1962.
[42] Slater J. C. and Kirkwood J. G., Phys. Rev. 37, 682, 1931.
[43] Singh R. K. and Khare P., J. Phys. Soc. Japan 51, 141, 1982.
[44] Sharma U. C. and Verma M. P., Phys. Status Solidi (b) 102, 487, 1980.
[45] Rajput B. D. and Browne D. A., Phys. Rev. B 53, 9052, 1996
[46] Smart C., Wilkinson G. R., Karo A. M. and Lattice Dynamics, edited by R. F. Wallis 1965 (Pergamon Press oxford).
[47] Peresada G. I., Soviet, Phys. Sol. Stat. 14, 1546, 1972.
[48] Ford P. J., Miller A. J., Saunder G. A., Yogurteu Y. K., Furdyana J. K. and. Jeezynski M. J, Sol. Stat. Phys. (C) 15, 657, 1982.

International Journal of Physics, 2016, Vol. 4, No. 6, 158-175
Available online at http://pubs.sciepub.com/ijp/4/6/3

DOI:10.12691/ijp-4-6-3

A New Principle for Elimination of Applied Defects in the Relativity Theory

Kexin Yao*

Xi'an Institute of Metrology, N0.12, Laodong South Road, Xi'an, P.R. China
*Corresponding author: yayydwpq@163.com

Abstract This paper puts forward the force equilibrium invariance axiom and derives the force transformation formula of the special relativity; puts forward the correlation analysis law and eliminates some problems resulted from the improper application of relativity; puts forward the principle of absolute velocity, determines the running speed of any moving object in real time, and solves the problem of twin paradox; puts forward the corresponding principle and determines the relationship between the rest mass and the reference frame; puts forward the concept of absolute transformation and relative transformation and clarifies two different natures of Lorentz transformation; puts forward the field similarity principle and determines the gravitational mass as a constant that has nothing to do with the velocity; infers that the equivalence principle is false and that the general relativity is only applicable to low speed moving objects; puts forward the gravity double equilibrium principle and concludes that Black Hole could not exist. It also analyzes the limiting speed of manned spaceship, and concludes that human beings cannot realize time travel of practical significance.

Keywords: *special relativity, general relativity, Lorentz transformation, Lelative velocity, absolute velocity, time running speed, relative transformation, absolute transformation, electric field, gravitational field, principle of equivalence, universal gravitation, black hole, time travel*

Cite This Article: Kexin Yao, "A New Principle for Elimination of Applied Defects in the Relativity Theory." *International Journal of Physics*, vol. 4, no. 6 (2016): 158-175. doi: 10.12691/jfe-4-6-3.

1. Introduction

Since the Theory of Relativity (including special relativity and general relativity) was proposed more than one hundred years ago, there are still some basic problems without scientific explanation or even with no explanation.

1.1 Many people don't understand the time transformation. Due to special relativity, A and B relatively move at the speed v, then A determines that the time of B t_B (the running speed of time, namely the speed of the clock) is smaller than the time of A t_A, that is, $t_B = t_A\sqrt{1-v^2/c^2}$. However, B also determines $t_A = t_B\sqrt{1-v^2/c^2}$, namely t_A is smaller than t_B. Obviously the judgment of A and B are contradictory, so we do not know which one is smaller.

There are many objects m_1, m_2, m_3 …, whose respective time is expressed as t_1, t_2, t_3 …, whose velocity relative to the object m is respectively expressed as v_1, v_2, v_3 …. According to special relativity, m_1 deduces the time of m as $t_{m1} = t_1\sqrt{1-v_1^2/c^2}$, m_2 deduces the time of m as $t_{m2} = t_2\sqrt{1-v_2^2/c^2}$, m_3 deduces the time of m as $t_{m3} = t_3\sqrt{1-v_3^2/c^2}$. Obviously, $t_{m1} \neq t_{m2} \neq t_{m3}$, that the real time of m is impossible to be equal to t_{m1}, t_{m2}, t_{m3}… at the same time. This example shows that, according to special relativity, it is not possible for arbitrary object to deduce the real time of another object from the relative velocity.

Through an imaginary experiment, it is proved that the real time of arbitrary object is independent of the relative motion of the other object. Launch a spacecraft A in a place on the Earth to revolve around the Earth in elliptical orbit, whose rotation cycle is T. After a period of $T/2$, launch spacecraft B in the same place to resolve around the Earth in elliptical orbit, whose rotation cycle is also T. If the people on Earth see the movement velocity of A and B at the speed v, spacecraft A or B both see the opposite spacecraft moving at the speed $2v$. According to special relativity, A and B both confirm that the time B and A is shortened. A concludes $t_B = t_A\sqrt{1-4v^2/c^2}$ while B concludes $t_A = t_B\sqrt{1-4v^2/c^2}$. After a period of time, A and B will return to the Earth at $T/2$ intervals. As A and B have exactly the same flight process, if there is a reduction process for t_A and t_B, the reduction extent of A and B must be the same. After return to the Earth, the time difference of A and B must be exactly the same as that before they were launched. This shows that based on special relativity, A and B in relative motion to deduce the conclusion that the time of the other one is shortened than its own time is wrong.

From the above analysis, let's discuss the twin paradox. In this problem, the twin A escapes from the Earth by spaceship. In the view of twin B, A moves relatively to B, and the time of A must be decreased, therefore B deduces that A must be younger than B when A returns to the Earth. However, A also sees that B moves relatively to A, A also deduces that the time of B is decreased, and finds out that B is younger than A when A returns to the Earth. Obviously, the judgment of A and B are contradictory.

Our previous analysis shows that for the two objects in relative motion, the conclusion of the time decrease of each other is not realistic, that is to say, the twin A and B could not determine whether the other is younger according to the relative velocity, namely there is no twin paradox. However, satellite time experiments show that the satellite clock is indeed slower than the Earth's clock, that is, t is decreased. This shows that, according to special relativity, it can deduce by the relative velocity that the time decrease in the satellite is in accord with the actual situation; on the other hand it also shows that it is wrong for people on the satellite to deduce the time decrease on Earth by the relative velocity. How to explain this phenomenon? The popular explanation currently is that the starting and accelerating process for the satellite to escape from the Earth leads to the time decrease of the satellite, that is, it makes twin A younger than twin B. Through the analysis, this explanation is not scientific, because for a satellite returning to Earth in one day, and a satellite returning to Earth after ten years, the starting and accelerating process is exactly the same. Does the satellite flying one day and flying ten years have the same effect? So, this explanation is not scientific, not to mention the following notes that the time of the clock on the flying aircraft can not only be decreased, but also increased (the clock goes faster). This can completely negate the explanation that the starting and accelerating causes the time decrease.

From the above analysis, we can see that the time transformation of special relativity has two basic problems that could not be explained: 1) the logical reasoning can draw the conclusion that it is not correct for an arbitrary object to deduce the real time of another object according to the relative velocity. If the conclusion is true, does it mean that the time transformation of special relativity does not fully meet the actual?, and 2) since people on Earth and people in the satellite have the same relative velocity, then, why it is realistic for the people on Earth to deduce the time decrease of satellite according to the relative velocity, while it is not consistent with the actual for the people in the satellite to deduce the time decrease of the Earth according to the same relative velocity (actually the time is relatively increased)?

1.2 Special relativity points out that there is a constant rest mass for any object. The rest mass is the mass of the object when the object is stationary relative to the Earth. However, the Earth is different from Mars, Saturn and the Moon and other celestial bodies. It may well be asked that whether the rest mass of the same object detected on Mars, Saturn and the Moon is different from the rest mass detected on the Earth. If the rest mass detected on each celestial body is different, then how to deduce the difference?

1.3 The mechanism has four basic physical quantities as length, quality, time and force. Now special relativity has identified transformation formula of the relation between the object's length, quality, time and movement velocity, but whether there is a relationship between the acting force and movement velocity is uncertain. If there is a relationship, how to transform has not been clearly explained, therefore, to determine the relationship between the acting force and movement velocity of the object is very necessary.

1.4 When analyzing some physical phenomena based on special relativity, we often get some wrong analysis results, for example:

The elliptical orbit of the planets revolving around the Sun basically is constant. An observer moving at high velocity relatively to the Sun sees that the Sun and the planets move at the same velocity relatively to him (without considering the slow movement of planets relative to the sun), but it does not change the motion of planetary orbits. However, according to special relativity, the mass of the Sun and planets at high speed should have obvious changes, for instance the mass of the Sun represented by M, the mass of the planet represented by m. According to the principle of equivalence, gravitational mass is equal to inertial mass. The inertial mass and gravitational mass of the Sun and planets in high-speed motion will be transformed to $M' = M\Big/\sqrt{1-v^2/c^2}$ and $m' = m\Big/\sqrt{1-v^2/c^2}$. Because the universal gravitation between the Sun and the planets is proportional to $M'\,1\Big/\left(1-v^2/c^2\right)$, that is, proportional to $1\Big/\left(1-v^2/c^2\right)$, while the centrifugal force of the planets to the Sun is only proportional to inertial mass $1\Big/\sqrt{1-v^2/c^2}$, that is, proportional to $1\Big/\sqrt{1-v^2/c^2}$. Obviously, $1\Big/\left(1-v^2/c^2\right) > 1\Big/\sqrt{1-v^2/c^2}$, the universal gravitation of the Sun to the planets is larger than the planets' centrifugal force, then the planets will be attracted to the sun. Apparently it does not conform to the fact that special relativity's judgment seems to be wrong code. If the equivalence principle is false that gravitational mass has nothing to do with the movement velocity, the observer should deduce that the gravitation of the Sun to the planets is independent of the velocity. However, the inertial mass of planets must be $m' = m\Big/\sqrt{1-v^2/c^2}$, so the centrifugal force of the planets to the Sun is larger than the universal gravitation of the Sun to the planets, then the planets will fly away from the sun, which is also inconsistent with the facts. From the above analysis, we conclude that according to special relativity, the universal gravitation of the Sun to the planets and the centrifugal force of the planets to the Sun in high-speed motion relatively to the Sun are not correct.

For another example, the fact shows that the displacement distance of object A with mass m, force F, through the time of t on object B must be $S = Ft^2/2m$. However, according to special relativity, in the view of the observer in motion at the velocity v parallel to F relative to B, m of A should be transformed to $m' = m\Big/\sqrt{1-v^2/c^2}$, t should be transformed to

$t' = t\sqrt{1-v^2/c^2}$, so the displacement distance of A on B should be $S' = Ft^2\left(1-v^2/c^2\right)^{3/2}/2m$. But according to the length transformation formula of special relativity, the actual distance on B S should be transformed to $S'' = S\sqrt{1-v^2/C^2} = Ft^2\sqrt{1-v^2/c^2}/2m$, obviously, $S' \neq S''$. That is to say, the inference of special relativity is self contradictory.

The above analysis shows that, according to the general analysis method of special relativity, the deduction of some basic physical phenomena does not accord with the actual conclusion.

1.5 The equivalence principle of general relativity assumes that gravitational mass is equal to inertial mass. For hundreds of years, in order to determine the relationship between gravitational mass and inertial mass, Galileo, Newton et al made a lot of experiments which show that, in general, the gravitational mass and inertial mass of an object have a constant ratio. Therefore, as long as select the appropriate proportion units, it can conclude that gravitational mass of the object is equal to inertial mass. But through the analysis of their experiments, it can be seen that all experiments obtained the results under the condition of low movement velocity of the object. No one has made the experiments about the ratio of gravitational mass and inertial mass under the condition of high movement velocity. Under the condition of high movement velocity, the object's inertial mass is obviously increased. According to special relativity, the inertial mass m_1 of the object in motion at high speed v increases to $m_1' = m_1/\sqrt{1-v^2/c^2}$. Numerous experiments have confirmed the conclusion undoubtedly. Set the object's gravitational mass as m_2. If gravitational mass and inertial mass are equal, there must be $m_2' = m_2/\sqrt{1-v^2/c^2}$. So far, no experiment has confirmed this conclusion, on the contrary, based on the simple logic analysis, it can prove $m_2' \neq m_2/\sqrt{1-v^2/c^2}$.

According to Figure 1, the object is composed of the cube A and B with the same mass m up and down, which is connected together with two springs. In our view of the inertial system Z, the shape of this object is constant. But in the view of people in motion at high speed V of the inertial system Z' relatively to Z, regarding the movement at high speed $-V$, the mass and length of the object are both changed. We do not discuss the changes of the length of the object, but only analyze the changes of the mass which is divided into two aspects of inertial mass and gravitational mass. According to special relativity, the inertial mass $2m_1$ of the object (without considering the spring mass) should be increased to $2m_1' = 2m_1/\sqrt{1-v^2/c^2}$. Its momentum is transformed to $2m_1'V$. The experiments show that such inference is consistent with the actual. The equivalence principle points out that gravitational mass and inertial mass are equal, therefore, gravitational mass should also be increased to $2m_2/\sqrt{1-v^2/c^2}$. Gravitational mass of object A and B must be increased to $m_2' = m_2/\sqrt{1-v^2/c^2}$ respectively. Since there is universal gravitation between A and B, which is in direct proportion to the product of gravitational mass of A and B, $m_2'm_2'/m_2m_2$ is equal to $1/\left(1-v^2/c^2\right)$, therefore, the people in Z' must deduce that the universal gravitation between A and B is increased by $1/\left(1-v^2/c^2\right)$. When V is very large, there will be significant compression for the spring. When V is approaching the speed of light, A and B should fit in one piece. Z sees that the spring cannot be deformed, Z' also cannot see the same spring deformation (the length vertical to V does not change), therefore, according to special relativity Z' can deduce that, gravitational mass cannot be in direct proportion to $1/\sqrt{1-v^2/c^2}$ when the object moves at the velocity V. That is to say, gravitational mass and inertial mass are not equal, so, it can be judged that the equivalence principle is false. As we all know, if the equivalence principle is not true, does general relativity also have problems?

The above part discussed from several aspects about some problems and defects may arise in the analysis of problems based on the relativity theory. Do these defects indicate that the theory of relativity is wrong? I don't think the relativity is wrong, but the deviations arise when use the relativity theory to analyze problems. The reasons for these deviations are the wrong analysis methods. Therefore I think that, in order to use the correct methods to apply the relativity theory, it is necessary to add some new analytical principles. Below I will describe some basic principles which should be added.

2. Invariance Axiom of Force Equilibrium

Place an object of 1 kilogram on the spring scale, the pointer of the spring scale will fix on the position of 1kg. The position of 1kg is not only the position of 1kg for the people who are relatively static to the spring scale, but also for other people in any motion. This fact shows that for a group of force in equilibrium in a reference frame, the observer of any other reference frames can also observe the group of force in equilibrium. In other words, a group of force in equilibrium will never change the state of equilibrium along with the different reference frames where the observer stays. This is the fact recognized by people in daily life. I call this fact as equilibrium invariance axiom. We can derive the formula of force transformation according to the force equilibrium invariance axiom.

2.1. Deduction of Force Transformation Formula

Figure 2a represents three forces F_A, F_B, F_C in a state of equilibrium. These three forces can be the electric

field force, also the universal gravitation or the spring force and so on. In the figure, the length of OA, OB, OC respectively represents the size of F_A, F_B, F_C, F_C is parallel to the X axis, F_A is equal to F_B, the angle between them and X axis are θ (not considering the positive or negative of θ). Due to the three forces in equilibrium, there will be $F_A\cos\theta + F_B\cos\theta = F_C$. Because of the equal size of F_A and F_B, to make the derivation simple, let $F_A = F_B = F$, there will be $2F\cos\theta = F_C$.

Figure 2b represents the three forces in Figure 1a to move parallel to X axis at the velocity v. According to special relativity, the length of direction v (direction X) should be shortened, while F_C in Figure 1a should be shortened to F_C', F_A and F_B should be shortened to F_A', F_B' respectively. According to the force equilibrium invariance axiom, F_C' and F_A', F_B' are still in a state of equilibrium, F_A' and F_B' are naturally equal. Let $F' = F_A' = F_B'$, similarly there will be $2F'\cos\theta' = F_C'$.

We infer the relationship between F_C and F_C' according to the changes of the electric field force in motion.

Figure 3a indicates that the charge Q is in a uniform electric field generated by the "infinite" charged flat plate; E indicates the electric field strength, AB represents a section of the charged plate. Obviously, the force of Q is F_Q. Figure 3 indicates that after AB moves parallel to E at the velocity v, AB becomes $A'B'$. According to special relativity, the length vertical to direction v maintains the same size after movement, therefore there will be $A'B' = AB$, naturally there will be the electric field strength of $A'B'$ $E' = E$. Therefore, the force of $A'B'$ in the electric field Q is $F_Q' = E'Q = EQ = F_Q$. From this fact, it is known that the force F_Q will not change after the movement in the direction parallel to ($F_C = E_Q$). For the force of Figure 2, there must be $F_C' = F_C$. Due to $F_C' = 2F'\cos\theta'$, $F_C = 2F\cos\theta$, there must be $F'\cos\theta' = F\cos\theta$.

$$F' = F\frac{\cos\theta}{\cos\theta'}$$

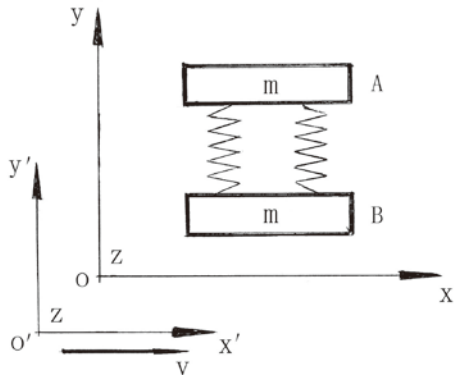

Figure 1. Spring compressed neither in Z nor in Z'

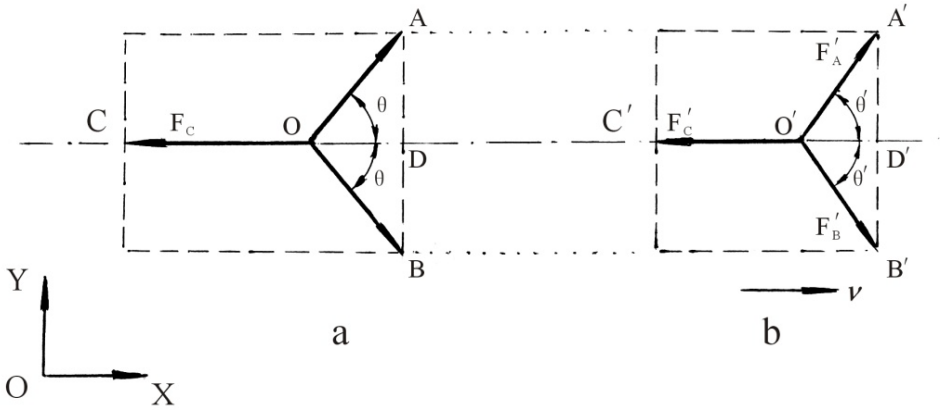

Figure 2. Changes of force in motion

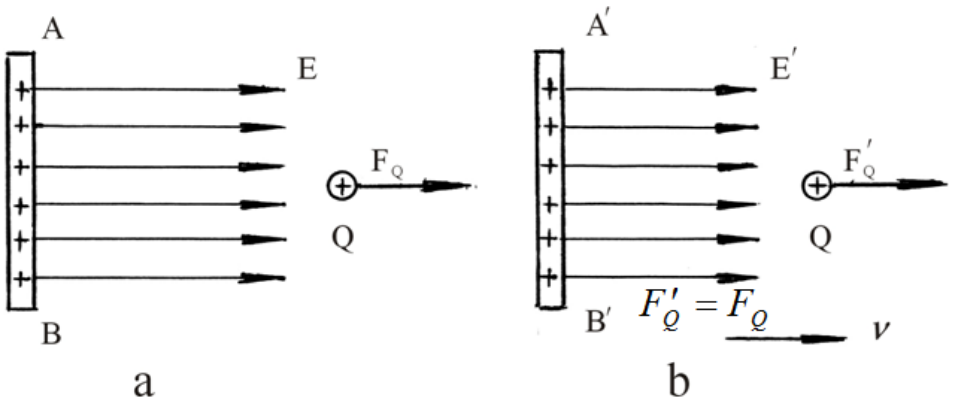

Figure 3. the electric field in motion parallel to the electric field strength line E

It can be seen in Figure 1 that

$$\cos\theta = \frac{OD}{\sqrt{OD^2 + AD}}, \cos\theta' = \frac{O'D'}{\sqrt{O'D'^2 + A'D'^2}}$$

Because the length vertical to direction v maintains the same size, there will be $A'D' = AD$. While the length $O'D'$ in the direction v has $O'D' = OD\sqrt{1-v^2/c^2}$ according to the length transformation formula of special relativity, based on the equation of $A'D'$ and $O'D'$, $\cos\theta'$ can be transformed to

$$\cos\theta' = \frac{OD\sqrt{1-v^2/c^2}}{\sqrt{OD^2\left(1-v^2/c^2\right)+AD^2}}$$

$$F' = F\frac{\cos\theta}{\cos\theta'}$$

$$= F\frac{OD}{\sqrt{OD^2+AD^2}}\cdot\frac{\sqrt{OD^2\left(1-v^2/c^2\right)+AD^2}}{OD\sqrt{1-v^2/c^2}}$$

$$= F\sqrt{\frac{\left(OD^2+AD^2\right)-OD^2\,v^2/c^2}{\left(OD^2+AD^2\right)\left(1-v^2/c^2\right)}}$$

Substitute $\cos\theta' = OD/\sqrt{OD^2+AD^2}$ to the above formula and conclude that

$$F' = F\sqrt{\frac{1-\cos^2\theta\,v^2/c^2}{1-v^2/c^2}} \tag{1}$$

Due to $F' = F\cos\theta/\cos\theta'$; $\cos\theta' = F\cos\theta/F'$ concludes

$$\cos\theta' = \cos\theta\sqrt{\frac{1-v^2/c^2}{1-\cos^2\theta\,v^2/c^2}}$$
$$\theta' = \cos\theta^{-1}\cos\theta\sqrt{\frac{1-v^2/c^2}{1-\cos^2\theta\,v^2/c^2}} \tag{2}$$

The above formula (1) and (2) are the transformation formula of force in motion at the speed v. The formula, like the transformation formula of length, time, mass, should be the basic transformation formula of special relativity.

2.2. Electric Field Distribution of Charged Particles in Motion Deduced by Force Transformation Formula

The positively charged particle Q in Figure 4 moves at the velocity v, the length l in static state will be contracted to $l' = l\sqrt{1-v^2/c^2}$ after movement. The height h vertical to direction v maintains the same before and after movement. r in static state will be contracted to r' after movement. It can be known by the figure that $l = r\cos\theta$, $l' = l\sqrt{1-v^2/c^2} = r\cos\sqrt{1-v^2/c^2}$, $h = r\sin\theta$ have

$$r' = \sqrt{l'^2+h^2} = \sqrt{r^2\cos^2\theta\left(1-v^2/c^2\right)+r^2\sin^2\theta}$$
$$= r\sqrt{1-\cos^2\theta\,v^2/c^2}. \tag{3}$$

Due to $h = r\sin\theta = r'\sin\theta'$ with $\sin\theta' = \sin\theta\, r/r'$, substitute formula (3) and conclude that

$$\sin\theta' = \sin\theta/\sqrt{1-\cos^2\theta\,v^2/c^2}. \tag{4}$$

The acting force of Q in the electric field with the electric field strength E is F=EQ, that is, the electric field strength E and the acting force F is directly proportional, so the force transformation type (1) can also be written as the electric field strength transformation type:

$$E' = E\sqrt{\frac{1-\cos^2\theta\,v^2/c^2}{1-v^2/c^2}}. \tag{5}$$

Transform formula (5) to

$$E' = E\sqrt{\frac{1-\cos^2\theta\,v^2/c^2}{1-v^2/c^2}}\cdot\frac{\left(1-\cos^2\theta\,v^2/c^2\right)\left(1-v^2/c^2\right)}{\left(1-\cos^2\theta\,v^2/c^2\right)\left(1-v^2/c^2\right)}E$$

$$= \frac{\left(1-\cos^2\theta\,v^2/c^2\right)^{3/2}}{\left(1-v^2/c^2\right)^{3/2}}\cdot\frac{1-v^2/c^2}{1-\cos^2\theta\,v^2/c^2}E$$

$$= \frac{1-v^2/c^2}{\left(\frac{1-v^2/c^2}{1-\cos^2\theta\,v^2/c^2}\right)^{3/2}}\cdot\frac{E}{1-\cos^2\theta\,v^2/c^2}.$$

Due to $1-v^2/c^2 = 1-\left(\sin^2\theta+\cos^2\theta\right)v^2/c^2$, the above formula can be transformed to

$$E' = \frac{1-v^2/c^2}{\left(1-\frac{\sin^2\theta\,v^2/c^2}{1-\cos^2\theta\,v^2/c^2}\right)^{3/2}}\cdot\frac{E}{1-\cos^2\theta\,v^2/c^2}.$$

Substitute formula (3) $\sqrt{1-\cos^2\theta\,v^2/c^2} = r'/r$ and formula (4) $\sin\theta' = \sin\theta/\sqrt{1-\cos^2\theta\,v^2/c^2}$ to this formula and conclude

$$E' = \frac{1-v^2/c^2}{\left(1-\sin^2\theta'\,v^2/c^2\right)^{3/2}}\cdot\frac{r^2}{r'^2}E.$$

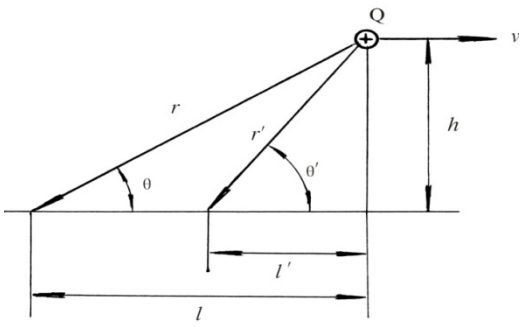

Figure 4. When the charged particles move with the velocity v, r becomes

Due to $E = kQ/r^2$, substitute to the this formula and conclude

$$E' = K\frac{1-v^2/c^2}{\left(1-\sin^2\theta' v^2/c^2\right)^{3/2}}\cdot\frac{Q}{r'^2}. \quad (6)$$

Formula (6) is the electric field distribution formula of the charged particles in motion at the speed v. By comparison, this formula is the same as the formula deduced by electrodynamics.

When the object moves, the force should be transformed with the length, time and mass. For example, when the charged particles move in a magnetic field, the Lorentz force of particles will be transformed. Detailed analysis is shown in references 3.

3. Correlation Analysis Law

Figure 5a, in the reference frame Z, the movement speed and the carrying capacity of the two positive charges are V_1, V_2 and Q_1, Q_2 respectively. According to the former formula (6), the electric field strength of Q_2 generated in Q_1 is (in the following formulas Y_0 represents the unit vector of direction Y).

$$E'_2 = k\frac{\left(1-V_2^2/C^2\right)Q_2}{\left(1-V_2^2\sin 0^{\circ 2}/c^2\right)^{3/2}\cdot r^2}(-Y_0) \quad (7)$$

Therefore, the force of Q_1 will be

$$F_1 = E'_2 Q_1 = \frac{\left(1-V_2^2/C^2\right)Q_1Q_2}{r^2}(-Y_0)$$

The electric field strength of Q_1 generated in Q_2 will be:

$$E'_2 = k\frac{\left(1-V_1^2/C^2\right)Q_1}{\left(1-V_1^2\sin 90^{\circ 2}/c^2\right)^{3/2}\cdot r^2}(Y_0) \quad (8)$$

The force of Q_2 will be:

$$F_2 = E'_2 Q_2 = \frac{Q_1Q_2}{\sqrt{1-V_1^2/C^2}\cdot r^2}(Y_0).$$

Obviously, the action and reaction force between $F_2 \neq F_1$, Q_1 and Q_2 are different, that is, the law of reaction is false.

If there is another observer in motion at the speed u relative to Z, in Figure 4b he will observe that the velocity of Q_1 is $V_{1v} = V_1 - u$, the velocity of Q_2 is transformed to $V_{2v} = V_2 - u$. It can be seen in Figure 5b that V_{1v} and V_{2v} are different and opposite, obviously the result is still $F_2 \neq F_1$, namely the law of reaction is false.

Because the law of reaction is recognized by the law, the law is also interrelated with the law of conservation of energy and other laws, its correctness is undoubted, and therefore, we can be sure that the analysis method above is wrong. Under the conditions not in violation of the law of reaction, how to analyze the interaction of Q_1 and Q_2 in Figure 5? Firstly we should take the law of reaction as the inevitable result, that the action and reaction are constant to be equal and opposite. Another form of equilibrium state of the force must be independent of the observer of any reference frames according to the force equilibrium invariance axiom, namely the interaction between Q_1 and Q_2 is independent of any observers. Q_1 is only related to Q_2, while Q_2 is only related to Q_1, that is to say, the physical function of Q_1 by Q_2 is only related to the physical quantities related to Q_2, which has nothing to do with any other observers. Of course, the physical function of Q_2 by Q_1 is only related to the physical quantities related to Q_1. Regarding Figure 5a, the force of Q_1 by Q_2 is only related to the movement velocity, distance of Q_2 relative to it, and the amount of electricity of Q_2. Q_1 observes that the movement velocity of Q_2 relative to it is $V_{21} = V_2 - V_1$, while Q_2 observes that the movement velocity of Q_1 relative to it is $V_{12} = V_1 - V_2$. Obviously, $V_{12} = -V_{21}$ [see Figure 5b]. Q_1 observes that the electric field direction of Q_2 is in the direction $-Y_0$ (unit vector in $Y_0 = Y$ direction), the distance from Q_2 to it is r.

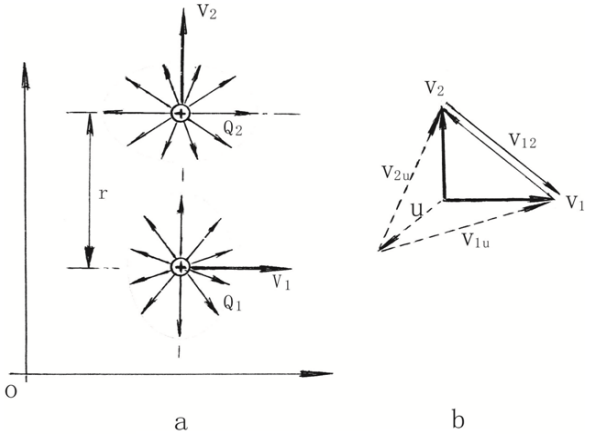

Figure 5. Interaction force of two moving charges

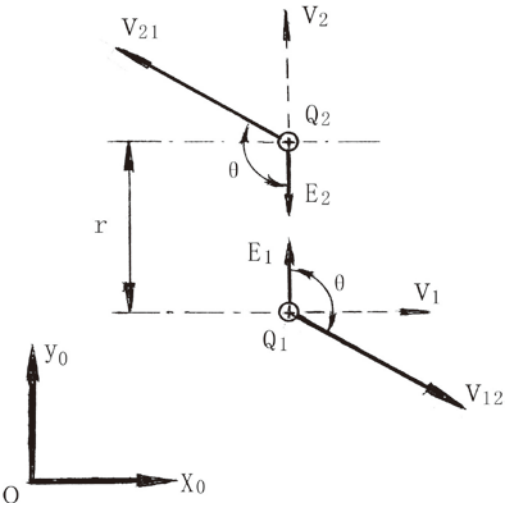

Figure 6. Respective physical parameters of Q_1 and Q_2

Q_1 observes the electric field strength of Q_2 to it as:

$$\mathrm{E}'_{21}=k\frac{\left(1-V_{21}^2/C^2\right)Q_2}{\left(1-V_{21}^2\sin\theta_1{}^2/c^2\right)^{3/2}\cdot r^2}\left(-\mathrm{Y}_0\right)\ (\theta_1 \text{ see Figure 6})$$

Q_1 force

$$\mathrm{F}_1=\mathrm{E}'_{21}Q_1=k\frac{\left(1-V_{21}^2/C^2\right)Q_1Q_2}{\left(1-V_{21}^2\sin\theta_1{}^2/c^2\right)^{3/2}\cdot r^2}\left(-\mathrm{Y}_0\right)\qquad(9)$$

Similarly, Q_2 observes the electric field strength of Q_1 to it as:

$$\mathrm{E}'_{12}=k\frac{\left(1-V_{12}^2/C^2\right)Q_1}{\left(1-V_{12}^2\sin^2\theta_2/c^2\right)^{3/2}\cdot r^2}\left(\mathrm{Y}_0\right)(\theta_2 \text{ - see Figure 6})$$

Q_2 force

$$\mathrm{F}_2=\mathrm{E}'_{12}Q_2=k\frac{\left(1-V_{12}^2/C^2\right)Q_1Q_2}{\left(1-V_{12}^2\sin^2\theta_2/c^2\right)^{3/2}\cdot r^2}\left(\mathrm{Y}_0\right)\qquad(10)$$

Since the direction of $\mathrm{V}_{12}=-\mathrm{V}_{21}$ E'_{21} (direction $-Y_0$) and E'_{12} (direction Y_0) is opposite, there must be $\theta_2=\theta_1$ and $\mathrm{V}_{12}^2=-\mathrm{V}_{21}^2$ must have

$$\mathrm{F}_2=-\mathrm{F}_1$$

That is to say, the acting force and reactive force of Q_1 and Q_2 are the same in the opposite direction, conforming to the law of reaction.

The former explains that, for an arbitrary observer moving at the velocity u relatively to Z, the movement velocity of Q_1 is $\mathrm{V}_{1u}=\mathrm{V}_1-\mathrm{u}$, the velocity of Q_2 is $\mathrm{V}_{2u}=\mathrm{V}_2-\mathrm{u}$. Q_1 observed the movement velocity of Q_2 as $\mathrm{V}_{21u}=\mathrm{V}_{2u}-\mathrm{V}_{1u}=\mathrm{V}_{21}$ [see Figure 5b] while Q_2 observed the movement velocity of Q_1 as $\mathrm{V}_{12u}=\mathrm{V}_{1u}-\mathrm{V}_{2u}=\mathrm{V}_{12}$. The relative velocity of Q_1 and Q_2 are still V_{21} and V_{12}, the interaction force of Q_1 and Q_2 F_1 and F_2 are still expressed by formula (9) and (10), namely still $\mathrm{F}_2=-\mathrm{F}_1$.

The above analysis shows that when the observer of any reference frame in accordance with the relevant physical quantity of Q_1 and Q_2 deduce the action and reaction between each other, the results are exactly the same, which is consistent with the law of reaction.

Generalize the reaction analysis results above to all physical phenomena, the conclusion is that the physical interactions of any two objects can only be analyzed by the physical quantity of two objects related to each other, which have nothing to do with any object outside the two objects. Define this conclusion as the correlation analysis law.

It should be pointed out that the former formula (7) and (8) are not the wrong formulas. According to the correlation analysis law, formula (7) is the correlation analysis between the observer in Z and the two related objects in Q_2, which is the real electric field distribution of Q_2 observed by the observer in Z. But this observation is not the observation of Q_1, the two cannot be confused. Similarly, formula (8) is the real electric field distribution of Q_1 observed by the observer in Z.

According to the correlation analysis law, it is easy to make explanation to the incorrect inferences on planetary orbits by the observer in motion at high speed relative to the Sun in the example in 1.4. According to this law, the observer's deduction of mass increase to the Sun and planets is just the relevant deduction result of the observer to the Sun and planets. Although this is a correct deduction, it is has nothing to do with the deduction of the Sun to the planets or the planets to the sun. The interaction between the Sun and planets is only related to the physics quantities related to each other. The rotation velocity, distance of the planets to the sun, the centrifugal force generated by its mass are equal to the universal gravitation of the Sun mass to the planets, therefore, the two are in a state of equilibrium.

For the example in 1.4, it is easy to explain the incorrect inferences on the displacement distance of A on B by the observer in motion at the speed V relatively to AB. According to the correlation analysis law, the observer's deduction of $S''=S\sqrt{1-v^2/C^2}$ is correct, but this deduction is just the correlation analysis between the observer and B, which is independent of the analysis of A to B. Similarly the observer's deduction of $m'=m\Big/\sqrt{1-v^2/c^2}$ and $t'=t\sqrt{1-v^2/c^2}$ is also correct, but this is just the correlation analysis between the observer and A, which is independent of the analysis of B to A. The displacement distance of A on B is only related to the relevant physical quantities of the two.

The correlation analysis law can not only deduce the problem correctly, but also simplify the problem.

For example, in Figure 7, ball A moves at high speed V_1, through the analysis of ball B's movement velocity $V_2=V_1\cos\theta_1/\cos\theta_2$, it can be known that, the displacement distance of ball A and B in direction X are the same within the limited time (without considering the gravity of the Earth). For the time $t=s/\left(V_2\sin\theta_2-V_1\sin\theta_1\right)$, the two balls will definitely collide. In order to deduce the collision results of the two balls in accordance with the general analysis methods, it needs to deduce ball A's $m'_A=m_A\Big/\sqrt{1-v_1^2/c^2}$ and ball B's $m'_B=m_B\Big/\sqrt{1-v_2^2/c^2}$, the momentum of ball A and B, the angle for the two to be equal etc.. The problem is complicated, and the result is not consistent with the actual. But to analyze this problem according to the correlation analysis law is very simple. It is easy to see that the relative velocity of AB is $V=V_2\sin\theta_2-V_1\sin\theta_1$. Then this problem is reduced to the head-on collision of AB at the relative speed V, and due to the relatively small V, there is no need to calculate m'_A and m'_A.

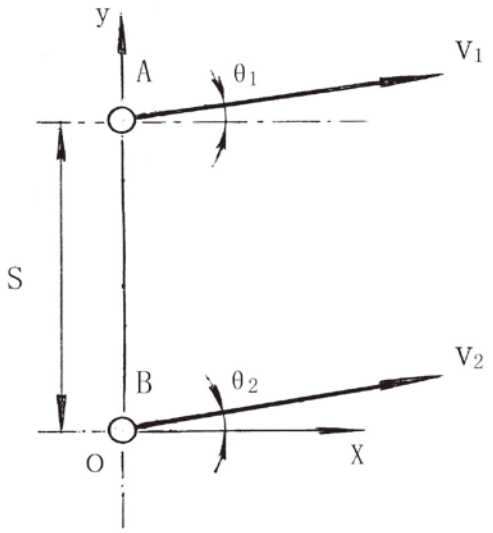

Figure 7. The collision results of the analysis of A and B

4. Absolute Velocity Principle

4.1. Relative Velocity and Absolute Velocity

In daily life, we often observe some relative motions; for example, we catch sight of another train in motion outside the window of our train, and this train may be in motion or may not be in motion, the reason for which is that our train is moving along the opposite direction; this is referred to as relative motion. Relative motion velocity is related to observer; if we sit in a motionless train and the motion velocity of the opposite train we get a sight of is V, then our train is moving at a velocity of $-V$ along the opposite direction; therefore, the motion velocity of the opposite train within our sight is $2V$; if our train and the opposite train keep pace with each other at V, then the opposite train we saw is motionless.

It is observed from the above mentioned example that relative motion velocity is the motion velocity of both parties in relative motion; however, a person in motion at a different velocity is to have a different result of measurement for the motion velocity of the same object; accordingly, it is impossible for us to deduce true motion velocity of any object based on relative motion velocity. Since there is only relative velocity between straight-line motions, we are unable to properly deduce the true velocity of any object in straight-line motion.

In addition to straight-line motion, objects may also be in curvilinear motion and any curve has radius of curvature; consequently, long-time curvilinear motion may certainly be circular motion that takes radius of curvature as a circle; the circular motion is the most common motion; the most familiar and obvious circular motion includes rotation of cabins around the ferris wheel center in amusement park and rotation of artificial satellite and Moon around the Earth. It is observed from in-depth analysis that all objects in universe are in circular motion (the ellipse is also taken as circle), with the exception of fixed stars likely to be motionless, e.g. the motion of the Earth around the Sun. Any object on the Earth is in motion around the Earth axis (motion of object relative to the ground is transitory, being additional motion to circular motion), which is to say that circular motion is the only form of motion of lasting object. Straight-line motion is impossible to be a type of lasting motion but a motion gone forever; as time goes on, all objects in straight-line motion will eventually fall into an infinite abyss.

Other than straight-line motion, circular motion velocity is an acknowledged motion velocity; for example, persons at ferris wheel center and persons motionless relative to ferris wheel center consider that the cabins of Ferris Wheel are rotating around the ferris wheel center, and persons inside the cabins of ferris wheel also think that they are rotating around the ferris wheel center, so the circular motion of the cabins of ferris wheel is an acknowledged motion rather than a relative motion. In addition, the motions including the Earth's rotation around the Sun and artificial satellite and Moon rotation around the Earth are also acknowledged motions. The analysis shows that any object has only one circular motion velocity, without a second different circular motion velocity; thereby we can determine the only circular motion velocity of object in order to express absolute velocity of object in true motion; the circular motion velocity of object is defined as true motion velocity of object, being absolute velocity principle.

4.2. Calculation of Absolute Velocity

Since there is no difference in top, bottom, left, right, front and back in universe, we may suppose that the fixed stars with their mutual positions unchanged by and large are motionless; namely the motion velocity of fixed stars is zero. In the solar system, the Sun's motion velocity is zero (since the Sun is in rotation and in fact the Sun's rotation axis motion velocity is zero) and the average rotational velocity of the Earth around the Sun is 29.78km/s, then the absolute velocity of the Earth axis is 29.78km/s; similarly, the absolute velocities of the planets including Venus, Mars, Mercury and Saturn can be obtained. However, the ground in every position on the Earth is rotating around the center of the Earth. The Moon and artificial satellite are also rotating around the center of the Earth; if the Moon has satellites rotating around the Moon, these objects do not rotate around the Sun in a direct way, then how to figure out their absolute velocity?

Let the motion velocity of Earth axis be V, the rotational velocity of artificial satellite and Moon or certain place on the Earth surface around the center of the Earth be V_m and the rotational velocity of the Moon's satellite around the Moon be V_n, we are able to determine the absolute velocity relevant to V_m and V_n based on time change formula given in the special relativity.

Let the time motion velocity of the Sun clock be t_0, then, according to time change formula given in the special relativity, the rotational velocity of the Earth axis around the Sun is V and its time t is $t = t_0\sqrt{1-V^2/c^2}$; if the rotational velocity of the Moon relative to the Earth is V_m, then the Moon's time $t_m = t\sqrt{1-V_m{}^2/c^2} = t_0\sqrt{1-V^2/C^2}\sqrt{1-V_m^2/C^2}$. Let the Moon's absolute velocity be V_m', then there will

be $t_m = t_0\sqrt{1-V_m'^2/c^2}$. It is observed from comparison between the two t_m formulae that

$$\sqrt{1-V_m'^2/c^2} = \sqrt{1-V^2/c^2}\sqrt{1-V_m^2/c^2}$$
$$= \sqrt{1-V^2/c^2-V_m^2/c^2+V^2V_m^2/c^4}$$

Since V and V_m are very small relative to C, $v^2v_m^2/c^4$ is extremely small and can be ignored; accordingly, it is observed from the above mentioned formula that

$$V_m' = V^2 + V_m^2, V_m' = \sqrt{V^2+V_m^2}. \quad (11)$$

The rotational velocity of the Moon's satellite around the Moon is V_n, and the time for the Moon's satellite is:

$$t_n = t_m\sqrt{1-V_n^2/C^2} = t_0\sqrt{1-V_m'^2/C^2}\sqrt{1-V_n^2/C^2}$$
$$= t_0\sqrt{1-\left(V_m'^2+V_n^2\right)/C^2}.$$

Let the absolute velocity of the Moon's satellite be V_n', then, there will be $t_n = \sqrt{1-V_n'^2/C^2}$ and the following expressions can be obtained:

$$V_n'^2 = V_m'^2 + V_n^2 = V^2 + V_m^2 + V_n^2$$
$$V_n'^2 = \sqrt{V^2+V_m^2+V_n^2} \quad (12)$$

We are able to calculate the absolute velocity of any object in universe based on above mentioned expressions.

4.3. Absolute Time

Length, mass, time and force are fundamental physical quantities for analysis of object motion and interaction. On the premise of invariable position, the length, mass, force and time motion velocity have constant values. However, since the clock for time measurement is not only used to measure time motion velocity but also to record total amount of time accumulated as time goes on, this total amount is to increase as time goes on, being an increasing physical quantity. Accordingly, if an object moves from certain point on the Earth to other position (such as Mars) and then returns to this original point on the Earth after a period of time, although the object remains unchanged in length, mass, force and time motion velocity before and after moving, the total amount of time recorded by clock has increased substantially; we draw a comparison between increment of the total amount of time recorded by the clock and the increment of total amount of time recorded by other clock without moving at the point so as to calculate the time motion velocity of the object in other position (such as Mars) based on the difference between the two increments, and figure out the absolute velocity of the other position. It can be seen that time is the only physical quantity available for us to determine change in position and motion velocity of object, given such a key role time plays, so we need to explain it in detail.

Since every point in universe is different in time and clock motion velocity, we need a standard clock as a reference for comparison of clock motion velocity. The Sun's absolute velocity is zero, so the Sun clock should be a standard clock, but as the Sun's temperature is too high, it cannot serve as a standard clock; therefore, for the sake of convenient comparison and analysis and consideration, the Earth clock should be the most suitable standard clock.

It is observed from the motion velocities V, V_m and V_n of the above mentioned Earth, Moon and Moon's satellite that if we let the Earth's pole (Earth axis) clock time t be standard time, then the Moon's time:

$$t_m = t\sqrt{1-V_m^2/C^2}. \quad (13)$$

The Moon's satellite time:

$$t_n = t_m\sqrt{1-V_n^2/C^2} = t\sqrt{1-V_m^2/C^2}\sqrt{1-V_n^2/C^2}$$
$$\approx t\sqrt{1-\left(V_m^2+V_n^2\right)/C^2}. \quad (14)$$

Given that the rotational velocity of terrestrial equator ground relative to Earth axis is 0.464km/s, the rotational velocity of the ground with any latitude θ on Earth is $V_\theta = 0.464\cos\theta$ km/s. V_θ is the velocity of any point on Earth's surface relative to V_m.

$$t_\theta = t\sqrt{1-0.2156\cos^2\theta/C^2} \quad (15)$$

Given that the Sun's time is t_0, the Earth's rotational velocity is V and $t = t_0\sqrt{1-V^2/C^2}$, then there is

$$t_0 = t/\sqrt{1-V^2/C^2} \quad (16)$$

Let the rotational velocity of any planet around the Sun be V_x, then the planet's time:

$$t_x = t_0\sqrt{1-V_x^2/C^2} = t\sqrt{1-V_x^2/C^2}/\sqrt{1-V^2/C^2} \quad (17)$$

As mentioned above, the absolute velocities of the Moon and its satellite are not V_m and V_n but V_m' and V_n', then are t_m and t_n in expressions (13)(14) also true times relative to the true absolute velocities V_m' and V_n' of the Moon and its satellite? As long as we substitute $t = t_0\sqrt{1-V^2/C^2}$ into expressions (13) and (14), there will be:

$$t_m = t_0\sqrt{1-V^2/C^2}\sqrt{1-V_m^2/C^2} = t_0\sqrt{1-V_m'^2/C^2} \quad (18)$$

$$t_n = t_m\sqrt{1-V_n^2/C^2} = t\sqrt{1-V_m^2/C^2}\sqrt{1-V_n^2/C^2}$$
$$= t_0\sqrt{1-V^2/C^2}\sqrt{1-V_m^2/C^2}\sqrt{1-V_n^2/C^2} \quad (19)$$
$$= t_0\sqrt{1-\left(V^2+V_m^2+V_n^2\right)/C^2} = t_0\sqrt{1-V_n'^2/C^2}.$$

It is observed from comparison between expressions (13)(14) and expressions (18) (19) that t_m and t_n obtained by calculation based on true absolute velocities V_m' and V_n' of object are t_m and t_n obtained by calculation based on V_m and V_n of object and Earth clock standard. It can

be seen that the times t, t_m, t_n and t_x are the intrinsic and true times of object. Relative to absolute velocity, we define true time of object as absolute time.

Given absolute time, we may take all places with same absolute time as one equal time zone; for example, all places with the same latitude are taken as one equal time zone.

According to the above mentioned analysis results, we can figure out the due absolute time process of an object having experienced various motions. For example, take h representing 1 hour of time on Earth axis as reference, put a clock in a place with latitude 45° on Earth for $n_1 h$, and then put it on the Moon for $n_2 h$, and then put it on a certain X planet of the Sun for $n_3 h$; if the time spent in traveling from the Earth to the Moon and then from the Moon to X planet is not taken into consideration, then the absolute time of the accumulative motion of the clock (where $\cos^2 45^\circ = 1/2$) is:

$$\begin{pmatrix} n_1\sqrt{1-0.2153/2C^2}+n_2\sqrt{1-V_m^2/C^2} \\ +n_3\sqrt{1-V_x^2/C^2}\Big/\sqrt{1-V^2/C^2} \end{pmatrix} h.$$

4.4. Experimental Verification of Absolute Velocity

J·C·Hafele and R·E·Keating made an experiment on relation between time change and object motion velocity in 1971. They put four caesium atomic clocks on plane over equator; when the plane flies around the Earth from east to west along equator, it is found that the four caesium atomic clocks on the plane gained 273×10^{-9} second in terms of average counting as compared with the caesium atomic clocks on the ground; namely the absolute time of atomic clock increased; when the plane flies around the Earth from west to east along equator, it is found that the four caesium atomic clocks on the plane ran 59×10^{-9} second behind in terms of average counting as compared with the caesium atomic clocks on the ground; namely the absolute time of atomic clock decreased (as shown in reference document 1). The reference document 1 points out that it is universally accepted that based on special relativity theory, the clock on the object flying above the Earth is certain to run slower than the clock on the ground; namely, the absolute time is short. However, the above mentioned experiment shows that the clocks on the plane flying towards west did not only run behind but also gain time; namely the absolute time increased. Of course, the experiment also shows that the clock on the plane flying toward east runs behind in deed and the absolute time has decreased. The question is why the absolute time of clock on the plane flying toward west increased and why the absolute time of clock on the plane flying toward east decreased.

The above mentioned experiment result can be explained by absolute velocity principle. The foregoing indicates that the rotational velocity of object and any point on the ground relative to Earth axis is V_m given in expression (13), suppose the rotational velocity of the ground along equator is υ and the travel velocity of plane is u, when plane flies toward east, the flying direction of the plane is identical to the rotational direction of equatorial ground around Earth axis; thus, the actual rotational velocity of the plane around Earth axis is $V_m' = \upsilon + u$. When the plane flies toward west, the flying direction of the plane is opposite to direction of rotation of the Earth; accordingly, the actual velocity of the plane is $V_m'' = \upsilon - u$. It is observed from the above mentioned expression (13) $t_m = t\sqrt{1-V_m^2/C^2}$ that the absolute time of equatorial ground is $t_\upsilon = t\sqrt{1-\upsilon^2/C^2}$, the absolute time when plane flies towards east is $t' = t\sqrt{1-(\upsilon+u)^2/C^2}$ and the absolute time when plane flies toward west is $t'' = t\sqrt{1-(\upsilon-u)^2/C^2}$. It is obvious that when t'' is larger than t_υ, the clock on the plane flying toward west gains time, and when t' is smaller than t_υ, the clock on the plane flying toward east runs behind, with time dilated.

J·C·Hafele and R·E·Keating figured out that the caesium atomic clock on the plane flying toward west should be 275×10^{-9} seconds faster than the caesium atomic clock on the ground along equator based on such difference, being consistent with actual reading by and large. They calculated that the caesium atomic clock on the plane flying toward west should be 40×10^{-9} seconds slower than the caesium atomic clock on the ground along equator, although the result seems to be different from actual reading of 59×10^{-9} seconds to a greater extent. But this is only the difference in comparison rather than true error in calculation; for example, the wall height is 300cm, tree height is 301cm and the tree is 1cm higher than wall, but the calculated tree height is 304cm, resulting in that tree is 4cm higher than wall, big difference between 4 and 1. However, this is the difference in comparison rather than error of calculation. The error in calculation is error between 304 and 301, within 1%. In a similar way, the difference between 59×10^{-9} and 40×10^{-9} in comparison is 19×10^{-9} seconds; if this difference is compared with the flight time of plane for more than 10^5 seconds, the error should be tiny; therefore, we may consider that the result of experiment by J·C·Hafele and R·E·Keating is consistent with the result of analysis of absolute velocity principle by and large.

Only one test result is not adequate to confirm that absolute velocity principle is correct, so we also need to carry out some other tests to further verify the principle. There are two simple and practicable tests available as follows:

1. We selected caesium atomic clocks with the same time operation velocity by and large in Singapore at $1^\circ09'$ north latitude: one clock is kept motionless in Singapore and the other one clock is transported to Reykjavik, the capital of Iceland at $64^\circ09'$ north latitude. Since the absolute velocity of Reykjavik is much smaller than absolute velocity of Singapore, the caesium atomic clock in Reykjavik is much faster than the caesium atomic clock in Singapore according to absolute velocity principle. When these two caesium atomic clocks are brought into

comparison in terms of reading by internet, the longer time will result in bigger difference between them according to absolute velocity principle.

2. Synchronous satellite is motionless relative to the Earth. Synchronous satellite is about 36000km away from the ground in height, and the Earth radius is about 6370 km. According to absolute velocity principle, the absolute velocity of synchronous satellite's rotation around the center of the Earth is 6 times larger than that of the ground's rotation around the center of the Earth; therefore, the clock on synchronous satellite should be slower than that on the ground; namely the absolute time is short, which can be verified by testing without difficulty.

And now, we can explain twin paradox in a simple way. The foregoing indicates that whether clock gains time or runs behind is dependent on absolute velocity of clock; therefore, if twin A is higher than twin B in absolute velocity, the t_m of twin A should be short, indicating that it is younger than twin B; otherwise, twin B is younger than twin A. For example, twin A taking the plane flying toward east is younger than twin B on the ground, and it is not when taking the plane flying toward west.

5. Correspondence Principle

Special relativity indicates that for an object moving at a velocity of V, its length l should be shortened to be $l' = l\sqrt{1-V^2/C^2}$, its mass m should be increased to be $m' = m\sqrt{1-V^2/C^2}$, its time t should be shortened to be $t' = t\sqrt{1-V^2/C^2}$. Namely l, m and t of object in motion be transformed to l', m' and t' at the same time; in other words, for every velocity V of an object in motion, l will transform to a unique l', m will transform to an unique m', and t will transform to an unique t'. According to foregoing absolute velocity, as every absolute velocity has one unique absolute time, they are certain to have corresponding absolute mass and absolute length. It is obvious that the absolute mass is rest mass, and the absolute length is rest length. Accordingly, our conclusion is that the rest mass, rest length, rest time and rest force of every object in universe are in one-to-one correspondence with absolute velocity of such object. The conclusion is defined as the correspondence principle.

According to the correspondence principle, for an object with rest mass of m in the South Pole or North Pole of the Earth, the absolute velocity of its rotation around the Sun is 30km/s; if it is moved to the Mars whose absolute velocity of rotation around the Sun is about 24km/s, as the mass is directly proportional to $1/\sqrt{1-V^2/C^2}$, its rest mass on the Mars is to decrease to $m_x = m_0\sqrt{1-(30)^2/C^2}\,/\sqrt{1-(24)^2/C^2}$. If it is moved to the moon, given that the rotational velocity of the Moon's rotation around the Earth is about 1km/s, it is observed from the previous expression (11) that the absolute velocity of the Moon is $V_m' = \sqrt{V_m^2+V^2} = \sqrt{1+(30)^2} = \sqrt{901}$, and the rest mass of the object is to increase to $m_m = m\sqrt{1-(30)^2/C^2}\,/\sqrt{1-901/C^2}$.

6. Relative Transformation and Absolute Transformation

Regarding to above mentioned flight experiment by J·C·Hafele and R·E·Keating, the experiment proved that t as clock time on the plane flying toward west along equator increased, which means the clock gained time, and that t as clock time on the plane flying toward east along equator decreased, which means the clock ran behind. We explained this experiment result by absolute velocity principle. However, the result observed by person on the ground along equator is different from the result of experiment; in his or her view, the flight velocity of the plane should be the same velocity u, no matter whether the plane flies to east or to west. According to Lorentz transformation in special relativity theory, one and the same velocity u should have identical length transformation $l' = l\sqrt{1-u^2/C^2}$, time transformation $t' = t\sqrt{1-u^2/C^2}$, mass transformation $m' = m/\sqrt{1-u^2/C^2}$ and vertical force transformation $F' = F/\sqrt{1-u^2/C^2}$.

This indicates that for the result observed by person on the equatorial ground, time t of the clock on the plane flying toward east and time t of the clock on the plane flying toward west are one t; it is different from the true time t of plane, so we wonder whether special relativity theory is wrong. Of course not, it is certain that special relativity theory is correct, and many experiments including μ particle life experiment, high velocity particle mass increase experiment, contraction experiment on electric field with electron in motion at high velocity have verified l', m' and t' deduced by special relativity theory. The only conclusion we drew based on these experimental results is that l', m' and t' of object in motion observed by person on the ground are different from the true l, m and t of object in motion.

It is observed from analysis that the result is inevitable. For example, we observe that length of an object in motion is reduced, with its mass increased and time shortened; however, the true length, mass and time of an object remain unchanged, just like a train in motion at a velocity of V on the ground, its velocity observed by a motionless person relative to the ground is V; its velocity observed by a person in motion at a velocity of V relative to the ground is 0; its velocity observed by a person in motion at a velocity of $-V$ relative to the ground is $2V$. These results of observation are true, but they are not true absolute velocity of the train.

According to the above mentioned analysis, an inevitable conclusion we draw is that the transformed values of time, mass, length and force of the object deduced based on special relativity theory and absolute velocity of the object are true values of the object itself,

being the result of observation by a motionless person relative to the object, and the transformed values of time, mass, length and force of the object deduced by relative velocity between observer and object according to special relativity theory are a reference system and the true result of observation of time, mass, length and force in another reference system in relative motion; one of them is observation at rest and another one is observation in motion; therefore, it is inevitable that results of observation are different.

We define Lorentz transformation deduced according to absolute velocity of the object as absolute transformation and Lorentz transformation deduced according to relative velocity of the object as relative transformation. The result of absolute transformation expresses true physical quantity of the object itself, and the result of relative transformation expresses true result of observation of the object in motion.

7. Field Similarity Principle

According to Coulomb's law, the acting force between two point charges in vacuum is in direct proportion to product of their electric quantities Q_1 and Q_2 and in reverse proportion to square of r as the range between them, with direction of acting force along their connecting line. The law's expression is as follows:

$$F = k\frac{Q_1 Q_2}{r^2} \qquad \text{(a)}$$

Where, k is proportional constant, also referred to as electrostatic force constant

According to the law of universal gravitation, all objects in university are in mutual attraction and the magnitude of gravitation between two objects is in direct proportional to product of m_1 and m_2 as their mass and in reverse proportional to square of the range between them. The law's expression is as follows:

$$F = G\frac{m_1 m_2}{r^2} \qquad \text{(b)}$$

Where, G is constant of universal gravitation

Obviously, G and K are also proportional constants; therefore, expression (a) and expression (b) are completely similar.

Electricity points out that F as force of Coulomb's law is electric field force, the electric field strength at Q_1 and Q_2 is $E = kQ_1/r^2$, the electric field is source to exert force on Q_2. And so, the force of universal gravitation is gravitational field force, the gravitational field strength at m_1 and m_2 is expressed by D, $D = Gm_1/r^2$ gravitational field is the source to exert a force on m_2.

Given that the generation of electric field is due to electric quantity of electric charge, in fact, it is as a result of electric quantity of negative electron or positive electron. An electric charge or a charged body has constant number of negative electrons or positive electrons, a charge or charge body will have constant number of electrons (negative or positive) regardless of motion and velocity, since electron is constant in electric quantity, therefore, the electric quantity of charge or charged body is unrelated to velocity.

Electric field is matter, gravitational field is certain to be matter. Electric field is due to negative electron or positive electron, it is certain that gravitational field is also as a result of source, it is obvious that the source is certain to be in atom of object, since there is only repulsion between negative electrons or between positive electrons, accordingly, it is impossible that there is repulsion and attraction between them at the same time, therefore, we suppose that gravitational field of object is unrelated to negative electron and positive electron in object, this gravitational field is only related to proton with negative electron removed and neutron with positive and negative electrons eliminated, according to existing noun, we define proton free of electron and neutron free of positive and negative electrons as graviton, graviton is source of gravitational field. Since negative electron and positive electron have mass, therefore, the mass of graviton in object is about millesimal smaller than total mass of object.

Since object in any motion and at any velocity has constant number of gravitons inside, namely object is unchanged in gravitational capacity, the gravitational mass of universal gravitation is derivable from gravitational capacity. Therefore, our conclusion is that the gravitational mass of object is unrelated to motion of object and gravitational mass is constant.

To say the least, supposing that there is attraction between negative electrons as well as between positive electrons, namely the entire atoms are graviton and object motion cannot change number of atoms, namely it cannot change gravitational capacity by and large, the conclusion is that gravitational mass of object is unrelated to motion of object, gravitational mass is constant.

The above mentioned analysis indicates that gravitational field and electric field have completely similar action pattern, the two fields are also derivable from certain field source matter. When electric field is in motion, the number of negative electrons or positive electrons in its field source matter keeps unchanged, namely, electric quantity is unchanged; when gravitational field is in motion, the number of gravitons in its field source matter is also unchanged, namely gravitational capacity is unchanged; by further deduction, when electron is in accelerated motion, its form of motion is to propagate from the near to the distant at light velocity and form electric wave in its electric field, quite as much, when graviton is in accelerated motion, its form of motion is also to propagate from the near to the distant at light velocity and form gravitational wave in its gravitational field; electric field has energy, gravitational field should also have energy, in other words, gravitational field and electric field are completely similar in physical property, which is referred to as field similarity principle.

Field similarity principle determines that gravitational mass of object is a constant unrelated to motion of object; however, experiment verifies that inertia mass of object is on the increase with the increase of its motion velocity; therefore, gravitational mass (in fact it is gravitational capacity) and inertial mass are two different physical quantities in terms of property, they are different in property and there is no comparison between them, just as

there is no comparison between velocity and displacement; therefore, the supposition that gravitational mass is equal to inertial mass is unscientific; in other words, strictly speaking, the equivalence principle is invalid.

We may also further explain that gravitational mass and inertial mass are different physical quantities in terms of property in the following respects:

Gravitational mass and inertial mass are equally derivable from elevator effect, when elevator suddenly goes up, person therein will feel that his or her weight is increased. Its seems that there is no difference between such weight increase and gravity increase; namely there is no essential difference between inertial force and universal gravitation, and then the deduction that gravitational mass is equal to inertial mass came into being; however, it is observed from further analysis that inertial force is energy transfer force, and universal gravitation is unrelated to energy transfer; because; if A exerts force F to move object B whose mass is m for a space S within time t, the energy output from A is FS, while object B is in motion at an acceleration of a under the action of F. Its motion space S.

As a result, $FS = Fat^2/2$. B is to get velocity $V = at$ within time t, the energy it gets is $mV^2/2 = m(at)^2/2$, it is certain that the energy outputted from A and energy B gets is identical, therefore, $Fat^2/2 = ma^2t^2/2$ with eliminated on both sides at the same time will be inertial force equation $F = ma$, indicating there is inertial force, with energy obtained by object, which is to say that inertial force is a type of energy transfer force, whereas, universal gravitation may act on motionless object forever, in other words, universal gravitation is not energy transfer force. It is obvious that energy transfer force and non energy transfer force are different in terms of property, namely, inertial force as energy transfer force is impossible to equal to universal gravitation as non energy transfer force, namely, inertial mass is impossible to equal to gravitational mass.

In addition, inertial force is force to move object, namely inertial force is in motion state forever, and universal gravitation may in stationary state forever, inertial force in motion may remain unchanged; since there is no absolutely uniform gravitational field for universal gravitation, universal gravitation in motion is certain to change all the time, the essential difference between inertial force and universal gravitation also indicates that inertial mass is not equal to gravitational mass.

In addition, if inertial mass is equal to gravitational mass and when object whose mass is m in motion at a velocity of V, according to special relativity theory, m is certain to increase to $m' = m/\sqrt{1-v^2/c}$. Gravitational mass is to increase from m to m', its gravitational field strength is certain to increase accordingly. However, the gravitational field is a matter and it is impossible to generate or vanish matter by any means in universe; accordingly, total capacity of gravitational field is impossible to increase, the source of gravitational field namely gravitational mass is also impossible to change, indicating that $m' = m/\sqrt{1-v^2/c}$ is not applicable to gravitational mass, namely gravitational mass is not equal to inertial mass.

In addition, the foregoing article 1.5 points out that if gravitational mass is equal to inertial mass of object, just like the object in motion at high velocity as shown in Figure 1. The spring will be compressed substantially, and it is obvious that this is not the fact, proving that gravitational mass is not equal to inertial mass.

The above mentioned analysis shows that gravitational mass is impossible to equal to inertial mass, namely equivalence principle fails to hold water in principle. We know that equivalence principle is theoretical basis for general relativity theory; equivalence principle is invalid in principle, naturally, general relativity theory is impossible to be a perfect truth.

When object is in motion at a velocity of V, being a tiny velocity compared with light velocity C, for example V < 1000km/s, there is $\sqrt{1-v^2/c} \approx 1$, under such condition, there will be $m' \approx m$, namely inertial mass of object is approximately equal to rest mass of object, indicating that inertial mass is constant, since gravitational mass is also constant; therefore, if we select suitable constant of proportionality to make inertial mass equal to gravitational mass, which are two different physical quantities in terms of property, just like a proportional constant may make length equal to pressure.

When the motion velocity of object is tiny compared with light velocity, inertial mass may be considered to be equal to gravitational mass, namely equivalent principle may be considered to hold water; therefore, when the motion velocity of object is tiny compared with light velocity, the deduction by general relativity theory is supposed to be correct. Since the motion velocity of every celestial body is tiny compared with light velocity, the general relativity theory is applicable to all celestial bodies in universe.

8. No Black Hole

8.1. Double Equilibrium Principle of Universal Gravitation

Figure 8a shows a planet whose mass is m is rotating around a fixed star M at a velocity of V, the range between m and M is l, physics points out universal gravitation between m and M is $F_0 = GMm/l^2$, centrifugal force generated by planet's rotation around M is $F_m = mV^2/l$, for ; since its centrifugal force F_m and its universal gravitation F_0 from M are equal and they are contrary in direction, m is in equilibrium state, whether M is also in equilibrium state?

The physics fails to analyze it. It is observed from Figure 8a that universal gravitation F_0 to M is the only force on M, according to Newton second law, there will be $F_0 = Ma$, namely there will be M which is to dash against m at an accelerated velocity of a, obviously,

such phenomenon has not occurred, therefore, it is certain that M will have a force F_M identical to F_0 in magnitude but opposite to F_0 in direction, reaching equilibrium with universal gravitation F_0 of m. It is certain that this force is not external; it must be generated by M, in additional to universal gravitation, and M is also to generate centrifugal force F_M by rotational motion; therefore, centrifugal force F_M by M through rotational motion is the only possibility for M to reach equilibrium. Our conclusion: for a fixed star M, it is certain to generate centrifugal force F_M to reach equilibrium.

Supposing that rotational velocity of M is V_M, since l as connecting line between m and M is constant; therefore, the only motion direction of V_M is contrary to direction of V_m; otherwise, V_M and V_m along the same direction will turn into M and m in parallel motion.

Figure 8b shows motion of M and m, since V_m and V_M are normal to l; therefore, centers of rotation of m and M are on l as connecting line between m and M. Since l is an invariable straight line, therefore, when motion of M and m rotates l to an angle θ, this θ will be rotation angle of m and M, if center of rotation of m and that of M are not on one point, then m and M cannot keep moving in a straight line at the same rotation angle, therefore; it is certain that m and M will have one center of rotation and that the center of rotation will be on l as connecting line between m and M, point O shown in Figure 8b indicates center of rotation of V_m and V_M, the range from point O to m is r_m, the range between point O and M is r_M, supposing that rotation angle of l is ω, there will be $V_m = r_m\omega$; $V_M = r_M\omega$. Since universal gravitation for m and M is one force, mV_m^2/r_m as centrifugal force of m will be identical to M MV_M^2/r_M as centrifugal force of M in terms of magnitude but they are contrary in terms of direction. Therefore, there will be:

$$\frac{m(r_m\omega)^2}{r_m} = \frac{M(r_M\omega)^2}{r_M}$$

The equation is simplified as follows:

$$mr_m = Mr_M \tag{20}$$

It is observed from equation (20) that $r_M = r_m m/M$, since $r_m + r_M = l$, therefore, there is:

$$r_m + r_M = r_m + r_m m/M = r_m(1+m/M) = l$$

$$r_m = \frac{l}{1+m/M} = \frac{Ml}{M+m} \tag{21}$$

$$r_M = l - r_m = \frac{ml}{M+m} \tag{22}$$

Centrifugal force generated by m in motion at a velocity of V_m

$$F_m = \frac{mV_m^2}{r_m} = \frac{m(M+m)V_m^2}{Ml} \tag{23}$$

Given that motion velocity of M is $V_M = r_M\omega$, and $V_m = r_m\omega$, therefore,

$$V_M = r_M V_m/r_m = \frac{r_M}{r_m}V_m = \frac{m}{M}V_m \tag{24}$$

Centrifugal force generated by M in motion at a velocity of V_M

$$F_M = \frac{MV_M^2}{r_M} = \frac{M(V_m m/M)^2}{ml/(M+m)} = \frac{(M+m)mV_m^2}{Ml}$$

It is obvious that centrifugal force of M is certain to equal to that of m, namely $F_M = F_m$. Since centrifugal force of m and M is certain to equal to universal gravitation of m and M, therefore, there is

$$G\frac{Mm}{l^2} = \frac{(M+m)mV_m^2}{Ml} \tag{25}$$

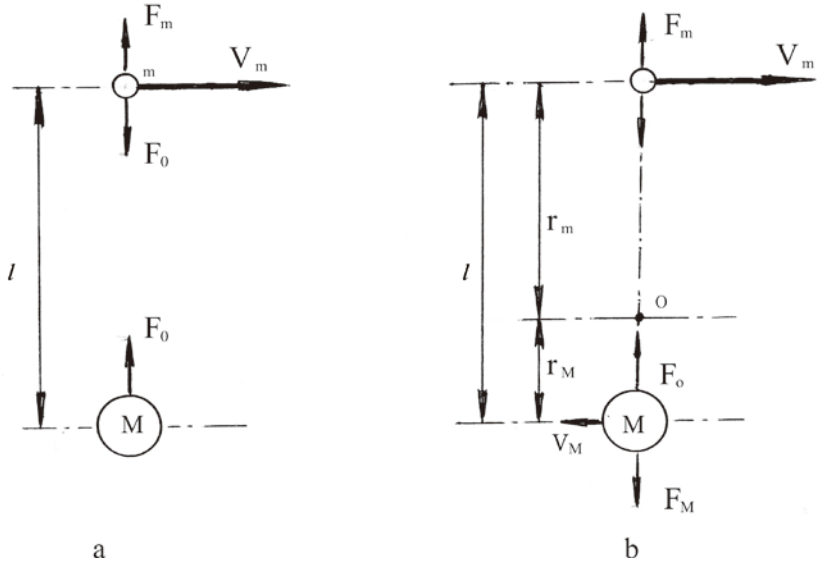

Figure 8. m and M are in force balance state

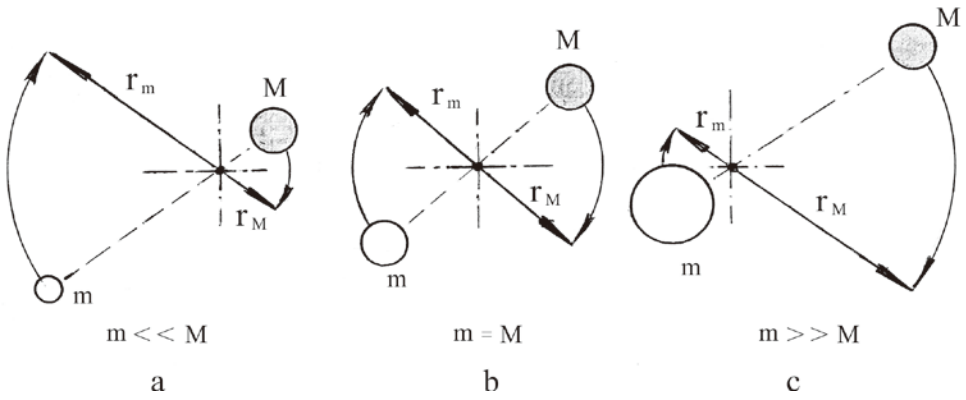

Figure 9. Relation between size proportion and motion of M and m

Equation (25) expresses acting force of both parties related to universal gravitation, being equilibrium equation in equilibrium state. We call such acting force of both parties related to universal gravitation in equilibrium state as double equilibrium principle for universal gravitation.

It is observed from comparison that there is obvious difference between equation (25) and $GMm/l^2 = mV_m^2/l$ given in physical text book. It is observed from equation (25) that the actual velocity of planet m 's rotation around fixed star M is as follows:

$$V_m = \sqrt{\frac{GM^2}{l(M+m)}} \tag{26}$$

It is observed from equation (22) and equation (24) that actual velocity of fixed star M is as follows:

$$V_M = \frac{m}{M}V_m = \sqrt{\frac{Gm^2}{l(M+m)}}. \tag{27}$$

It is worth mentioning that the previous equation (21) $r_m = Ml/(M+m)$ and equation (22) $r_M = ml/(M+m)$ are one equation in fact; one is to indicate the range from m to center of rotation of M and m and the other is to indicate the range from M to O; they are equation to calculate position of O. According to these two equations, we may estimate motional orbit of m and M based on their size proportion.

Figure 9 shows relation between size proportion and motion orbit of M and m. According to Figure 9a, when $m << M$, it may be taken as m 's rotation around M; according to Figure 9b, when $m = M$, $r_m = r_M$, M and m have same radius of rotation; according to Figure 9c, when $m >> M$, r_M is much larger than r_n, it may be taken as fixed star's rotation around planet.

The above mentioned analysis is carried out on the premise that fixed star M has only one planet m, if M has two m, with two m located on both sides of M symmetrically, then the universal gravitation of two m to M will cancel out, therefore M is in equilibrium state; if two m is asymmetrical to M, or just like the Sun has many planets, it is necessary to analyze the result of composition of all universal gravitations of all planets to fixed star.

The foregoing equation (22) $r_M = ml/(M+m)$ indicates radius of circle of fixed star M in circular motion. It is observed from the equation that when the Sun has only one planet namely the Earth, the radius of rotation of the Sun is about 448.7km, this radius is tiny as compared with 695000km as the radius of the Sun but the radius of rotation of the Earth is large relative to the moon, the Earth 81times the Moon in terms of mass, by calculation, the Earth's $r_M \approx 4687.8$km, compared with 6371km as the radius of the Earth, the r_M is about 73.6% of the radius of the Earth, namely the center of rotation for the Moon and Earth is only 1683.3km away from the Earth's surface, therefore, the Earth's circular motion relative the Moon will substantially influence the orbit of the Earth's rotation around the Sun (it is necessary to take the change in universal gravitation from the Sun to the Earth into consideration when we calculate the change of the Earth orbit, the orbit change should not be considerate as simple composition of small circle and great circle), making the orbit of the Earth's rotation around the Sun cease to be a smooth elliptical curve.

Taking rotational velocity of the Moon as an example to explain why there is difference between our feeling and actual condition, the actual length from the Moon to the Earth l = 384402km, the actual angular velocity of the Moon is ω, the rotational velocity of the Moon we observed is $V = l\omega =$ 1020m/s, however, according to the previous equation (22), the actual radius of rotation of the Moon is $r_m = ML/(M+m) = 379714$ km, the actual rotational velocity of the Moon should be $V_m = r_m\omega = 1008$ m/s. Why is the actual V_m different from V we observed? Because the Earth has a V_M opposite to V_m in direction, the Earth radius of rotation $r_M = 4687.8$ km, $V_M = r_M\omega = 12$ m/s. V as the rotational velocity of the Moon we observed is certain to be the sum of V_m and V_M, namely $V = V_m + V_M$ = 1008m/s+12m/s=1020m/s.

8.2. Black Hole is Impossible to be Object in Motion

Supposing that there is black hole and that black is an object in motion, and then what kind of motion the black hole is likely to go through? It is obvious that the motion

is not a straight line motion, since straight line motion is to go forward and never go backward, it will go into the infinite abyss, therefore, black hole will only go through motion in cycles, supposing that the black hole's mass is m and that the radius of circular motion is r and that the rotational velocity is v, it is certain that black hole will generate centrifugal force $F_m = mv^2/r$. In order to balance the force, black hole will need a force identical to F_m in magnitude but contrary to F_m in direction, this force will only be universal gravitation. Supposing that there is a fixed star with a mass of M to balance the centrifugal force of black hole, the length from M to m is l, and then the universal gravitation generated by M to black hole is $F = GMm/l^2$, the equilibrium between M and m is expressed by the previous equation (25).

Given that the largest fixed star A_1 in universe is 150 times the Sun in terms of mass, supposing that there is a fixed star whose mass is identical to that of A_1 to balance the centrifugal force of black hole. The existing data show that the smallest diameter of black hole is 24km, but the black hole theory points out that the mass of a black hole whose size is similar to that of a football court (to calculate based on sphere whose diameter is 120m) is about the mass of 4 suns. It is observed from the calculation that m as the mass of the minimum black hole is 213000 times the M as the mass of the largest fixed star, namely m=213000M. It is observed from the foregoing equation (21) $r_M = Ml/(M+m)$ and equation (22) $r_m = ml/(M+m)$ that the radius of rotation of fixed star M is $r_M \approx l$.

However, the radius of rotation of black hole is $r_m = 4.6\times10^{-6} l$, indicating that if we adopt the universal gravitation from largest fixed star M to the smallest black hole m to balance centrifugal force generated by rotational velocity of black hole, the only possibility is that the fixed star is to rotate around the black hole and that the black hole is motionless by and large. It is obvious that there will be no such fixed star rotating around the black hole, and there will be no black hole in rotary motion. Therefore, our conclusion is that black hole is impossible to be an object in motion, namely the motion velocity of black hole is 0. It is observed from the conclusion that even if equivalence principle is valid, on the premise that the motion velocity of black hole is on, no one could make a deduction that black hole is existent, namely, under the condition of $V = 0$, block hole theory is invalid, we will verify that black hole is not an actual matter in terms of matter structure of black hole as follows:

8.3. Black Hole is Impossible to be Matter Composed of Atom

Black hole theory points out that a spherical black hole with a diameter of 120m is equal to four suns in terms of mass, being equivalent to the mass of 1.32 million Earths, and the volume of the Earth is 10^{15} times larger than the sphere with a diameter of 120m, indicating that the density of black hole is 10^{21} times larger than that of the Earth, according to calculation based on such proportion, the one thousand times of the total mass of 7 billion people (according to 50kg per person) on Earth is also smaller than the mass of a block hole whose size is equivalent to a grain of rice.

It is known that every matter in universe is composed of several elements in 118 elements. Up to now, there has been no exception in celestial bodies. However, according to the above mentioned calculation of black hole matter density, the size of atom of black hole is only 10^{21} that of the Earth. Obviously, this is impossible, the reason for which is that if we suppose that black hole is composed of atom, as black hole theory says that the black hole atoms have collapsed, with electrons around atom falling onto protons and turning into neutrons. These neutrons box up to become a large neutron; it is observed from calculation that such large neutron is also one million times larger than theoretical volume of black hole; if atoms of black hole do not collapse, it will be ten trillion times larger than theoretical volume of black hole, so it is impossible for actual atom; therefore, we conclude that black hole is impossible to be composed of actual atoms, namely, black hole is not an actual matter.

Why did black hole theory make such an impractical deduction? It is observed from analysis that black hole theory is derivable from general relativity theory, and the theoretical basis for general relativity theory is equivalence principle. The foregoing has shown that equivalence principle is invalid in principle; only if object's motion velocity is tiny as compared with light velocity, the equivalence principle may be considered to be approximately valid. Black hole theory takes equivalence principle as absolute truth; misunderstanding of equivalence principle resulted in the improper conclusion that it is applicable to any velocity and that visional black hole is existent.

The above mentioned shows that black hole is impossible to be actual matter, and black hole theory is invalid under the condition of $V = 0$, indicating that the black hole is not only visionary but also inexistent in theory.

9. It is Impossible for Human to Realize Significant Time Travel

The foregoing indicates that time is significant, being the time operation velocity. The higher time operation velocity means clock gains time; to be specific, the time quickens. The low time operation velocity means clock runs behind, to be specific, the time dilates. It is obvious that time dilation to more vivid to express low time operation velocity compared with that time decreases, but it is improper to say that increase in time operation velocity is time dilation. We will only discuss the issue about time decrease, and we will use time dilation to express the issue as follows:

Human is able to accelerate the absolute velocity of particle to the velocity approximate to light velocity by synchrocyclotron so as to prolong the life of particle by tens of times; however, for an object with certain mass, even if the mass is only 1g, up to now, human cannot accelerate its velocity to the velocity approximate to light velocity. It is observed from calculation that it is more difficult to accelerate the velocity of an object of 1g in

mass to 0.1C than to send a heavy of 1000kg into the moon. However, we cannot eliminate the possibility that human can accelerate the velocity of heavy to the velocity approximate to light velocity by advanced technology; it is possible for human to take spaceship at a velocity of being approximate to light velocity to achieve time travel to prolong human life by several times, but the in-depth analysis shows that it is impossible for human to achieve time travel to prolong human life by several times.

The foregoing shows that only the object in circular motion will have absolute velocity and absolute time, and only circular motion will have motion state in cycles, such as planets of the Moon and the sun, whose motions are eternal. Straight-line motion is transient motion, having relative velocity and relative dilation, being the motion to go forward and never to return; in other words, straight line motion is unrelated to human's time travel, accordingly. We discuss time dilation only by analysis of circular motion.

Synchrocyclotron is able to accelerate the motion velocity of particle to the velocity approximate to light velocity, but the spaceship for human cannot achieve motion at high velocity by similar synchrocyclotron, the reason for which is that human cannot bear the centrifugal force due to circulation motion at high velocity other than difficulty in production of great accelerator for spaceship. It is observed from calculation that if human is in motion at a velocity of ten thousandth of light velocity in cyclotron, namely velocity is V=30km/s, given that human mass is 50kg and supposing that radius of cyclotron is 50km, the centrifugal force human bear is up to 900000 Newton, being about 1800 times the gravity of human (about 500 Newton), and such huge centrifugal force cannot be borne by human, let alone velocity further accelerated by 10000 times.

Since universal gravitation of celestial bodies in universe (their mass is expressed by M) can balance out the centrifugal force in circular motion, human in spaceship's rotation around celestial body in universe means that human obtain absolute velocity, absolute time, being an practical approach to achieve actual time dilation. Suppose human's mass is m, and radius of rotation of m around M is r, rotation velocity is V, then, when m's rotation around M is in stable state, there will be centrifugal force mV^2/r equal to universal gravitation GMm/r^2, as shown in foregoing modified equilibrium equation between universal gravitation and centrifugal force;

$$G\frac{Mm}{r^2}=\frac{(M+m)mV^2}{Mr}$$

m at the left end of the above mentioned equation is gravitational mass, being a constant and m at the right end thereof is inertial mass; in case of high V, m is to become $m'=m\Big/\sqrt{1-V^2/C^2}$, accordingly, the above mentioned equation will become:

$$G\frac{Mm}{r^2}=\frac{\left(M+m\Big/\sqrt{1-V^2/C^2}\right)m\Big/\sqrt{1-V^2/C^2}}{Mr}V^2$$

Since the m of spaceship is tiny compared with M of celestial body, even if $m'=100$ m, m' is still tiny as compared with M; therefore, there will be $\left(M+m\Big/\sqrt{1-V^2/C^2}\right)\Big/M$ approximate to 1, and the above mentioned equation can be simplified as:

$$G\frac{Mm}{r^2}=\frac{mV^2}{r\sqrt{1-V^2/C^2}}.$$

After elimination of m/r from both ends of equation, there will be $GM/r=V^2\Big/\sqrt{1-V^2/C^2}$, $V^2=GM\sqrt{1-V^2/C^2}\Big/r$, to solve the equation to obtain:

$$V=\frac{1}{\sqrt{2}}\left[\frac{G^2M^2}{C^2r^2}+\left(\frac{G^4M^4}{C^4r^4}+4\frac{G^2M^2}{r^2}\right)^{1/2}\right]^{1/2}. \quad (28)$$

It is observed from the equation (28) that the solution to select large M and small r as radius of rotation will be adopted to improve velocity of spaceship's rotation around celestial body.

The above mentioned analysis is based on the premise that black hole with super huge mass is eliminated. Therefore, the only way is to look for a celestial body with huge mass and medium radius (large radius will lead to large r) in universe. celestial observation only found fixed star A_1 is huge in mass and medium in radius; its mass is 150 times that of the sun and its diameter is 114 times that of the Sun, (reference documents 6); suppose there is human living on the planet adjacent to it and that spaceship can rotate around the fixed star surface, according to calculation by equation (28), the spaceship velocity is up to 510km/s. It is obvious that 510km/s is limit flight velocity for human and human flight for one year at this limiting velocity will prolong life for 271seconds. It is observed that the life prolonged by spaceship is limited, falling short of the goal to prolong life for several times; therefore, it is insignificant travel.

10. Conclusion

The analysis in the paper shows that up to now, there has been no comprehensive elucidation about special relativity theory and general relativity theory in books and data. As they ignored some key and necessary explanation, the relative velocity and absolute velocity have not been properly understood, and there has been no clear understanding about actual time operation velocity of object and observed time operation velocity of object, nor has there been idea about whether there is relation between rest mass, rest length and reference system, failure to understand that Lorentz transformation should be differentiated based on relative velocity and absolute velocity. In addition, human is accustomed to analysis based on subjective standpoint, making a false deduction in analysis of physical phenomena unrelated to observation according to relativity theory; general relativity theory takes energy transfer force and acting force of various fields as one type of force, so it puts forward unscientific equivalence principle.

In order to solve the above mentioned problems, the paper puts forward axiom of equilibrium and invariability to deduce Lorentz transformation equation and proposes the correlation analysis method, stating that analysis on physical interaction between two objects will only be carried out according to physical quantities related to the two objects to avoid problem as a result of subjective analysis based on special relativity theory, that every object in universe will have unique circular motion velocity unrelated to reference system, that circular motion velocity is absolute velocity and presenting calculation method for absolute velocity, that the time of Lorentz time transformation deduced based on absolute velocity is absolute time, and that experiment on relation between velocity and time conducted by J·C·Hafele and R·E·Keating can verify the absolute velocity is valid.

This paper puts forward correspondence principle, determines that rest mass and rest length is associated with reference system, presents relevant calculation methods as well as concept about relative transformation and absolute transformation, points out that Lorentz transformation based on absolute velocity is absolute transformation and Lorentz transformation based on relative velocity is relative transformation, raises field similarity principle, points out that gravitational field and electric field are completely similar in terms of physical property and that the electric quantity of electric field is unrelated to velocity, and the gravitational capacity of gravitational field is also unrelated to velocity so as to deduce that gravitational mass is constant unrelated to motion velocity of object and that equivalence principle is invalid in principle.

It makes a deduction that only when the motion velocity of object is tiny as compared to light velocity, may the equivalence principle be approximately valid. The general relativity theory will have proper analysis conclusion, present double equilibrium principle of universal gravitation, and point out that two celestial bodies having universal gravitation will be in equilibrium state. According to the principle, in case that black hole is existing, it will not be in motion state; namely, the motion velocity of black hole is zero, and $V = 0$, indicating that black hole theory is invalid.

The density of black hole is calculated in detail, pointing out that if all atoms of black hole collapsed and became neutrons, the density of these neutrons will still be one million times smaller than theoretical density of black hole. A deduction is made that black hole is not composed of atoms; namely, black hole is not existent as an actual matter. In the end, the issue on time travel is discussed, pointing out only circular motion may have actual time dilation and spaceship for human is only to rotate around fixed star to eliminate centrifugal force to be borne by human. The calculated limiting velocity of spaceship for human is 510km/s; this limiting velocity is much smaller than light velocity; therefore, it is impossible for human to achieve significant time travel.

References

[1] Wu Shouhuang Basics of Theory of Relativity (1987). Shaanxi Science & Techology Press.
[2] Fudan University, Physics (1985). China Higher Education Press
[3] Yao. K.X (2015). A New Explanation of Deflection Results of Charged Particles in High-Velocity Motion in Magnetic Field. Correction of Lorentz Force. Applied Physics Research. Vo1.7. No.5. October 2015.
[4] Yao.K.X (2015). Complenent of Special Relativity and Linitation of General Pelativity. LAMBERT Academic Publishing.
[5] Stephen Hawking (2002). The Universe in A Nutshell.
[6] Carl-Saghn (2012). Universe.
[7] Kip S. Thome (1994). Black hole with time to bend.

International Journal of Physics, 2016, Vol. 4, No. 6, 176-180
Available online at http://pubs.sciepub.com/ijp/4/6/4

DOI:10.12691/ijp-4-6-4

Characterization of Environmental Radioactivity Level in Al-Basrah City (Iraq)

Muhannad Kh. Mohammed[1], Nabeel H. Ameen[2,*], Mohammad Sh. Naji[1]

[1]Ministry of Higher Education and Scientific Researches, Al-Mustansiriyh University, College of Basic Education, Baghdad, Iraq
[2]Ministry of Science and Technology, Radiation & Nuclear Safety Directorate, Baghdad, Iraq
*Corresponding author: nabeelhameen@googlemail.com

Abstract Soils and earth-derived building materials contain radioactive materials provide external exposure to nearby individuals and result in detrimental health effects including cancer. The risk of cancer incidence (morbidity) and mortality to individuals in Al-Basrah's population (south of Iraq) related to external exposure to ambient gamma radiation is evaluated in this study. The risk estimations include delayed radiation effects (cancer morbidity, mortality and hereditary genetic damages). Radiation exposure rates were measured using BGS-4 gamma-ray scintillation (Scintrex, Canada) for the period 2012-2013. Absorbed dose rates in air and in human tissues are determined by applying typical conversion factors available in the literature. Age-dependent radiation dose is calculated for infants, children, and adults. Dose-to-risk conversion factors are applied to estimate potential risk to various body organs and tissues as a result of exposure to ambient gamma radiation. The findings of this study report that about 0.26% of Al-Basrah population are expected to be diagnosed with radiation-induced cancer over there lifetime. The lifetime fatal cancer probability (mortality) is found to be occurs at a rate of 0.19%. The risk of developing fatal stomach cancer is found to be occurs at a largest extent in comparison with other exposed body organs and tissues. Children and infants are found to be at a greater radiation risk than adults due to lower body weight. Other consequences of radiation injury such as genetic effects transmitted to succeeding generations are expected to occur at a rate of 0.03% in the offspring of Al-Basrah population as a result of changes transmitted via the genetic mechanisms due to irradiation of gonads.

Keywords: *environmental radioactivity level, Al-Basrah city*

Cite This Article: Muhannad Kh. Mohammed, Nabeel H. Ameen, and Mohammad Sh. Naji, "Characterization of Environmental Radioactivity Level in Al-Basrah City (Iraq)." *International Journal of Physics*, vol. 4, no. 6 (2016): 176-180. doi: 10.12691/ijp-4-6-4.

1. Introduction

Al-Basrah city, located to the south of Iraq, has been widely contaminated by depleted uranium (DU) particles during the 1991 and 2003 Gulf wars. Cancer, birth defects, hereditary genetic effects and other radiation-derived biological diseases have been widely observed among the population of Al-Basrah city.

Gamma energy is a high-energy electromagnetic radiation that can penetrate most substances. Because of its high energy, gamma radiation can penetrate the human body from the outside and damage cells, which would lead to cancer later in life [1]. Humans are exposed to many sources of radiation in the environment of which natural sources are the most important ones [2]. Natural sources deliver the highest radiation dose that people normally receive. The average annual dose from natural sources is 2.4 mS_v, which is a reference level representing the average 1-5 mS_v, and in extreme cases to 1 S_v or more [3].

The term natural radiation background is used to designate naturally occurring radioactive materials and high-energy radiations. The various members of the uranium and thorium families and a radioactive isotope of potassium are the most important naturally occurring radioactive materials. Naturally occurring radiations are due partly to these natural radioactive materials and partly to the cosmic radiation. The total background radiation levels to which people may be exposed are of considerable interest. Measurements are usually made with ionization chambers and the results expressed in milli-roentgens per year, i.e. in terms of the rate of energy absorption. The sea-level value is about 0.01 mR/h (88 mR/y) in regions of low background but will be considerably higher in many places [4].

The aims of this study are:-

(1) Make quantitative estimations of the biologically damaging effects associated with exposure of Al-Basrah inhabitants to natural background radiation by using a hypothetical linear no threshold (LNT) statistical model. The specific risks concerned in this study focus on the ionizing radiation as the cause, cancer morbidity, mortality (an abnormal process in which cells begin a phase of uncontrolled growth and spread) and genetic effects transmissible to progeny as the response. The assessed harmful consequences of ionizing radiation include somatic effects (risk of cancer, leukemia, sterility, cataracts, reduction in lifespan) and genetic damage (increasing the mutation rate in chromosomes and genes, affects future generations).

(2) Investigate the effect of the type of dwellings (single family house or flat) and materials of construction on the dose received by its occupants.

(3) To determine which population group (infants, children or adults) should be the primary target for radiation protection.

2. Materials and Methods

The exposure rates were measured 1m above the ground by using BGS-4 survey instrument. The measuring instrument utilized in this study is owned by Ministry of Science and Technology/ Hazardous Materials and Environmental Researches Directorate. The display in counts per second (c.p.s) was converted to exposure rates in μ R/hr using equation below [5]:

$$c.p.s \times \frac{1}{8.27} = \mu R / hr. \quad (1)$$

One roentgen (R) of exposure dose to a specific volume of air at standard conditions results in the absorbed dose of 0.87 rad. One rad (radiation absorbed dose) is equivalent to 0.01 Gray (Gy). A coefficient of 0.7 Sv/Gy is used to convert absorbed dose rate in air to effective dose equivalent. UNSCEAR 1993 report provides coefficients for exposure to terrestrial gamma rays for adults (0.72 Sv/Gy), children (0.80 Sv/Gy) and for infants (0.93 Sv/Gy) [6].

The standard error of the arithmetic mean S.E $(\bar{x})$ for the exposure rate readings is estimated by using equation below [7]:

$$S.E(\bar{x}) = \frac{S_x}{\sqrt{n}} \quad (2)$$

where S_x is the standard deviation of the exposure rate readings of size (n).

Exposure is defined as contact of an organism, such as humans or endangered species with a contaminant. Exposure assessment is the estimation of the magnitude, frequency, duration, and route of exposure [8]. The purpose of exposure assessment is the estimation of the contaminant concentrations and dosages to the population at risk [9].

Observed radiation affects (or effects the other types of noxious agents) may be broadly classified into two categories, stochastic and non-stochastic effects. In the context of radiation protection, the main stochastic effects are cancer and genetic effects. The results of exposure to a carcinogen or to a mutagen are an increase in the probability of occurrence of the effect with the increase in probability being directly proportional to the size of the dose. Radiation doses to exposed individuals in Al-Basrah population are estimated by using equation below:

$$\bar{H}_i = \mathrm{ER} \times 10^{-3} \times 0.87 \times 0.01 \times 0.7 \times 24 \times 365 \quad (3)$$

Where $\bar{H}_i$ represent radiation dose rate in mSv/y, ER represent exposure rate in µR/h, 10^{-3}, 0.87 rad/R, 0.01 Gy/rad, 0.7 Sv/Gy, 24 hr/day, and 365 day/y are conversion factors.

The collective effective dose equivalents S_E (human-Sv/y) were assessed according to the following expression [10]:

$$S_E = \bar{H}_i . N(\bar{H})_i \quad (4)$$

where $\bar{H}_i$ is the effective dose equivalent and $N(\bar{H})_i$ is the number of individuals in population subgroup i receiving dose equivalent of $\bar{H}_i$.

3. Risk Characterization

Toxicity Assessment is the acquisition and evaluation of toxicity data for each contaminant, a procedure that is performed for both non-carcinogens and carcinogens. The final step in a risk assessment is to bring the various studies together into an overall risk characterization. Public health risk for individual members in Al-Basrah population is modeled in this study as a linear function of radiological dose:

$$\mathrm{Risk} = \mathrm{Dose}\left(\frac{mSv}{y}\right) \times 10^{-3} \left(\frac{Sv}{mSv}\right) \times \mathrm{Lifetime}\,(\mathrm{y}) \times \mathrm{Risk\ Factor}\left(\frac{Risk}{Sv}\right) \quad (5)$$

where Risk = the probability of carcinogenic risk (dimensionless), lifetime exposure is taken to be 70 y (standard exposure duration for an adult exposed to a carcinogen) [11].

Table 1. Risk factors to various body organs and tissues (1 Sv=100 rem) [14]

Cancer	Radiation mortality (risk per rem)	Radiation inecidence (risk per rem)	Lethality
Bladder	0.00003	0.00006	0.5
Bone surface	0.000005	0.00001	0.7
Breast	0.00002	0.00004	0.5
Colon	0.000085	0.00015	0.55
Leukemia (Bone marrow)	0.00005	0.00005	0.99
Liver	0.000015	0.00002	0.95
Lung and Bronchus	0.000085	0.00009	0.95
Oesophagus	0.00003	0.00003	0.95
Ovary	0.00001	0.00001	0.7
Skin	0.000002	0.001	0.002
Stomach	0.00011	0.00012	0.9
Thyroid	0.000008	0.00008	0.1
Remainder	0.00005	-	-

Estimation of the potential risk from low levels of ionizing radiation requires application of dose-to-risk conversion factors to the estimation of the dose. For external sources of linear energy transfer (LET) radiation that provide nearly uniform irradiation of the body, the risk of cancer incidence (morbidity) and mortality as a function of external dose can be closely approximated using the conversion factors of 8×10^{-2} and 6×10^{-2} risk per sievert (Sv), respectively [12]. Morbidity and mortality risks to specific body organs and tissues can be estimated by means of the risks factors listed in Table 1. The risk coefficient for genetic effects in all generations following the radiation exposure of adults is 0.01 Sv^{-1} [13].

The genetic injury or damage to Al-Basrah population from radiation exposure is estimated in this study from the total number of human-sieverts delivered to the gonads. It is thought that in the majority of cases the inherited change will have a deleterious effect on the individual. This may be premature death, inability to produce offspring, susceptibility to disease, or any number of changes of lesser or greater importance [13]. The genetic risk coefficient for gonads is taken to be 4×10^{-3} Sv^{-1} for the first 2 generations (Cember, 1987) and 0.01 Sv^{-1} for all generations [14].

4. Results and Discussion

Multi-step risk assessment process is used in this study to predict the biologically damaging effect of public exposure to ambient background radiation. The 1st step is making quantitative measurements of the ability to produce ionization in air or the exposure dose to individuals in Al-Basrah population living in the area of the study by using BGS-4 Gamma-ray Scintillation Counter (SCINTREX, Canada) and the results are expressed in micro roentgen per hour ($\mu R/hr$). Extensive measurements of the natural γ-radiation background in the outdoor air spaces are made. The 2nd step is estimation of the absorbed dose rate in air (in μrad/hr) and biological dose in human tissues and organs (in mSv/y) for local inhabitants by using a series of conversion factors available in the literature. The last step is making a correlation between the dose administered and the radiation injury produced by using a linear, no-threshold (LNT) dose-response statistical model.

Results of gamma exposure rates measurements are presented in Table 2. All field measurements were conducted in the period 2012–2013. The standard error of the exposure rate readings listed in Table 2 for outdoor exposure is estimated to be 0.33 μR/h. Step-by-step computation of the effective dose equivalent from the exposure rates is shown in Table 3. The natural background γ-radiation level in Al-Basrah City (8.87 μR/hr) is comparable to that in the USA (8 μR/hr) ersity, 2003]. The whole-body effective dose equivalent inferred from measurement (0.472 mSv/y) is found to be greater than the annual effective dose equivalent of 0.01 mSv, which corresponds to the National Council on Radiation Protection and Measurement (NCRP) concept of negligible individual risk level [15,16]. This result indicates that public exposure to natural background radiation causes considerable possible long term bioeffects include increased incidence of somatic and hereditary genetic effects (increased incidence of genetic abnormalities in humans) to a large number of individuals in Al-Basrah population.

Effective dose equivalent to infants, children, and adults arising from external exposure to indoor and outdoor gamma radiation are listed in Table 4. Infants are at greater risk than adults and children due to lower body weight.

The likelihood or probability of radiation risk to Al-Basrah population is evaluated in Table 5 by using a linear, no-threshold (LNT) dose-response model (Eq.(5)) and the risk factors listed in Table 1. The biological effects of natural background radiation are expressed in statistical terms due to biological variability accounts for a difference in sensitivity among individuals and a wide variation in susceptibility to radiation damage exists among different types of cells and tissues. The probabilities of cancer risks to various body organs and tissues are calculated and the results are listed in Table 5. The results of quantitative risk assessment are written in Table 5 in the following form (Risk = Number of injuries or deaths per number of people exposed to hazard). The risk of developing blood cancer (leukemia) as a result of the irradiation of the bone marrow is calculated to be 1 in 6060 exposed individuals, while the risk of developing bone cancer is evaluated to be 1 in 62500. The fatality rate in Al-Basrah population owing to natural γ-radiation exposure is evaluated at 28 extra fatal cancer case/million people/year. The gonad dose of 0.472 mSv/y is found to be less than the population dose limit for genetic effects of 1.7 mSv/y proposed by the National Council on Radiation Protection and Measurements (NCRP) [17] and less than the dose limits for gonads of 5 mSv/y recommended by the International Commission on Radiological Protection (ICRP) [18].

Table 2. Results of gamma exposure rates measurements

No.	Location/district	Mean exposure rate (μR/hr)
1	Al-Tameemiya (Al-Robat Youth Center)	9.12
2	Al-Jamhuriya (near football stadium)	10.48
3	Al-Barakhiya (near educational hospital)	8.2
4	Bab Al- Zubair (near economic and management college)	9.7
5	Al-Zubair (near Al-Zubair hospital)	11.2
6	Al-Zubair	12
7	Al-Basrah University (Karmat Ali)	7.8
8	Karmat Ali (center)	8
9	Al-Ma'aqal (near rain station)	8.0
10	Al-Tanoma	6.8
11	Al-Seba	7.6
12	Abi-Al-khasib	6.6
13	Hamdan	9.12
14	Safwan (center)	10.25
15	Safwan (farms)	10.95
16	Safwan (Salam mountain)	11.40
17	Al-Hartha (center)	7.5
18	Al-Deer (center)	9.4
19	Al-Kurna (center)	7.8
20	Al-Huwair (center)	7.2
21	Talha (near petroleum wells, west of Al-Kurna)	10.0
22	Ahmad Ebn-Ali (Talha center)	7.8
23	Al-Mdayna (center)	7.1
Mean ± standard deviation		8.87 ± 1.61
Range		6.6 - 12

Table 3. Exposure rates, effective doses, morbidity and mortality risks from lifetime (70 year) external exposure to indoor and outdoor ambient γ-radiation level in Al-Basrah city

Parameters	Value
Ambient γ-radiation level, outdoor (μR/hr)	8.87 (6.6 – 12)
Absorbed dose rate in air (μrad/hr)	7.71
Absorbed dose rate in air (μGy/hr)	0.0771
Effective dose equivalent (mSv/y)	0.472
Lifetime morbidity health risk (extra cancer case per no. of exposed individuals)	1 per 377
Lifetime mortality health risk ((extra fatality case per no. of exposed individuals))	1 per 503

Table 4. Ranking of exposed groups in Al-Basrah population on the basis of the radiation dose administered (mSv/y) (age-dependent radiation dose)

Rank	Group	Radiation dose (mSv/y)
1	Infants (1<age(y)<2)	0.628
2	Children (2<age(y)<18)	0.540
3	Adults (age(y)>18)	0.472

Table 5. Lifetime (70 years) cancer mortality and morbidity risks to various body organs and tissues as a result of external exposure to indoor and outdoor gamma radiation

No.	Body organ or tissue	Mortality risk	Morbidity risk
1	Bladder	99 per million	198 per million
2	Bone surface	16 per million	33 per million
3	Breast	66 per million	132 per million
4	Colon	280 per million	495 per million
5	Leukemia (Bone marrow)	165 per million	165 per million
6	Liver	49 per million	66 per million
7	Lung and Bronchus	280 per million	297 per million
8	Esophagus	99 per million	99 per million
9	Ovary	33 per million	33 per million
10	Skin	6 per million	3304 per million
11	Stomach	363 per million	396 per million
12	Thyroid	26 per million	264 per million
13	Remainder	165 per million	–

5. Conclusions

(1) Al-Basrah City is situated in an area of low background radiation since the ambient γ-radiation level is found to be <10 μR/hr. The environmental γ-radiation background level in Al-Basrah City is classified as "unhealthy" since the mean γ-radiation exposure rate inferred from measurement (8.87 μR/hr) is found to be between 33 and 66% of the EPA's external gamma radiation criterion of 20 μR/hr for habitable structures [20,21].

(2) The effective dose equivalent is found to be less than the recommended dose limit to the public (1 mSv/yr) [22]. However, the results indicate that population exposure to natural background radiation causing considerable carcinogenic risks and genetic damage to a large number of people.

(3) Population exposure to natural background radiation is found to be causing considerable carcinogenic risks and genetic damage to a large number of people. The lifetime fatal cancer risk to a person receives 0.472 mSv/y is 0.19% (about 2 chances in a thousand exposed individuals, or there is one additional death in a group of 503 people if they would all receive 0. 472 mSv/y instantaneously).

(4) The chronic excess cancer risk estimates attributed to external exposure to natural background γ-radiation level is found to be exceed the EPA's 1×10^{-5} risk level of concern [21] for all receptors evaluated.

(5) The various body organs and tissues differ in their sensitivity to the ionizing radiation emitted from natural sources.

(6) Possible long-term bioeffects related to exposure of Al-Basrah population to natural background radiation include increased incidence of hereditary genetic abnormalities in humans at a rate of 0.03% due to irradiation of gonads.

(7) Children and infants are at greatest risk than adults ($Risk_{infant}>Risk_{child}>Risk_{adult}$) (Table 4) due to lower body weight.

(8) The appearance of cases such as cancer, inability to produce offspring, premature death, susceptibility to disease, and abnormal offspring among residents of Al-Basrah City is an evidence of the harmful consequences and biologically damaging effects associated with chronic doses of natural background ionizing radiation and public exposure to other carcinogens.

6. Recommendation

(1) The radioactivity of local and imported building materials needs to be monitored in Iraq to prevent dwellings from becoming a major source of radiation hazard.

(2) National radiation protection guides or criteria system for radioactive materials content in local and imported building materials are need to be established in Iraq in order to protect the public health from harmful consequences associated with exposure to natural background radiation and to maintain the radiological exposure of the public at the lowest practicable value (as low as reasonably achievable).

References

[1] CDC, Radioisotope Brief: Cesium-137, the Center for Disease Control and Prevention, CDC Radiation Emergencies, Emergency Preparedness and Response, 2003.

[2] ICRP, A Compilation of the Major Concepts and Quantities in Use by ICRP, ICRP Publication 42, Pergamon Press, 1984.

[3] Gonzalez, A. J. and J. Anderer, Radiation Versus Radiation, Nuclear Energy in Perspective, I.G.E.A, Bull, 1969, 21-29.

[4] Blatz, H., Radiation Hygiene Handbook, McGraw-Hill, New York, 1959.

[5] Marouf, B.A., Mohamad, A.S., and Taha, J.S., Assessment of Exposure Rate and Collective Effective Dose Equivalent in the City of Al-Basrah Due to Natural Gamma Radiation, The Science of the Total Environment, Elsevier Science Publishers B.V., Amsterdam, 0048-9697/93, 133, 1993, 133-137.

[6] UNSCEAR, Sources and Effects of Ionizing Radiation, United Nations Scientific Committee on the Effects of Ionizing Radiation, Report to the general assembly, with Scientific Annexes, United Nations, 1993.

[7] Al-Mashhadani, Mahmood H., Hormez, Ameer H., Statistics, Iraqi Ministry of Higher Education and Scientific Research, Baghdad University, Wisdom Home, pp.476.

[8] Patton, D. E., 1993. The ABCs of Risk Assessment, EPA Journal, 1989, 10-15.

[9] Watts R., Hazardous Wastes, Sources, Pathways, Receptors, John Wiley and Sons, Inc., 1998, 521-530.

[10] ICRP, Principles for Limiting Exposure of the Public to Natural Sources of Radiation, ICRP Publication 39, Pergamon Press, UK, 1984.

[11] Masters, Gilbert M., Introduction to Environmental Engineering and Science, Prentice-Hall, Inc., 1991, 299-300.

[12] ISCORS, A Method for Estimating Radiation Risk from TEDE, International Steering Committee on Radiation Standards, ISCORS Technical Report No.1, 2002.

[13] IAEA, Radiation and Society: Comprehending Radiation Risk, Proceeding Series, Vol.1, Prepared by the Swedish Risk Academy, International Atomic Energy Agency, Vienna, 1994.

[14] Idaho State University, Radiation and Risk, Radiation Information Networks, 2003.

[15] Marshall, W., Nuclear Power Technology, Nuclear Radiation, Claredon Press, Volume.3, Oxford, 1983, 21-30.

[16] Peterson, S. Ring, Appendix A. Methods of Dose Calculations, Lawrence Livermore National Laboratory (LLNL) Environmental Report for 1999.

[17] Eisenbud, M., Environmental Radioactivity, 2nd Edition, Academic Press, A subsidiary of Harcourt Brace Jovanovich, Publishers, 1973.

[18] Cember, H., Introduction to Health Physics, Pergamon Press, pp.178, 1987.

[19] EPA, Technical Basis for a Candidate Building Materials Radium Standard, National Risk Management, Research Laboratory, EPA/600/SR-96/022, March 1996.

[20] DOE, Environmental Implementation Guide for Radiological Survey Procedure, U.S. Department of Energy, Assistant Secretary for Environmental Safety and Health, Washington, D.C., 20585, 1997.

[21] Rutherford, P., Radiation Risk, A Critical Look at Real and Perceived Risks from Radiation Exposure, 2002.

[22] EPA, Combustion Human Health Risk Assessment for Angus Chemical Company, Sterington, Louisiana, U.S. Environmental Protection agency, Center for Combustion Science and engineering, Dallas, Texas, Region 6, 2000, 10.

International Journal of Physics, 2016, Vol. 4, No. 6, 181-186
Available online at http://pubs.sciepub.com/ijp/4/6/5

DOI:10.12691/ijp-4-6-5

Control of Roll Motion of Fishing Vessel by Fin-Stabilizer Using PID Controller

Hassan Ghassemi*, Hamid Malekizade, Arash Ashrafi

Department of Maritime Engineering, Amirkabir University of Technology, 424 Hafez Ave, Tehran, Iran
*Corresponding author: gasemi@aut.ac.ir

Abstract The aim of this study is to diminish the roll motion of the fishing vessel using fin-roll stabilizer. In this regard, lift coefficient of the fin and the hydrodynamic coefficients of the roll equation are calculated by empirical formulas. In effect, constrained LQR (Linear Quadratic Regulator) controller is designed and used to control the roll motion in the presence of operational constraints of fin's actuator. In order to boost the validity of our results, the performance of this controller is compared with a conventional PID (Proportional-Integral-Derivative) controller. Finally, simulation results indicate the significant amount of reduction in roll amplitude.

Keywords: *PID controller, fishing vessel, fin roll stabilizer*

Cite This Article: Hassan Ghassemi, Hamid Malekizade, and Arash Ashrafi, "Control of Roll Motion of Fishing Vessel by Fin-Stabilizer Using PID Controller." *International Journal of Physics*, vol. 4, no. 6 (2016): 181-186. doi: 10.12691/ijp-4-6-5.

1. Introduction

Among the motions of a ship at sea, roll motion is the most important one. The accelerations due to wave-induced roll motions negatively influence on a fishing vessel performances by making limitation in comfort, workability and safety. The roll stabilization systems have been widely studied for more than three decades and various types of anti-rolling devices have been introduced to reduce the undesirable roll motion [1,2]. The active fin stabilizer has been considered as the most effective anti-rolling technique for ships which normally operates above certain speeds. It reduces roll motion by controlling the mechanical angle of the fin according to the ship roll angle and roll rate [3].

The studies of the nonlinear roll motion model have been done by Taylan [4]. In those models, nonlinear restoring terms were considered as a third order polynomial; likewise, nonlinear damping was regarded as a second-order polynomial. In research of Surendran et. al. [5], the roll dynamics of a Ro–Ro ship taking into account the many types of combinations of loads in linear and nonlinear forms. A lift feedback fuzzy-PID control method was developed to better deal with these problems, and this lift feedback fin stabilizer system was simulated under different sea condition [6]. The roll amplitude of the fishing vessel under the wave effect was analyzed using the nonlinear mathematical model in Alarçin's paper [7].

The PID controller has mainly been used in the ship fin stabilizers. The results of using a combined neural network and PID for roll control of ship with small draught were presented [8]. Modified PID control design was presented for roll fin actuator of nonlinear modeling of the fishing boat [9], roll damping characteristics of a trimaran displacement ship [10]. However, because of difficulty, non-linearity, and constriction of fin stabilizers in this method, attaining the optimal performance for control system is very intricate [11]. A multi-input multi-output (MIMO) optimal control system that has two control inputs such as fin stabilizers and pod propellers is designed. The linear quadratic regulator (LQR) control algorithm is applied to reduce the roll motion of cruise ships in regular waves [12]. A robust fin controller based on L2 gain design is proposed, in order to reduce the roll motion of surface ships. The plant consists of the ship roll dynamics and that of the fin actuator [13].

The purpose of this paper is the nonlinear modeling and its coefficients extraction as well as designing constrained controller for fin-roll stabilizer in a fishing vessel. To achieve this goal, the active fin stabilizer with NACA0015 section is used as the fin-roll stabilizer. Also, CFD method is used for the flow analysis so that the lift coefficient would be extracted which, in turn, is validated by use of empirical formulas. The roll motion model is derived in the presence of irregular waves. In this model, the nonlinear restoring moment is considered as a 3rd order polynomial and its coefficients are calculated by the GZ curve and the empirical formulas. A nonlinear term is also considered for the roll damping moment. Furthermore, the linear damping coefficient, mass moment of inertia and added mass moment of inertia are calculated by using the Free Roll decay test and empirical formulas.

Finally, the constrained LQR is designed as optimal stabilizer to control the roll motion. In order to fortify the results of this study, the performance of this controller is compared with a conventional PID controller. Simulation results, demonstrated in time domain, are presented to show the effectiveness of the constrained LQR.

2. Nonlinear Modeling

It is assumed that the fin stabilizer is approximately located in amidships close to the center of gravity and there is a minimum coupling with the other motions. Consequently, the coupling with other motions can be regarded and just one degree of freedom can be considered. The model of roll motion can be represented as

$$I_{xx}\ddot{\phi} = \tau_d - \tau_f - \tau_h \qquad (1)$$
$$p = \dot{\phi}$$

where ϕ, p, I_{xx}, τ_f, τ_h and τ_d are roll angle, roll rate, roll moment of inertia, moment created by fins, hydrodynamic moment and wave excitation moment, respectively. The moment due to the fins and the hydrodynamic moment are calculated for a fishing vessel with characteristics which presented in the Table 1 and the body plane illustrated in the Figure 1.

Table 1. The specifications of the fishing vessel

Item	Value
Length (m)	20
Breadth (m)	5.714
Draft (m)	2.854
Vertical center of gravity (m)	2.4
Metacentric height (m)	0.57
Service speed (m/s)	12.5
Block coefficient	0.457

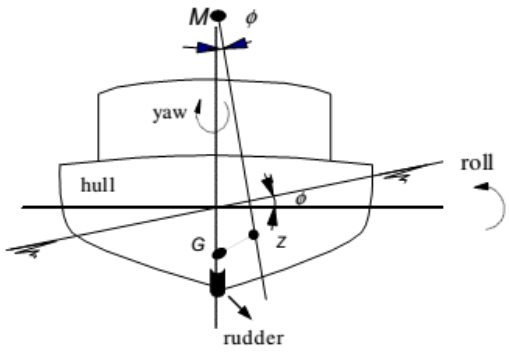

Figure 1. Fishing vessel at roll angle

2.1. Fin Data

The coefficients of fin stabilizer which conisdered in this study are presented in Table 2.

Table 2. Characteristics of the fin

Item	Value
Fin area (m^2)	3.7
Fin span (m)	1.4
Mean chord (m)	2.2
Fin lever (m)	5.8
Aspect ratio	0.72
Fin section	NACA0015

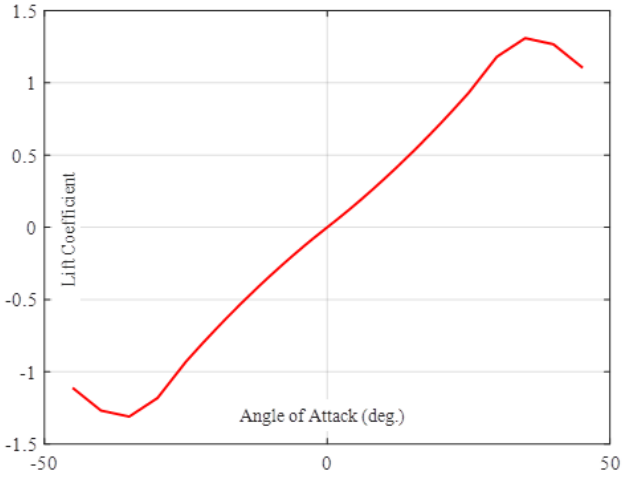

Figure 2. Lift coefficient of the fin

The fins moment can be determined by the Eq. (2).

$$\tau_f = \rho V^2 A_f R_f C_L(\alpha_e) \qquad (2)$$

where ρ, V, A_f, R_f and $C_L(\alpha_e)$ are the density of the flow, ship speed, fin area, fin lever, and lift coefficient respectively. It should be noted that lift coefficient is a function of the effective angle of attack between the flow and the fin (Figure 2).

2.2. The Hydrodynamic Moment

The hydrodynamic moment due to the interaction between fluid and ship is defined by Eq. (3).

$$\tau_h = K_{\dot{p}}\dot{p} + f_1(\phi,\dot{\phi}) + f_2(\phi) \qquad (3)$$

where $K_{\dot{p}}\dot{p}$ regards a hydrodynamic moment in roll due to pressure variation that is proportional to the roll accelerations and the coefficient $K_{\dot{p}}$, called roll added mass. The $f_1(\phi,\dot{\phi})$ is damping term and it can be represented as Eq. (4).

$$f_1(\phi,\dot{\phi}) = k_p\phi + k_{p|p|}\dot{\phi}|\dot{\phi}| \qquad (4)$$

where $k_p\phi$ is a linear damping term which includes forces due to wave-making and linear skin-friction. Besides, the coefficient k_p is denoted a linear damping coefficient. The $k_{p|p|}\dot{\phi}|\dot{\phi}|$ is a nonlinear damping term, which contains moments due to viscous effects, alike nonlinear skin friction and eddy making due to flow separation. Also, the coefficient $k_{p|p|}$ is denoted a nonlinear damping coefficient. the $k_{p|p|}$ is about 60% of k_p at an advance speed of zero knots, $k_{p|p|}$is reduced to 5% of k_p at an advance speed of 15 knots, and $k_{p|p|}$ is practically zero at an advance speed of 30 knots. The $f_2(\phi)$ is the restoring moment term due to gravity and buoyancy and it can be specified as Eq. (5).

$$f_2(\phi) = \Delta GZ(\phi) \qquad (5)$$

where Δ is the ship's displacement and $GZ(\phi)$ is the restoring moment arm that it is function of the roll angle.

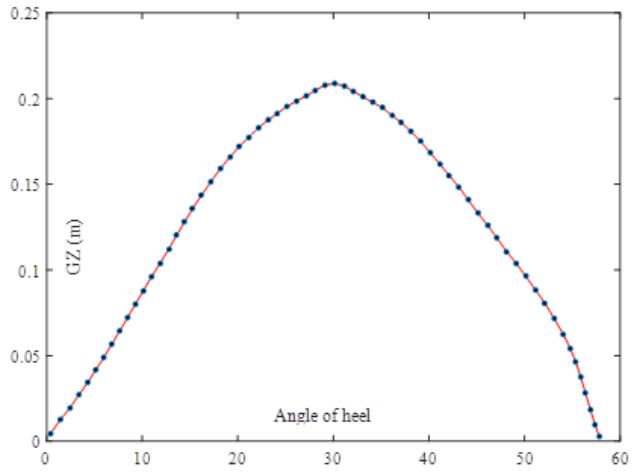

Figure 3. GZ curve of fishing vessel

The GZ curve is an odd function and therefore represent with odd order polynomial. Meanwhile, GZ curve of the fishing vessel is shown in Figure 3. The GZ-curve for the restoring moment arm has been defined by the following polynomial formula

$$GZ(\phi) = c_1\phi + c_3\phi^3 + c_5\phi^5 \tag{6}$$

where the coefficients c_1, c_3, and c_5 defined by Taylan [4]:

$$c_1 = \frac{d(GZ)}{d\phi} = GM$$
$$c_3 = \frac{4}{\phi_v^4}(3A_{\phi v} - GM\phi_v^2) \tag{7}$$
$$c_5 = -\frac{3}{\phi_v^6}(4A_{\phi v} - GM\phi_v^2)$$

where GM, ϕ, and $A_{\phi v}$ are, respectively, the metacentric height, angle of vanishing stability, and undersurface the GZ curve.

2.3. Calculation of Hydrodynamic Coefficients

The non-dimensional damping coefficient can be calculated as follows:

$$\zeta_\phi \cong \frac{\ln(\phi_1/\phi_2)}{2\pi}. \tag{8}$$

Based on the results above and the following standard relationships, the hydrodynamic coefficients may be calculated by the following formulas

$$\omega_\phi = \frac{2\pi}{T_\phi} \tag{9}$$

$$I_{xx} + K_{\dot{p}} = \frac{\Delta GM}{\omega_\phi^2} \tag{10}$$

$$k_p = 2\zeta_\phi\sqrt{\Delta GM(I_{xx} + K_{\dot{p}})} \tag{11}$$

The wave exciting moment is defined by

$$\tau_d = I_{xx}\omega_e^2\alpha_{\max}\cos(\omega_e t) \tag{12}$$

where α_{max} the maximum wave slope and ω_e is the wave encounter frequency that is described as

$$\omega_e = \omega\left(1 - \frac{\omega}{g}V\cos\mu\right) \tag{13}$$

where ω and μ are the wave frequency and the wave encounter angle.

2.4. Fin Dynamic Model

Block diagram of the fin-roll closed loop control system is summarized in Figure 4. The roll angle and roll rate are measured by gyroscope. The active fin is actuated by Electro-Hydraulic Servomechanism which is called fin's actuator. Fin's actuator has a first order dynamic model as Eq. (14).

$$T_e\dot{\alpha}_m + \alpha_m = K_{dc}\alpha_c \tag{14}$$

where, K_{dc} is dc gain of the actuator and T_e is time constant due to the delay between α_c and α_m.

The relationship between mechanical and effective angle of attack is as Eq. (15).

$$\alpha_e = -\alpha_f - \alpha_m$$
$$\alpha_f = arc\tan\left(\frac{R_f p}{V}\right) \approx \frac{R_f p}{V} \tag{15}$$

where α_f is flow angle which derived by the combination of the local roll-induced velocity together with the forward velocity of the fishing vessel.

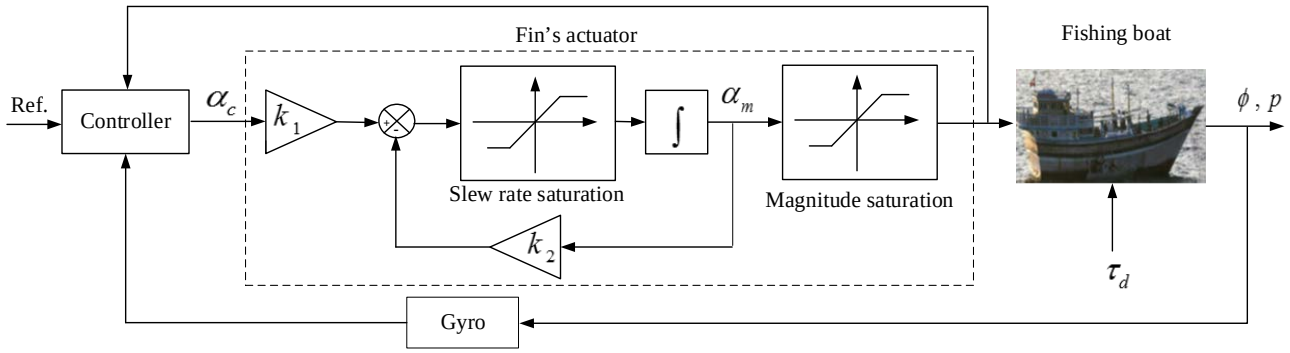

Figure 4. Block diagram of the fin-roll closed loop control system

2.5. State Space Model

According to Eqs. (1) and (15), the nonlinear model of roll motion can be summarized as following equation:

$$\begin{aligned}&\left(I_{xx}+K_p\right)\ddot{\phi}+k_p\dot{\phi}+K_{p|p|}\dot{\phi}\left|\dot{\phi}\right|\\&+\Delta\left(c_1\phi+c_3\phi^3+c_5\phi^5\right)=\tau_d-K_\alpha\alpha_e\\&\alpha_e=-\frac{R_f\,p}{V}-\alpha_m\\&T_e\,\dot{\alpha}_m+\alpha_m=K_{dc}\alpha_c.\end{aligned}\tag{16}$$

Also, based on the assumptions listed in section 2.3, it is considered linear model roll motion. A linear state space model to describe the dynamic of the roll motion can be presented by

$$\begin{aligned}\dot{x}_1(t)&=x_2(t)\\\dot{x}_2(t)&=\frac{-\Delta GM}{I_{xx}+K_p}x_1(t)+\frac{(k_\alpha R_f/V)-k_p}{I_{xx}+K_p}x_2(t)\\&+\frac{k_\alpha}{I_{xx}+K_p}u(t)+\frac{1}{I_{xx}+K_p}\tau_d(t)\\\dot{x}_3(t)&=k_2x_3(t)+k_1u(t)\end{aligned}\tag{17}$$

where $x(t)=[x_1(t),x_2(t),x_3(t)]^T$ is $[\phi(t),p(t),\alpha_m(t)]^T$ and $u(t)$ is $\alpha_c(t)$. As well as $k_1=k_{dk}/T_e$ and $k_2=1/T_e$. Also, the operational constraints should be considered as:

• Input constraints which reflect the saturation of the mechanical fin angle:

$$|\alpha_c|\le\alpha_{sat}\tag{18}$$

• State constraint that is used in order to preventing the dynamic stall:

$$|\alpha_e|=\left|\frac{R_f}{V}P+\alpha_m\right|\le\alpha_{stall}.\tag{19}$$

3. Controller Design

In this section, a constrained LQR as an optimal controller for stabilizing the ship in roll motion was designed. The aim of controller is regulating the state variables with minimum control action. Therefore, it is considered the continuous-time linear time-invariant system as:

$$\dot{x}(t)=A_cx(t)+B_cu(t).\tag{20}$$

And it is sampled discrete-time version as Eq. (21).

$$x(t+1)=Ax(t)+Bu(t)\tag{21}$$

where $x\,\varepsilon\,R^3$ and $u\,\varepsilon\,R$.

The optimal control input, $u(t)$, should minimize the cost function, J.

$$\begin{aligned}&J\left(u(t),u(t+1),\ldots,x(t)\right)\\&=\sum_{\tau=t}^{\infty}x(\tau)^T\,Qx(\tau)+u(\tau)^T\,Ru(\tau)\end{aligned}\tag{22}$$

Also, it is subjected to the linear constraints as Eq. (23).

$$\begin{aligned}&G\,x(\tau+1)\le g\\&H\,u(\tau)\le h.\end{aligned}\tag{23}$$

For all $\tau\ge t$, where $R>0$, $Q\ge0$ and $G\,\varepsilon\,R^{1\times3}$ and $H\,\varepsilon\,R$. The pair (A, B) is controllable, and it is assumed that $g,\,h>0$ to ensure that the origin is an interior point in the acceptable region. The optimal cost function is defined as

$$F(x(t))=\min_{u(t),u(t+1),\ldots}J(u(t),u(t+1),\ldots,x(t))\tag{24}$$

where the minimization is subject to the dynamics of the system (Eq. 21), and the constraints (Eq. 23) are imposed at every time $\tau\ \varepsilon\ \{t,\ t+1,\ t+2,\ldots\}$ on the trajectory. There are different methods for solving these kinds of problems. It has been done the constrained LQR design using Sequential Quadratic Programming (SQP) methodology with quadratic objective functions that is an effective algorithm.

4. Simulation Results and Discussion

The sailing condition is assumed for a random sea and beam sea condition at the forward speed 20 knots. Such a profile corresponding to a regular wave with period of 10s with a steepness of 1/60 is assumed for the calculation of exciting moment. The exciting moment was derived from a MATLAB code, and is depicted in Figure 5.

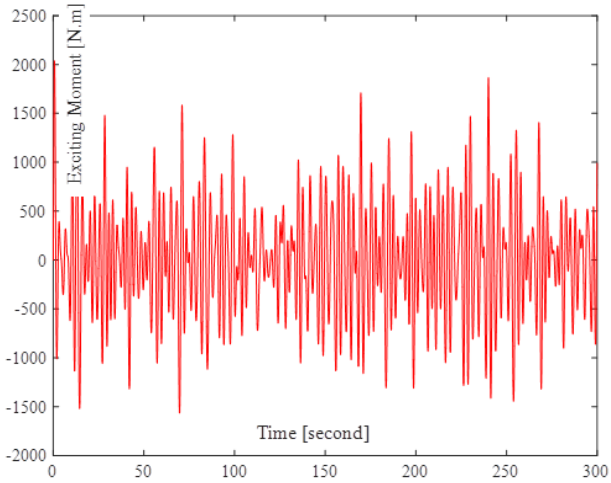

Figure 5. Plot of exciting moment

Table 3. The calculated coefficients of the vessel

Item	Value
$c_1\,(kg\,m^2\,s^{-2})$	0.73
$c_3\,(kg\,m^2\,s^{-2})$	-0.0504
$c_5\,(kg\,m^2\,s^{-2})$	0.1912
$k_p\,(kg\,m^2\,s^{-1})$	8.75
$I_{xx}+k_p\,(kg\,m^2)$	53.65
$k_{p\|p\|}\,(kg\,m^2)$	0.4375

According to the empirical formulas and the specifications of the fishing vessel, with fin and in the linear region of the lift curve, obtained values are $C_L = 0.61$, $dC_L/d\alpha_e = 1.762\ (rad^{-1})$ and $\alpha_{stall} = 0.62\ (rad)$. Also, the fins moment is $\tau_c = 2047.83\ (N.m)$. By using of the roll decay test, the first two peaks are $\phi_1 = 8^\circ$ and $\phi_2 = 5.7^\circ$. The non- dimensional damping coefficient and roll natural period obtain $\zeta_\phi = 0.054$ and $T_\phi = 5.5$ sec. by using Eq. (8). The calculated restoring and damping moment coefficients for the fishing vessel are expressed in Table 3. Some other data are given as follows: Sea water density: $\rho = 1025\ (kg/m^3)$, Gravity constant: $g = 9.81(m/s^2)$, $k_{p|p|}$: 5% of k_p, Added mass moment of inertia: 20% of displacement.

The open loop roll system is simulated using MSS toolbox. The roll responses for two state linear and nonlinear models for initial roll angle 5° are shown in Figure 6 and Figure 7. The results show the nonlinear terms cause deviation of linear model but the amplitude of these deviations, in order to design controller, is negligible.

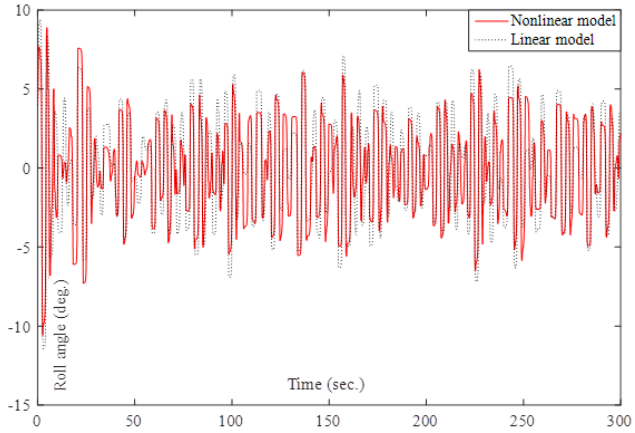

Figure 6. Comparison of open loop response for linear and nonlinear models with initial roll angle 5°

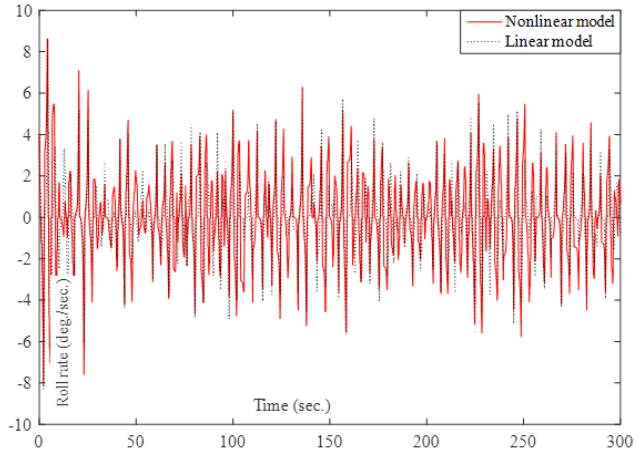

Figure 7. Comparison of open loop response for linear and nonlinear models

The closed loop fin-roll system is simulated by employing the constrained LQR controller with fin for initial roll angle 5°. Simulation results were compared with the results of the PID controller presented by [14] and the uncontrolled system. Figure 8 and Figure 9 show that the amplitude of the roll angle and roll rate in the constrained LQR controller is smaller and smoother than PID controller.

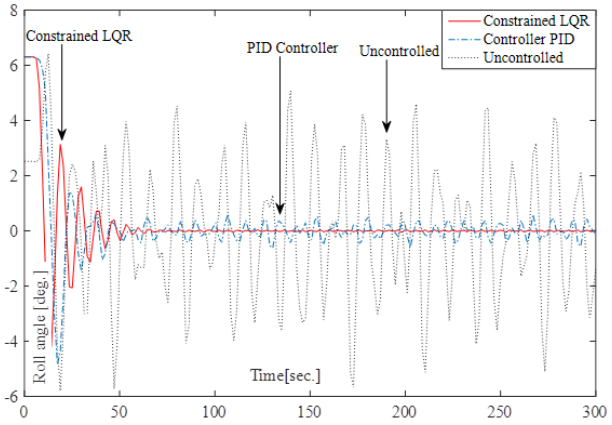

Figure 8. Comparison of roll angle response for the constrained LQR, PID controller and uncontrolled with initial roll angle 5°

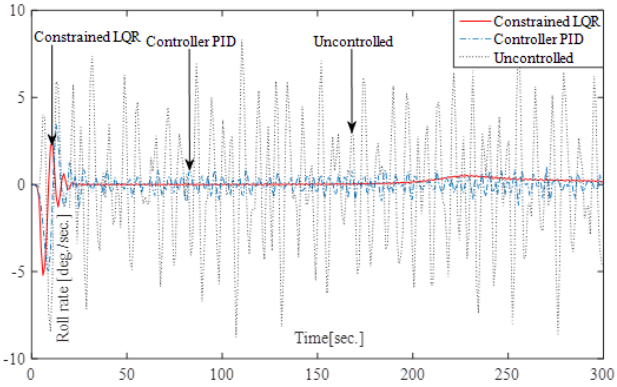

Figure 9. Comparison of roll rate response for the constrained LQR, PID controller, and uncontrolled

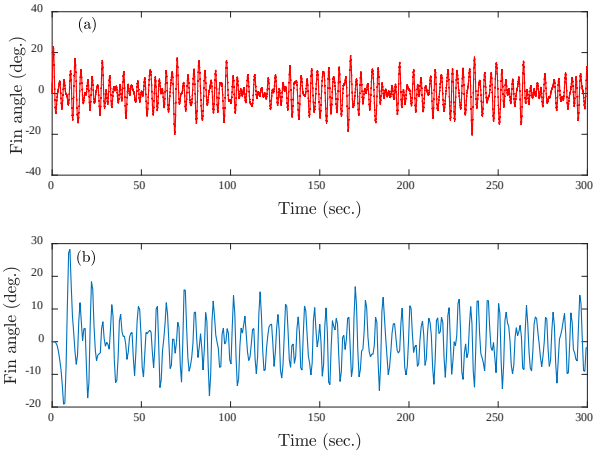

Figure 10. Variations of the fin regarding to the two controllers, a) Constrained LQR, b) PID controller

The mechanical angles of the fin in the simulations for two LQR and PID controller have been shown in Figure 10. The characteristics of simulation results for two controllers are summarized in table (4) which shows roll angle and roll rate, by using constrained LQR control are improved about 50% in comparison with the results of PID controller.

Table 4. Comparison of the controller's performance

Controller	Max. roll angle (deg.)	Max. roll rate (deg./s)
Uncontrolled	6.5	8
PID Controller	2	2.5
Constrained LQR	1	0.7

5. Conclusion

In this paper, the nonlinear modeling was derived for the fin-roll motion. The coefficients of nonlinear model, the nonlinear damping, and restoring terms were computed by means of the empirical formulas and numerical calculations by using the CFD method and MATLAB software. By considering the NACA0015 section, flow analysis and lift coefficient computation are presented by CFD method. Also, a constrained LQR was designed to satisfy the operational constraints of the roll motion including the mechanical fin angle and the dynamic stall saturations in order to achieve the desired performance. The simulation results for two constrained LQR and PID controllers were presented and compared in the presence of irregular wave. All in all, the simulation results showed that the constrained LQR reduced the RMS value of the roll motion.

References

[1] Perez T, 2005. Ship motion control: course keeping and roll stabilization using rudder and fins, Springer Pub., London.

[2] Perez T., Blanke M., 2012. Ship roll damping control. Annual Reviews in Control, 36, 129-147.

[3] Sellars F.H., Martin J.P., 1999. Selection and evaluation of ship roll stabilization systems. Mar. Tech., SNAME, 29, 84-101.

[4] Taylan M., 2000. The effect of nonlinear damping and restoring in ship rolling, Ocean Eng., 27, 921–932.

[5] Surendran S., Venkata Ramana Reddy R., 2002. Roll dynamics of a Ro–Ro ship. Int. Shipbuilding Prog., 49, 301-320.

[6] Liang Y. H., Jin H. Z., Liang L.H., 2008. Fuzzy-PID controlled lift feedback fin stabilizer, J. Mar. Sci. and App., 7(2), 127-134.

[7] Alarçin, F., 2014. Nonlinear modelling of a fishing boat and Fuzzy Logic Control Design for electro-hydraulic fin stabilizer system, Nonlinear Dyn., 76, 581-590.

[8] Ghassemi, H., Dadmarzi, F., Ghadimi, P., & Ommani, B., 2010. Neural network-PID controller for roll fin stabilizer. Pol. Mar. Res., 17, 23-28.

[9] Alarçin F., Demirel H., Ertugrul Su M., Yurtseven A., 2014. Modified PID control design for roll fin actuator of nonlinear modeling of the fishing boat, Pol. Mar. Res. 21(81), 3-8.

[10] Zhang, J. W., Andrews D J., 1999. Roll damping characteristics of a trimaran displacement Ship, Int. shipbuilding Progress, 46, 445-472.

[11] Moradi M., Malekizade H., 2013. Robust adaptive first-second-order sliding mode Control to stabilize the uncertain fin- roll dynamic, Ocean Eng. 69, 18-23.

[12] Sungkyun Lee, Key-Pyo Rhee, 2011. Design of the roll stabilization controller, Using fin stabilizers and pod propellers, Applied Ocean Res., 33, 229-239.

[13] Hinostroza M.A., Luo W., Guedes Soares C., 2015. Robust fin control for ship roll Stabilization based on L2-gain design, Ocean Eng. 94, 126-131.